

UNIVERSAL  
LIBRARY

OU 166830

UNIVERSAL  
LIBRARY





OUP—707—25-4-81—10,000.

**OSMANIA UNIVERSITY LIBRARY**

Call No. 669  
B275

Accession No. 27236

Author

Title

This book should be returned on or before the date last marked below



**METALLURGY AND METALLURGICAL ENGINEERING SERIES**

**ROBERT F. MEHL, PH.D., D.Sc., *Consulting Editor***

## **Structure of Metals**

*The quality of the materials used in the manufacture  
of this book is governed by continued postwar shortages.*



# Structure of Metals

## CRYSTALLOGRAPHIC METHODS, PRINCIPLES, AND DATA

BY

CHARLES S. BARRETT, PH.D.

*Associate Professor of Metallurgical Engineering and Member  
of Staff of the Metals Research Laboratory  
Carnegie Institute of Technology*

FIRST EDITION

FIFTH IMPRESSION

McGRAW-HILL BOOK COMPANY, INC.  
NEW YORK AND LONDON

1943

STRUCTURE OF METALS

COPYRIGHT. 1943, BY THE  
MCGRAW-HILL BOOK COMPANY, INC.

— - -

PRINTED IN THE UNITED STATES OF AMERICA

*All rights reserved. This book, or  
parts thereof, may not be reproduced  
in any form without permission of  
the publishers.*

## P R E F A C E

This book is intended to serve both as a text and as a reference book. The portions intended for classroom use have been written for courses in crystallography, particularly the courses offered to students of metallurgy. It is primarily intended for graduate courses, but a number of chapters are at a level appropriate for advanced undergraduate courses in applied x-rays, crystallography, and physical metallurgy (Chaps. I to IV, IX to XI, XIII). In an effort to make the book more readable, certain advanced topics on x-ray diffraction and various tables of data have been placed in appendixes, and laboratory manipulations that would not interest the general reader have been printed in smaller type.

The first four chapters of this book explain the fundamentals of crystal lattices and projections, and the general principles of the diffraction of x-rays from crystals. Chapters V to VII cover the technique of x-ray diffraction, presenting the operating details of the methods that are in common use. Several chapters are included on the applications of x-ray diffraction in the field of physical metallurgy, covering techniques for determining constitution diagrams, identifying unknown materials, determining crystal structures, determining the orientation of single crystals, detecting and analyzing preferred orientations, and measuring stresses.

One chapter is devoted to electron diffraction, its metallurgical uses, and the precautions to be observed in interpreting electron diffraction data. The electron microscope receives only a brief mention because at the time the manuscript was written the metallographic technique for this instrument was still being rapidly developed and, except for particle-size determinations, the instrument had not yet achieved the status of a widely accepted tool in metallographic or crystallographic research.

The last half of the book is devoted to the results of research and contains extensive reviews of fields that are of current interest. In assembling these summaries, an effort has been made to include an adequate number of references to the literature, to cover thoroughly the subjects that have not been extensively reviewed in readily available publications, and to maintain a critical but unbiased attitude toward the data and conclusions that are reviewed. The subjects treated include the following: principles governing the crystal structure of metals and

alloys; superlattices and their effect on properties; imperfections in crystals; the structure of liquid metals; the processes of slip, twinning, and fracture and modern theories of these processes, including the current "dislocation theory"; the effects of cold work and annealing on the structure of metals, including the effects on diffraction patterns of static and fatigue stressing, rolling, grinding, and polishing; the results of x-ray studies of internal stresses; preferred orientations resulting from cold work, hot work, recrystallization, freezing, electrodeposition, evaporation, and sputtering; directionality in commercial products and in single crystals and its relation to crystal orientation.

The author is indebted to many colleagues and graduate students who have assisted directly and indirectly in the preparation of this book. He particularly wishes to thank Dr. R. F. Mehl, head of the Department of Metallurgy and director of the Metals Research Laboratory at Carnegie Institute of Technology, who guided the organization of the courses out of which the book evolved, encouraged publication of the material, and offered valuable criticisms of the manuscript.

The author is also grateful for original prints furnished by a number of investigators and manufacturers. These are acknowledged individually in the text. Permission has been given to reproduce numerous illustrations and extracts from books and journals, for which the writer wishes to express his appreciation to the authors and publishers. Figure 15/I is from W. L. Bragg, "The Crystalline State," by permission of The Macmillan Company; Fig. 20/I is from R. W. James, "X-Ray Crystallography," by permission of E. P. Dutton & Company; Figs. 4/XI and 5/XI are from W. Hume-Rothery, "Structure of Metals," by permission of The Institute of Metals; Figs. 5/V, 6/V, 7/V, and 14/VII are from R. W. G. Wyckoff, "The Structure of Crystals," by permission of Reinhold Publishing Corporation; Figs. 9/III, 16/XI, and 17/XI are from G. L. Clark, "Applied X-Rays," and Figs. 11/VI, 12/VI, 13/VI, 15/VII, and 16/VII from W. P. Davey, "A Study of Crystal Structure and Its Applications," both published by McGraw-Hill Book Company, Inc.; Figs. 10, 12 to 14, 17 to 21 of Chap. IV and Figs. 1/X and 13/XXII are from the "Metals Handbook" of the American Society for Metals; Fig. 2/V is from the "Symposium on Radiography and X-Ray Diffraction," of the American Society for Testing Materials; and much of the material in Chap. X is from an article by the author in the *Journal of Applied Physics*. Appropriate references to the source of illustrations and data from the technical journals are given in the text.

CHARLES S. BARRETT.

PITTSBURGH, PA.  
June, 1943.



# CONTENTS

	Page
PREFACE . . . . .	v
CHAPTER	
I. THE FUNDAMENTALS OF CRYSTALLOGRAPHY. . . . .	1
Space-lattices and Crystal Systems . . . . .	2
Miller Indices. . . . .	7
Hexagonal Indices . . . . .	9
Transformation of Indices . . . . .	11
Law of Rational Indices . . . . .	12
Zones and Zone Axes; Crystal Geometry. . . . .	12
Symmetry Classes and Point Groups. . . . .	13
Space Groups . . . . .	19
Glide Planes and Screw Axes . . . . .	21
Space-group Notation . . . . .	22
Tables of Equivalent Points . . . . .	24
II. THE STEREOGRAPHIC PROJECTION . . . . .	25
Reference Sphere and Its Stereographic Projection . . . . .	25
Projection of Great and Small Circles . . . . .	27
Ruled Globe and Stereographic Nets. . . . .	29
Rotation with the Nets . . . . .	31
Angle Measurement. . . . .	32
Properties of Stereographic Projection . . . . .	33
Standard Projections of Crystals . . . . .	33
Orientation of Single-crystal Wires and Disks . . . . .	34
Applications to Metallography . . . . .	37
Other Perspective Projections . . . . .	42
III. X-RAYS. . . . .	44
The Continuous Spectrum . . . . .	46
The Characteristic Spectrum . . . . .	47
Moseley's Law . . . . .	48
Origin of Characteristic Radiation and Absorption . . . . .	49
Dependence of Line Intensities on Voltage . . . . .	52
Absorption of X-rays . . . . .	53
Filtering . . . . .	56
The Scattered Radiation . . . . .	58
X-ray Tubes . . . . .	59
Electrical Equipment for Diffraction Tubes. . . . .	62
X-ray Protection . . . . .	64
Photographic Efficiency of X-rays . . . . .	65
IV. DIFFRACTION OF X-RAYS BY CRYSTALS. . . . .	69
Scattering of X-rays by Atoms . . . . .	69
Bragg's Law . . . . .	70

CHAPTER	PAGE
The Laue Equations. . . . .	71
Interplanar Spacings. . . . .	76
Relation of Atom Arrangement to the Diffraction Pattern . . . . .	77
Relation of Atom Arrangement to Diffracted Intensities . . . . .	78
The Structure-factor Equation . . . . .	78
X-ray Diffraction Methods. . . . .	80
The Laue Method. . . . .	80
The Rotating-crystal Method . . . . .	82
The Powder Method. . . . .	83
 V. THE LAUE METHOD . . . . .	 88
Determination of Symmetry . . . . .	89
Assigning Indices to Spots by Gnomonic Projection . . . . .	90
Analysis of Crystal Structure from Laue Photographs . . . . .	93
The Shapes of Laue Spots . . . . .	93
 VI. ROTATING-CRYSTAL METHODS. . . . .	 97
Interpretation of Rotation Photographs . . . . .	98
Assigning Indices to Spots . . . . .	100
Identifying Face-centered and Body-centered Lattices . . . . .	101
The Reciprocal Lattice. . . . .	101
Diffraction and the Reciprocal Lattice . . . . .	103
Relation of the Reciprocal Lattice to the Film . . . . .	106
Determining Unit-cell Dimensions . . . . .	107
Assigning Indices to Reflections . . . . .	108
Oscillating-crystal Photographs . . . . .	109
The Weissenberg Goniometer. . . . .	111
 VII. THE POWDER METHOD. . . . .	 115
Cylindrical Cameras. . . . .	115
Choice of Camera Dimensions . . . . .	119
High-temperature Cameras . . . . .	119
Low-temperature Cameras . . . . .	120
Focusing Cameras . . . . .	121
Back-reflection Cameras . . . . .	122
Choice of Radiation. . . . .	125
Interpretation of Powder Patterns. . . . .	125
Graphical Methods of Solving Patterns. . . . .	127
Precision Determinations of Lattice Constants . . . . .	132
Errors and Corrections in Debye Cameras . . . . .	132
Graphical Extrapolation Methods for Debye Films . . . . .	134
Extrapolation for Cylindrical Back-reflection Cameras. . . . .	135
Cohen's Method. . . . .	136
Scale of Wavelengths Used. . . . .	138
Chemical Analysis by X-ray Diffraction . . . . .	139
Field of Application of Diffraction Analysis. . . . .	141
Particle-size Determination. . . . .	142
 VIII. THE DETERMINATION OF CRYSTAL STRUCTURE. . . . .	 144
Determination of Symmetry Class. . . . .	144
Determination of the Unit Cell . . . . .	145
Determination of Space-lattice and Space Group . . . . .	146

CHAPTER	PAGE
Number of Atoms or Molecules per Unit Cell. . . . .	148
Determination of Atomic Positions . . . . .	149
Sizes of Atoms and Ions . . . . .	150
Example of Structure Determination. . . . .	151
<b>IX. POLE FIGURES AND ORIENTATION DETERMINATIONS . . . . .</b>	<b>154</b>
Detection of Preferred Orientations . . . . .	154
Stereographic Projection of Data . . . . .	155
Fiber Textures . . . . .	156
Plotting of Pole Figures . . . . .	158
Specimens and Cameras for Texture Studies . . . . .	162
Orientation of the Axis of Single-crystal Rods. . . . .	163
Complete Orientation of Single Crystals . . . . .	165
Back-reflection Laue Method for Determining Crystal Orientation .	167
The Transmission Laue Method. . . . .	172
The Determination of Orientations by Etch Pits . . . . .	173
<b>X. DETERMINATION OF CONSTITUTION DIAGRAMS WITH X-RAYS . . . . .</b>	<b>178</b>
Comparison of Methods . . . . .	178
Binary Diagrams—Disappearing-phase Method. . . . .	179
Parametric Method . . . . .	182
Accuracy of the Parametric Method. . . . .	183
Ternary Diagrams. . . . .	185
Disappearing-phase Method in Ternary Diagrams. . . . .	187
Parametric Method in Ternary Diagrams. . . . .	187
Laborsaving Principles . . . . .	188
Quasi-binary Systems . . . . .	193
Complexities . . . . .	195
<b>XI. THE STRUCTURE OF METALS AND ALLOYS. . . . .</b>	<b>196</b>
<i>Structures of the Elements</i> . . . . .	197
The 8 — N Rule . . . . .	199
Allotropy. . . . .	201
<i>Solid Solutions</i> . . . . .	201
Types of Solid Solution . . . . .	201
Determination of the Type of Solid Solution . . . . .	205
Generalizations Concerning Solubility . . . . .	205
<i>Intermediate Phases</i> . . . . .	208
Structures of Compounds with Normal Valency. . . . .	208
Structurally Analogous Phases and Hume-Rothery's Rule . . . . .	211
Norbury's Electron-Atom Ratios . . . . .	215
Interstitial Compounds. . . . .	216
Phases Containing Alkali and Alkaline-earth Elements . . . . .	217
Periodic Relations in Iron Alloys . . . . .	219
Imperfections in Crystals. . . . .	219
<i>The Structure of Liquid Metals.</i> . . . .	224
Earlier Methods of Analysis . . . . .	224
The Radial-distribution Method. . . . .	224
Liquid Metals. . . . .	227
Liquid Alloys. . . . .	228
The Amorphous State . . . . .	229

XII. SUPERLATTICES . . . . .	230
Common Types of Superlattices. . . . .	231
Elements of Superlattice Theory . . . . .	235
Short-range Order. . . . .	238
Dependence of $T_c$ on Composition. . . . .	240
Phenomena Related to Superlattices. . . . .	241
Specific Heats of Superlattices . . . . .	242
Electrical Resistivity of Superlattices . . . . .	243
Other Physical Properties of Superlattices . . . . .	246
The Rate of Approach to Equilibrium . . . . .	248
Compounds, Superlattices, and Solid Solutions Compared . . . . .	249
XIII. THE ELECTRON THEORY OF METALS AND ALLOYS . . . . .	251
Metallic Binding . . . . .	251
Cohesive and Repulsive Forces in Metals. . . . .	251
Electron Energies in a Metal . . . . .	254
The Zone Theory of Solids . . . . .	257
Zones in Conductors and Insulators . . . . .	259
Factors Affecting Electrical Resistance of Metals . . . . .	260
Energy Levels and Ferromagnetism . . . . .	261
Paramagnetism and Diamagnetism . . . . .	264
Zone Theory of Alloy Phases . . . . .	265
XIV. STRESS MEASUREMENT BY X-RAYS . . . . .	267
Elastic Stress-Strain Relations . . . . .	268
Method for Sum of Principal Stresses ( $\sigma_1 + \sigma_2$ ) . . . . .	270
Equations for the Ellipsoid of Strain and of Stress. . . . .	272
Two-exposure Method for $\sigma_\phi$ . . . . .	273
Correction for Oscillation of Film (Two-exposure Method) . . . . .	275
Single-exposure Method for $\sigma_\phi$ . . . . .	275
Methods for Determining $\sigma_1$ and $\sigma_2$ When Their Directions Are Known . . . . .	276
Method Giving Magnitude and Direction of Principal Stresses . . . . .	277
Values of the Elastic Constants. Anisotropy. . . . .	278
Equipment for Stress Measurement . . . . .	279
Applications . . . . .	280
X-ray vs. Other Methods of Residual-stress Analysis . . . . .	286
XV. THE PLASTIC DEFORMATION OF METALS . . . . .	288
<i>Slip in Metal Crystals</i> . . . . .	288
Slip Planes and Directions . . . . .	288
Slip Lines . . . . .	291
Critical Resolved Shear Stress for Slip. . . . .	294
Dependence on Temperature . . . . .	298
Strain Hardening . . . . .	298
Dependence of Strain Hardening on Temperature. . . . .	300
Lattice Rotation with Simple Slip. . . . .	302
Duplex Slip. . . . .	304
Rotation from Duplex Slip . . . . .	304
Deformation Bands . . . . .	305
Lattice Bending. . . . .	307

CHAPTER	PAGE
<i>Twinning</i> . . . . .	307
Deformation Twins . . . . .	308
Crystallography of Twins . . . . .	311
Orientations from Twinning . . . . .	311
Atom Movements in Twinning . . . . .	313
Critical Stress for Twinning . . . . .	315
Deformation by Twinning . . . . .	315
<i>Fracture</i> . . . . .	317
Brittle Cleavage . . . . .	317
Theoretical Calculations of Cleavage Strength . . . . .	319
Furth's Theory . . . . .	321
Shearing Fracture . . . . .	321
Relative Stresses for Slip, Twinning, and Cleavage . . . . .	322
<i>Plastic Flow in Polycrystalline Metal</i> . . . . .	325
Grain Boundaries and Their Effect on Plastic Flow . . . . .	325
The Effect of Grain Size on Plastic Flow and Hardness . . . . .	326
The Hardness of Solid Solutions . . . . .	326
The Effect of Fineness of Microstructure in Steels . . . . .	328
The Bauschinger Effect and the Elastic Aftereffect . . . . .	329
Taylor's Theory of Flow in Aggregates . . . . .	330
XVI. THEORIES OF SLIP . . . . .	332
Stress Concentrations . . . . .	332
Becker-Orowan Theory . . . . .	333
<i>The Theory of Dislocations</i> . . . . .	334
Nature of a Dislocation . . . . .	334
Strain Hardening . . . . .	335
Slip Lines . . . . .	338
Temperature Effects . . . . .	339
Residual Energy from Cold Work . . . . .	339
Solid-solution Hardening . . . . .	340
Age Hardening . . . . .	340
Internal Friction . . . . .	341
Creep . . . . .	344
Summary . . . . .	347
XVII. THE STRUCTURE OF COLD-WORKED METAL . . . . .	349
<i>Asterism</i> . . . . .	350
The Optical Analogy for Asterism . . . . .	350
Interpretation of Asterism in Terms of Range of Orientation . . . . .	351
Asterism and Internal Stresses . . . . .	354
Crossed-grating Theory for Cold-worked Metals . . . . .	356
Asterism from Thermal Vibration . . . . .	357
Asterism from Structural Irregularity . . . . .	358
Local Curvature . . . . .	359
Tests of the Local-curvature Theory . . . . .	361
Inhomogeneous Distortion in Polycrystalline Aggregates . . . . .	362
<i>Diffraction-line Widths and Intensities</i> . . . . .	363
Lattice Constants Varying from Block to Block . . . . .	364
Atomic Displacements within a Block . . . . .	366
Measurements of Line Broadening . . . . .	367
Intensities of Diffraction Lines from Cold-worked Metals . . . . .	372

Recovery of Line Sharpness during Annealing . . . . .	375
X-ray Studies of Fatigue . . . . .	377

<b>XVIII. PREFERRED ORIENTATIONS RESULTING FROM COLD WORK . . . . .</b>	<b>381</b>
Textures of Polycrystalline Wires . . . . .	382
Textures of Eutectic Wires . . . . .	385
Compression Textures . . . . .	385
Theories of Tension and Compression Textures . . . . .	387
Deformation Bands in the Compression of Iron . . . . .	391
Deformation Bands in the Compression of Aluminum . . . . .	393
Deformation Bands in the Elongation of Iron . . . . .	394
<i>Rolling Textures</i> . . . . .	395
Face-centered Cubic Rolling Textures . . . . .	395
Surface Textures in Face-centered Metals . . . . .	401
Deformation Bands in Rolled Face-centered Cubic Metals . . . . .	402
Body-centered Cubic Rolling Textures . . . . .	402
Theories of the Rolling Textures . . . . .	406
The Layer Structure of Rolled Steel . . . . .	407
Variables Affecting the Texture of Steel . . . . .	408
Hexagonal Close-packed Rolling Textures . . . . .	410
Cross Rolling . . . . .	415
Hot Rolling . . . . .	416
Torsion Textures . . . . .	417
Cold-drawn Tubes . . . . .	417
Textures in Deep Drawing . . . . .	417
Textures from Machining and Polishing . . . . .	418
Summary . . . . .	419
<b>XIX. PREFERRED ORIENTATIONS AFTER RECRYSTALLIZATION . . . . .</b>	<b>420</b>
Recrystallized Face-centered Cubic Fiber Textures . . . . .	421
Recrystallized Body-centered Cubic Fiber Textures . . . . .	424
Face-centered Cubic Rolling Recrystallization Textures . . . . .	424
The Cube Texture . . . . .	425
Body-centered Cubic Rolling Recrystallization Textures . . . . .	431
Hexagonal Close-packed Rolling Recrystallization Textures . . . . .	433
Summary . . . . .	434
<b>XX. ORIENTATIONS IN CASTINGS AND IN DEPOSITED FILMS . . . . .</b>	<b>435</b>
Textures in Cast Metal . . . . .	436
Orientations in Electrodeposits . . . . .	437
Evaporated and Sputtered Metal Films . . . . .	439
Films Deposited on Single Crystals . . . . .	441
<b>XXI. ANISOTROPY . . . . .</b>	<b>443</b>
Directionality in the Strength Properties . . . . .	443
Miscellaneous Tests for Anisotropy . . . . .	449
Anisotropy of Elastic Properties of Crystals . . . . .	453
Elastic Moduli in Aggregates . . . . .	456
Anisotropy of Physical Properties in Crystals . . . . .	458

# CONTENTS

xiii

CHAPTER	PAGE
XXII. AGE HARDENING AND TRANSFORMATIONS . . . . .	461
Theories of Age Hardening . . . . .	461
Microstructures Resulting from Precipitation . . . . .	464
Lattice Relationships in Widmanstätten Structures . . . . .	466
Plane of Precipitation . . . . .	469
Shape of Precipitated Particles . . . . .	470
Diffraction in the Early Stages of Aging. . . . .	470
Phase Transformations in Pure Metals . . . . .	474
Structures in Steel. . . . .	475
Orientations from the Decomposition of Austenite . . . . .	480
Habit Planes for Austenite Decomposition Products . . . . .	484
Orientations in Other Reactions. . . . .	491
XXIII. ELECTRON DIFFRACTION . . . . .	493
Electron Waves . . . . .	493
Apparatus . . . . .	494
Specimens . . . . .	496
Identification of Polycrystalline Materials . . . . .	497
Preferred Orientations . . . . .	502
Polished Surfaces . . . . .	503
Diffraction from Single Crystals. . . . .	505
Intensity of Scattering . . . . .	508
Secondary Effects . . . . .	508
APPENDIX	
I. CRYSTAL GEOMETRY. . . . .	511
II. EMISSION AND ABSORPTION WAVELENGTHS . . . . .	516
III. ABSORPTION COEFFICIENTS . . . . .	520
IV. REFLECTING PLANES OF CUBIC CRYSTALS. . . . .	522
V. THE INTENSITY OF X-RAY REFLECTIONS . . . . .	524
VI. DETERMINATION OF CRYSTAL STRUCTURE WITH FOURIER SERIES . . . . .	542
VII. CRYSTAL STRUCTURES OF THE ELEMENTS . . . . .	552
VIII. INTERNATIONAL ATOMIC WEIGHTS . . . . .	555
IX. PHYSICAL CONSTANTS AND NUMERICAL FACTORS. . . . .	556
INDEX . . . . .	557





# STRUCTURE OF METALS

## CHAPTER I

### THE FUNDAMENTALS OF CRYSTALLOGRAPHY

A crystal consists of atoms arranged in a pattern that repeats periodically in three dimensions. The regular repetition of the unit of structure in a crystal is analogous to a pattern of wallpaper. The design of the wallpaper consists of a fundamental unit of the design placed in parallel fashion at each point of a two-dimensional lattice; the structure of a crystal consists of a unit of structure—an atom or group of atoms—placed in parallel fashion at each point of a three-dimensional lattice.

Crystallinity is completely absent in a **gas**, owing to the kinetic and random motion of the atoms, but in a **liquid** the velocity of atomic movement is less, and some tendency to take a regular arrangement is apparent. If an instantaneous photograph of a liquid could be taken that would show the individual atoms, it would disclose several clusters in which the atoms have the close packing characteristic of the crystalline state. These clusters are potential nuclei of the solid phase, but above the melting point they are unable to maintain their close-packed near-crystalline arrangement against the severe thermal agitation of the atoms of which they are composed and the bombardment of the impinging atoms. In some substances the liquid arrangement may be frozen in by rapid cooling, and the material hardens into the **glassy state** and is a supercooled liquid. The vitreous state acquired in this way then persists until the atoms are given an opportunity to rearrange themselves; annealing below the melting point permits a glass to crystallize (devitrify) and become a true solid.

Molten metals do not supercool to the glassy state, but it is possible to produce an amorphous or nearly amorphous condition in many metals by electrodeposition. Bridgman has also succeeded in disrupting almost completely the crystallinity of certain metals by extreme amounts of twisting, and there is some evidence (perhaps wrongly interpreted) that polished layers on metals are amorphous. It is safer to say that the grain size in these controversial cases is extremely small. The individual crystals in a polycrystalline aggregate may have any size from macroscopic dimensions down to the unit of structure or less. Obviously, there

can be no regular repetition in the atomic pattern if the grain size is of the order of one structural unit, and so the crystallinity would really be zero at the lower limit of grain size. It is thus inconsistent to speak of the crystal structure of a glass or of an amorphous body, even though a fundamental configuration can be found in it, for there is no periodicity to the configuration. Intermediate degrees of crystallinity are possible as the grain size increases above this lower limit.

Carbon and various organic and inorganic substances may exist in semicrystalline states that possess periodicity in one or two dimensions but lack it in others. The **mesomorphic state** possessed by certain long-chain organic substances (also called "liquid crystals") affords examples of various intermediate types of regularity. A lack of periodicity in one dimension has been discovered in some varieties of mica and is characteristic of the early stages of age-hardening in certain alloys.

**Space-lattices and Crystal Systems.**<sup>1</sup>—The atomic array in a crystal is conveniently described with respect to a three-dimensional net of straight

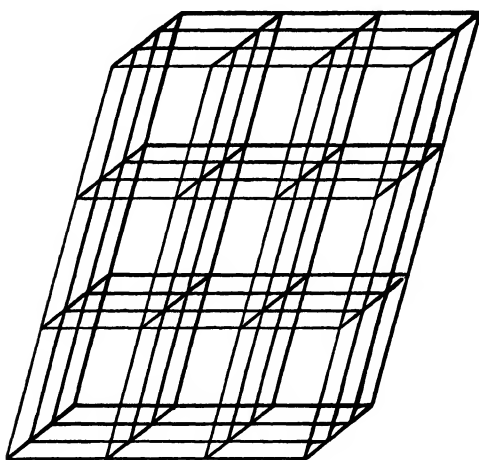


FIG. 1.—A space lattice.

lines. Imagine a lattice of lines, as in Fig. 1, dividing space into equal-sized prisms which stand side by side with all faces in contact so as to fill space with no voids. The intersections of the lines are points of a space-lattice. These points are of fundamental importance in descriptions of crystals, for they may be the positions occupied by atoms in crystals—as they are in the common metals—or they may be points about which several atoms are clustered. Since prisms of many different shapes can be

drawn through the points of a space-lattice to partition the crystal into cells, the manner in which the network of reference lines is drawn is arbitrary. They need not be drawn so that lattice points lie only at the corners of the unit prisms; in fact, it is found more convenient to describe some crystals with respect to prisms in which points lie not only at prism corners but also at prism centers or at the centers of prism faces.

The important characteristic of a space-lattice is that *every point of a space-lattice has identical surroundings*. The grouping of lattice points about any given point is identical with the grouping about any other point

<sup>1</sup> The space-lattices are also called "translation groups" because there are certain movements—"primitive translations"—which by repetition will lead from one lattice point to any other. Space-lattices are also referred to as "Bravais lattices."

in the lattice. If it were possible for a tiny observer to hop about on the lattice points, he would be unable to distinguish one from another, for the rows and planes of points near each point would be identical; and if he wandered among the atoms of a solid metal or a chemical compound, he would find the outlook from any lattice point just like that from any other.

There are 14 space-lattices. No more than 14 ways can be found in which points can be arranged in space so that each point has identical surroundings. There are, of course, many more than fourteen ways in which actual crystals may be built up of atoms piled together; *i.e.*, there are a great many **crystal structures**. However, each of the structures consists of some fundamental pattern repeated at each point of a space-lattice. The schemes of repetition, the *space-lattices*, are very limited in number while the possible *crystal structures* are almost unlimited. Not infrequently the term "lattice" has been loosely used as a synonym for "structure," a practice that is incorrect and likely to be confusing.

To specify a given arrangement of points in a space-lattice or of atoms in a structure, it is customary to give their coordinates with respect to a set of coordinate axes chosen with an origin at one of the lattice points. Cubic crystals, for example, are referred to a cubic set of axes, three axes of equal length that stand perpendicular to one another and that form three edges of a cube. Each space-lattice has some convenient set of axes that is conventionally used with it, some axes being equal in length and others unequal, some standing at right angles and others not. Seven different **systems of axes** are used in crystallography, each possessing certain characteristics as to equality of angles and equality of lengths. These are the basis of the seven **crystal systems** employed, for instance, in the classification of minerals. Referring to Fig. 2, the lengths of the three axes of a system are  $a$ ,  $b$ , and  $c$ , respectively; the angles are  $\alpha$ ,  $\beta$ , and  $\gamma$ , with the angle  $\alpha$  opposite the  $a$  axis, etc. The crystal systems are listed in Table I, together with their axial lengths, angles, and some examples of crystals belonging to each classification. When a crystal structure is determined, definite values are found for the axial lengths, angles, and ratios  $c/a$  and  $b/a$ ; different substances crystallizing in a given system will have different values for these variables.

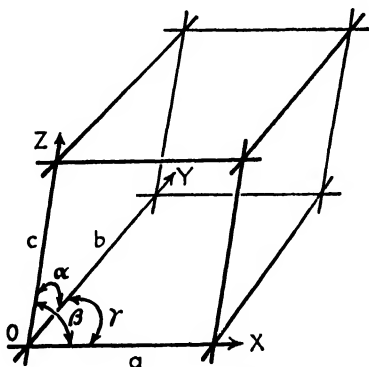


FIG. 2.—Crystal axes.

The network of lines through the points of a space-lattice, as in Fig. 1, divides it into prisms called **unit cells**. Each unit cell in a space-lattice is identical in size, shape, and orientation with every other. It is the

TABLE I.—THE CRYSTAL SYSTEMS

System	Axes and interaxial angles	Examples
Triclinic	Three axes not at right angles, of any lengths $a \neq b \neq c$ $\alpha \neq \beta \neq \gamma \neq 90^\circ$	$K_2CrO_7$
Monoclinic	Three axes, one pair not at right angles, of any lengths $a \neq b \neq c$ $\alpha = \beta = 90^\circ \neq \gamma$	$\beta$ -S $CaSO_4 \cdot 2H_2O$ (gypsum)
Orthorhombic (rhombic)	Three axes at right angles; all unequal $a \neq b \neq c$ $\alpha = \beta = \gamma = 90^\circ$	$\alpha$ -S Ga $Fe_3C$ (cementite)
Tetragonal	Three axes at right angles; two equal $a = b \neq c$ $\alpha = \beta = \gamma = 90^\circ$	$\beta$ -Sn (white) $TiO_2$
Cubic	Three axes at right angles; all equal $a = b = c$ $\alpha = \beta = \gamma = 90^\circ$	Cu, Ag, Au Fe NaCl
Hexagonal	Three axes coplanar at $120^\circ$ , equal Fourth axis at right angles to these $a_1 = a_2 = a_3 \neq c$ (or $a_1 = b \neq c$ , $\alpha = \beta = 90^\circ$ , $\gamma = 120^\circ$ )	Zn, Cd NiAs
Rhombohedral (trigonal)	Three axes equally inclined, not at right angles; all equal $a = b = c$ $\alpha = \beta = \gamma \neq 90^\circ$	As, Sb, Bi Calcite

building block from which the crystal is constructed by repetition in three dimensions. Each face of a unit cell is a parallelogram (Fig. 2); the cell is a parallelepiped with the axes  $a$ ,  $b$ , and  $c$  as edges. In the hexagonal system, two axes,  $a_1$  and  $a_2$ , are equal in length and are at  $120^\circ$  to each other. These two, together with the  $c$  axis that stands  $90^\circ$  to each, form the edges of the unit cell; there is also a third axis,  $a_3$ , that is coplanar with  $a_1$  and  $a_2$  and  $120^\circ$  from each, which is used when one wishes to show the full symmetry of the lattice.

Unit cells are drawn with lattice points at all corners. Unit cells in some lattices are drawn so as to have lattice points at the center of certain faces or at the center of volume in addition to the points at the corners. This is done as a matter of convenience so that the symmetry of the unit cell will be more closely that of the crystal. It is customary to specify the positions of the points in a unit cell by means of **lattice coordinates**, in which each coordinate is a fraction or a multiple of the axial length,  $a$ ,  $b$ , or  $c$ , in the direction of the coordinate. The origin of coordinates is

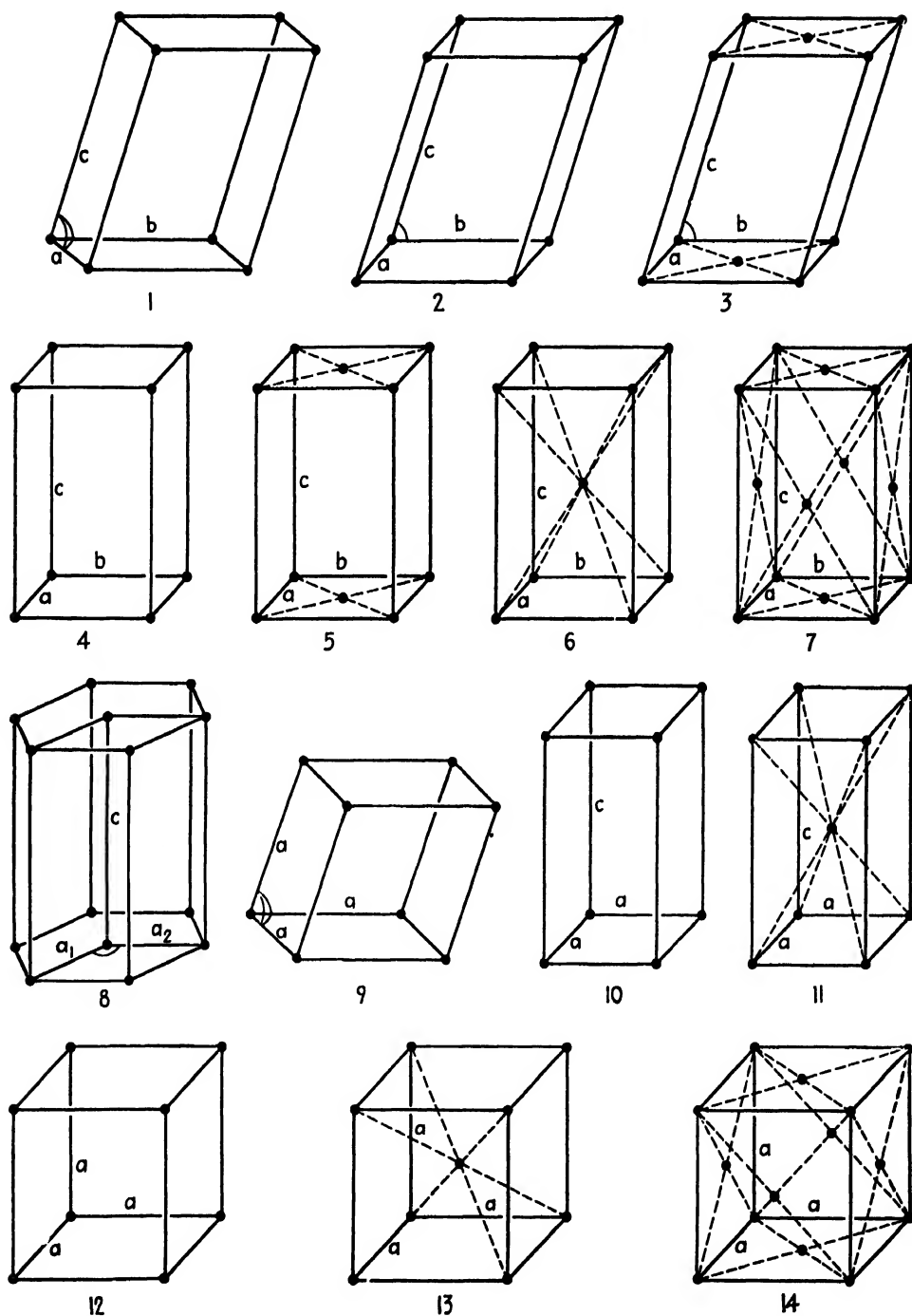


FIG. 3.—The 14 space lattices illustrated by a unit cell of each: (1) triclinic, simple; (2) monoclinic, simple; (3) monoclinic, base centered; (4) orthorhombic, simple; (5) orthorhombic, base centered; (6) orthorhombic, body centered; (7) orthorhombic, face centered; (8) hexagonal; (9) rhombohedral; (10) tetragonal, simple; (11) tetragonal, body centered; (12) cubic, simple; (13) cubic, body centered; (14) cubic, face centered.

taken at the corner of a cell. A point at any other cell corner then has coordinates  $m, n, p$ , where these numbers are all integers. All points at the centers of unit cells have coordinates  $m + \frac{1}{2}, n + \frac{1}{2}, p + \frac{1}{2}$ , and in the cell at the origin this central point is at  $\frac{1}{2}\frac{1}{2}\frac{1}{2}$ . Points at the center of the  $c$  face (the face containing the  $a$ - and  $b$ -axes) have coordinates  $m + \frac{1}{2}, n + \frac{1}{2}, p$ ; in the cell at the origin this point is at  $\frac{1}{2}\frac{1}{2}0$ . The other face-centered positions are  $\frac{1}{2}0\frac{1}{2}$  and  $0\frac{1}{2}\frac{1}{2}$ . Some writers enclose coordinates in double square brackets thus:  $[[mnp]]$ .

The 14 space-lattices are pictured in Fig. 3 and listed in Table II, together with standard notations for them.

TABLE II.—THE SPACE-LATTICES

System	Space-lattice	Hermann-Mauguin symbol	Schoenflies symbol
Triclinic	Simple	$P$	$\Gamma_{tr}$
Monoclinic	Simple	$P$	$\Gamma_m$
	Base-centered <sup>†</sup>	$C$	$\Gamma_{m'}$
Orthorhombic	Simple	$P$	$\Gamma_o$
	Base-centered *	$C$	$\Gamma_{o'}$
	Face-centered	$F$	$\Gamma_{o''}$
	Body-centered	$I$	$\Gamma_{o'''}$
Tetragonal	Simple	$P$	$\Gamma_t$
	Body-centered	$I$	$\Gamma_{t'}$
Hexagonal	Simple	$P$	$\Gamma_h$
Rhombohedral	Simple	$R$	$\Gamma_{rh}$
Cubic	Simple	$P$	$\Gamma_c$
	Face-centered	$F$	$\Gamma_{c'}$
	Body-centered	$I$	$\Gamma_{c''}$

\* The face that has a lattice point in its center may be chosen as the  $c$  face (the  $XY$  plane) denoted by the symbol  $C$ , or the  $a$  or  $b$  face denoted by  $A$  or  $B$ , since the choice of axes is arbitrary and does not alter the actual translations of the lattice.

It will be noted that one space-lattice in each system is a "simple" one in that it has lattice points only at the corners. In the newer notation all these, except the rhombohedral, are given the symbol  $P$ , meaning "primitive." In the monoclinic system there is also a base-centered cell, in the tetragonal a body-centered, in the orthorhombic all types, and in the cubic all types save the base-centered.

It might be supposed that a face-centered tetragonal lattice should be added to this list, since such an arrangement fulfills the requirements for a

space-lattice. If one makes a sketch of this arrangement, however, it will become clear that with a different choice of axes the lattice may be described as a body-centered tetragonal lattice and thus it is not different from one of those listed. Similarly, it is unnecessary to list a base-centered tetragonal lattice or an orthorhombic lattice centered on four sides, for these are equivalent to lattices already listed.

The hexagonal unit cell is drawn as a parallelepiped having edges parallel to  $a_1$ ,  $a_2$ , and  $c$ , the heavier lines in Fig. 4. It is thus constructed like all the others, and it is not immediately apparent from the unit cell why it is called hexagonal. But if a number of these cells are packed together with axes parallel to one another, as in a space-lattice, a hexagonal prism can be carved out of them as shown in Fig. 4. This prism will contain two whole unit cells and two halves and is in no sense a true unit

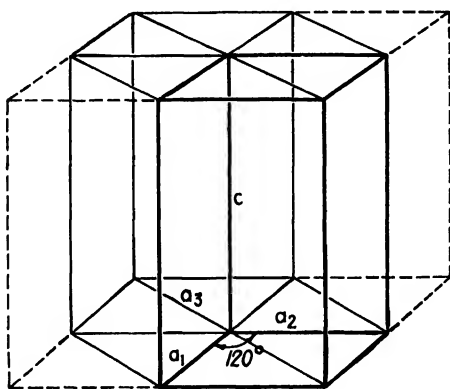


FIG. 4.—Relation of the unit cell in the hexagonal system (heavy lines) to a prism with hexagonal symmetry.

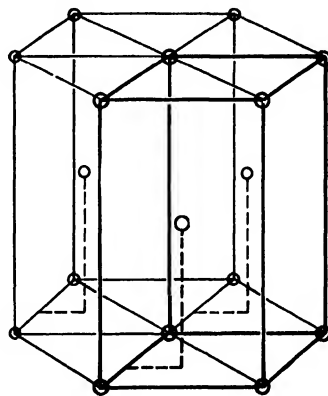


FIG. 5.—The hexagonal close-packed structure.

cell itself, for a parallel repetition of it will not build up the extended lattice.

A common crystal structure among the metals is the **hexagonal close-packed structure** possessed by zinc, cadmium, and magnesium. In this structure the coordinates of atom positions are 000 and  $\frac{2}{3}\frac{1}{3}\frac{1}{2}$ , as shown in Fig. 5. A study of the drawing will reveal that the atom positions in this structure do not constitute a space-lattice, since the surroundings of the interior atom are not identical with those of the corner atoms. The actual space-lattice is *simple hexagonal* with a pair of atoms ( $000; \frac{2}{3}\frac{1}{3}\frac{1}{2}$ ) associated with each lattice point.

**Miller Indices.**—It is necessary to have a system of notation for the faces of a crystal, and for the planes within a crystal or a space-lattice, that will specify *orientation* without giving *position* in space. Miller indices are universally used for this purpose. These indices are based on the intercepts of a plane with the three crystal axes (three edges of the unit

cell). The intercepts are measured in terms of the dimensions of the unit cell, which are the unit distances along the three axes, and not in centimeters. For example, a plane that cuts the  $X$  axis at a distance from the origin equal to half the  $a$  dimension of the cell is said to have the  $X$  intercept  $\frac{1}{2}$ ; and if it cuts the  $Y$  axis at  $\frac{1}{2}b$ , its  $Y$  intercept is  $\frac{1}{2}$ , regardless of the relative sizes of  $a$  and  $b$ . If a plane is parallel to an axis, it intersects it at infinity. To determine the Miller indices of a plane, the following steps are necessary:

1. Find the intercepts on the three axes in multiples or fractions of the unit distances on each axis.
2. Take the reciprocals of these numbers.
3. Reduce to the three smallest integers having the same ratio.
4. Enclose in parentheses,  $(hkl)$ .

Thus the plane shown cutting the axes in Fig. 6 has intercepts 1, 1, 1 and therefore indices  $(111)$ . A plane that has intercepts 2,  $\infty$ , and 1 has

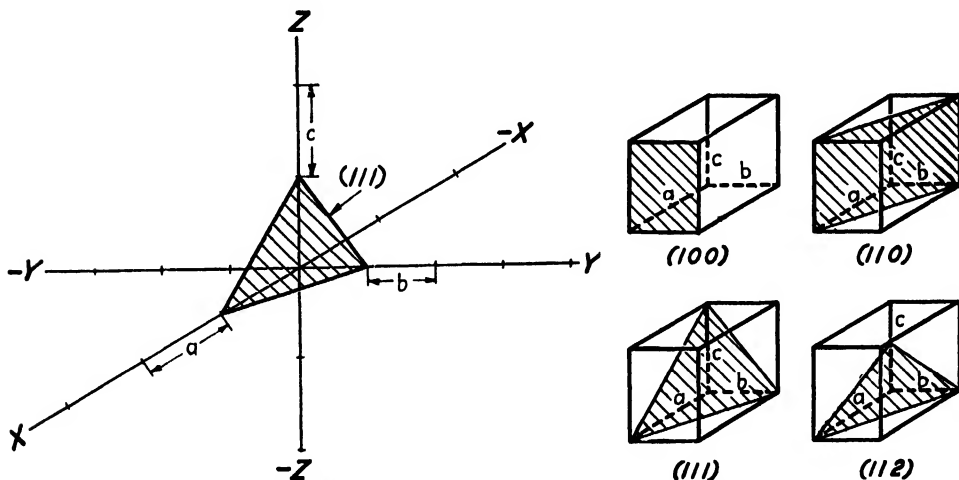


FIG. 6.—Miller indices of some important planes.

reciprocal intercepts  $\frac{1}{2}$ , 0, 1 and Miller indices  $(102)$ . The figure shows some of the most important planes in relation to the unit cell, but it should be remembered that planes parallel to the crosshatched ones have the same indices. If a plane cuts any axis (for example, the  $X$  axis) on the negative side of the origin, the corresponding index will be negative and is indicated by placing a minus sign above the index:  $(\bar{h}kl)$ .

Parentheses,  $(hkl)$ , around Miller indices signify a single plane or set of parallel planes. Curly brackets (braces) signify planes of a "form"—those which are equivalent in the crystal—such as the cube faces of a cubic crystal:  $\{100\} = (100) + (010) + (001) + (\bar{1}00) + (0\bar{1}0) + (00\bar{1})$ .

The **indices of a direction** are derived in a different way. Consider a point at the origin of coordinates which must be moved in a given direction by means of motion parallel to the three crystal axes. Suppose the



desired motion can be accomplished by going along the  $X$  axis a distance  $u$  times the unit distance  $a$  on this axis, along the  $Y$  axis a distance  $v$  times the unit distance  $b$ , and along the  $Z$  axis a distance  $w$  times the unit distance  $c$ . If  $u$ ,  $v$ , and  $w$  are the smallest integers that will accomplish the desired motion, they are the indices of the direction and are written with square brackets,  $[uvw]$ .

*Examples:* The  $X$  axis has indices  $[100]$ , the  $Y$  axis  $[010]$ , and the  $Z$  axis  $[001]$ ; a face diagonal of the  $XY$  face of the unit cell has indices  $[110]$ , and a body diagonal of the cell has indices  $[111]$ . Negative indices occur if any of the translations are in the negative directions of the axes; for example, the  $-X$  direction has indices  $[\bar{1}00]$ . A full set of equivalent directions (directions of a form) are indicated by carets:  $\langle uvw \rangle$ .

It should be noted that reciprocals are not used in computing indices of a direction. A frequent source of error is to assume that a direction will always be perpendicular to a plane having the same indices. This happens to be true for all planes in the cubic system but is not true for other systems (except for a few planes of the tetragonal system).<sup>1</sup>

**Hexagonal Indices.**—Two methods are in common use for specifying planes and directions in the hexagonal system, one using three numbers (Miller indices) and the other using four (Miller-Bravais indices). To determine the indices of a plane in the three-indices system consider only the axes  $a_1$ ,  $a_2$ , and  $c$ . The reciprocals of the intercepts on these three axes, reduced to smallest integers, are the three required indices, just as with any other system of axes. The indices of a direction are determined by finding the magnitude of the translations along the directions  $a_1$ ,  $a_2$ , and  $c$ , respectively, that will cause motion from the origin in the required direction. The translations must be the smallest integers that will do this and are always expressed as multiples of the unit distances along the respective axes. This, too, is identical with the procedure for other systems.

Miller indices are often used for hexagonal crystals but are open to the objection that equivalent planes do not have similar indices. For instance, the planes  $(100)$  and  $(\bar{1}10)$  are both "prism planes of type I" and are equivalent. The same objection applies to the indices of directions. For these reasons many crystallographers have preferred the Miller-Bravais system.

The rules for determining Miller-Bravais indices are similar to those enumerated above except that attention is given to all four axes,  $a_1$ ,  $a_2$ ,  $a_3$ , and  $c$ . When reciprocal intercepts of a plane on all four axes are found and reduced to smallest integers, the Miller-Bravais indices will be of the

<sup>1</sup> Indices of a direction may be described as the lattice "coordinates" of a point on a line in the given direction through the origin. When the coordinates are lowest integers, this is equivalent to the definition in the text above.



axes, and both kinds of indices are given for the principal directions. The axes  $a_1$ ,  $a_2$ , and  $a_3$  are often called "digonal axes of type I" and are the directions of close-packed rows of atoms in the hexagonal close-packed structure. Directions of the type  $[10\bar{1}0]$ , which bisect the principal axes, are "digonal axes of type II."

**Transformations of Indices.**—It is frequently desirable to change from one set of axes to another and to transform the indices of a crystallographic plane accordingly. This presents no problem when changing the indices of planes of hexagonal crystals from the Miller to Miller-Bravais indices, for the index  $i$  in the notation  $(hkil)$  is always given by the equation  $i = -(h + k)$ . To transform from Miller-Bravais to Miller merely requires dropping the third index,  $i$ .

A direction in the hexagonal system may be written with either three or four indices, as explained in the previous section, and  $[UVW]$  in the one case will have the indices  $[uvw]$  in the other if<sup>1</sup>

$$\begin{array}{lll} U = u - t & V = v - t & W = w \\ u = \frac{1}{3}(2U - V) & v = \frac{1}{3}(2V - U) & t = -(u + v) \quad w = W \end{array}$$

Some crystals can be described on the basis of either hexagonal or rhombohedral axes. If the  $(10\bar{1}1)$  plane in the hexagonal cell is made the  $(100)$  face of the rhombohedral cell, then any plane  $(hkil)$  in the hexagonal system will be the plane  $(HKL)$  in the rhombohedral system if

$$\begin{array}{lll} H = 2h + k + l & K = k - h + l & L = -2k - h + l \\ h = \frac{1}{3}(H - K) & k = \frac{1}{3}(K - L) & i = -(h + k) \quad l = \frac{1}{3}(H + K + L) \end{array}$$

In the hexagonal system it is sometimes useful to refer planes to axes at right angles, **ortho-hexagonal axes**. These define a unit cell, shown in

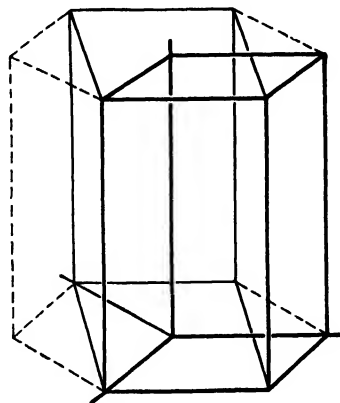


FIG. 9.—Relation of the simple hexagonal cell (heavy lines) to the ortho-hexagonal cell (light full lines) and the hexagonal prism.

<sup>1</sup>These relations may be derived by considering the vector,  $\mathbf{R}$ , in the given direction, which is the vector sum of the components along the crystal axes as follows:

$$\begin{array}{l} \mathbf{R} = u\mathbf{a}_1 + v\mathbf{a}_2 + t\mathbf{a}_3 + w\mathbf{c} \\ \mathbf{R} = U\mathbf{a}_1 + V\mathbf{a}_2 + W\mathbf{c} \end{array}$$

Since the three vectors  $\mathbf{a}_1$ ,  $\mathbf{a}_2$ , and  $\mathbf{a}_3$  build an equilateral triangle, it follows that

$$\mathbf{a}_3 = -(\mathbf{a}_1 + \mathbf{a}_2),$$

which, together with the expressions for  $\mathbf{R}$  and the relation  $t = -(u + v)$ , gives the relations  $U = u - t$ , etc. For a comprehensive treatment of transformation of indices see M. J. Buerger, "X-ray Crystallography," Wiley, New York, 1942.

Fig. 9, which is actually orthorhombic and for which the indices of a plane ( $pqr$ ) are related to hexagonal indices for the same plane ( $hkl$ ) by the relations

$$\begin{array}{llll} p = k + 2h & q = k & r = l \\ h = \frac{1}{2}(p - q) & k = q & i = -(h + k) & l = r \end{array}$$

**Law of Rational Indices.**—Figure 10 represents a single plane of a lattice, say the plane containing the  $X$  and  $Y$  axes. Many sets of parallel planes extend through the lattice in different directions, and a number are indicated in the figure by parallel lines with different orientations. If all the planes indicated are parallel to the  $Z$  axis, their indices will be as given on the drawing. Each complete set of parallel planes will pass through every point on the lattice, and, as a consequence of this, the set of planes that is most widely spaced will contain the fewest planes; each plane of this set will be more densely studded with lattice points than

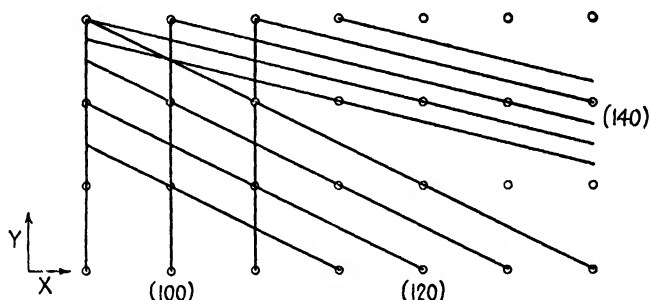


Fig. 10.—Sketch of different sets of planes in a lattice, showing interplanar spacings which decrease in the sequence (100), (120), (140).

planes of any other set. Planes listed in the order of decreasing spacing will be in the order of decreasing numbers of lattice points per plane.

In the natural growth of crystals it is the planes that are densely packed with lattice points that tend to become the crystal faces. Consideration of the example in Fig. 10 or of a three-dimensional model will show that these are always planes of low indices. Hence it is an empirical law—the law of rational indices—that the commonly occurring crystal faces have indices that are small whole numbers. These are usually 1, 2, or 3 and rarely exceed 6. This law can be considered the result of a tendency for crystal faces to be relatively closely packed layers of atoms, for atoms or groups of atoms are located on lattice points.

**Zones and Zone Axes; Crystal Geometry.**—Certain sets of crystal planes meet along a line or along parallel lines. For example, the vertical sides of a hexagonal prism intersect along lines that are parallel to the  $C'$  axis. Such planes are known as planes of a zone, and the direction of their intersection is the zone axis. Any two nonparallel planes will intersect and will thus be planes of a zone, for which their line of intersection is the

zone axis; but the important zones in a crystal will be those to which many different sets of planes belong. On the surface of a crystal the faces of a zone form a belt around the crystal; and, by placing the crystal on the graduated circle of a goniometer with the zone axis parallel to the goniometer axis, the angles between all faces of the zone can be measured directly on the circle. Zones are also useful in interpreting x-ray diffraction patterns and in making projections of a crystal.

There are simple rules governing the Miller indices of planes of a zone, given in Appendix I, which are a great convenience to crystallographers. They apply to all crystal systems. For example, the plane  $(hkl)$  belongs to the zone  $[uvw]$  (*i.e.*, is parallel to  $[uvw]$ ) if  $hu + kv + lw = 0$ .

Formulas are given in Appendix I for computing spacings between planes and along crystallographic directions, angles between planes and directions, and unit-cell volumes—quantities that are useful in x-ray work and in various crystallographic problems.

**Symmetry Classes and Point Groups.**—A crystal possesses definite symmetry in the arrangement of its external faces, if the faces are developed, and also in the value of its physical properties in different directions, such as its thermal expansion, elastic moduli, and optical constants. The nature of the symmetry revealed by measurements of these features is the basis of the classification of the crystals into 32 symmetry classes. These can be understood best if one dissects the total symmetry of a crystal into simple fundamental symmetry elements, which when grouped together at a point within the crystal combine to yield the total symmetry of the crystal. A group of symmetry elements at a point constitutes a point group, and the 32 possible point groups in crystallography correspond to the 32 classes of crystal symmetry.

A symmetry element is an operation, like a rotation about an axis or a reflection across a plane, which will bring the crystal into a position indistinguishable from its former one, *i.e.*, bring it into coincidence with itself. In this connection it is the tilt—the orientation—of the crystal faces or of the atomic planes within the crystal that is important, and not the size and shape of the faces and planes, for their size and shape are matters of accidents of growth and subsequent handling, while the orientation of the faces and internal planes is a consequence of the regular and symmetrical arrangement of atoms inside the crystal. To describe the symmetry elements, however, we may assume an ideal crystal in which all equivalent faces are equally developed.

When this ideal crystal can be brought into self-coincidence (into an equivalent position) by a rotation around an axis, it is said to possess a **rotation axis** of symmetry. The symmetry elements of this kind that have been found to occur in crystals are one-fold, two-fold, three-fold, four-fold, and six-fold axes, which bring about self-coincidence by the

operations, respectively, of a full turn, a half turn, a third turn, a fourth turn, and a sixth turn about the rotation axis. A square is an example of a figure having four-fold rotation axis, the axis standing perpendicular to the plane of the square and passing through its center. A regular

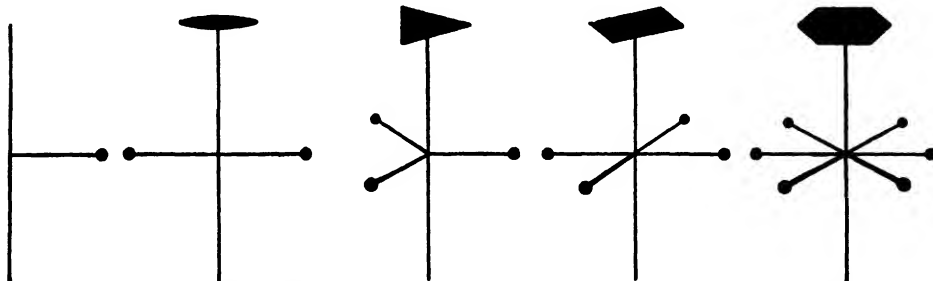


FIG. 11.—Rotation axes of symmetry, one-, two-, three-, four-, and six-fold.

pentagon, similarly, has a five-fold rotation axis, but this symmetry axis does not occur in crystals, nor does an axis of greater multiplicity than 6. The one-fold axis represents, of course, no symmetry at all. Each rotation axis is indicated in Fig. 11 as a vertical line; the symmetry is indicated

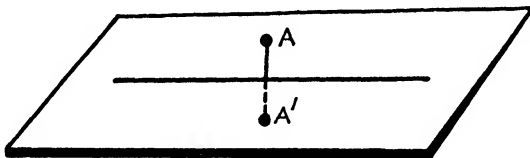


FIG. 12.—Plane of symmetry.

by a geometrical figure at the top and a group of points at the ends of arms extending out from the axis.

If a plane can be drawn through the center of a crystal so that one half of the crystal is the reflection of the other half in this plane, the crystal possesses a **plane of symmetry**. Figure 12 illustrates this symmetry where the point  $A'$  is produced from the point  $A$  by the operation of reflection in the plane as if in a mirror.

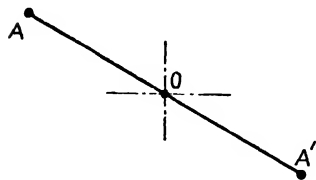


FIG. 13.—Center of inversion.

A crystal has a **center of inversion** if to every point on one side of the crystal there is a corresponding point on the other side of the crystal that is located an equal distance from the center and on the same line through the center. This is illustrated in Fig. 13, where the operation of the center of inversion at  $O$  produces the point  $A'$  from the point  $A$ , with  $AOA'$  a straight line and  $OA = OA'$ .

A crystal has a **rotation-inversion axis** if it is brought into self-coincidence by a combined rotation and inversion. The operation is indicated

in Fig. 14, which shows a two-fold rotation-inversion axis standing vertically with its center at  $O$ , operating on the point  $A$  by rotating it  $180^\circ$  into the intermediate position  $A'$  and then inverting it through the center to the point  $A''$ . It will be seen that the points  $A$  and  $A''$  in this figure have a plane of symmetry between them, the plane standing perpendicular to the axis and passing through point  $O$ ; so it follows that the two-fold rotation-inversion axis is exactly equivalent to a reflection plane of symmetry. A similar construction will show that a one-fold rotation-inversion axis is equivalent to a center of symmetry. Crystals can possess one-, two-, three-, four-, and six-fold rotation-inversion axes. The copper mineral, copper pyrites ( $\text{CuFeS}_2$ ), is a common example of a crystal with a four-fold rotation-inversion axis. In Fig. 15 this axis is in a vertical position.

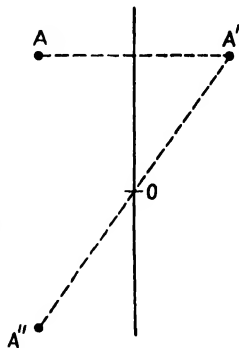


FIG. 14. Two-fold rotation-inversion axis.

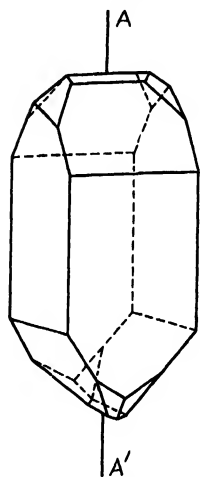


FIG. 15.—Crystal of copper pyrites having a vertical 4-fold rotation-inversion axis. (Bragg.)

The symmetry elements that have been enumerated above, rotation axes, reflection planes, inversion centers, and rotation-inversion axes, occur singly and in groups in crystals and define their external symmetry, the symmetry of faces and of physical properties. They are known as the **macroscopic symmetry elements** (to distinguish them from certain others having to do only with the microscopic internal structure). Some classes of crystals have the symmetry of a single rotation axis, others have the symmetry of several rotation axes that intersect at a point, and many crystals have the symmetry of a complex group of symmetry elements at a point. There are in all **32 classes** of crystal symmetry. Each class is defined by a group of symmetry elements at a point, appropriately called a **point group**. To reiterate, there are 32 point groups of symmetry elements that define the 32 classes of macroscopic symmetry of crystals.

Several notations have been devised for the symmetry classes, but crystallographers have agreed to standardize on two, the **Schoenflies** and the newer **Hermann-Mauguin notations**. In the Schoenflies system the symbols are  $C$ ,  $S$ ,  $D$ ,  $V$ ,  $T$ , and  $O$ , with certain subscripts,  $C_2$ , for example, standing for the "cyclic" class having only a two-fold rotation axis of symmetry,  $C_{3h}$  denoting the class having a three-fold rotation axis and a reflection plane, and  $D_2$  or  $V$  denoting the "dihedral" class having 3 two-fold axes at right angles. In the

Hermann-Mauguin notation, the point-group symbol is derived from the space-group symbol (this is discussed under Space Groups) and indicates the symmetry elements associated with three important directions of a crystal. The macroscopic symmetry elements in this notation are as follows:

Element	Hermann-Mauguin Symbol
1-, 2-, 3-, 4-, and 6-fold rotation axes	1, 2, 3, 4, and 6
Reflection plane	<i>m</i> (for "mirror" plane)
Axes of rotation-inversion	$\bar{1}$ , $\bar{2}$ , 3, $\bar{4}$ , and 6
Center of inversion	$\bar{1}$ (equivalent to 1-fold rotation-inversion)

The 32 crystal classes are divided among the seven crystal systems in such a way that each system has a certain minimum of symmetry elements, as follows:

Triclinic: None

Monoclinic: A single 2-fold rotation axis or a single plane

Orthorhombic: Two perpendicular planes or three mutually perpendicular 2-fold axes of rotation

Tetragonal: A single 4-fold axis of rotation or of rotation-inversion

Rhombohedral: A single 3-fold rotation axis

Hexagonal: A single 6-fold rotation axis

Cubic: Four 3-fold rotation axes (along cube diagonals)

These elements may coexist with others, but they are sufficient to identify the system to which any crystal belongs. In each system there are several classes differing from one another; thus in the triclinic system there is a class having no symmetry, and a second class having only a center of symmetry. The class having the highest possible symmetry of the system to which it belongs is called the **holohedral** class of that system, and classes of lower symmetry than the maximum are called **hemihedral** or, in some cases, **tetartohedral**. **Enantiomorphic** crystals are those of which two varieties are possible in a single class, a right-handed and a left-handed variety. An example is quartz. The arrangement of faces on a crystal of one enantiomorphic variety is the mirror image of the arrangement on the other, and neither can be turned about so as to coincide with the other. Eleven of the 32 classes are enantiomorphic. **Hemimorphic** crystals contain axes of symmetry that are different at their two ends. The opposite ends of such **polar axes** show different physical properties—for example, they may develop electric charges of opposite sign when heated (**pyroelectricity**) or when mechanically stressed (**piezoelectricity**).

When a crystal is built up of atoms located only at the corners of unit cells, the crystal will have the highest symmetry possible in its class, and this will also be true if the crystal has highly symmetrical groups of atoms



at the lattice points. But if a low-symmetry group of atoms surrounds each lattice point, the symmetry of the crystal will be lower. Thus, it is possible for several classes of symmetry to exist in a single system.

There is no need to discuss in detail all the 32 individual classes. These are listed briefly in Table III together with the notations commonly

TABLE III.—THE 32 SYMMETRY CLASSES OR POINT GROUPS WITH THEIR SCHOENFLIES AND HERMANN-MAUGUIN NOTATION\*

System	Classes
Triclinic	$C_1 = 1$
	$C_2 = \bar{1}$
Monoclinic	$C_2 = m = \bar{2}$
	$C_2 = 2$
	$C_{2h} = 2/m$
Orthorhombic	$V = 222 (= Q)$
	$C_{2v} = 2/mm$
	$V_h = mmm (= Q_h)$
Tetragonal	$C_4 = 4$
	$S_4 = \bar{4}$
	$D_4 = 42$
	$C_{4h} = 4/m$
	$C_{4v} = 4/mmm$
	$V_d = \bar{4}2/m (= Q_d)$
Cubic	$D_{4h} = 4/mmm$
	$T = 23$
	$O = 43$
	$T_h = m\bar{3}$
	$T_d = \bar{4}3/m$
Rhombohedral	$O_h = m\bar{3}m$
	$C_3 = 3$
	$D_3 = 32$
	$C_{3v} = 3/m$
	$C_{3i} = 3$
Hexagonal	$D_{3d} = \bar{3}/m$
	$C_{3h} = \bar{6}$
	$D_{3h} = \bar{6}/m$
	$C_6 = 6$
	$D_6 = 62$
	$C_{6h} = 6/m$
	$C_{6v} = 6/mmm$
	$D_{6h} = 6/mnmm$

\* In the Hermann-Mauguin notation the symmetry axes parallel to and the symmetry planes perpendicular to each of the "principal" directions in the crystal are named in order. When there is both an axis parallel to and a plane normal to a given direction, these are indicated as a fraction; thus  $6/m$  means a sixfold rotation axis standing perpendicular to a plane of symmetry, while  $\bar{4}$  means only a fourfold rotary inversion axis.

used to designate them and to indicate their symmetry elements; full details will be found in the standard reference books and tables.<sup>1</sup>

As an introduction to these tabulations one of the classes of lower symmetry will be mentioned, the one whose elements are sketched in Fig. 16, possessing a vertical four-fold axis and a horizontal plane of symmetry.

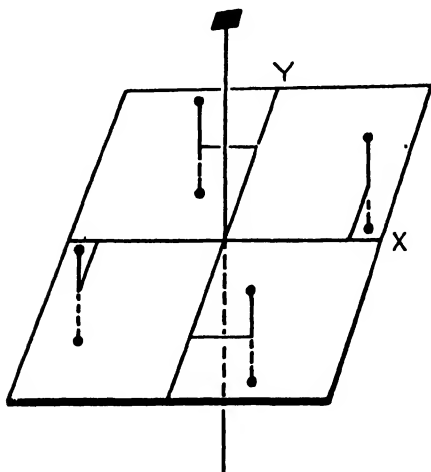


FIG. 16.—Symmetry elements of class  $C_{4h}-4, m$  (4-fold axis normal to a plane of symmetry).

The symmetry in Schoenflies notation is  $C_{4h}$  and in the Hermann-Mauguin notation  $4/m$ . The figure shows a set of points which come into coincidence by the operation of the symmetry elements—the **equivalent points**. The coordinates of one of these points, referred to the  $X$ ,  $Y$ , and  $Z$  axes of the tetragonal system to which this point group belongs, may be chosen at random and are written in the general form  $xyz$ . The coordinates of all the other equivalent points are then written in terms of these three coordinates; thus  $\bar{y}xz$  refers to the point whose coordinate along the  $X$  axis is  $-y$ , along the  $Y$  axis is  $x$ , and along

the  $Z$  axis is  $-z$ , respectively. The full list of equivalent points for this class is as follows:  $xyz, \bar{y}xz, \bar{x}\bar{y}z, y\bar{x}z, \bar{x}\bar{y}\bar{z}, y\bar{x}\bar{z}, x\bar{y}\bar{z}, \bar{y}x\bar{z}$ .

The different forms and the number of equivalent faces in each form can be derived from these equivalent points<sup>2</sup> (since the points can be taken as the intercepts of the planes) and are listed in crystallographers' tables. In the example chosen, ( $C_{4h} - 4/m$ ), there is a form containing the two planes (001) and (00 $\bar{1}$ ), and another containing faces whose indices are ( $hk0$ ), ( $\bar{h}\bar{k}0$ ), ( $k\bar{h}0$ ), and ( $\bar{k}h0$ ); these are "special" forms, containing fewer equivalent faces than the "general" form  $\{hkl\}$ , which has all indices unequal and different from zero. The equivalent faces of  $\{hkl\}$  are ( $hkl$ ), ( $\bar{h}\bar{k}\bar{l}$ ), ( $\bar{h}k\bar{l}$ ), ( $h\bar{k}l$ ), ( $k\bar{h}l$ ), ( $\bar{k}hl$ ), ( $\bar{k}\bar{h}l$ ), ( $kh\bar{l}$ ). The more complete tables also list the symmetry properties possessed by each face of the crystal; for example, in our illustration the faces (001) and (00 $\bar{1}$ ) have each the symmetry of a four-fold rotation axis. This is, therefore, the symmetry which would be expected in etch pits or other crystallographic markings on these faces.

<sup>1</sup> "International Tabellen zur Bestimmung von Kristallstrukturen," Bornträger, Berlin, 1935. R. W. G. WYCKOFF, "The Structure of Crystals," pp. 41-44, Chemical Catalog Co., New York, 1931. WHEELER P. DAVEY, "A Study of Crystal Structure and Its Applications," McGraw-Hill, New York, 1934.

<sup>2</sup> R. W. G. WYCKOFF, "The Structure of Crystals," Chemical Catalog Co., New York, 1931.

Names have been assigned to the various forms by Groth and are occasionally encountered in metallurgical literature. **Pinacoids** are forms consisting simply of two parallel faces. **Prisms** are forms with faces parallel to the principal, or vertical, axis (the  $Z$  axis in the above illustration). **Domes** have faces parallel to one (horizontal) axis and intersecting the other two. **Pyramids** have faces intersecting all three axes.

**Space Groups.**—In the preceding section the symmetry of the external faces of crystals and of their anisotropic physical properties permits a classification of all crystals into 32 *crystal classes*, which are divided among the 7 *systems*. The symmetry of each of these classes is described by macroscopic symmetry elements grouped at a point, termed a *point group*. It may also be described by a group of *equivalent points* that can be written in the form  $xyz$ ,  $\bar{x}\bar{y}\bar{z}$ , etc. The operation of all the symmetry elements of the point group upon any one of the equivalent points will produce all the others. We now consider another classification of crystals that has become of primary importance since the advent of x-ray analysis of crystals, a classification that specifies the symmetry of the arrangement of *atoms* in a crystal.

A **space group** is an array of symmetry elements in three dimensions on a space lattice. Just as a point group is a group of symmetry elements at a *point*, a space group is a group in *space*. Each element of symmetry has a specific location in a unit cell as well as a specific direction with respect to the axes of the cell, and each unit cell in the crystal has an identical array of symmetry elements within it. The elements are always arranged so that the operation of any one of them brings all others into self-coincidence, and thus they may be said to be self-consistent. The group of symmetry elements at and around every lattice point is identical throughout a crystal.

A large number of the possible space groups consist simply of point groups placed at the points of the 14 space lattices. This procedure, however, does not produce all possible space groups, for there are certain symmetry elements possible in a space group that are not possible in a point group; these are commonly termed the **microscopic symmetry elements** since they involve translations through distances of the order of a few angstrom units. Every self-consistent arrangement of all macroscopic and microscopic symmetry elements in space leads to a total of 230 space groups, to one or more of which every crystal must belong.

The symmetry elements of a space group, operating on a point located at random in a unit cell of the lattice, will produce a set of **equivalent points** in the cell. In an actual crystal, if an atom is located at one of these equivalent points, identical atoms should be found at each of the other equivalent points. The complete tabulation of coordinates of

equivalent points in all the space groups is thus of great convenience to crystallographers when they are determining complex crystal structures, for it is a *description of all possible atomic groupings in crystals*.

Consider as an example the space group derived by placing a center of inversion at the lattice points of the simple triclinic space-lattice. The lattice is represented by a unit cell in Fig. 17a; a center of inversion is indicated by a small circle at the origin which turns a point  $A$  into a point  $A'$ , the former having coordinates  $xyz$ , the latter  $\bar{x}\bar{y}\bar{z}$ , where  $x$ ,  $y$ , and  $z$  may be any fractions of the axial lengths,  $a$ ,  $b$ , and  $c$ . The translations of the lattice produce symmetry centers and pairs of equivalent points identical with  $A$  and  $A'$  at all other points of the space-lattice, as will be seen from Fig. 17b.

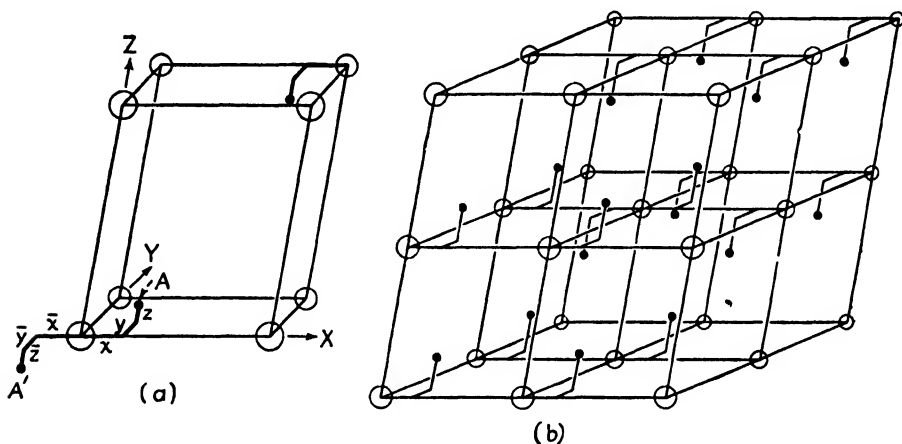


FIG. 17.—The space group  $C_1-P\bar{1}$ . (a) Unit cell with center of inversion at 000 indicated by open circle. Points  $xyz$  and  $\bar{x}\bar{y}\bar{z}$  are equivalent. (b) Showing repetition of unit cell in the crystal. Additional symmetry elements are present but are not indicated on the drawing.

It will be seen by studying this figure that additional symmetry elements are to be found in this arrangement of equivalent points, for the full symmetry includes symmetry centers at the mid-points of each edge and of each face of the unit cell, as well as one at the center of the cell. The coordinates  $xyz$  of an equivalent point are always expressed as fractions of the axial lengths  $a$ ,  $b$ , and  $c$ ; these fractions may have any value whatever without altering the symmetry properties of the group of points derived from it by the operation of the symmetry elements of the space groups. The value of the coordinates does alter the *number* of equivalent points in special cases, however, for if a point is located on an axis of symmetry it is obvious that no new equivalent points will be produced by the operation of rotation around that axis. Similarly, in the example of Fig. 17a, if the point  $A$  lies at the special position 000, where a center of inversion is located, all the equivalent points will be at

the corners of the unit cells, and there will be only half as many as for the general position.

**Glide Planes and Screw Axes.**—In the point groups the operation of a symmetry element located at the origin on a point  $xyz$  will always produce equivalent points that are equidistant from the origin; but in the space groups it is possible to have symmetry elements in which a translation is involved, and equivalent points will consequently be at different distances from the origin.

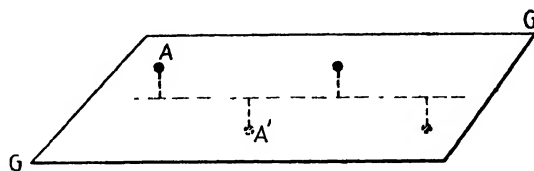


FIG. 18.—Glide plane.

A glide plane combines a reflection plane with a translation parallel to the plane so that the structure is brought into coincidence by reflection across the plane and simultaneous movement along the plane a specified distance. This is illustrated in Fig. 18, where the point  $A'$  is produced from point  $A$  by the action of glide plane  $GG$ . In the different kinds of glide planes the translations are half the axial lengths, half the face diagonals, or one-fourth the face diagonals.

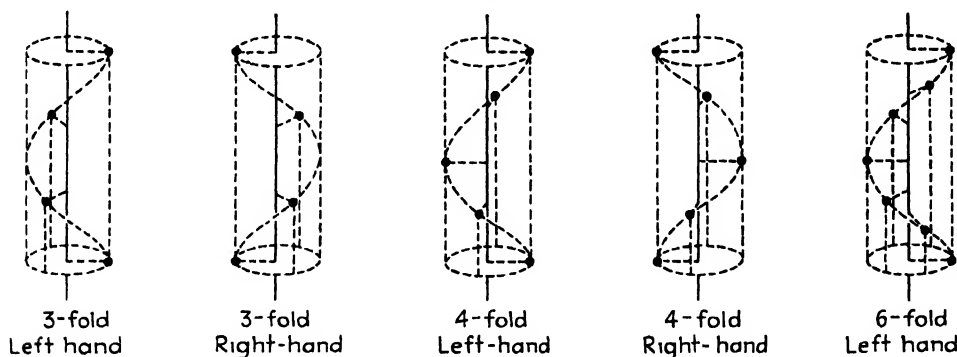


FIG. 19.—Examples of screw axes.

In the Hermann-Mauguin notation glide planes with a glide of  $a/2$ ,  $b/2$ , and  $c/2$  are represented by the symbols  $a$ ,  $b$ , and  $c$ , respectively, one with a glide of half a face diagonal by  $n$ , and one with a glide of one-fourth a face diagonal by  $d$ ; in each of these the translation is parallel to the axis or the diagonal concerned.

A **screw axis** combines rotation with translation parallel to the axis. A three-fold screw axis parallel to the  $Z$  axis, for instance, involves a rotation of one-third turn around  $Z$  and a translation of one-third the axial length  $c$ , as indicated in Fig. 19. An  $n$ -fold screw axis combines a

rotation of  $2\pi/n$  with a translation parallel to the axis amounting to a certain fraction of the distance between lattice points in the direction of the axis; the translation is one-half this distance for a two-fold screw axis, one-third in the case of a three-fold, one-fourth or one-half in the case of a four-fold, and one-sixth, one-third, or one-half in the case of a six-fold. Several of these axes can be either right-handed or left-handed, since the equivalent points are on spirals that advance either as a right-handed or a left-handed screw (see Fig. 19). The following table lists the screw axes and their Hermann-Mauguin symbols.

Symbol	Multiplicity	Translation	Nature
$2_1$	2-fold	$1/2$	
$3_1$	3-fold	$1/3$	Right-handed
$3_2$	3-fold	$1/3$	Left-handed
$4_1$	4-fold	$1/4$	Right-handed
$4_2$	4-fold	$1/2$	Includes rotation axis 2
$4_3$	4-fold	$1/4$	Left-handed
$6_1$	6-fold	$1/6$	Right-handed
$6_2$	6-fold	$1/3$	Right-handed
$6_3$	6-fold	$1/2$	Includes rotation axis 3
$6_4$	6-fold	$1/3$	Left-handed
$6_5$	6-fold	$1/6$	Left-handed

As far as the *external* symmetry of crystals is concerned, glide planes cannot be distinguished from reflection planes, nor can screw axes be distinguished from rotation axes of the same multiplicity. For example, the orthorhombic crystal class having three mutually perpendicular two-fold axes,  $V-222$ , has a number of possible internal arrangements of two-fold rotation and screw axes, leading to different space groups pictured in Fig. 20. While the internal structures of the crystals belonging to these space groups are all different, their macroscopic symmetry properties are identical.

**Space-group Notation.**—The symmetry elements of each of the 230 space groups have been tabulated many times.<sup>1</sup> The content of space-group tables will be illustrated with reference to Fig. 20c. The notation for this space group is  $D_2^3-P2_12_12$ , the symbol in front of the dash being the Schoenflies and the second the newer Hermann-Mauguin symbol. In the older system the symbol for the point group is retained as the symbol

<sup>1</sup> R. W. G. Wyckoff, *The Analytical Expression of the Results of the Theory of Space Groups*, *Carnegie Inst. Wash. Pub.* 318, 1922, 1930. "International Tabellen zur Bestimmung von Kristallstrukturen," Bornträger, Berlin, 1935.

for all space groups belonging thereto, and a superscript is added to designate the serial number of the space group belonging to that particular point group; the one under discussion is thus the third space group of the point group  $D_2$ . The symbols in the newer notation indicate the type of lattice and the symmetry elements associated with the principal crystallographic directions. The object of the international committee in urging the simultaneous and eventually the exclusive use of the new

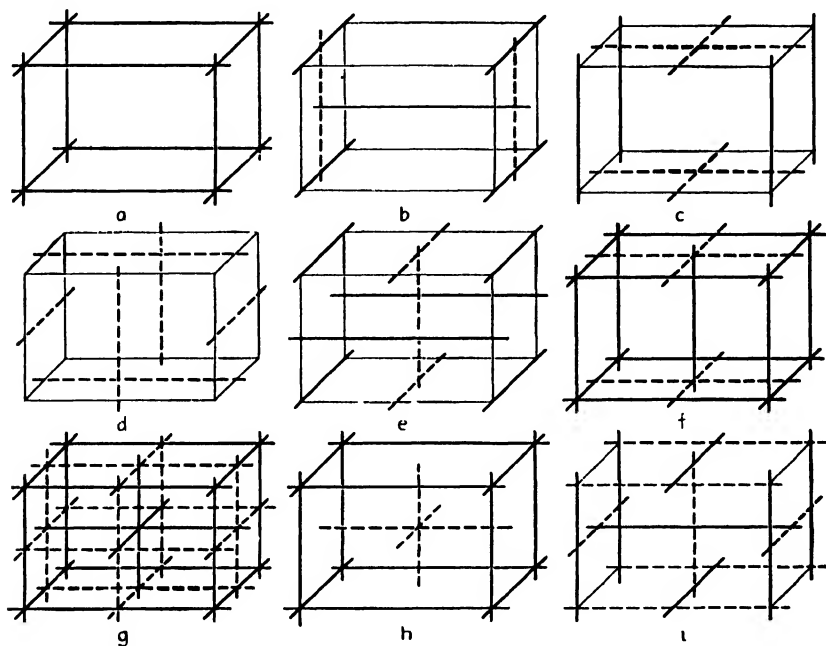


FIG. 20.—Space groups of Class  $D_2$ —222, showing  $1/8$  of unit cell of each. Dashed and heavy lines are  $2_1$  and  $2_2$  axes, respectively. (Other portions of unit cell are similar to these.) (James.)

notation was to provide a shorthand from which all the symmetry properties of a space group would be self-evident.

Rules that must be kept in mind for an understanding of this notation are as follows:<sup>1</sup>

The designation of the lattice is given by a capital letter.  $P$  denotes a simple lattice,  $A$  or  $B$  or  $C$  a lattice centered on the  $a$ ,  $b$ , or  $c$  face (i.e., a cell of a  $C$  lattice has a point  $\frac{1}{2}\frac{1}{2}0$  equivalent to the corner point 000), and  $F$  a lattice centered on all faces.

In this system of notation cells are chosen so as to be as nearly rectangular as possible, the hexagonal lattice being denoted by the letter  $C$  (an orthohexagonal cell centered on the  $c$  face with  $a:b = 1:\sqrt{3}$ ) or by the letter  $H$  if a cell is chosen having an axial ratio  $a:b = \sqrt{3}:1$ . The simple rhombohedral cell having equal axes at equal angles is given a special symbol,  $R$ , since it is not conveniently drawn using rectangular axes.

<sup>1</sup> The system is presented in detail in "International Tabellen zur Bestimmung von Kristallstrukturen," Bornträger, Berlin, 1935; and in *Z. Krist.*, vol. 79, p. 495, 1931.

The remaining symbols in the space-group notation give the symmetry elements associated with special directions in the crystals. These are: in the monoclinic system the axis normal to the others; in the orthorhombic system the three mutually perpendicular axes; in the tetragonal system the "principal" axis, the "secondary" axis, and the "tertiary" axis  $90^\circ$  from the principal and  $45^\circ$  from the secondary; in the rhombohedral and hexagonal systems the principal axis, the secondary axis, and the tertiary axis, which lies  $90^\circ$  from the principal and  $30^\circ$  from the secondary; and in the cubic system the directions [001], [111], and [110]. The symbols for rotation axes, screw axes, or axes of rotary inversion along these directions are written in the symbol, as are also the symbols for the reflection planes and glide planes that stand perpendicular to the directions. If two symmetry elements belong to one direction, their two symbols may be combined as a fraction;  $2/m$  thus denotes a two-fold axis normal to a reflection plane. Only the necessary minima of symmetry elements are given, for the remainder follow as a consequence of those given.

*Example:* The space group  $O_h^3 - Fm\bar{3}m$  is based on a face-centered lattice and has reflection planes normal to [100] and [110] with three-fold axes along the secondary axes [111], an arrangement possible only in the cubic system. It should be mentioned that the crystal axes sometimes can be chosen in different ways with respect to the symmetry elements; these different orientations are distinguished from one another in the notation, and a normal, or standard, orientation is chosen from the various possible ones and is used in space-group tables.

**Tables of Equivalent Points.**—The equivalent points in each space group are listed in tables in such a way as to show clearly the number of equivalent points belonging to each set (the "multiplicity") and thus the number of equivalent atoms that could be located at these points in a crystal. For the example we are considering (Fig. 20c) the points that lie on no symmetry elements form a set of four equivalent points known as the "general" set, while two sets of "special" point positions are possible in which the points lie on rotation axes; the sets are labeled (a), (b), and (c) for convenience in working with the tables. The information is tabulated as follows:

EQUIVALENT POINT POSITIONS OF SPACE GROUP  $D_2^3 - P2_12_12$

Multiplicity	Set
2:	(a) $00z; \frac{1}{2}\frac{1}{2}\bar{z}$
	(b) $0\frac{1}{2}z; \frac{1}{2}0\bar{z}$
4:	(c) $xyz; \bar{x}\bar{y}\bar{z}; \frac{1}{2}+x, \frac{1}{2}-y, \bar{z}; \frac{1}{2}-x, \frac{1}{2}+y, \bar{z}.$



## CHAPTER II

### THE STEREOGRAPHIC PROJECTION

Mineralogists have used the stereographic projection for many years in the description of symmetry classes and crystal planes, for it presents an accurate, easily understood plot of angular relations in crystals with all unessential features eliminated (such as the accidentally determined size and shape of crystal faces). Metallurgists are making use of the stereographic projection to a steadily increasing extent. In metallography and physical metallurgy the projection is much used for the analysis of markings appearing on polished grains, such as slip lines, twins, cracks, structures formed by precipitation, magnetic powder patterns, and etch pits. Data from certain types of x-ray photograms are most conveniently analyzed by its use, particularly those for determining the orientation of single crystals or the preferred orientation of grains in an aggregate. Calculations of the angular relationships involved in tilting or cutting a crystal parallel to a certain crystallographic plane or in reflecting x-rays from a certain plane are rapidly carried out. It has been adopted almost universally to the exclusion of other methods by those studying the deformation of metallic crystals, except where the accuracy required is greater than a few tenths of a degree. Any directional property in a crystal or polycrystalline material can be shown on a stereographic projection, for example, the modulus of elasticity and the yield point.

**Reference Sphere and Its Stereographic Projection.**—Crystallographic planes, axes, and angles are conveniently represented on a sphere. The crystal is assumed to be very small compared with the sphere (known variously as the reference sphere or polar sphere) and to be located exactly at the center of the sphere. Planes on the crystal can then be represented by extending them until they intersect the sphere, as in Fig. 1, where the plane *F* intersects the sphere along the circle *M*. The crystal is assumed to be so small that each of these planes passes through

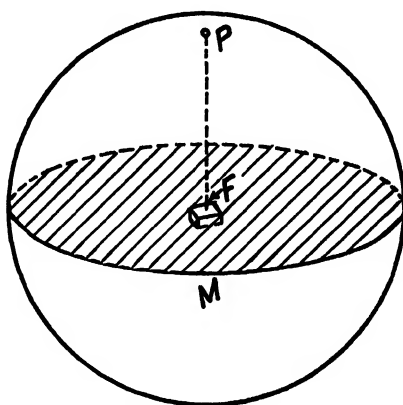


FIG. 1.—Projection of crystal plane upon reference sphere. Plane *F* represented on sphere by great circle *M* or pole *P*.

the center of the sphere; this results in the plane's intersecting the sphere

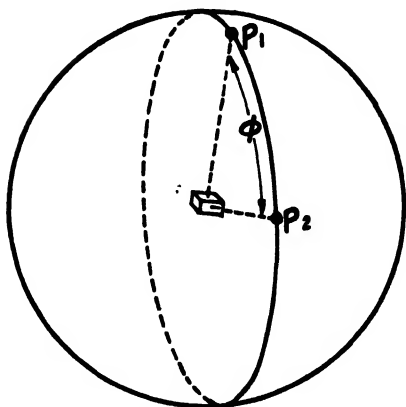


FIG. 2.—Angle  $\phi$  between poles  $P_1$  and  $P_2$  is measured on great circle through poles.

in a circle of maximum diameter—a great circle. If all planes of the crystal are projected upon the sphere in this manner, it will be found that the great circles intersect each other at the same angles as do the planes of the crystal and so exhibit without distortion all the angular relations of the crystal.

Crystal planes can also be represented on the reference sphere by erecting perpendiculars to the planes. These plane normals are made to pass through the center of the sphere and to pierce the spherical surface at a point known as the pole of the plane. This is illustrated in

Fig. 1, where the plane  $P'$  and its pole  $P$  are shown. The array of poles on the sphere, forming a **pole figure**, represents the orientation of the crystal planes without, of course, indicating the size and shape of the crystal planes. The angle between any two planes is equal to the angle between their poles and is the number of degrees between the poles measured on a great circle through them, as indicated in Fig. 2.

The applications discussed in this chapter can be carried through by using the spherical projection just described, but in practice it is usually more convenient to use a map of the sphere, so that all the work can be done on flat sheets of paper. The stereographic projection is one of the methods—and generally the most satisfactory one—by which the sphere may be mapped without distorting the angular relations between planes or poles.

In Fig. 3 it will be seen that there is a simple relation between the sphere and its stereographic projection. If the sphere is transparent and a source of light is located at a point on its surface, the markings on the surface of the sphere will be projected as shadows upon a plane erected as shown. The plane is perpendicular to the diameter of the sphere that

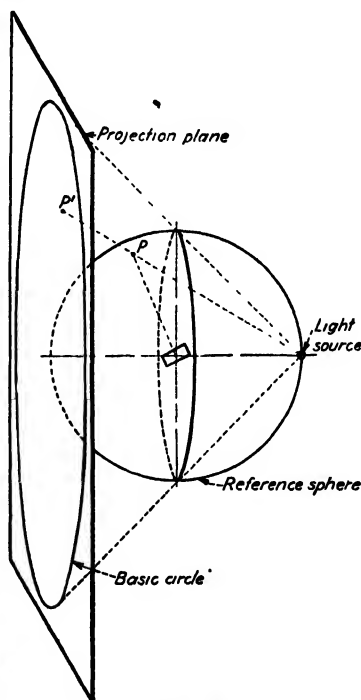


FIG. 3.—Stereographic projection. Pole  $P$  of crystallographic plane projects to  $P'$  on projection plane.

passes through the light source. The pattern made by the shadows is a stereographic projection of the sphere; the point  $P'$  is the stereographic projection of the pole  $P$ . The distance of the plane ("projection plane") from the sphere is immaterial, for changing the distance will merely change the magnification of the map and will not alter the geometrical relations (in fact, the plane is frequently considered as passing through the center of the sphere).

Obviously, only the hemisphere opposite the source of light will project within the **basic circle** shown in the figure. The hemisphere con-

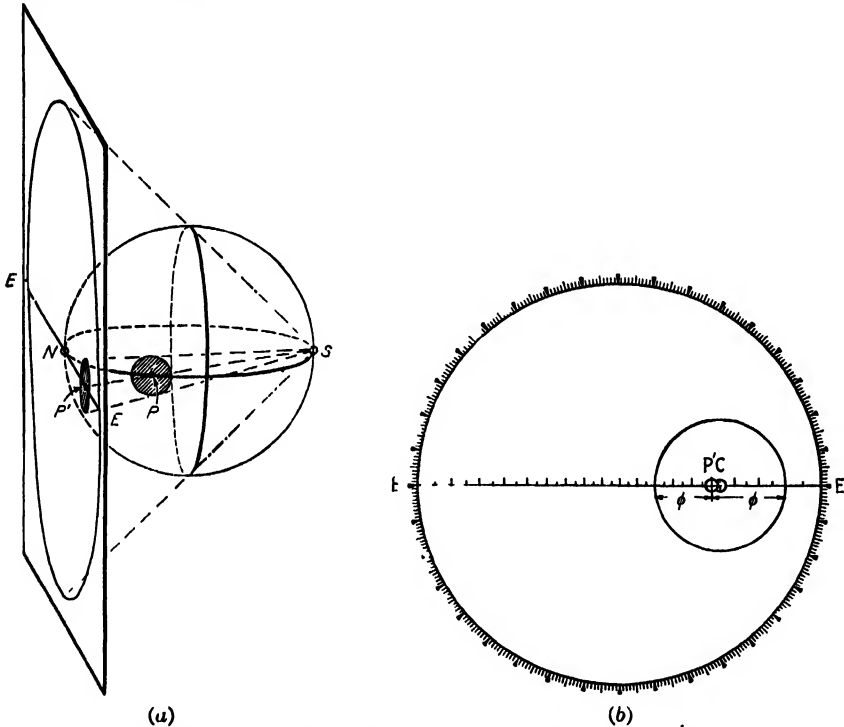


FIG. 4.—Stereographic projection of small circle. Projection of great circle through  $N$  is  $EE'$ ; projection of small circle (shaded) is circle having center displaced from  $P'$ , which is the projection of  $P$ .

taining the source of light will project outside the basic circle and extend to infinity. It is possible, however, to represent the whole sphere within the basic circle if two projections are superimposed, the one for the left-hand hemisphere constructed as in Fig. 3 and the one for the right-hand hemisphere constructed by having the light source on the left and the screen on the right. The same basic circle is used for both projections, and the points on one hemisphere are distinguished from those on the other by some notation such as plus and minus signs.

**Projection of Great and Small Circles.**—Let us consider how great circles and small circles inscribed on the sphere will appear on the projection (Fig. 4a). Any great circle that passes through the point  $N$  will

project to form a straight line passing diametrically through the basic circle on the projection; thus *SPNS* projects to *EE*. That this is true will be seen from the fact that the great circle *SPNS* and its projection *EE* are in fact lines of intersection of a plane with the sphere and projection plane, respectively. If the great circle is graduated in degrees, its projection *EE* will be a scale of stereographically projected degree points and will be useful for reading angular distances on the projection; it is shown with  $5^\circ$  graduations in Fig. 4b. Penfield<sup>1</sup> engraved a scale of this type for a projection of a basic circle of 14 cm. diameter, and such a scale is inherent in the stereographic nets that are discussed in the next section.

A small circle inscribed about a point such as *P* (Fig. 4a) that lies on the great circle *SPNS* will cut the great circle at two points, each of which is  $\phi^\circ$  from *P*.

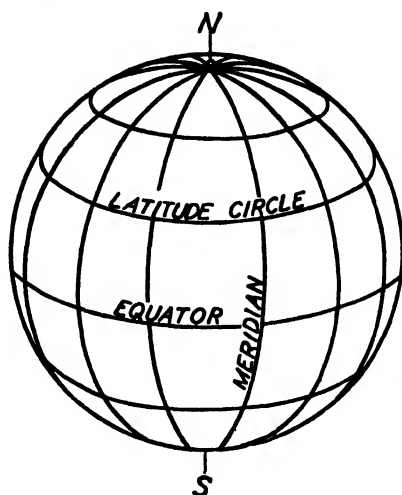


FIG. 5.—Ruled globe. Projections of this form the stereographic nets of Figs. 6 and 7.

The point *P* will project to *P'*. The bundle of projection lines for the small circle will form an elliptical cone with its apex at *S*, and the cone will intersect the plane in a true circle of which the center is on the line *EE*, either inside or outside the basic circle. The point *P'* will not be at the center of area of this projected circle but will lie on the line *EE* at a point distant an equal number of *stereographically projected* degrees from all points of the projected circle. The scale of projected degrees enables the size of the projected circle to be determined quickly, as indicated in Fig. 4b: the scale *EE* is laid diametrically across the basic circle so as

to pass through *P'*; then two points are laid down at a distance of  $\phi^\circ$  from *P'* in each direction, and a circle, centered on *EE*, is drawn through the two points thus located. (In Fig. 4b,  $\phi = 30^\circ$  and the center of area on the projected circle is at *C*.)

If the radius of the small circle about *P* is increased, it finally becomes a great circle. Since this great circle does not pass through the point *N*, its projection will not be a straight line. It will be a circle with a large radius having its center on an extension of *EE*; it will cut the basic circle

<sup>1</sup> S. L. PENFIELD, *Am. J. Sci.*, vol. 11, pp. 1, 115, 1901. The Penfield scales and protractors may be purchased from Penfield Stereographic Supplies, Mineralogical Laboratory, Yale University, New Haven, Conn. Penfield's protractors give the radii of stereographically projected small and great circles directly; these circles may however, be determined by trial; many will be found on the stereographic nets discussed in the next section and can be traced directly from the nets.

at two diametrically opposite points, and it will cut the line  $EE$  at the point  $90^\circ$  from  $P'$ . Its position and radius will thereby be uniquely determined.

**Ruled Globe and Stereographic Nets.**—A ruled globe is useful in crystallographic work, just as it is in geography, and the method of ruling is the same in both cases. Great circles are drawn through the north and south poles of the sphere for meridians, connecting all points of equal

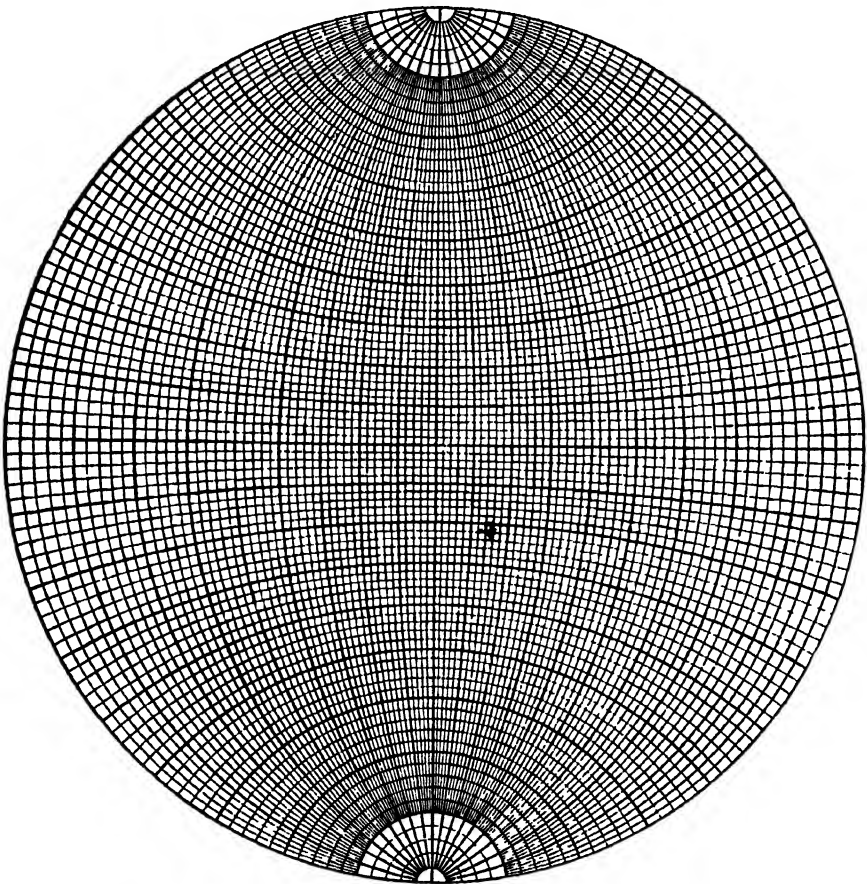


FIG. 6.—Stereographic net, Wulff or meridional type, with  $2^\circ$  graduations.

longitude. Another set of circles is drawn concentric with the north and south poles to connect points of equal latitude (since they have diameters less than the great circles, these are *small circles*). A globe ruled with latitude and longitude lines is shown in Fig. 5.

If the net of latitude and longitude lines on the reference sphere is projected upon a plane, it will form a stereographic net much resembling the rulings of the globe in appearance. When the north-south axis of the

sphere is *parallel to the projection plane*, the latitude and longitude lines form the stereographic net of Fig. 6, frequently referred to as a **Wulff net**. The meridians extend from top to bottom, the latitude lines from side to side (compare with Fig. 5). If, on the other hand, the north-south axis is perpendicular to the projection plane, the net of Fig. 7 will be formed,

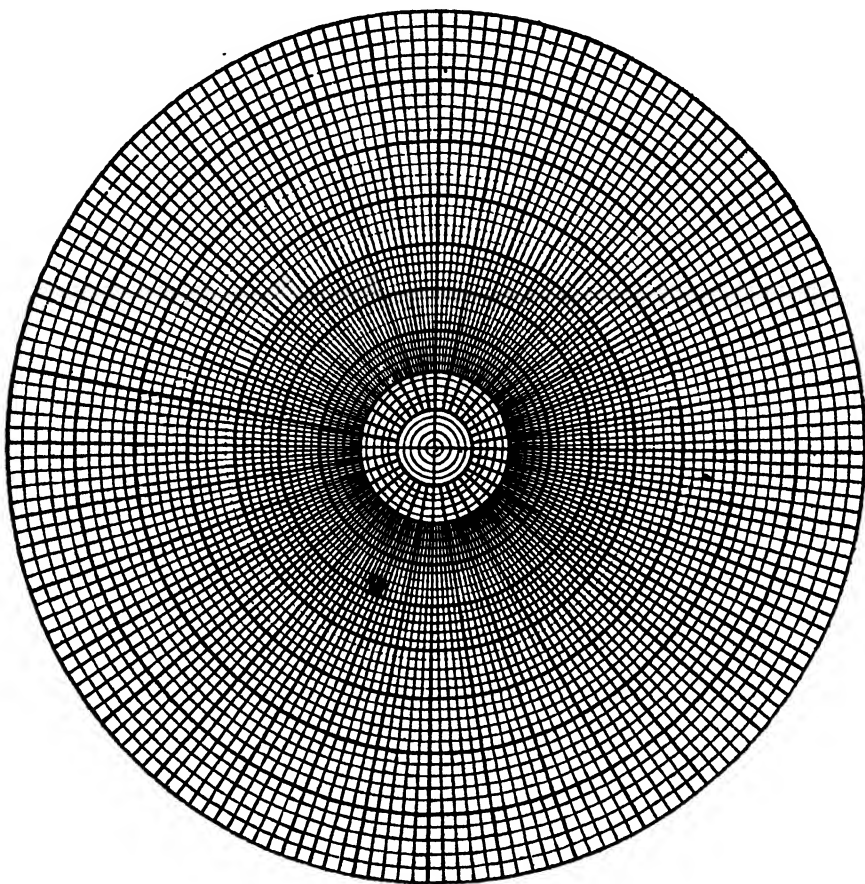


FIG. 7.—Polar stereographic net with  $2^\circ$  graduations.

which is known as the **polar net** or **equatorial net**. In this case the meridians radiate from the pole in the center, and the latitude lines are concentric circles.

The nets reproduced here are graduated in intervals of  $2^\circ$ . Larger nets of greater precision have been published repeatedly.<sup>1</sup> Nets of

<sup>1</sup> An accurate stereographic net,  $15\frac{3}{4}$  in. diameter, of the type reproduced in Fig. 6, was engraved by Admiral Sigsbee for the Hydrographic Office of the United States Navy, known as *H.O. Miscellaneous 7736*. Nets are sold by Penfield Stereo-

reasonable size will enable problems to be solved with an error of a degree or at best a few tenths of a degree; for greater precision it is necessary to resort to mathematical analysis.

**Rotation with the Nets.**—For the solution of crystallographic problems on a ruled globe it is necessary to use a device similar or equivalent to the one sketched in Fig. 8, consisting of a transparent cap fitting accurately over the globe but free to rotate with respect to it. Poles marked on the cap, such as  $P_1$  and  $P_2$ , may be studied with reference to the underlying net of latitude and longitude lines. Rotating this cap about the north-south axis of the globe will cause each point on the cap to move along a circle of constant latitude on the globe, as shown, and in so doing each point will cross the same number of meridians; *i.e.*, each point will retain its latitude, and each will alter its longitude equally.

An exactly analogous rotation may be carried out with stereographic nets. A transparent sheet of tracing paper replaces the transparent spherical cap, and the stereographic net laid under the paper replaces the ruled globe. An array of poles on the tracing paper is rotated with respect to the net by moving each point along the latitude line that passes through it, counting off along that line the required difference in longitude. With the Wulff net of Fig. 6, the poles shift to the right or left, whereas with the polar net of Fig. 7 they rotate about the center.

A greater freedom of rotation is possible with the cap-and-globe device than with the nets, for the axis of rotation in the former case can be chosen at random, while in the latter rotation must always be done about the north-south axis of a net. It is possible, however, to rotate first about the axis of one net and then about the axis of the other and by thus combining rotations to effect a rotation about an axis inclined to both. In this way,

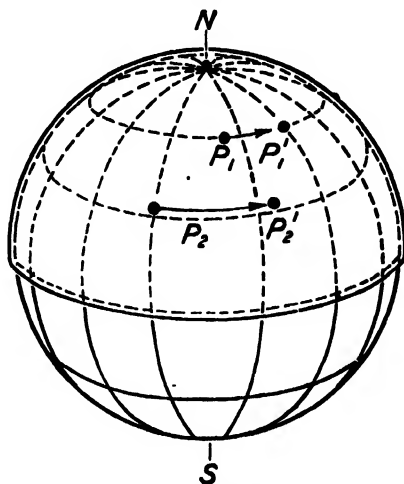


FIG. 8.—Ruled globe with transparent cap. Rotation of cap about  $NS$  axis moves  $P_1$  to  $P_1'$  and  $P_2$  to  $P_2'$ .

graphic Supplies, Mineralogical Laboratory, Yale University, New Haven, Conn. (14 cm. diameter), and the University Press, Cambridge, Mass. (12 in. diameter). Reproductions appear in the following references: F. RINNE, "Einführung in die kristallographische Formenlehre," Leipzig, 1922 (12 cm.); H. E. BOEKE, "Die Anwendung der stereographischen Projektion bei kristallographischen Untersuchungszeichnung," Bornträger, Berlin, 1914 (14 cm.); B. GOSSNER, "Kristallberechnung und Kristallzeichnung," Leipzig and Berlin, 1914 (20 cm.); G. WULFF, *Z. Krist.*, vol. 36, p. 1, 1902 (20 cm.); F. RINNE, *Z. Krist.*, vol. 65, p. 83, 1927 (10 cm.); D. JEROME FISHER, *Bull. Am. Assoc. Petroleum Geol.*, vol. 22, p. 1261, 1938.

rotations of *any* amount about *any* axis, whatever its inclination to the projection, can be made. The method amounts to resolving the rotation into components; one component is rotation about the axis parallel to the plane of the paper and is carried out by the Wulff net, and the other component is rotation about the axis normal to the paper and is accomplished by using the polar net.

In practice, rotation about an inclined axis can be accomplished without transferring the tracing paper from one net to the other, for obviously the circular rotation with the polar net can be performed simply by rotating the tracing paper about a pin at the center of its basic circle. Rotations of both types can be carried out conveniently with the tracing paper lying on the Wulff net and free to swing about a central pin.

**Angle Measurement.**—As has been stated in connection with Fig. 2, the angle between two points on a sphere is the number of degrees separating them on the great circle through them. The angle can be read on the spherical-cap and ruled-globe apparatus by so rotating the cap that the two points are made to lie on the same meridian of the globe, for all meridians are great circles (they all pass through two diametrically opposite points—the north and south poles). With the two points on the same meridian the angle between them is their difference in latitude, directly read with the help of the latitude lines ruled on the globe. Angles are measured with a stereographic net in exactly the same way by bringing the points to the same meridian of the stereographic net and counting their difference in latitude. Any two points can be brought to the same meridian merely by rotating them a certain amount about the center (swinging the tracing paper about the central pin of a Wulff net).

The most frequent source of error in students' work with the projection comes from misunderstanding or forgetting this principle, that *the angle between two points is equal to their difference in latitude only when they lie on the same meridian*. It is also true, of course, that the angle between two points is equal to their difference in *longitude* when, and only when, they lie on the *equator*, the equator of the Wulff net then serving as the scale of projected degrees that was mentioned earlier.

The operation of angle measurement described above is, of course, identical whether the points on the projection represent poles of crystallographic planes, crystallographic directions, or points on a sphere.

When planes appear in a stereographic projection as great circles, like the circle *M* of Fig. 1, it is easy to plot the poles of the planes and then to measure the angle between the poles. To plot the projection of pole *P* (Fig. 1) it is necessary merely to turn the tracing paper about the central pin in a Wulff net until the projection of great circle *M* falls on a meridian of the Wulff net; then the point on the equator 90° from that meridian is the pole *P* of the plane.



**Properties of Stereographic Projection.**—Elaborate treatises have been written on the properties and uses of the stereographic projection for crystallographic work,<sup>1</sup> and the reader is referred to these for details not mentioned in the present discussion and for mathematical proofs. We may summarize as follows the items that have been found most useful in metallurgical problems:

1. The reference sphere is projected as it would appear to the eye at a point on the spherical surface; hence it is a "perspective projection." It is also the "shadow projection" when a source of light is on the sphere, as has been discussed above.

2. Small circles on the sphere appear as circles on the projection; however, the centers of these circles on the sphere will not project to the center of the area of the projected circles but will be displaced radially an amount sufficient to correspond to equal *angular* distances from the center to all points on the circumference.

3. Great circles on the sphere appear on the projection as circles cutting the basic circle at two diametrically opposite points; a great circle lying in a plane perpendicular to the projection plane becomes a diameter on the projection, while great circles in inclined positions on the sphere may be made to coincide with one of the meridians of a Wulff net.

4. Angles between points are measurable and may be read as a difference of latitude on a net so rotated as to give the points the same longitude. The *linear* distance on the projection representing  $1^\circ$  of arc varies from the center to the basic circle by a factor of 2.

5. The projection is angle true; the angle between intersecting planes equals the angle at which the projection of the planes intersect. (However, see page 32 for a more suitable method of determining the angle.)

6. Angular relations between points on the projection remain unchanged by rotation of the points about the axis of a stereographic net as described earlier (page 31).

7. Half of a sphere is projected within a basic circle; the other half is projected on a plane of infinite extent but is more conveniently projected within the basic circle and distinguished from the first by some notation.

**Standard Projections of Crystals.**—A stereographic projection of the poles of all the important planes in a crystal is indispensable in metallographic studies. When such a projection is prepared with a plane of low indices as the plane of projection, it is called a standard projection.

<sup>1</sup> S. L. PENFIELD, *Am. J. Sci.*, vol. 11, pp. 1, 115, 1901; vol. 14, p. 249, 1902; *Z. Krist.*, vol. 35, p. 1, 1902. E. BOEKE, "Die Anwendung der stereographische Projektion bei kristallographischen Untersuchungen," Bornträger, Berlin, 1911. F. E. WRIGHT, *J. Optical Soc. Am.*, vol. 20, p. 529, 1930; *Am. Mineral.*, vol. 14, p. 251, 1929. A. HUTCHINSON, *Z. Krist.*, vol. 46, p. 225, 1909. D. JEROME FISHER, A New Projection Protractor, *J. Geol.*, vol. 49, pp. 292, 419, 1941; reprints and protractors sold by University of Chicago Bookstore, Chicago, Ill.

Figure 9 is a simple example representing a cubic crystal with a cube face parallel to the projection plane; the  $X$  and  $Y$  axes of the crystal lie in the projection plane so that the poles of the planes (100) and (010), respectively, are on the basic circle, and the  $Z$  axis is normal to the plane of projection so that the pole of the plane (001) is at the center of this circle. The plot is constructed by calculating the angles between the poles and

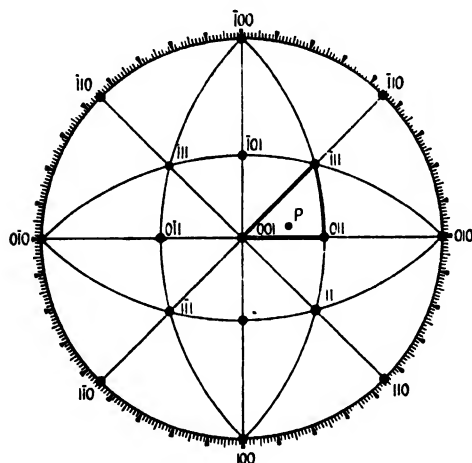


TABLE IV.—ANGLES BETWEEN CRYSTALLOGRAPHIC PLANES IN CRYSTALS OF CUBIC SYSTEM

{ <i>HKL</i> }	{ <i>hkl</i> }	Values of angles between planes of forms { <i>HKL</i> } and { <i>hkl</i> }					
100	100	0°	90°				
	110	45°	90°				
	111	54°44'					
	210	26°34'	63°26'	90°			
	211	35°16'	65°54'				
	221	48°11'	70°32'				
	311	25°14'	72°27'				
110	110	0°	60°	90°			
	111	35°16'	90°				
	210	18°26'	50°46'	71°34'			
	211	30° 1'	54°44'	73°13'	90°		
	221	19°28'	45°	76°22'	90°		
	311	31°29'	64°47'	90°			
111	111	0°	70°32'				
	210	39°14'	75° 2'				
	211	19°28'	61°52'	90°			
	221	15°48'	54°44'	78°54'			
	311	29°30'	58°30'	79°58'			
210	210	0°	36°52'	53° 8'	66°25'	78°28'	90°
	211	24° 6'	43° 5'	56°47'	79°29'	90°	
	221	26°34'	41°49'	53°24'	63°26'	72°39'	90°
	311	19°17'	47°36'	66° 8'	82°15'		
211	211	0°	33°33'	48°11'	60°	70°32'	80°24'
	221	17°43'	35°16'	47° 7'	65°54'	74°12'	82°12'
	311	10° 0'	42°24'	60°30'	75°45'	90°	
221	221	0°	27°16'	38°57'	63°37'	83°37'	90°
311	311	0°	35° 6'	50°29'	62°58'	84°47'	

ever, to draw the whole standard projection before plotting the axis in it, for the axis may just as well be referred to the three neighboring poles of (100), (110), and (111) planes. If poles of these three types are joined by great circles, there results (for the cubic system) a pattern of 24 equivalent triangles, one of which is outlined with heavy lines in Fig. 9, and it is common practice to draw only one of these triangles or two adjacent triangles before plotting the specimen orientation.

It is easy to show by means of a projection of this sort (using one triangle or sometimes two adjacent ones) how the orientation of the lattice changes during deformation of the crystal, for deformation causes a cer-

tain rotation of the axis with respect to the lattice and causes the point  $P$  (Fig. 9) to move along a definite path on the standard projection.<sup>1</sup> It will be noted that plotting the specimen axis in this way leaves unspecified the orientation of the lattice with respect to rotation around the specimen axis, but in many problems this is unimportant, for example, in tensile

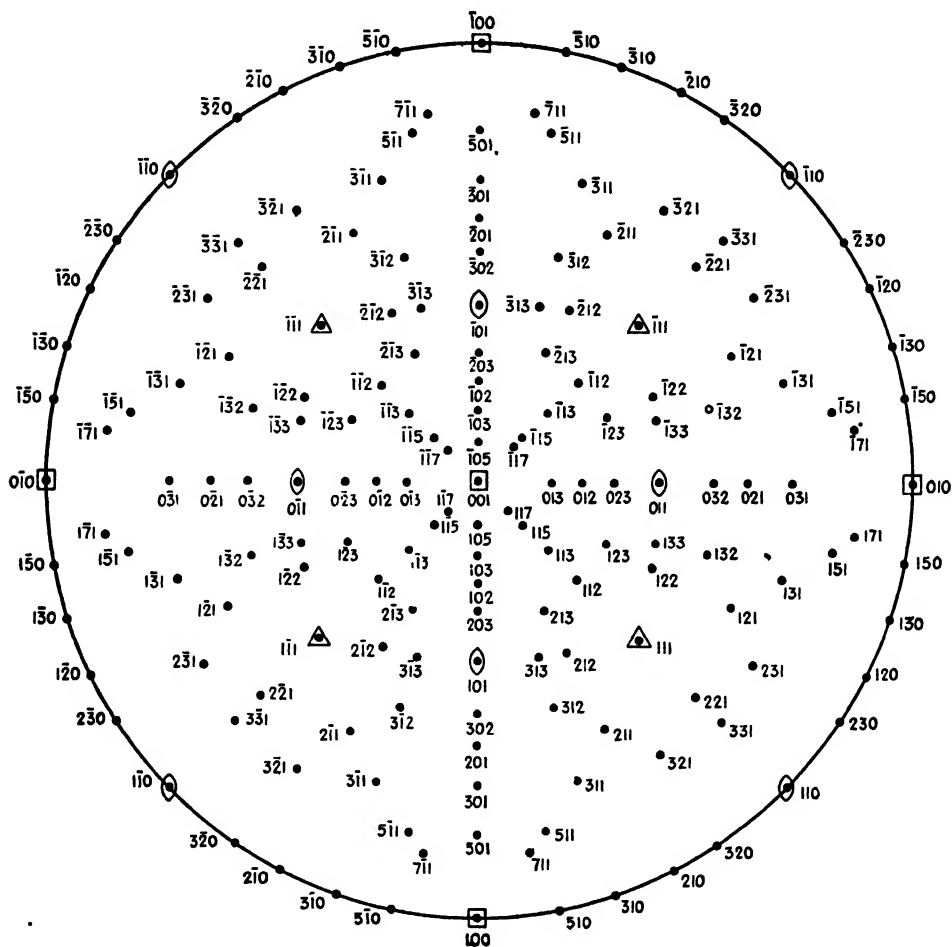


FIG. 10.—Standard (001) projection for cubic crystals.

tests of a wire. A number of investigators have made use of this kind of plot to show the variation of physical properties with lattice orientation; measurements of a physical property of a wire can be written beside the point representing the wire orientation, and points of equal magnitude can be joined by contours.

<sup>1</sup> G. I. TAYLOR and C. F. ELAM, *Proc. Roy. Soc. (London)*, vol. A102, p. 643, 1923; vol. A108, p. 28, 1925. G. I. TAYLOR, *Proc. Roy. Soc. (London)*, vol. A116, p. 16, 1927. H. J. GOUGH, Edgar Marburg Lecture, *Proc. A.S.T.M.*, vol. 33, pt. 2, p. 3, 1933.

**Applications to Metallography.**<sup>1</sup>—The combination of standard projection and stereographic net is particularly convenient for analyzing the crystallographic features of the deformation of crystals by slip, twinning, and cleavage or the growth habits of crystals precipitated within a crystal, forming a Widmanstätten pattern. Such studies deal with the orientation of planes in space, the angles between these planes, and the intersections of these planes with one another, matters readily visualized

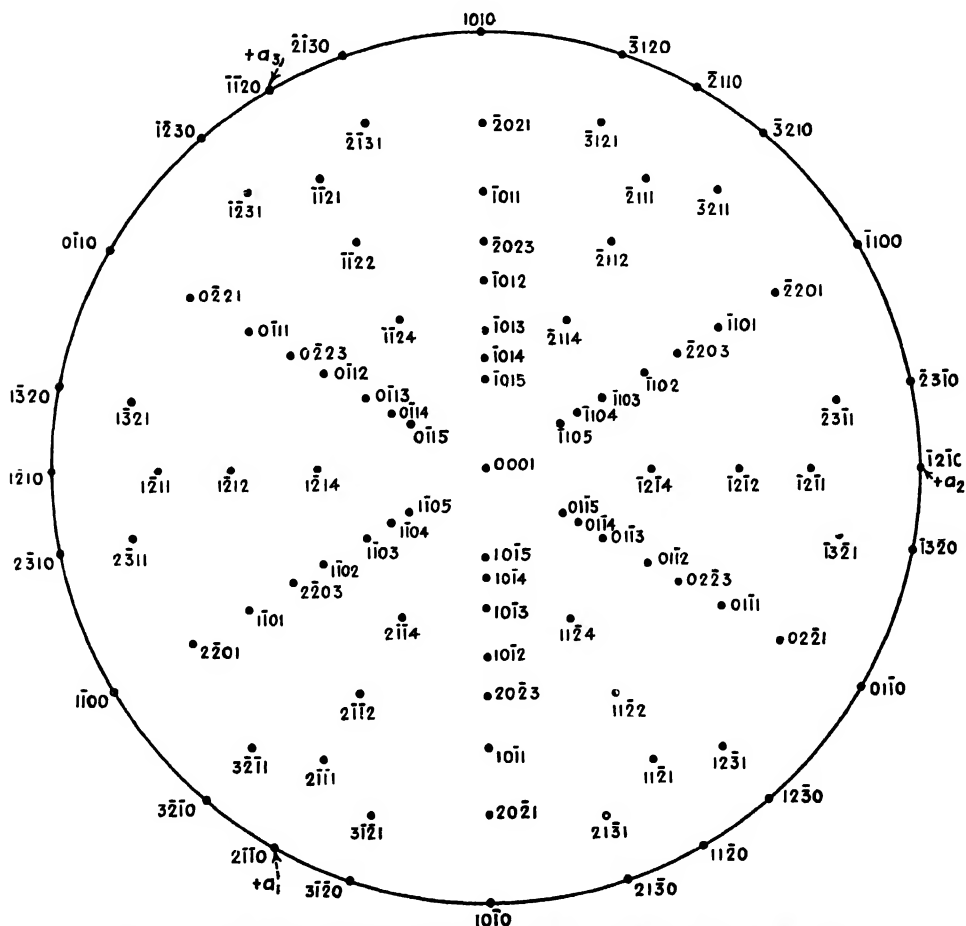


FIG. 11.—Standard (0001) projection for zinc (hexagonal,  $c/a = 1.86$ ).

and handled on the stereographic projection. To aid the beginner it is desirable to list the more common problems and to give the operations by which they are graphically solved, but it should be borne in mind that as soon as one is accustomed to think clearly of the sphere and its "picture," the stereographic net, these operations become self-evident.

Obviously, the solutions are independent of the choice of projection plane and are applicable to problems in pure spherical trigonometry; but,

<sup>1</sup> C. S. BARRETT, *Trans. A.I.M.E.*, vol. 124, p. 29, 1937.

to make the operations more easily understood by the metallographer, we shall present them from his standpoint rather than in the abstract. We shall speak of polished surfaces of specimens and of traces of crystallographic planes in these surfaces (lines of intersection), and we shall generally consider the projection plane to lie in one of the surfaces.

1. ORIENTATION OF PLANES CAUSING A GIVEN TRACE IN A SURFACE.—Let us consider the stereographic projection of a polished surface containing the trace of a crystal plane, the projection being made on a sheet of paper laid parallel to the polished surface. The surface will then be represented on the paper by the basic circle, and markings on the surface will be plotted as points on the circumference of this basic circle. A trace in the surface that runs lengthwise of the page ("vertically") will be plotted in the projection as the diametrically opposite points  $T$  and  $T'$  at the top and bottom of the basic circle (Fig. 12). A trace in any other direction in the

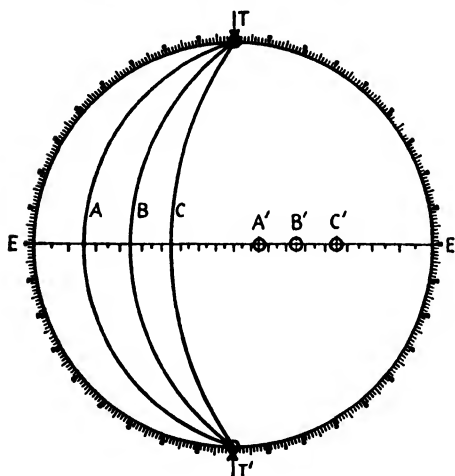


FIG. 12.—Planes  $A$ ,  $B$ ,  $C$ , with poles  $A'$ ,  $B'$ ,  $C'$ , and all other poles along  $EE'$  intersect projection plane in trace  $TT'$ .

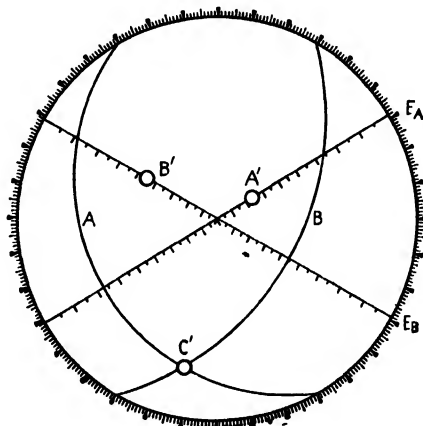


FIG. 13.—Planes  $A$  and  $B$ , with poles  $A'$  and  $B'$ , intersect along direction  $C'$ .

surface would be plotted similarly, as the end points of a diameter parallel to the given direction.

To find the planes that would intersect the surface in the direction  $TT'$ , the points  $TT'$  are superimposed on the  $N$  and  $S$  poles of a Wulff net. It will then be seen that all the meridians of the net—such as the meridians  $A$ ,  $B$ , and  $C$  of Fig. 12—are projections of the required planes, since they intersect the basic circle at  $T$  and  $T'$ . Similarly, any other plane whose pole lies on the equator of the Wulff net will intersect the surface in the direction of the  $NS$  axis.

Conversely, if the pole of a plane is given, such as  $A'$ , its trace in the projection plane is readily found. The transparent sheet on which the pole is plotted is laid on a Wulff net and turned until the pole falls on the equator, in which position the required trace will be parallel to the  $NS$  axis of the net.

2. TRACE OF ONE PLANE IN ANOTHER WHEN BOTH ARE INCLINED TO THE PROJECTION PLANE.—Given two poles  $A'$  and  $B'$  (Fig. 13), the planes  $A$  and  $B$  are first plotted. This is accomplished for  $A$  by rotating the projection over a Wulff net so that the pole  $A'$  lies on the equator  $E_A$  and then tracing on the projection the meridian lying at  $90^\circ$  to the pole  $A'$ . The operation is repeated for the second pole,  $B'$ , with

the net turned so that its equator is in the position  $E_B$ . The point of intersection,  $C'$ , of the two planes thus plotted is the projection of the required line of intersection of the planes.

**3. DIRECTION NORMAL TO TWO GIVEN DIRECTIONS (OR ZONE AXIS OF TWO PLANES WHOSE POLES ARE GIVEN).**—Referring again to Fig. 13, let us assume that the directions  $A'$  and  $B'$  are given and that the direction normal to both is required. This may be given by the construction described in the preceding paragraph, for obviously every line in plane  $A$  is normal to the direction  $A'$  and every line in  $B$  is normal to  $B'$ ; hence, the line common to  $A$  and  $B$  is normal to both  $A'$  and  $B'$ .

An alternative solution is shown in Fig. 14. The projection is rotated over a Wulff net until both  $A'$  and  $B'$  lie on the same meridian; then the point  $C'$  on the equator and  $90^\circ$  from this meridian is the projection of the required direction. If  $A'$  and  $B'$  are poles of planes,  $C$  is the zone circle and  $C'$  is their zone axis.

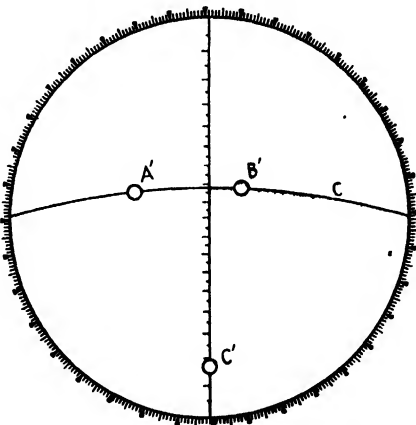


FIG. 14.—Alternative method of locating  $C'$ , which is normal to  $A'$  and  $B'$ .

**4. DETERMINATION OF ORIENTATION OF PLANE FROM ITS TRACES IN TWO SURFACES.**—The surfaces are first plotted on the projection as in Figs. 15a and 15b, one surface lying in the plane of projection and forming the basic circle  $A$  of Fig. 15b, the other surface,  $B$ , coinciding with the meridian of the stereographic net that lies  $\phi'$  from the first about the axis  $NS$ . (To draw this meridian the net is rotated so that the direc-

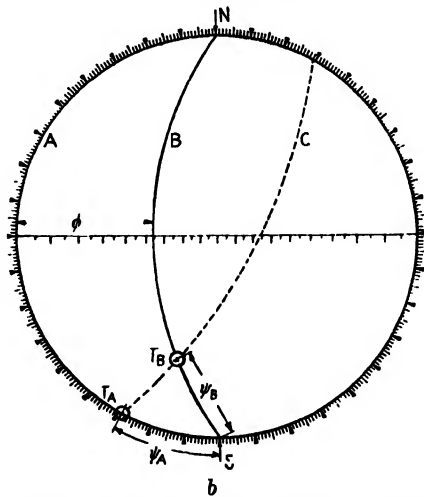
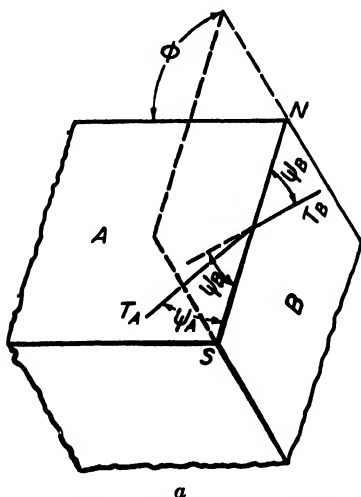


FIG. 15.—Determination of orientation of plane from its traces in two surfaces. Traces are  $T_A$  and  $T_B$  in surfaces  $A$  and  $B$ , respectively. Plane causing these is  $C$ .

tion  $NS$  is parallel to the line of intersection of the two surfaces.) On the planes  $A$  and  $B$  thus plotted in Fig. 15b are then located the points  $T_A$  and  $T_B$ , which represent the directions of the traces in the two surfaces, respectively; they will lie at angles laid off from the edge  $NS$  to correspond with the angles on the specimen, the angles being measured as differences of latitude,  $\psi_A$  and  $\psi_B$ , on the stereographic net. The traces

$T_A$  and  $T_B$  having been plotted, the plane that causes them can be drawn by rotating the net so that some single meridian of the net will pass through both points; this meridian (the dashed circle  $C$  in the figure) is then the projection of the required plane.

5. DETERMINATION OF CRYSTAL ORIENTATION FROM TRACES OF  $\{hkl\}$  PLANES WHEN  $h$ ,  $k$ , AND  $l$ , ARE KNOWN. (a) *Traces in One Surface Only*.—On tracing paper a basic circle is drawn representing the specimen surface; through this circle are drawn diameters perpendicular to the directions of traces seen on the specimen surface.

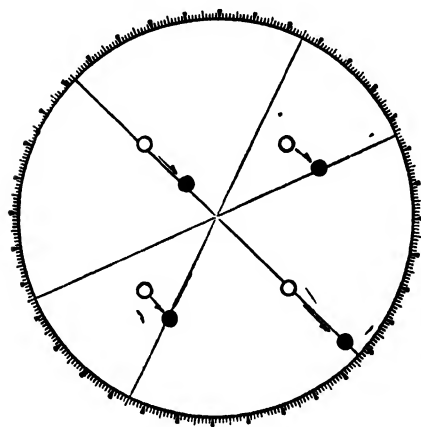


FIG. 16.—Orientation of cubic crystal determined from traces of  $\{111\}$  planes. Indicated on projection are normals to traces (diameters);  $\{111\}$  poles of standard projection (○);  $\{111\}$  poles in orientation explaining traces (●).

These diameters are then the loci of all poles capable of forming the traces. A standard projection on a transparent sheet of all poles of the given form  $\{hkl\}$  is then superimposed on this plot and on a Wulff net, and a pin is put centrally through all three sheets. By trial the relative position of the three sheets is found in which each pole of the standard projection may be rotated into coincidence with one of the diameters by the same amount of rotation about the axis of the net. This position of the sheets is illustrated in Fig. 16, in which appear the  $\{111\}$  trace normals (diameters), the  $\{111\}$  poles of the standard projection (○), and the position of these poles on the trace normals after the rotation with the net (●). This final array of poles (●) describes an orientation of the crystal consistent with the observed traces; it may not be, however, the only consistent orientation. In fact, if traces on only one surface are studied, the crystal may have the orienta-

tion shown or a mirror image of this orientation in the plane of projection, the poles lying in either of the hemispheres.

The example in Fig. 16 is an orientation determination in which a method of this sort was necessary, for the crystal in which the traces originated had decomposed. (The traces were formed by decomposition of a  $\gamma$ -iron crystal into  $\alpha$ -iron crystals which formed lamellae on  $\{111\}$  planes.<sup>1</sup>)

5.(b) *Traces in Two Surfaces*.—The solution is more direct and rigorous if traces can be followed from one surface around the edge to the other surface, thus eliminating any uncertainty as to the proper pairing of traces on the two surfaces. If this is possible, the first operation is to plot the orientation of each plane by method 4 above. The poles thus plotted give the crystal orientation. If the orientations of other poles of the same crystal are required, they may be obtained by rotation of the standard projection, as in the previous method—the plotted poles on one sheet and the standard projection on another being rotated with respect to the net until a difference of  $\phi^\circ$  of longitude and no difference of latitude exists between each  $\{hkl\}$  pole of the standard and a corresponding plotted pole. Rotation of  $\phi^\circ$  then puts any pole of the standard into its proper position in the plot.

<sup>1</sup> R. F. MEHL and D. W. SMITH, *Trans. A.I.M.E.*, vol. 113, p. 203, 1934. In this work, traces on two surfaces were used, but for simplicity the author has shown in the present chapter the data from only one surface.



When the pairing of traces on the two surfaces is uncertain, it is necessary to make a plot of poles for all possible pairings. Among this array of poles there will be one or more groupings having the angular relations appropriate for  $\{hkl\}$  planes, and these may be singled out from the whole number by trial rotations of the  $\{hkl\}$  poles of the standard, possible solutions being those for which  $\phi^\circ$  rotation about the net axis brings the standard poles into coincidence with the sets of plotted poles.

6. DETERMINING INDICES OF SET OF PLANES CAUSING TRACES ON ONE OR MORE SURFACES. (a) *Crystal Orientation Unknown*.—The poles of the planes (or of all possible planes in cases of uncertain pairing) are plotted as in the preceding problem. Trial rotations are then performed, using different sets of standard projection poles, until a set is brought into coincidence with the plotted poles. For example, traces on two polished surfaces were found to be consistent with  $\{111\}$  planes by the analysis

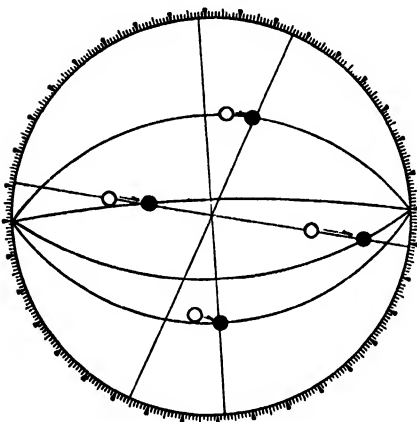


FIG. 17.—Orientation of cubic crystal determined from traces on two surfaces. Normals to traces are full lines; standard projection  $\{111\}$  poles (O);  $\{111\}$  poles in orientation explaining traces (●).

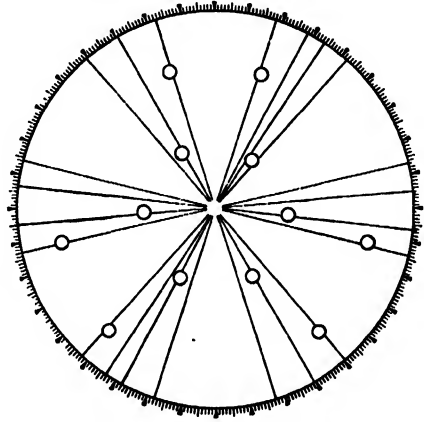


FIG. 18.—Determination of indices when crystal orientation is known. Traces on one surface available. Diameters are normals to traces of precipitated plates of iron nitride in polished surface. Circles (O) are  $\{210\}$  poles, located by x-rays, which account for traces.

shown in Fig. 17.<sup>1</sup> Normals to traces on the plane of projection appear in this figure as diameters, while normals to traces on a second plane of polish appear as great circles. The dots are poles of  $\{111\}$  planes that have been rotated from a standard projection in such a way as to lie at or near the intersections of diameters and circles and that are therefore capable of explaining the traces in both surfaces.

The procedure in this problem is laborious and leads to uncertain results unless traces are measured on two surfaces and unless the planes are of low indices. It is frequently possible to save labor by noting the number of different directions of traces on each surface, for in this way certain planes may be eliminated from further consideration. If, for example, a single crystal of a cubic metal exhibits more than three directions of traces,  $\{100\}$  slip planes alone could not be responsible; if more than four directions are found, neither  $\{100\}$  nor  $\{111\}$  planes alone could have produced them; if more than six directions, neither  $\{100\}$ , nor  $\{111\}$ , nor  $\{110\}$ , etc. Numerous applications of this principle have been made, particularly in Widman-

<sup>1</sup> R. F. MEHL and C. S. BARRETT, *Trans. A.I.M.E.*, vol. 93, p. 78, 1931.

stätten studies, both for determining the indices of planes and for excluding planes of certain indices.

6.(b) *Crystal Orientation Known*.—If x-ray data or other observations have already given the orientation of a crystal, a standard projection of all likely planes can be rotated to their positions for this crystal orientation. By the methods presented above, the traces that each set of planes will make in the plane of polish may then be

plotted. The coincidence of predicted and observed traces will then single out the sets of planes best able to explain the data.

Figure 18 illustrates the method for traces in one surface.<sup>1</sup> The directions of "nitride needles" in a single crystal of iron were measured, and diameters were drawn perpendicular to these directions. The poles of various low-index planes of the matrix crystal of iron were then plotted on the projection in positions determined by x-rays. The poles of {210} planes lay on or near the trace normals without exception and were thus adequate to explain them. One becomes convinced that planes of no other index could be involved, however, only after several individual examples have been analyzed in this way.

That "nitride needles" are plates formed on {210} planes in  $\alpha$ -iron was proved more rigorously by analyzing traces that appeared simultaneously on two surfaces. Poles of the

FIG. 19.—Determination of indices when crystal orientation is known. Traces on two surfaces available. Circles are poles of nitride plates appearing simultaneously on two surfaces; crosses are {210} poles, located by x-rays, which account for traces.

plates could then be plotted by method 4. These are shown as circles in Fig. 19. These observed poles agreed well with the poles of {210} planes located by x-ray diffraction, shown as crosses in the figure.

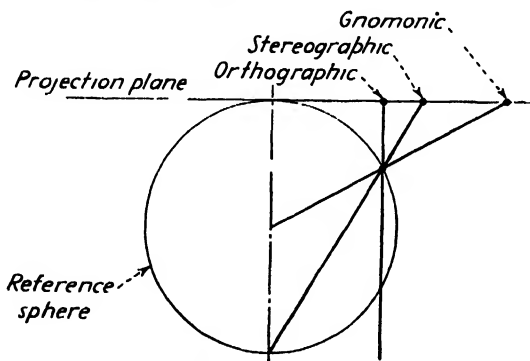


FIG. 20.—Relations among orthographic, stereographic, and gnomonic projections.

**Other Perspective Projections.**—The stereographic projection is but one of a series of projections that are "perspective," *i.e.*, that represent what the eye sees when placed at a definite position with respect to the reference sphere. The eye (or a light source) placed on the *surface* of the

<sup>1</sup> R. F. MEHL, C. S. BARRETT, and H. S. JERABEK, *Trans. A.I.M.E.*, vol. 113, p. 211, 1934.

reference sphere gives the **stereographic** projection. When it is at infinity, it gives the **orthographic** projection so widely used in mechanical drawing. And when it is at the *center* of the sphere, it gives the **gnomonic** projection. These relations are sketched in Fig. 20, which represents a section through the center of the sphere normal to the projection plane. It will be seen that the hemisphere adjacent to the projection plane is mapped within a basic circle in the case of the stereographic projection, but it extends to infinity in the case of the gnomonic. The gnomonic is accordingly less useful in crystallographic problems [see applications of the gnomonic to the Laue method in Chap. V]. All perspective projections have the property that the azimuthal positions around the central ray (the dot-dash line in Fig. 20) are the same on the sphere and its projection. Other related projections have sometimes been employed<sup>1</sup>—for example, the **equiangular**—but they are not conventional for crystallographic problems and would be likely to lead to confusion if occasionally adopted for this purpose by investigators. The reflection of x-rays from a crystal plane forms a projection on a photographic film which has been called a **reflection projection**.

<sup>1</sup> F. E. WRIGHT, *The Methods of Petrographic Microscopic Research*, *Carnegie Inst. Wash. Pub.* 158, 1911.

## CHAPTER III

### X-RAYS

When Laue suggested to his assistant, Friedrich, in 1912 that x-rays should be of the right wavelength to diffract from the atoms within crystals, he started a train of experiments that has been of incalculable aid to the development of crystallography. In the hands of W. H. Bragg and his son, W. L. Bragg, x-rays were immediately put to work in the solution of crystal structures. Practically every structure determination since that time has employed x-rays; applications of x-rays to chemistry, physics, and metallurgy have been continuous. No laboratory in these fields is now considered complete without equipment for x-ray diffraction. It is desirable, therefore, to devote a considerable portion of this volume to the methods of x-ray diffraction. In order that x-rays may be employed most effectively it is first necessary to cover in some detail their nature and the methods of producing them. The fundamental principles of radiography are discussed briefly but not the practical art; the same is done for chemical analysis by x-rays, which has been so well covered in von Hevesy's book.<sup>1</sup>

X-rays were discovered in 1895 when Prof. W. K. Röntgen was experimenting at the University of Würzburg, Germany, with highly evacuated tubes in which cathode rays were being generated. It had already been shown by Sir William Crookes that the cathode rays in these tubes are streams of negative electricity—electrons—impelled and directed by the electric field within the evacuated bulb. Röntgen discovered that the impact of the cathode rays on the wall of the bulb generates an invisible, penetrating radiation which in many respects resembles light. The rays spread outward from the source in straight lines and cast sharp shadows; they darken photographic plates that have been wrapped in black paper; they excite barium platinocyanide to brilliant fluorescence; and, like ultraviolet light, they ionize air.

The interest in this discovery was tremendous, especially among the physicists, who were anxious to learn the exact relation of the rays to light, and among the technologists, who within a few months had begun to apply them to medical and industrial uses. The concentrated efforts of physicists in many laboratories disclosed additional properties of the

<sup>1</sup> G. VON HEVESY, "Chemical Analysis by X-Rays and Its Application," McGraw-Hill, New York, 1932.

rays analogous to the properties of light and other electromagnetic radiation: their path can be bent by refraction when passing through a substance; they can be polarized; they can be reflected from a smooth surface if the glancing angle between the beam and the surface is less than about  $\frac{1}{2}^\circ$ ; they can be diffracted (very slightly) by a slit, a grating, or a crystal; they can stimulate, "burn," or kill living matter, depending on dosage; they can eject electrons from an absorbing substance which becomes, in turn, an emitter of fluorescent x-rays; they are scattered by the atoms of a substance, and if the atoms are arranged in a regularly repeating pattern the scattered rays cooperate to build up diffracted rays. In addition to following the laws of wave propagation and diffraction,

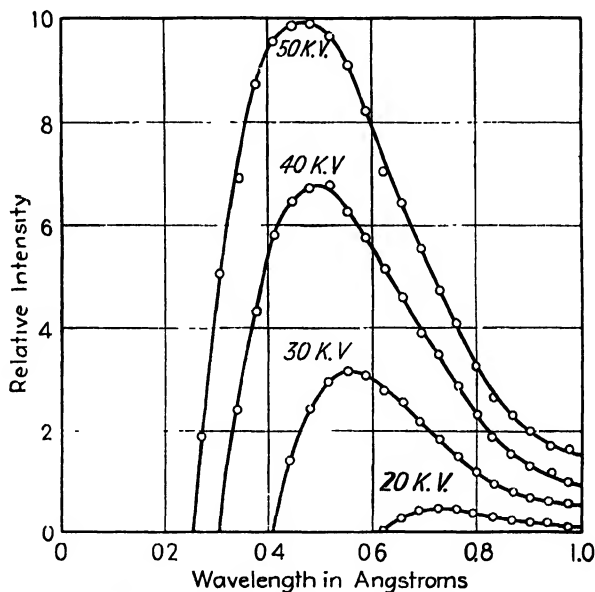


FIG. 1.—Distribution of energy in the continuous x-ray spectrum of tungsten at different voltages. (Urey.)

the rays also act as discrete particles, quanta, possessing definite energy and momentum.

When electrons are driven at high speed into the metal target of an x-ray tube, about 2 percent of their energy is converted into x-rays; the balance is converted into heat in the target. The distribution of the x-ray energy in the different wavelengths of the spectrum is a matter of first importance in the various methods of crystal analysis and the different techniques of industrial radiography.

The radiation consists of a continuous spectrum—radiation spread over a wide band of wavelengths—and a superimposed line spectrum of high-intensity single-wavelength components. The former corresponds to white light and is frequently called the **white radiation**. The latter corresponds to monochromatic light; and because the wavelength of each

component is characteristic of the metal emitting the rays, it is called the **characteristic radiation**. The continuous spectrum can be produced without the characteristic if the tube is operated at a low voltage, but as soon as the voltage is increased beyond a critical value the characteristic spectral lines appear in addition to the white radiation.

**The Continuous Spectrum.**—Figure 1 shows the distribution of energy in the continuous or white radiation emitted from a tungsten-target tube operating at a series of voltages. The important features of the spectra in Fig. 1 are the abrupt ending of each spectrum at a minimum wavelength, the maximum at longer wavelengths, and the gradual decrease in intensity on the long wavelength end of the spectrum. Increasing the operating voltage shifts both the minimum wavelength (the **short-wavelength limit**) and the point of maximum intensity to the left and increases the intensity of all wavelengths.

The radiation originates when an electron that is moving with a high velocity encounters an atom in the target. If it converts its entire kinetic energy into x-rays at a single encounter, the frequency of the rays produced will be given by the quantum relation

$$eV = h\nu$$

where  $e$  is the charge on the electron,  $V$  the voltage applied to the tube,  $h$  a universal constant (Planck's constant), and  $\nu$  the frequency of the radiation. While all electrons strike the target with energy  $eV$ , only rarely are they stopped in a single encounter so as to convert their entire energy into one quantum. More frequently they dissipate their energy in a series of glancing encounters with a number of atoms and generate heat or quanta of lower frequency than the maximum. From varied encounters an entire continuous spectrum is produced which extends from the limiting frequency given in the above equation down to very low frequencies. In terms of the operating potential of the tube in volts and the wavelength of the radiation (which is equal to the velocity of light divided by the frequency) the above relation for the short-wavelength limit for the continuous spectrum is

$$\lambda_{\min} = \frac{12,430}{V} \quad \text{angstroms}$$

If the voltage impressed on the tube is pulsating between limits or is alternating, it is the peak value and not the root-mean-square value that must be used in this formula to give the minimum wavelength. For x-ray diffraction the wavelengths used are  $0.2\text{\AA}$  or more and thus do not require potentials in excess of 60,000 volts; but for industrial radiography much shorter waves are needed, and voltages are raised to 200, 400, and even 1000 kv.

The efficiency of an x-ray tube as a generator of white radiation is greatly influenced by the metal used for the target and the voltage employed. The total energy emitted increases directly as the atomic number of the target material and roughly as the square of the applied voltage.<sup>1</sup> Increased emission with increasing voltage is evident in the curves of Fig. 1, where the area under the curves is proportional to the total energy in the continuous spectrum. The intensity at the highest point of the curve also increases rapidly with voltage; doubling the voltage may result in as much as a sixteenfold increase in the maximum intensity.

The wavelength at which the intensity is a maximum is about 1.5 times the minimum wavelength and shifts to shorter wavelengths with increasing voltages. For radiographic purposes requiring high intensities and short wavelengths it is therefore necessary to use very high voltages, not only to reduce the value of the short-wave limit, but also to shift the effective mean wavelength to the short-wave end of the spectrum;



FIG. 2. —Spectrum of radiation from molybdenum. Characteristic lines of the  $K$  series are superimposed on continuous spectrum.

it is also necessary to use a metal of high atomic number for the target in order to increase the efficiency of the tube. Tungsten is universally chosen for the purpose because its atomic number is high (74) and because it has a high melting point and good thermal conductivity, which permits the heat arising from the impact of the electrons to flow through the target and be dissipated without melting or vaporizing the target.

**The Characteristic Spectrum.**—In addition to the continuous spectrum, an x-ray tube operating at a sufficiently high potential will also emit a line spectrum that is characteristic of the kind of atoms in the target. The nature of the characteristic spectrum is illustrated by Fig. 2, in which a portion of the spectrum from a molybdenum target is reproduced. The sharp lines in the spectrum are classified into series ( $K$ ,  $L$ ,  $M$ , etc.) and are named with Greek letters and subscripts in accordance with their origin in the atoms of the target. The most important lines for x-ray diffraction work, the  $K$  series, are shown in this figure. In the order of decreasing wavelength these are the  $K\alpha$  line, which is a close doublet composed of  $K\alpha_2$  and  $K\alpha_1$ , and a weaker  $K\beta$  line, a close doublet of  $K\beta_3$  and  $K\beta_1$ , which is rarely resolved. There is sometimes also a weak  $K\gamma$ , now known as  $K\beta_2$ , which is also a very close

<sup>1</sup> W. W. Nicholas finds the energy emitted is proportional to  $V^{1.5}$  for high voltages and a tungsten target. (*J. Research Natl. Bur. Standards*, vol. 5, p. 853, 1930.)

(unresolved) doublet. Unless special precautions are taken to eliminate some of these lines,  $K\alpha$ ,  $K\beta$ , and possibly  $K\gamma$  will appear on x-ray diffraction patterns. A plot of intensity vs. wavelength for a tube emitting the  $K$  series is shown in Fig. 3; the strong  $K\alpha$  and  $K\beta$  peaks appear in this plot, but the weaker  $K\gamma$  and the longer wavelength  $L$  and  $M$  lines do not.

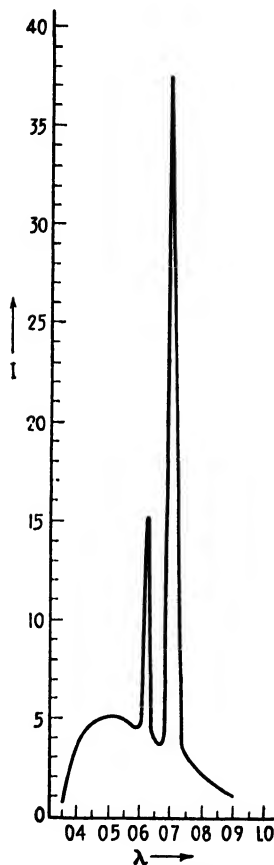


FIG. 3.—Spectrum of molybdenum at 35,000 volts showing  $K\alpha$  and  $K\beta$  lines superimposed on continuous spectrum.

There are a number of lines in the  $L$  series,  $M$  series, etc., particularly with the heavier elements, but these are always of longer wavelength, as illustrated in Fig. 4, and are less penetrating. They contribute to diffraction photographs only when they are emitted by very heavy atoms such as tungsten and mercury, unless a special vacuum camera is used to prevent absorption in the glass of the x-ray tube and in the air surrounding it. These longer wavelength lines are of importance in chemical analysis by x-rays, but in crystal analysis they are avoided. Appendix II lists the strongest lines in the  $K$  and  $L$  spectra and their wavelengths. The relative intensities of the lines of a series vary with atomic number, with the exception of  $K\alpha_2$  and  $K\alpha_1$ , which are always very close to the ratio  $K\alpha_2:K\alpha_1 = 1:2$ . With a molybdenum target the intensity ratio is  $K\beta:K\alpha = 1:7.7$  (with the doublets unresolved); with a target of high atomic number the ratios  $K\alpha_2:K\alpha_1:K\beta_3 + K\beta_1:K\beta_2$  are approximately 50:100:35:15. The relative intensities of the more intense lines of the  $L$  series in tungsten are  $\alpha_2:\alpha_1:\beta_1:\beta_2:\beta_3:\beta_4:\gamma_1 = 12:100:52:20:8:5:9$ .\*

The targets most used for diffraction purposes produce  $K\alpha$  rays in the wavelength range from 0.56 to 2.29 Å; these are Ag, Mo, Cu, Ni, Co, Fe, and Cr. Elements of lower atomic number emit long waves that are largely absorbed in the windows of an ordinary x-ray tube, while elements heavier than these give white radiation that is too intense to be useful when only line radiation is wanted.

**Moseley's Law.**—The wavelengths of the lines in the characteristic spectra vary in a regular manner from one element to another, as was first shown by Moseley. He discovered that for corresponding lines of the spectrum, the higher the atomic number of the emitting atom, the

\* Additional measurements are summarized in A. H. Compton and S. K. Allison, "X-rays in Theory and Experiment," pp. 638ff., Van Nostrand, New York, 1935.



shorter the wavelength (the higher the frequency). The quantitative relation is illustrated in Fig. 5 and is known as Moseley's law: The square root of the frequency of corresponding lines from different elements

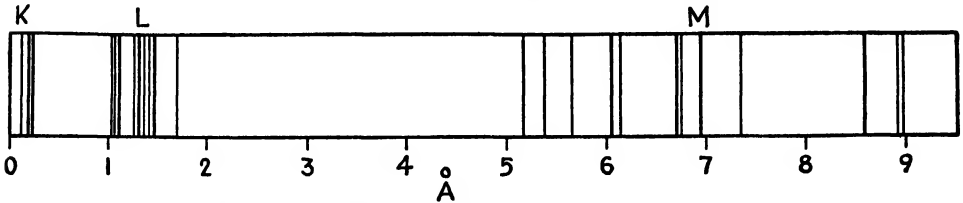


FIG. 4.—Plot of  $K$ -,  $L$ -, and  $M$ -series lines of tungsten with wavelength scale below.

increases linearly with atomic number  $Z$ . This can be expressed by the formula

$$\sqrt{\nu} = K(Z - \sigma)$$

where  $\nu$  is the frequency,  $K$  is a constant for corresponding lines from all elements, and  $\sigma$  is another constant. This law applies not only to lines of the  $K$  series but also to lines of other series with appropriate changes in the constants  $K$  and  $\sigma$ . The regular increase in frequency on the plot of one of the lines, as illustrated in Fig. 5, enables an investigator to detect missing elements of the periodic table and to identify them by means of their emission spectra when they have been discovered. Original surveys of this type disclosed gaps at the atomic numbers 43, 61, 72, 75, 85, and 87, and later research has resulted in the identification of x-ray spectra of masurium (43), illinium (61), hafnium (72), and rhenium (75). X-ray spectra are much simpler than optical spectra and are consequently much more convenient for identification work of this sort.

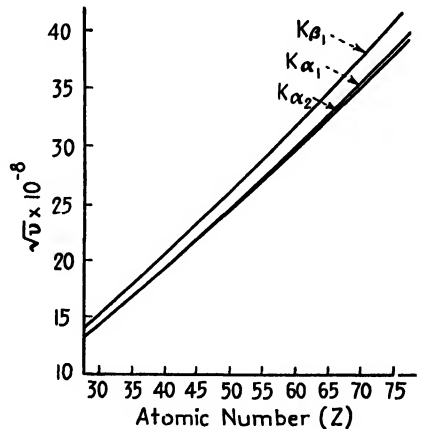


FIG. 5.—Chart showing Moseley's law relating atomic number of x-ray emitter to the square root of the frequency of emission lines.

**Origin of Characteristic Radiation and Absorption.**—The remarkable regularities in x-ray spectra are best understood by considering the states of energy in which an atom can exist, after the manner proposed by Bohr. In the Bohr theory an atom is capable of remaining indefinitely in a state of minimum energy unless an amount of energy is imparted to it that is capable of raising it to one of a set of higher energy states. In the higher energy state (excited state) there is no radiation or loss of energy until the atom reverts suddenly to a lower energy state. At this time, the atom throws out a unit of energy, a quantum, in the

form of radiation, and the frequency of the radiation,  $\nu$ , is related to the loss in energy of the atom,  $E$ , by the equation

$$h\nu = E$$

where  $h$  is Planck's constant. Since the energy states, or "levels," are discrete and sharp, the transitions between them give rise to sharp lines in the spectrum.

It will be recalled that, on the Bohr model of the atom, the charge on the central nucleus of the atom holds the electrons surrounding the nucleus in definite shells,  $K$ ,  $L$ ,  $M$ , etc. When electrons from the filament of an x-ray tube are driven into the target with sufficient energy,

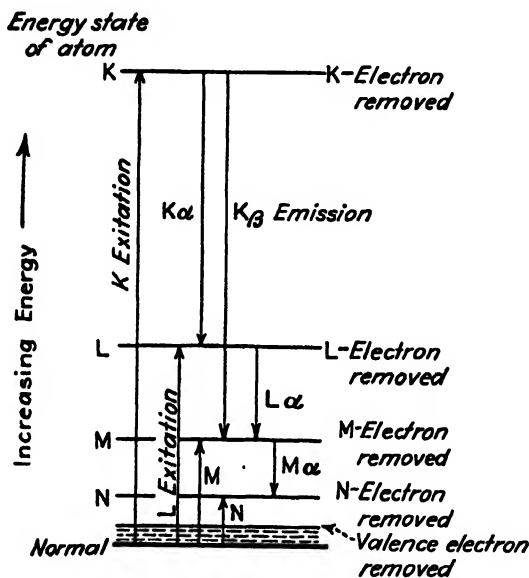


FIG. 6.—Energy-level diagram for an atom (schematic). Excitation and emission processes indicated by arrows.

they eject an electron from one of these shells and thereby raise the atom to an excited state. A characteristic ray is emitted when an electron from an outer shell falls into the shell vacated by the ejected electron. If it is an electron from the  $K$  shell that has been ejected and if the  $K$ -shell vacancy is filled by an electron from the adjacent  $L$  shell, the atom will emit  $K\alpha$  radiation. If the  $K$ -shell vacancy is filled by an  $M$  electron, the  $K\beta$  line will be emitted. From the various atoms of the target the various lines of the  $K$  series will be emitted. Similarly, vacancies in the  $L$  shells of the atoms are filled by transitions from outer shells, and  $L$ -series lines are emitted.

The customary way of showing these relations on a diagram is to make a one-dimensional plot of the energy states of an atom with energy increasing vertically above the normal state (Fig. 6). Reference to this



energy change for  $K$  absorption is greater than the energy change in the emission of any  $K$  series line; *i.e.*, the wavelength of the  $K$  absorption edge is less than any  $K$  emission wavelength. A similar relation holds for the various  $L$  and  $M$  absorption processes and the emission lines resulting from them. The frequency of each emission line is equal to the difference in frequency between two absorption edges. When radiation results from the excitation of an atom by the absorption of x-rays, it is known as **fluorescent radiation**, just as in the analogous case with visible light, and is composed almost exclusively of line radiation.<sup>1</sup> It would serve as an excellent source of rays for diffraction if it were not of such low intensity compared with other sources.

Thorough investigation of the absorption edges and emission lines for the elements has disclosed a complex array of energy levels; while there is only a single  $K$  absorption edge, there are three  $L$  absorption edges, five  $M$  absorption edges, and many  $N$  and  $O$  levels (in the heavier atoms). The complete energy-level diagram for one of the heavy elements is reproduced in Fig. 7 with the transitions marked that give rise to the x-ray emission lines.

**Dependence of Line Intensities on Voltage.**—Emission lines are not excited unless the voltage exceeds the critical value  $V_0$  necessary to remove an electron entirely from an atom of the target. This occurs when

$$eV_0 = h\nu_a$$

where  $\nu_a$  is the frequency of the absorption edge. The intensity  $I$  of a spectral line increases with voltage  $V$ , and the current through the x-ray tube,  $i$ , approximately according to the relation

$$I = ci(V - V_0)^n$$

where  $c$  is a proportionality constant and  $V_0$  is the excitation voltage for the line. The value of  $n$  is slightly less than 2 if a tube is operated with constant-potential direct current and moderate voltages; *i.e.*, the intensity is nearly proportional to the square of the voltage in excess of the critical. The exponent decreases toward unity at higher voltages, and the squared relation should be considered a good approximation only at voltages less than two or three times the excitation potential.<sup>2</sup>

The critical excitation voltage for molybdenum  $K$  radiation is about 20,000 volts, but because of the relations discussed above it is advantageous to operate considerably above this voltage to obtain a line spectrum that is intense in comparison with the continuous spectrum,

<sup>1</sup> A. H. COMPTON, *Proc. Natl. Acad. Sci.*, vol. 14, p. 549, 1928.

<sup>2</sup> G. VON HEVESY, "Chemical Analysis by X-rays and Its Applications," p. 72, McGraw-Hill, New York, 1932.

which is always present. Molybdenum tubes are usually operated between 35 and 60 kv., while tubes with targets similar to copper and chromium are operated near 35 kv. The ratio of line intensities to white radiation at a given voltage becomes more favorable as the atomic number decreases, since the lighter elements are inefficient generators of white radiation.

**Absorption of X-rays.**—An x-ray beam loses intensity in traversing matter both by “true” absorption, which is a transformation from x-rays into kinetic energy of ejected electrons and atoms, and by “scattering,” a transfer of radiant energy from the primary beam to scattered beams originating in the atoms of the absorbing matter. An understanding of these processes is important both in radiography and in x-ray diffraction.

Consider a monochromatic beam of x-rays penetrating a sheet of material of thickness  $x$ . If a beam of energy  $I$  traverses a thin layer of thickness  $dx$  and diminishes in energy by the fraction  $dI/I$ , then

$$\frac{dI}{I} = -\mu dx$$

where  $\mu$  is a constant, the **linear absorption coefficient**, which depends on the wavelength of the rays and the nature of the absorber. Integration of this equation gives the absorption equation

$$I = I_0 e^{-\mu x}.$$

The energy, or intensity, decreases from the initial value  $I_0$  exponentially, the more rapidly the greater the linear absorption coefficient. It is convenient to put this equation in terms of the mass traversed rather than the thickness. This can be done by replacing the term  $x$  by  $\rho x$ , where  $\rho$  is the density of the absorbing material. The quantity  $\mu$  must then be replaced by  $\mu/\rho$ , which is the **mass absorption coefficient**, and the equation becomes

$$I = I_0 e^{-\frac{\mu}{\rho} \rho x}.$$

Most tables list  $\mu/\rho$  rather than  $\mu$  because  $\mu/\rho$  is independent of the physical state (solid, liquid, or gas), whereas  $\mu$  is not. The mass absorption coefficient of an alloy can readily be calculated from the weight percentages  $w_1, w_2, \dots$  and the values  $(\mu/\rho)_1, (\mu/\rho)_2, \dots$  for the individual elements in the alloy by the formula

$$\frac{\mu}{\rho} = \frac{w_1}{100} \left( \frac{\mu}{\rho} \right)_1 + \frac{w_2}{100} \left( \frac{\mu}{\rho} \right)_2 + \dots$$

In the absorption formula this over-all absorption coefficient  $\mu/\rho$  is multiplied by the density of the alloy and the thickness penetrated.

These absorption equations are fundamental to the practice of **radiography**. When a beam of x-rays or gamma-rays from radioactive material passes through an object, it emerges with an intensity that is dependent upon the thickness and absorption coefficient of the material it penetrates. A beam that encounters a cavity in a metal casting, forging, or weld emerges with greater intensity than a beam that encounters only sound metal. An image of the cavity is registered on a photographic film placed behind the object. To radiograph thick metal objects it is necessary to make the absorption coefficient small, while to increase the sensitivity to small defects it is necessary to make the absorption coefficient large. Hence the radiography of heavy steel objects is done with high-voltage x-ray tubes or with radium, sources which yield short-wavelength, highly penetrating radiation; the radiography of aluminum, magnesium, and all small or thin objects is done with low-voltage x-rays of longer wavelength and higher absorption coefficient. The nature of a defect is recognized from the appearance of its image on the radiograph. An experienced radiographer has no difficulty in recognizing by the appearance of the film such defects as blowholes, sand and oxide inclusions, shrinkage cavities (pipes), interdendritic shrinkage (capillary piping), hot tears, cracks, unfused chills and chaplets, cold shuts, and lack of fusion in a weld.

Since the loss of intensity is due to the combined effects of true absorption and scattering,  $\mu/\rho$  is really made up of two separable terms, the **true absorption coefficient**,  $\tau/\rho$ , and the **scattering coefficient**,  $\sigma/\rho$ :

$$\frac{\mu}{\rho} = \frac{\tau}{\rho} + \frac{\sigma}{\rho}.$$

The second term is the less important of the two and contributes a relatively small amount to the total absorption for elements of greater atomic number than iron (26). It does not vary greatly with changes in wavelength or atomic number, as will be seen from selected values listed in Table V.

TABLE V.—MASS SCATTERING COEFFICIENTS  $\sigma/\rho$ \*

Wavelength, Å	Scatterer			
	Al	Cu	Ag	Pb
0.12	0.14	0.18	0.35	0.67
0.71	0.20	0.29	0.47	0.82

\* Additional values will be found in Landolt-Börnstein, "Physikalisch-chemische Tabellen," Springer, Berlin, 1923, 1935.

The true absorption coefficient varies markedly with wavelength and atomic number, for it depends on the efficiency of the rays in ejecting photoelectrons. Between absorption edges,  $\tau/\rho$  varies with the cube of the wavelength and the cube of the atomic number:

$$\frac{\tau}{\rho} = cZ^3\lambda^3.$$

At each absorption edge there is an abrupt change in the constant  $c$ . This results from the fact that an absorption edge marks the place on the frequency scale where the radiation is just able to eject an electron from one of the electron shells. For example, radiation of longer wavelength than the  $K$  edge cannot eject  $K$  electrons, while waves shorter than the  $K$  edge are able to do so. Owing to the fact that true absorption predominates over scattering in all except the light elements and the very short x-ray wavelengths, the total absorption varies approximately according to the relation

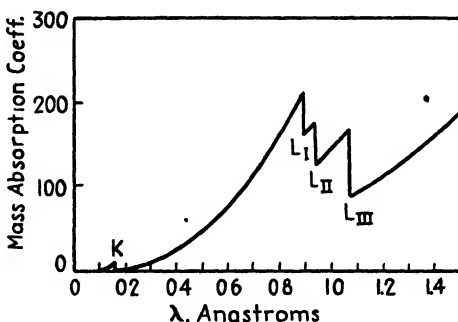


FIG. 8.—Variation of absorption in platinum with wavelength, showing  $K$  and  $L$  absorption edges.

$$\frac{\mu}{\rho} = cZ^3\lambda^3.$$

Here again the constant changes at each absorption edge. In the curve of  $\mu/\rho$  against wavelength reproduced in Fig. 8 the absorption edges are very prominent; in most elements  $\mu/\rho$  differs by a factor of about 5 on the two sides of the  $K$  absorption edge. Appendix III lists values of  $\mu/\rho$  for a number of wavelengths frequently encountered.

It is often convenient to know for common materials the thickness that will reduce the intensity of a beam to a certain fraction of its initial value, say one-half. The "half-value thickness" that will reduce  $I$  to  $\frac{1}{2}I_0$  can be computed from the absorption equation by taking natural logarithms; this yields the equation

$$x_{\frac{1}{2}} = \frac{0.69}{\mu}$$

where  $x_{\frac{1}{2}}$  is the half-value thickness in centimeters. Some values are given in Table VI.

TABLE VI.—THICKNESS OF ABSORBER IN CENTIMETERS TO REDUCE INTENSITY TO HALF VALUE

Wavelength, Å	Absorber				
	Air at 0°C., 760 mm.	Cellophane	Al	Cu	Pb
0.1	...	4.3	1.6	0.21	0.016
0.7	410	0.4	0.050	0.0016	0.00044
1.5	62	0.11	0.0056	0.0016	
2.0	26	0.049	0.0025	0.00071	

**Filtering.**—An absorbing layer may be used to render a heterogeneous beam more monochromatic. Even with white radiation this tendency can be observed, because the longer wavelength components, which are “softer,” diminish more rapidly than the “harder” short waves, and thus the energy is concentrated in the harder components. Figure 9

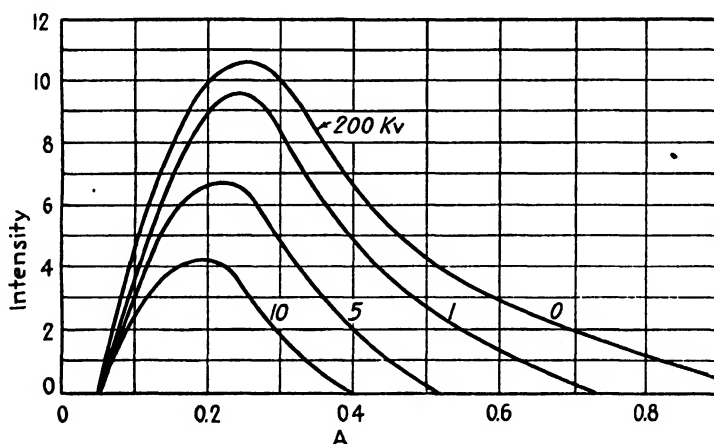


FIG. 9.—Spectra showing effect of filtering x-rays from a tungsten target through 1, 5, and 10 mm. of aluminum.

illustrates the filtering of a typical continuous spectrum by aluminum sheets 1, 5, and 10 mm. thick.<sup>1</sup> Filtering is important in medical diagnosis and therapy, for it removes the soft components, which would be completely absorbed in the outer layers of the skin and would cause severe burns.

Filtering is frequently used in diffraction work to remove unwanted components of the characteristic spectrum together with some of the white radiation. For this purpose, advantage is taken of the absorption discontinuity at the *K* absorption edge; the wavelengths are listed in Appendix II. An element is chosen for the filter which has its *K* edge

<sup>1</sup> GEORGE L. CLARK, “Applied X-rays,” p. 145, McGraw-Hill, New York, 1940.



just to the short-wave side of the  $K\alpha$  emission line of the target material (see Fig. 10). A sheet of this material is then relatively transparent to the  $K\alpha$  line and relatively opaque to the  $K\beta$  and  $K\gamma$  lines and to the white radiation in their vicinity. A filter containing zirconium is suitable for a molybdenum target; a screen of  $ZrSiO_4$  0.35 mm. in thickness will reduce the  $K\beta$  line in the ratio 39 to 2 while reducing the  $K\alpha$  only from 62 to 21.

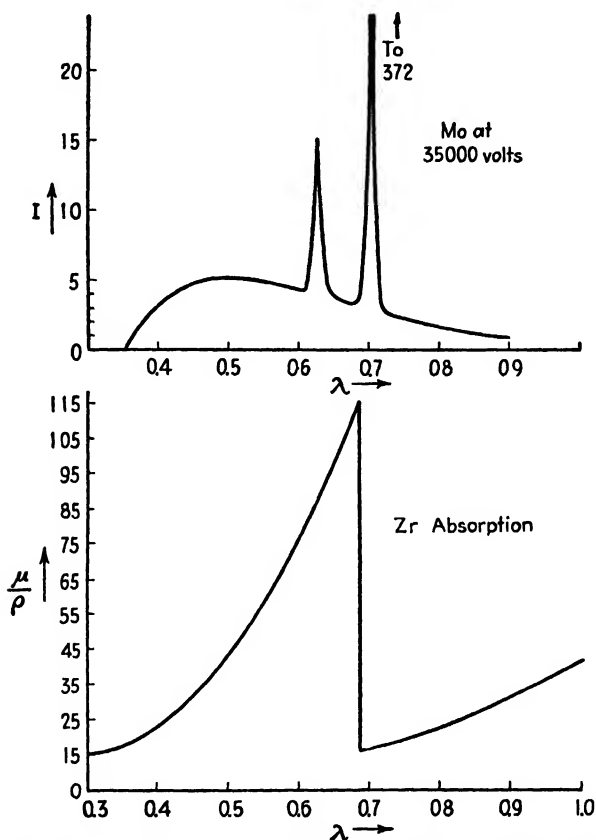


FIG. 10.—Emission and absorption spectra for molybdenum target and zirconium filter.

A sheet of nickel 0.001 cm. thick will absorb 40 percent of Cu  $K\alpha$  radiation and 94 percent of Cu  $K\beta$ ; a sheet 0.002 cm. thick will absorb 50 percent of Cu  $K\alpha$  and 99 percent of Cu  $K\beta$ .<sup>1</sup> Manganese is the proper filter for iron radiation and can be deposited electrolytically on aluminum foil for this purpose.<sup>2</sup> Effective filtering will result if a filter is adjusted so that the exposure time is increased to about  $1\frac{1}{2}$  the normal.

For certain research problems the **differential filter** originated by Ross has advantages. Two filters are prepared using adjacent elements in the

<sup>1</sup> F. HALLA and H. MARK, "Röntgenographische Untersuchung von Kristallen," p. 3, Barth, Leipzig, 1937.

<sup>2</sup> W. A. WOOD, *Proc. Phys. Soc. (London)*, vol. 43, p. 275, 1931.

periodic series. Their thicknesses are adjusted until they transmit equal intensities of all wavelengths except those between their  $K$  absorption limits. Intensity measurements are made with one filter in the beam, then with the other, and the two intensity readings are subtracted. The intensity difference is due entirely to radiation between the  $K$  absorption limits.<sup>1</sup> If this wavelength band is made to include the  $K\alpha$  emission line from the target, a strong monochromatic beam is obtained;<sup>2</sup> and if careful balancing is carried out by methods explained by P. Kirkpatrick,<sup>3</sup> undesired components can be made to cancel with remarkable accuracy.

**The Scattered Radiation.**—Two scattering processes contribute to the term  $\sigma/\rho$  of the absorption formula. **Coherent scattering** results from the back-and-forth acceleration of an electron by the primary radiation and is identical in wavelength with the original radiation. When this coherent radiation from the electrons of one atom is superimposed on the rays from other atoms arranged on a space lattice, reinforcement occurs and diffracted beams are formed. A second type of scattering also occurs which is not coherent and which does not take part in diffraction; this is the **modified radiation**.

A. H. Compton showed that the modified radiation may be understood as being the result of an encounter of a quantum with a loosely bound or a free electron, the electron recoiling under the impact and the quantum being deflected with a partial loss of energy (the Compton effect). The laws of conservation of energy and of momentum govern the encounter, and it is therefore possible to derive a formula relating the angle of deflection of the quantum to the loss of energy in the encounter and thus to the increase in wavelength of the quantum. The equation giving the increase of wavelength in angstroms is

$$\begin{aligned}\Delta\lambda &= \frac{h}{mc} (1 - \cos \phi) \\ &= 0.024(1 - \cos \phi)\end{aligned}$$

where  $h$  is Planck's constant,  $m$  is the mass of the electron,  $c$  is the velocity of light, and  $\phi$  is the angle between the scattered ray and the original beam. The modified radiation forms a decreasing proportion of the total scattered radiation as the wavelength of the primary beam is increased and as the angle between primary beam and the direction of measurement of the scattered ray is decreased, other conditions remaining the same. In the heavier elements more of the electrons are tightly bound and contribute to the coherent rather than the modified scattering.

<sup>1</sup> P. A. ROSS, *Phys. Rev.*, vol. 28, p. 425, 1926; *J. Optical Soc. Am.*, vol. 16, p. 433, 1928.

<sup>2</sup> C. S. BARRETT, *Proc. Natl. Acad. Sci.*, vol. 14, p. 20, 1928.

<sup>3</sup> P. KIRKPATRICK, *Rev. Sci. Instruments*, vol. 10, p. 186, 1939.

**X-ray Tubes.**—A great variety of x-ray tubes is used for diffraction purposes and still others for radiography, but all are of two general types: (1) **gas tubes** ("ion tubes"), in which electrons are supplied by an electrical discharge through low-pressure gas within the tube; and (2) **electron tubes** ("Coolidge tubes"), in which a hot filament maintained under high vacuum supplies the electrons. Both tubes have been supplied in two types: a demountable tube, which can be taken apart for cleaning and for changing targets; and a sealed-off tube, which is evacuated and sealed off during manufacture.

1. **GAS TUBES.**—Gas tubes were originally sealed off and equipped with a device for controlling the gas pressure, but they were exceedingly temperamental. Modern gas tubes are invariably operated with vacuum pumps attached and are usually maintained at the proper gas pressure by balancing the rate of pumping against the rate of influx of air through a controlled leak. The pressure must be kept within a certain range near 0.01 mm. of mercury in order to permit operation; this range is best judged by the operating characteristics of the tube as recorded on the electrical meters, rather than by direct measurement. The necessity for strict pressure control in a gas tube is a matter of great annoyance to anyone who uses a tube only occasionally, for a gas tube is particularly unstable during the outgassing period, but when a tube is kept well outgassed by frequent operation it is fairly stable and reliable. There are two advantages of gas tubes over other types: they are the most inexpensive tubes that can be built, and they produce the purest spectra, since the target is not contaminated with materials evaporated from a hot filament.

A number of suitable designs<sup>1</sup> have appeared in the scientific literature, and several are available on the market. The essential features appear in the accompanying figure (Fig. 11). The whole anticathode assembly should be water-cooled, and the cathode should also be cooled by running water or by a stream of cool air. The target should be readily removable, and it is desirable to mount several different metals on different sides of a single water-cooled target in such a way that the tube may be set for different radiations by merely turning the target. The glass or porcelain insulator separating the cathode from the anticathode must be removed for cleaning at intervals, and the tip of the cathode (which is an aluminum insert) must be reconditioned on a lathe

<sup>1</sup> R. W. G. WYKOFF and J. B. LAGSDIN, *Radiology*, vol. 15, p. 42, 1930; *Rev. Sci. Instruments*, vol. 7, p. 35, 1936. C. J. KSANDA, *Rev. Sci. Instruments*, vol. 3, p. 531, 1932. G. HÄGG, *Rev. Sci. Instruments*, vol. 5, p. 117, 1934. I. FANKUCHEN, *Rev. Sci. Instruments*, vol. 4, p. 593, 1933. Bulletins of American Instrument Co., Silver Spring, Md. Bulletins of Baird Associates, Cambridge, Mass. Bulletins of A. Hilger, London.

when it becomes too pitted for steady operation. To obtain a sharp focal spot, the cathode is hollowed out slightly and adjusted to a proper distance from the target; a radius of curvature of 2 cm., a cathode distance of 3.5 cm., and a gas pressure of  $15 \times 10^{-3}$  mm. of mercury have been recommended by Clay.<sup>1</sup> A suitable groove in the cathode can be used to produce a line focus of electrons on the target.<sup>2</sup> Two to four windows are generally provided for the exit of radiation and are covered with aluminum foil 0.001 in. thick or less. In general, it is better to avoid innovations and to build or purchase an exact replica of some tube that has given satisfactory service, thereby eliminating at least some of the many sources of trouble that are characteristic of this device.

A mercury diffusion pump is not recommended for gas tubes since it is necessary to use a liquid-air trap and considerable care to prevent contamination of the target with mercury. An oil diffusion pump is

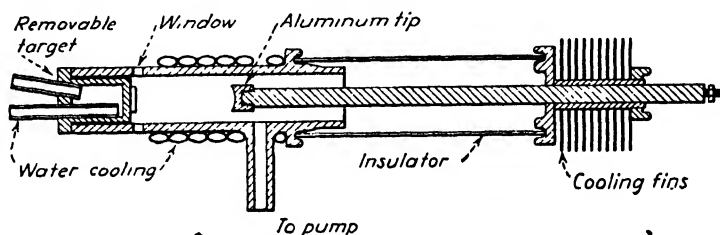


FIG. 11.—A gas tube with air-cooled cathode.

frequently used and introduces no spurious lines into the spectrum, but the simplest arrangement is to operate the tube directly from a good rotary oil pump, since a pump of intermediate size is able to reach and maintain a suitable pressure without the aid of a diffusion pump. Numerous devices have been designed to stabilize operation by controlling the pumping speed, but these are likely to add to the possible sources of trouble. The simplest method of maintaining the right pressure is (1) to provide a large reservoir that is pumped down occasionally to the operating pressure or (2) to balance a constant rate of pumping with a constant rate of leak. The second method can be made to work reliably over long periods with nothing more elaborate than a rotary pump operating against an air leak consisting of a length of rubber hose squeezed between the jaws of an adjustable clamp.

**2. DEMOUNTABLE ELECTRON TUBES.**—A gas tube can be converted into an electron tube by replacing the cold cathode with a hot filament of tungsten suitably mounted in a focusing cup so as to direct a stream of electrons at a point or a line on the target. Since high vacuum must

<sup>1</sup> R. E. CLAY, *Proc. Phys. Soc. (London)*, vol. 40, p. 221, 1928.

<sup>2</sup> R. B. COREY, J. B. LAGSDIN, and R. W. G. WYKOFF, *Rev. Sci. Instruments*, vol. 7, p. 193, 1936.

be provided to prolong filament life and to prevent rapid contamination of the target by the filament, a diffusion pump or its equivalent is necessary. A demountable electron tube offers the advantages of better control of x-ray intensity and of focal-spot size and shape and may be operated at larger currents, usually at 20, 30, or 40 ma., the limit being set by melting or excessive pitting of the target. On the other hand, the equipment requirements are greater than for the gas tube, and there is danger of contamination of the spectrum by tungsten *L* lines (and mercury *L* lines if a mercury pump is used). For the life of a filament to exceed a week or so it is necessary to have internal parts well out-gassed and free from contaminating greases and vapors and to eliminate leaks from the system. In addition to tubes of conventional design,<sup>1</sup>

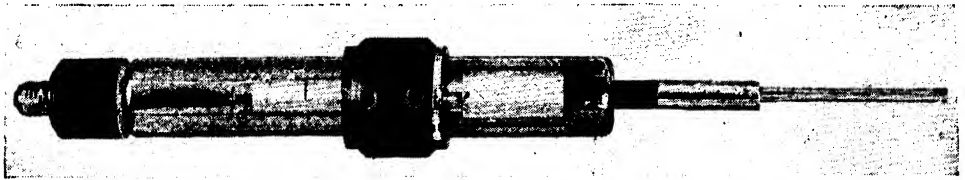


FIG. 12.—Sealed-off x-ray tube manufactured by General Electric X-ray Corporation.

there are now in operation tubes containing rotating targets<sup>2</sup> that are capable of operation at upwards of five or ten times the usual input.

3. SEALED-OFF TUBES.—X-ray tubes of the Coolidge type are manufactured in quantities for medical purposes, industrial radiography, and diffraction. The diffraction tubes illustrated in Figs. 12 and 13 are available in a number of target materials. They are equipped with beryllium windows approximately 0.010 in. thick, which are much more transparent to the rays than the special Lindemann glass previously used.<sup>3</sup> The line-focus principle is used to spread out the focal spot without losing the effectiveness of a point source of radiation.

Some diffraction tubes have been manufactured with ray-proof and shockproof housings integral with the body of the tube. Tubes of the type shown in Figs. 12 and 13 can be mounted in a simple iron pipe

<sup>1</sup> H. OTT, *Physik. Z.*, vol. 27, p. 598, 1926. J. EGGERT and E. SCHIEBOLD, "Ergebnisse der technischen Röntgenkunde," vol. 1, Akademische Verlagsgesellschaft m.b.H., Leipzig, 1930. V. E. PULLIN and C. CROXSON, *J. Sci. Instruments*, vol. 8, p. 282, 1931. W. M. ROBERTS, *Rev. Sci. Instruments*, vol. 1, p. 473, 1930. E. A. OWEN and G. D. PRESTON, *J. Sci. Instruments*, vol. 4, p. 1, 1926. L. G. PARRATT, *Phys. Rev.*, vol. 41, p. 553, 1932.

<sup>2</sup> A. MÜLLER, *Brit. J. Radio.*, vol. 3, p. 127, 1930; *Proc. Roy. Soc. (London)*, vol. A117, p. 30, 1927; vol. A125, p. 507, 1929; vol. A132, p. 646, 1931. A. MÜLLER and R. CLAY, *J. Inst. Elec. Eng. (London)*, vol. 84, p. 261, 1939. J. W. M. DU MOND, B. B. WATSON, and B. HICKS, *Rev. Sci. Instruments*, vol. 6, p. 183, 1935. A. BOUWERS, *Physica*, vol. 10, p. 125, 1930. H. STINZING, *Physik. Z.*, vol. 27, p. 844, 1926.

<sup>3</sup> R. R. MACHLETT, *J. Applied Phys.*, vol. 13, p. 398, 1942.

(Fig. 14) which is provided with four ports and centered on a table for supporting diffraction cameras. The housing is grounded, and the high-

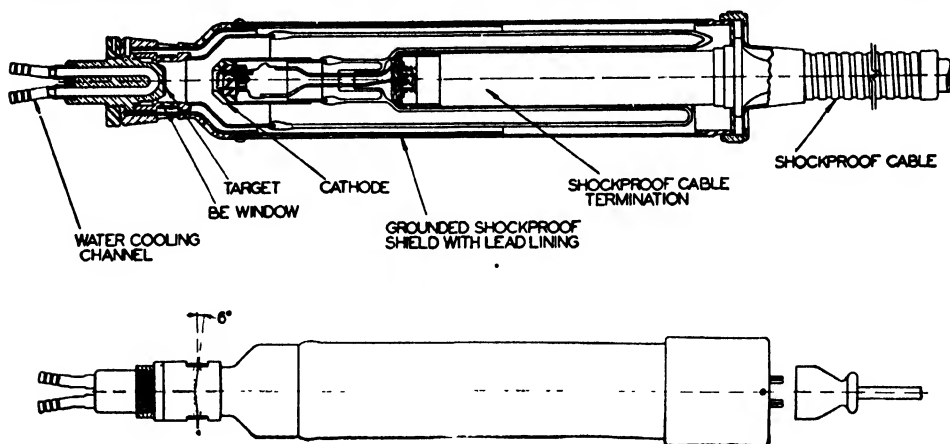


FIG. 13.—Sketch of sealed-off, shielded tube manufactured by Machlett Laboratories.

voltage wires leading to the tube are fully insulated from the operator.

It is advisable to install a water-pressure switch or a thermostatic device to turn off the tube current if the cooling water is interrupted. While rotating target types are available as sealed-off tubes, these are not designed (at the present time) for continuous operation and are of little value for diffraction.

The convenience of having x-rays immediately available at the snap of a switch makes the sealed-off type a great favorite in laboratories where diffraction work is intermittent or laboratory technicians are inexperienced. Installation and maintenance costs are higher, of course, and purity of spectrum must be watched, but the results with sealed-off tubes are usually quite satisfying. For radiography and medical work they are indispensable and are under rapid development in the million-volt range.

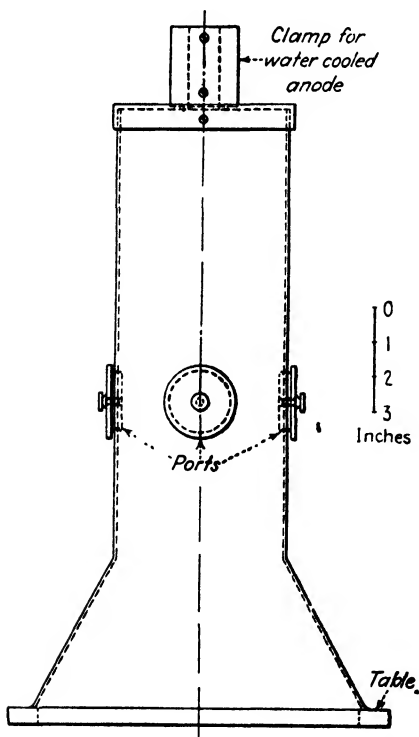


FIG. 14.—A housing for sealed-off tubes. High-voltage transformers are beneath table.

**Electrical Equipment for Diffraction Tubes.**—The elaborate high-voltage installations with rectifying and filtering circuits that are necessary for radiography are unnecessary for diffraction work unless precise

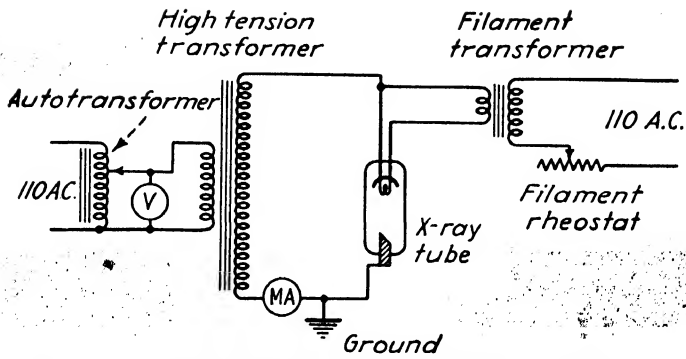


FIG. 15.—A wiring diagram for self-rectifying x-ray tube.

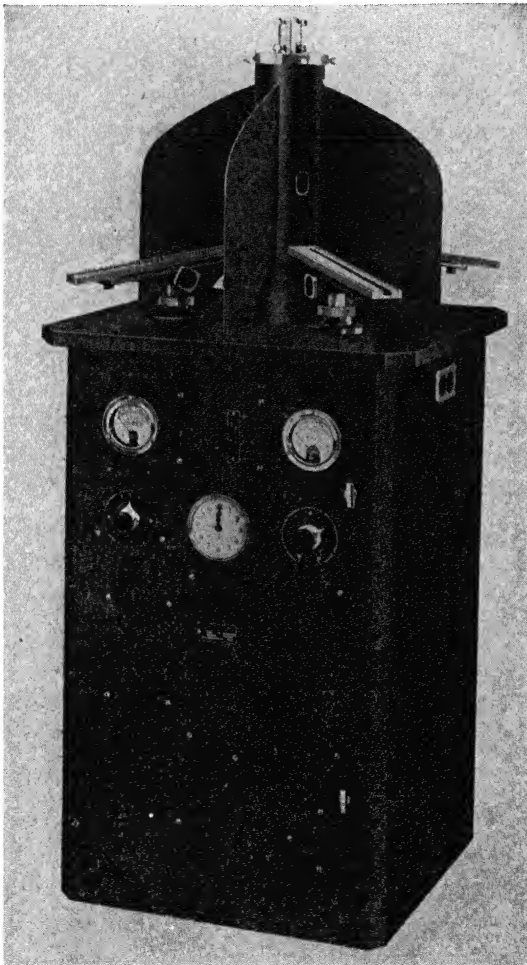


FIG. 16.—Diffraction unit manufactured by General Electric X-ray Corporation.

intensity measurements are required. The usual research problems need only the minimum equipment: a transformer giving 30 to 50 kv., a rheostat or an autotransformer to regulate the voltage, and a voltmeter, milliammeter, and filament transformer with control (Fig. 15). Both gas and electron tubes can be operated as self-rectifying units, although the use of a rectifier tube contributes to the stability and performance of both types. An overload relay and a telltale lamp to indicate when the tube is running are desirable additions to the circuit. The essentials can be assembled at low cost from outmoded medical or dental equipment, or a complete assembly can be purchased (see, for example, Fig. 16).

If electron-diffraction studies are to be conducted in the same laboratory or if ionization measurements are to be made on diffracted x-rays, it is well to provide a source of controlled-voltage alternating current (voltage regulators or synchronous motor-driven motor generators are used), a high-voltage circuit containing rectifier tubes for half- or full-wave rectification, and high-tension condensers to provide constant-voltage direct current. Data on the various wiring circuits and their characteristics may be obtained from the manufacturers of x-ray equipment and are available in numerous publications.<sup>1</sup> Much care should be exercised in providing safeguards against the high voltages used. Complete enclosure of high-voltage circuits is best.

**X-ray Protection.**—Soft radiation of the type used for diffraction work is readily absorbed in the tissues of the body and is consequently a source of grave danger to the careless operator. A brief exposure of the hands to the direct radiation can cause an x-ray burn that is extremely painful and that will require many weeks to heal, if it can be healed at all, and yet the operator may be conscious of no sensation at the time he is exposed or for several days thereafter. Just as severe burns have been received from *scattered rays* by operators who avoided the direct beam but put their hands or faces in the way of the radiation scattered by some piece of apparatus they were demonstrating or adjusting. In these days when dangers of this sort are fully understood there need be no further tragedies of the sort that were common in the pioneer days of x-ray history if only operators will exercise constant care and take pains to develop safe habits in manipulating their apparatus.

Diffraction tubes should be mounted so that only a narrow pencil of rays emerges, and this only when a camera is in place before the opening.

<sup>1</sup> See, for example: GEORGE L. CLARK, "Applied X-rays," McGraw-Hill, New York, 1940. "Symposium on Radiography and X-ray Diffraction," A.S.T.M., Philadelphia, 1936. R. GLOCKER, "Materialprüfung mit Röntgenstrahlen," Springer, Berlin, 1936. H. M. TERRILL and C. T. ULREY, "X-ray Technology," pp. 76-98, Van Nostrand, New York, 1930. A. ST. JOHN and H. R. ISENBERGER, "Industrial Radiography," pp. 58-69, Wiley, New York, 1934. L. G. SANSFIELD, "Electrical Engineering in Radiology," Instruments Publishing Co., Pittsburgh, 1936.



A red light to signify that the tube is operating will eliminate much of the hazard from carelessness. There is also a danger from weaker exposures over larger areas of the body, and these, like the local burns, are cumulative over several weeks. A general dosage may be accumulated that will cause a serious lowering of the white blood count and other destructive effects. To guard against this danger the protective shields around the tube must be designed to absorb properly the unused radiation. A test for this is to place a piece of x-ray film in a lighttight envelope near the tube during an operating time of a few days and to look for fog on the film after development. A radiologist often carries such a film in his pocket during his work and has periodic blood counts made; this is hardly necessary with a properly designed diffraction outfit.

#### Photographic Efficiency of X-rays.

The intensity of an x-ray beam can be measured by an ionization chamber connected to an electrometer or to an amplifier and microammeter; alternatively, it can be measured by a Geiger counter or by photographic films. The last is the most convenient. With care, all but the most difficult diffraction problems can be solved with photographically measured intensities, but an understanding of the laws of film darkening by x-rays is required for this work.

The density  $D$  of a photographic emulsion after exposure and development is measured by the intensity of the light incident upon it and transmitted through it, and is defined by the relation

$$D = \log_{10} \frac{\text{incident light}}{\text{transmitted light}}.$$

The **characteristic curve** for a photographic film is the curve of  $D$  plotted against the intensity of the rays causing the exposure, or more properly against the product of the intensity  $I$  and the time of exposure  $t$ , since it is the product  $I \cdot t$  that actually measures the amount of **exposure**. It is important to keep in mind the fact that the characteristic curve is different for every type of emulsion and that it varies even with different samples of film of a given type and with any variation in developing technique. Therefore, intensity measurements from films must be preceded by a calibration of each *individual* film before densities can be interpreted in terms of x-ray intensities. Typical curves for x-ray films

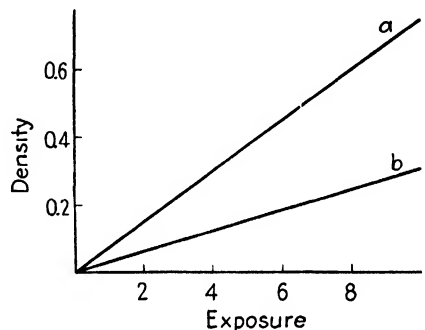


FIG. 17.—Characteristics of a screenless-type x-ray film (a), and of a standard x-ray film (b), with filtered Mo radiation.

and filtered molybdenum radiation are plotted in Fig. 17.<sup>1</sup> Densities on this plot are densities corrected for the background fog, *i.e.*,

$$D_{\text{corr}} = \log_{10} \frac{\text{light through unexposed spot}}{\text{light through exposed spot}}$$

Densities usually increase linearly with exposure up to a value of about 0.7. When plotted on a semilogarithmic scale, the characteristic curves for x-ray films are usually of the type illustrated in Fig. 18.<sup>2</sup> They show a certain minimum density from "fog" in the emulsion, an insensitive region at very low densities, a working range in which density increases

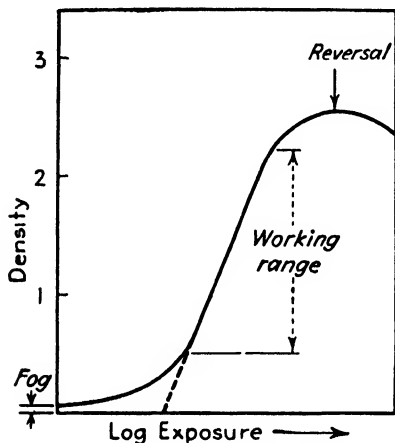


FIG. 18.—Typical characteristic curve for an x-ray film.

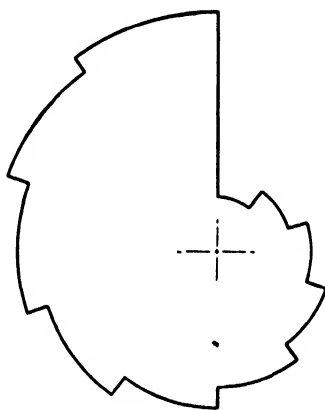


FIG. 19.—Rotating metal disk for calibrating films.

with the logarithm of the exposure, sometimes in a linear fashion, and a region of overexposure where "reversal" takes place, additional exposure reducing the density. A density of 2.0 appears very black to the eye, but densities as high as 3 are still useful in double-coated x-ray films. The slope of the characteristic curve in the working range defines the **contrast**, which increases rapidly with increasing time of development. If an intensifying screen of zinc sulphide or calcium tungstate is placed in contact with the film during the exposure to speed the action of the rays, the characteristic curve for the combination will be entirely different from that for the film alone.

In practice, it is not always necessary to plot the curve, for the densities to be measured can be compared directly with a graded series of densities representing known exposures. For example, a series of spots

<sup>1</sup> C. GAMERTSFELDER and N. S. GINGRICH, *Rev. Sci. Instruments*, vol. 9, p. 154, 1938.

<sup>2</sup> Symposium on Radiography and X-ray Diffraction, A.S.T.M., Philadelphia, Pa., 1936. R. B. WILSEY and H. A. PRITCHARD, *J. Optical Soc. Am.*, vol. 11, p. 661, 1926; *Rev. Sci. Instruments*, vol. 12, p. 661, 1926.

along one edge of the film can be exposed to weak radiation of constant intensity for periods such as 2, 4, 8, 16, 32 sec., and these can be compared by eye with the spots of unknown density on the film. A rotating disk with sectors cut out as illustrated in Fig. 19 can be placed in front of the film to provide the graded exposures without accurate timing. Calibration of the film in this way is possible because film darkening by x-rays obeys the **reciprocity law** that exposure is proportional to intensity times time, regardless of the length of exposure and whether it is continuous or interrupted. The eye is capable of judging equal densities rather well but cannot judge density ratios; when ratios are required, the film must be measured on a densitometer or a microphotometer or compared with a graded series of exposures.

A series of spots in a diffraction pattern can be graded in intensity with sufficient precision for many purposes by the expedient of using two superimposed films in the same film holder. The rays will be absorbed a definite amount in the first film and will thus blacken the second film to a density that is a definite fraction of the density of the first film. The ratio of densities on the two films can be determined for a particular wavelength of radiation and can be used as a basis for judging approximate intensities of the entire series of spots. Intensities can also be determined by counting the number of silver grains in a spot or in a given area of the emulsion. This method is useful only for low densities and in emulsions where the grains do not clump together; to attain an accuracy of 1 percent for a single reading may require two or three hours of grain counting.<sup>1</sup>

To increase the speed of blackening, most x-ray films are made with an emulsion on each side of the cellulose acetate base. This must be kept in mind when using a diffraction camera in which the rays strike the film obliquely, for the records on the two sides of the film will not exactly coincide, and it may be necessary to resort to the slower single-emulsion films. All high-speed x-ray films have large-grained emulsions, and so for applications requiring maximum detail in the image a slower, finer grained x-ray film must be substituted.

When maximum detail and precision are not needed, it is possible to decrease exposure time by the use of intensifying screens placed in intimate contact with the film. For short-wavelength radiation a calcium tungstate screen will reduce exposure time for a standard x-ray film to  $\frac{1}{10}$  normal, but the efficiency rapidly diminishes, and such a screen is no longer useful above 0.6 or 0.7 Å; the newer zinc sulphide screens<sup>2</sup> con-

<sup>1</sup> G. VON HEVESY, "Chemical Analysis by X-rays and Its Applications," McGraw-Hill, New York, 1932.

<sup>2</sup> L. LEVY and D. W. WEST, *Brit. J. Radio.*, vol. 8, p. 191, 1934. Symposium on Radiography and X-ray Diffraction, p. 206, A.S.T.M., Philadelphia, Pa., 1936.

tinue to be effective up to a wavelength of  $1.5\text{\AA}$  or more. For Mo  $K\alpha$  radiation ( $0.71\text{\AA}$ ) a zinc sulphide screen sold under the name Fluorazure increases the speed of standard film by a factor of 5. However, the advantages of intensifying screens have lately been much lessened by the introduction of new kinds of films, which do not require screens and yet compare very favorably with the fastest film-screen combinations. These, sold under the trade names of No-Screen, Industrial No-Screen, Non-Screen, and the like, contain thick emulsions of remarkable speed.

## CHAPTER IV

### DIFFRACTION OF X-RAYS BY CRYSTALS

This chapter presents a brief survey of the fundamental principles and the several methods by which x-rays are employed to investigate the inner structure of crystals. Simple sketches are given for each of the common types of cameras and films. Subsequent chapters are devoted to more detailed treatments of the individual methods and the techniques used in various applications.

A beam of x-rays is diffracted from a crystal when certain geometrical conditions are satisfied, which may be stated either by Bragg's law or alternatively by Laue's equations. With the aid of these relationships the positions of the diffracted beams forming the diffraction pattern can be analyzed to give the size, shape, and orientation of the unit cell. To determine the manner in which the atoms are arranged within the unit cell it is necessary to analyze the intensities of the reflected beams. This is done using the structure-factor equation, which relates the position of each atom to the intensities of all reflections. In an actual determination of crystal structure by x-rays it is often necessary to apply certain correction factors to the intensities as read from the film in order to reduce them to true intensities. The corrections are presented in Appendix V.

**Scattering of X-rays by Atoms.**—When a beam of x-rays passes over an atom, the electric field of the beam acts upon each electron of the atom, accelerating each with a vibratory motion. Any electric charge undergoing an oscillation of this sort becomes the source of a new set of electromagnetic waves, just as the alternating electric current in the antenna of a radio transmitter sends out electromagnetic waves of radio frequency. The waves radiating out from the vibrating electrons have the same frequency and wavelength as the incident beam that is responsible for the vibration. (We are concerned in this chapter only with the coherent scattered radiation, not with the modified radiation that is altered in wavelength.) In effect, each electron subtracts a small amount of energy from the impinging beam and broadcasts it in all directions, "scatters" it. The various scattered waves from the individual electrons of an atom combine and may be treated as a single set of radiating waves which, for most purposes, can be considered as originating from a point. Actually, the difference in the nature of the scattering by a num-

ber of electrons grouped at a point and the same number distributed in a cloud around the nucleus of an atom is sufficiently marked so that an analysis of the scattering gives the dimensions of the cloud and the distribution of the electrons within it. An introduction to this type of analysis of the structure of individual atoms is given in Appendix V.

The superposition of waves scattered by individual atoms results in diffraction. The waves that radiate from the atoms of a crystal combine in an additive way in certain directions from the crystal but annul one another in other directions, the intensity in any direction depending on whether or not the crests of the waves from each of the atoms superpose, *i.e.*, whether or not the individual scattered waves are in phase. The relation of the regularly repeating pattern of atoms in a crystal to the directions of the reinforced diffracted beams is given in the sections immediately following.

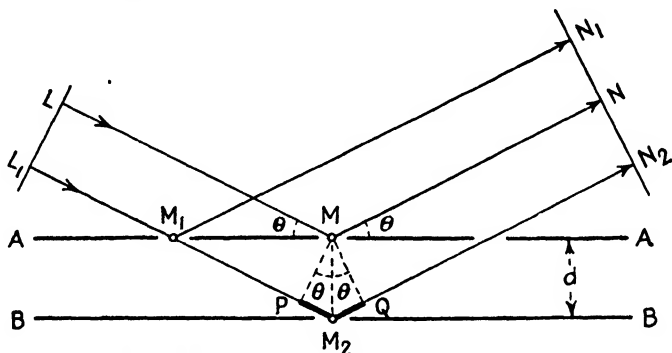


FIG. 1.—Illustrating Bragg's law of reflection from planes of atoms in a crystal.

**Bragg's Law.**—Consider a set of parallel planes of atoms in a crystal, two of which are represented by the lines  $AA$  and  $BB$  in Fig. 1, and suppose a beam of monochromatic x-rays is directed at the planes in the direction  $LM$ , which makes an angle  $\theta$  with the planes. The line  $LL_1$  is drawn to represent one of the crests in the approaching waves and is perpendicular to the direction of propagation of the waves. As this crest reaches each of the atoms in the crystal, it generates a scattered wave crest. We shall see that the various scattered waves reinforce in the direction  $MN$ , their crests coinciding along the line  $N_1N_2$ . There will be a certain number of complete wavelengths in the path  $LMN$  along which a ray proceeds that is scattered by an atom at  $M$ . Now if the ray scattered by an atom at  $M_1$  travels the same distance (*i.e.*, if the distance  $L_1M_1N_1$  is equal to  $LMN$ ), then the scattered rays from the two atoms will be in phase and will reinforce each other. It will also be true that any other atom lying anywhere in the plane  $AA$  will also reinforce the beam in this direction. This reinforcement will take place when the incident and the scattered rays make equal angles with the atomic

plane. It is then possible to regard the plane of atoms as a mirror that is reflecting a portion of the x-rays at an angle of reflection equal to the angle of incidence. Let us now consider the condition for reinforcement of the waves from successive planes in the crystal that lie parallel to  $AA$ . The requirement to be met is that the difference in the length of the path for rays reflected from successive planes be equal to an integral number of wavelengths. In Fig. 1 this corresponds to the condition that the distance  $PM_2Q$  is one wavelength or a multiple of it, since  $PM$  is drawn perpendicular to  $LM$  and  $MQ$  is drawn perpendicular

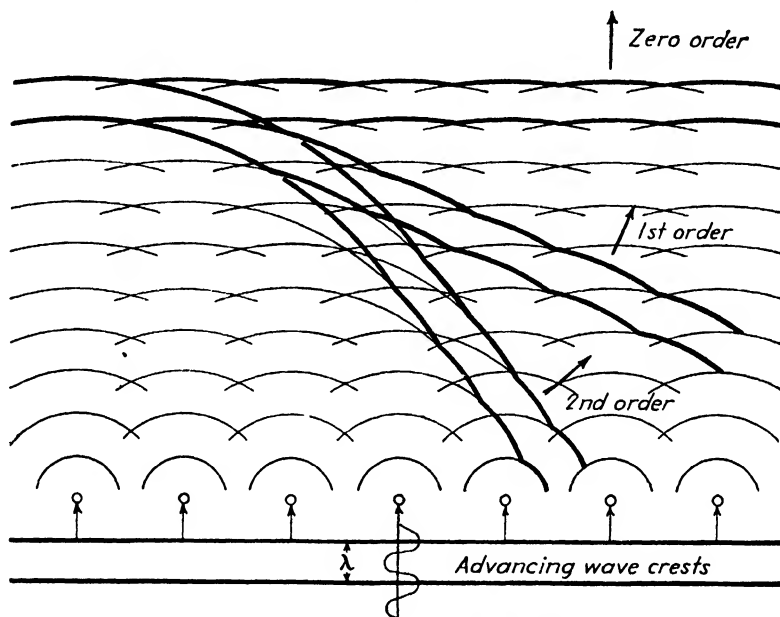


FIG. 2.—Reinforcement of scattered waves producing diffracted beams in the different orders.

to  $MN$ , making the paths of the rays from  $L$  and  $L_1$  the same except for the distance  $PM_2Q$ . It will be seen from the figure that

$$PM_2 = M_2Q = d \sin \theta.$$

Thus the condition for reinforcement of all the reflected rays is

$$n\lambda = 2d \sin \theta$$

where  $n = 0, 1, 2, 3$ , etc.,  $\lambda$  is the wavelength, and  $d$  is the spacing of the planes. This is Bragg's law. The integer  $n$ , which gives the number of wavelengths' difference in path for waves from successive planes, is the **order of reflection**.

**The Laue Equations.**—Diffraction from a crystal, as indicated above, is analogous to reflection from a series of semitransparent mirrors, but it is also to be understood as diffraction from a three-dimensional grating.

analogous to the diffraction of light from a one-dimensional optical grating.

If an x-ray beam is directed at a row of equally spaced atoms, as represented in Fig. 2, each atom will be a source of scattered waves spreading spherically, which reinforce in certain directions to produce the zero-, first-, second-, and higher order diffracted beams. Successive waves are indicated on the drawing by concentric arcs, which are linked

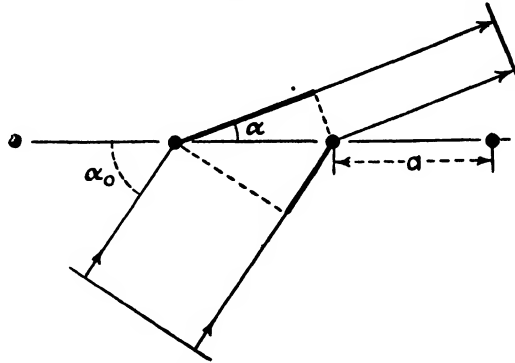


FIG. 3.—Conditions for reinforcement leading to one of the Laue equations.

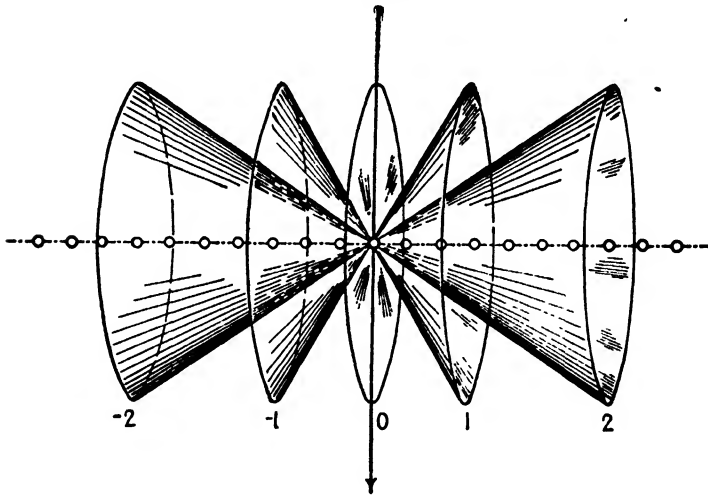


FIG. 4.—Cones of diffracted beams around a row of atoms, with direction of primary beam indicated by the arrow. Orders of diffraction indicated by numbers.

together to show how the various orders are built up. The condition for reinforcement can be derived from Fig. 3, which shows the path difference for rays scattered by two adjacent atoms in the row. If the incident beam makes an angle  $\alpha_0$  with the row, and the diffracted beam leaves at the angle  $\alpha$ , then the path difference is  $a(\cos \alpha - \cos \alpha_0)$ . This path difference must be an integral number of wavelengths if the scattered waves are to be in phase, so the following relation must hold:

$$a(\cos \alpha - \cos \alpha_0) = h\lambda$$



where  $h$  is an integer and  $\lambda$  is the wavelength. This equation will be satisfied by all the generators of a cone that is concentric with the line of atoms and that has the semiapex angle  $\alpha$ . Thus for any given angle of incidence there will be a series of concentric cones surrounding the row of atoms, each cone being made up of one order of diffracted rays. A set of cones of this type is indicated in Fig. 4.

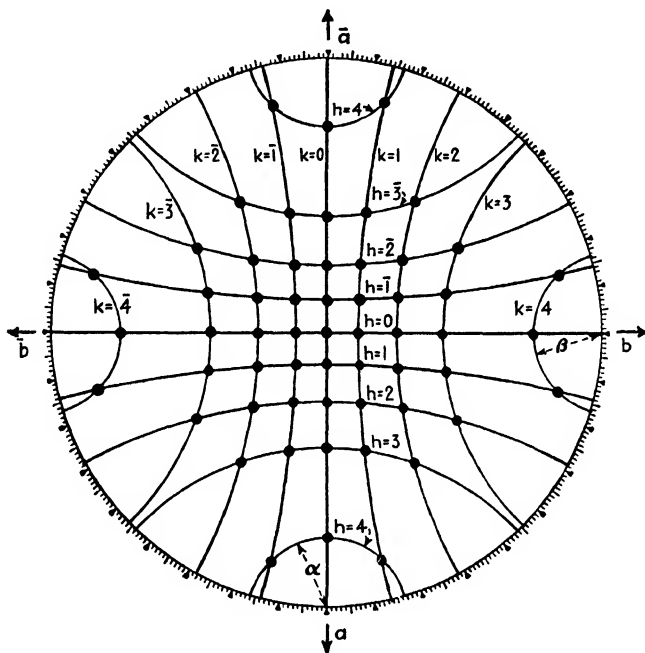


FIG. 5.—Stereographic projection of diffracted beams from a two-dimensional square network. Cones are concentric with  $a$  and  $b$  axes; intersections are strong diffracted beams.

If there is a two-dimensional network of atoms with spacings  $a$  in one direction and  $b$  in another, there will be two simultaneous equations to be fulfilled for intense diffracted beams:

$$\begin{aligned} a(\cos \alpha - \cos \alpha_0) &= h\lambda. \\ b(\cos \beta - \cos \beta_0) &= k\lambda. \end{aligned}$$

In these relations,  $\alpha_0$  and  $\alpha$  are the angles the incident and diffracted beams make with the  $a$  rows, while  $\beta_0$  and  $\beta$  are the corresponding angles for the  $b$  rows;  $h$  is the integer giving the order of reflection with respect to the  $a$  rows, and  $k$  is the order for the  $b$  rows. These equations correspond to two sets of cones, a set around the  $a$  axis and another concentric with the  $b$  axis. The most intense diffracted beams will travel out along the intersections of these two sets. The geometry of these beams can be illustrated neatly on a stereographic projection. The projection of Fig. 5 illustrates diffraction from a square network of atoms in the plane

of the projection, with  $a$  and  $b$  axes as indicated; the incident beam is coming toward the observer and striking the atom plane perpendicularly. The diffracted rays coming out of the atom plane toward the observer are indicated by dots at the intersections of the cones. Projections of this type aid in visualizing what changes would result from various alterations in the quantities of the two equations; for instance, increasing the wavelength spreads out the pattern of cones and intersections and reduces the number of diffracted beams.

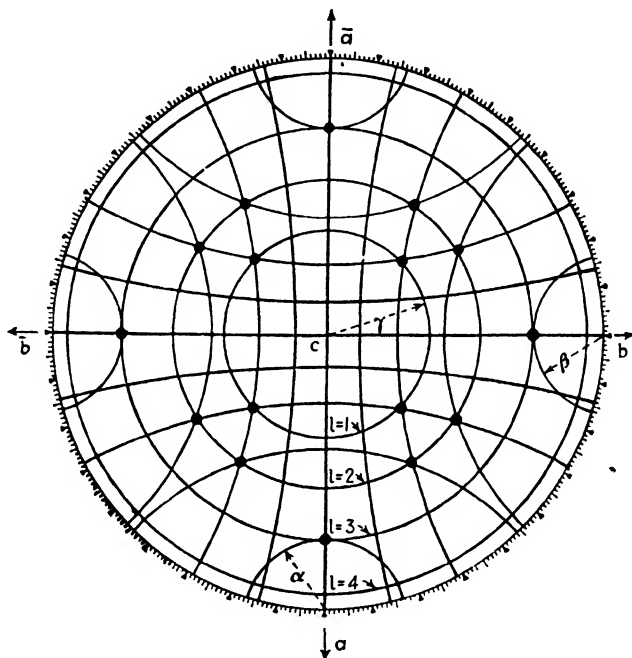


FIG. 6.—Stereographic projection of diffracted beams from a three-dimensional cubic lattice. Dots indicate strong diffracted rays.

A crystal is a three-dimensional network of atoms, and there are, accordingly, three conditions to be met simultaneously for diffraction:

$$a(\cos \alpha - \cos \alpha_0) = h\lambda.$$

$$b(\cos \beta - \cos \beta_0) = k\lambda.$$

$$c(\cos \gamma - \cos \gamma_0) = l\lambda.$$

These are the Laue equations; the first two have the same significance as before, and the third relates to the periodicity in the third dimension, the  $c$  axis of the crystal, with which the incident beam makes the angle  $\gamma_0$  and the diffracted beam the angle  $\gamma$ . The integer  $l$  is the order of diffraction with respect to the third axis, and  $hkl$  can be called the indices of the diffracted beam. The sets of cones around  $a$ ,  $b$ , and  $c$ , respectively, are illustrated in the projection shown in Fig. 6 for a particular wavelength and a cubic lattice. It will be noted that all three cones can intersect

along a single line only if there are special values for the variables. In other words, the requirement that all three equations be satisfied simultaneously acts as a severe limitation to the number of diffracted beams.

Bragg<sup>1</sup> has shown that fulfilling the Laue equations is equivalent to reflecting from a lattice plane. Reference to the unit cell of the lattice in Fig. 7 shows that a diffracted ray having indices  $hkl$  will be built up of waves scattered by atoms at the unit-cell corners  $A$ ,  $B$ , and  $C$ , if these waves are  $h$ ,  $k$ , and  $l$  wavelengths ahead, respectively, of the waves scattered by  $O$ . If we now draw a crystal plane such that its intercepts are  $OA' = a/h$ ,  $OB' = b/k$ , and  $OC' = c/l$ , then the wave scattered by every atom on this plane  $A'B'C'$  will be one wavelength ahead of the wave scattered by  $O$ . All waves scattered by the plane  $A'B'C'$  will thus be in phase; this is the condition for reflection from the plane  $(hkl)$ .

It is a great convenience to distinguish between indices of a reflected beam and the indices of a reflecting plane in a crystal. It will be remembered that indices of crystal planes never have a common factor. We are therefore free to use indices with a common factor to express the order of reflection,  $n$ . The first-order reflection is given the same indices as the plane. For example, the first order from (110) is written 110. The second order is written with the indices of the reflecting plane multiplied by two—220. The third order is 330, etc. To avoid confusion, the indices of the reflections are written without parentheses.

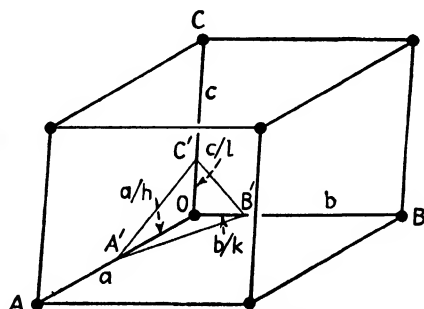


FIG. 7.—A reflecting plane  $(hkl)$  in a unit cell.

This scheme of notation for reflections is more than a mere convention, for it simplifies the interpretation of diffraction patterns. Its usefulness depends on the fact that  $n$ th-order reflection from a plane  $(hkl)$  is equivalent to first-order reflection from an imaginary set of planes spaced  $1/n$ th the spacing of the  $(hkl)$  planes. If the intercepts of the  $(hkl)$  plane nearest the origin are  $1/h$ ,  $1/k$ , and  $1/l$ , then the intercepts of the first plane of the new set will be  $1/nh$ ,  $1/nk$ , and  $1/nl$ . All reflections can be considered as first-order reflections from this new set of planes, and if their spacing is  $d'$  the Bragg equation can be simplified to

$$\lambda = 2d' \sin \theta.$$

The reflecting angles are computed by the equations in the following section, in which this convention is used.

<sup>1</sup> W. L. BRAGG, "The Crystalline State," vol. I, p. 18, Macmillan, New York, 1934.

**Interplanar Spacings.**—From the foregoing sections it is apparent that the *directions* of the diffracted beams are governed entirely by the *geometry of the lattice* (by the orientation and spacing of the planes of atoms, from the point of view of Bragg's law, or by the periodicity of the lattice in three dimensions, from the point of view of the Laue equations). In other words, the size and shape of the unit cell determine where the diffracted beams will go. The distribution of atoms within the unit cell has no effect on these directions but determines, on the other hand, the *intensities* of the diffracted beams. This will be discussed later.

Given a unit cell of known dimensions, the diffracted beams can be predicted if the various interplanar spacings,  $d$ , are computed and inserted in Bragg's law. Consider as an example a hypothetical crystal composed

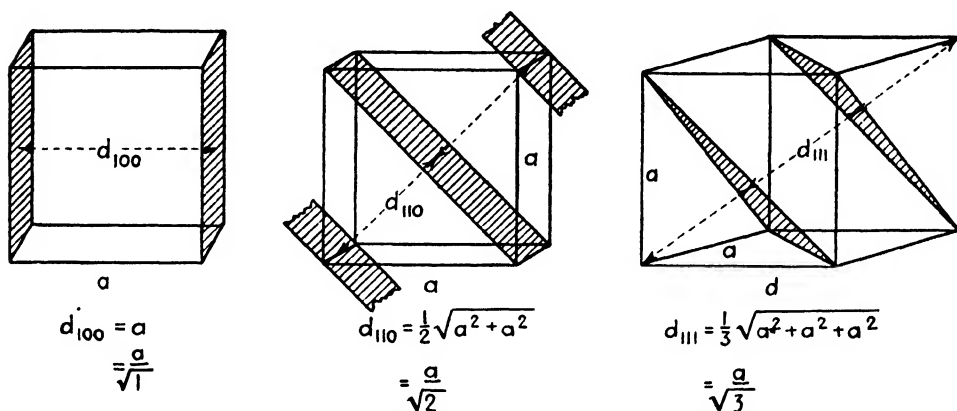


FIG. 8.—Some reflecting planes in a simple cubic lattice and their spacings.

of atoms only at the corners of simple cubic unit cells. Reference to Fig. 8 will show that the most widely spaced atomic planes are those that are spaced at intervals equal to the edge of the cell,  $a$ , which are the (100) planes. This spacing is  $d_{100} = a/\sqrt{1}$ . The reflected beam from these planes will have the least value of  $\theta$  and will thus be least deviated by reflection. The next planes in order of spacing will be the (110) planes which bisect the face diagonal and for which  $d_{110} = a/\sqrt{2}$ . The third set, illustrated at the right of Fig. 8, which cuts the body diagonal into three parts, has  $d_{111} = a/\sqrt{3}$ .

The general rule for these spacings is

$$d_{hkl} = \frac{a}{\sqrt{h^2 + k^2 + l^2}}.$$

This formula can be inserted in the Bragg equation, which can most conveniently be written in the squared form

$$\sin^2 \theta = \frac{n^2 \lambda^2}{4} \cdot \frac{1}{d^2}.$$

Using the convention that the  $n$ th-order reflection from a plane has indices that are  $n$  times the Miller indices, it is possible to predict the angles for all the possible reflections from **cubic** crystals by the formula

$$\sin^2 \theta_{hkl} = \frac{\lambda^2}{4a^2} (h^2 + k^2 + l^2).$$

The equations for the other systems can also be derived by inserting the proper spacing formulas (see Appendix I); for example,

### **Tetragonal**

$$\sin^2 \theta = \frac{\lambda^2}{4} \left( \frac{h^2 + k^2}{a^2} + \frac{l^2}{c^2} \right)$$

### **Orthorhombic**

$$\sin^2 \theta = \frac{\lambda^2}{4} \left( \frac{h^2}{a^2} + \frac{k^2}{b^2} + \frac{l^2}{c^2} \right)$$

### **Hexagonal**

$$\sin^2 \theta = \frac{\lambda^2}{4} \left[ \frac{4}{3} \frac{(h^2 + k^2 + hk)}{a^2} + \frac{l^2}{c^2} \right]$$

These are special cases of the more complicated formula for the triclinic lattice which involves the interaxial angles  $\alpha$ ,  $\beta$ ,  $\gamma$ , as well as the axial lengths  $a$ ,  $b$ , and  $c$ . These equations hold for all types of diffraction patterns and are the principal means of deciphering the patterns. For the less symmetrical crystals, however, there are so many reflections that these relations alone cannot be relied upon to unravel the patterns, and additional geometrical relations are required, which are taken up in later chapters.

**Relation of Atom Arrangement to the Diffraction Pattern.**—The *positions* of the diffracted beams from a crystal are determined by the size and shape of the unit cell, but the *intensities* of the beams are independent of these dimensions and are affected only by the distribution of electrons within the cell. The diffracted beams are built up by the combination of the scattered rays from each of the electrons in the unit cell. (The nuclei of the atoms contribute a negligible amount to the total scattering and need not be considered.) The scattering power of an individual electron is the natural unit to which to refer all quantitative treatments of intensities; so we shall first discuss the cooperative scattering of the electrons in an atom, using the scattering from an individual electron as a unit, and then the cooperative scattering of the various atoms in the unit cell.

It is customary to use a quantity  $f$ , the **atomic scattering factor**, to express the efficiency of an atom in scattering x-rays. The atomic scattering factor is simply the ratio of the amplitude of the wave scattered

by an atom to that scattered by an electron under the same conditions. In other words, since the intensity of a wave is the square of its amplitude,  $f^2$  is the ratio of the intensity of the scattering from an atom to that from an electron. The atomic scattering factor varies with angle—an atom scatters less efficiently at large angles from the incident beam than at small. This is because the individual scattered waves from the various electrons in the atom are nearly in phase and reinforce each other for directions near the incident beam, while they are out of phase and reinforce each other less effectively at the larger angles. Values of  $f$  have been tabulated for all atoms and will be found in Appendix V. It will be noted that at small diffraction angles where reinforcement is nearly complete  $f$  is nearly proportional to the atomic number.

**Relation of Atom Arrangement to Diffracted Intensities.**—Let us now consider the intensity of the diffracted beam that results from the combination of the waves scattered by a number of atoms in a unit cell.

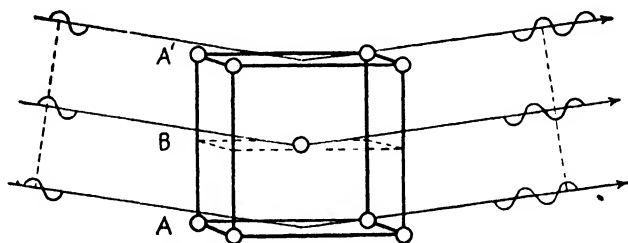


FIG. 9.—Interference in 100 reflection from a body-centered cubic lattice.

Each atom scatters a wave of amplitude  $f$ , which is wholly or partly in phase with the waves from the other atoms of the group. Consider the atomic arrangement in Fig. 9, for example, with a beam reflecting in the first order from the planes marked  $A$  and  $A'$ . The wave from  $A'$  will therefore be one wavelength ahead of the wave from  $A$  and will reinforce it. On the other hand, the beam from the plane of atoms marked  $B$  will be one-half wavelength ahead and will be exactly out of phase; thus the reflections from alternate planes annul each other,  $B$  canceling  $A$ , etc., throughout the crystal—provided that the scattering power of plane  $B$  is equal to that of  $A$ . If the scattering powers are unequal or if  $B$  is not midway between  $A$  and  $A'$ , the interference will not lead to complete annihilation of this reflection. Furthermore, if the reflection is of the second order from  $A$  and  $A'$ , then it will be of the first order from  $A$  and  $B$ , so that complete reinforcement will occur.

**The Structure-factor Equation.**—To compute quantitatively the total intensity of a reflection it is necessary to sum up the waves that come from all the atoms. Mathematically, this is the problem of adding sine waves of different amplitude and phase but of the same wavelength to determine

the amplitude of the resultant wave. The square of this resultant amplitude is the required intensity.

The summation for the total intensity may be accomplished by inserting the coordinates and  $f$  values of each atom in the unit cell in the structure-factor formula for  $I$ , which is proportional to the square of the absolute value of the amplitude of the diffracted ray:

$$I \propto |F|^2 = [f_1 \cos 2\pi(hu_1 + kv_1 + lw_1) + f_2 \cos 2\pi(hu_2 + kv_2 + lw_2) + \dots]^2 \\ + [f_1 \sin 2\pi(hu_1 + kv_1 + lw_1) + f_2 \sin 2\pi(hu_2 + kv_2 + lw_2) + \dots]^2$$

where  $I$  is the intensity of the reflection,  $F$  is the structure factor,  $u_1v_1w_1$ ,  $u_2v_2w_2$ , etc., are the coordinates of atoms having structure factors  $f_1, f_2$ , etc., respectively, and  $hkl$  are the indices of the reflection being computed. This may be written

$$|F|^2 = \left[ \sum_i f_i \cos 2\pi(hu_i + kv_i + lw_i) \right]^2 + \left[ \sum_i f_i \sin 2\pi(hu_i + kv_i + lw_i) \right]^2.$$

The formula applies to all crystal systems and lattices. A derivation is included in Appendix V.

We shall illustrate the use of the structure-factor equation by applying it to a body-centered lattice having identical atoms at the coordinates 000 and  $\frac{1}{2}\frac{1}{2}\frac{1}{2}$  in the unit cell, as in Fig. 9. The formula for this case becomes

$$I \propto f^2 \left[ \cos 2\pi \cdot 0 + \cos 2\pi \left( \frac{h}{2} + \frac{k}{2} + \frac{l}{2} \right) \right]^2 \\ + f^2 \left[ \sin 2\pi \cdot 0 + \sin 2\pi \left( \frac{h}{2} + \frac{k}{2} + \frac{l}{2} \right) \right]^2$$

Thus

$$I \propto [1 + \cos \pi(h + k + l)]^2 + \sin^2 \pi(h + k + l),$$

and it will be seen that  $I = 0$  for every reflection having  $(h + k + l)$  an odd number. This is true regardless of the system to which the body-centered crystal belongs. Thus when a diffraction pattern of a crystal has been assigned indices, the absence of all reflections for which the sum  $(h + k + l)$  is odd indicates a body-centered lattice, while the presence of any reflection of this type proves that the lattice is not body-centered. Other rules hold for lattices centered on one or more faces. If we apply the formula to a crystal of cesium chloride in which a cesium atom is at 000 and a chlorine atom is at  $\frac{1}{2}\frac{1}{2}\frac{1}{2}$ , quite a different result is obtained, for although cesium chloride has what might be called a body-centered cubic type of structure the  $f$  values of the two atoms are not the same. The formula becomes

$$I \propto [f_{cs} + f_{cl} \cos \pi(h + k + l)]^2 + [f_{cl} \sin \pi(h + k + l)]^2$$

and thus

$$\begin{aligned} I &= c(f_{cs} + f_{cl})^2 && \text{when } (h + k + l) \text{ is even} \\ I &= c(f_{cs} - f_{cl})^2 && \text{when } (h + k + l) \text{ is odd} \end{aligned}$$

where  $c$  is a constant. There are no reflections missing in the diffraction patterns of this crystal, though the reflections that are missing in a true body-centered lattice are present in this case with very low intensity. This is illustrated in the structure of Fig. 9 when the  $B$ -plane atoms scatter less strongly than the  $A$ -plane atoms, or vice versa, and are unable to reduce the 100 reflection to zero intensity.

### X-RAY DIFFRACTION METHODS

If a monochromatic beam of x-rays is directed at a single crystal, the angle of incidence may not be correct for reflection from any of its planes. To ensure that Bragg's law is satisfied it is necessary to provide a range of values of either  $\lambda$  or  $\theta$ . The various ways of doing this form the bases of the standard methods of diffraction used in crystal analysis.

1. In the **Laue method** a single crystal is held stationary in a beam of white radiation usually from a tungsten target. The variable is provided by the range of wavelengths in the beam.

2. In the **rotating-crystal method** a single crystal is rotated (or oscillated) in a beam of monochromatic x-rays. The rotation brings different atomic planes, in turn, into reflecting position. Thus  $\theta$  is the variable.

3. In the **powder method**  $\theta$  is again the variable, for powdered crystal-line material is placed in a monochromatic beam, and among the myriad particles with random orientations certain particles will be properly oriented to reflect from each of the possible reflecting planes.

The elements of these three methods are presented below, and a more detailed treatment of each is given in later chapters.

**The Laue Method.**—A Laue camera (Fig. 10) consists of a pinhole system which collimates the beam into a narrow pencil of rays, a goniometer head or other device to hold the crystal in a definite orientation, and a flat film in a lightproof envelope placed to receive either the rays diffracted through the crystal or those reflected back from its surface. Each reflecting plane in the crystal reflects a portion of the beam, and the diffraction pattern (Fig. 11) is a pattern of spots that can be visualized simply as a pattern made by reflection from a number of mirrors inclined at different angles.

The spots in a **Laue transmission pattern** (on a film placed at  $A$ , Fig. 10) are arranged on ellipses that have one end of their major axes at the central spot on the film. All spots on any one ellipse are reflections from planes of a single zone (planes parallel to a single zone axis). This



characteristic can be demonstrated easily by the corresponding experiment with mirrors and a beam of light: a set of small mirrors fastened to the surface of a cylindrical rod will produce an elliptical pattern of spots on the wall—or the polished surface of the cylindrical rod will reflect an ellipse. On a Laue **back-reflection pattern** (on a film placed at *B*, Fig. 10) these zones of spots lie on hyperbolas.

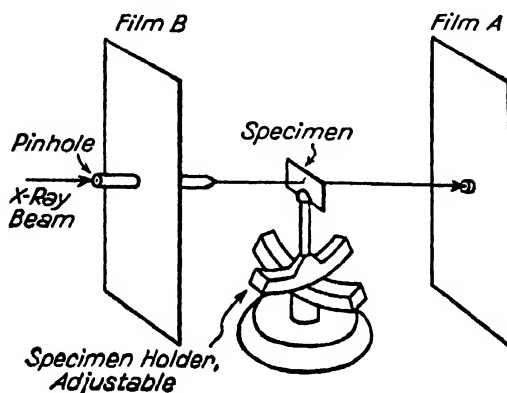


FIG. 10.—Laue camera. Film *A* records the transmission pattern, or Film *B* may be substituted for recording the back-reflection pattern.

Laue patterns reflect the *symmetry* of a crystal; when the x-ray beam is directed parallel to a fourfold axis of symmetry, for example, the pattern will have fourfold symmetry about the central point and a quarter turn will bring coincidence of all the spots. Any other macroscopic symmetry element parallel to the beam will also be evident on the pattern. The method has been widely used as an aid in determining symmetry classes of crystals although it is not capable of fully establishing the symmetry.

In the relation  $n\lambda = 2d \sin \theta$  each plane selects a wavelength that satisfies the equation, and as a wide range of wavelengths is present (from  $0.2\text{\AA}$  to over  $2\text{\AA}$  when a tube is operated at 65,000 volts) there may be two wavelengths reflecting from a single plane. Thus two or more different orders of reflection may superimpose on a single spot. This makes the method an awkward one for determining the relative *intensities*

of the reflected beams. The differing intensities of the various wavelengths in the beam as well as their differing efficiencies in blackening a photographic film are additional factors that make it difficult to measure the intensities of the reflections. Consequently, the Laue method is not

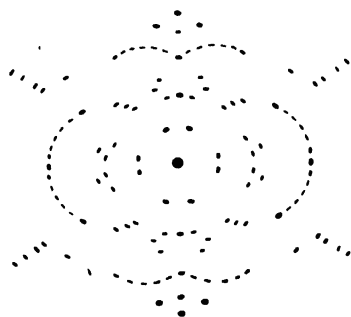


FIG. 11.—A Laue pattern, transmission type, with two-fold symmetry. X-ray beam parallel to a two-fold axis of symmetry of an undistorted crystal.

widely used for crystal structure determination and is mainly of importance for determining symmetry and orientations of crystals. In the metallurgical field it is also useful for revealing imperfections resulting

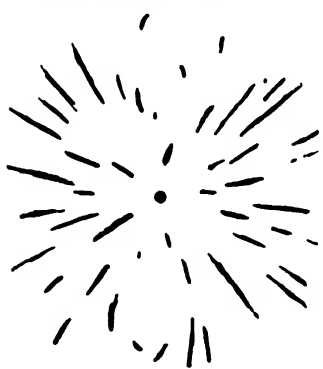


FIG. 12.—A Laue pattern of a distorted crystal, showing asterism.

from accidents of crystal growth or from deformation. The Laue spots from perfect crystals are sharp, but those from imperfect or deformed crystals are blurred or elongated, giving the appearance known as **asterism** illustrated in Fig. 12. Asterism corresponds to the reflection of light from bent mirrors. If several grains of a polycrystalline metal are struck by the beam from the x-ray tube, their Laue patterns will superimpose, as shown in Fig. 13, and from the number of spots or their average size it is possible to estimate the grain size in the metal.

**The Rotating-crystal Method.**—The elements of a simple rotating-crystal camera are sketched in Fig. 14. In the simpler instruments of this class the crystal is rotated continuously about an axis that is perpendicular to the beam of rays from the pinhole system. The diffracted beams flash out when the angle of incidence on a certain plane is correct for the monochromatic radiation employed. It will be seen by reference to Fig. 14 that all planes parallel to the vertical axis of rotation will reflect rays horizontally.

A cylindrical film taken from such a camera is illustrated in Fig. 15.

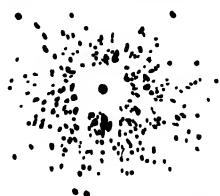


FIG. 13.—A Laue pattern of undistorted polycrystalline material. Typical of recrystallized metal.

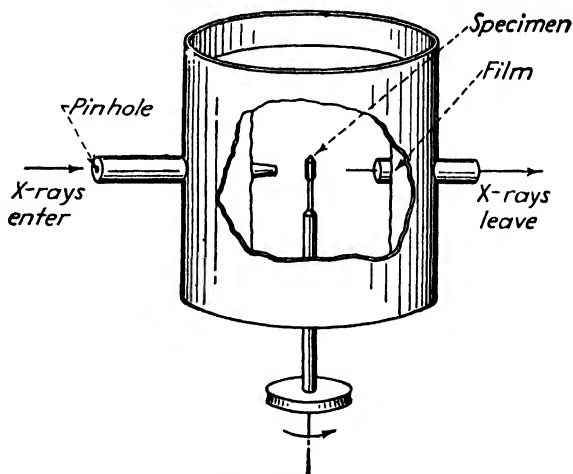


FIG. 14.—Rotating crystal camera.

strated in Fig. 15. The reflections are arranged on **layer lines**. The spots on the central layer line are reflections from planes whose normals are in a horizontal plane; the spots on any other layer line are from planes that have the same intercept on the axis of rotation. It is not difficult to assign indices to all of the spots if the crystal has been placed in the camera with an important zone axis along the axis of rotation.

Since all spots are made with a single wavelength, it is easier to determine the relative intensities from rotation photographs than from Laue photographs. The various modifications of this method (oscillating crystal, Weissenberg, etc.) are the crystallographer's most important tools for the determination of crystal structures.

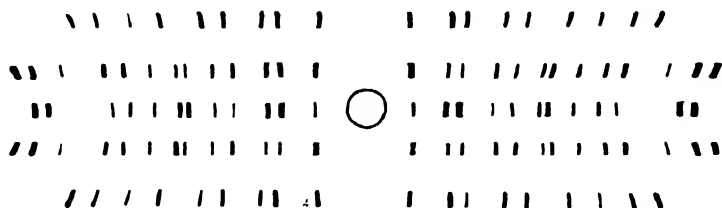


FIG. 15.—Rotating crystal pattern. Axis of rotation vertical, layer lines horizontal.

The **ionization spectrometer** ("Bragg spectrometer") is closely related to the rotating-crystal method and also uses a single crystal and monochromatic radiation (Fig. 16). The crystal is set in a reflecting position in the beam through slit  $S_1$ , and the reflected beam is caught in an ionization chamber connected to an electrometer. The intensity of reflection is measured by the ionization produced in the chamber. A wide slit,  $S_2$ , in front of the chamber may be used so that the whole beam is received, or a narrow slit may be used if it is desired to plot the intensities at intervals every few minutes of arc across the reflection. The advantages of the method are the accuracy with which intensities can be determined and the fact that the reflected intensities can be referred to the intensity of the incident beam as a standard so as to yield **absolute reflecting powers** of the different planes. For the latter purpose the incident beam is rendered monochromatic by reflection from a crystal before it strikes the crystal being studied. Absolute intensities are needed only when the crystal structure is too complex to be solved by the less laborious photographic methods or when the electron distribution in an atom is to be determined.

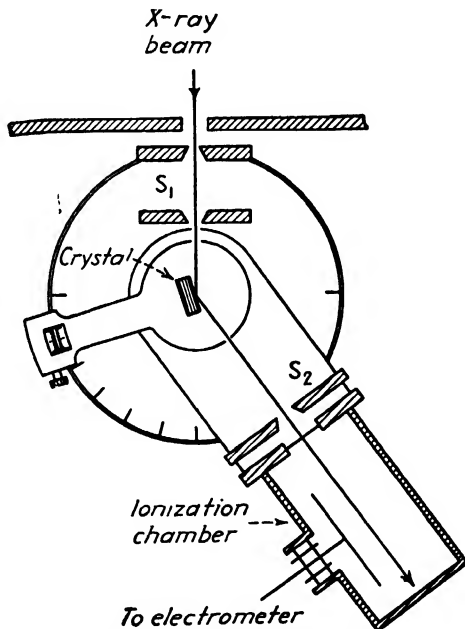


FIG. 16.—Ionization spectrometer.

**The Powder Method.**—The powder method employs monochromatic radiation falling on a finely powdered specimen or a fine-grained poly-

crystalline specimen. The usual type of camera is shown in Fig. 17 and consists of a pinhole collimating system, a wire-shaped specimen, and a cylindrical film. A cup to catch the undiffracted beam or a tube to

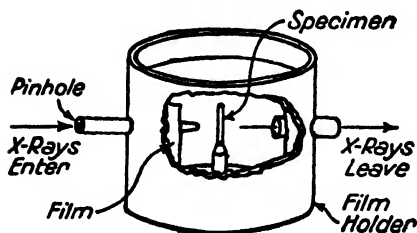


FIG. 17.—Powder camera (Debye-Scherrer-Hull method).

conduct it out of the camera prevents fogging of the film. Diffracted rays leave the specimen along the generators of cones concentric with the primary beam, each cone having a semiapex angle equal to twice the Bragg angle  $\theta$ . When the film is laid out flat, it has the appearance of Fig. 18; the cones make a series of concentric rings around the central spot, and the Bragg angles

can be determined quickly from the maximum diameter of these Debye rings. If  $2S$  is the maximum diameter of a ring on a film of the type sketched in Fig. 18 and if  $R$  is the radial distance from specimen to film, then the angle  $\theta$  in radians is  $S/2R$ , and in degrees the angle is  $57.30$

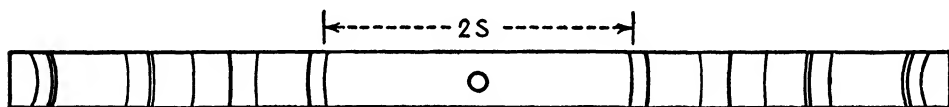


FIG. 18.—Powder diffraction pattern.

times this. If a camera holds a film on only one side of the central spot, it is necessary to determine the  $\theta$  value by calibrating the film with the diffraction pattern from a standard substance having known diffracting angles.

**Focusing cameras** are also cylindrical but are designed so that the specimen, slits, and photographic film all lie on the circumference of the cylinder, as shown in Fig. 19. This arrangement causes diffracted rays from all parts of the specimen to focus on the film in sharp lines. Since a large area of the specimen contributes to the pattern, exposure times with focusing cameras are usually shorter than with cameras of the Debye type; they also have higher dispersion—more widely spaced lines—than Debye cameras of similar diameter.

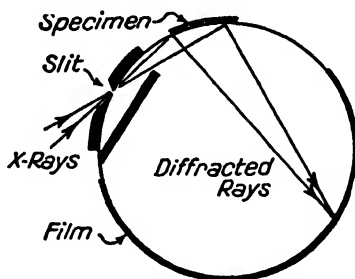


FIG. 19.—Focusing camera.

The indices of the lines on a powder pattern are determined by trial. From the positions of the lines the spacings of the corresponding atomic planes are computed by Bragg's law, and observed spacings are compared with the spacings that would exist in unit cells of various dimensions and angles. In the highly symmetrical crystal systems this trial procedure

is relatively simple, but when there are many variable parameters, as for example in orthorhombic, monoclinic, or triclinic crystals, the procedure becomes unworkable because of the tremendous number of trials that are required. Prediction of the lines for a given unit cell is carried out by inserting all combinations of  $h$ ,  $k$ , and  $l$  in the corresponding formula for  $\sin^2 \theta$  (page 76). Effective graphical aids for shortening the procedure with cubic, hexagonal, rhombohedral, and tetragonal crystals are described in Chap. VII. Intensities of the various lines can be measured on powder patterns very precisely but only the simplest crystals can be completely determined by the powder method alone.

Powder cameras are operated with x-ray targets that emit strong characteristic radiation. Molybdenum targets are good if a zirconium filter is used. Best results are obtained with targets of Fe, Co, Ni, Cr, or Cu (or in special cases with alloys of these). White radiation, which fogs the film, is then of low intensity compared with the characteristic lines. If the characteristic spectrum contains  $K\beta$  as well as  $K\alpha$  radiation, the diffraction pattern will contain reflections of both wavelengths, and the  $K\beta$  diffraction pattern will be superimposed on the  $K\alpha$ . The lines of the  $K\beta$  pattern may be recognized by the following characteristics:

1. They are all single lines, whereas the  $K\alpha$  pattern consists of close doublets resolved at the higher diffraction angles.

2. The  $K\beta$  lines are always weaker than the  $K\alpha$  lines from the same planes.

3. The ratio of  $\sin \theta$  values for  $K\alpha$  and  $K\beta$  radiation reflecting from a given atomic plane always equals the ratio of the wavelengths.

It is best to choose the target of the x-ray tube so that the  $K\alpha$  emission line has a longer wavelength than the  $K$  absorption limit of the principal chemical elements in the specimen, for unless this is done the specimen will become a strong emitter of fluorescent radiation, which will fog the film. For eliminating  $K\beta$  radiation a properly chosen filter can be placed in front of the pinholes, but more effective filtering will be obtained if the filter is made in the form of a uniform sheet and placed between sample and film, for in this position it can filter out fluorescent rays from the sample.

**Back-reflection cameras** (precision cameras) make use of the fact that diffraction lines at large angles are extremely sensitive to slight changes of interplanar spacings. If the spacing  $d$  in the equation  $n\lambda = 2d \sin \theta$  is varied, it will produce variations in  $\theta$  according to the relation

$$\Delta d \sin \theta + d \cos \theta \Delta \theta = 0,$$

$$\frac{\Delta \theta}{\Delta d} = - \frac{\tan \theta}{d}.$$

Therefore, as  $\theta$  approaches  $90^\circ$ , the quantity  $\Delta\theta/\Delta d$  becomes very great. The slight changes in  $d$  caused by elastic stress can be measured in a camera designed to record these high-angle lines to best advantage, and lattice alterations accompanying the change in composition of a solid solution can be determined. With ordinary care a precision of 0.02 percent is obtained, and with extreme care 0.003 percent can be reached. The small cylindrical cameras of the Debye type usually yield results with an accuracy of 0.1 to 0.02 percent.

**Identification of phases** by their powder patterns is an important practical use of the method. This may be done without solving the crystal structure or assigning indices to the reflections, simply by comparing the patterns of the unknown material with patterns of known

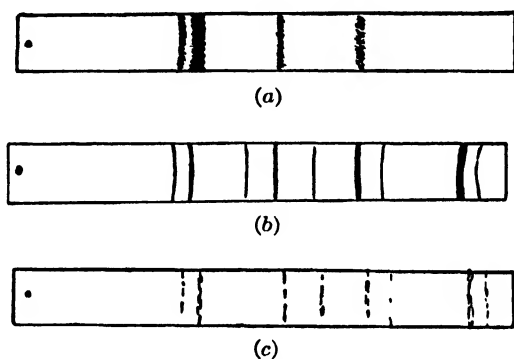


FIG. 20.—*a*, pattern from cold-worked iron. Lines widened and weakened by “microscopic” internal stresses; from camera of Fig. 17, with  $\text{FeK}\alpha$  and  $\text{FeK}\beta$  radiation; increasing  $\theta$  from left to right. *b*, powder pattern of annealed iron. *c*, pattern from recrystallized iron, the large unstrained grains forming spotty lines.

substances. The films are laid side by side or superimposed, and the similarities are observed directly. For this work, many lines should be recorded on the film, and every individual line of the pattern of the unknown must be accounted for. Identification is often possible when the specimen contains as many as three or more different substances provided that each substance represents an appreciable fraction of the mass of the sample, for each produces its spectrum independently, and the pattern consists of superimposed spectra with relative intensities dependent on the relative amounts of the different phases present. If a series of alloys is prepared consisting of various compositions spaced across a binary constitutional diagram, the powder patterns will follow the alternate single and two-phase regions of the diagram.

**Cold work, recovery, and recrystallization** are readily recognized by their effect on the patterns. Cold work is shown by a blurring of individual spots on the diffraction rings, by broadening of the rings, and by a reduction of their intensity relative to the background—especially at the

higher diffraction angles. Figure 20a illustrates this for a cold-worked sample, compared with Fig. 20b for the annealed condition. Recovery from the strained condition is indicated by sharpening of the lines (Fig. 20b), and recrystallization (the growth of strain-free grains) by a spotty type of pattern indicative of large grains, sketched in Fig. 20c.

The distribution of intensity around a diffraction ring reveals the presence or absence of a **preferred orientation** of the grains. Random

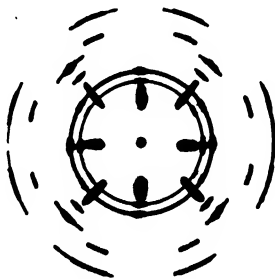


FIG. 21.—Pinhole pattern of sheet steel having a preferred orientation from cold rolling (rolling direction vertical, sheet surface perpendicular to the x-ray beam).

orientations produce rings that are uniformly black all around, while the presence of a texture is indicated by intense spots at certain points on the rings. A flat film in a camera of the Laue type (Fig. 10, Film A), which is well suited to this type of work, is often referred to as a **pinhole camera**. A typical pattern for highly oriented grains is illustrated in Fig. 21.

Subsequent chapters present more detailed information on each of the methods outlined here.

## CHAPTER V

### THE LAUE METHOD

The Laue method is now used chiefly for the determination of crystal orientation and symmetry, and in metallurgical work for revealing crystalline imperfection, distortion, and recrystallization. While it has been brought to a high state of development<sup>1</sup> as a method of crystal-structure determination, its use for this purpose is rapidly diminishing and will be discussed only briefly here. Crystal orientation by Laue photographs is discussed in Chap. IX.

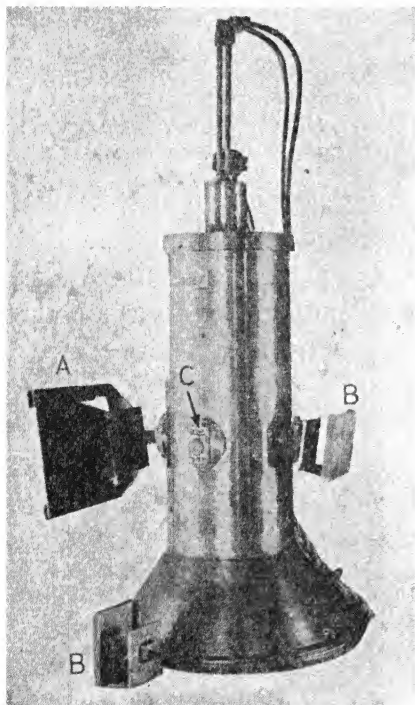


FIG. 1.—Simple Laue cameras which plug into prealigned socket in x-ray-tube housing. A, 5- by 7-in. camera; B, 2- by 2-in. cameras; C socket filled with plug when not in use.

A simple Laue apparatus is illustrated in Fig. 1. Four cameras plug into openings in the side of the tube housing and are automatically aligned. Each camera consists merely of a frame supporting a film and pinhole system. The film is enclosed in a lightproof envelope and is mounted so that it is perpendicular to the axis of the pinholes. The specimen is mounted with a bit of laboratory wax or clay to the end of the pinhole system, which is a brass rod drilled with a hole of 0.5 to 1.0 mm. diameter. A limited amount of control of the angular setting of the sample is possible on simple cameras of this sort (for example, by providing a set of wedges

that fasten over the rear of the pinhole and tilt the crystal known amounts), but for precise and convenient setting a Laue camera must be provided with a goniometer head (see Fig. 10, page 81). It is advantageous to use a camera that combines Laue and rotating-crystal or Weissenberg features, so that the crystal can be oriented by Laue

<sup>1</sup> R. W. G. WYCKOFF, "The Structure of Crystals," Chemical Catalog Co., New York, 1931. E. SCHIEBOLD, "Die Lauemethode," Akademische Verlagsgesellschaft m.b.H., Leipzig, 1932.



photographs and then employed for one of the other methods. Figure 2 shows a universal camera for Laue, rotating-crystal, oscillating-crystal, and powder photographs.<sup>1</sup>

Samples for the transmission Laue method are small single crystals 1 mm. or less in diameter or crystals cut thin enough to transmit the beam without excessive absorption. White radiation from a tube with a tungsten target is usually employed, with operating voltages of 40 to 60 kv.

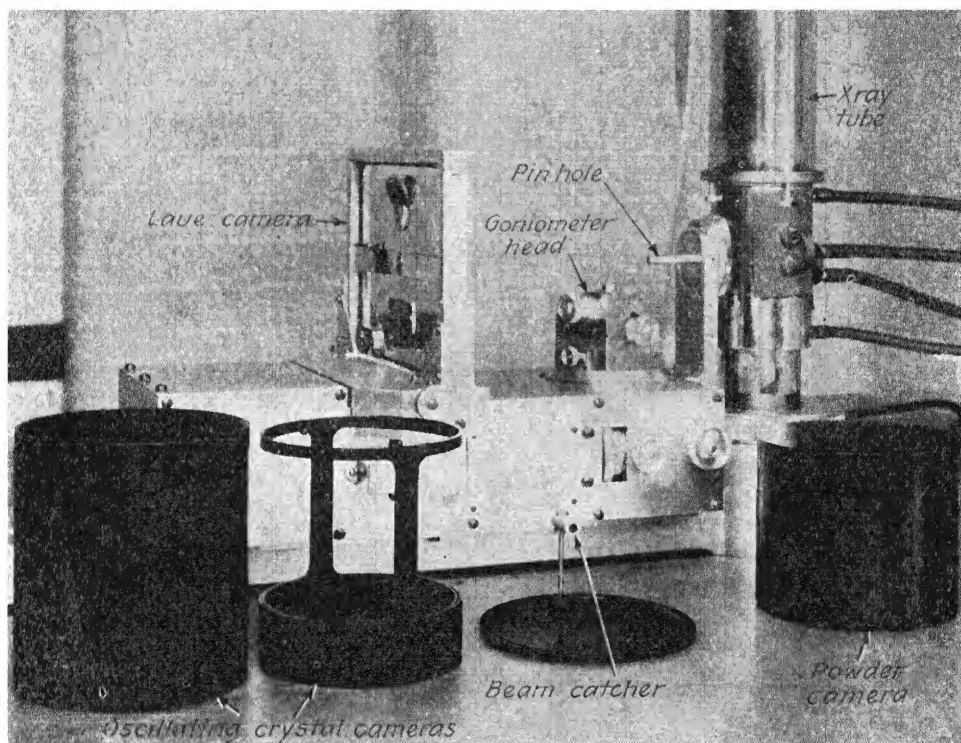


FIG. 2. Universal camera with provision for Laue, Debye, and oscillating crystal methods and demountable x-ray tube. (Research Laboratories of the Aluminum Company of America.)

**Determination of Symmetry.**—Any rotation axes of symmetry or planes of symmetry that lie parallel to the incident beam produce corresponding symmetry around the center of the Laue photograph. The pattern reproduced in Fig. 3, for example, exhibits sixfold symmetry around the center because the sample was a hexagonal crystal in which the beam was directed along the hexagonal axis. Owing to the fact that the face  $(hkl)$  and the parallel face  $(\bar{h}\bar{k}\bar{l})$  reflect to the same spot and cannot be distinguished, all crystals seem to have a center of inversion as judged by the symmetry of diffraction effects (**Friedel's law**). From

<sup>1</sup> Blueprints of this and other cameras constructed in the Aluminum Research Laboratory have been made available to crystallographers at nominal cost.



point, all spots on any one ellipse being reflections from planes of one zone. The most convenient method of interpreting Laue photographs is to employ a projection that transforms these ellipses into straight lines. The gnomonic projection does this and is almost universally used for the purpose. It is illustrated in Fig. 4, which represents a crystal  $C$  at the center of a reference sphere, a reflecting plane oriented as indicated by the dotted lines, and an x-ray beam reflecting from the crystal to form a Laue spot,  $F$ , on a film perpendicular to the beam. The line  $GC$  through the center of the reference sphere and normal to the reflecting plane intersects the plane of projection at the point  $G$ , which is the gnomonic projection of the Laue spot. Thus

$$\frac{GC'}{CC'} = \frac{CC'}{C'D} = \cot \theta.$$

The distance  $CC'$  is usually taken as 5 cm., and so the projection of any Laue spot is given by the relation  $GC' = 5 \cot \theta$ . In practice, it is convenient to construct a ruler that can be laid on the Laue photograph to locate directly the position of the gnomonic projection of any spot (Fig. 5). The left side of the ruler is graduated in millimeters from the point  $C'$ , which superimposes on the central point ( $C'$ ) of the film, and the right side is graduated to give the corresponding distances on the gnomonic projection; *i.e.*, the left side reads the distance  $C'F$  of Fig. 4, and the right side reads  $C'G$ . If the left side is graduated directly in values of  $\sin \theta$  for the spots instead of millimeters and the right side is graduated accordingly, this saves an additional computation.<sup>1</sup>

When the  $a$ ,  $b$ , or  $c$  axis of a crystal is normal to the plane of projection, it is possible to read the indices of spots directly from the gnomonic projection. In Fig. 6, for instance, a Laue photograph of magnesium oxide (cubic) shown in the center circle is projected gnomonically. The photograph, taken with the beam parallel to the  $c$  axis, is oriented so that  $a$  is horizontal and  $b$  is vertical. All spots for which the  $h$  index is zero lie on the central vertical line of the projection, since they belong to

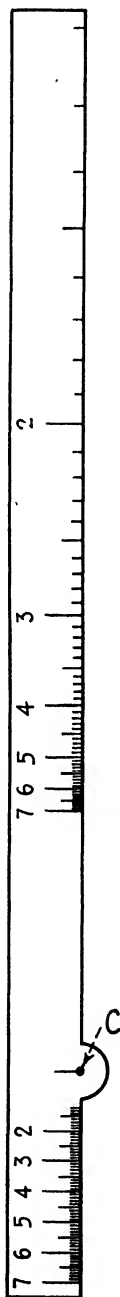


FIG. 5.—Ruler for plotting gnomonic projection of Laue spots. (Wyckoff.)

scattering that makes it possible to distinguish (111) from ( $\bar{1}\bar{1}\bar{1}$ ), etc., as has been demonstrated in experiments with zinc blende (ZnS).

<sup>1</sup> M. L. HUGGINS, *J. Optical Soc. Am.*, vol. 14, p. 55, 1927.

the zone  $[100]$ ; similarly, all spots with  $k = 0$  lie on the central horizontal line. The zone lines for  $h = 1$ ,  $h = 2$ ,  $k = 1$ ,  $k = 2$ , etc., form a coordinate network of squares that are 5 cm. on a side (if the projection sphere has a radius of 5 cm.). The indices of any spot can be read from this network by simply reading the two coordinates from the plot, assuming the third to be unity, and then clearing of fractions. For example, the spot  $R$  has coordinates  $2, -\frac{1}{2}, 1$  and indices  $4\bar{1}2$ .

When the crystal axes parallel to the plane of the projection are of unequal length, the network will still be orthogonal, provided that the crystal is orthogonal, but will be rectangular instead of square. With

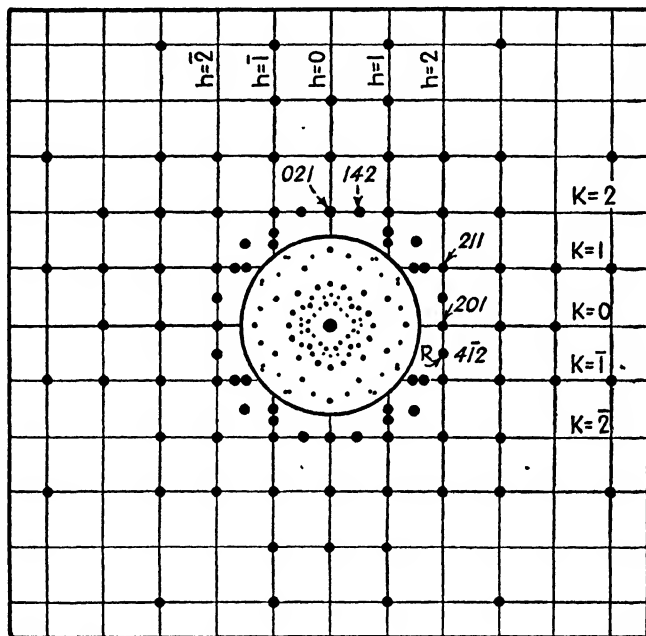


FIG. 6.—Gnomonic projection of Laue photograph of  $\text{MgO}$  (cubic). Photograph is within central circle. X-ray beam parallel to  $c$  axis.

the beam along the  $c$  axis of an orthorhombic crystal each rectangle will have the dimensions  $5c/a$  in the direction of the  $a$  axis and  $5c/b$  in the direction of the  $b$  axis. Similar principles hold for other orientations and other orthogonal axes. For example, if a crystal has  $a$  parallel to the beam, the network will have lines of constant  $k$  and  $l$  values that divide the projection into rectangles with sides  $5a/b$  and  $5a/c$ . Inclined axes, as in triclinic crystals, project into parallelograms on a gnomonic projection, and so both parallelograms and rectangles are encountered with projections of monoclinic crystals.

Converging lines replace parallel lines if a crystal is not oriented with the incident beam exactly along an axis. It is often possible to tell by inspection how much a crystal must be rotated to bring it from an

unsymmetrical to a symmetrical position. After the adjustment has been made, a second photogram should then yield a symmetrical pattern and a simple gnomonic projection. As an alternate procedure, Wyckoff<sup>1</sup> has used a gnomonic rotation net that rotates the gnomonic projection directly and eliminates the necessity for resetting the crystal.

**Analysis of Crystal Structure from Laue Photographs.**—After a gnomonic projection of a Laue photograph has been made, the crystallographer frequently cannot deduce immediately the unit cell in his crystal, for there are many cells of different size and orientation that could be chosen to account for the data. For example, in an orthorhombic crystal a unit cell could be chosen having any or all of its sides an integral multiple of the correct unit cell. The possible unit cells for other systems have been listed by Wyckoff.<sup>2</sup>

For each unit cell there is a new system of indices for the Laue spots. The correct unit cell among those possible is determined by measuring  $\theta$  and computing the value of  $\lambda$  for each spot from the appropriate Bragg equation. The correct unit cell will be the one for which the calculated values of  $\lambda$  will range down to the short-wavelength limit of the continuous spectrum but will not go below this minimum wavelength. In this test one must guard against being misled by a strong absorption edge in the crystal that might introduce a false minimum wavelength.

Laue photographs can be used to determine the relative intensities of the different reflections, but the procedure is difficult and the results are less accurate than can be obtained by other methods. There is first the difficulty introduced by the fact that the intensity in the continuous spectrum varies with wavelength. The photographic efficiency of the film also varies with wavelength. These two factors together produce an effective spectrum of the sort shown in Fig. 7. The absorption of the rays in passing through the specimen varies with the shape of the specimen and with the angle of diffraction. Finally there is the uncertainty introduced by the possibility that any given spot may be caused by the superposition of different orders of reflection.<sup>3</sup>

**The Shapes of Laue Spots.**—The shapes of the spots in a Laue pattern are determined by crystal imperfection and by geometrical conditions such as the nature of the convergence or divergence of the primary beam of x-rays. It is possible for patterns of polycrystalline samples to contain spots of such a nature that they give the pattern the

<sup>1</sup> R. W. G. WYCKOFF, *Am. J. Sci.*, vol. 50, p. 317, 1920.

<sup>2</sup> R. W. G. WYCKOFF, "The Structure of Crystals," 2d ed., pp. 143–145, Chemical Catalog Co., New York, 1931.

<sup>3</sup> This can be minimized by operating the tube at 50 to 60 kv. so that the maximum photographic effect lies between 0.48 and half this value, for then strong first- and second-order reflections cannot be obtained from any one plane.

appearance of a preferred orientation when actually there is only a random orientation of crystals in the sample. It is well, therefore, to have some understanding of the shapes frequently encountered. The

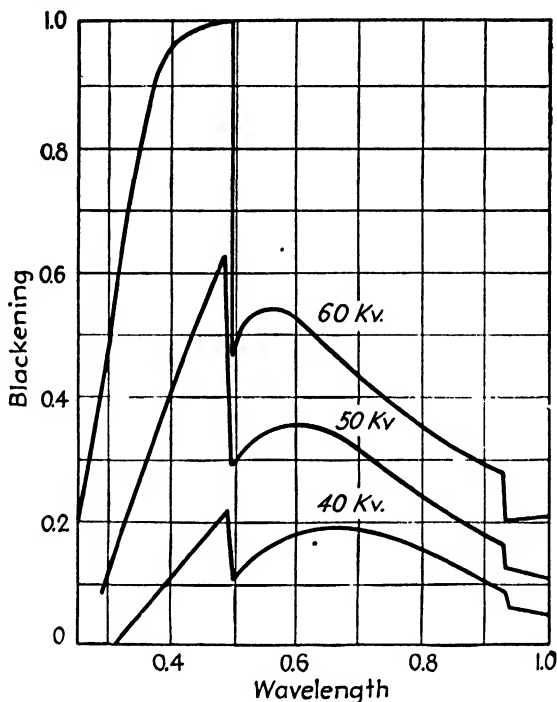


FIG. 7.—Photographic effect of white radiation from a tungsten tube at 40, 50, and 60 kilovolts. Discontinuities occur at K absorption edge of Ag and Br in the photographic emulsion. (Wyckoff.)

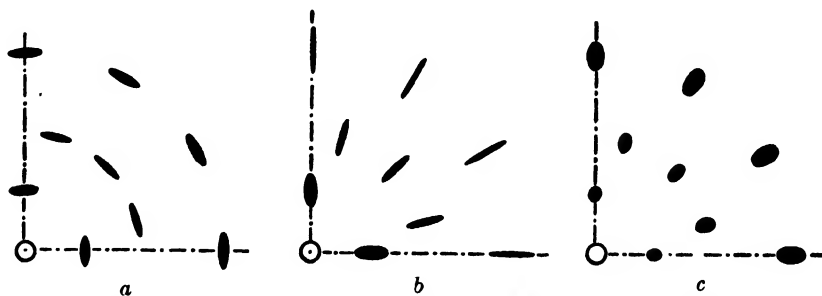


FIG. 8.—Laue spot shapes. *a*, divergent cone of x-rays striking large crystal; *b*, converging cone of x-rays striking large crystal; *c*, converging cone of x-rays striking small crystal.

discussion below applies to transmission Laue photographs of single crystals and polycrystalline samples.<sup>1</sup>

1. If the primary beam is a divergent circular cone of rays, as if it were originating at a point, and if the reflecting crystal covers the entire cone, then the Laue pattern will appear as in Fig. 8*a*. The spots will be

<sup>1</sup> J. LEONHARDT, *Z. Krist.*, vol. 63, p. 478, 1926.

elliptical with the minor axes of the ellipse radial. The ellipse will be smallest when the distance of the spot from the crystal is equal to the distance from the crystal to the point of origin of the conical incident beam, for the diffracted beams focus here. A small pinhole uniformly filled with rays can produce this type of pattern.

2. If the beam is a converging circular cone of rays, the spots will be elliptical, with their major axis radial, and the diffracted rays will diverge rather than come to a focus. If the crystal is large enough to fill the conical beam, the pattern will resemble Fig. 8*b*. On the other hand, if a very small crystal is located at the apex of a conical incident beam, the pattern will resemble Fig. 8*c*. The latter is very common in practice, because the individual grains of a polycrystalline specimen are so small they are effectively a point and the rays that pass a circular pinhole

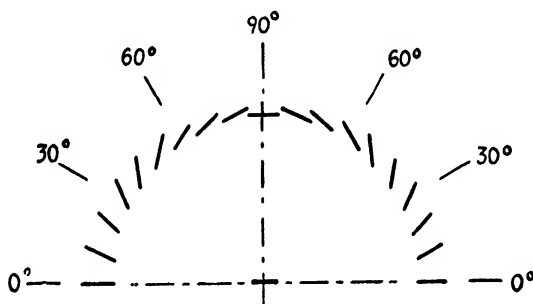


FIG. 9.—Laue spots from beam converging fanwise in a horizontal plane; small crystal.

effectively converge to this point (*i.e.*, all rays that are reflected by that grain do so).

3. If the beam converges fanwise, the spots will be streaks pointed in directions dependent on their azimuth around the central beam. The directions of the streaks for a beam that converges in the horizontal plane are plotted in Fig. 9. This condition is frequently encountered when an x-ray tube is used in which the target is horizontal and the camera is placed to take a beam that is going only slightly upward from the horizontal; the focal spot may then be foreshortened into a line which fills the pinhole openings in the camera horizontally but not vertically. The effect will be noted in the polycrystalline pattern of Fig. 10, although it is partly obscured by arcs from characteristic radiation (molybdenum  $K\alpha$  and  $K\beta$ ) that cut across the streaks.

4. Fanwise convergence with a large crystal is similar to Fig. 9 except that the streaks are longer near the  $0^\circ$  azimuth than near  $90^\circ$ .

5. Fanwise divergence with a large crystal gives shorter streaks near  $0^\circ$  than near  $90^\circ$  and somewhat different directions of streaks from those in Fig. 9.

Undesirable effects among the types listed above may be avoided by using pinholes that limit the beam to small convergence or divergence and by seeing that the pinhole system is completely filled with radiation. To test this, a fluorescent screen is placed at a considerable distance

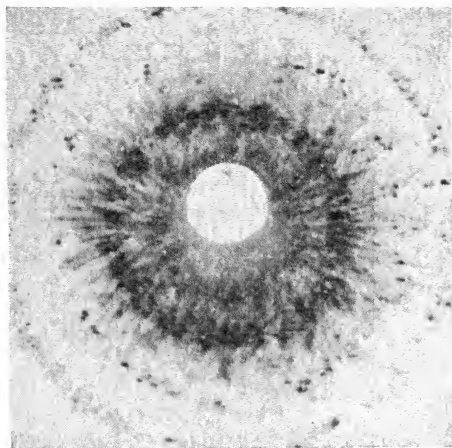


FIG. 10.—X-ray photograph illustrating shapes of Fig. 9. Molybdenum tube, annealed steel samples; beam from horizontal line focus incompletely fills circular pinholes.

from the pinhole system. If the pinholes are properly filled with radiation, the spot on the fluorescent screen will be circular rather than elliptical.

Laue spots from distorted and imperfect crystals produce “asterism,” which is superimposed on the above effects; this is discussed further in Chap. XVII.



## CHAPTER VI

### ROTATING-CRYSTAL METHODS

Crystal structures can be determined with greater certainty by using the rotating-crystal method and its modifications than by any other method. The apparatus can be very simple, as shown in Chap. IV

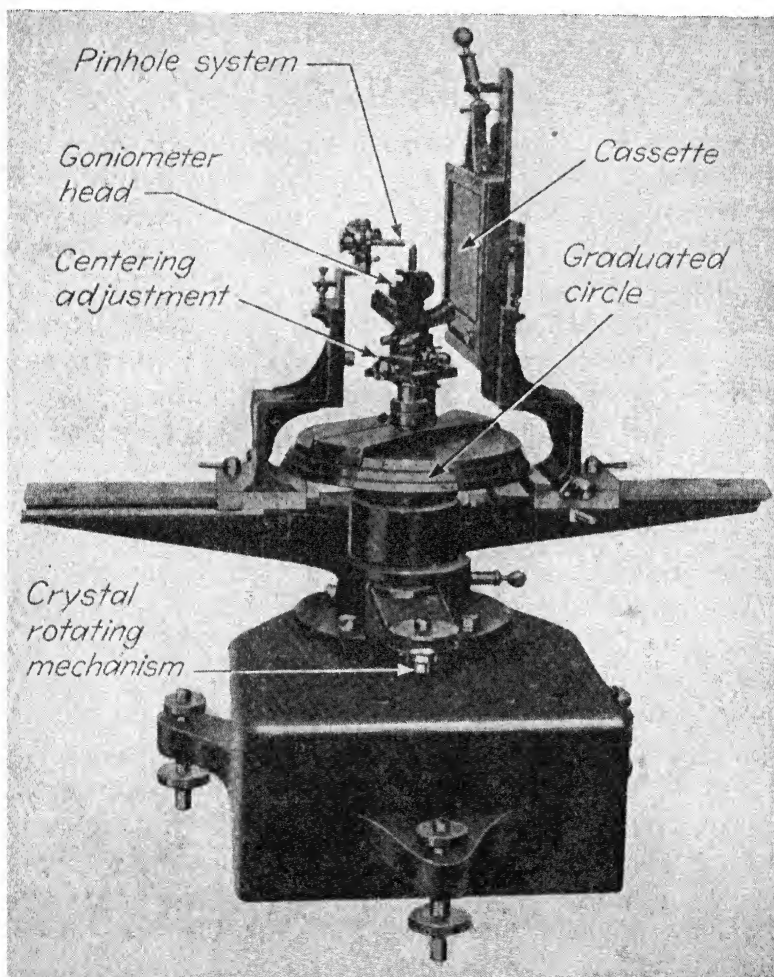


FIG. 1.—Bernal's universal camera set up with flat film. Cylindrical film holder is interchangeable. Base contains motor. (*W. G. Pye & Company.*)

(page 82), and consists essentially of a rotating spindle on which a single crystal is mounted, a cylindrical film around the crystal (the axis of the cylinder coinciding with the spindle axis), and a set of pinholes to

collimate the x-ray beam. It is essential to place an important zone axis of the crystal parallel to the axis of rotation, and for this purpose the apparatus should have a goniometer head that provides small angular and lateral adjustments of the crystal. A telescope and collimator are usually employed so that the small crystals (preferably 0.1 to 0.5 mm in average dimension) can be visually adjusted to a setting in which an important crystal edge lies along the axis of rotation, or the planes of an important zone lie perpendicular to the axis. Optical adjustment of the crystal is often supplemented by x-ray patterns; one or two Laue photographs serve to determine the orientation of the crystal and to predict the angle through which the crystal must be turned to reach the desired setting. Laue photographs can be made on the same instrument if an interchangeable film holder is used or on another camera to which the goniometer head can be transferred.

An elaborate universal camera has been designed by Bernal and marketed by W. G. Pye & Co. of Cambridge, England; it is shown with some of the attachments in Fig. 1. Any camera of the Weissenberg type is admirably suited to rotation and oscillation photographs. A number of suitable designs of this type have been published,<sup>1</sup> the most convenient probably being that of Buerger.<sup>2</sup> A low-temperature camera is described by Keesom and Taconis,<sup>3</sup> and a high-temperature camera by Goetz and Hergenrother.<sup>4</sup> The construction and operation of many types of stationary-film and moving-film cameras are covered in detail in Buerger's recent book.<sup>5</sup>

Long-wavelength radiation, such as copper  $K\alpha$  and  $K\beta$ , is desirable in order to gain high dispersion; it is unnecessary to employ a filter, for the  $K\beta$  spots are readily recognized from their position on the film.

**Interpretation of Rotation Photographs.**—Figure 2 is a typical rotation photograph showing prominent horizontal **layer lines** of spots and approximately vertical rows of spots (**row lines**). If a crystal is mounted for rotation around the  $a$ ,  $b$ , or  $c$  axis, the spacings of the layer lines give immediately the spacing between lattice points, the identity distance ( $a$ ,  $b$ , or  $c$ , respectively) in the direction of the rotation axis. This can be seen from the Laue equations, for each layer line is produced by diffracted rays forming the generators of a cone coaxial with the rotation axis (Fig. 3). The cone is actually the cone along which reinforcement occurs according to one of the three Laue equations, *viz.*, the Laue equa-

<sup>1</sup> K. WEISSENBERG, *Z. Physik*, vol. 23, p. 229, 1924. J. BOHM, *Z. Physik*, vol. 39, p. 557, 1926.

<sup>2</sup> M. J. BUEGER, *Z. Krist.*, vol. 94, p. 87, 1936.

<sup>3</sup> W. H. KEESOM and K. W. TACONIS, *Physica*, vol. 2, p. 463, 1935.

<sup>4</sup> A. GOETZ and R. C. HERGENROTHER, *Phys. Rev.*, vol. 40, p. 643, 1932.

<sup>5</sup> M. J. BUEGER, "X-ray Crystallography," Wiley, New York, 1942.

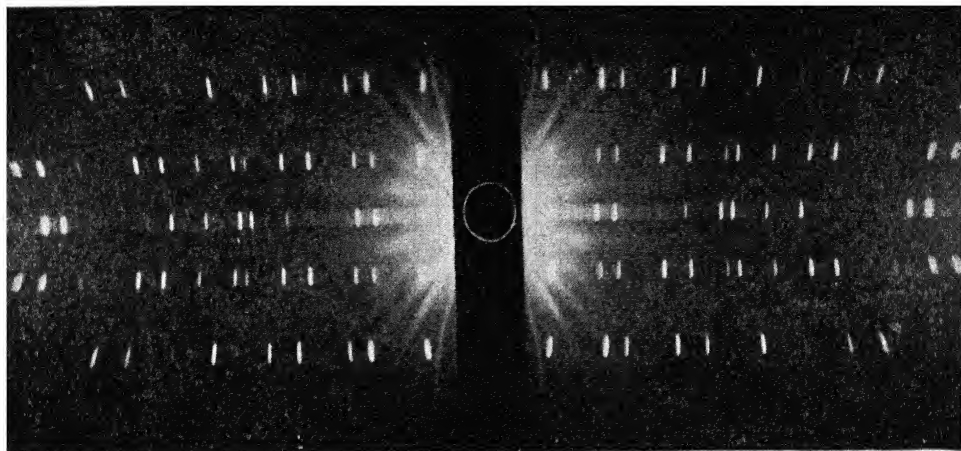


FIG. 2.—Rotating crystal pattern of quartz, cylindrical film. Axis of rotation vertical. Filtered radiation. (Warren.)

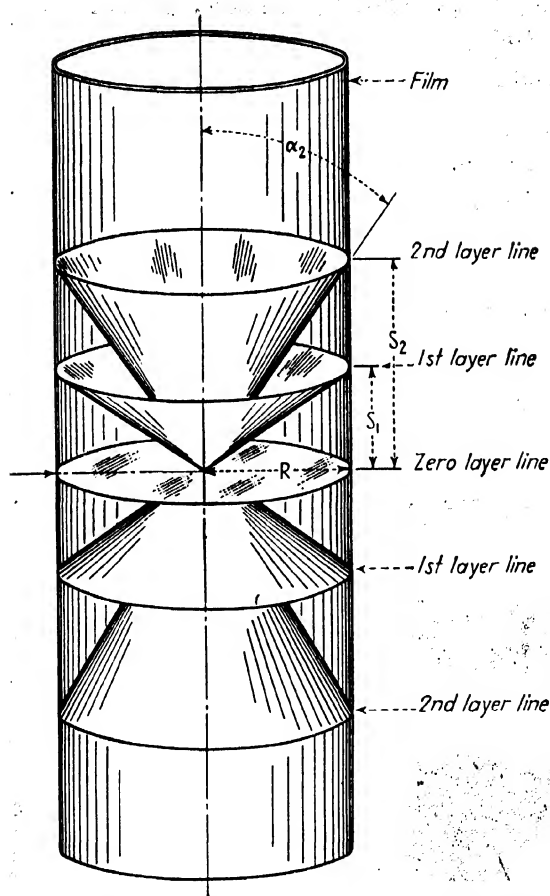


FIG. 3.—Formation of layer lines from cones of diffracted rays.

tion concerned with the periodicity along the axis of rotation. If the crystal is rotated around the  $a$  axis, the Laue equation that applies is

$$a(\cos \alpha - \cos \alpha_0) = h\lambda;$$

and if the incident beam is perpendicular to the axis of rotation, this reduces to

$$a = \frac{h\lambda}{\cos \alpha}$$

where  $a$  is the identity distance along the rotation axis,  $\alpha$  is the semiapex angle of the diffracted cone,  $\lambda$  is the wavelength, and  $h$  is an integer (the order of reflection for the cone) which is 0 for the horizontal layer line through the central spot, 1 for the first layer line above this, 2 for the second layer line, etc. Similar equations hold for rotation about any other direction in the crystal. We may therefore generalize the equation to apply to the identity distance in any direction that is chosen as the rotation axis, and if we insert the measured distance,  $S_n$ , on the film (Fig. 3) from the zero layer line to the  $n$ th layer line we have the formula

$$I = \frac{n\lambda}{\cos \alpha_n}$$

where  $\alpha_n$  is determined by the relation  $\cot \alpha_n = S_n/R$ ,  $R$  is the radius of the cylindrical film, and  $I$  is the identity distance in the chosen direction.

Perhaps the greatest advantage of the rotating-crystal method is the fact that the dimensions of the unit cell can be obtained unequivocally from photographs taken with each of the unit-cell axes in turn serving as the rotation axis. With other diffraction methods it is not uncommon to derive a unit cell that is half the true unit cell in some dimension. In rotation photographs this error could be made only by overlooking entire layer lines, which is easily avoided, particularly if attention is directed to the higher order layer lines. The precision of the determinations is usually about 1 percent and is much inferior to determinations by the powder method.

**Assigning Indices to Spots.**—Each spot on a rotation photograph satisfies not only the Laue equation discussed in the preceding section but also the two other Laue equations and consequently Bragg's law. Thus each spot is located on an invisible Debye ring for which the Bragg angle,  $\theta$ , is given by an appropriate formula (quadratic form) on page 77. Thus, indices can be assigned to the spots by the method of calculating the  $\theta$  values for all possible reflections and then comparing these calculated values with the ones read from the film by the aid of an appropriate chart.

A great advantage of the rotating-crystal method is its separation of the reflections into layer lines. Not only does this prevent some overlapping of reflections that would superimpose in powder photographs, but it makes assigning indices much easier. All planes that are parallel to the rotation axis reflect to the zero layer line. On a photograph with the  $a$  axis as the axis of rotation in the crystal these will be planes of the type  $(0kl)$ . Similarly planes of the type  $(1kl)$  will reflect to the first layer line above the central one,  $(2kl)$  to the second,  $(\bar{1}kl)$  to the first one below, etc. The general rule is that reflections on the  $n$ th layer line will have indices  $hkl$  that satisfy the equation

$$hu + kv + lw = n$$

where  $[uvw]$  are the indices of the axis about which the crystal is rotated.

**Identifying Face-centered and Body-centered Lattices.**—Rotating a crystal about the direction  $[110]$  gives the identity distance in this direction. If this is compared with the  $a$  and  $b$  dimensions of the cell, it will be evident at once whether the  $(001)$  face of the unit cell has a lattice point at its center or not. Similar photographs for  $[011]$ ,  $[101]$ , and  $[111]$  directions will disclose space lattices with  $a$  or  $c$  face-centered and body-centered lattices, respectively.<sup>1</sup>

**The Reciprocal Lattice.**—The indexing of spots on rotation photographs is nearly always done by methods based on the reciprocal lattice, a concept originally developed by Ewald<sup>2</sup> and applied to rotation photographs by Bernal.<sup>3</sup> The reciprocal lattice is the best basis for the analysis of many types of x-ray and electron diffraction patterns and results in such savings in time over other methods of solving diffraction patterns that it is indispensable to the research worker; many recent theoretical papers employ the concept extensively. It provides an easy visualization of the slopes of lattice planes in a crystal and at the same time shows the spacings of these planes. It is based on the use of a normal to each parallel set of planes, the direction of the normal indicating the orientation of the planes just as in the projections discussed in Chap. II. However, it goes further than the other projections in that the spacing of the set of planes is also indicated. This is accomplished by measuring off a certain distance along the normal.

The reciprocal lattice is a lattice of points, each of which represents a reflecting plane in the crystal and each of which is given the same indices as the corresponding reflecting plane. By "reflecting planes" is

<sup>1</sup> The type of space lattice can be determined also without taking these additional photographs if indices are assigned to all spots and "characteristic absences" noted. This is discussed in Chap. VIII.

<sup>2</sup> P. P. EWALD, *Z. Krist.*, vol. 56, p. 129, 1921.

<sup>3</sup> J. D. BERNAL, *Proc. Roy. Soc. (London)*, vol. A113, p. 117, 1926.

meant not only the true atomic planes with Miller indices such as  $(hkl)$ , but also the fictitious planes with spacings that are submultiples of these, which give the reflections in higher orders with indices that are multiples of the Miller indices. Each reciprocal lattice point is located on a line through the origin perpendicular to the corresponding planes of the crystal and at a distance from the origin inversely proportional to the spacing of these crystal planes. It is convenient in x-ray work to choose the constant of proportionality equal to  $\lambda$ , the wavelength of the x-rays used; the reciprocal relation is then

$$\rho = \frac{\lambda}{d}$$

where  $\rho$  is the distance from the origin to the reciprocal lattice point and  $d$  is the spacing of the corresponding planes in the crystal, as indicated in Fig. 4. By carrying out this construction for all other sets of

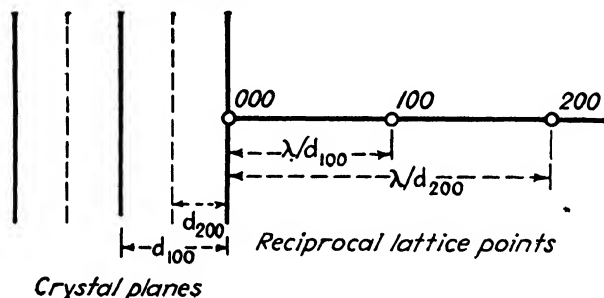


FIG. 4.—Relation between crystal lattice planes and their reciprocal lattice points.

crystal planes a three-dimensional lattice of reciprocal points is constructed representing all true and fictitious crystal planes.

The points of a reciprocal lattice always form a simple space lattice regardless of the type of space lattice possessed by the crystal that it represents. That is, the points lie at the corners of unit cells. If we designate the unit-cell edges in the reciprocal lattice by the starred quantities  $a^*$ ,  $b^*$ , and  $c^*$ , then the relation between these axial lengths and the crystal axial lengths  $a$ ,  $b$ ,  $c$ , and interaxial angles  $\alpha$ ,  $\beta$ , and  $\gamma$  will be given by the following equations:

$$a^* = \frac{\lambda bc}{V} \sin \alpha \quad \text{and is perpendicular to the } bc \text{ plane}$$

$$b^* = \frac{\lambda ac}{V} \sin \beta \quad \text{and is perpendicular to the } ca \text{ plane}$$

$$c^* = \frac{\lambda ab}{V} \sin \gamma \quad \text{and is perpendicular to the } ab \text{ plane}$$

where  $V$  is the volume of the unit cell in the crystal.<sup>1</sup>

<sup>1</sup> To derive these relations consider the volume of the unit cell,  $V$ , which equals

Several planes of a crystal lattice are illustrated by the solid lines and filled circles of Fig. 5. The dashed lines in this figure are drawn perpendicular to these planes and contain rows of open circles, the reciprocal lattice points. Along the  $a^*$  direction in the reciprocal lattice are the points 100, 200, 300, etc., which have coordinates  $a^*$ ,  $2a^*$ ,  $3a^*$ , etc. These correspond to the (100) planes in the crystal, which reflect in the first, second, and third order with reflection indices 100, 200, and 300. Similarly, all other planes in the crystal are represented in the different orders by other rows of points which extend out radially from the origin in reciprocal coordinate space. Along the  $b^*$  axis lie the points 010, 020, etc., and along the negative  $b^*$  axis lie  $0\bar{1}0$ ,  $0\bar{2}0$ , etc. All points of the reciprocal lattice have coordinates that are integral multiples of  $a^*$ ,  $b^*$ , and  $c^*$ . These integral multiples are both the coordinates of the

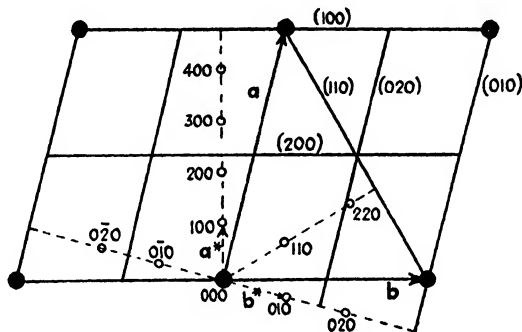


FIG. 5.—A portion of a single layer of a reciprocal ( $^{\circ}$ ) and crystal ( $\odot$ ) lattice, for a monoclinic crystal.

points and the indices of the points; thus the point having coordinates  $1a^*, 1b^*, 0$ , which in terms of the unit axes can be written  $110$ , has indices  $110$  and represents the  $110$  reflection.

In Fig. 5 a portion of one layer of the reciprocal lattice for a monoclinic crystal is shown; other layers will lie above and below the one shown and will have their points directly over or under these, the point  $hk1$  lying above the point  $hk0$  and the point  $hk\bar{1}$  lying immediately under it. This will also be true for all orthogonal crystals (cubic, tetragonal, orthorhombic, orthohexagonal). A perspective view of a typical reciprocal lattice for an orthogonal crystal is shown in Fig. 6.

**Diffraction and the Reciprocal Lattice.**—A simple geometrical construction in the reciprocal lattice gives the condition that corresponds to reflection. Consider a sphere that touches the origin of the lattice and that has a unit radius. Any crystal plane will reflect if the corresponding reciprocal lattice point lies on the surface of this sphere,

the area of the base of the cell times its altitude. In the first formula the area of the base is  $bc \sin \alpha$  and the altitude is  $d_{100}$ ; hence,  $d_{100} = V/(bc \sin \alpha)$  and since  $a^* = \lambda/d_{100}$  it follows that  $a^* = (\lambda bc/V)(\sin \alpha)$ .

provided that the diameter of the sphere is along the direction of the incident x-ray beam. This may be seen from Fig. 7, which represents

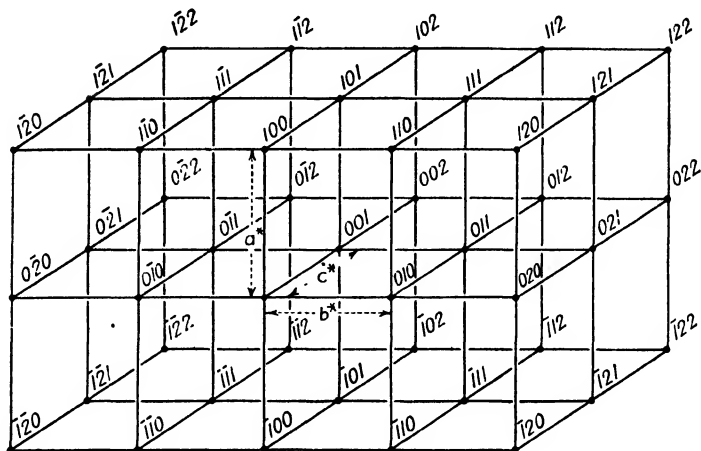


FIG. 6.—Reciprocal lattice for an orthorhombic crystal.

a set of crystal planes at  $O$  having its reciprocal lattice point at  $P$ , and an incident beam along  $QO$ . The “sphere of reflection” is drawn with  $QO$  as its diameter, the distance  $QO$  being twice the distance that has

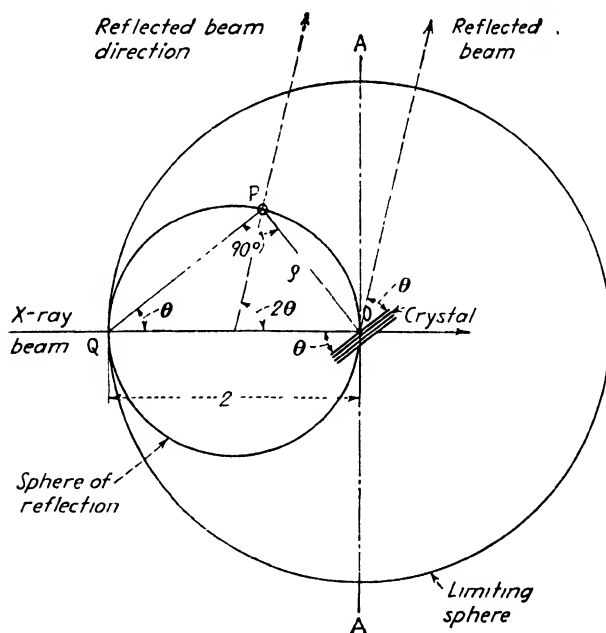


FIG. 7.—Sphere of reflection in a reciprocal lattice.

been chosen as the unit distance for plotting the reciprocal lattice. For example, if the scale used for  $\rho = 1$  is 1 cm. (so that a point for which  $\rho = \lambda/d = 1.26$  is plotted as 1.26 cm. on a plot of the reciprocal lattice),



the unit distance is 1 cm. and therefore  $QO$  is 2 cm. Now reference to the figure will show that the point  $P$  will lie on the sphere of reflection if

$$\sin \theta = \frac{\rho}{2},$$

and, upon substituting the value for  $\rho$ , this is seen to be equivalent to the condition for reflection as stated in Bragg's law

$$\sin \theta = \frac{\lambda}{2d}.$$

The reflected ray will lie in the plane with  $Q$ ,  $O$ , and  $P$ . The reflected beam will go out from the crystal at an angle  $2\theta$  from the incident beam,

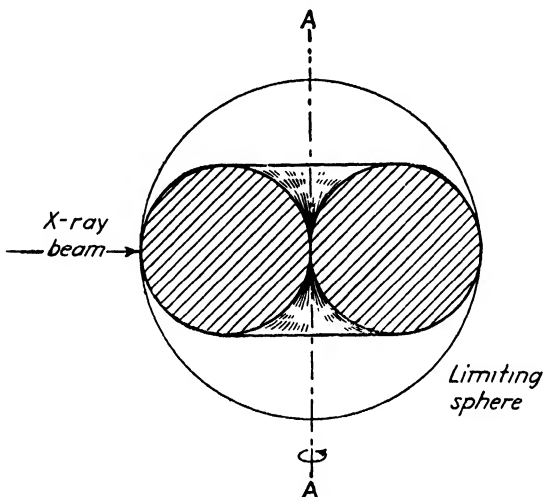


FIG. 8.—Section through tore swept out by sphere of reflection rotating through reciprocal lattice.

and from the construction of Fig. 7 it may be seen that the direction of the reflected beam is along the line from the center of the reflection sphere through the lattice point  $P$ .

At any one setting of the crystal, few if any points will touch the sphere of reflection, but if the crystal is rotated the reciprocal lattice will rotate with it and will bring many points into contact with the sphere. At each contact of a point with the sphere an x-ray reflection will occur. All planes that can be made to reflect have their reciprocal lattice points within two unit distances of the origin, *i.e.*, within the "limiting sphere" shown. Rotation of the crystal with respect to the beam can be represented by rotating the sphere of reflection and keeping the lattice fixed; if the axis of rotation is  $AA'$ , the sphere of reflection will sweep out a tore whose cross section is shown in Fig. 8. During a complete rotation of the crystal each point within this tore will pass through the surface of the

sphere twice and will produce two reflections, one on the right and one on the left side of the rotating crystal pattern. For each point  $hkl$  that yields spots in the upper quadrants of the film there will be a corresponding point  $\bar{h}\bar{k}\bar{l}$ , on the opposite side of the origin, that will also pass through the sphere twice and yield similar reflections in the lower quadrants of the rotation photograph. Thus if the axis of rotation is normal to the beam, the photograph will be symmetrical about horizontal and vertical lines through the center.

**Relation of the Reciprocal Lattice to the Film.**—Suppose the “limiting sphere” in Fig. 7 were a spherical photographic film. Rotation of the crystal would cause reflections which would be recorded on the film in a certain pattern. Now this pattern would be identical with the pattern

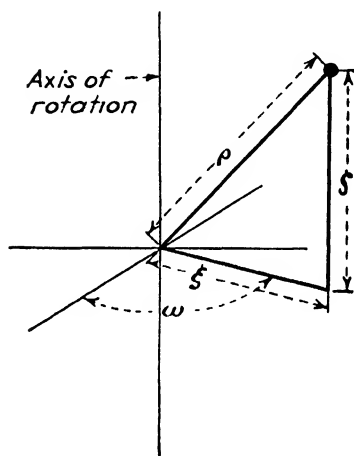


FIG. 9.—Cylindrical coordinates for reciprocal lattice points.

formed on the smaller “sphere of reflection” if each reciprocal lattice point, as it moves around the axis during the rotation, were to leave a spot where it touches the sphere of reflection. The film pattern could thus be interpreted as if the reciprocal lattice punctured it during rotation. In practice, of course, spherical films would be inconvenient and cylindrical or flat films are used, with the result that the pattern of reflected spots on the film is a distorted version of this pattern on the sphere. It is interesting to note, however, that, when the reflection sphere is very large compared with the spacings of the reciprocal lattice points, then the portion of the sphere near the origin is almost a plane surface. The pattern on the sphere is then like the pattern on a flat film. This is the situation when electrons of very short wavelength are diffracted; the electron diffraction pattern on a flat film appears to be made by swinging the film through the reciprocal lattice.

To relate spots on a film to points in the reciprocal lattice it is best to use the **cylindrical coordinates** of the lattice points. These coordinates are indicated in Fig. 9 where  $\xi$  (xi) is the perpendicular distance from the axis of rotation to a lattice point,  $\zeta$  (zeta) is the distance parallel to the axis from the origin to the point, and  $\omega$  (omega) is the angular position with respect to some reference line. Since  $\omega$  acquires all values during a complete rotation, this coordinate is not determined in a rotation photograph, but  $\xi$  and  $\zeta$  can be computed for each lattice point by measurements of the position of the corresponding spot on the film.

The  $\xi$  and  $\zeta$  coordinates can be found quickly, without computation, by superimposing the film on a chart of appropriate size ruled with lines of constant  $\xi$  and  $\zeta$  values. Figure 10 is a chart of this type for cylindrical

films of 57.3 mm. diameter.<sup>1</sup> Other camera sizes can be fitted by suitable enlargement. The chart covers  $\xi$  values from 0 to 1.6 and  $\zeta$  values from 0 to approximately 0.9.

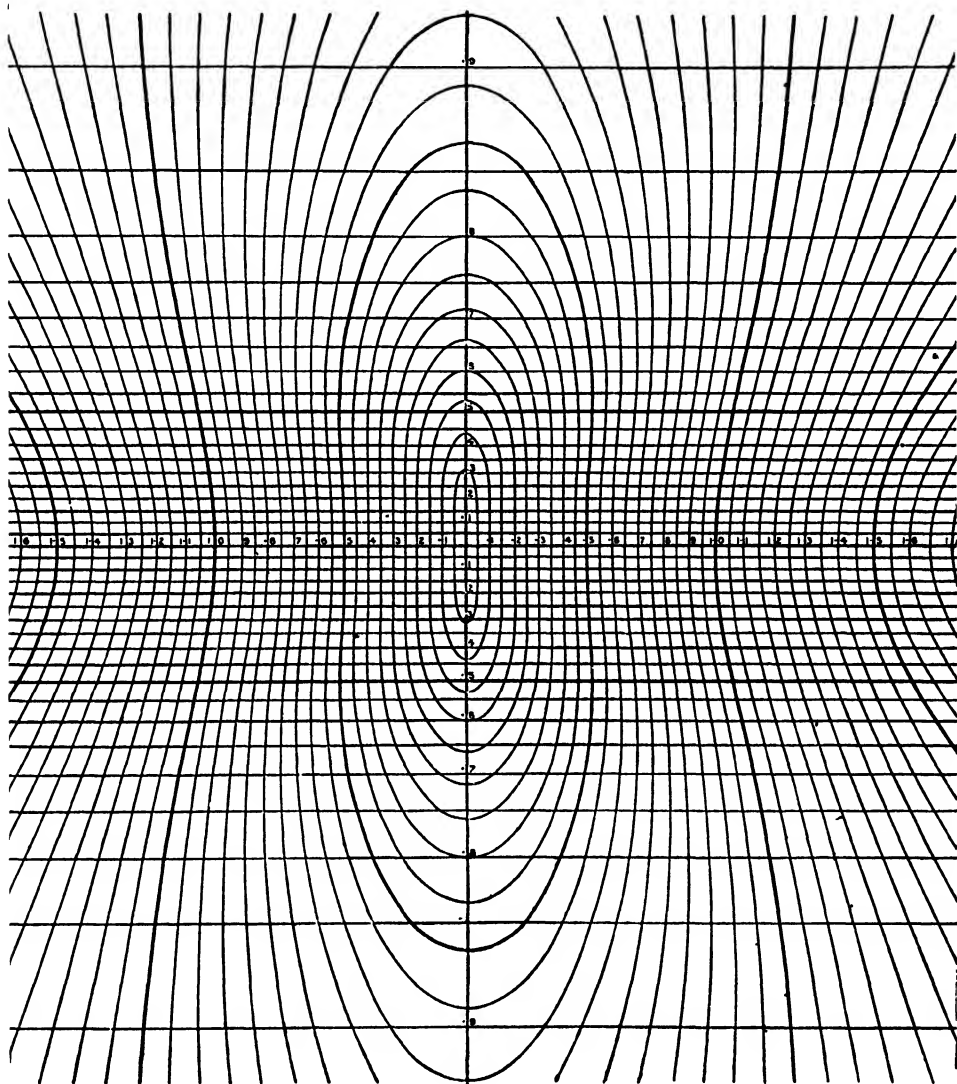


FIG. 10.—Bernal's chart for reading reciprocal lattice coordinates  $\xi$  and  $\zeta$  from cylindrical films. Scaled to fit camera of 57.3 mm. diameter. Layer lines run horizontally on this chart.

**Determining Unit-cell Dimensions.**—The cell dimensions are readily determined for any crystal that yields layer lines when rotated about its  $a$ ,  $b$ , and  $c$  axes (cubic, tetragonal, orthorhombic, orthohexagonal). The

<sup>1</sup> J. D. Bernal has published this chart on tracing paper for a 10-cm.-diameter camera and has published also a chart for flat films [*Proc. Roy. Soc. (London)*, vol. A113, p. 117, 1926].

points in a single layer of the reciprocal lattice have a constant  $\zeta$  value and form one layer line on the film. Since the axes of the reciprocal lattice for these crystals are parallel to the crystal axes, it follows that a rotation photograph with rotation around the  $a$  axis has a succession of layer lines at  $\zeta$  values corresponding to the  $a^*$  spacing of the layers in the reciprocal lattice, so that

$$\zeta_a = ha^* = \frac{h\lambda}{a}$$

where  $h = 1$  for the first layer line, 2 for the second, etc. Similarly, for rotation around  $b$ ,

$$\zeta_b = kb^* = \frac{k\lambda}{b};$$

and, for rotation around  $c$ ,

$$\zeta_c = lc^* = \frac{l\lambda}{c}.$$

Therefore, the  $a$  dimensions of the unit cell can be determined unequivocally from the  $\zeta$  values read by means of the chart from the layer lines of an  $a$  rotation photograph. By choosing the rotation axes along  $a$ ,  $b$ , and  $c$ , in turn, all dimensions of the cell are determined.

**Assigning Indices to Reflections.**—The relations between reciprocal lattice coordinates and indices of reflections are simple if the crystal has orthogonal axes (cubic, tetragonal, orthorhombic, or orthohexagonal) and is rotated around these. First the  $a^*$ ,  $b^*$ , and  $c^*$  dimensions of the reciprocal lattice are determined by the equations of the previous section. These data make it possible to plot the reciprocal lattice (this is usually done a layer at a time). Indices are assigned to each of the points in the lattice in the simple manner that has been illustrated in Fig. 6. Then the  $\xi$  and  $\zeta$  coordinates of the spots on the film are compared, graphically, with  $\xi$  and  $\zeta$  coordinates of points on the plot. A spot on the film is identified when a point is found that has the same coordinates as the spot; the indices of the spot and its corresponding point are the same. Instances sometimes occur in which two or more reciprocal lattice points have the same  $\xi$  and  $\zeta$  coordinates, and the corresponding reflection may have the indices of any of these—or all of these if reflections have overlapped.

An alternate method of assigning indices to reflections is to compute the  $\xi$  and  $\zeta$  values.<sup>1</sup> The increased accuracy of computed over graphically measured values is seldom needed, however.

<sup>1</sup> For an orthogonal crystal rotated about the  $a$  axis,

$$\begin{aligned}\zeta_a &= ha^* \\ \xi &= \sqrt{k^2b^{*2} + l^2c^{*2}},\end{aligned}$$

and similar equations apply to rotation photographs around  $b$  and  $c$  axes. Formulas

The reciprocal lattice layers of monoclinic and triclinic crystals do not lie directly over each other;  $a^*$  is not at right angles to  $b^*$  and  $c^*$ . Hence the rotation axis, which is the origin of  $\xi$  coordinates and passes through the point 000, does not pass through the points 100, 200, etc., on the upper levels. This must be taken into account in working out the coordinates.

**Oscillating-crystal Photographs.**—One method of avoiding overlapping reflections, which lead to uncertainties in indexing and in determining the intensities of reflections, is to limit the range through which the crystal is rotated. This reduces the number of reciprocal lattice points that come into contact with the reflection sphere and so reduces the number of reflections. The crystal is set as for a rotation photograph, and with a known face exactly perpendicular to the x-ray beam the crystal is oscillated through a 5, 10, or 15° range of angles around this position; by means of an azimuth circle on the camera a new azimuth setting is made and a new oscillation photograph is made around it, etc., until all typical reflections have been obtained. The ranges of oscillations are made small enough to prevent overlapping spots.

A graphical construction predicts which reflections will occur, by showing which reciprocal lattice points touch the sphere of reflection. Assume, for convenience, that the reciprocal lattice remains stationary while the x-ray beam and the reflection sphere revolve around the axis of rotation in the sense opposite to the actual crystal rotation. The sphere swings through the angle of oscillation and sweeps out two cup-shaped regions in reciprocal space, instead of the entire torus as it would in a rotation photograph. Figure 11 illustrates an oscillation of 30° about the  $a$  axis of an orthogonal crystal. The reflection circle has  $XO$  and  $X'O$  as diameters at the extremities of its oscillation. The reciprocal lattice plane containing the origin cuts the sphere of reflection in a circle of unit radius that sweeps through the shaded areas of Fig. 11a. All points lying in the shaded areas correspond to planes that will reflect in the oscillation photograph; and since these points are on the layer for which  $h$  is everywhere zero, all these reflections will fall on the zero layer line on the photograph—the equatorial layer line.

Points on one of the layers above this one will lie on a plane that intersects the sphere of reflection in a circle of smaller radius. A side view of the sphere of reflection is shown in Fig. 11b, where it will be seen that the radius of the circles for these higher sections can be readily scaled from the drawing or computed analytically and varies with each value of  $\zeta$ . To determine the possible reflecting planes for the second layer line the construction of Fig. 11c is used. Here it is assumed that

---

for less symmetrical crystals are given in J. D. Bernal, *Proc. Roy. Soc. (London)*, vol. A113, p. 117, 1926.



because of crystal imperfection and angular divergence in the primary beam of x-rays.

In an interesting variation of the oscillating-crystal method Buerger rocks a crystal in such a way that a crystal axis sweeps over the surface of a cone coaxial with the incident beam. The pattern obtained on a stationary film is then an almost undistorted picture of the reciprocal lattice; the diffraction spots can be assigned indices by inspection, without computation; and the symmetry of the photograph is the symmetry of the crystal axis that oscillates about the direct beam.

**The Weissenberg Goniometer.**—An ingenious camera first designed by Weissenberg<sup>1</sup> completely eliminates overlapping reflections and has other advantages as well, making it highly desirable for the analysis of complex crystals. The principle of the instrument is illustrated by Fig. 12. A cylindrical film, *F*, moves back and forth longitudinally in exact synchronism with the oscillation of the crystal; this is accomplished by a pulley arrangement, as indicated, or by an appropriate set of gears. A stationary metal shield, *S*, surrounds the crystal and contains a circumferential slot that permits the recording of a single layer line of spots at one setting. The shifting of the film during the oscillation of the crystal causes the spots from a single layer line to be spread out over the whole of the film (Fig. 13). The vertical distance between two spots of Fig. 13 is directly proportional to the angle through which the crystal turns in going from one reflecting position to another.

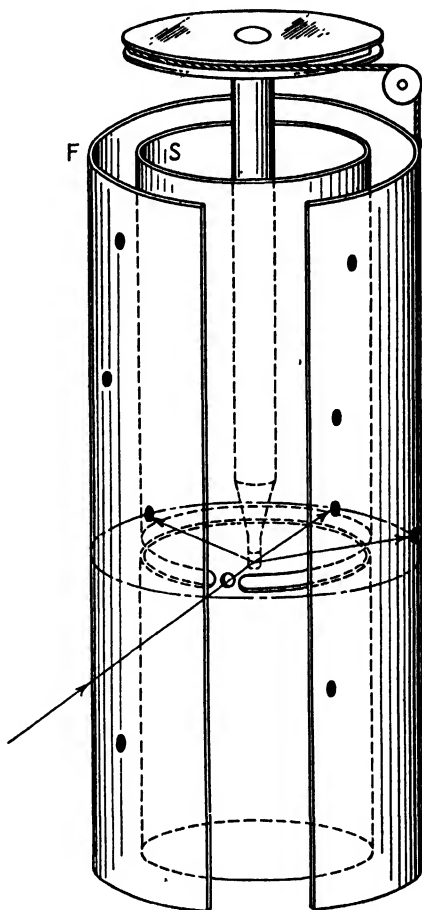


FIG. 12.—Illustrating the principle of the Weissenberg x-ray goniometer.

The indexing of spots on Weissenberg photographs has been worked out in various ways.<sup>2</sup> In the method of Wooster and Wooster<sup>3</sup> the polar

<sup>1</sup> K. WEISSENBERG, *Z. Physik*, vol. 23, p. 229, 1924. J. BOHM, *Z. Physik*, vol. 39, p. 557, 1926.

<sup>2</sup> For a detailed treatment of moving-film techniques and methods of interpretation see M. J. Buerger, "X-ray Crystallography," Wiley, New York, 1942.

<sup>3</sup> W. A. WOOSTER and NORA WOOSTER, *Z. Krist.*, vol. 84, p. 327, 1933.

coordinates ( $\xi$ ,  $\omega$ ) of the spots are read from a chart that is laid over the film, and the reciprocal lattice is constructed graphically ( $\zeta$  is determined

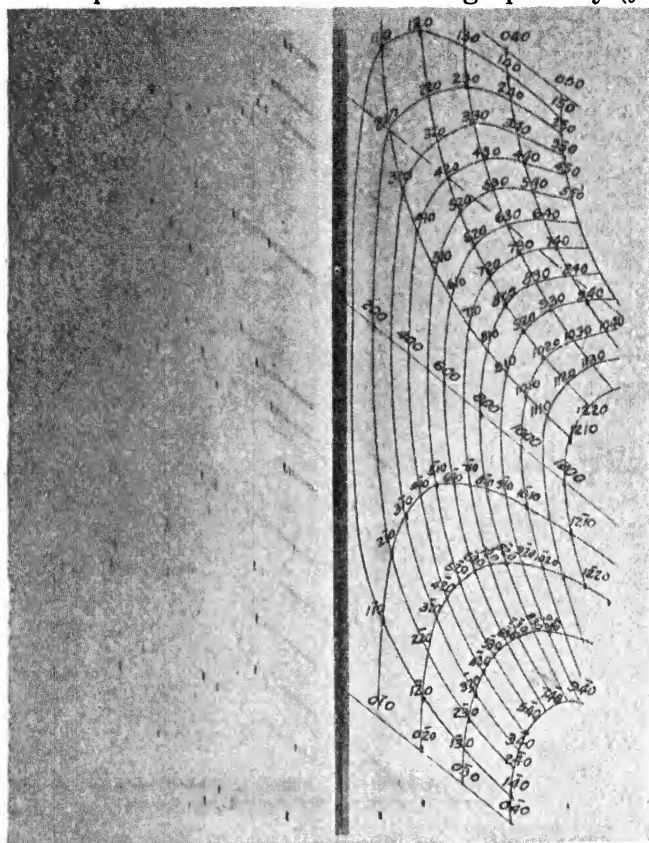


FIG. 13.—Weissenberg photograph of a monoclinic crystal rotated about the  $c$  axis, with unfiltered copper radiation. Lines along which one index changes are sketched at right.

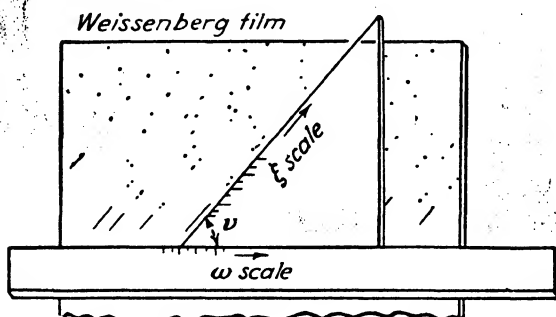


FIG. 14.—Buerger's method for reading Weissenberg films.

when the layer line is chosen; it is the same for all spots of one photograph). In the reciprocal lattice any row of points that passes through the origin is represented on the film as a straight line of spots. The



inclination,  $\nu$ , of the line to the longitudinal direction on the film is

$$\nu = \tan^{-1} \left( \frac{\text{circumference of camera}}{\text{translation for } 180^\circ \text{ rotation}} \right).$$

These lines on the film are marked out by white radiation streaks and are the lines that contain different orders of reflection from a single plane.

Buerger constructed a reading device (see Fig. 14) that slides over the film and provides convenient scales for reading spot coordinates. A celluloid triangle with an angle  $\nu$  slides along a ruler on which the azimuth coordinate  $\omega$  has been marked (the coordinates are those of Fig. 9). Along the edge of the triangle is marked a scale that gives  $\xi$  values when the edge is made to touch a spot; the  $\omega$  value for the spot is then read from the intersection of the edge of the triangle with the  $\omega$  scale. One  $\xi$  scale applies to all zero layer-line photographs, but for nonzero layer-line photographs other scales of  $\xi$  must be marked on the triangle.

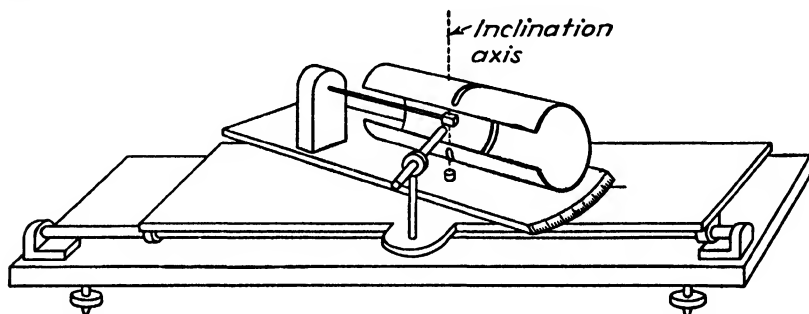


FIG. 15.—Simplified sketch of Buerger's design for Weissenberg camera, with variable inclination of rotation axis.

In making photographs of the higher layer lines, Buerger has pointed out the convenience of adjusting the incident beam so that both incident and diffracted beams make equal angles with the axis of rotation, giving what is termed an **equi-inclination photograph**. Figure 15 is a diagrammatic sketch of his equi-inclination camera (rotating and shifting mechanisms are not indicated).

A Weissenberg photograph is simply a two-dimensional projection of one of the reciprocal lattice levels. The rows of points of the reciprocal lattice appear in a distorted form on the photograph and can be recognized with experience or with the aid of appropriate charts.<sup>1</sup> (Note the lines of constant  $k$  and  $l$  indices in Fig. 13.) When the lines are recognized on the film, indexing of spots can be done simply by inspection and is a matter of five minutes or so as compared with an hour or two by the method of Wooster and Wooster. In equi-inclination photographs the

<sup>1</sup> M. J. BUEGER, *Z. Krist.*, vol. 88, p. 356, 1934; "X-ray Crystallography," Wiley, New York, 1942.

rows of reciprocal lattice points fall on curves of similar shape on the films for all layers of the reciprocal lattice. Hence a single transparent template can be employed to mark the rows on the film.<sup>1</sup>

Sauter<sup>2</sup> designed a camera in which a flat film is rotated instead of being shifted, as in the Weissenberg camera. It is inferior to the Weissenberg camera because some reflections cannot be picked up. The **de Jong-Bouman camera**<sup>3</sup> also has blind areas where reflections cannot be obtained, but it has the remarkable characteristic that a photograph made in the camera is a direct enlargement, without distortion, of a level of the reciprocal lattice. To accomplish this desirable result, the camera is provided with a flat film that rotates in its own plane in synchronism with the rotation of the crystal. The axis of rotation of the film is parallel to the axis of rotation of the crystal but is displaced from it by such an amount that the center of film rotation is at the origin of the reciprocal lattice layer being photographed. A shield between crystal and film absorbs all but one layer line of reflections, as in the other moving-film cameras.

<sup>1</sup> In a further development of Weissenberg photograph technique M. J. Buerger shows that it is possible to determine the space-lattice type and the space group of a crystal by the simple inspection of a properly chosen set of Weissenberg photographs, without indexing any of the spots. This is possible by recognizing the symmetry properties of the reciprocal lattice from the appearance of the photographs. There are 15 possible types of spot arrangements in equi-inclination photographs, which have been catalogued and related to the possible arrangements of reciprocal lattice points in a given level. From a series of equi-inclination Weissenberg photographs it is possible to recognize not only the arrangement of points in a level but also the stacking of the levels over one another; glide planes and screw axes are also recognized.

However, there are limitations to space-group determination by diffraction data alone; for example, a simple monoclinic crystal would give the same pattern of spots whether it belonged to space groups  $Pm$ ,  $P2$ , or  $P2/m$ ; space group  $I222$  cannot be distinguished from  $I2_12_12_1$ , nor  $I23$  from  $I2_13$ ; left-handed screw axes cannot be distinguished from right-handed screw axes. A total of 121 diffraction pattern types is possible out of the 230 space groups.

<sup>2</sup> E. SAUTER, *Z. Krist.*, vol. 84, p. 461, 1933; vol. 85, p. 155, 1933; *Z. Physik. Chem.*, vol. B23, p. 70, 1933. F. SCHIEBOLD, *Z. Krist.*, vol. 86, p. 377, 1933.

<sup>3</sup> W. F. DE JONG and J. BOUMAN, *Z. Krist.*, vol. 98, p. 456, 1937-1938; *Physica*, vol. 5, pp. 220, 817, 1938. See also discussion in M. J. Buerger, "X-ray Crystallography," Wiley, New York, 1942.

## CHAPTER VII

### THE POWDER METHOD

The powder method, devised independently by Debye and Scherrer<sup>1</sup> and by Hull,<sup>2</sup> is by far the most useful method in the field of applied x-rays. Many special cameras and techniques have been developed, and it well repays the user to keep informed of the more important advances as they appear. A comprehensive treatment of all the past developments in the field is neither possible nor desirable here, but an attempt is made

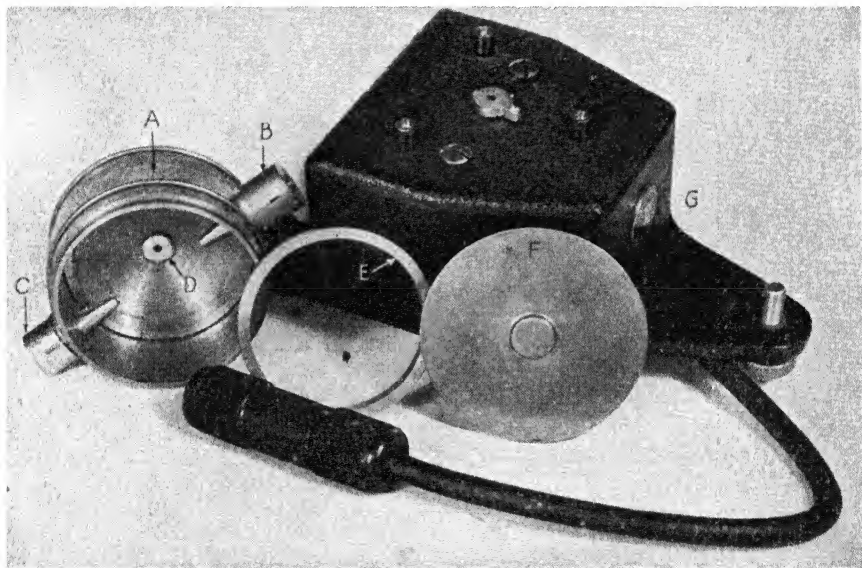


FIG. 1.—Powder camera. *A*, camera; *B*, cap with pinholes for incident beam; *C*, cap over exit hole; *D*, rotating spindle for specimen; *E*, ring for clamping film; *F*, cover; *G*, base with motor for rotating specimen. (*Baird Associates.*)

to cover the more important ones that are now in widespread use. The fundamental principles of the method have been presented in Chap. IV and need not be repeated here.

**Cylindrical Cameras.**—Figure 1 illustrates a typical Debye-Scherrer camera.<sup>3</sup> The incident beam enters the chamber *A* through pinholes in cup *B* and on the exit side is trapped by a tube *C* in which a fluorescent

<sup>1</sup> P. DEBYE and P. SCHERRER, *Physik. Z.*, vol. 18, p. 291, 1917.

<sup>2</sup> A. HULL, *Phys. Rev.*, vol. 10, p. 661, 1917.

<sup>3</sup> Manufactured by Baird Associates, Cambridge, Mass.

screen may be mounted to aid in lining up the camera. The specimen is accurately centered in the camera on an axis  $D$  that can be rotated by a motor in the base  $G$ . The film is inserted in a slot and clamped in such a way that it conforms accurately to the circumference of the brass cylinder. Holes are punched in the film so that it will fit over the projecting tubes.

Another instrument is illustrated in Fig. 2.<sup>1</sup> A wedge-shaped specimen can be rocked by the motor fastened to the side of the instrument;

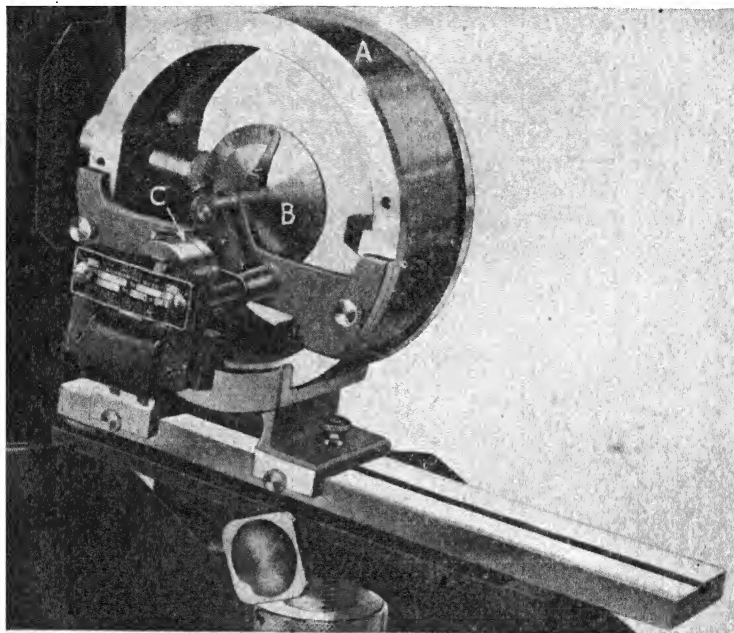


FIG. 2.—Powder camera arranged for oscillation of a wedge specimen.  $A$ , cylindrical film and cover;  $B$ , specimen mount;  $C$ , motor for oscillating specimen. (*General Electric X-ray Corporation.*)

another specimen mount, interchangeable with this, provides complete rotation of the specimen, and a septum can be used so that two spectra can be photographed side by side.

A camera<sup>2</sup> developed in Sir Lawrence Bragg's laboratories is sketched in Fig. 3. The customary cylindrical film is replaced by two semicircular films that extend from the inlet tube on the left to the outlet on the right (Fig. 3a). Knife-edges at these two ends furnish an abrupt end to the fogged region on the film and thus furnish reference marks from which diffraction angles can be measured. Figure 3b shows the inner part of the camera around the edge of which the film is held by elastic bands.

<sup>1</sup> Sold by General Electric X-ray Corporation, Chicago, Ill.

<sup>2</sup> A. J. BRADLEY, W. L. BRAGG, and C. SYKES, *J. Iron Steel Inst.*, vol. 141, p. 63, 1940. A. J. BRADLEY, H. LIPSON, and N. J. PETCH, *J. Sci. Instruments*, vol. 18, p. 216, 1941.

A lightproof case (Fig. 3c) fits over the internal part and provides for rotation of the specimen; the slits and the thumbscrew centering device for the specimen are indicated in Figs. 3d and 3e, respectively.

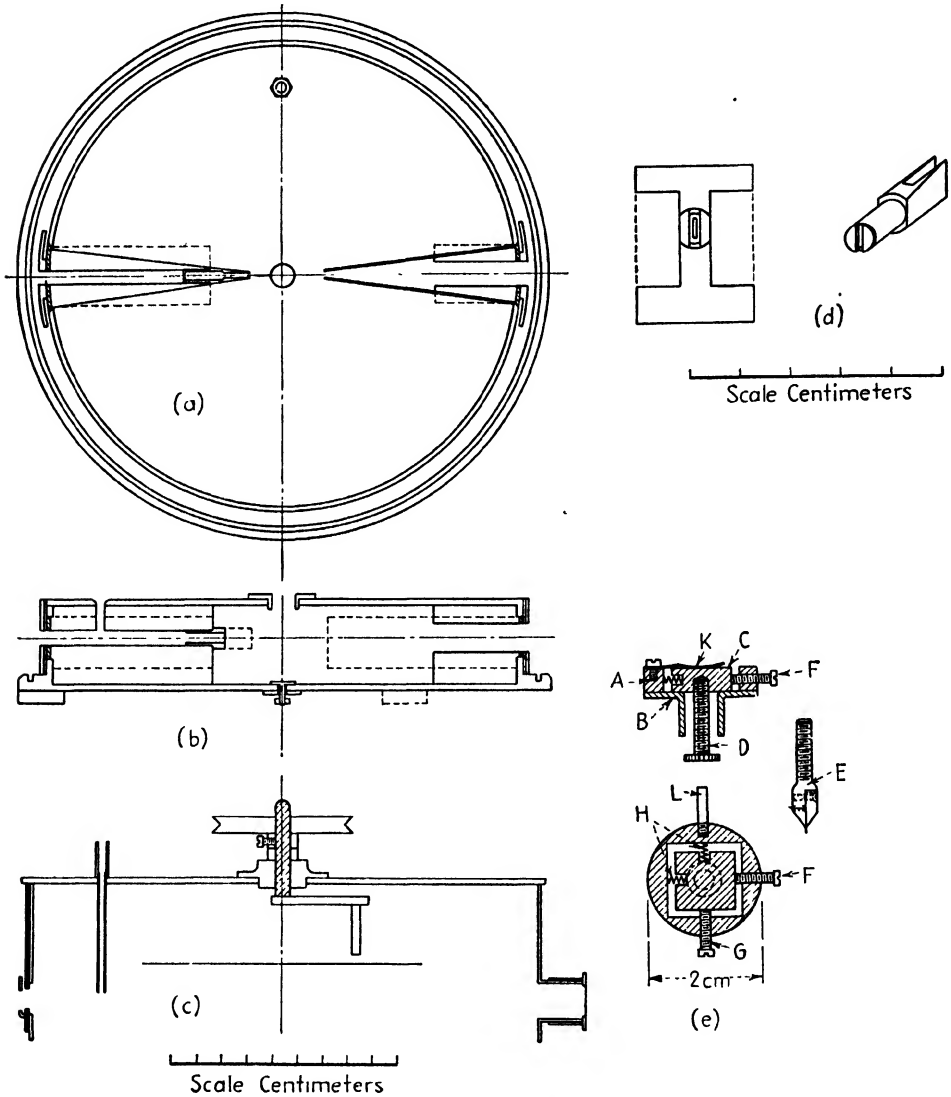


FIG. 3.—Powder camera designed by Bradley and collaborators. (a) Horizontal section of camera, (b) vertical section, (c) lighttight cover with pulley and arm to rotate specimen mount, (d) slit system, (e) specimen mount with screws F and G for centering specimen.

The slit arrangement in any camera is important. There should be three openings properly cut and spaced so that the first two limit the divergence of the beam and the last one just misses the beam but stops the diffracted rays arising from the metal at the second opening, as

indicated in Fig. 4. If rays are taken from a target at grazing angle so that they effectively diverge from a line source, the first slit of Fig. 4 is unnecessary.

The usual specimen for Debye cameras is a thin-walled capillary tube 0.3 to 0.5 mm. in diameter of lithium borate glass, silica, or cellophane, which is filled with powder that has been passed through a sieve of about 250 mesh. Davey<sup>1</sup> has recommended diluting the more absorbent specimens with amorphous materials like wheat flour, the amount of dilution increasing with the atomic number of the specimen to keep the linear-absorption coefficient in the powder about constant. Excellent specimens can be prepared by mixing powder with collodion, dilute shellac, or the like, packing it into a small tube, and then extruding it by pushing a wire through the tube. Small-bore stainless-steel tubes can be purchased for the purpose,<sup>2</sup> and if the mixture is only partly extruded

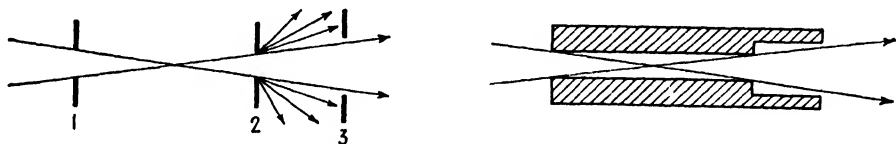


FIG. 4.—Design of slits. Primary beam through openings 1 and 2 should not touch 3.

from these they will serve as excellent mounts to fasten into the camera. Powders can also be coated on a fine fiber using an adhesive.

A polycrystalline solid formed into a wire may be used in Debye cameras, but these must be used with caution owing to the preferred orientations that are likely to be generated in the wire by the forming process. If a block of material has a sharp edge, this can be placed so as to cut across the beam from the slits and provide a thin line of diffracting material—the so-called “wedge technique.” The purpose of oscillating or rotating a specimen is to reduce spottiness of the diffraction rings by bringing a greater number of particles into reflecting positions.

Cameras have been specifically designed for flat sheet specimens<sup>3</sup> and for other special shapes, but they are not in general use. Some investigators have mounted a rock salt crystal as a monochromator on Debye cameras. This is advantageous for work with vitreous materials as it reduces the background blackening markedly and renders weak and diffuse lines more visible, but unfortunately it multiplies the exposure times manyfold.

<sup>1</sup> WHEELER P. DAVEY, “A Study of Crystal Structure and Its Applications,” p. 117, McGraw-Hill, New York, 1934.

<sup>2</sup> The Superior Tube Co., Norristown, Pa., is one source; 19-gauge  $\frac{1}{8}$ -in. lengths are convenient.

<sup>3</sup> R. A. STEPHEN and R. J. BARNES, *Nature*, vol. 136, p. 793, 1935. J. C. M. BRENTANO, *Proc. Phys. Soc. (London)*, vol. 47, p. 932, 1935.

**Choice of Camera Dimensions.**—For rapid exposures and for materials of poorly developed crystallinity a small camera is favored, usually one of about 5 cm. diameter, but for complicated patterns or other problems where high dispersion is required it is better to use larger ones. A camera of 19 cm. diameter ( $\theta = 5$  to  $85^\circ$ ) is useful in alloy studies,<sup>1</sup> and cameras of even 35 cm. diameter serve for occasional special problems.

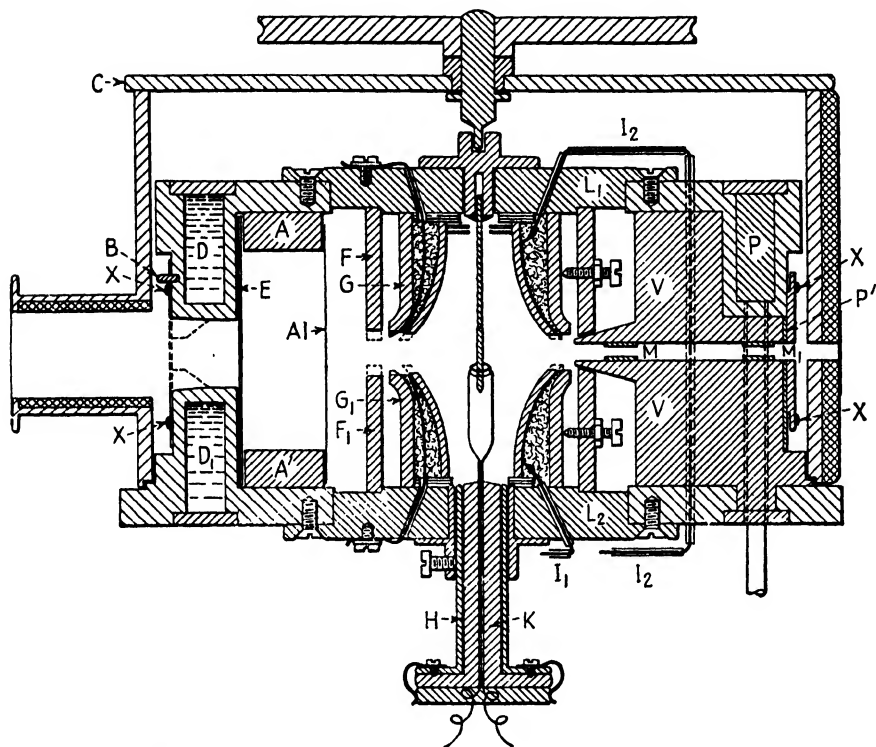


FIG. 5.—High-temperature powder camera. (Hume-Rothery and Reynolds.)

The exposure time increases roughly as the cube of the diameter, and in addition it is advisable to fill the largest cameras with hydrogen to reduce absorption and scattering from the air, yet these disadvantages are frequently overcome by the advantage of greater contrast between background and lines and greater dispersion.<sup>2</sup>

**High-temperature Cameras.**—A number of designs have been published for cameras that operate with the specimen at an elevated temperature.<sup>3</sup> One of the most suitable designs for precision work is that of

<sup>1</sup> A. J. BRADLEY, W. L. BRAGG, and C. SYKES, *J. Iron Steel Inst.*, vol. 141, p. 63, 1940. A. J. BRADLEY, H. LIPSON, and N. J. PETCH, *J. Sci. Instruments*, vol. 18, p. 216, 1941.

<sup>2</sup> A. J. BRADLEY and H. LIPSON, *Proc. Roy. Soc. (London)*, vol. A167, p. 421, 1928.

<sup>3</sup> A. WESTGREN and G. PHRAGMÉN, *Z. physik. Chem.*, vol. A102, p. 1, 1922. W. COHN, *Z. Physik*, vol. 50, p. 123, 1928. O. RUFF and F. EBERT, *Z. anorg. Chem.*,

Hume-Rothery and Reynolds<sup>1</sup> illustrated in Fig. 5. The sample of metallic filings is sealed in a thin-walled silica capillary tube which may be sealed off in a vacuum or filled with inert gas. It is mounted on the axis of the camera, which consists principally of a pair of rings *AA'* machined in one piece with the connecting block *VV* and a pair of disks, supported by these, which contain circular cooling-water channels *DP*. The film is held in contact with the outer circumference of the disks by rubber bands *XX*. The beam of x-rays enters through tubes *M* and *M*<sub>1</sub> of 2 mm. inside diameter and leaves through the port at the left.

The furnaces mounted on the disks *L*<sub>1</sub> and *L*<sub>2</sub> are bell-shaped to minimize thermal gradients. They consist of heating wire wound on silica forms and fastened with alundum cement. They are fixed in the outer quartz tubes *G* and *G*<sub>1</sub> with tightly packed lagging and are centered and clamped by adjusting screws in the brass shields *F* and *F*<sub>1</sub>. The leads to the heating elements are *I*<sub>1</sub> and *I*<sub>2</sub>. A black-paper shield at *E* protects the film from the heat, and at high temperatures an aluminum-foil shield (0.0075 mm. thick) is added at *Al*. Temperatures are measured by a 3-mm.-diameter platinum ring welded to a platinum and platinum-rhodium thermocouple mounted in the holder *H*. This is adjustable vertically to explore the temperature at various points. With a 3-mm. gap between the two furnaces it is possible to reduce the thermal gradient in the irradiated region to 1°C. at 1000°C. Temperatures can be regulated by hand or by a potentiometric regulator. Diffraction lines from silver are satisfactory at 943°C., though the general background is more intense than at lower temperatures; lattice parameters appear to be reproducible to 0.0001Å. The specimen is rotated by means of the pulley at the top.

**Low-temperature Cameras.**—Powder photographs have been made at low temperatures by blowing cold air over a specimen or by attaching a specimen to a copper conductor cooled by liquid air,<sup>2</sup> but the simplest and perhaps the most effective scheme for maintaining the specimen at

vol. 180, p. 19, 1929. H. BRAEKKEN and L. HARANG, *Z. Krist.*, vol. 75, p. 538, 1930. N. P. GOSS, *Metal Progress*, vol. 28, p. 163, October, 1935. A. GOETZ and R. C. HERGENROTHER, *Phys. Rev.*, vol. 40, p. 643, 1932. R. BERTHOLD and H. BÖHM, *Metallwirtschaft*, vol. 11, p. 567, 1932. A. H. JAY, *Z. Krist.*, vol. 86, p. 106, 1933; *Proc. Phys. Soc. (London)*, vol. 45, p. 635, 1933.

<sup>1</sup> W. HUME-ROTHERY and P. W. REYNOLDS, *Proc. Roy. Soc. (London)*, vol. A167, p. 25, 1938.

<sup>2</sup> M. WOLF, *Z. Physik*, vol. 53, p. 72, 1929. R. F. MEHL and C. S. BARRETT, *Trans. A.I.M.E.*, vol. 89, p. 575, 1930. O. KRATKY and P. LOSADA in F. HALLA and H. MARK, "Röntgenographische Untersuchung von Kristallen," p. 149, Barth, Leipzig, 1937. F. FEHER and F. KLÖTZER, *Z. Elektrochem.*, vol. 41, p. 850, 1935. W. H. BARNES and W. F. HAMPTON, *Rev. Sci. Instruments*, vol. 6, p. 342, 1935. N. W. TAYLOR, *Rev. Sci. Instruments*, vol. 2, p. 751, 1931.



the temperature of liquid air seems to be merely to cause a fine stream of liquid air to flow continuously over the specimen in an ordinary powder camera. The specimen may be mounted on a glass rod (about 0.5 mm. in diameter) and enclosed in a small cellophane tube that is connected to a storage reservoir of liquid air.<sup>1</sup>

**Focusing Cameras.**—Cameras in which the slits, specimen, and film all lie on the circumference of the same cylinder (Fig. 19, page 84) have been much used since their development by Seemann and Bohlin.<sup>2</sup> Since all the diffracted rays from a large area of the specimen are focused

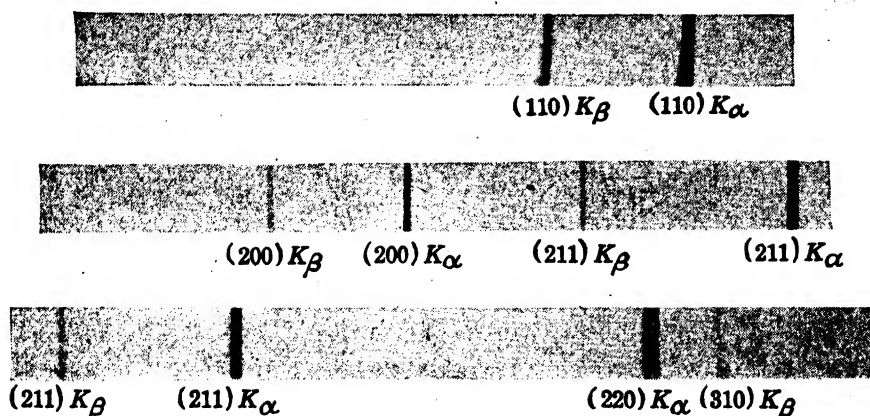


FIG. 6—Powder pattern of  $\alpha$ -iron in Phragmén focusing cameras with overlapping ranges. Diffraction angle increases from left to right. Unfiltered iron radiation.

to a sharp line, the exposure times are relatively short; a second advantage is the fact that dispersion of these cameras is twice that of a Debye camera of the same radius. Westgren and Phragmén in their extensive studies of alloy constitution have used focusing cameras in which the range from 16 to 82° is covered by three separate cameras in order to obtain optimum conditions in each range.<sup>3</sup> Figure 6 illustrates the films obtained from these. Jette covers the range from 17.5 to 77° in a single camera of high dispersion,<sup>4</sup> illustrated in Fig. 7. The specimen is held on an oscillating arm, pivoted at the center of the camera.

Focusing cameras of this type are calibrated by taking photographs of standard materials. The position of a diffraction line is measured from

<sup>1</sup> The tube may be made by dissolving cellophane cuttings in a 50–50 solution of amyl acetate and acetone until the solution becomes fairly viscous, then dipping a soft copper wire in the solution. After drying for 2 days, the wire is reduced in size by stretching and can then be removed from the cellophane tube. (K. LONSDALE and H. SMITH, *J. Sci. Instruments*, vol. 18, p. 133, 1941.)

<sup>2</sup> H. SEEMANN, *Ann. Physik*, vol. 59, p. 455, 1919. H. BOHLIN, *Ann. Physik*, vol. 61, p. 421, 1920.

<sup>3</sup> A. F. WESTGREN, *Trans. A.I.M.E.*, vol. 93, p. 13, 1931.

<sup>4</sup> Built by George C. Wyland, Ramsey, N.J.

the shadow of one of the knife-edges at the ends of the film. The distance from a knife-edge shadow to a line is corrected for shrinkage or expansion of the film by multiplying by the distance between knife-edges on the standard film and dividing by the distance between knife-edges on the film being measured, thus effectively reducing each film to standard length. Single emulsion films must be used because of the oblique incidence of the diffracted rays. Specimens may be prepared by coating a layer of powder on a strip of paper with a small amount of an adhesive

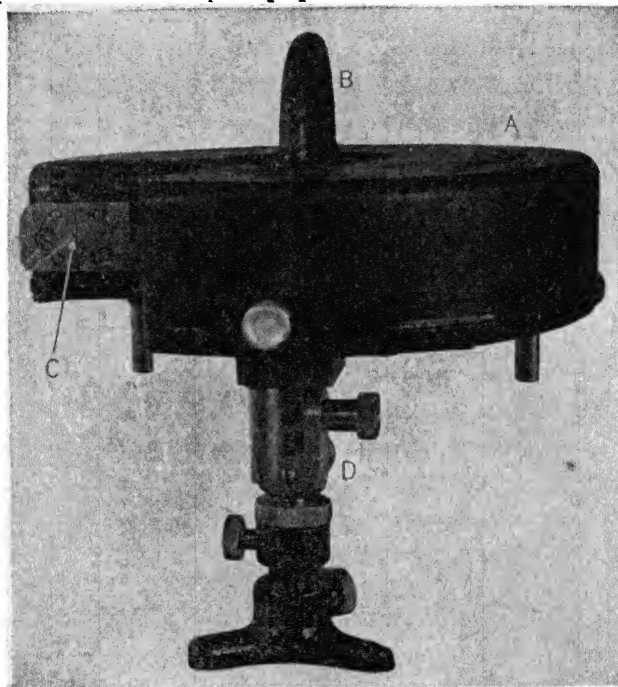


FIG. 7.—Focusing camera designed by Jette. A, cover; B, handle; C, adjustable slit on circumference of film cylinder; D, adjustable stand. (George C. Wyland.)

or by placing a layer of powder on paper and covering it with Scotch tape. The specimen is clamped in place so that it accurately fits the cylindrical surface of the camera. Symmetrical back-reflection focusing cameras are discussed in the following section.

**Back-reflection Cameras.**—Precision determinations of lattice constants are best made at high diffraction angles because of the greater dispersion in this range. Cameras for this purpose using flat films or photographic plates<sup>1</sup> are usually provided with means for rotating the specimen and film, as in Fig. 8, to make smoother lines. By placing a shield over the film and exposing a segment at a time, it is possible to put

<sup>1</sup> G. SACHS and J. WEERTS, *Z. Physik*, vol. 60, p. 481, 1930. G. SACHS, *Trans. A.I.M.E.*, vol. 93, p. 39, 1931. F. WEVER and A. ROSE, *Mitt. Kaiser-Wilhelm Inst. Eisenforsch. Düsseldorf*, vol. 17, p. 33, 1935.

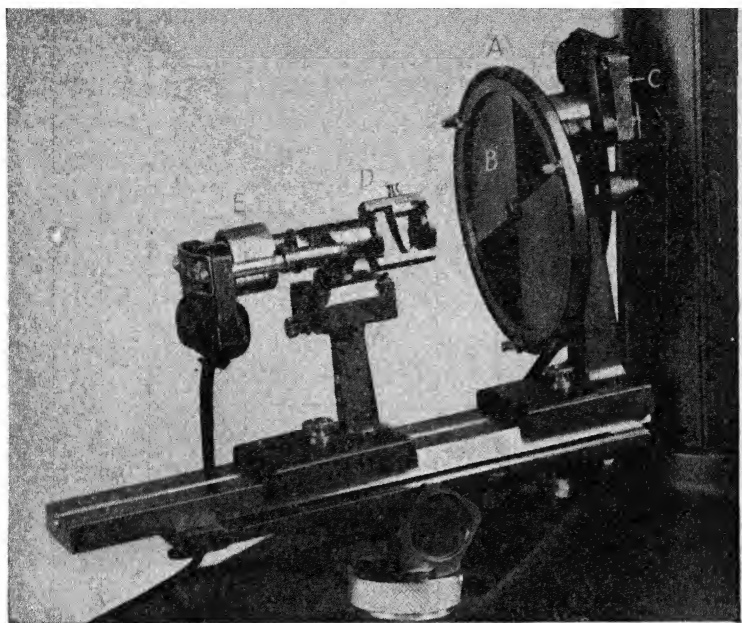


FIG. 8.—Focusing camera with flat film. A, film cassette; B, shield over portion of film, C, film-rotating motor; D, specimen holder rotated by motor E. (*General Electric X-ray Corporation.*)

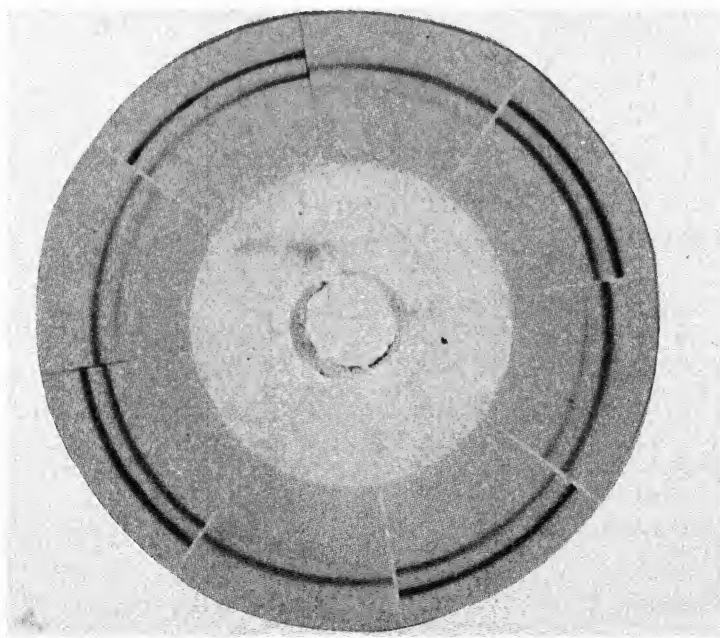


FIG. 9.—Back-reflection powder pattern on a flat film. Alternate segments are from solid-solution alloys of different composition and different lattice parameter.  $K\alpha_1$  and  $K\alpha_2$  lines are fully resolved.

several exposures on one film (see Fig. 9). Film-to-specimen distances can be measured by micrometers or determined by calibration spectra.<sup>1</sup> By setting the pinhole at the proper place along the axis of the film carriage it is possible to obtain a focusing condition on one line of the spectrum (the pinhole, specimen, and line on film must lie on the circum-

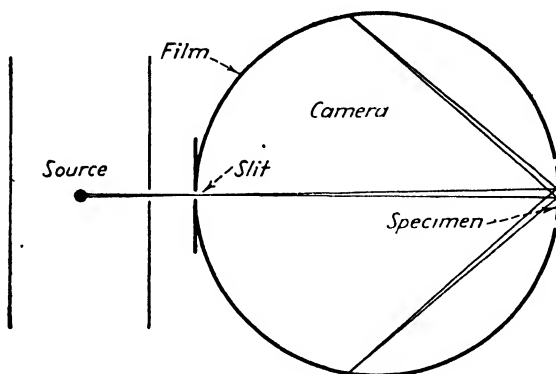


FIG. 10.—Symmetrical back-reflection focusing camera.

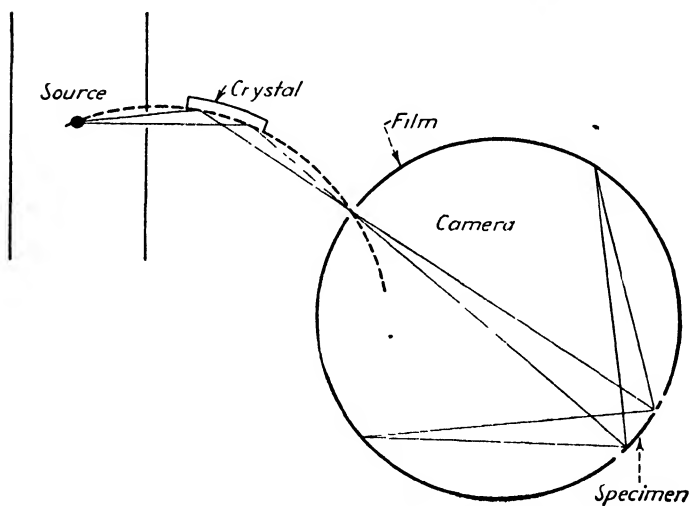


FIG. 11.—Crystal monochromator for a focusing camera.

ference of a circle). However, the focusing condition does not extend over the entire film in a camera of the flat-film type.

**Cylindrical back-reflection cameras** of the type indicated in Fig. 10 provide focusing over their entire range and are very effective in precision studies of noncubic metals, as Jette and Foote have shown.<sup>2</sup> A movable

<sup>1</sup> Cameras of this type have been sold by General Electric X-ray Corporation, Chicago, Ill., and by the American Instrument Company, Washington, D.C.

<sup>2</sup> E. R. JETTE and F. FOOTE, *J. Chem. Phys.*, vol. 3, p. 605, 1935. A camera of their design has been marketed by George C. Wyland, Ramsey, N.J. Cylindrical cameras are also supplied by Baird Associates, Cambridge, Mass.

arm for shifting the specimen is advantageous but must be so constructed that friction of the moving parts does not raise the temperature of the specimen more than  $1^{\circ}\text{C}$ . The camera can be calibrated by direct measurement of its diameter, and the films can be corrected by proper extrapolation to  $\theta = 90^{\circ}$ . This is discussed in a later section (page 135).

Bozorth and Haworth,<sup>1</sup> find that a **bent-crystal monochromator** (Fig. 11) will reduce the intensity of the background to one-eighth that of the usual focusing camera yet will require exposure times scarcely double the normal ones.<sup>2</sup> Synthetic rock salt crystals are more suitable than natural crystals for this purpose.<sup>3</sup>

**Choice of Radiation.**—To produce satisfactory photographs it is necessary to avoid fogging the film with fluorescent radiation from the sample. One way of doing this is to employ molybdenum radiation, which has a fairly short wavelength, and to filter the fluorescent radiation by placing a zirconium filter between the specimen and the film. This technique gives satisfactory films for most materials,<sup>4</sup> and suitable filter strips are available on the market.<sup>5</sup> But longer wavelengths are often needed, and it is then important to choose a target that emits a line spectrum of longer wavelength than the  $K$  absorption edge of the sample, if this is practicable. A filter to remove the  $K\beta$  radiation is optional. This is ordinarily placed between the tube and the camera, but if it is placed between the sample and the film it will serve also to filter out fluorescent radiation. Radiations of Cr, Mn, Fe, Co, Ni, Cu, and Zn are commonly used, and some have also used Au  $L\alpha_1$  and  $L\alpha_2$  ( $1.27377$ ,  $1.28502\text{\AA}$ ) after removing the  $L\beta$  and  $L\gamma$  lines with a Ga filter.<sup>6</sup> In precision work, radiation is chosen to yield diffraction lines at high angles, preferably above  $\theta = 70^{\circ}$ , and to give sufficient lines in this neighborhood it is helpful to use alloy targets.<sup>7</sup> A table of wavelengths is given in Appendix II.

**Interpretation of Powder Patterns.**—A powder or polycrystalline specimen has crystalline particles at all orientations. Consequently the

<sup>1</sup> R. M. BOZORTH and F. E. HAWORTH, *Phys. Rev.*, vol. 53, p. 538, 1938.

<sup>2</sup> They used a rock salt crystal 3.3 by 1.7 by 0.24 cm. which was clamped between cylindrical forms while immersed in a concentrated solution of sodium chloride. The crystal was bent to a radius of 20 cm., then dried, and the concave side ground to a radius of 10 cm. and etched with water until clear.

<sup>3</sup> CHARLES S. SMITH, *Rev. Sci. Instruments*, vol. 12, p. 312, 1941. Crystals are obtainable from Harshaw Chemical Company, Cleveland, Ohio.

<sup>4</sup> J. D. HANAWALT, H. W. RINN, and L. K. FREVEL, *Ind. Eng. Chem.*, anal. ed., vol. 10, p. 457, 1938.

<sup>5</sup> The Patterson Screen Company, Towanda, Pa.

<sup>6</sup> O. S. EDWARDS and H. LIPSON, *J. Sci. Instruments*, vol. 18, p. 131, 1941.

<sup>7</sup> E. R. JETTE and F. FOOTE (*J. Chem. Phys.*, vol. 3, p. 605, 1935) have used 50 atomic percent alloys of Fe-Mn, Fe-Ni, Fe-Cr, Cu-Ni, Fe-Co, Ni-Cr, Ni-Co, and Cu-Mn.

diffracted rays from it travel outward in all directions that make an angle of  $2\theta$  with the direct beam, where  $\theta$  is the Bragg angle. Thus each order of reflection from each set of planes forms a cone of semiapex angle  $2\theta$  concentric with the primary beam and produces a diffraction line on the film. The  $\theta$  values are computed for all the reflecting planes from measurements of the line positions. Identification of the lines is a simple matter with cubic crystals but is difficult with crystals of lower symmetry and generally impossible with monoclinic or triclinic crystals. Fortunately, most of the metals and alloys are cubic, tetragonal, or hexagonal.

Identification of the lines in a powder pattern is always based on comparing the measured list of  $\theta$  values with a list predicted for a unit cell of assumed dimensions. Given the parameters  $a, b, c, \alpha, \beta, \gamma$  of a cell and the wavelength to be used, one can quickly compute all possible reflections by using the quadratic forms on page 77 and inserting all possible values of  $h, k$ , and  $l$ . With cubic crystals the equation is

$$\sin^2 \theta = K(h^2 + k^2 + l^2) \quad (1)$$

where  $K = \lambda^2/4a^2$ . It will be noted that reflections 100, 010, and 001 all fall on the same ring; likewise, reflections from all planes of the general form  $\{hkl\}$  superimpose. However, this is not true of noncubic crystals, as can be seen, for example, from the quadratic form for the orthorhombic class:

$$\sin^2 \theta = \frac{\lambda^2}{4} \left( \frac{h^2}{a^2} + \frac{k^2}{b^2} + \frac{l^2}{c^2} \right). \quad (2)$$

The quantity  $(h^2 + k^2 + l^2)$  in Eq. (1) has small integral values—in fact, by a proper choice of indices this quantity can have any value from 1 through 6, 8 through 14, 16 through 22, etc. To identify the lines of a cubic pattern it is necessary merely to choose a set of these integers so that  $(\sin^2 \theta)/(h^2 + k^2 + l^2)$  will have the same value for every line in the pattern. The value of the constant  $K$  is then  $\lambda^2/4a^2$ . It is obvious, of course, that Eq. (2) and other noncubic formulas do not permit a simple identification of this sort.

To facilitate computations of the lattice constant or, conversely, to speed the calculation of cubic patterns when  $a$  is known, a table of reflecting planes is included in Appendix IV with logarithms of  $(h^2 + k^2 + l^2)$ .<sup>1</sup>

Only with simple cubic lattices will there be reflections for all possible values of  $(h^2 + k^2 + l^2)$ ; other space lattices will have characteristic

<sup>1</sup> For more extensive tables see "Internationale Tabellen zur Bestimmung von Kristallstrukturen," vol. II, Bornträger, Berlin, 1935. L. W. MCKEEHAN, *Am. J. Sci.*, vol. 17, p. 548, 1929.

**absences** by means of which it is possible to distinguish body-centered cubic from face-centered cubic. Consider the structure-factor formula

$$|F|^2 = [\sum f \cos 2\pi(hu + kv + lw)]^2 + [\sum f \sin 2\pi(hu + kv + lw)]^2 \quad (3)$$

discussed in Chap. IV. If this is applied to a unit cell of any **simple space lattice**, the coordinates of the only atom in the cell are  $uvw = 000$ ; hence,  $|F|^2 = f^2$  for any reflection, regardless of indices, and there will be no missing reflections. On the other hand, if it is applied to a **body-centered** cell with atoms at  $000$  and  $\frac{1}{2}\frac{1}{2}\frac{1}{2}$ , we see that  $|F|^2 = 0$  whenever  $(h + k + l)$  is odd and so these reflections will be absent, for example,  $100$ ,  $111$ ,  $210$ , etc. In a **face-centered** lattice one can easily show in the same way that all reflections will be missing for which the indices  $h$ ,  $k$ ,  $l$

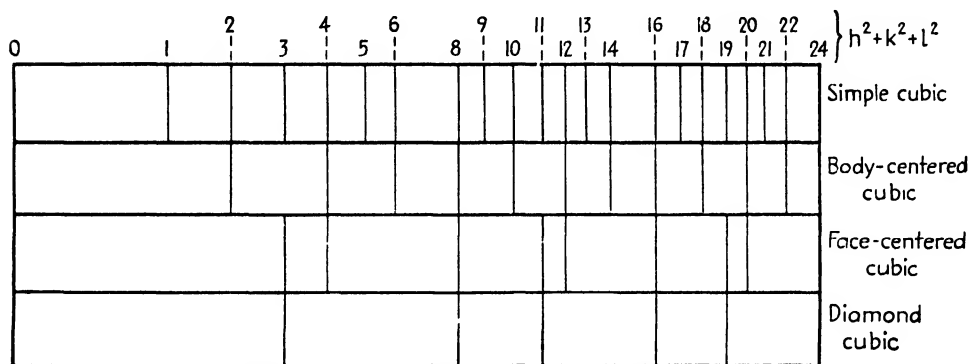


FIG. 12.—Powder patterns for different cubic crystals, illustrating characteristic reflections for each type.

are mixed odd and even, for example,  $100$ ,  $211$ , etc. These rules apply to all crystal systems. There are also characteristic absences for the **diamond cubic** structure.<sup>1</sup> The characteristic sequence of lines in cubic crystals is illustrated in Fig. 12, where  $h^2 + k^2 + l^2$  is indicated for each line that is observed in simple, body-centered, face-centered, and diamond cubic spectra.

**Graphical Methods of Solving Patterns.**—The logarithmic scales of a **slide rule** provide a rapid means of solving cubic patterns. Various arrangements have been proposed,<sup>2</sup> one of the best being illustrated in Fig. 13,<sup>3</sup> in which four logarithmic scales are used,  $A$ ,  $B$ ,  $C$ ,  $D$ . Along the log scale  $A$  are marked all wavelengths to be used, including  $K\beta$  as well as  $K\alpha$ . Scale  $B$  is an ordinary log scale for reading the cube

<sup>1</sup> The structure of diamond, silicon, germanium, and gray tin, with atoms at  $000$ ,  $\frac{1}{2}\frac{1}{2}0$ ,  $\frac{1}{2}0\frac{1}{2}$ ,  $0\frac{1}{2}\frac{1}{2}$ ,  $\frac{1}{4}\frac{1}{4}\frac{1}{4}$ ,  $\frac{3}{4}\frac{3}{4}\frac{3}{4}$ ,  $\frac{2}{4}\frac{2}{4}\frac{2}{4}$ ,  $\frac{1}{4}\frac{3}{4}\frac{3}{4}$ . The reflections that can be obtained for each of these lattices are indicated in the table, Appendix IV.

<sup>2</sup> E. SCHIEBOLD, *Z. Physik*, vol. 28, p. 355, 1924. G. KETTMAN, *Z. Physik*, vol. 53, p. 198, 1929; vol. 54, p. 596, 1929. WHEELER P. DAVEY, "A Study of Crystal Structure and its Applications," McGraw-Hill, New York, 1934.

<sup>3</sup> D. F. THOMAS, *J. Sci. Instruments*, vol. 18, p. 205, 1941.

dimension  $a$ . Distances along  $C$  are proportional to  $\log \sqrt{h^2 + k^2 + l^2}$  and are marked with the corresponding  $hkl$  indices; it would be better to add  $B$ ,  $F$ , and  $D$  notations to each of these to indicate reflections for body-centered, face-centered, and diamond cubic structures. Scale  $D$  has distances proportional to  $\log \sin \theta$  with graduations in  $\theta$  values ( $\sin \theta$  graduations would also be useful). The four scales are laid out so that the equality  $(\sin \theta) / \sqrt{h^2 + k^2 + l^2} = \lambda / 2a$  is represented by one setting. If a series of  $\theta$  values is marked along the  $D$  scale, their indices will be found when the rule is adjusted to the position for which they simultaneously match the marks on scale  $C$ , and at this setting of the slide the  $a$  value (scale  $B$ ) will appear under the wavelength used (scale  $A$ ). If

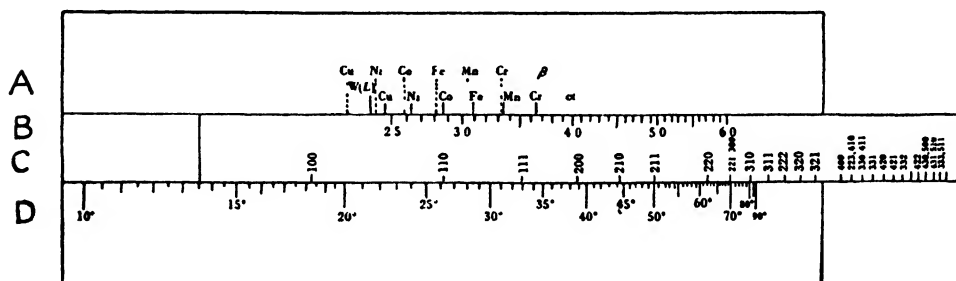


FIG. 13.—Slide rule for solving powder patterns of cubic crystals. The wavelength scale (A), lattice parameter scale (B), indices scale (C), and  $\theta$  scale (D) are set for Co  $K\alpha$  radiation and iron specimen with  $a_0 = 2.86$ . (Thomas.)

both  $K\alpha$  and  $K\beta$  lines appear on the pattern, these require independent settings of the slide.

Powder patterns for lattices with two parameters (tetragonal, hexagonal, and rhombohedral) can be solved with the aid of **charts** devised by Hull and Davey, giving the relative spacings for unit cells having all possible axial ratios within their range.<sup>1</sup> The charts are made with lattice-plane spacings plotted along the axis of abscissas according to a logarithmic scale, as indicated in Fig. 14, and different axial ratios  $C = c/a$  appear at different vertical levels on the chart. At a given axial ratio the distances from left to right are given by the formula

$$\log d = \log \left( \frac{a}{\sqrt{h^2 + k^2 + \frac{a^2}{c^2} l^2}} \right) = \log a - \log \sqrt{h^2 + k^2 + \frac{a^2}{c^2} l^2}. \quad (4)$$

A strip of paper is marked with the spacings calculated from a diffraction pattern and is moved over the chart to various horizontal positions until

<sup>1</sup> A. W. HULL and W. P. DAVEY, *Phys. Rev.*, vol. 17, p. 549, 1921. W. P. DAVEY, *Gen. Elec. Rev.*, vol. 25, p. 564, 1922.



the marks coincide with curves on the chart (see Fig. 14). Doing so amounts to trying various  $c/a$  and  $a$  values until the predicted pattern agrees with the observed one. Indices for each of the lines are then read from the curves. Figure 15 is the chart for simple tetragonal lattices.<sup>1</sup>

It is desirable to have a graphical method in which the scale can be much larger than in the Hull-Davey charts as reproduced, for curves are

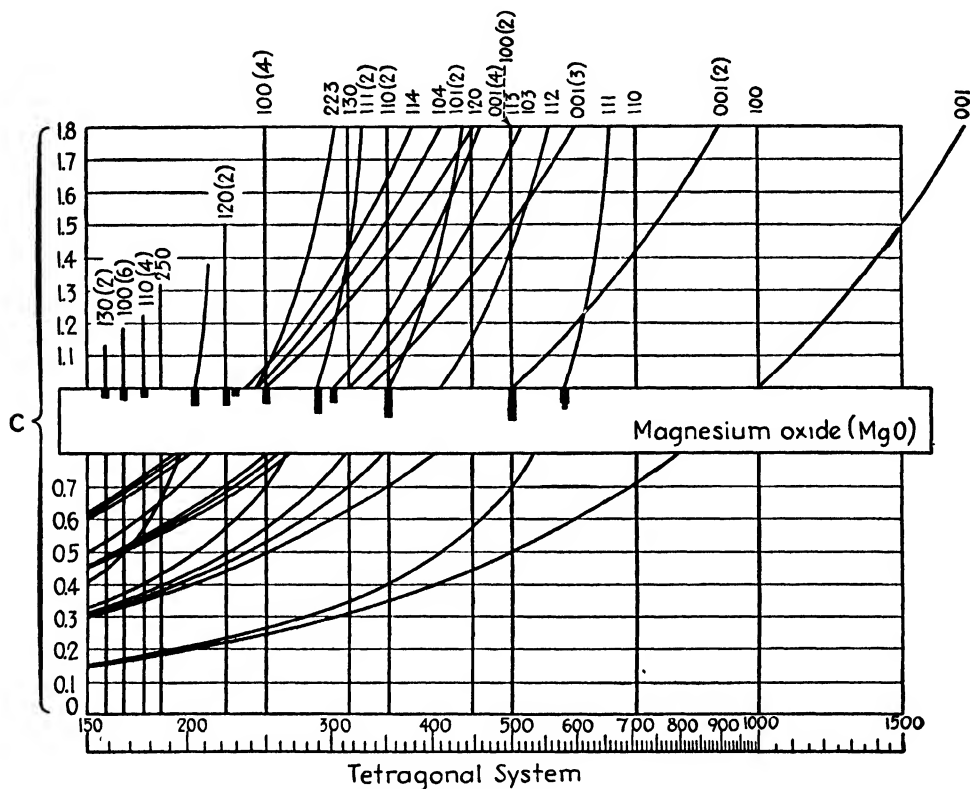


FIG. 14.—Illustrating a Hull-Davey chart and its use in indexing the powder pattern of MgO. (Wyckoff.)

too densely packed in some regions of the charts. An ingenious ruler, illustrated in Fig. 16, has been devised by Bjurström for this purpose.<sup>2</sup> For the hexagonal system, lines are drawn parallel to  $AB$  at distances above  $AB$  that are proportional to the observed  $\sin^2 \theta$  values. Points are marked off along the ruler  $CD$  so that the distances from  $00$  are proportional to  $h^2 + k^2 + hk$  for various  $h$  and  $k$  values. From these marked points, parallel strings are stretched to a second straightedge,

<sup>1</sup> Others appear in the preceding references (Hull and Davey) and in W. P. Davey, "A Study of Crystal Structure and Its Applications," McGraw-Hill, New York, 1934, and Fairbanks, "Laboratory Investigation of Ores," McGraw-Hill, New York, 1928.

<sup>2</sup> T. BJURSTRÖM, *Z. Physik*, vol. 69, p. 346, 1931.



and points are marked on the strings for  $l^2$  values, at distances proportional to  $1^2, 2^2, 3^2, 4^2$ , etc., from the edge  $CD$ . The straightedge is then laid so the point  $00$  rests on  $AB$ , and the angle between the edge  $CD$  and the strings is varied together with the angle between  $CD$  and  $AB$  until a mark on a string lies on each of the horizontal lines. The indices are then read off: the  $h$  and  $k$  values are taken from the ruler and the  $l$  values

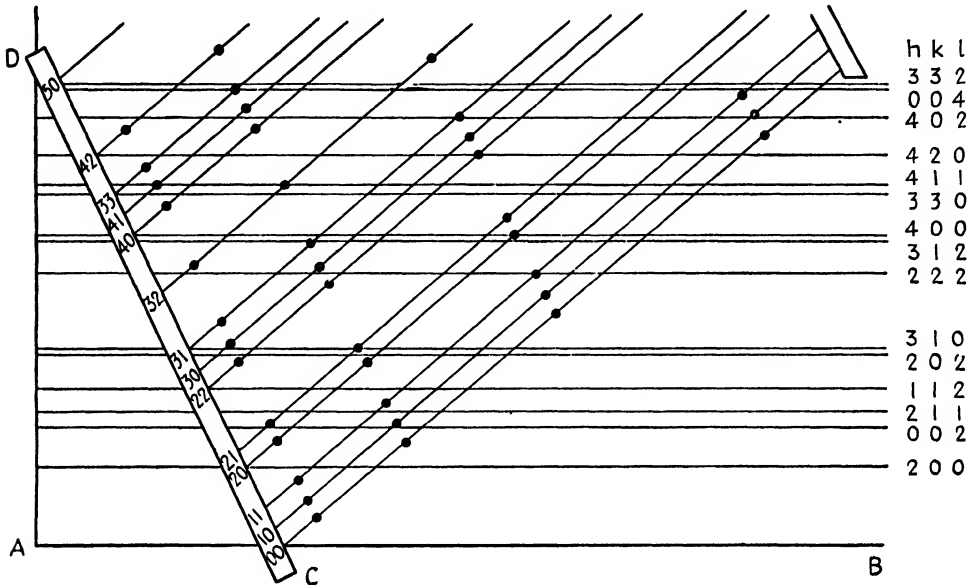


FIG. 16.—Bjurstrom's ruler for solving powder patterns. The indices at the right will be obtained if the strings are tilted at a slightly greater angle.

from the marks on the strings. It will be seen that this procedure amounts to varying the quantities  $K_1$  and  $K_2$  in the quadratic form

$$\sin^2 \theta = K_1(h^2 + k^2 + hk) + K_2l^2 \quad (\text{hexagonal system}) \quad (5)$$

An analogous procedure is used for tetragonal crystals, for which the quadratic form is

$$\sin^2 \theta = K_1(h^2 + k^2) + K_2l^2 \quad (\text{tetragonal system}) \quad (6)$$

A modification of this device will operate for the orthorhombic system, where one seeks three sets of lines from the entire list, each set satisfying one of the equations

$$\left. \begin{aligned} \sin^2 \theta &= K_1h^2 - K_2k^2 \\ \sin^2 \theta &= K_1h^2 - K_3l^2 \\ \sin^2 \theta &= K_2k^2 - K_3l^2 \end{aligned} \right\} \quad (\text{orthorhombic system}) \quad (7)$$

The distances on the straightedge from the point  $00$  are made proportional to  $1^2, 2^2, 3^2$ , etc., and on the strings the distances to the marks are also proportional to these numbers. When the marks on the strings

are made to coincide with a certain series of lines on the paper, two indices are tentatively determined; three series are sought that give consistent values of  $K_1$ ,  $K_2$ , and  $K_3$ .

The purpose of all graphical methods is to aid in tentatively identifying the diffraction lines. They should not be trusted for the final assignment of indices or for the accurate determination of the lattice constants, which should be done by putting the tentative indices and the observed  $\theta$  values in the appropriate formulas and making the computations with logarithms.

**Precision Determinations of Lattice Constants.**—Precise lattice-constant determinations are important for the determination of solubility limits in constitution diagrams. Other applications in research include determinations of the coefficients of thermal expansion of metals and alloys, studies of precipitation from solid solution, and determination of diffusion rates in solids.

Much work in the past has been done with Debye cameras, but they are inherently less precise than back-reflection cameras, which operate in the sensitive range of  $\theta$  values near  $\theta = 90^\circ$ . Precision work with Debye cameras is hampered by many factors: (1) film shrinkage, (2) errors in measuring the camera radius, (3) displacement of the specimen from the center of the camera by improper adjustment, (4) displacement of the effective center of the specimen from the center of the camera by absorption of the rays in the sample, (5) x-ray beam divergence, (6) finite height of slits, and (7) deviations from Bragg's law due to refraction of x-rays. Careful design of cameras and careful technique reduce many types of error, and correction formulas have been employed to eliminate some, but the greatest improvements have come from the more recent methods for eliminating systematic errors by extrapolation.

**Errors and Corrections in Debye Cameras.**—When a film is put through the developing, fixing, and washing baths, it undergoes expansion or contraction of uncertain amounts. Further alteration occurs in storage and while it is being measured. This **film shrinkage** alters the apparent circumference of the camera. A remedy for it is to print a scale on the film at the time the photograph is made. Subsequent measurement of this scale then reveals the amount of shrinkage that has taken place. Unless the film has been mishandled or has dried unevenly, it can be assumed that shrinkage is uniform throughout the length of the strip; hence, the same percentage correction can be applied to all measured distances on the film.

One method is to allow the film to wrap completely around the camera and overlap; the inner end is then in position to cast a sharp shadow on the overlapping end at a distance along the film that equals the effective circumference of the camera. If the film subsequently shrinks, this

distance also shrinks in proportion. Since a diffraction ring for  $\theta = 90^\circ$  would cause two spots on the film separated by a full circumference it follows that

$$\frac{\theta^\circ}{90^\circ} = \frac{S}{S_0} \quad (8)$$

where  $S$  is the distance from one arc of a diffraction line to its mate and  $S_0$  is the effective circumference.

Another common method of marking a standard distance on the film is to build two knife-edges into the camera so that they will form sharp limits to the exposed (darkened) portion of the film. The camera then requires calibration experiments to determine the camera dimensions. The preceding formula is then replaced by

$$\frac{\theta^\circ}{\theta_1^\circ} = \frac{S}{S_1}, \quad (9)$$

where  $\theta_1$  is the diffraction angle for a line exactly at the knife-edges and  $S_1$  is the circumferential distance between them.<sup>1</sup>

The principle of calibration can be applied to individual films if the powders of the unknown sample and the standard substance are mixed and the superimposed spectra are obtained. The angles of reflection from the standard powder, which are known accurately, are plotted against the measurements of the corresponding lines to give a calibration curve for the film. Then the corrected angles for other lines are read from the curve.<sup>2</sup> Some cameras contain a septum that divides the interior into two independent compartments, one for the standard specimen and one for the unknown. To attain precision with this type of instrument the operator must be careful to center the specimens in the axis of the camera and to equalize the absorption of rays in the two specimens by diluting with an amorphous material like flour.<sup>3</sup>

<sup>1</sup> This may be done by measuring the camera directly or, alternatively, by taking a photograph of a substance of known lattice spacings [see A. J. Bradley and A. H. Jay, *Proc. Phys. Soc. (London)*, vol. 44, p. 563, 1932].

Quartz (the clear variety, not smoky) is recommended for a calibrating substance. The quartz spectrum has been listed by A. J. Bradley and A. H. Jay, *Proc. Phys. Soc. (London)*, vol. 45, p. 507, 1933, but their spacing values have been criticized and amended by H. Lipson and A. J. C. Wilson, *J. Sci. Instruments*, vol. 18, p. 144, 1941. Much attention must be given to the question of the purity of any calibration substance, for dissolved impurities alter the spacing.

<sup>2</sup> Interpolation formulas have also been used for this procedure (see F. Wever and O. Lohrmann, *Mitt. Kaiser-Wilhelm Inst. Eisenforsch. Dusseldorf*, vol. 14, p. 137, 1932).

<sup>3</sup> See W. P. DAVEY, "A Study of Crystal Structure and Its Applications," McGraw-Hill, New York, 1934.

Attempts have been made to correct for the **radius of the specimen** by using correction formulas, though the results are less reliable than are obtained by calibration methods.<sup>1</sup> The simplest formula, which assumes that the incident rays are parallel and are completely absorbed in the specimen, is

$$S_c = S' - \delta \quad (10)$$

where  $S'$  is the film measurement between outer edges of the two arcs of a Debye ring,  $\delta$  is the diameter of the cylindrical specimen, and  $S_c$  is the corrected value of the ring measurement from which  $\theta$  is obtained ( $\theta = S_c/4R$  radians if  $R$  is the camera radius). ♦

**Graphical Extrapolation Methods for Debye Films.**—To compute the error in lattice spacing,  $\Delta d$ , that results from an error of  $\Delta\theta$  in the measurement of  $\theta$  we may put Bragg's law in the form

$$d \sin \theta = \frac{n\lambda}{2} \quad (11)$$

which by differentiation yields

$$d \cos \theta \Delta\theta + \sin \theta \Delta d = 0 \quad (12)$$

from which

$$\frac{\Delta d}{d} = -\cot \theta \Delta\theta \quad (13)$$

Thus the percentage error in spacing measurement caused by a given error in angle measurement approaches zero as  $\cot \theta$  approaches zero, hence as  $\theta$  approaches  $90^\circ$ . Kettmann<sup>2</sup> used this fact to eliminate errors by simply plotting the apparent lattice constant determined from each line against the value of  $\theta$  for that line; a smooth curve drawn through the plotted points and extrapolated to  $\theta = 90^\circ$  gave the corrected value of the lattice constant.

Bradley and Jay<sup>3</sup> have improved upon Kettmann's method by handling the data in such a way that the extrapolated curve is approximately a straight line. From the geometry of a forward-reflection Debye camera they show that two important systematic errors can be effectively treated. Fractional errors in lattice spacings,  $\Delta d/d$ , that arise from incorrect centering (**eccentricity**) of the specimen in the camera depend upon  $\theta$  in the following way:

$$\frac{\Delta d}{d} = C_1 \cos^2 \theta \quad (14)$$

<sup>1</sup> F. WEYER and O. LOHRMANN, *Mitt. Kaiser-Wilhelm Inst. Eisenforsch. Dusseldorf*, vol. 14, p. 137, 1932.

<sup>2</sup> G. KETTMANN, *Z. Physik*, vol. 53, p. 198, 1929.

<sup>3</sup> A. J. BRADLEY and A. H. JAY, *Proc. Phys. Soc. (London)*, vol. 44, p. 563, 1932.

where  $C_1$  is a constant for all lines of a given film. Similarly, the fractional spacing errors arising from the **absorption** of rays in the sample are given by the approximate equation

$$\frac{\Delta d}{d} = C_2 \frac{1}{\theta} \cos^2 \theta \quad (15)$$

where  $C_2$  is another constant for all lines of one photograph. Both errors approach zero at  $\theta = 90^\circ$ , as does the sum of the two, and both vary approximately in proportion to the factor  $\cos^2 \theta$ . Therefore by plotting computed values of  $d$  against  $\cos^2 \theta$ , as in Fig. 17, a curve through the points approximates a straight line at high values of  $\theta$ . This line extrapolates to the true  $d$  value at  $\cos^2 \theta = 0$ . The linear extrapolation becomes the more precise the nearer the points are to  $\theta = 90^\circ$  and the smaller the systematic errors.

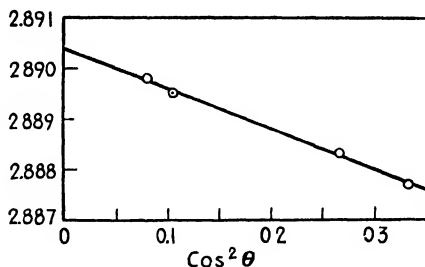


FIG. 17.—Extrapolation of lattice parameters to  $\theta = 90^\circ$  by plotting against  $\cos^2 \theta$ . Specimen was 85.5 percent Fe, 14.5 percent Al. (Bradley and Jay.)

**Shrinkage** and **radius** errors do not lead to a straight line on a plot of this kind,<sup>1</sup> for they produce spacing errors of magnitude

$$\frac{\Delta d}{d} = \frac{\Delta R}{R} \theta \cot \theta \quad (16)$$

where  $\Delta R$  is the error in equivalent radius,  $R$ , caused by shrinkage or by incorrect measurement of the camera radius. If shrinkage errors of any importance are present, the curve on a Bradley and Jay plot approaches  $\cos^2 \theta = 0$  with a marked slope which makes extrapolation very uncertain. Therefore, an essential element of Bradley and Jay's technique for Debye films is to *calibrate the camera and correct for shrinkage in the film before plotting the results*.

**Extrapolation for Cylindrical Back-reflection Cameras.**—The differentiated form of Bragg's law given in Eq. (13) shows that the percentage error in the determination of a lattice spacing is least when  $\theta$  is greatest, for the term  $\cot \theta$  approaches zero as  $\theta$  approaches  $90^\circ$ . Back-reflection cameras utilize this principle. With no more than ordinary care these cameras can equal the precision attained by Debye cameras that are operated with the most painstaking technique.

The correction of systematic errors by extrapolation is very effective in back-reflection cameras,<sup>2</sup> which admit the beam from the x-ray tube

<sup>1</sup> M. J. BUEGER, "X-ray Crystallography," Wiley, New York, 1942.

<sup>2</sup> W. STENZEL and J. WEERTS, *Z. Krist.*, vol. 84, p. 20, 1933. J. WEIGEL, *Helv. Phys. Acta*, vol. 7, pp. 46, 51, 1934. M. U. COHEN, *Z. Krist.*, vol. 94, p. 288, 1936. M. J. BUEGER, "X-ray Crystallography," Wiley, New York, 1942.

through a hole in the center of the film. As sketched in Fig. 18, the angle  $2\phi$  rather than  $2\theta$  or  $4\theta$  is measured and  $\theta$  is obtained from the relations  $\phi = \pi - 2\theta$  or  $\phi/2 = (\pi/2 - \theta)$ . The equation for **radius** and **shrinkage** errors then becomes

$$\frac{\Delta d}{d} = \frac{\Delta R}{R} \left( \frac{\pi}{2} - \theta \right) \cot \theta. \quad (17)$$

Therefore, if a film contains only errors of this type, the computed spacings will fall on a straight line when plotted against  $[(\pi/2) - \theta] \cot \theta$ . They will also fall on a line that is approximately straight if plotted against  $\cos^2 \theta$  owing to the fact that this trigonometric function varies almost linearly with  $[(\pi/2) - \theta] \cot \theta$  in the range of  $\theta$  values that is useful for extrapolation. Since **eccentricity** errors are also linear on a  $\cos^2 \theta$  plot, they too are eliminated by linear extrapolation to  $\theta = 90^\circ$ . **Absorption** errors are not linear on this plot and can therefore introduce some curvature into the line that is extrapolated. Buerger points out that if eccentricity is eliminated by accurate instrument construction, and if shrinkage errors are corrected for by calibrating the film, then the

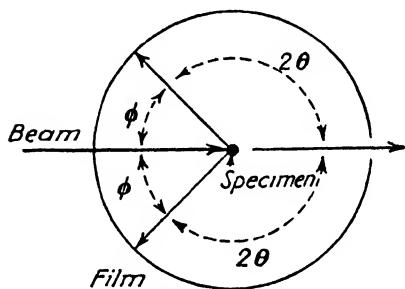


FIG. 18. Angles in a back-reflection Debye camera.

remaining absorption errors can be eliminated by a linear extrapolation provided that the computed spacings are plotted against the function  $\cot \theta \cos^2 \theta$ .\*

**Cohen's Method.**—Cohen has developed an analytical method for extrapolating to eliminate systematic errors.<sup>1</sup> The method is particularly valuable for noncubic crystals and for least squares computations of the errors.<sup>2</sup> The eccentricity and absorption errors in **cylindrical cameras** of the Debye type may be written in the approximate form

$$\frac{\Delta d}{d} = D \cos^2 \theta \quad (18)$$

where  $D$  is a constant [see Eqs. (14) and (15)]. This is applicable to  $\theta$  values above  $\theta = 60^\circ$ . From Bragg's law, by squaring and taking

\* M. J. BUEGER, "X-ray Crystallography," p. 426, Wiley, New York, 1942. The function  $\cot \theta \cos^2 \theta$  replaces Bradley and Jay's  $(1/\theta)(\cos^2 \theta)$  of Eq. (15).

<sup>1</sup> M. U. COHEN, *Rev. Sci. Instruments*, vol. 6, p. 68, 1935; vol. 7, p. 155, 1936; *Z. Krist.*, vol. 94, pp. 288, 306, 1936.

<sup>2</sup> E. R. JETTE and F. FOOTE, *J. Chem. Phys.*, vol. 3, p. 605, 1935. M. J. BUEGER, "X-ray Crystallography," p. 426, Wiley, New York, 1942.



logarithms we have

$$2 \log d = -\log \sin^2 \theta + 2 \log \left( \frac{n\lambda}{2} \right)$$

and differentiating gives

$$2 \frac{\Delta d}{d} = - \frac{\Delta \sin^2 \theta}{\sin^2 \theta}$$

Substituting Eq. (18) in this expression leads to

$$\Delta \sin^2 \theta = D \sin^2 2\theta \quad (19)$$

where  $D$  is a constant. Thus the important systematic errors give values of  $\sin^2 \theta$  that are incorrect by an amount  $D \sin^2 2\theta$  where  $D$  is different from film to film but is constant throughout any one film. If this corrective term is added to the quadratic form for **cubic crystals**, we have

$$\sin^2 \theta = K(h^2 + k^2 + l^2) + D \sin^2 2\theta \quad (20)$$

where  $K = \lambda^2/4a^2$ . An equation of this type is written for each line of the pattern. The least squares values of the constants  $K$  and  $D$  are obtained from the entire series of lines by setting up two normal equations<sup>1</sup>

$$\left. \begin{aligned} K \Sigma \alpha_i^2 + D \Sigma \alpha_i \delta_i &= \Sigma \alpha_i \sin^2 \theta_i \\ K \Sigma \alpha_i \delta_i + D \Sigma \delta_i^2 &= \Sigma \delta_i \sin^2 \theta_i \end{aligned} \right\} \quad (21)$$

where  $\alpha_i = h^2 + k^2 + l^2$  and  $\delta_i = 10 \sin^2 2\theta_i$ . The factor 10 is used merely so that the coefficients of the normal equations will be of the same magnitude. The summations extend over all the equations for the separate lines. Solution of the two simultaneous normal equations gives the corrected value of  $K$  and thus the lattice constant. This method of calculation is readily extended to other systems with additional parameters; for **hexagonal crystals**, Eq. (20) is replaced by

$$\sin^2 \theta = \alpha K_1 + \gamma K_2 + \delta D \quad (22)$$

where  $\alpha = h^2 + hk + k^2$ ,  $\gamma = l^2$ ,  $\delta = 10 \sin^2 2\theta$ ,  $K_1 = \lambda^2/3a^2$ ,  $K_2 = \lambda^2/4c^2$ . Orthorhombic crystals are handled in a similar way.

Cohen finds that **symmetrical focusing cameras** have systematic errors in  $\Delta d/d$  that in the range  $\sin^2 \theta > 0.7$  are proportional to  $\phi \tan (\phi/2)$ , where  $\phi/2 = \pi/2 - \theta = L/8R$ . In this equation  $L$  is the distance between reflections from the same plane on opposite sides of the center and  $R$  is the camera radius. This leads to corrected quadratic forms as follows:

$$\sin^2 \theta = K(h^2 + k^2 + l^2) + D\phi \sin \phi \quad (\text{cubic}) \quad (23)$$

$$\sin^2 \theta = K_1(h^2 + hk + k^2) + K_2 l^2 + D\phi \sin \phi \quad (\text{hexagonal}) \quad (24)$$

<sup>1</sup> J. W. MELLOR, "Higher Mathematics," Longmans, New York, 1926.

which are employed as in the Debye case. It is convenient to use  $5\phi \sin \phi$  as  $\delta$  in the computation. For cubic crystals the lattice constant may be plotted against  $\phi \tan (\phi/2)$  and a straight-line extrapolation to  $\phi \tan (\phi/2) = 0$  gives the corrected value. To make use of Cohen's method the camera must be constructed so that the x-ray beam *enters* rather than *leaves* the camera through the center of the film. Jette and Foote<sup>1</sup> have discussed the evaluation of standard errors and fiduciary limits of results from a single film and from a set of films when computed by Cohen's method.

Deviations from Bragg's law due to refraction of the x-rays are small (roughly 0.01 percent) and are usually neglected. Jette and Foote, however, believe a detectable improvement results from applying a **refraction correction**, and they use the correction

$$\Delta \sin^2 \theta = \frac{4.895\rho Z\lambda^2}{M} \cdot 10^{-6} \quad (25)$$

where  $\rho$  is the density,  $Z$  the atomic number,  $\lambda$  the wave length in angstroms, and  $M$  the atomic weight. Results obtained on cubic and hexagonal crystals with a 10-cm symmetrical focusing camera gave five significant figures; fiduciary limits were  $\pm 2$  to 7 parts per 100,000 when the limits were computed so the chance that the correct value of the lattice constant falls within the limits is 19 out of 20. Temperature corrections are important, for a temperature difference of 1°C. introduces a detectable change in the data.

Different laboratories favor different film-reading instruments, varying from a simple glass scale to precision comparators and microphotometers. All workers seem to agree that magnifications of 1 to 3 are best for visual work, since high magnification renders the lines almost invisible.

Charts have been published<sup>2</sup> by which the proper radiation or combination of radiations for precision photographs may be selected quickly when approximate lattice constants are known.

**Scale of Wavelengths Used.**—For many years the scale of wavelengths used in precision x-ray work has been based on Siegbahn's values<sup>3</sup> (Appendix II) for which the spacing  $d_{100}$  of calcite was assumed to be  $3.02945\text{\AA}$  at 18°C. and Avogadro's number  $N$  was assumed to be  $6.0594 \times 10^{23}$ . It is now known that this scale of wavelengths is not a true scale. Consequently, densities computed from x-ray measurements

<sup>1</sup> E. R. JETTE and F. FOOTE, *J. Chem. Phys.*, vol. 3, p. 605, 1935.

<sup>2</sup> L. A. CARAPPELLA, *J. Applied Phys.*, vol. 11, p. 510, 1940 (for cubic crystals); vol. 11, p. 800, 1940 (for hexagonal, rhombohedral, and tetragonal crystals).

<sup>3</sup> M. SIEGBAHN, "Spectroscopie der Röntgenstrahlen," 2d ed., Springer, Berlin, 1931.

based on it disagree with measured values. Nevertheless, it seems inadvisable at present to discard this scale since it would require recalculation of all the precision lattice constants determined to date and would make them inconsistent with future ones based on an absolute scale.

Foote and Jette<sup>1</sup> suggest that the fundamental equation of density of a crystal be written

$$\rho = \frac{KnM}{V'} \quad (26)$$

where  $V'$  is the volume of the unit cell calculated on the basis of lattice dimensions computed with Siegbahn's wavelengths,  $n$  is the number of atoms (molecules) per cell,  $M$  is the atomic (molecular) weight, and  $K$  is a constant that is chosen to make observed and calculated densities agree. The best value of  $K$  is computed from precision measurements of the rhombohedral angle of calcite, its measured density, and Siegbahn's value  $d_{100} = 3.02945$ . When  $K$  is computed to make calculated and observed densities of calcite agree, it also serves to bring agreement to all other properly measured values. Foote and Jette's value of  $K$  is

$$K = 1.650_{23} \pm 0.00015$$

(Standard deviation =  $14.7 \times 10^{-5}$ )

**Chemical Analysis by X-ray Diffraction.**—The possibility of chemical analysis by the powder method was clearly stated by Hull<sup>2</sup> in 1919 when he pointed out that every crystalline substance gives a diffraction pattern; that the same substance always gives the same pattern; that in a mixture each substance produces its pattern independently of the other, just as if each of the components had been exposed separately for the same length of time; and that quantitative analysis could be made by suitable measurements of the relative intensities of the lines from the various components. Hanawalt and his coworkers at the Dow Company added another useful fact to this list—*viz.*, that the thousands of patterns representing the thousands of different chemical substances can be classified so as to be readily usable for the identification of an unknown substance or even a mixture of unknowns.<sup>3</sup> The classification system they adopted as the result of carrying out several thousand analyses in a period of many years is highly effective and is being made the basis of a "Recommended Practice," by the American Society for Testing

<sup>1</sup> F. FOOTE and E. R. JETTE, *Phys. Rev.*, vol. 58, p. 81, 1940.

<sup>2</sup> A. W. HULL, *J. Am. Chem. Soc.*, vol. 41, p. 1168, 1919.

<sup>3</sup> J. D. HANAWALT and H. W. RINN, *Ind. Eng. Chem.*, anal. ed., vol. 8, p. 244, 1936. J. D. HANAWALT, H. W. RINN, and L. K. FREVEL, *Ind. Eng. Chem.*, anal. ed., vol. 10, p. 457, 1938.

Materials (A.S.T.M.). The reader is referred to the article by Hanawalt, Rinn, and Frevel<sup>1</sup> for details of the technique.

The problem was to devise a classification system somewhat analogous to that employed for filing fingerprints, so that any pattern similar to an unknown could be quickly located in the file and compared with the unknown; this was successfully accomplished by using the *interplanar spacings*,  $d$ , of the lines together with their relative *intensities*. The spectra are classified according to the spacing of the three strongest lines. A set of diffraction data has been prepared by an A.S.T.M. subcommittee, in which is recorded the spacing and intensity data for over a thousand substances.<sup>2</sup> Three cards are included for each substance, one giving the strongest line first, one giving the second strongest line first, and one the third strongest. All cards are arranged in a file in the order of the spacing of the first line listed. On the cards are printed spacings and relative intensities,  $I/I_1$ , for all lines of the spectrum, referred to the intensity of the strongest line. An example taken from the original article,<sup>1</sup> in which 1000 patterns were published, is given in Table VII. In addition to the relative intensities  $I/I_1$ , the approximate absolute intensities are given for a few lines in order to provide a basis for judging relative proportions of components in a mixture of two substances.

TABLE VII.—POWDER DIFFRACTION SPECTRUM FOR FeO (SERIAL NUMBER 425 OF HANAWALT, RINN, AND FREVEL<sup>1</sup>)

$d$	$I$ Absolute intensity	$I/I_1$ Intensity relative to strongest line
2 47	(20)	0.50
2 14	(40)	1.00
1.51	(25)	0.63
1 293		0.15
1 238		0.08
1 072		0.03
0 984		0.03
0.959		0.05
0 876		0.03

The steps in conducting an analysis are as follows:

1. Calculate  $d$  values for all lines of the unknown spectrum, and estimate their relative intensities.

<sup>1</sup> J. D. HANAWALT, H. W. RINN, and L. K. FREVEL, *Ind. Eng. Chem.*, anal. ed., vol. 10, p. 457, 1938.

<sup>2</sup> Obtainable from the A.S.T.M., Philadelphia, Pa.

2. Search the section of the card file containing all substances with the strongest line having  $d$  values near that of the unknown.

3. Locate the entries in this section that have the second strongest line near the second strongest of the unknown (usually a range of  $d$  values  $0.01\text{\AA}$  on each side of the measured value should be searched).

4. Check the third strongest and all the weaker lines against the spectra thus located. The best check is always to compare the films of the known and unknown substances.

When the unknown is a single phase this procedure will find it if listed, but when the unknown is a mixture there will be lines left over that are not explained by the printed spectrum. These leftovers must be treated similarly, as the pattern of one or more additional substances. Another difficulty arises if the constituent giving the strongest line of the unknown pattern is not listed or if the strongest line should happen to be so by virtue of the superposition of weaker lines. Then one must proceed by using the second strongest line to locate the material in the file, etc. Superimposed lines can often be detected by anomalous intensities in the unknown compared with the standard spectra. The procedure when properly conducted should not fail to locate any and all components of a mixture that are listed in the file, provided that the components are present in sufficient quantity to yield readable patterns.

The apparatus with which these standard patterns were prepared consisted of an early-model multiple-diffraction unit employing molybdenum radiation;  $K\beta$  filters of zirconium dioxide were used in front of the film and Fluorazure intensifying screens were placed immediately behind the double-emulsion film. Intensities were judged by comparison with narrow blackened strips that were given exposures in the ratios 1, 2, 4, 8, 10, 15, 20, 30, 50, 75, 125, 175, 250, 325.

**Field of Application of Diffraction Analysis.**—It was found that some substances will produce a pattern in a mixture if they represent only 1 percent or so of the material being examined; but many will not show at less than 10 percent, and some will not show plainly even in a 50 percent mixture. Elements present in solid solution may not be detected by the method as described; their presence can sometimes be inferred from precision measurements of lattice constants or other means. About 5 percent of the solid inorganic substances give only an amorphous pattern with no distinct lines. Liquids can be analyzed only if they can be photographed in the solid state at low temperatures.

Special advantages of the diffraction method of analysis are that it identifies conclusively amounts of material even as small as 0.1 mg.; that it differentiates different phases of the same composition and different states of chemical combination; that it supplies a permanent record of the original data; and that it does not destroy the sample.

**Particle-size Determination.**—The determination of the size of colloidal particles using x-ray diffraction needs but a brief mention, for the great majority of problems in this field can be attacked more successfully by the electron microscope. Elaborate techniques have been worked out for the x-ray method,<sup>1</sup> but these are unnecessary when experiments are confined to particles of about 200Å diameter or less and when no attempt is made to determine the distribution of sizes or the shape of particles. This discussion will therefore be limited to the simplest procedure, the method of mixtures.<sup>2</sup>

Because of the lack of resolving power of very small crystallites each diffraction line is broadened. A plot of intensity vs. angle for such a line will have the shape of an error curve when conditions are favorable for the simplest technique. The breadth of this curve, in radians, is measured from one side of the curve to the other at the level midway between base and peak. Let this measured breadth be  $B_m$ . To correct this width for the many factors arising from the finite width and height of the camera slits, the wavelength distribution in the x-ray beam, the divergence of the beam through the slits, and the penetration of the rays below the surface of the sample, a calibration substance is mixed with the sample. A substance is chosen in which there is no widening of lines from particle size, the substance having particles in the range of  $10^{-4}$  to  $10^{-5}$  cm. A line from this substance is chosen that lies near the previously measured line; let its breadth be  $B_s$ . Under the above conditions the broadening due to particle size alone will then be

$$B_{ps}^2 = B_m^2 - B_s^2$$

and the corrected quantity  $B_{ps}$  may be put in the Scherrer formula

$$L_{hkl} = \frac{0.89\lambda}{B_{ps} \cos \theta}$$

where  $L_{hkl}$  is the thickness of the particles in angstroms in the direction normal to the reflecting plane ( $hkl$ ),  $\lambda$  is the wavelength in angstroms, and  $\theta$  is the Bragg reflecting angle.<sup>3</sup>

<sup>1</sup> For summaries, see GEORGE L. CLARK, "Applied X-rays," 3d ed., McGraw-Hill, New York, 1940. Symposium on Radiography and X-ray Diffraction, A.S.T.M., Philadelphia, 1936. J. T. RANDALL, "The Diffraction of X-rays and Electrons by Amorphous Solids, Liquids and Gases," Wiley, New York, 1934. R. BRILL, *Kolloid-Z.*, vol. 69, p. 301, 1934; vol. 55, p. 164, 1931. C. C. MURDOCK, *Phys. Rev.*, vol. 31, p. 304, 1928; vol. 35, p. 8, 1930.

<sup>2</sup> Details are given of the method as used by B. E. Warren at the Massachusetts Institute of Technology.

<sup>3</sup> Scherrer's original formula contained the constant 0.94 instead of 0.89. For a simple derivation of the constant 0.89 see W. L. Bragg, "The Crystalline State," G. Bell, London, 1933. The exact value of the constant is of little importance in most applications.

It is necessary, of course, that the standard substance (for example, copper powder) produce no lines overlapping those of the sample which are to be measured, that the slits be narrow enough for  $B_s$  to be small compared with  $B_m$ , and that the intensity curve be the shape of an error curve (a partly resolved  $K\alpha$  doublet cannot be used without further correction).

Line broadening begins to be detectable when particle size is reduced below about  $1000\text{\AA}$ . A back-reflection camera with narrow slits of the order of  $0.001$  in. in width is necessary with this range of sizes, while particles  $200\text{\AA}$  or less in diameter may be studied in a Debye camera, preferably with radiation from copper or a similar element.

## CHAPTER VIII

### THE DETERMINATION OF CRYSTAL STRUCTURE

Metals and alloys tend to assume the simpler crystal structures, which can be solved by relatively simple x-ray investigations. It is sometimes possible to guess the structure and to confirm the guess by a few photographs; the position of the alloying elements in the periodic table is usually the background for such a guess, as will be discussed in Chap. XI. On the other hand, many organic and inorganic compounds have crystal structures so complex that they have resisted years of research without being deciphered. Intermediate between these two extremes are the many structures that can be solved by the methods discussed in the preceding chapters. The steps that are generally followed in such a crystal-structure determination are briefly outlined in this chapter.

There is no completely standardized procedure for determining a structure, for each crystal presents new difficulties that may have to be overcome by devising new methods of attack. To do effective work in this field of research requires a critical attitude toward experimental data and inferences drawn from them and a generous expenditure of patience, understanding, and ingenuity.

In solving crystal structures of great complexity it is possible to obtain great benefits from the mathematical device of using Fourier series to analyze the diffraction data. As this is a special development that is infrequently used with alloys, it has been treated in Appendix VI rather than in the present chapter.

The usual steps in determining the structure of a crystal are as follows:

1. Determination of symmetry class (macroscopic symmetry).
2. Determination of size of unit cell.
3. Determination of space lattice.
4. Calculation of number of atoms or molecules in the unit cell.
5. Determination of space group.
6. Tabulation of all possible atomic arrangements and choice of correct one; determination of parameters of this arrangement that fix the exact positions of the atoms within the cell.

With crystals of great complexity, it is sometimes impossible to complete all these steps, although the first five can generally be completed if suitable specimens are available.

**Determination of Symmetry Class.**—Macroscopic symmetry is evident in the arrangement of the growth faces of a crystal. The angles



between well-formed growth or cleavage faces are measured on an optical goniometer. It is convenient to plot the data stereographically so as to recognize more readily the presence of symmetry axes and planes. Measurements of these faces must be interpreted with care, however, for certain faces may be suppressed or the sample may be twinned, with the result that the specimen may appear to have higher symmetry than it actually possesses. The danger of this is lowered by critical examination of several crystals. A study of etch pits on the faces reveals the presence or absence of some symmetry elements that would otherwise be in doubt.

Important information on symmetry is obtained from the optical constants of a crystal when it is transparent. Other physical properties (pyroelectricity, piezoelectricity, etc.) are also useful. Standard books on crystallography and petrography cover the various aspects of this field. The important compilation of crystal forms and crystal properties presented by Groth in his "Chemische Krystallographie" has been the starting point for countless structure determinations. Laue photographs are widely employed to determine symmetry, and Weissenberg photographs can also be used, though x-ray methods are usually unable to distinguish between the presence and absence of a center of symmetry.

**Determination of the Unit Cell.**—The rotating-crystal method is preferred when choosing the correct unit cell from the various cells that can be imagined, for there is then less likelihood of adopting a cell in which some edge is a multiple of the true unit cell. Rotation photographs around each cell edge in turn give the edge lengths directly from layer-line spacings. Laue photographs may also be used and serve as a check on the determination. For precise measurement of axial lengths the powder method is usually preferred, although it is possible to achieve precision in a rotating-crystal photograph with back-reflection technique.<sup>1</sup>

To prevent confusion it has been necessary to adopt conventional rules regarding the choice of axes for the unit cell and the labeling of these axes. It is the custom among crystallographers to choose the shortest three axes that will give a unit cell having the symmetry of the crystal. If orthogonal axes are desired in spite of the symmetry (*e.g.*, orthohexagonal axes), the shortest three orthogonal axes are chosen. A test for the proper unit cell is that each cell edge must be shorter than the face diagonals of all faces touching it. Base-centered or face-centered tetragonal cells are discarded in favor of smaller cells that are simple or body-centered tetragonal; hexagonal and rhombohedral cells are always chosen so as to be simple, and monoclinic cells either simple or base-

<sup>1</sup> M. J. BUEGER, *Z. Krist.*, vol. 97, p. 433, 1937; "X-ray Crystallography," Wiley, New York, 1942.

centered. Triclinic crystals are referred to axes giving smallest simple cells.<sup>1</sup>

**Determination of Space-lattice and Space Group.**—If a unit cell is not simple but is centered on one or more faces or is body-centered, then certain reflections will be absent. From the structure-factor equation, it can be seen that the following criteria hold:

*I*—body-centered lattices: reflections absent if  $h + k + l$  is odd.

*F*—face-centered lattices: reflections absent if  $h, k, l$  are mixed odd and even.

Base-centered lattices:

*A*—face-centered: reflections absent if  $k + l$  is odd.

*B*—face-centered: reflections absent if  $h + l$  is odd.

*C*—face-centered: reflections absent if  $h + k$  is odd.

*P*—simple primitive space-lattices: no systematic absences.

These characteristics result from the fact that in the directions corresponding to missing reflections the waves scattered by body- or face-centered atoms are exactly out of phase with those scattered by the atoms at the cell corners. That is, the spacings of certain planes are halved, and odd-order reflections from such planes are consequently destroyed.

Microscopic symmetry elements likewise reduce certain spacings and destroy corresponding reflections. A glide plane halves the spacings in the direction of glide. A twofold screw axis halves the spacings along the screw axis, while a threefold screw axis reduces spacings along itself to thirds, etc. Table VIII summarizes the reflection characteristics of lattices and symmetry elements. The reflections that are present are listed, rather than those that are absent.

A systematic application of these principles to each of the 230 space groups has now been completed, and characteristic extinctions have been tabulated for each.<sup>2</sup> To determine the space group or the several possible space groups to which a crystal belongs, the crystallographer first assigns indices to his observed reflections, lists them, notes the characteristic absences, and then searches the tables for space groups

<sup>1</sup> For the triclinic system there are 24 possible ways of attaching the labels  $a$ ,  $b$ , and  $c$  to the axes—there would be 48 ways if crystallographers did not universally adhere to right-handed coordinate axes. There has been no universal convention; some writers have chosen the long dimension of an acicular crystal as the  $c$  axis; some have followed a rule that  $c < a < b$ . M. J. Buerger recommends that for consistency the following rules be followed in the future: (1) Label axes so that  $a < b < c$ , and (2) choose the positive directions along these axes so that the interaxial angles  $\alpha$ ,  $\beta$ , and  $\gamma$  are all obtuse.

<sup>2</sup> "International Tabellen zur Bestimmung von Kristallstrukturen," Bornträger, Berlin, 1935. W. T. ASTBURY and K. YARDLEY, *Phil. Trans. Roy. Soc. (London)*, vol. A224, p. 221, 1924. C. HERMANN, *Z. Krist.*, vol. 68, p. 257, 1928. J. D. H. DONNAY and D. HARKER, *Naturaliste canadien*, vol. 67, p. 33, 1940.

TABLE VIII.—REFLECTION CHARACTERISTICS OF LATTICES AND SYMMETRY ELEMENTS

Class of reflection	Condition for reflection ( $n = \text{an integer}$ )	Lattice or symmetry element	Symbol
$hkl$	$h + k + l = 2n$	Body-centered lattice	$I$
	$h + k = 2n$	$C$ —face-centered lattice	$C$
	$h + l = 2n$	$B$ —face-centered lattice	$B$
	$k + l = 2n$	$A$ —face-centered lattice	$A$
	$h, k, l$ all even or all odd	Face-centered lattice	$F$
	$-h + k + l = 3n$	Rhombohedral lattice indexed according to hexagonal axes	$R$
	$h + k + l = 3n$	Hexagonal lattice indexed according to rhombohedral axes	$H$
	All values $h, k, l$	Simple primitive lattice	$P$
$0kl$	$k = 2n$	(100) glide plane with glide of $b/2$	$b$
	$l = 2n$	(100) glide plane with glide of $c/2$	$c$
	$k + l = 2n$	(100) glide plane with glide of $b/2 + c/2$	$n$
	$k + l = 4n$	(100) glide plane with glide of $b/4 + c/4$	$d$
$h0l$	$h = 2n$	(010) glide plane with glide of $a/2$	$a$
	$l = 2n$	(010) glide plane with glide of $c/2$	$c$
	$h + l = 2n$	(010) glide plane with glide of $a/2 + c/2$	$n$
	$h + l = 4n$	(010) glide plane with glide of $a/4 + c/4$	$d$
$hk0$	$h = 2n$	(001) glide plane with glide of $a/2$	$a$
	$k = 2n$	(001) glide plane with glide of $b/2$	$b$
	$h + k = 2n$	(001) glide plane with glide of $a/2 + b/2$	$n$
	$h + k = 4n$	(001) glide plane with glide of $a/4 + b/4$	$d$
$hhl$	$l = 2n$	(1 $\bar{1}$ 0) glide plane with glide of $c/2$	$c$
	$h = 2n$	(110) glide plane with glide of $a/2 + b/2$	$b$
	$h + l = 2n$	(1 $\bar{1}$ 0) glide plane with glide of $a/4 + b/4 + c/4$	$n$
	$2h + l = 4n$	(1 $\bar{1}$ 0) glide plane with glide of $a/2 + b/4 + c/4$	$d$
$h00$	$h = 2n$	[100] screw axis of types $2_1, 4_2$	
	$h = 4n$	[100] screw axis of types $4_1, 4_3$	
$0k0$	$k = 2n$	[010] screw axis of types $2_1, 4_2$	
	$k = 4n$	[010] screw axis of types $4_1, 4_3$	
$00l$	$l = 2n$	[001] screw axis of types $2_1, 4_2, 6_3$	
	$l = 3n$	[001] screw axis of types $3_1, 3_2, 6_2, 6_4$	
	$l = 4n$	[001] screw axis of types $4_1, 4_2$	
	$l = 6n$	[001] screw axis of types $6_1, 6_2$	
$hh0$	$h = 2n$	[110] screw axis of type $2_1$	

having similar absences. In so doing he must bear in mind that his choice of  $a$ ,  $b$ , and  $c$  edges may be interchanged with respect to those listed in the tables and must take precautions to avoid being misled by this. (For example, he may list the absences in terms of every possible permutation of  $a$ ,  $b$ , and  $c$  axes.) A large number of indexed reflections should be available in order to show the characteristic absences well.

Properly done, this procedure yields a list of every possible space group to which the crystal could belong. Prism-face reflections (one index zero) are studied carefully to distinguish between systematic absences and "accidental" extinctions arising from the particular position of certain atoms in the cell, and an attempt is made to single out the space group that explains all systematic absences. If it is known to which of the 32 classes a crystal belongs, it is generally possible to establish the space group unequivocally, but when the symmetry class is in doubt this may not be possible. Reflection planes and rotation axes do not cause extinctions, and therefore the presence or absence of them cannot be determined from lists of reflections. Another source of ambiguity should be mentioned: the shielding of some characteristic extinctions by a more general class of extinctions. When there is a characteristic set of extinctions in some general class of reflections, this includes corresponding extinctions in a less general class. For example, a body-centered lattice produces extinctions in  $hkl$  reflections whenever  $h + k + l$  is odd, but it also extinguishes  $h0l$  reflections when  $h + l$  is odd and  $h00$  reflections when  $h$  is odd. If the body-centered crystal in this example contained a screw axis  $2_1$ , this could not be detected, for it also would extinguish  $h00$  reflections when  $h$  is odd.

Certain sets of special atomic positions occur in many different space groups. Such a set is called a **lattice complex**. For example, the body-centered cubic set of points (coordinates  $000, \frac{1}{2}\frac{1}{2}\frac{1}{2}$ ) is a special position of the space group  $O_h^2-Im\bar{3}/m$ , but it is found also in space group  $O_h^1-Pm\bar{3}/m$ . Heavy atoms may be located at such a set of points and give strong reflections, while light atoms, scattering weakly, may be at places corresponding to only one of these space groups. Lists of lattice complexes are used by some crystallographers to aid in recognizing the various possibilities.

Another convenience in space-group tables is a list of **point symmetries**, which gives the symmetry of the group of atoms that exists around a given point position in the crystal. A study of such a list shows possible positions for a group of atoms, such as a silicate group, and eliminates incompatible positions.

**Number of Atoms or Molecules per Unit Cell.**—The number of molecules in the unit cell is determined from the measured density of the substance,  $\rho$ , the known mass of each molecule,  $M$ , and the volume

of the cell,  $V$ . The obvious relation is  $\rho = nM/V$ , where  $n$  is the number of molecules in the cell and  $M$  is the molecular weight multiplied by the mass of an atom of unit molecular weight ( $1.65 \times 10^{-24}$  g.). In a chemical compound with definite molecular formula,  $n$  is integral and is determined as the integer that most nearly satisfies the relation  $n = \rho V/M$ . In alloys a modified formula must be used, which is given in Chap. XI.

**Determination of Atomic Positions.**—If the space group or possible groups have been identified and the number of atoms of each kind in the cell is known, the space-group tables give at once the possible arrangements of the atoms. If it is found, for example, that there are four atoms of a certain kind in the unit cell, it can be assumed that they will lie on a set of equivalent positions containing four atom positions. (In alloys, however, there are exceptions to this rule which are discussed in Chaps. XI and XII.) There are usually several arrangements to be considered, and each is likely to involve one or more variable parameters. The choice of atom arrangement and the fixing of parameters depend upon relative intensities of different reflections and are accomplished by finding the atom positions that give the best match between calculated and observed intensities throughout a long list of reflections. Relative intensities are computed by the structure-factor equation (preferably modified by the other intensity factors of Appendix V). Simplified formulas for the structure factor will be found in space-group tables, particularly Lonsdale's.<sup>1</sup>

Crystals with one or two parameters can be solved rather directly (graphical aids are useful in this work),<sup>2</sup> and more parameters can be handled if they happen to be separable into independent pairs. In complicated structures it is impossible to guess or to deduce by straightforward methods what values of the many parameters are likely because there is a multiple infinity of atom positions to be considered. For these crystals the methods of Fourier series are of great value in fixing parameters and indicating atomic arrangements. These are discussed in Appendix VI. In complex crystals it often happens that atoms of a certain kind, owing to their restricted number, must occupy special positions in the cell, as specified by the space group. These are frequently heavy atoms which make a large contribution to the structure factor, and the analysis can begin with these, using preliminary computations which are followed by successive approximations until all atoms are located. An example is West's analysis of potassium dihydrogen

<sup>1</sup> K. LONSDALE, "Simplified Structure Factor and Electron Density Formulae for the 230 Space Groups of Mathematical Crystallography," G. Bell, London, 1936.

<sup>2</sup> W. L. BRAGG, *Nature*, vol. 138, p. 362, 1936. W. L. BRAGG and H. LIPSON, *Z. Krist.*, vol. 95, p. 323, 1936. J. M. ROBERTSON, *Nature*, vol. 138, p. 683, 1936.

phosphate.<sup>1</sup> Very complex crystals have been solved, when they are one of an isomorphous series of compounds, by substituting a different element for one of the elements of the compound. This frequently can be done without altering atomic positions in the unit cell, thus changing the intensities of certain reflections and thereby revealing the positions of the substituted atoms.

A knowledge of atomic and ionic sizes and of the habitual groupings of atoms—coordination and the factors governing it—can aid the crystallographer by forming a basis for judging whether a given atomic arrangement is possible.

**Sizes of Atoms and Ions.**—The distances between atom centers in crystals can be interpreted as the sum of the radii of the two neighboring atoms, as if they were tightly packed spheres. After lengthy study of crystallographic data it was found that a consistent set of radii can be

TABLE IX.—RADII OF ATOMS IN METALLIC CRYSTALS ACCORDING TO GOLDSCHMIDT<sup>1</sup> FOR COORDINATION NUMBERS 12, 8, AND 4

Element	Coordination number			Element	Coordination number		
	12	8	4		12	8	4
Li	1.37	1.52		Ru	1.32	1.28	
Be	1.13	1.10		Rh	1.34	1.30	
C	..	..	0.77	Pd	1.37	1.33	
Na	1.92	1.86		Ag	1.44	1.40	
Mg	1.60	1.55		Cd	1.52	1.47	
Al	1.43	1.39		In	1.57	1.52	
Si	..	..	1.17	Sn	1.58	1.53	1.40
K	2.36	2.29		Sb	1.61	1.56	
Ca	1.97	1.91		Cs	2.74	2.66	
Ti	1.45	1.41		Ba	2.25	2.18	
V	1.36	1.32		Ce	1.81	1.76	
Cr	1.28	1.24		Hf	1.59	1.53	
Mn	1.30	1.26		Ta	1.46	1.42	
Fe	1.27	1.24		W	1.41	1.37	
Co	1.26	1.22		Re	1.37	1.34	
Ni	1.24	1.21		Os	1.34	1.30	
Cu	1.28	1.24		Ir	1.35	1.31	
Zn	1.37	1.34		Pt	1.38	1.34	
Ge	1.39	1.34	1.22	Au	1.44	1.40	
As	1.40	1.35		Hg	1.55	1.50	
Rb	2.53	2.46		Tl	1.71	1.66	
Sr	2.16	2.10		Pb	1.74	1.69	
Zr	1.60	1.55		Ti	1.82	1.77	
Mo	1.40	1.36		Th	1.80	1.75	

<sup>1</sup> V. M. GOLDSCHMIDT, *Trans. Faraday Soc.*, vol. 25, p. 253, 1929.

assumed so a given element always has approximately the same radius when in the same valence state and in similar surroundings. Sizes depend on whether an atom is closely bonded to 1, 2, 3, 4, 6, 8, or 12 neighbors; as the coordination (number of nearest neighbors) increases, the radius

<sup>1</sup> J. WEST, *Z. Krist.*, vol. 74, p. 306, 1930.

of an atom or ion increases. Sizes also depend upon the nature of the binding forces in the crystal—ionic, covalent, van der Waals, or metallic. Variations are also introduced by the valence state of neighboring ions and by their sizes (radius ratio effect). For tables of radii and discussions of how they apply in crystal-structure determination, the crystallographer should refer to original papers on empirical and theoretical radii<sup>1</sup> or to recent summaries.<sup>2</sup> Table IX lists values for radii of atoms in metallic crystals for coordination numbers 4, 8, and 12.

**Example of Structure Determination.**—Jacob and Warren's determination<sup>3</sup> of the structure of uranium will serve to illustrate many of the steps in a determination of crystal structure. It is an unusual example in that powder diffraction data alone are sufficient to solve the structure, even though it is orthorhombic.

Thirty-nine lines were measured on a powder pattern<sup>4</sup> and were graded in intensity as strong, medium, weak, or very weak. From the table of interplanar spacings it was immediately noted that the structure could not be cubic. No satisfactory agreement was obtained on the hexagonal and tetragonal Hull-Davey charts. It was therefore concluded that the symmetry was orthorhombic or lower, and the fact that the pattern was not particularly complicated suggested that the symmetry was not lower than orthorhombic.

A procedure for assigning indices was followed that is analogous to Bjurström's (page 131). The orthorhombic reciprocal-lattice points and the crystal spacings are related by the equation

$$\frac{1}{d^2} = h^2 a^{*2} + k^2 b^{*2} + l^2 c^{*2}.$$

Any plane network of points in this lattice that contains the  $a^*$ ,  $b^*$ , or  $c^*$  axes will be an orthogonal net, and the lattice can be considered as constructed of a series of these nets. A Hull type chart was made for two-dimensional orthogonal nets by using the logarithm of this expression

<sup>1</sup> V. M. GOLDSCHMIDT, *Trans. Faraday Soc.*, vol. 25, p. 253, 1929. I. PAULING, *J. Am. Chem. Soc.*, vol. 49, p. 765, 1927; vol. 50, p. 1036, 1928; vol. 53, p. 1367, 1931; *Proc. Roy. Soc. (London)*, vol. A114, p. 181, 1927. W. H. ZACHARIASEN, *Z. Krist.*, vol. 80, p. 137, 1931. I. PAULING and M. L. HUGGINS, *Z. Krist.*, vol. 87, pp. 205, 222, 1934.

<sup>2</sup> C. W. STILLWELL, "Crystal Chemistry," McGraw-Hill, New York, 1938. "International Tabellen zur Bestimmung von Kristallstrukturen," Bornträger, Berlin, 1935. R. W. G. WYCKOFF, "The Structure of Crystals," Chemical Catalog Co., New York, 1931.

<sup>3</sup> C. W. JACOB and B. E. WARREN, *J. Am. Chem. Soc.*, vol. 59, p. 2588, 1937.

<sup>4</sup> Copper radiation was filtered through nickel to remove  $K\beta$ , and 0.002 in. aluminum covered the film to remove fluorescent  $M$  radiation from the sample. Copper filings were mixed with the uranium filings in some exposures for calibration.

with one term equal to zero, in the form

$$-2 \log d = 2 \log a^* + \log \left[ h^2 + \left( \frac{c^*}{a^*} \right)^2 l^2 \right].$$

The experimental  $d$  values, plotted on a strip, were moved about on the chart in the usual way. Several positions were found at which about six  $d$  values fitted lines of the chart. Each of these positions, if it is not accidental and spurious, indicates two possible axes of the reciprocal lattice—at least one of which must be a principal axis,  $a^*$ ,  $b^*$ , or  $c^*$ . Among a series of values so obtained the principal axes will occur most often. Three of the positions that appeared particularly important led to the following three pairs of possible reciprocal axes:

$$(a) \ 0.1696, 0.2023 \qquad (b) \ 0.1696, 0.3510 \qquad (c) \ 0.2023, 0.3901$$

Since 0.3901 could be a diagonal of a rectangle having sides 0.3510 and 0.1696, the latter were assumed to be two of the principal axes and 0.2023 the third. In this way, tentative values for the axes were found. These reciprocal lattice axes were confirmed when computation showed that an orthorhombic unit cell having crystal axes  $a = 2.852$ ,  $b = 5.865$ , and  $c = 4.945 \text{ \AA}$  predicts all observed spacings satisfactorily.

Indices were assigned to each reflection, and the following characteristics could be noted:

General reflections  $hkl$  occur only for  $(h + k)$  even (111, 131, etc.).

Prism reflections  $h0l$  occur only for  $h$  and  $l$  even (202, 204, etc.).

Prism reflections  $0kl$  occur only for  $k$  even (021, 022, 040, etc.).

Prism reflections  $hk0$  occur only for  $(h + k)$  even (110, 130, 220, etc.).

Reference to space-group tables shows that these are found among the orthorhombic space groups only in  $D_{2h}^{17}$ — $Cmcm$ .

The number of uranium atoms in the unit cell was calculated from the measured density,  $\rho$ , by

$$n = \frac{V\rho N}{A} = \frac{2.852 \times 5.865 \times 4.945 \times 18.9 \times 0.606}{238} = 4.0$$

where  $N/A$  is Avogadro's number divided by the atomic weight. The four atoms could be placed at special positions  $4a$ ,  $4b$ , or  $4c$ :

$$4a: 000; 00\frac{1}{2}; \frac{1}{2}\frac{1}{2}0; \frac{1}{2}\frac{1}{2}\frac{1}{2}$$

$$4b: 0\frac{1}{2}0; 0\frac{1}{2}\frac{1}{2}; \frac{1}{2}00; \frac{1}{2}0\frac{1}{2}$$

$$4c: 0y\frac{1}{4}; 0\bar{y}\frac{3}{4}; \frac{1}{2}y + \frac{1}{2}, \frac{1}{4}; \frac{1}{2}, \frac{1}{2} - y, \frac{3}{4}$$

Special positions  $4a$  and  $4b$  were excluded because they would halve the  $c$  spacings and  $hkl$  would then occur only if  $l$  were even; so special position  $4c$  was left as the only possibility. The structure factor for space group



$D_{2h}^{17}$ — $Cmcm$ , which has also been labeled  $V_h^{17}$ , reduces to

$$F = \sum f \cos^2 2\pi \frac{h+k}{4} \cos 2\pi hx \cos 2\pi \left( ky - \frac{l}{4} \right) \cos 2\pi \left( lz + \frac{l}{4} \right).$$

For the reflections listed above and for atom positions  $4c$  this reduces further to

$$\begin{aligned} F &= 4f \sin 2\pi ky, & \text{when } l \text{ is odd,} \\ F &= 4f \cos 2\pi ky, & \text{when } l \text{ is even.} \end{aligned}$$

In fixing the parameter  $y$  it is unnecessary to consider values beyond the range 0 to 0.25, for other values will be seen to be equivalent to these when the origin of coordinates is shifted.

From the fact that 020 and 022 are very weak it follows that  $\cos 2\pi 2y$  is nearly zero or  $y$  is approximately  $\frac{1}{8}$ . By trial it was found that assuming  $y = 0.105 \pm 0.005$  made calculated and observed intensities agree satisfactorily. In comparing calculated and observed intensities there was a strong absorption correction to be considered; this was avoided by comparing relative intensities of neighboring lines only.

After the coordinates of the atoms are determined it is usually necessary to plot the atoms or to construct a model in order to comprehend their true arrangement in space, which is the fundamental information sought. In fact, axes, space-lattices, space groups, atom coordinates, parameter values, number of atoms per unit cell, etc., can

be considered merely as aids to the crystallographer in reaching this end and in reporting his results to others

The data for uranium are plotted in Fig. 1, which shows a plan and an elevation view of the structure. The atoms are indicated by circles, and the fractions within the circles give the height of the atoms above the plane of the drawing in terms of the axial length. By studying this drawing (or an extension of it to several unit cells) it will be found that the orthorhombic structure, with atom positions  $4c$  where  $y = 0.105$ , can be considered as a distorted hexagonal close-packed structure in which 4 of the 12 nearest neighbors of the hexagonal array are moved in to appreciably closer distances.

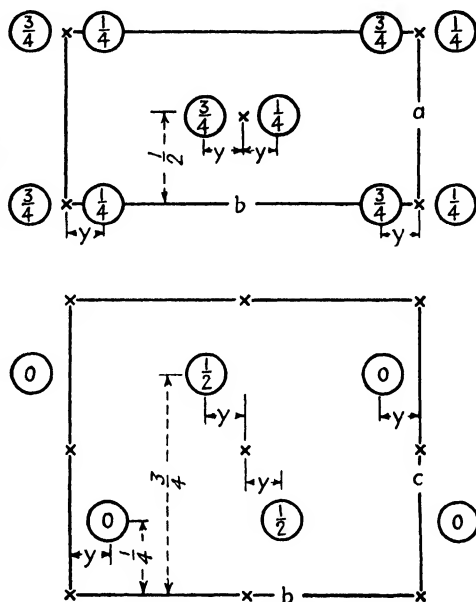


FIG. 1.—Uranium. (Jacob and Warren.)

## CHAPTER IX

### POLE FIGURES AND ORIENTATION DETERMINATION

The orientations of single crystals and aggregates are of such importance in laboratory investigations of metals and other crystalline materials that it seems appropriate to devote a chapter to a detailed explanation of orientation methods. The plotting of pole figures which show the preferred orientations in polycrystalline aggregates is covered first, since it is of most general interest, and is followed by a treatment of x-ray

methods and etch-pit methods applicable to single crystals.

#### Detection of Preferred Orientations.

When the grains of a poly-crystalline metal are oriented at random, a photograph made by passing a "pinhole" beam through the metal will show Debye rings of uniform intensity all around their circumference. On the other hand, if the grains cluster around certain orientations so the metal has a **texture** or **preferred orientation**, then more grains will be in position to reflect to certain segments of the diffraction rings than to others, and the rings will have maxima.

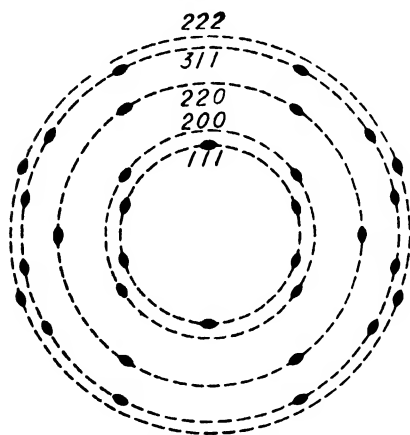


FIG. 1.—Pattern of cold-drawn aluminum wire. Radiation of a single wavelength incident perpendicular to the wire axis, which is vertical.

Figure 1 illustrates the pattern that is obtained with monochromatic x-rays from a cold-drawn wire of aluminum, which is a face-centered cubic metal that becomes oriented with the  $[111]$  direction in each grain parallel to the axis of the wire. The dashed circles represent Debye rings that would be present if the metal had a random orientation, with all orientations present. The limited number of orientations that are present in the wire permit only a few spots in the Debye rings to appear strongly, as indicated in the figure. A common axis in all grains or crystalline fragments is parallel to the wire, but all other axes have a random distribution around the wire; *i.e.*, all azimuthal orientations around the axis are equally probable. An x-ray photograph of the wire is in effect a rotating-crystal photograph in which the axis of rotation

of the crystal corresponds to the axis of the wire.<sup>1</sup> The textures of wires are appropriately called **fiber textures**, for they resemble the structure of fibrous materials. The axis of symmetry of the texture (the longitudinal axis of a wire) is the **fiber axis**. In a rolled sheet, on the other hand, there is no longer an equal probability of all orientations around the direction of elongation (the direction of rolling), and a more detailed analysis is necessary. The stereographic projection is almost universally used for this purpose.

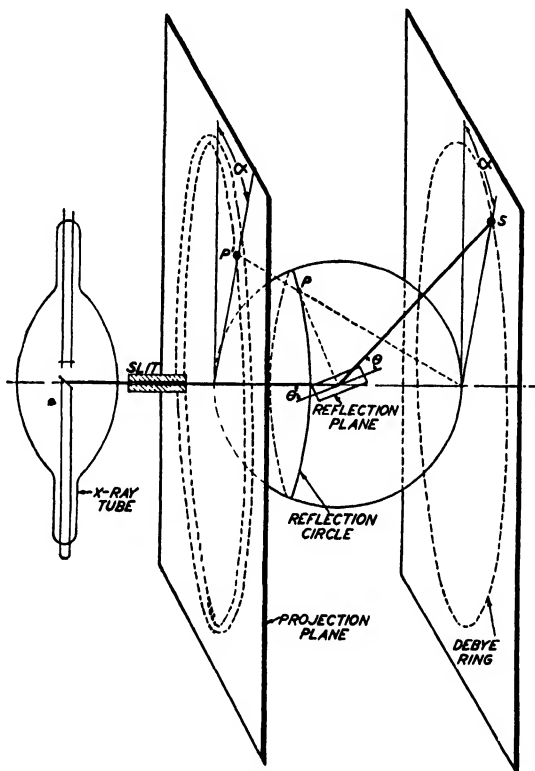


FIG. 2.—Relation between crystal plane, diffracted beam, and stereographic projection. Pole  $P$ , diffracted spot  $S$ , and projection  $P'$  all lie in a plane, which also contains the incident beam.

**Stereographic Projection of Data.**—There is a simple and direct relation between spots on a preferred orientation pattern and their stereographic projection. This is illustrated in Fig. 2. A crystal plane is here shown in position to reflect a beam of x-rays to form a spot  $S$  on the film. The plane normal intersects the reference sphere, which is inscribed about it, at the point  $P$ , which projects stereographically to the point  $P'$  in the projection plane. The incident beam, the reflected beam, and

<sup>1</sup> The intense spots on the Debye rings are actually on layer lines. If the axis of the wire has indices  $[uvw]$  in each oriented grain, then the  $n$ th layer line will contain the spots  $hkl$  for which  $hu + kv + lw = n$ .

the pole of the reflecting plane all lie in the same plane tipped at an angle  $\alpha$  from the vertical. Thus, when the film and projection plane are placed normal to the beam as shown, it will be seen that the angle  $\alpha$  on the projection will be exactly equal to  $\alpha$  on the film.

Since the angle of incidence,  $\theta$ , of the beam on the crystal plane is determined by the Bragg law  $n\lambda = 2d \sin \theta$  whenever reflection occurs, it follows that the poles of all planes capable of reflecting must lie at a constant angle  $90 - \theta$  from the incident beam and must therefore intersect the reference sphere only along the circle known as the "reflection circle," a circle on the projection  $90 - \theta$  from the centrally located beam. Both the azimuthal and radial positions on the pole figures are thus determined.

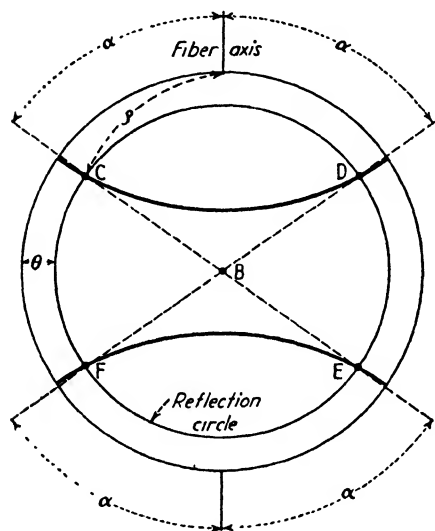


FIG. 3.—Ideal pole figure for (100) planes in a wire of a cubic metal having a [111] fiber texture. Poles at  $C, D, E, F$  can reflect when x-ray beam is at  $B$ .

tions would fall upon the film at equal angles,  $\alpha$ , from the projection of the fiber axis.

It was remarked earlier that the angle  $\alpha$  is identical on projection and film, but Fig. 3 shows that this is not exactly equal to the angle  $\rho$  between the pole of the reflecting plane and the fiber axis. From the geometry of the figure when the beam is normal to the fiber axis, it follows that

$$\cos \rho = \cos \alpha \cos \theta$$

which approaches the relation  $\alpha = \rho$  as  $\theta$  approaches 0.\* If the fiber axis is inclined so it makes an angle  $\beta$  with the incident beam, the corre-

\* A plot of this function and of the corresponding one for the fiber axis inclined at a certain angle to the beam has been worked out by R. M. Bozorth, *Phys. Rev.*, vol. 23, p. 764, 1924.

**Fiber Textures.**— Let us consider an ideal fiber texture in which all grains have a certain crystallographic direction, say [111], parallel to the fiber axis. The stereographic projection of the (100) planes would then form the pole figure of Fig. 3, in which (100) poles of various grains lie at various spots along the latitude lines shown as heavy lines at an angle  $\rho = 54^\circ 44'$  from the fiber axis, since this is the angle between [111] and [100] poles. Now if a beam entered the reference sphere at  $B$ , perpendicular to the fiber axis, and reflected from the planes at the Bragg angle  $\theta$ , reflections would occur at the intersections  $C, D, E$ , and  $F$ . All reflections

sponding equation is

$$\cos \rho = \cos \beta \sin \theta + \sin \beta \cos \theta \cos \alpha.$$

Thus a series of  $\rho$  values can be computed for the observed spots on a film, and from these the indices of the fiber axis may be deduced with the aid of tables of angles between crystallographic directions. Some textures are composed of two fiber textures superimposed; for example, iron after compression has some grains with [111] parallel to the fiber axis and others with [100], forming a **duplex fiber texture** [111] + [100].

A graphical determination of fiber axis from a series of  $\rho$  values is shown in Fig. 4. On a stereographic projection the point is found (F.A.) that is the proper angle  $\rho$  from the pole of each reflecting plane; such a point is then the projection of the fiber axis and can be identified by reference to a standard projection. In Fig. 4 the fiber axis coincides with [112]. Note that the arcs in the figures are loci of points at equal *angles* from reflecting poles, not equal *distances*. If

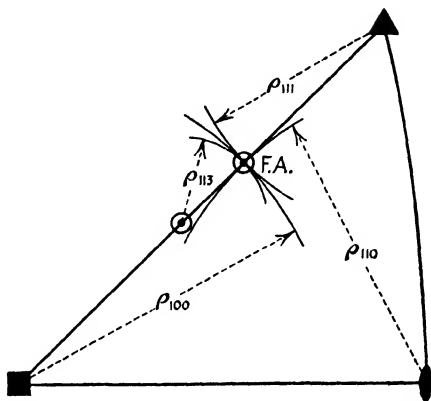


FIG. 4.—Method of determining fiber axis (F.A.) on a standard stereographic projection of a cubic crystal. Angle  $\rho$  for each reflection is laid off from a corresponding pole of projection.

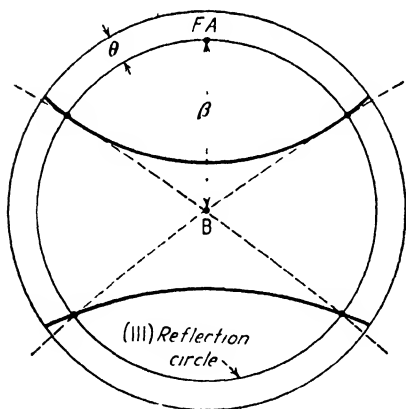


FIG. 5.—Stereographic projection showing fiber axis tilted to cause strong reflection from planes normal to F.A. Beam is at B.

there is a considerable range of orientation in the specimen, both maximum and minimum  $\rho$  values may be plotted and an *area* determined on the standard projection rather than a *point*.

If a plane ( $hkl$ ) is perpendicular to the fiber axis in each grain, it is advantageous to tilt the wire with respect to the x-ray beam so as to reflect from this plane. A tilt of  $\theta_{hkl}$  will obviously do this, since the reflection circle will then touch the fiber axis. For the case of aluminum wire, the fiber axis is [111] and for molybdenum rays  $\theta_{100} = 10.1^\circ$ .

The tilted condition is represented in the (111) pole figure of Fig. 5. The reflection in the vertical plane is very strong, since all grains of the texture contribute to it, while only a small fraction of the grains contribute to the other reflections. Thus, for example, a weak texture in iron after compression can readily be

shown by this kind of tilting of the specimen,<sup>1</sup> although it has been overlooked in some less sensitive tests.

**Plotting of Pole Figures.**—Preferred orientations produced by deformation other than simple uniaxial elongation or compression are complex. While they are often described in terms of **ideal orientations** with certain crystal axes parallel to the principal axes of strain, the choice of indices is often arbitrary and the description is incomplete. **Pole figures** provide a complete description of the texture and provide a safer basis for studies of the underlying mechanism, for they represent the observational data in an unprejudiced manner.<sup>2</sup>

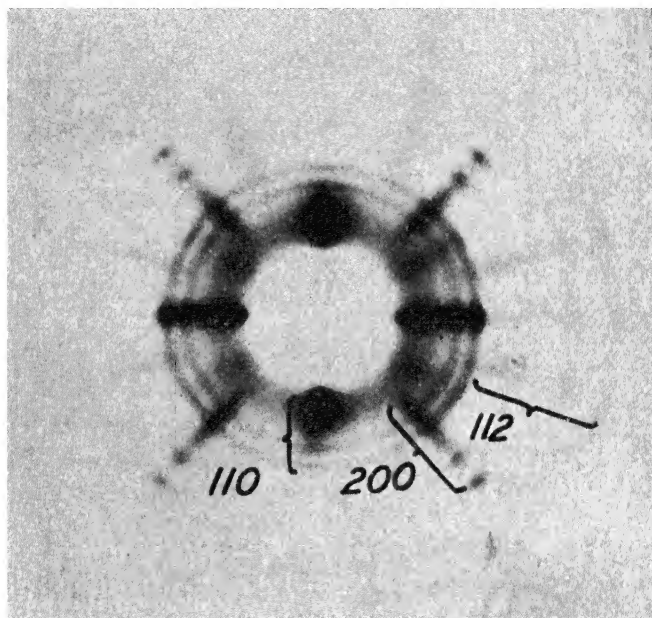


FIG. 6.—Diffraction pattern of cold-rolled steel. Mo radiation perpendicular to rolled surface, rolling direction vertical. Shows  $K\alpha$ ,  $K\beta$  and white radiation reflections from (110), (200), and (112) planes.

To plot a pole figure, the relations of Fig. 2 are kept in mind. All the intensity maxima on a single diffraction ring (Debye ring) are plotted on a single reflection circle on the pole figure. When the circle cuts through heavily populated regions on the pole figure, the diffraction ring will show intense blackening at the same azimuth; when it cuts through lightly populated regions, the corresponding arc of the diffraction ring will be weak. To determine the true extent of the areas on the pole figure it is necessary to plot a series of reflection circles that form a network covering the projection. This is accomplished by taking a series

<sup>1</sup> C. S. BARRETT, *Trans. A.I.M.E.*, vol. 135, p. 296, 1939.

<sup>2</sup> F. WEVER, *Mitt. Kaiser-Wilhelm Inst. Eisenforsch. Düsseldorf*, vol. 5, p. 69, 1924; *Z. Physik*, vol. 28, p. 69, 1924; *Trans. A.I.M.E.*, vol. 93, p. 51, 1931.

of diffraction patterns with the specimen tilted increasing amounts in steps of 5 or 10°. The number of exposures in such a series may vary from 5 to 20, depending upon the detail required in the pole figure. An oscillating-film arrangement can be used in texture cameras so that one exposure gives the information ordinarily obtained from many individual exposures of the stationary type (see later section on cameras, page 163).

The plotting of the data will be illustrated, using rolled steel as an example. If the radiation from molybdenum is used, the photographs will resemble Fig. 6, with concentric Debye rings (incomplete) from  $K\alpha$  and  $K\beta$  characteristic radiation and an inner band from white radiation. The diffraction from the ferrite {110} planes will occur at  $\theta = 10^\circ$ , and the reflection circle will lie  $90 - \theta = 80^\circ$  from the center of the pole figure. If the first photogram is made with the beam normal to the surface of the specimen, the surface will appear on the projection as the basic circle and the reflection circle will lie concentric with it.

Let us suppose that the specimen is then rotated about a vertical axis and a new photogram taken with the specimen turned, say 30°, the near side rotating to the left as we look away from the x-ray tube. We first plot the data as before, with the projection plane again normal to the beam and the reflection circle again concentric. This is illustrated in Fig. 7, where the reflection circle is shown as a dashed circle and an intensity maximum is indicated between the limits A and B. But with this setting of the specimen its surface will lie at a tilt of 30° from the projection plane (the right side tilted up from the projection plane), and all data from this setting must be rotated 30° back to the right in order to plot a pole figure in which the plane of the specimen is the projection plane. The rotation is done with the Wulff net, each point on the reflection circle being moved to the right along its latitude line a distance of 30° of longitude. This is shown in Fig. 7, where the reflection circle with the intensity maximum on it is plotted after rotation as a full line. Part of the rotated reflection circle on the right-hand side passes to the negative hemisphere and is shown as a broken line. The process is repeated with different settings of the specimen and corresponding rotations of the data until the areas on the pole figure are sufficiently well defined.

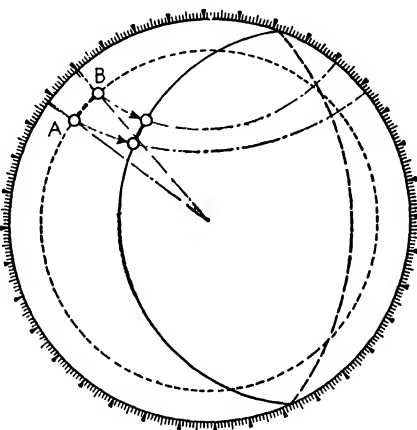


FIG. 7.—Plotting a pole figure. (-----), reflection circle with beam normal to projection plane. (—) and (— —), reflection circle with plane of specimen as projection plane.

Much of the labor of plotting may be eliminated if a chart is made up in which the series of reflection circles are shown in the position they would have after rotation back to the normal setting, *i.e.*, their position with respect to the surface of the specimen as the projection plane. A different chart is required, of course, for every different value of  $\theta$  that is used, thus for different wavelengths, different specimen materials, and different reflecting planes. Wever<sup>1</sup> has published charts for copper  $K\alpha$  radiation reflecting from {001} and from {111} planes of aluminum and for iron  $K\alpha$  radiation

<sup>1</sup> F. WEVER and W. E. SCHMID, *Mitt. Kaiser-Wilhelm Inst. Eisenforsch. Düsseldorf*, vol. 11, p. 109, 1929. F. WEVER, *Trans. A.I.M.E.*, vol. 93, p. 51, 1931.

reflecting from  $\{110\}$  of iron. Figure 8 presents a chart for molybdenum  $K\alpha$  radiation reflecting from  $\{110\}$  planes of iron ( $\theta = 10^\circ$ ) with reflection circles plotted for every  $5^\circ$  rotation interval from 0 to  $90^\circ$ . The azimuthal positions on all the circles are given by their intersections with the latitude lines that are drawn on the chart and labeled with values of the angle  $\alpha$  (the numbers around the circumference). When the reflection circles lie on the back hemisphere, they are shown as dashed lines, but the same lines of constant  $\alpha$  apply as on the near hemisphere. This same chart will serve for plotting the  $\{200\}$  reflections from iron if one reads the intensity maxima on

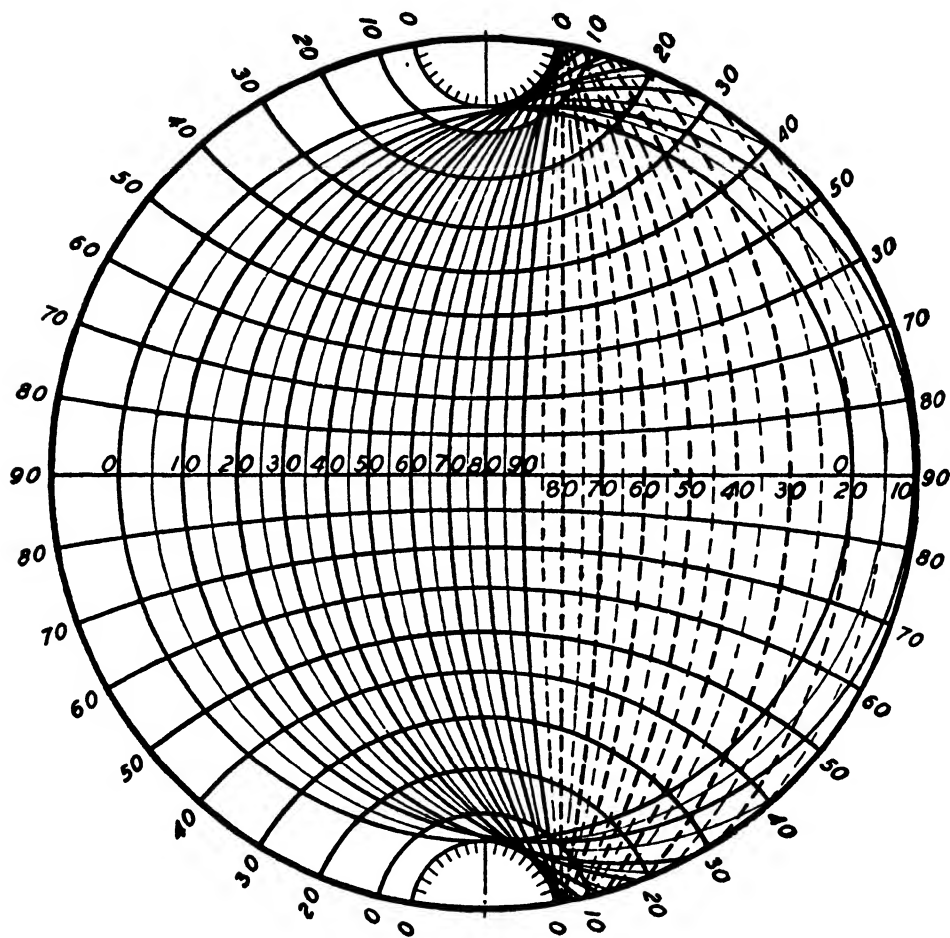


FIG. 8.—Pole-figure chart for Mo  $K\alpha$  radiation reflecting from  $\{110\}$  planes of iron ( $\theta = 10^\circ$ ).

the broad ring caused by general (white) radiation. In this instance, the most intense portion of the  $\{200\}$  reflection of the general radiation from a tube operating at 30 or 40 kv. is in the neighborhood of  $\theta = 10^\circ$ . The maximum intensity of general radiation from  $\{110\}$  planes is around  $\theta = 7^\circ$  and is particularly suitable for pole-figure work, for it is free from overlapping  $\{200\}$  reflections and shows clearly the slight differences of intensity that are sometimes important. A chart for plotting the  $\{200\}$  reflections of molybdenum  $K\alpha$  from iron ( $\theta = 14^\circ 20'$ ) is reproduced in Fig. 9.

Areas near the top and bottom of the pole figure are not crossed by any reflection circles on the chart. To fill in these areas the specimen may be turned  $90^\circ$  on its own



plane and then rotated a small amount about the vertical axis, as before. (This requires turning the pole figure plot  $90^\circ$  with respect to the reflection-circle chart.) The number of exposures may be reduced by making use of the symmetry of the orientations in the structure; in rolled sheet, for example, a symmetry plane may be anticipated normal to the rolling direction and another normal to the transverse direction in the sheet, but it is always advisable to test for these symmetry planes before assuming them.

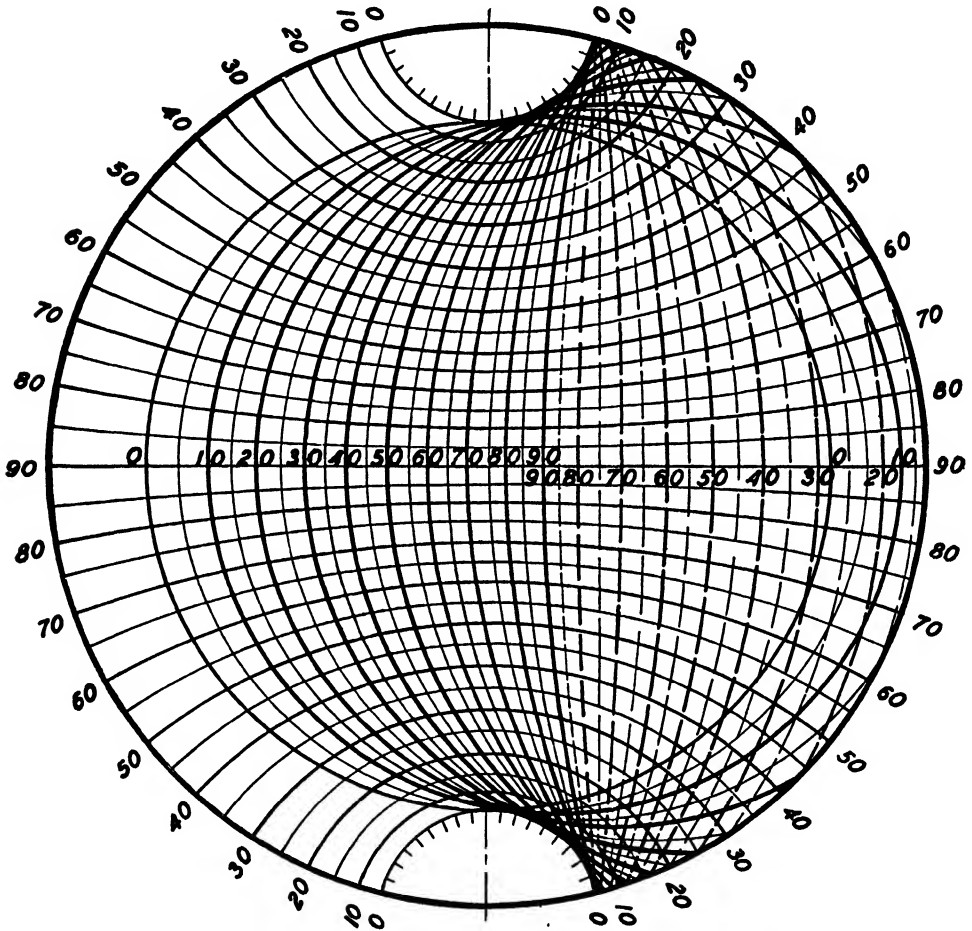


FIG. 9.—Pole-figure chart for Mo  $K\alpha$  radiation reflecting from (200) planes of iron ( $\theta = 14^\circ 20'$ ).

A pole figure for a mild-steel sheet rolled to a reduction of thickness of 85 percent and etched so that the surface layers are removed is shown in Fig. 10.<sup>1</sup> The rolling plane is parallel to the projection plane, with the rolling direction at the top. This figure illustrates why it is that preferred orientations appear more prominently in photograms made with the beam along or near to the transverse axis of a rolled-steel sheet than with the beam normal to the rolling plane. The (110) reflection circle for a beam of white radiation normal to the rolling plane is shown as a dotted circle near the periphery and nowhere passes into regions of greatly differing intensity.

<sup>1</sup> M. GENSAMER and R. F. MEHL, *Trans. A.I.M.E.*, vol. 120, p. 277, 1936.

On the other hand, the reflection circle for a beam along the transverse direction appears as a dotted line extending from top to bottom near the center of the projection and passes through regions of both maximum and minimum intensity, which would yield more pronounced maxima and minima on the (110) diffraction rings.

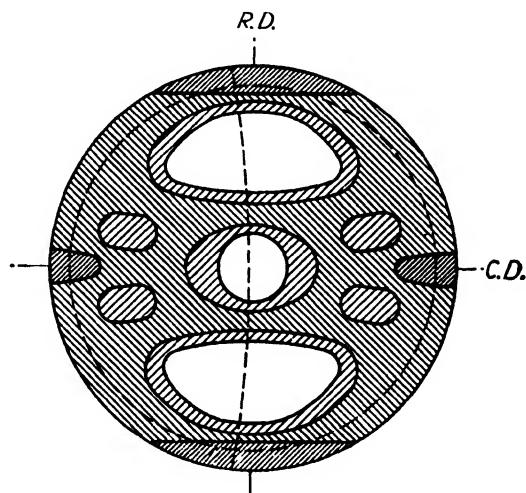


FIG. 10.—Pole figure for  $\langle 110 \rangle$  poles of mild steel reduced 85 per cent in thickness by cold-rolling. Two reflection circles shown (dashed). (*Gensamer and Mehl.*)

**Specimens and Cameras for Texture Studies.**—When a sheet specimen is used for pole-figure studies, there is an absorption correction that depends markedly on the angle of setting in the camera. Bakarian<sup>1</sup>

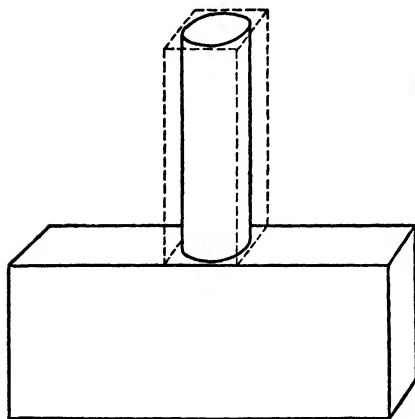


FIG. 11.—Specimen for preferred orientation photograph of sheet material. (*Bakarian.*)

has improved the technique by cutting a stem out of the sheet metal with a jeweler's saw, then grinding the stem to a cylindrical shape, as in Fig. 11. Rotation of this specimen around its axis does not change the absorption. With adequate calibration of the films for exposure, it is then possible to make a fairly reliable estimate of the relative number of grains in each orientation region of the pole figure.

Large-grained specimens must be exposed in cameras that bring more than the usual number of grains into reflecting position in the beam. This can be done by oscillating the specimen through a slight range of angles on an oscillating-crystal camera or by shifting the specimen in its own plane during the exposure. The importance of this is not often appreciated by beginners, and several incorrect conclusions have resulted

<sup>1</sup> P. W. BAKARIAN, *Trans. A.I.M.E.*, vol. 147, p. 266, 1942.

from photographs of specimens in which the grains were too large. An elaborate integrating camera to sweep the beam over large areas of sheet specimens is described by D. W. Smith,<sup>1</sup> but simple shifting devices will often serve.

**Texture goniometers** have been designed in which a single exposure with an oscillating film gives the information ordinarily obtained from many individual exposures. The camera<sup>2</sup> illustrated in Fig. 12 provides a film  $F$ , which shifts longitudinally in synchronism with the oscillation of the specimen  $P$ . The incident beam is parallel to the axis of the cylinder and strikes the specimen which is oscillating about the vertical axis  $D$ . A single Debye ring is allowed to reach the film through the slit  $S$  in a shield  $A$  surrounding the specimen. It will be seen that a chart can easily be prepared to convert positions on the film to positions on a pole figure. Another design<sup>3</sup> is sketched in Fig. 13, with a film shifting behind a shield that is cut to let part of a single Debye ring pass. Moving the shield closer to the specimen adjusts it for Debye rings of higher  $\theta$ . In an alternate design the shield and film are in the

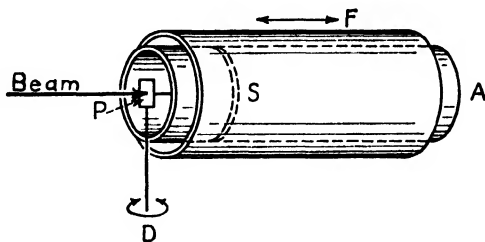


FIG. 12.—Principle of texture goniometer with cylindrical film shifted longitudinally in synchronism with oscillation of specimen.

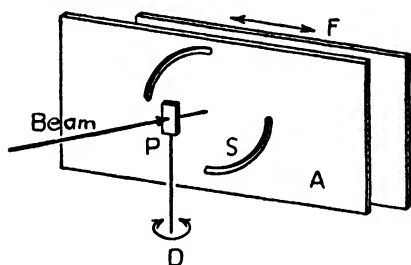


FIG. 13.—Texture goniometer with flat film shifted laterally.

shape of cylinders concentric with the axis of rotation, in which case the specimen and film may be mounted on a single carriage.

**Back-reflection cameras** are not very well suited to pole-figure work. While they have been used in special cases, they have the disadvantage that little information is obtained from an individual film, and to combine the information from a series of films requires careful control of the exposure throughout the series. The reflection circle for a high-angle Debye ring is small compared with those discussed in this chapter and may lie entirely outside of important maxima on the pole figure.

**Orientation of the Axis of Single-crystal Rods.**—The orientation of the axis of a cylindrical specimen may be determined by taking a photo-

<sup>1</sup> D. W. SMITH, "Symposium of Radiography and X-ray Diffraction," A.S.T.M., Philadelphia, Pa., 1937. Blueprints of this camera have been made available by the Research Laboratories of the Aluminum Company of America.

<sup>2</sup> O. KRATKY, *Z. Krist.*, vol. 72, p. 529, 1930.

<sup>3</sup> W. E. DAWSON, *Physica*, vol. 7, p. 302, 1927; *Phil. Mag.*, vol. 5, 7th ser. p. 756, 1928. C. S. BARRETT, *Trans. A.I.M.E.*, vol. 93, p. 75, 1931.

graph with the crystal rotating about its axis, which yields a rotating crystal pattern. Since the axis of rotation is usually a crystallographic direction of high or irrational indices, the usual methods for solving

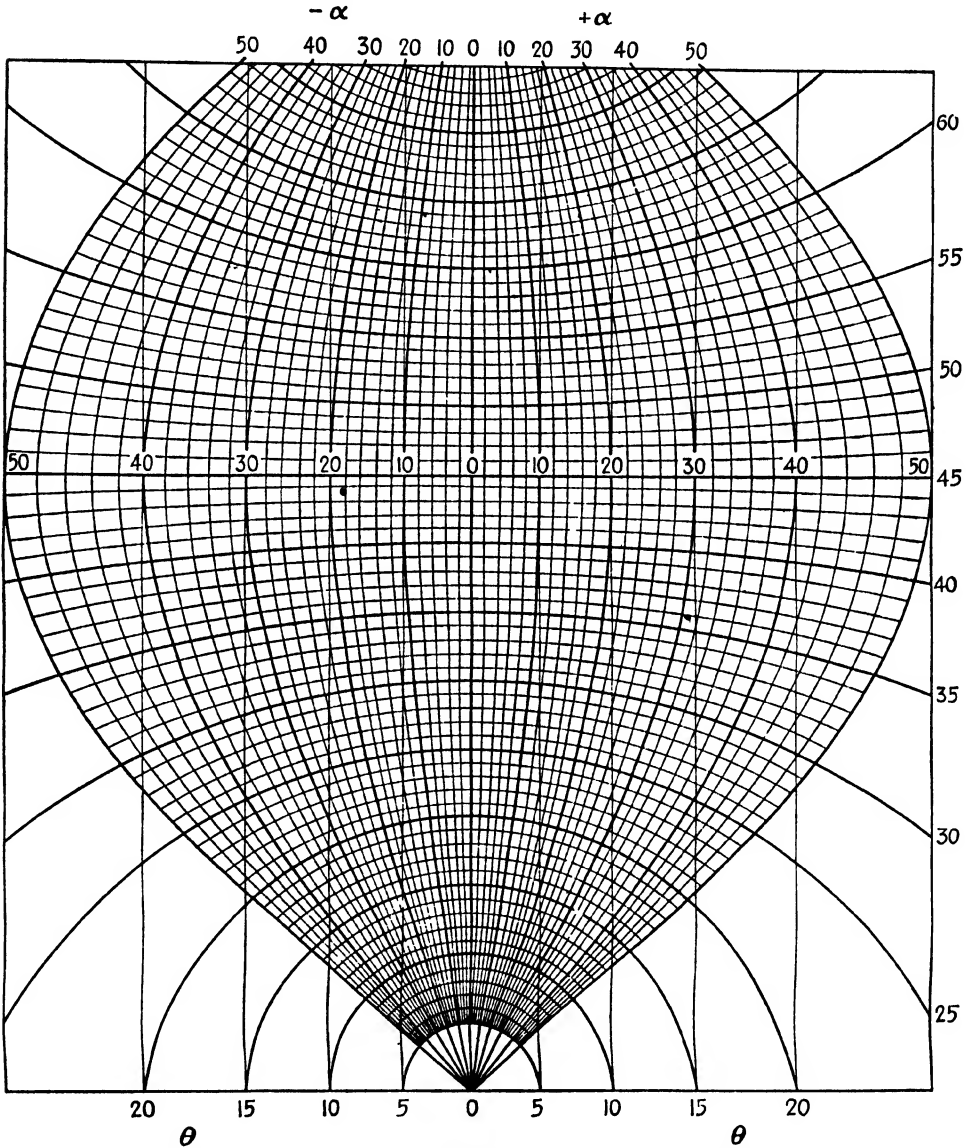


FIG. 14.—Chart for reading  $\alpha$  and  $\theta$  from stationary cylindrical film. Axis of cylinder is horizontal. Chart must be enlarged until distance from  $\theta = 0$  to  $\theta = 45^\circ$  is  $\frac{1}{4}$  of film circumference.

rotating-crystal patterns are unsatisfactory. But the graphical analysis discussed in the earlier section on fiber textures (Fig. 4) will apply, for the rotation axis is a “synthetic” fiber axis. The orientation of the axis only is determined, of course, but this is all that is required for some research, such as mechanical tests.

**Complete Orientation of Single Crystals.**—An oscillating-crystal method developed by Davey<sup>1</sup> and described in detail by Wilson<sup>2</sup> (often referred to as the Davey-Wilson method) has proved valuable for determining orientations of single crystals and individual grains in metallographic specimens. It makes possible the solution of complex orientation problems such as one encounters when investigating the many orientations that may exist in an oriented overgrowth or among precipitated crystals within a grain. It has also been used to study the distortion of grains during freezing, deformation, and recrystallization.

Two concentric cylindrical films are used, the rays passing through the inner one to the outer one and making a record on both. The inner film is mounted on the carriage that holds the specimen and oscillates back and forth with the specimen, while the outer film remains stationary. Each spot is identified by its  $\theta$  value, which is read from the stationary film with a

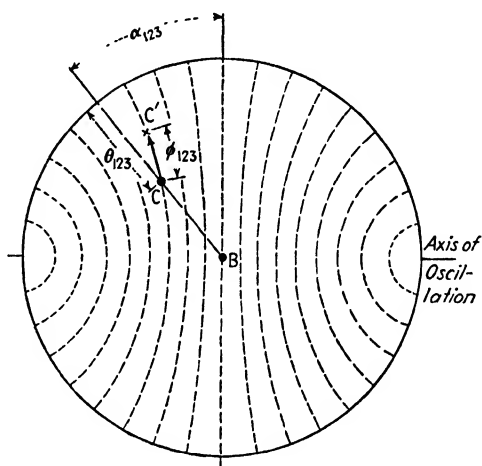


FIG. 15.—Plotting a (123) reflection from known  $\theta$  and  $\alpha$  values. Position after rotating  $\phi$  is shown by cross.

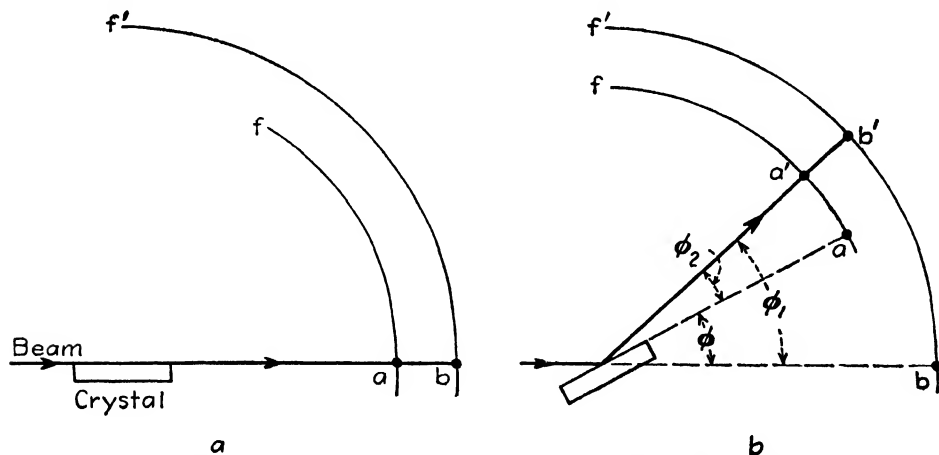


FIG. 16.—Arrangement of films in Davey-Wilson orientation goniometer. (a) Initial setting, (b) after rotating into reflecting position.

chart on which  $\theta$  values are marked, as in Fig. 14. The same chart may be graduated to read the angle  $\alpha$  (see Fig. 2) giving the azimuthal position of the reflected and incident beams.

<sup>1</sup> W. P. DAVEY, *Phys. Rev.*, vol. 23, p. 764, 1924.

<sup>2</sup> T. A. WILSON, *Gen. Elec. Rev.*, vol. 31, p. 612, 1928.

The spot may be plotted immediately on a stereographic projection, as in Fig. 15 at a point  $\theta^\circ$  in from the basic circle and  $\alpha^\circ$  from the vertical. The point  $C$  on this projection represents the reflecting plane as it was when reflection occurred, and it is then necessary to correct for the amount of rotation of the specimen that permitted

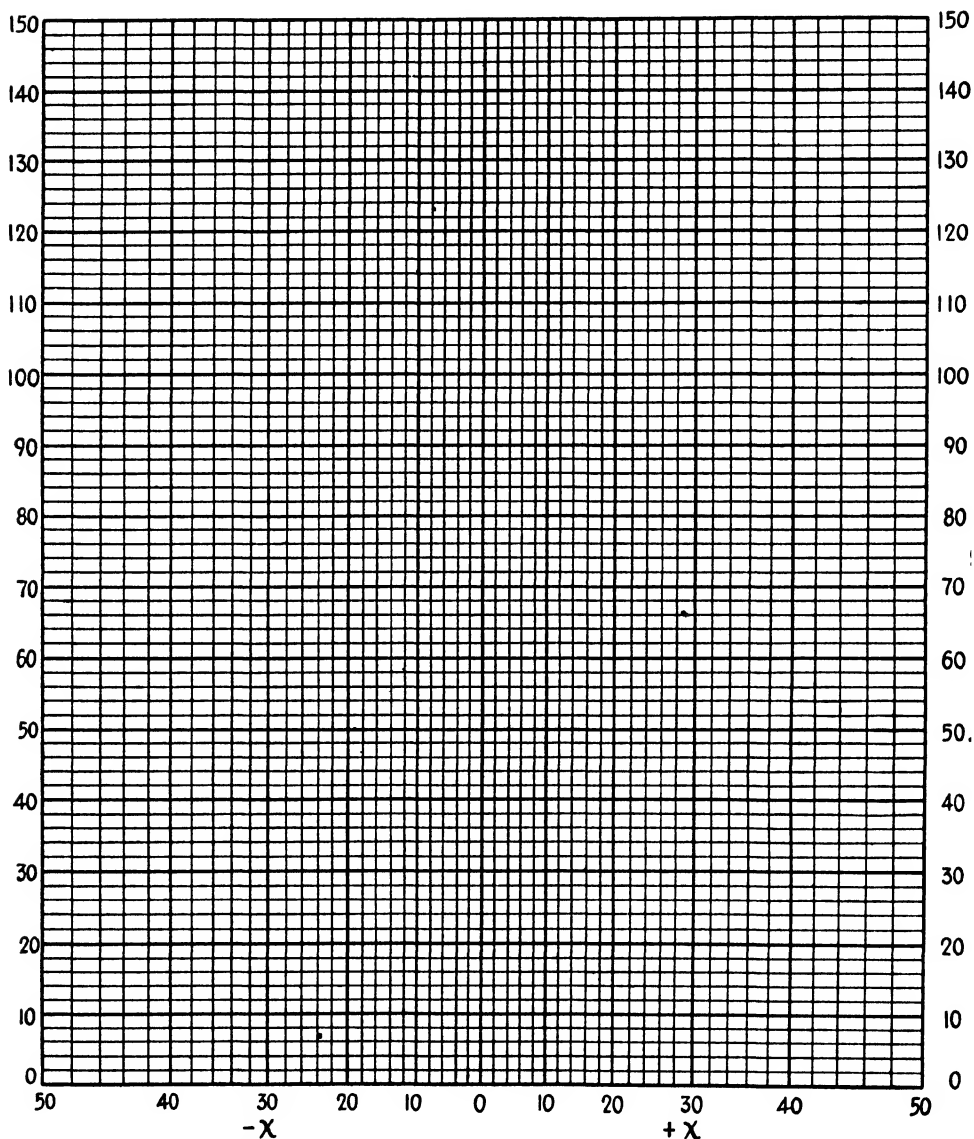


FIG. 17.—Chart for reading  $\phi$  and  $\chi$  coordinates from cylindrical films of Davey-Wilson camera. Axis of film cylinder is horizontal. Chart must be enlarged until the distance from  $\phi$  to 0 to  $\phi = 90^\circ$  is  $\frac{1}{4}$  of film circumference.

the reflection to occur. Suppose a crystal is adjusted on the oscillating carriage so that the x-ray beam just grazes the surface at the end of the oscillation, as in Fig. 16a, and in so doing makes a spot at  $a$  on the oscillating film and at  $b$  on the stationary film. Then, when a reflection occurs, the specimen will have rotated from this position and the reflection ray will cause spots  $a'$  and  $b'$  on the two films, respectively. The

amount of this rotation,  $\phi$ , will be given by the difference of the angles  $\phi_1$ , measured on the stationary film, and  $\phi_2$  on the moving film (Fig. 16b):

$$\phi = \phi_1 - \phi_2.$$

The  $\phi$  values can be read with charts of the type illustrated in Fig. 17 enlarged to the proper size for each film. The point on the stereographic projection is then rotated  $\phi^\circ$ , point  $C$  going to  $C'$  in Fig. 15 along the latitude line of a Wulff net. This procedure is followed for a number of reflections, each being identified by its  $\theta$  value, plotted, and rotated the amount  $\phi$  determined for it, giving a final plot resembling Fig. 18. The position of any other poles can then be found by rotating a standard projection of the crystal into coincidence with the plotted poles.

In this method it is necessary to pair off the spots on the two films correctly. Often this can be accomplished by noting the shape of the spots, but it may be necessary to rely upon measurements. For this purpose it is convenient to use the vertical lines of the chart in Fig. 17. These measure a coordinate,  $\chi$ , that is the same for both spots of a pair—i.e., if a spot on the moving film lies on a certain  $\chi$  line of the moving film chart, then the related spot on the stationary film must lie on the same  $\chi$  line on the stationary-film chart.

### Back-reflection Laue Method for Determining Crystal Orientation.

—One of the most convenient and accurate methods of determining the orientation of a single crystal or an individual grain in an aggregate is the back-reflection Laue method.<sup>1</sup> It is a method that is useful not only for laboratory research but also in the production of commercial crystals, such as quartz crystals cut for piezoelectric control of radio circuits. An exceedingly simple camera will yield accuracies of the order of  $\frac{1}{2}^\circ$ , and cameras for more precise work are not elaborate, as will be seen from the one illustrated in Fig. 19. The interpretation of a photograph may be carried out in a few minutes by making use of the chart developed by Greninger<sup>2</sup> together with a stereographic net and a standard projection of the crystal. When the incident beam in a back-reflection Laue camera is made to straddle a boundary between two grains, two components of a twin, or two imperfect regions of a crystal so that the two are jointly

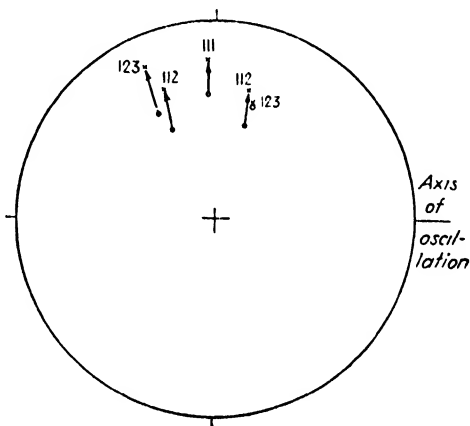


FIG. 18.—Projection showing final positions of reflections after rotation of each point the amount  $\phi$  determined for it.

<sup>1</sup> L. CHROBAK, *Z. Krist.*, vol. 82, p. 342, 1932. W. BOAS and F. SCHMID, *Metallwirtschaft*, vol. 10, p. 917, 1931. A. B. GRENINGER, *Trans. A.I.M.E.*, vol. 117, p. 61, 1935; *Z. Krist.*, vol. 91, p. 424, 1935.

<sup>2</sup> A. B. GRENINGER, *Trans. A.I.M.E.*, vol. 117, p. 61, 1935; *Z. Krist.*, vol. 91, p. 424, 1935.

recorded on the film, it is possible to determine their relative orientations to within a few minutes of arc.<sup>1</sup>

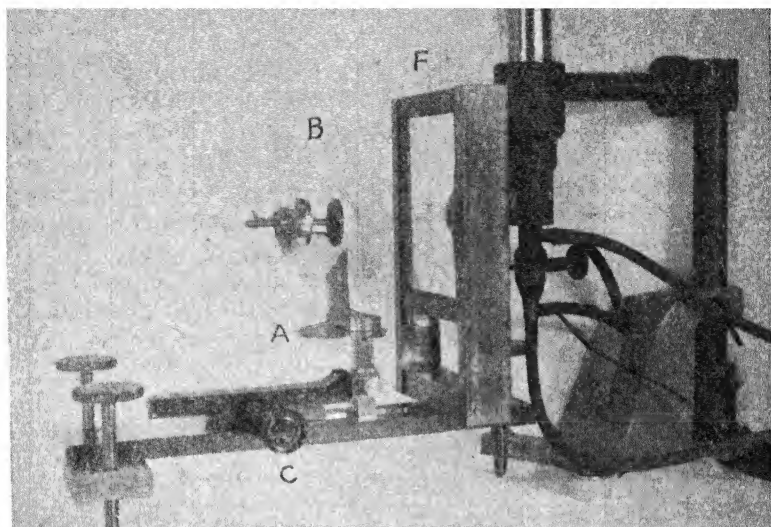


FIG. 19.—Camera for back-reflection Laue photographs. Crystal is adjustable with horizontal and vertical graduated circles *A* and *B*; its distance from film in cassette *F* is adjusted by *C*. Portion of gas x-ray tube shown. (Greninger.)

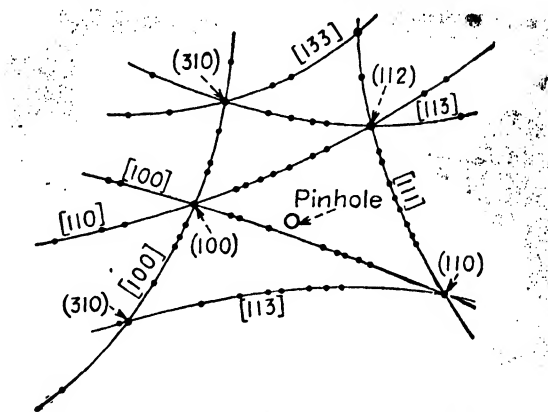


FIG. 20.—Back-reflection Laue pattern of  $\alpha$ -iron with principal zones and spots identified.

Tungsten target x-ray tubes are best suited for the work, but any tube giving appreciable general radiation with or without characteristic radiation will serve.<sup>2</sup> A back-reflection pattern of a body-centered cubic

<sup>1</sup> A. B. GRENINGER, *Trans. A.I.M.E.*, vol. 117, p. 75, 1935; vol. 122, p. 74, 1936.

<sup>2</sup> In typical experiments a tungsten tube with a 2-mm. focal spot operating at 8 ma., 40 kv. requires exposures of 15 to 60 min. with a pinhole 0.8 mm. diameter, 6 cm. long, and crystal-to-film distance of 3 cm., with standard x-ray film and Fluor-azure intensifying screens. A 5- by 7-in. film is convenient at this distance. For metals such as Cu, Zn, Fe, etc., there is considerable fogging from fluorescent radiation, but this may be reduced by a filter, for example by 0.01-in. aluminum sheet.



crystal ( $\alpha$ -iron) is shown in Fig. 20. The circle at the center indicates the hole that is punched to enable the film to slip over the pinhole system. It will be seen that the Laue spots lie on hyperbolas. The spots on each of these rows are reflections from various planes of a given zone, *i.e.*, planes parallel to a line that is the zone axis. The geometrical conditions are sketched in Fig. 21. A cone of reflected rays is formed for each zone of planes in the crystal, such as the one shown in the drawing, and each cone intersects the flat film to form a row of spots (*C, D, E*) along a

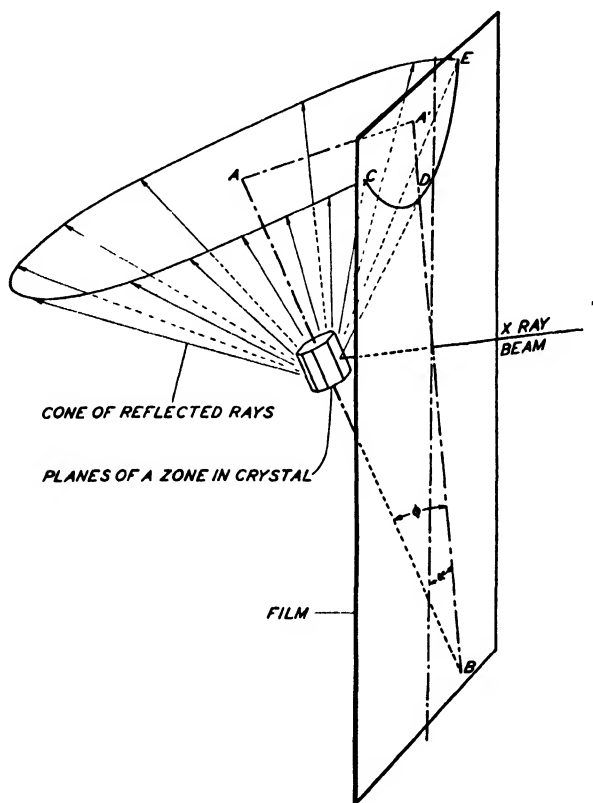


FIG. 21.—Back-reflection Laue pattern of planes of a zone in a crystal.

hyperbola. If the zone axis *AB* is inclined to the film, the hyperbola will lie at a distance from the center of the film an amount that is related to the angle of inclination,  $\phi$ <sup>1</sup>; if *AB* is parallel to the film ( $\phi = 0$ ), the hyperbola will degenerate into a line passing through the center of the film. If the axis of the cone is projected perpendicularly upon the film, forming the line *A'B*, it is obvious that the hyperbola will be symmetrical with respect to this line.

<sup>1</sup> The closest approach of the hyperbola to the center of the film is given by the relation  $S = R \tan 2\phi$ , where  $R$  is the distance from the specimen to the film, and  $S$  is the minimum distance of the hyperbola from the center.

In determining the orientation of a crystal from a pattern of this type it is necessary to assign the proper indices to some of the zones causing these hyperbolas or to some of the individual spots. The technique for doing this is much simplified if attention is directed merely to the hyper-

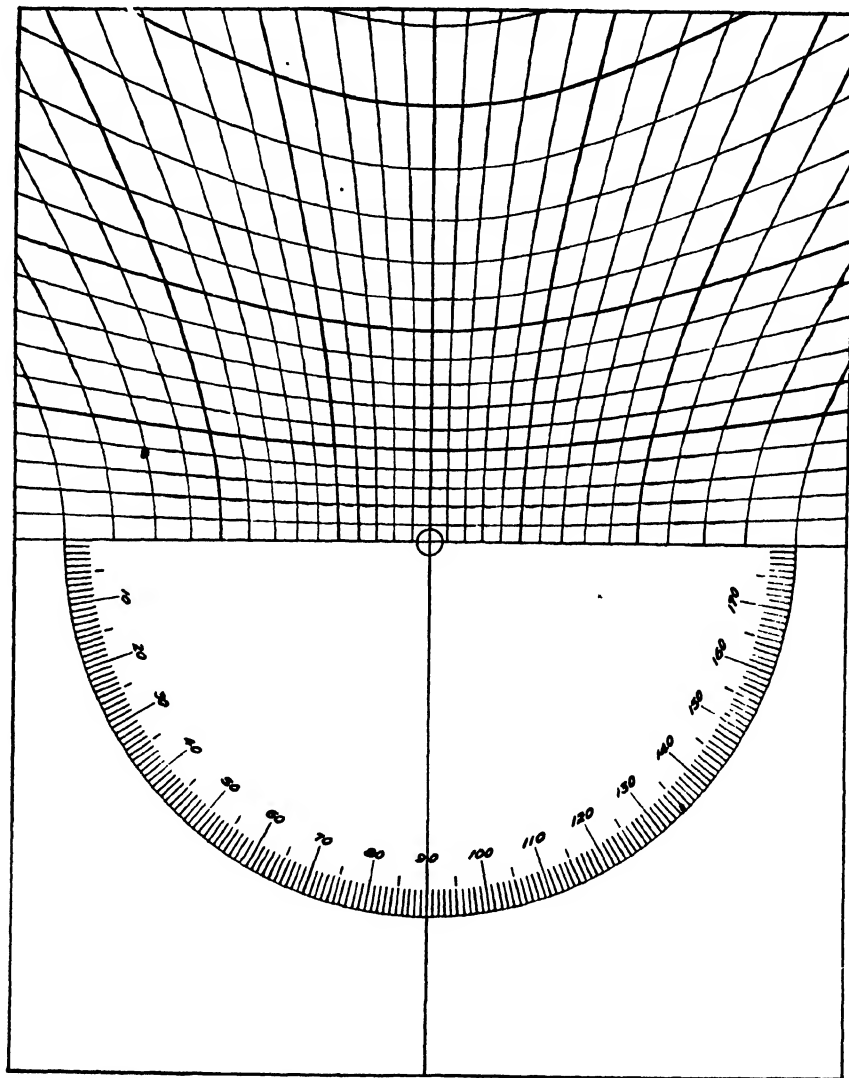


FIG. 22.—Chart for back-reflection photographs. Printed for 3-cm. distance from specimen to film; graduated in  $2^\circ$  intervals.

bolae which are the most densely packed with spots and to those spots which lie at the intersections of three or more prominent hyperbolas, for then only low indices are involved.

On every film of a cubic crystal will be found prominent rows of spots from the zones  $[100]$ ,  $[110]$ , and  $[111]$  and less prominent ones from the zone  $[113]$ . Many other zones also appear but are not easily recognized.

The spots at the intersections of these principal hyperbolas are reflections from the planes common to the principal zones in the crystal; in the body-centered cubic patterns they are (100), (110),<sup>\*</sup>(112), and others of higher indices, which are less prominent. In the face-centered cubic patterns, (111) appears in addition to these. These important spots with low indices are always of high intensity and are somewhat isolated from their neighbors on the hyperbola (see Fig. 20).

Figure 22 is Greninger's chart for reading angular relations on back-reflection films and is reproduced in the proper size for a 3-cm. separation of specimen and film. Any row of spots on the film can be made to

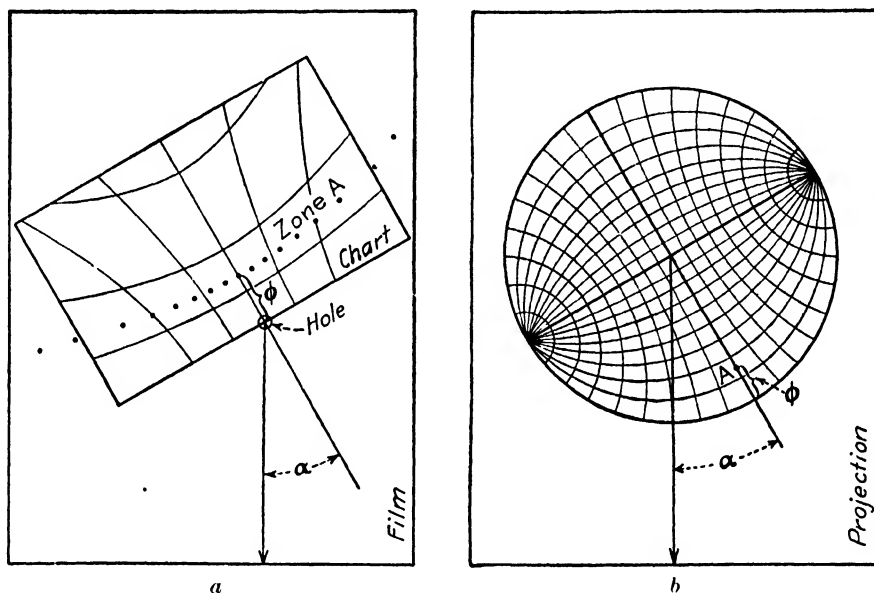


FIG. 23.—(a) Back-reflection Laue film superimposed on chart. (b) Stereographic projection paper superimposed on net; the zone of spots is plotted at  $A$ .

coincide with a hyperbola extending across the chart horizontally by suitably turning the film about its center when it is placed centrally on the chart. The angle of inclination,  $\phi$ , of the zone axis to the film is given directly from the chart; hyperbolas have been drawn for each  $2^\circ$  of  $\phi$ , with heavy lines each  $10^\circ$ . The amount of rotation of the film that is required to get a row to coincide with a horizontal hyperbola on the chart is a direct measure of the azimuthal angle  $\alpha$  (see Fig. 21), for it is the angle between the line  $A'B$  and the vertical reference line.

It is most convenient to solve the films by plotting a stereographic projection; this can be done rapidly by a method which will be described with reference to Fig. 23. The plane of the projection is made perpendicular to the primary x-ray beam (parallel to the plane of the film), and the film is read from the side opposite to that on which the reflected rays were incident, so as to give a projection of the crystal that corresponds to viewing it from the position of the x-ray tube. An arrow is marked on the

film parallel to some fiducial mark on the specimen, and the film is superimposed on the chart, as in Fig. 23*a*, with its central hole at the center of the chart. A piece of tracing paper is then placed on a stereographic net and pivoted at the center of it with a pin. An arrow is drawn on the paper radially outward from the central pin. The zones recorded on the film are then plotted on the paper, as indicated in Fig. 23*b*, by turning the paper and film together so that both arrows are parallel and point to the same angle  $\alpha$  and by plotting the angle  $\phi$  upward from the basic circle of the projection. The point *A* thus plotted is the projection of the zone responsible for the entire row of spots on the film.

Tentative indices are assigned by determining the angles between prominent zones and comparing the angles with a table (see the table on page 35). This tentative assignment of one or more possible sets of indices is merely for the purpose of saving time in the final operation, which is that of finding a position of a standard projection of zone axes and an amount of rotation of the standard such that its points will coincide with all the plotted ones and thus will disclose their indices. When a match has been found between each zone and a corresponding zone from a rotated standard projection, it is possible, of course, to rotate any other zone or any pole of the standard by the same amount and thus to show its position in the crystal. The final plot expresses the crystal orientation graphically; in addition, it can also be described in terms of the angles between the crystallographic axes and convenient marks or surfaces on the crystal.

The above technique is but one of several by which one may deduce the indices of the zones and spots. No use has been made in this procedure of the vertical curves of the chart (Fig. 22). These have been drawn to measure angular relations between spots on a given hyperbola and are spaced at  $2^\circ$  intervals just as are the others; i.e., two planes of the same zone in a crystal that lie at an angle of  $2^\circ$  to each other will reflect to form two spots separated by one of the intervals marked out by two adjacent vertical curves. The angle between the two principal spots of Fig. 20, for example, can be measured directly from the chart and will be found to be  $45^\circ$ ; this suggests at once that the indices of one of the spots are (100) and of the other are (110), although it does not tell which spot is which.

If the spots thus partly identified are plotted on the projection, they will greatly reduce the number of trial rotations of the standard projection that are necessary to find the complete solution. The pole of a plane causing a spot is plotted by a procedure analogous to that of Fig. 23, except that the spot is made to lie on the *central vertical line* of the chart, and the corresponding pole is plotted  $\phi^\circ$  up from the center of the projection, rather than  $\phi^\circ$  up from the circumference (since the pole is normal to its zone axis). Poles thus plotted are useful for a rapid solution of the film, but zones can be read from the film more accurately.

**The Transmission Laue Method.**—It has been mentioned in Chap. V that a transmission Laue pattern has a symmetry around the center similar to the symmetry of the axis or plane in the crystal along which the x-ray beam is directed. If a cubic crystal is mounted on a goniometer head and turned until the Laue pattern has four-fold symmetry, it becomes at once obvious that the incident beam is parallel to a cube axis, [100]; similarly, three-fold symmetry indicates that the beam is parallel to a cube diagonal, [111]. With crystals of high reflecting power and with intense radiation it is possible to see these patterns on a fluorescent screen and to adjust the crystal quickly to a symmetrical position, though it is

necessary to work in a darkened room with the eyes fully accommodated to the dark.

To find the orientation of an unsymmetrically oriented crystal one can transfer each of the spots on a transmission photograph to a stereographic projection. The prominent zones then appear as points along great circles of the projection and can be identified either by the symmetry of their arrangement or by the angles between them.

**The Determination of Orientations by Etch Pits.**—Various orientation methods have been employed for the reflection of light from crystallographic etch pits. Bridgman's method<sup>1</sup> consists in attaching the specimen to a sphere (a transparent sphere is convenient<sup>2</sup>), holding it at arm's length, and marking a spot on it when it has been turned so that the etch pits reflect light into the eye of the observer from a lamp standing behind him. It has an accuracy of about 2° and is extremely rapid. A greater accuracy can be obtained by causing the reflected light to fall on a screen, as has been done by Czochralski,<sup>3</sup> Chalmers,<sup>4</sup> and Schubnikov.<sup>5</sup> Tammann and his coworkers<sup>6</sup> developed a method for estimating the number of grains in a polycrystalline aggregate having orientations in a given region of the stereographic triangle and thus obtained statistical information about deformation and recrystallization textures. While the method has had some use in recent years,<sup>7</sup> it is not applicable to the majority of problems in physical metallurgy. Smith and Mehl<sup>8</sup> determined orientations by plotting the directions of the sides of individual etch pits on a stereographic projection. The accuracy is limited to about 3°, and the method requires careful polishing and high magnification.

The most useful methods involve the measurement of the angles between the etch-pit faces using a goniometer. Weerts<sup>9</sup> has given a lengthy discussion of a technique using a three-circle goniometer and polarized light. A less elaborate method, which gives an accuracy that is sufficient for the great majority of investigations, consists simply in measuring the orientations of the etch-pit faces on a two-circle optical goniometer.<sup>10</sup> It has an accuracy of  $\frac{1}{2}$  or 1°. The method operates

<sup>1</sup> P. W. BRIDGMAN, *Proc. Am. Acad. Arts Sci.*, vol. 60, p. 305, 1925.

<sup>2</sup> J. B. BAKER, B. B. BETTY, and H. F. MOORE, *Trans. A.I.M.E.*, vol. 128, p. 118, 1938.

<sup>3</sup> J. CZOCHRALSKI, *Z. anorg. allgem. Chem.*, vol. 144, p. 131, 1925.

<sup>4</sup> B. CHALMERS, *Proc. Phys. Soc. (London)*, vol. 47, p. 733, 1935.

<sup>5</sup> A. SCHUBNIKOV, *Z. Krist.*, vol. 78, p. 111, 1931.

<sup>6</sup> G. TAMMANN, *J. Inst. Metals*, vol. 44, p. 29, 1930. G. TAMMANN and H. H. MEYER, *Z. Metallkunde*, vol. 18, p. 339, 1926.

<sup>7</sup> K. J. SIXTUS, *Physics*, vol. 6, p. 105, 1935.

<sup>8</sup> D. W. SMITH and R. F. MEHL, *Metals & Alloys*, vol. 4, pp. 31, 32, 36, 1933.

<sup>9</sup> J. WEERTS, *Z. tech. Physik*, vol. 9, p. 126, 1928.

<sup>10</sup> L. W. MCKEEHAN, *Nature*, vol. 119, p. 705, 1927. L. W. MCKEEHAN and H. J. HODGE, *Z. Krist.*, vol. 92, p. 476, 1935. H. H. POTTER and W. SUCKSMITH, *Nature*,

satisfactorily with grains as small as 0.1 mm. diameter and has been used with cold-worked and annealed grains and single crystals.<sup>1</sup>

1. A GONIOMETER.—An inexpensive two-circle goniometer may be constructed from an old surveyor's transit (Fig. 24). It consists of the horizontal circle of the transit *H*, a vertical circle *V* (formerly the compass circle of the transit) mounted on the rotating cover of the horizontal circle, a shaft through the vertical circle for supporting the specimen *S*, a light source and collimator *C*, and the transit telescope *T*, all mounted on a base plate. The specimen *S* is mounted with modeling clay on the faceplate *F*. The specimen is illuminated by parallel light from the collimator *C*, which contains a lamp and lens, and is observed in the transit telescope *T*, fitted with cross hairs. For ordinary measurements of single crystals or large grains a magnification of two or three times is used in the telescope.

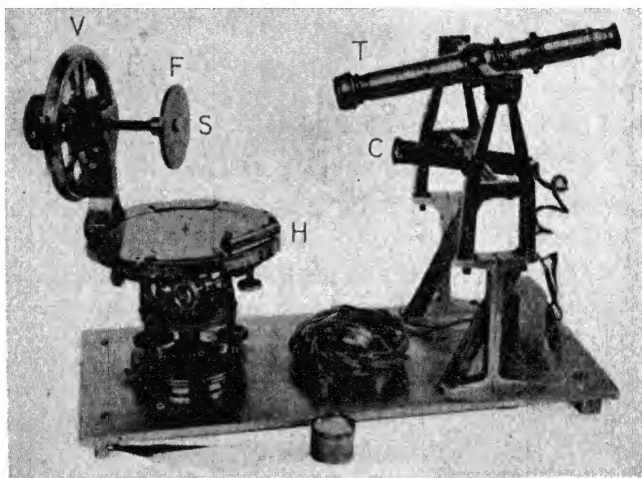


FIG. 24.—A two-circle goniometer. *V*, vertical circle; *H*, horizontal circle; *F*, specimen mount; *S*, specimen; *C*, collimator; *T*, telescope.

The grain to be measured is placed at the intersection of the vertical and horizontal axes of the instrument, and the axes of the telescope and collimator are made to intersect at this point. The axes of the collimator and telescope lie in a vertical plane and make equal angles of about  $10^\circ$  with the horizontal; with this arrangement, light that is multireflected from the three faces of an etch pit of cubic shape is returned in the incident direction and is not seen in the telescope.

2. ETCHING TECHNIQUE.—An ideal etchant would be one that develops etch pits or facets with plane faces accurately parallel to crystallographic planes of low index. The etched metal specimen would then appear intensely bright when the normals to these planes bisected the angle between telescope and collimator and perfectly black in all other positions. Actually, however, the etch-pit faces are always more or less rounded, causing the intensity of the reflected light gradually to build up to and drop off from a maximum as the reflecting plane approaches and recedes from the reflecting position. For the same metal and etchant the position and sharpness of the maxima

vol. 119, p. 924, 1927. C. S. BARRETT and L. H. LEVENSON, *Trans. A.I.M.E.*, vol. 137, p. 112, 1940.

<sup>1</sup> C. S. BARRETT, *Trans. A.I.M.E.*, vol. 135, p. 296, 1939. C. S. BARRETT and L. H. LEVENSON, *Trans. A.I.M.E.*, vol. 137, p. 76, 1940.

vary with the etching time and the temperature of the etchant. When the maxima are sharp enough to be reproducible within  $\frac{1}{2}^\circ$ , their positions usually coincide with the crystallographic poles, but sometimes they tend to fall a degree or two away from true crystallographic poles. For example, maximum reflections from cubic etch pits are often  $88$  or  $89^\circ$ , rather than  $90^\circ$ , apart. Since only two poles are necessary to determine the orientation and three can usually be measured, the observed poles can be corrected by moving them a minimum amount to make them mutually perpendicular. Occasionally, a few large noncrystallographic pits are developed; these may

TABLE X.—DIRECTIONS FOR ETCHING

Metal	Purity, per cent	Etchant*	Etch- ing time, min- utes	Planes developed	Remarks
Aluminum	99.95	9 parts HCl 3 parts HNO <sub>3</sub> 2 parts HF 5 parts H <sub>2</sub> O	2	{100}	Use large quantity of etchant with respect to surface of specimen, and avoid heating of etchant
$\alpha$ -iron	H <sub>2</sub> purified de-carburized mild steel	1 part HNO <sub>3</sub> 4 parts H <sub>2</sub> O	4	{100}	Avoid heating, as above; wipe during etching
Copper	Oxygen-free high-conductivity copper	1 part HCl 1 part H <sub>2</sub> O; mixture saturated with FeCl <sub>2</sub> ·6H <sub>2</sub> O	10	{100}	
Brass	Cartridge brass (70-30)	1 part etch for Cu 1 part H <sub>2</sub> O	20	{100} and {111}	Agitate etchant at 2-min. intervals
Lead	99.9	3 parts H <sub>2</sub> O <sub>2</sub> 2 parts glacial acetic acid 2 parts H <sub>2</sub> O	10	{100}	
Tin	99.991	1 part etch for Cu 1 part H <sub>2</sub> O	10	{100} and {110}	Wipe off at 2-min. intervals
Tungsten		100 parts saturated K <sub>2</sub> Fe(CN) <sub>6</sub> 5 parts saturated KOH 95 parts H <sub>2</sub> O	15	{110}	Agitate etchant at 2-min. intervals. Composition of etch is critical
Zinc	99.99	7 parts saturated CuCl <sub>2</sub> ·2H <sub>2</sub> O 3 parts HCl 90 parts H <sub>2</sub> O	3	{10 $\bar{1}$ l}, l having many values	Wipe off deposited copper at 30-sec. intervals. Maximum reflections lie in three planes intersecting at pole of basal plane. Hexagonal axes lie $90^\circ$ from the intersection and midway between these planes

\* For other etchants that have been used by various investigators see references in C. S. Barrett and L. H. Levenson, *Trans. A.I.M.E.*, vol. 137, p. 76, 1940.

be readily recognized as such, since they have no definite maximum. In Table X directions are given for etching various metals for orientation work. The etching times are for etchants at room temperature and for strain-free metals of the purity indicated; for cold-worked metals the etching time usually must be reduced.

3. METHOD OF PLOTTING.—The readings on the two circles of the goniometer corresponding to a reflection maximum (a cube pole in this discussion) can be plotted directly as a point on a stereographic projection. The data are plotted on tracing paper fastened over a stereographic net by a pin at the center of the net, the paper being left free to turn about the pin.

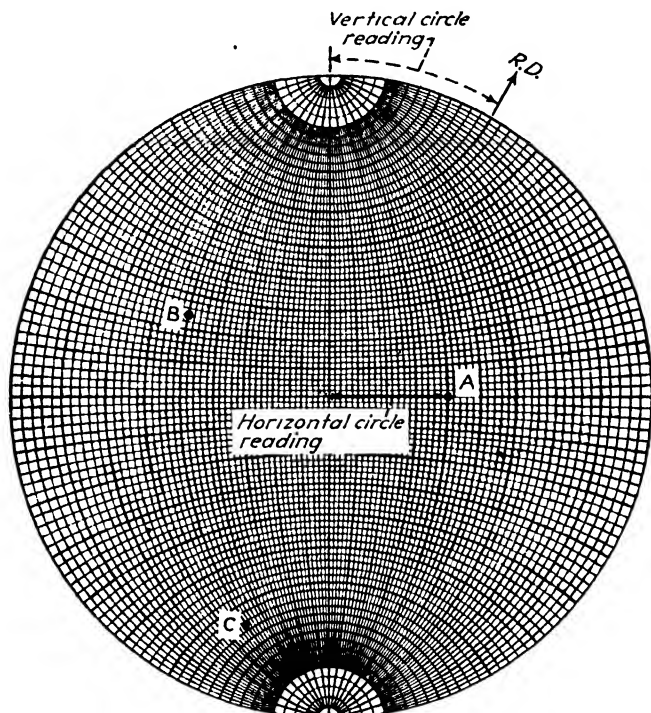


FIG. 25.—Stereographic projection of data. Poles of cube faces of etch pits are *A*, *B*, and *C*; specimen surface normal is at center.

Transferring data from the goniometer to the projection is direct and simple, for readings on the horizontal circle of the goniometer correspond to radial distances from the center of the projection and readings on the vertical circle correspond to azimuthal positions around the center if one makes the plane of projection parallel to the surface of the specimen.

Let us illustrate with an example using a portion of a grain in a rolled specimen in which it is desired to find the orientation of the cube poles with respect to the rolling direction and the normal to the rolling plane. Let the zero setting of the instrument be the one for which the rolling direction is vertical and the rolling plane is in the reflecting position (this can be found by holding a small mirror on the surface). Assume that to bring the specimen into a position of maximum reflection requires a 30° clockwise rotation of the vertical circle (as seen from the telescope) and a 40° clockwise (looking down) rotation of the horizontal circle. The pole of this reflecting plane is plotted by rotating the tracing paper 30° clockwise about the center of the net from the position in which *RD* is at the north pole and marking a point 40° to the right



of the center on the equatorial line of the net. The pole *A* in the projection of Fig. 25 is plotted thus, with the rolling direction indicated on the boundary circle at *RD*. The same plane can also be brought into its reflecting position by a  $150^\circ$  counterclockwise rotation of the vertical circle and a  $40^\circ$  counterclockwise rotation of the horizontal circle from the zero setting. Thus for each of the faces of an etch pit there are two settings for maximum reflected intensity  $180^\circ$  apart on the vertical circle and symmetrical with respect to the zero position of the horizontal circle. The closeness with which these two plotted points agree on the projection is a check on the alignment of the apparatus and the reliability of the readings. The other two cube poles, *B* and *C*, are found and plotted similarly and, as shown in Fig. 25, lie  $90^\circ$  apart on a great circle  $90^\circ$  from *A*. The third pole might have been plotted at once  $90^\circ$  from the other two, but it is better to use its experimentally observed position as a check on the accuracy of the orientation determination.

4. APPLICATION TO DEFORMED METALS.—The optical goniometer has especial value in the study of lattice orientations in deformed grains and single crystals, in which fields x-ray work is difficult. In general, with either single crystals or grains of a polycrystalline aggregate, the orientation after deformation varies considerably and in an irregular manner over each grain. In determining the range of orientation, a grain is divided into a number of areas, and the orientation of each area is measured separately and transferred to a standard projection.<sup>1</sup> The grouping of points on the final projection gives a pole figure of the preferred orientations present. This technique has been used to prepare pole figures of polycrystalline specimens, both in cold-worked and recrystallized states,<sup>2</sup> the individual grains of which were a few millimeters in diameter; but it does not, of course, detect the fragments of microscopic or submicroscopic size that can be registered by x-rays.

<sup>1</sup> C. S. BARRETT and L. H. LEVENSON, *Trans. A.I.M.E.*, vol. 137, p. 112, 1940.

<sup>2</sup> C. S. BARRETT, *Trans. A.I.M.E.*, vol. 137, p. 128, 1940.

## CHAPTER X

### DETERMINATION OF CONSTITUTION DIAGRAMS WITH X-RAYS

The variety of properties encountered in different alloys or that may be induced in one alloy by different heat-treatments makes it almost essential to have a guide to each alloy system in the form of a constitution diagram showing the various solid solutions and compounds which exist in the system and the ranges of temperature and composition within which they are stable. The diagram guides the practical metallurgist in his melting and heat-treating and aids the research laboratories in selecting alloys for particular uses or alloys that seem capable of improvement.

X-ray diffraction has been of great value in the determination of the constitution of alloys. At the present time, only a small fraction of the great number of possible binary alloy systems and almost no systems with three or more component metals have been investigated with the care necessary to provide accurate phase diagrams; most of the existing diagrams must be considered merely as approximations. Many of the errors and inconsistencies in these have resulted from the use of impure materials; some from a lack of appreciation of the faults of the methods used in their determination; others from a failure to apply the most suitable methods; some from failure to regard the phase rule; and some, of course, from incomplete experimental work.

**Comparison of Methods.**—A brief listing and discussion of the various methods employed in phase-diagram work will aid in showing the x-ray method in a proper perspective. **Thermal analysis** (the use of heating and cooling curves) is particularly valuable for determining the beginning and end of freezing. **Dilatometric measurements** are excellent for determining the presence of transformations in the solid state. **Microscopic observations** of polished and etched sections are often sufficient to establish all phases and transformations in the solid state and are more widely used than electrical, magnetic, or other **physical properties** in determining the boundaries of the single- and polyphase regions on the diagram. The microscope reveals the distribution of the products of a reaction, which none of the other methods can do, and makes it possible to determine the nature of most of the high-temperature reactions by inference from the microstructures they produce. **X-ray diffraction** is capable of determining not only the phases present in an alloy but also the crystal structure of the phases. It excels the other methods in its ability to detect metastable and transitional states and to relate these

to the phases preceding and following them in a transformation—permitting in some cases a detailed understanding of the mechanism of transformation and of the strains accompanying it (this is treated in Chap. XXII). A diffraction pattern of a polyphase alloy can be made to yield, by comparison with alloys of known compositions, the compositions of the individual phases present, since the spectra of the phases are superimposed in the diffraction pattern for the aggregate.

Conversely, we may summarize the **principal limitations** of these methods as follows: Thermal analysis is a poor method of studying sluggish reactions; the heat of reaction is evolved over such an extended period of time that it is difficult to detect or measure. This method is also likely to fail if the heat of reaction is small. Dilatometric curves are sometimes better than cooling curves for studies of transformations in the solid state, but neither thermal nor dilatometric data are suitable for determining the range of composition of single-phase or polyphase regions in the solid state. Mechanical strength is a good method for determining the beginning of melting and is coming into wide use for this purpose, but otherwise the mechanical methods find little service in phase-diagram work. The valuable microscopic method runs into difficulties when the grain size of a sample is too small or when the products of a reaction are too finely dispersed. This is likely to occur with reactions in the solid state that take place at low temperatures. It depends upon room-temperature observations and consequently gives only indirect evidence of phases that are not retained by quenching to room temperature. The microscopic method fails in occasional instances for lack of a suitable etching reagent that will distinguish between the various phases present.

The x-ray method also has its limitations. It is capable of disclosing conditions in an alloy at elevated temperatures in two ways: (1) by quenching the alloy to room temperature and taking a diffraction pattern at that temperature, in which case it is limited to alloys in which the high-temperature condition is adequately retained at room temperature by the quenching action, and (2) by applying the method at the elevated temperature, a procedure requiring special cameras, temperature-control equipment, and inert atmospheres for protecting the sample against oxidation. It is not possible to recognize extremely small quantities of a second phase in a binary or polyphase alloy, and so x-rays are usually inferior to the microscope in this respect. This is not a serious limitation in phase-diagram work, however, as will be discussed later (page 187). The x-ray method reveals practically nothing about the distribution of phases, which is evident in microscopic examination and is of vital importance in practical problems.

**Binary Diagrams—Disappearing-phase Method.**—The accepted manner of presenting data on the constitution of alloys is to plot a diagram

on which single-phase and polyphase regions are plotted against composition as abscissa and temperature as ordinate, as in Fig. 1. It will be remembered that, when such diagrams represent equilibrium in the alloys, they must be drawn in accord with the relations embodied in Gibbs's phase rule.<sup>1</sup>

It follows that, in an equilibrium diagram for binary alloys at atmospheric pressure, there will be regions of single- and two-phase equilibria alternating with each other across the diagram at any constant temperature. If x-ray diffraction patterns are made of a series of alloys in such a system, the films will show single patterns with single-phase alloys and

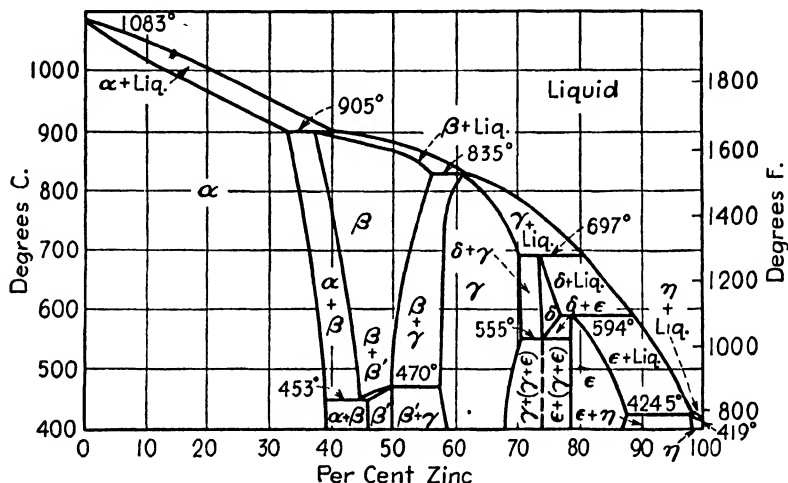


FIG. 1.—Constitution diagram for copper-zinc alloys. Compositions in weight percent. (*National Metals Handbook.*)

two superimposed patterns with two-phase alloys. Figure 2 is a reproduction of typical powder diffraction patterns for one- and two-phase specimens. This principle alone could be used to establish the solid portion of the diagram in a rough fashion, but much labor is saved by using the "lever principle" in the two-phase regions. Reference to Fig. 3 shows that an alloy of composition  $P$  in equilibrium at a certain tempera-

<sup>1</sup> This states that, if the equilibrium between the phases is influenced only by temperature and pressure and not by gravitational, electrical, or magnetic forces or by surface conditions, then  $P + F = C + 2$ , where  $P$  is the number of stable phases present,  $F$  is the number of degrees of freedom, and  $C$  is the number of components. A phase may be defined as any physically distinct part of a system that is separated from the other parts of the system by definite bounding surfaces. The number of degrees of freedom of a system is the number of independently variable factors (such as temperature and pressure of the system and composition of any phase) that must be specified completely to define the conditions in the system. The number of components of a system is the smallest number of independently variable substances by means of which the composition of any phase present can be expressed. In most alloy systems this is the number of elemental metals present in the alloy.

ture in the two-phase region  $\alpha + \beta$  contains the  $\alpha$  and  $\beta$  phases in the proportions given by the relative lengths of the lines  $Px$  and  $Py$ ; i.e., amount of  $\alpha$ : amount of  $\beta = Py:Px$ ; or, equivalently,  $Py/xy$  of the total

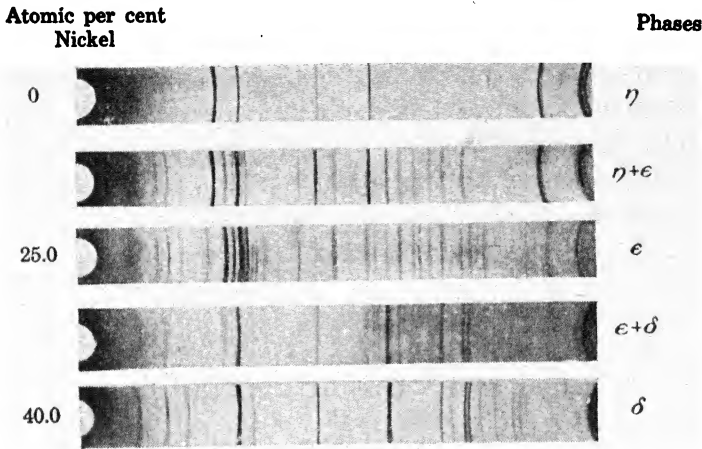


FIG. 2.—Powder-diffraction patterns of alternating one-phase and two-phase regions in aluminum-rich aluminum-nickel alloys. (A. J. Bradley and A. Taylor, *Proc. Roy. Soc., (London)*, vol. A159, p. 53, 1937.)

alloy is  $\alpha$  and  $Px/xy$  is  $\beta$ . The intensity of the diffraction pattern of a phase is proportional to the quantity of that phase present in the alloy (barring disturbing effects). It follows, therefore, that as the boundary of a two-phase region is approached the diffraction pattern of the disap-

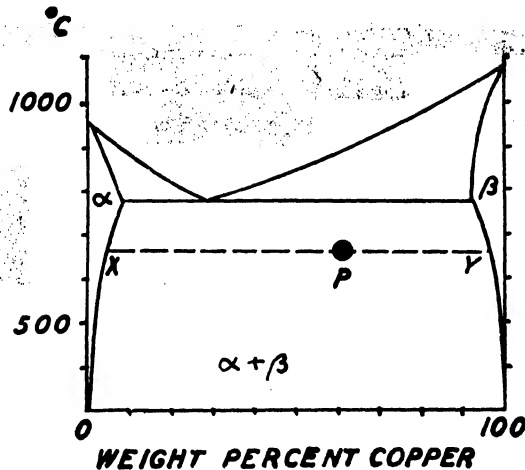


FIG. 3.—The level principle illustrated in the two-phase region of the copper-silver diagram.

pearing phase will steadily diminish in intensity; the boundary can thus be located by extrapolation to the point of disappearance on a plot of intensity vs. composition. This has been called the **disappearing-phase method**.

**Parametric Method.**—The most precise location of the phase boundaries by x-rays involves the use of lattice-spacing measurements. Within a single-phase region the lattice spacings (lattice parameters) usually follow a smooth curve when plotted against composition and not infrequently vary linearly, as in Fig. 4. Variation with composition is to be expected whenever there is an appreciable range of composition within which there exist homogeneous single-phase alloys, regardless of whether the single-phase region is a solid solution at an extremity of the diagram—a terminal solid solution—or within the diagram and whether the solute atom replaces one of the solvent atoms to form a substitutional solid solution, or fits interstitially between the solvent atoms to form an

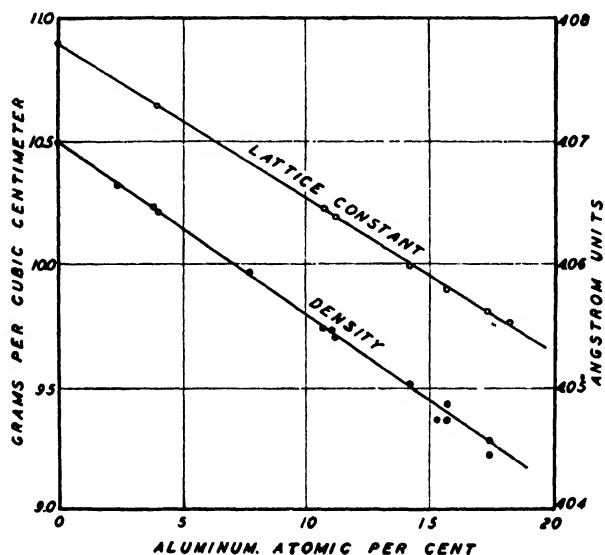


FIG. 4.—Lattice constants and densities of silver-aluminum alloys. (Footé and Jellé.)

interstitial solid solution, or replaces more than one solvent atom to form a defect lattice. Within a two-phase region of a binary diagram, on the other hand, the lattice spacings of each phase are invariant with composition at constant temperature. The spacings of each phase are those corresponding to alloys with compositions at the ends of the tie line<sup>1</sup> drawn on the binary diagram through the point representing the two-phase alloy. For example, in Fig. 3 the alloy *P* will yield the superimposed diffraction spectra of the  $\alpha$  phase of composition *x* and the  $\beta$  phase of composition *y*, which are at the ends of the tie line through *P*. The lattice parameter of the  $\alpha$  phase in this alloy will match some point on the lattice-parameter curve for the  $\alpha$  field, a curve that is determined by quenching from the temperature at which solubility is a maxi-

<sup>1</sup> A tie line is a line joining the two points that give the composition of the two coexisting phases in equilibrium.

mum; the composition corresponding to the point of equal lattice parameter will be the composition of the  $\alpha$  phase on the boundary of the  $\alpha$  field at the temperature chosen. To locate the entire curve giving the limit of solubility for the  $\alpha$  phase, it is merely necessary to homogenize alloys in the two-phase region at a series of temperatures, to determine the corresponding lattice parameters after quenching from these temperatures, and to compare these parameters with the parameter curve for the solid solution. For example, in an investigation of the Ag-Al system the data in Fig. 4 were first assembled, then the parameters were deter-

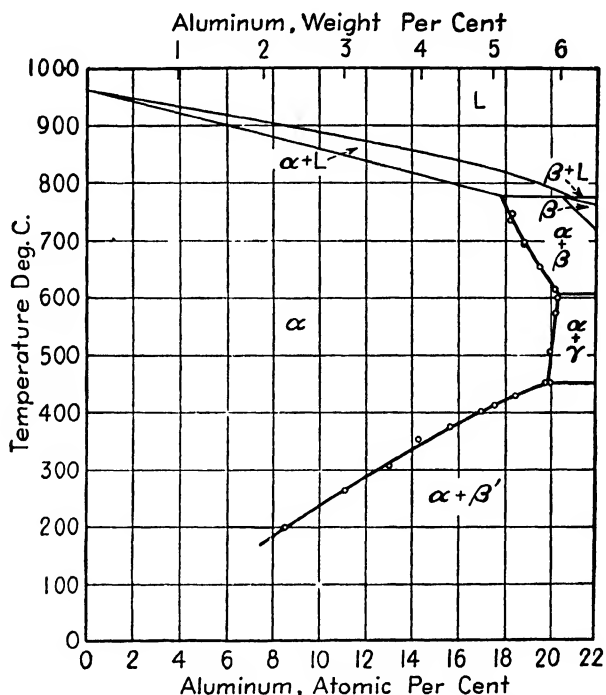


FIG. 5.—Constitution diagram of silver-rich silver-aluminum alloys determined with the aid of Fig. 4. (Foote and Jette.)

mined for alloys in the adjoining two-phase field after quenching from the homogenizing temperature. Comparison of the quenched parameters with Fig. 4 gave the solubility limits shown in Fig. 5.<sup>1</sup>

**Accuracy of the Parametric Method.**—It is well to review the difficulties that may be encountered with this parametric method. The accuracy with which the solubility limits can be determined is directly proportional to the slope of the lattice-parameter curve in the single-phase region; the method is unworkable when there is no variation in lattice dimensions with composition as, for example, in aluminum-rich Ag-Al alloys. Unless suitable precautions are taken, this parametric

<sup>1</sup> F. FOOTE and E. R. JETTE, *Trans. A.I.M.E.*, vol. 143, p. 151, 1941.

curve may be in error as a result of (1) improper removal of segregation in the sample; (2) oxidation; (3) sublimation; (4) contamination by diffusion from adjoining solids or by reaction with vapors; (5) internal strains resulting from quenching, filing, or grinding the samples; and (6) alteration of surface composition by the selective action of an etchant. The data from the two-phase region is subject to the same errors, especially those arising from the lack of equilibrium in the specimen. When the degree of supersaturation in a two-phase alloy is slight and the rate of diffusion is slow, it sometimes requires prohibitive annealing times to reach equilibrium; it is then advantageous to speed up the equilibration by cold-working the alloy before the annealing treatment. In other cases, reaction rates are so fast that it is difficult or impossible to retain the high-temperature state by quenching.

The devices used to minimize these difficulties are varied and must be altered to fit particular cases. A technique that gives excellent results when it can be employed is as follows: The alloy is first homogenized, then powdered by filing (or crushing) and sealed into small capsules of glass or silica. The capsules are annealed at the required temperatures for a sufficient number of hours to produce equilibrium and are then plunged into water and smashed immediately, so that the hot particles of powder are individually brought into contact with the quenching medium and are cooled instantly. The powder is then collected, dried, and mounted for use in the x-ray camera. Internal strains from quenching are avoided by the small size of the individual particles, and decomposition of the high-temperature state is minimized by the drastic quench.

Anyone who finds he is not critical of the technique used in the average x-ray investigation of an alloy diagram should read a discussion by Hume-Rothery and Raynor<sup>1</sup> in which it is pointed out that filings from a two-phase alloy are likely to consist chiefly of single-phase particles, and these quite commonly are different-size particles from the different phases. In such cases the composition of the filings varies with the fineness of the sieve through which they are passed. In an extreme case only one phase of a two-phase alloy passed a 250-mesh screen. Chemical analyses of filings require particular care. Computing the percentage of one element by difference is wholly unreliable, for dust, moisture, etc., may amount to as much as 1.0 percent when filing is done under ordinary conditions. Filing and screening under argon is recommended. Inadequate quenching of filings permits decomposition of phases and causes incorrect results like those shown by the dotted lines in Fig. 6. The solid lines were determined by methods in which precipitation was prevented.

<sup>1</sup> W. HUME-ROTHERY and G. V. RAYNOR, *J. Sci. Instruments*, vol. 18, p. 74, 1941.



Naturally, the accuracy attained in any diagram is dependent upon the accuracy of the x-ray technique, which means that back-reflection powder cameras should be used, with proper corrections for film shrinkage and other instrumental errors. The design of slits to give diffraction lines of suitable sharpness without excessively long exposures is a matter of some importance; the details of camera design are also of considerable importance when the method of disappearing phases is employed.

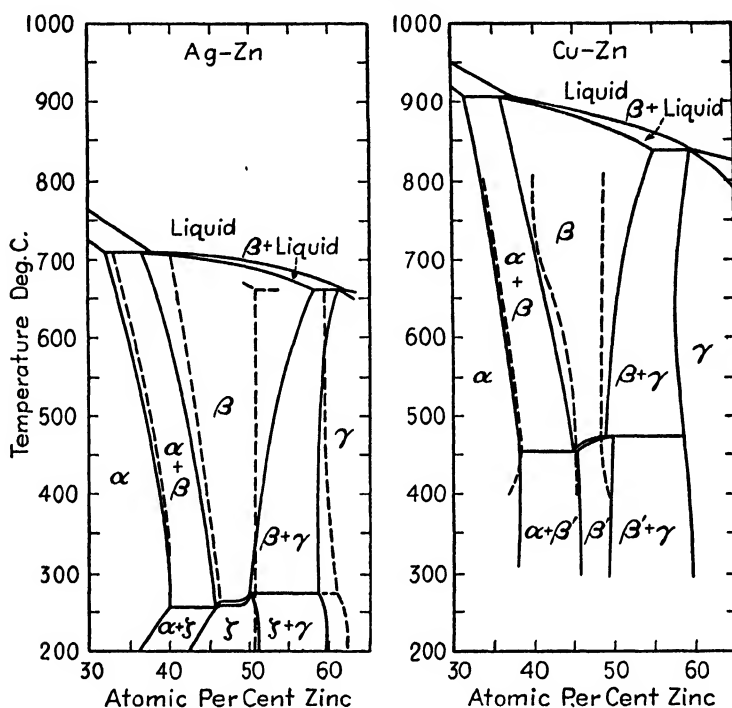


FIG. 6.—Phase diagrams of  $\beta$ -phase regions of Ag-Zn and Cu-Zn alloys. Dotted lines: resulted from unsatisfactory x-ray technique, solid lines from satisfactory technique. (Hume-Rothery and Raynor.)

**Ternary Diagrams.**—The commercial importance of ternary and more complex alloys has focused an increasing amount of attention on them in recent years. X-ray methods have proved very fruitful with ternary alloys, both in rough survey work and in more precise determinations of diagrams. Owing to the fact that the individual regions within a ternary equilibrium diagram may represent single-phase, two-phase, or three-phase equilibria, the principles governing ternary diagrams and their determination necessarily differ somewhat from those employed with binary alloys.

To plot the phases in a three-component system, it is best to use an equilateral-triangle plot. The three pure metals are represented by the corners of the diagram, as indicated by the letters *A*, *B*, *C* in Fig. 7. All the binary alloys of these metals will be represented by points along

the boundaries of the triangle, and alloys containing all three components will lie within the triangle. The location of a point within the triangle

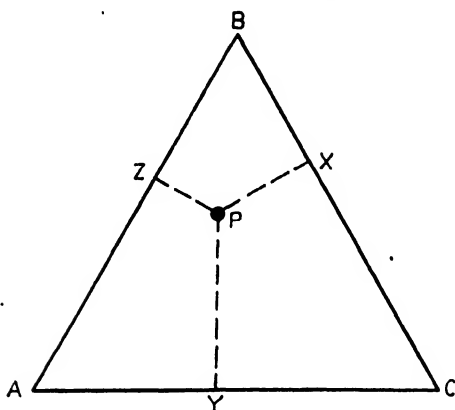


FIG. 7.—Triangular plot for ternary systems.

gives its composition; thus the alloy *P* in Fig. 7 contains amounts of metals *A*, *B*, and *C* in proportion to the perpendicular distances *PX*, *PY*, and *PZ* respectively.<sup>1</sup> The same principle holds, of course, for points along the boundaries where the alloys contain only two metals. Atomic percentages are of more significance than weight percentages in determining the extent of phase fields and are usually preferred in research work.

Figure 8 illustrates a possible disposition of phase fields in a ternary diagram and gives the equilibrium relations for one temperature. It is an isothermal section through a three-dimensional plot having the composition triangle as a base and temperature as the ordinate. A succession of such plots for different temperature levels would be necessary for a full specification of the ternary constitution, but usually only a few are of sufficient practical importance to be mapped out in detail.

The geometry of an isothermal diagram is important, for the x-ray method depends upon it. Three-phase fields are always triangular. They always have boundaries in common with two-phase fields and corners that touch one-phase fields at cusps on the one-phase boundaries.<sup>2</sup>

The tie lines within the two-phase fields, which give the compositions of the two coexisting phases, are straight lines that never cross each other and that change in direction gradually from one side of the area to the

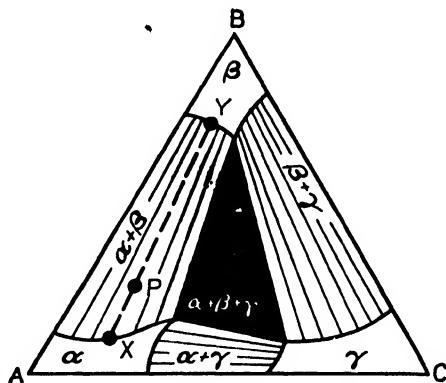


FIG. 8.—Isothermal section of a hypothetical ternary diagram showing one-, two-, and three-phase fields as open, ruled, and black areas respectively.

<sup>1</sup> This method of plotting is possible because the sum of the perpendicular distances from any interior point to the three sides is always the same, a length which is taken as 100 percent.

<sup>2</sup> Certain rules govern the angle relationships that are permitted at these corners. Extrapolation of the single-phase boundaries at a corner should result either in two lines extending into the three-phase triangle or in two lines extending into the two-phase regions, but not in one line extending into each.

other. The relative proportion of two phases in equilibrium is given by the lever relation just as with binary alloys. Referring to Fig. 8, the lever principle applied to alloy  $P$  gives

$$\frac{\text{Amount of } \alpha}{\text{Amount of } \beta} = \frac{\text{length of } Py}{\text{length of } Px'}$$

or, equivalently,  $Py/xy$  of the total alloy is  $\alpha$ .

In any three-phase region the compositions of the coexisting phases are given by the three corners of the three-phase triangle and are independent of the over-all composition of the alloy. The relative proportion of the phases present in a three-phase region may be found by the construction shown in Fig. 9, where an alloy  $P$  lies within a three-phase region containing  $\alpha$ ,  $\beta$ , and  $\gamma$  phases. The amounts of the individual phases are given by drawing a line through  $P$  and one corner of the three-phase triangle and setting up equations of the type

$$\frac{\text{Amount of } \beta}{\text{Amount of } (\alpha + \gamma)} = \frac{\text{length of } Px}{\text{length of } P\bar{v}}$$

and

$$\frac{\text{Amount of } \alpha}{\text{Amount of } \gamma} = \frac{\text{length of } xw}{\text{length of } xu}$$

**Disappearing-phase Method in Ternary Diagrams.**—Boundaries of two-phase regions and corners of three-phase regions can be located by applying the above relations to the relative intensities of the spectra of the individual phases. This procedure is analogous to the disappearing-phase method discussed in connection with binary diagrams. It has been employed with marked success by Bradley and his associates<sup>1</sup> in various ternary systems of iron, nickel, aluminum, and copper, although it has not been held in high regard by many investigators, perhaps for the reason that full use is not often made of intensity data and the lever relations mentioned above, and perhaps because imperfectly crystallized transition lattices may exist that lead to diffuse spectra of the minor constituent. Bradley and Lipson succeeded in detecting a phase when it was only  $\frac{1}{800}$  of the total alloy and regularly used films showing a phase that constituted only  $\frac{1}{100}$  of the specimen, usually employing for this purpose a cylindrical camera of 19 cm. radius, nicely adjusted, with suitably chosen radiation that had been passed through a filter.

**Parametric Method in Ternary Diagrams.**—While the method of disappearing phases is useful for survey work, there seems no doubt

<sup>1</sup> A. J. BRADLEY, H. J. GOLDSCHMIDT, H. LIPSON, and A. TAYLOR, *Nature*, vol. 140, p. 543, 1937. A. J. BRADLEY and H. LIPSON, *Proc. Roy. Soc. (London)*, vol. A167, p. 421, 1938. A. J. BRADLEY, W. L. BRAGG, and C. SYKES, *J. Iron Steel Inst.*, vol. 141, p. 63, 1940.

that lattice-parameter measurements are required for precision determinations of ternary diagrams, just as with binaries. The principles involved have been summarized by Bradley and his coworkers<sup>1</sup> and in greater detail by Andersen and Jette.<sup>2</sup>

The investigator first determines the variation of the lattice spacings within the single-phase regions of the three binary constitution diagrams, then over the single-phase regions of the ternary diagram. He then prepares diffraction patterns for alloys in the three-phase regions and uses the principle that each phase in any three-phase alloy will have the same lattice spacings as the alloy at the corresponding corner of the three-phase triangle. For example, the alloy *P* in Fig. 9 will contain an  $\alpha$  phase with the same parameter as alloy *u*. Thus comparison with the

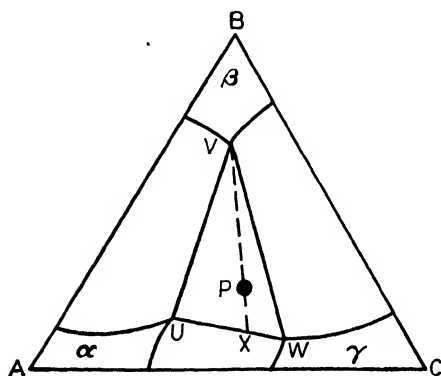


FIG. 9.—The lever principle in three-phase ternary fields.

spacings of the one-phase regions touched by the triangle corners will immediately locate the position of the corners and thereby the whole triangular region. By locating the three-phase triangles in this way, the investigator has also located some of the boundaries of the contiguous two-phase regions. The remaining boundaries of each two-phase area are located by measurements on a series of alloys within the area. Each alloy will give the superimposed spectra of

the two alloys at the ends of the tie line through the point representing the alloy. Turning again to Fig. 8, for example, the alloy *P* will yield the spectra of alloys *x* and *y*. The lattice spacings of *x* and *y*, of course, will coincide with the spacings for certain compositions in the single-phase regions and will thereby determine the compositions of the ends of the tie line. With a series of alloys in the two-phase region, a series of points will be determined on the curved boundaries of the region. The fixing of all boundaries of three-phase and two-phase regions completes the diagram, for the one-phase regions are then fully outlined.

**Labor-saving Principles.**—Let us now consider how the labor can be minimized in this procedure. By judicious choice of alloys the number that must be studied to work out a ternary system can be greatly reduced. Bradley and Taylor,<sup>3</sup> for example, used 130 alloys spaced as much as possible near the boundaries of one-phase regions and obtained results

<sup>1</sup> A. J. BRADLEY, H. J. GOLDSCHMIDT, H. LIPSON, and A. TAYLOR, *Nature*, vol. 140, p. 543, 1937.

<sup>2</sup> A. G. H. ANDERSEN and E. R. JETTE, *Trans. A.S.M.*, vol. 24, pp. 375, 519, 1936.

<sup>3</sup> A. J. BRADLEY and A. TAYLOR, *Proc. Roy. Soc. (London)*, vol. A166, p. 353, 1938.

comparable in accuracy with those that would have been obtained with 741 alloys equally spaced at 2.5 atomic percent intervals. Their choice of alloys for an x-ray investigation of the system Fe-Ni-Al is shown in Fig. 10, with open, half-filled, and filled circles indicating alloys that were found to contain one, two, and three phases, respectively. The ternary diagram derived from these data is reproduced in Fig. 11.

As a rule, the phases along the three binaries extend considerable distances into the interior of the triangle, and there are relatively few single-phase regions that are entirely divorced from the boundaries.

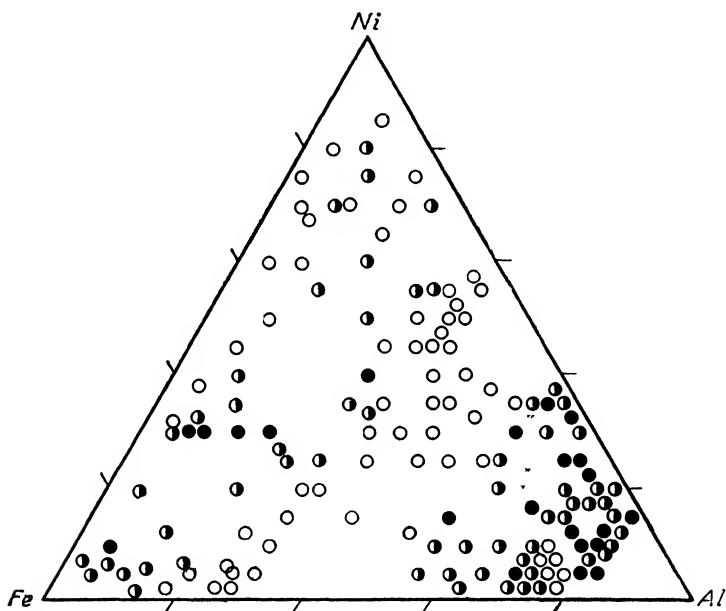


FIG. 10.—Plot of alloy compositions used in an x-ray investigation of the iron-nickel-aluminum system. Open, half-filled, and filled circles represent alloys found to contain one, two, and three phases, respectively. (A. J. Bradley and A. Taylor, *Proc. Roy. Soc. (London)*, vol. A166, p. 353, 1938.)

There also appears to be a tendency in some ternary diagrams for the phase boundaries and the tie lines to run roughly parallel to the lines of equal ratios of valence electrons to atoms—an extension of the Hume-Rothery rule in binary alloys. When similar structures occur at similar electron-to-atom ratios on two of the binaries, it is not unlikely that a single-phase region will extend entirely across the ternary triangle from one to the other, as in the case, for example, in the Fe-Ni-Al system where a phase exists that has a cubic structure with aluminum atoms at cube corners and iron or nickel atoms at cube centers and extends from the composition NiAl across to the composition FeAl (see Fig. 11). These rough generalizations enable the investigator to guess somewhat more readily the possible configuration of the phase fields and thereby

minimize the number of alloys to be made. It has been remarked that the mapping of a ternary is often less laborious—after the component binaries are known—than mapping out a single complicated binary system.

Interpolation is important if one is to reduce the labor of the lattice-parameter method of fixing the phase boundaries. Andersen and Jette<sup>1</sup> have developed a convenient way of interpolating in ternary diagrams based on plotting the lattice parameters for any phase as ordinate on the composition triangle as a base. In such a three-dimensional plot, the

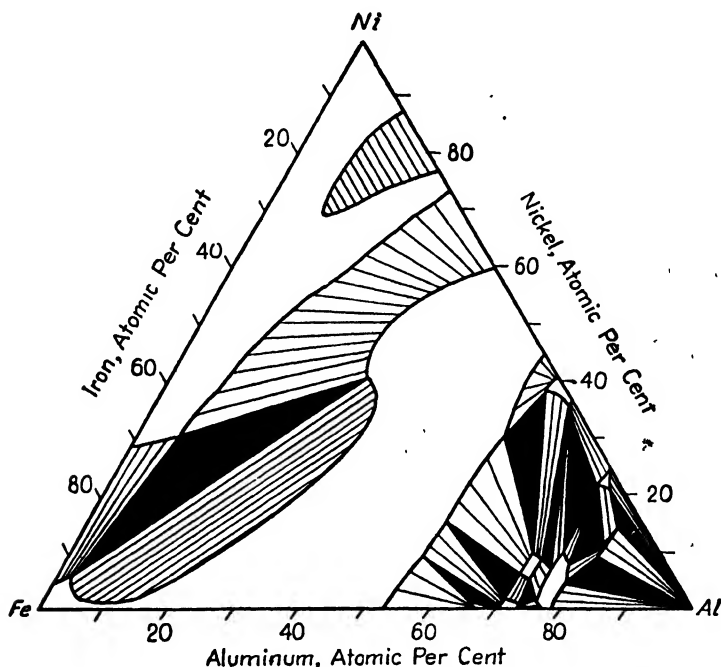


FIG. 11.—Diagram based on the data of Fig. 10. Single-phase fields are unshaded, two-phase fields are ruled with tie lines, three-phase regions are black. Superlattices are present but are not indicated.

parameters will form a surface—the “parametric surface.” This surface will have the following properties illustrated by the drawing in Fig. 12, which is supposed to represent the  $\alpha$ -phase parametric surface for Fig. 8. In three-phase regions it will be a horizontal plane of constant parameter. In two-phase areas it will be, in general, a curved surface; horizontal sections through this will be straight lines identical with tie lines. In one-phase regions, the parametric surface is generally curved and need not contain any sections that are straight lines. The surface for a single-phase region must intersect the surface for the adjoining two-phase region along the boundary line between these regions (generally a curved

<sup>1</sup> A. G. H. ANDERSEN and E. R. JATE, *Trans. A.S.M.*, vol. 24, pp. 375, 519, 1936.

line) and must touch the three-phase parametric plane at the corner of the three-phase triangle..

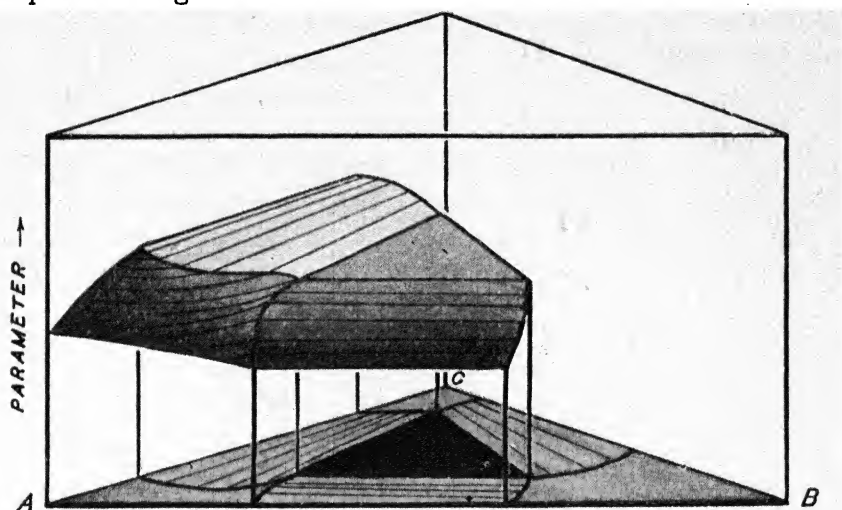


FIG. 12.—Sketch of  $\alpha$ -phase parametric surface for the hypothetical diagram of Fig. 8.

With these facts in mind, it is not difficult to interpret the parameter measurements in terms of phase boundaries or to devise schemes for

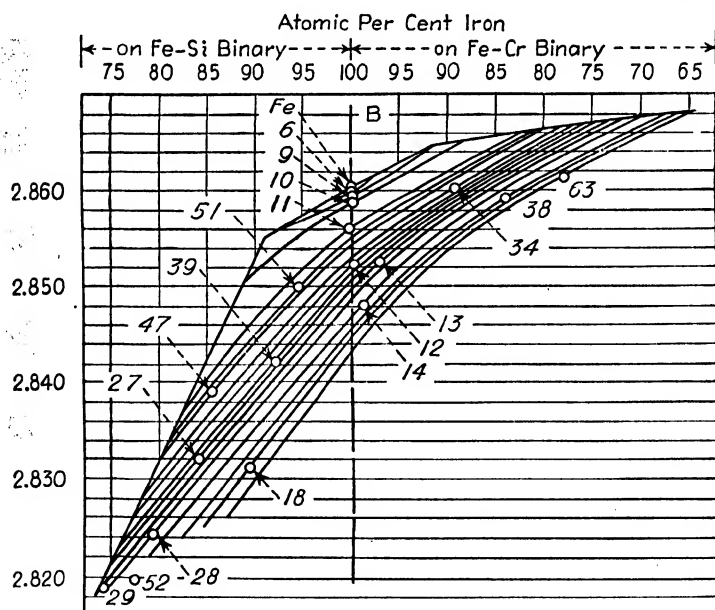


FIG. 13.—Parameters along sections of constant iron content in iron-chromium-silicon alloys, projected on a plane of constant iron content. (A. G. H. Andersen and E. R. Jette, *Trans. Am. Soc. Metals*, vol. 24, pp. 375, 519, 1936.)

interpolation. Andersen and Jette recommend instead of a solid model of the surface, which is a cumbersome device to use, a series of vertical sections of the surface projected orthogonally upon a plane. Figure 13

illustrates this procedure for the phase in the iron corner of the Fe-Cr-Si system, where a family of similarly shaped parameter curves have been drawn through the experimental points labeled Fe, 6, 9 . . . 63. It will be seen that the method of drawing these parameter curves amounts to graphical interpolation both in the plane of constant iron content and in the direction perpendicular to this plane. A horizontal section through this plot gives the compositions along a contour of the parametric surface, which can then be plotted as a contour map on the composition triangle, as in Fig. 14. The solid lines in this figure indicate the single-phase region and the dotted lines the adjacent two-phase regions whose contours

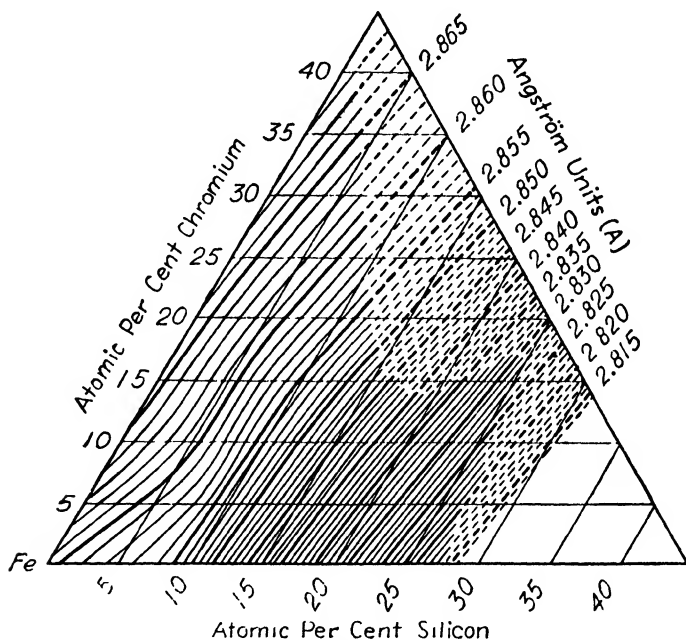


FIG. 14.—Parametric surface indicated by contours of equal parameter derived from Fig. 13.

must connect at the phase boundary with those in the single-phase region. When these two surfaces intersect at an appreciable angle the boundary can be fixed with accuracy, but when the contours pass from one to the other without a distinct change in direction the investigator must resort to the method of disappearing phases to place the boundary. When it is found that the tie lines of a two-phase field converge to a point, it must be concluded that a compound of substantially invariant composition occurs at that point, and from the degree of convergence the extent of the homogeneity range of this phase can be estimated. A suitable choice of vertical sections through the parametric surfaces near a phase boundary aids in making the exact position of the boundary evident.



The iron corner of the Fe-Cr-Si diagram determined by x-rays is reproduced in Fig. 15. Solubility limits are shown for three temperatures, obtained by quenching the powdered samples from homogenizing temperatures of 600, 800, and 1000°C., respectively.

**Quasi-binary Systems.**—Consider the case of a binary system  $A-B$  containing an intermediate phase that melts congruently, *i.e.*, with liquidus and solidus meeting at a maximum, say at the composition  $A_mB_n$ . It usually occurs that the phase at  $A_mB_n$  divides the binary diagram into two independent partial systems, *viz.*,  $A-A_mB_n$  and  $A_mB_n-B$ , each of which is represented by a diagram obeying all the rules of a true

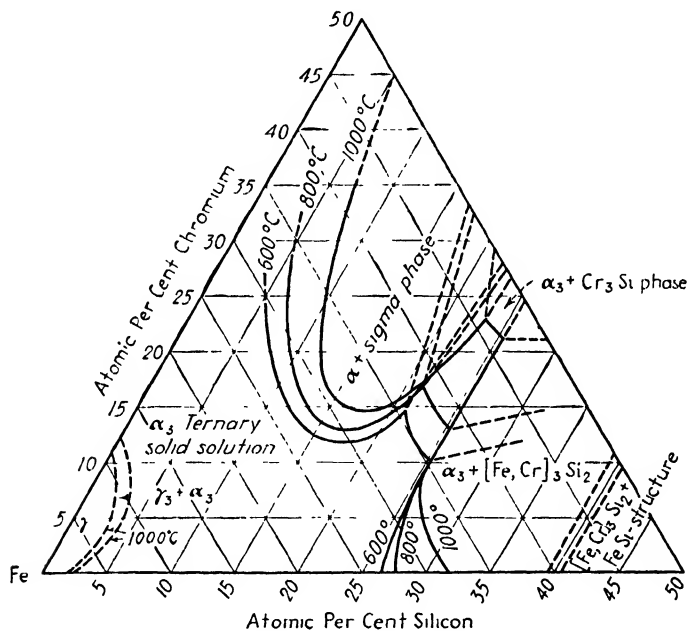


FIG. 15.—The iron-rich corner of the iron-chromium-silicon system determined by x-rays; isothermal sections at 600, 800, and 1000°C.

binary system, the compound or intermediate phase taking the place of an element. Now if this binary is one system in a ternary diagram,  $A-B-C$ , it may occur that the  $A_mB_n$  phase also acts as an element in the ternary, dividing the diagram into independent partial diagrams. In such an event there will be a quasi-binary system between the phase  $A_mB_n$  and some other element or intermediate phase. If  $A_mB_n-C$  is such a quasi-binary system, then the line between  $A_mB_n$  and  $C$  will be a tie line in any two-phase region on this line, and no tie lines will cross it. X-ray spectra of any alloy on one side of this line will show only the spectra of phases on the same side of the line and none from phases on the other side. The division of the ternary diagram into two partial diagrams by the quasi-binary line simplifies the work of interpretation.

If congruently melting compounds occur on two or more binary diagrams of a ternary diagram, then a number of quasi binaries may exist. A rapid survey of the diagram is possible by first locating which of the possible ones, if any, actually exist. A short-cut method of accomplishing this was worked out by Guertler (*Klärkreuzverfahren*) and is illustrated in the isothermal section sketched in Fig. 16. The method is based on the rule that *quasi-binary lines cannot cross each other*. Thus the quasi binaries in Fig. 16 may be any of those shown as dashed lines except that  $AB-C$  and  $AC-B$  cannot both exist. Therefore, examination of an alloy  $P$  at the intersection of two possible quasi binaries will reveal which of these two systems, if any, actually exist. For example, if the alloy  $P$  shows by microscopic or x-ray examination only the phases  $AC$  and  $B$ ,

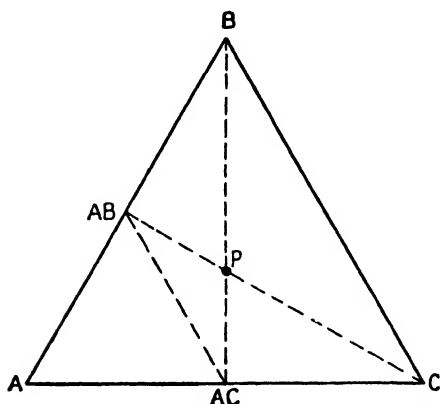


FIG. 16.—Possible quasi-binary lines in a ternary diagram with congruently melting compounds  $AB$  and  $AC$ .

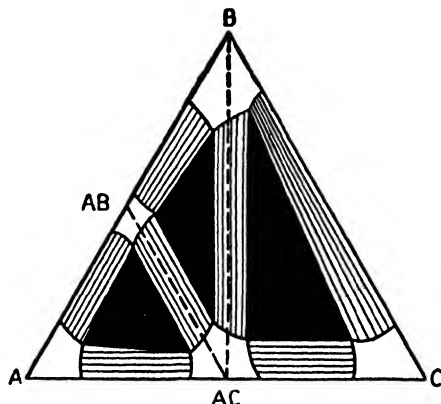


FIG. 17.—A simple isothermal section based on quasi-binary  $AB-AC$  and  $AC-B$ .

then it is inferred that  $AC-B$  is a quasi binary. Then if another alloy is examined on the line  $AC-AB$  and shows only phases  $AC$  and  $AB$ , it can be inferred that the isothermal section has three partial diagrams and may appear as in Fig. 17, or it may contain other fields in addition to these. Naturally, merely the examination of one isothermal section cannot establish whether or not a quasi binary exists between two components at all temperatures or only over a limited range of temperatures.<sup>1</sup> A complete exploration of a diagram, either binary or more complex, requires the use of the older methods, particularly in the range of temperatures near the liquidus and solidus.

<sup>1</sup> If ternary compounds exist within a ternary diagram, these may also act as components of various quasi-binary systems, connecting them with other compounds or with the corners of the ternary. The distributions that are possible are discussed in R. Vogel, *Der Heterogenen Gleichgewichte*, vol. II, "Handbuch der Metallphysik," Akademische Verlagsgesellschaft m.b.H., Leipzig, 1937, and in J. S. Marsh, "Principles of Phase Diagrams," McGraw-Hill, New York, 1935. An analogous short-cut method is useful in quaternary diagrams.

**Complexities.**—It might be well to remind the reader that alloys often are not so simple as they might be. If they have not been brought to equilibrium, they may not obey the phase rule. They may contain transition structures that disappear on further annealing, as, for example, martensite, the familiar transition structure forming from the eutectoid inversion in the Fe-C system; or the  $\theta'$  phase that forms during the first stages of precipitation from the aluminum-rich matrix in Al-Cu alloys and later decomposes to the stable precipitate. These transition states may be fully developed three-dimensional crystallites, or they may be segregated layers or imperfectly formed structures capable of developing only two-dimensional grating diffraction, as in the case of binary Al-Ag alloys<sup>1</sup> and the ternary alloys of Fe, Cu, and Ni.<sup>2</sup> Alloys that have not been brought to equilibrium may contain phases that are supercooled from a region of stability at higher temperatures. The presence of coring in crystals that solidified from the melt may cause weak and diffuse x-ray diffraction lines that are seen with difficulty.

The observer may find the atoms in his alloy distributed on the atomic sites of a phase in any degree of order from complete randomness to complete order; *i.e.*, he may find a superlattice of one of the types discussed in Chap. XII. When he inserts superlattice data on his phase diagram and draws the boundaries of the temperature-composition region in which it exists, he is usually at a loss to know whether the lines obey the phase rule or not. Actually it remains uncertain whether the lines should obey the phase rule—whether, for instance, there should be regions where two phases having different compositions are in equilibrium with each other, the one partially ordered and the other disordered. Data appear inadequate to decide the question and the observer is free to draw conventional lines obeying the phase rule, as in the  $\beta'$  phase of the Cu-Zn diagram of Fig. 1 (which is a superlattice), or he may draw in dotted lines of highly unconventional character that violate the phase rule but that represent the diffraction data nicely. In either case, his choice will probably enrage some serious student of phase diagrams; but, in either case, if the work has been done with care, the published diagram will be worth while and a needed contribution to our very limited knowledge of the constitution of alloys.

<sup>1</sup> C. S. BARRETT, A. H. GEISLER, and R. F. MEHL, *Trans. A.I.M.E.*, vol. 143, p. 134, 1941.

<sup>2</sup> A. J. BRADLEY, W. L. BRAGG, and C. SYKES, *J. Iron Steel Inst.*, vol. 141, p. 63, 1940.

## CHAPTER XI

### THE STRUCTURE OF METALS AND ALLOYS

Numerous summaries of crystal structures have been published, the most extensive being the various volumes of "Strukturbericht" by P. P. Ewald and C. Hermann,<sup>1</sup> which contain abstracts of all x-ray crystal-structure determinations from 1913 to 1936. More condensed listings of structures are available in numerous recent books.<sup>2</sup> Phase diagrams for metallic systems are covered in the extensive book by Hansen<sup>3</sup> and elsewhere.<sup>4</sup> The treatment in this chapter and the two following chapters does not attempt a complete listing of structures but is directed toward a correlation of the structures and an understanding of the principles underlying the structures of the metallic phases.

Crystals may be classified as to types of binding forces as follows:

1. **Metallic** crystals consist of positive ions immersed in a "gas" of negative electrons. The attraction of the positive ions for the negative electrons holds the structure together and balances the repulsive forces of the ions for one another and of the electrons for other electrons. The electrons move freely through the lattice and provide good electrical and thermal conductivity.

2. **Ionic** crystals are bound together by the electrostatic attraction between positive and negative ions. They are combinations of strongly electronegative and electropositive elements. In NaCl, for example, the electron affinity of chlorine atoms causes a transfer of electrons from the electropositive sodium atoms to yield  $\text{Na}^+$  and  $\text{Cl}^-$  ions.

3. **Covalent** crystals ("homopolar," or "valency," crystals) are held together by the sharing of electrons between neighboring atoms. Diamond

<sup>1</sup> Published serially in *Z. Krist.* and also as separate volumes by Akademische Verlagsgesellschaft m.b.H., Leipzig, 1931 ff.

<sup>2</sup> R. W. G. WYCKOFF, "The Structure of Crystals," 2d ed., 1931, and "Supplement to the Second Edition," Reinhold, New York, 1935. R. GLOCKER, "Materialprüfung mit Röntgenstrahlen," Springer, Berlin, 1936. C. H. DOUGLAS CLARK, "The Fine Structure of Matter," Wiley, New York, 1937. W. HUME-ROTHERY, "The Structure of Metals and Alloys," Institute of Metals, London, 1936. U. DEHLINGER, "Gitteraufbau metallischer Systeme," "Handbuch der Metallphysik," vol. I, Akademische Verlagsgesellschaft, m.b.H., Leipzig, 1935.

<sup>3</sup> M. HANSEN, "Der Aufbau der Zweistofflegierung," Springer, Berlin, 1936.

<sup>4</sup> Metals Handbook, A.S.M., Cleveland, Ohio, 1939. G. SACHS and K. R. VAN HORN, "Practical Metallurgy," A.S.M., Cleveland, Ohio, 1940. E. JANECKE, "Kurzgefasstes Handbuch aller Legierungen," Otto Spamer, Leipzig, 1937. Alloys of Iron Research, Monograph Series, McGraw-Hill, New York.

is a typical example, in which each carbon atom shares its four valence electrons with the four nearest neighbors and thus completes an outer shell of eight electrons in each atom. The crystals are characterized by poor conductivity and great hardness.

4. **Molecular** crystals are composed of inactive atoms or neutral molecules bound by weak van der Waals forces. They have low melting points. Typical examples are the rare gases.

Many crystals are intermediate between these "ideal" types. For example, some alloy phases have metallic conductivity and other properties associated with metallic binding yet at the same time resemble covalent crystals.

### STRUCTURES OF THE ELEMENTS

The crystal structures of the elements are listed in Appendix VII. We are concerned here with the more common types and their relation to the periodic table.

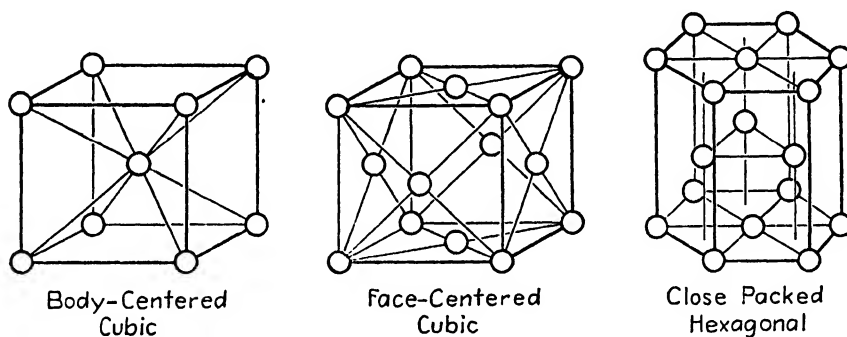


Fig. 1.— The principal structures of the metals.

The structures of most metals are face-centered cubic (f.c.c.), hexagonal close-packed (h.c.p.), or body-centered cubic (b.c.c.) (Fig. 1). These are structures in which each atom is surrounded by 12 or 8 near neighbors in one of the simple ways of packing spheres. Elements in the same group of the periodic table tend to have the same structures—for example, the alkali metals Li, Na, K, Rb, Cs are all b.c.c.; Be, Mg, Zn, Cd are h.c.p.; Cu, Ag, Au are f.c.c., as are most of the eighth-group elements in at least one of their modifications.

The electropositive elements, those toward the left of the periodic table (Fig. 2), tend to have these structures. In this class are the alkali metals with one valence electron, the alkaline-earth elements with two valence electrons (Be, Mg, Ca, Sr, Ba), and most of the transition elements in which the process of forming a new shell of electrons awaits the filling of interior shells. The latter are boxed in the figure and include 21 Sc to 28 Ni in the first long period, 39 Y to 46 Pd in the second, and 57

La through the rare earths to 78 Pt in the third. Because of their low electron affinity, these elements give up their valence electrons to the electron gas.

Hexagonal close-packed and face-centered cubic crystals are much more closely related than would appear from Fig. 1. Both are structures that represent spheres in closest packing. In the h.c.p. structure the

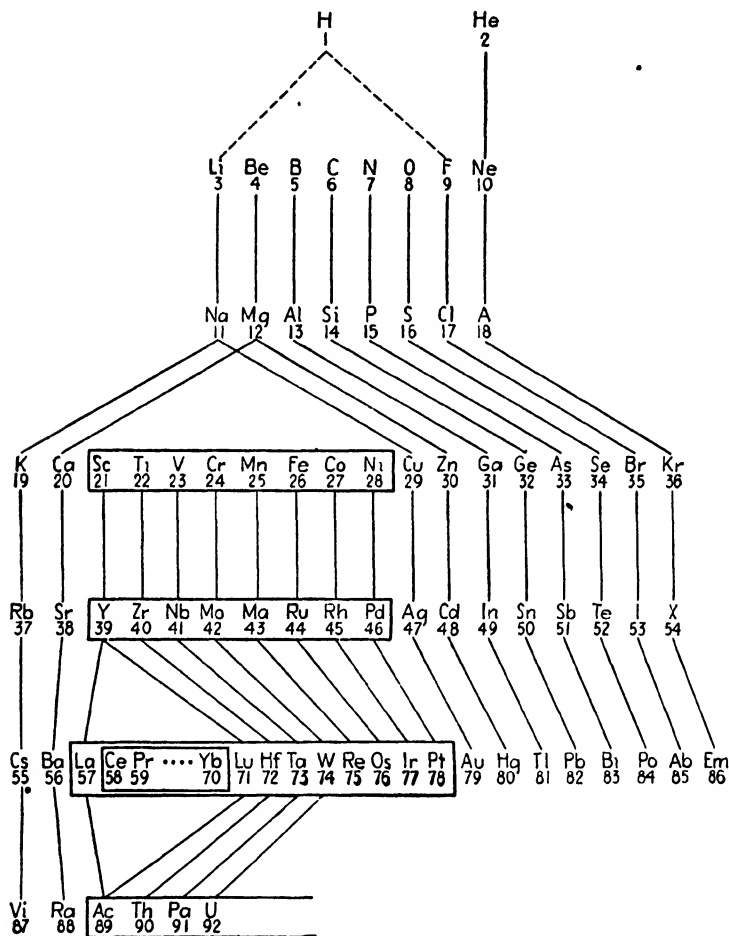


FIG. 2.—The periodic table.

close-packed (0001) layers are stacked above each other in the sequence *ABAB* . . . ; *i.e.*, atoms of the third layer are directly above those of the first. In the f.c.c. structure the [111] planes have the same h.c.p. array of atoms and are stacked in the sequence *ABCABC* . . . so that the fourth layer is directly above the first. The atoms in each layer fit in the hollows of the layer beneath. Tightly packed rows of atoms run in six directions through h.c.p. and f.c.c. structures and in four directions through the less densely packed b.c.c. lattice.

**The 8 -  $N$  Rule.**—The  $B$  subgroup elements, in which the outer shells are again in the process of being filled, are in general less closely packed. The binding becomes more a covalent binding between certain neighboring atoms instead of a binding among positive ions and electrons. The homopolar character increases toward the end of the periods until it is a true covalent bond in the diatomic molecules  $F_2$ ,  $Cl_2$ ,  $Br_2$ , and  $I_2$ .

Most of the structures in the  $B$  subgroups follow Bradley and Hume-Rothery's interesting "8 -  $N$  rule," which states that each atom has 8 minus  $N$  close neighbors, where  $N$  is the number of the group to which the element belongs.

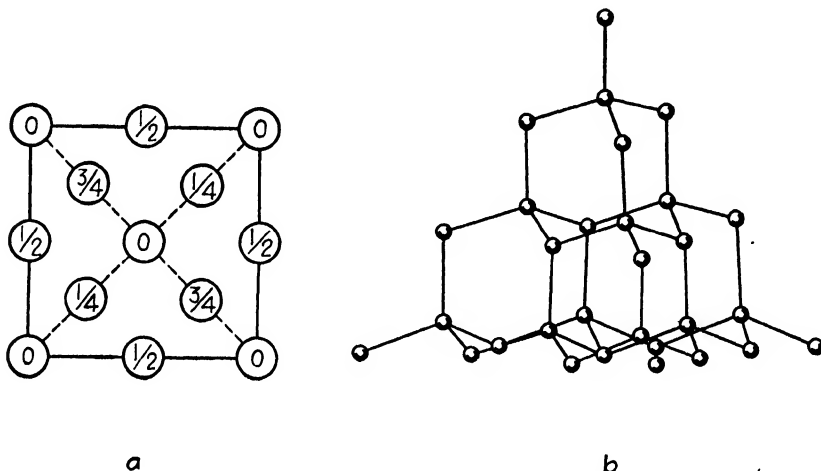


FIG. 3.—The structure of diamond. (a) Projection on the basal plane. Fractions in circles indicate heights above the basal plane. (b) Perspective drawing, showing that each atom has four nearest neighbors.

Consider first the structure of diamond, Fig. 3. The atoms are arranged on two interpenetrating f.c.c. lattices. Projected upon the basal plane the atom positions are as indicated in Fig. 3a, where the fractions give the coordinate normal to the plane of projection. A perspective view of the structure, Fig. 3b, shows more clearly that each atom has four near neighbors.<sup>1</sup> Gray tin, Si, and Ge of Group  $IV_B$  also have this diamond cubic structure with coordination number 4.

In Group  $V_B$ , As, Sb, and Bi have rhombohedral structures with each atom surrounded by three (Fig. 4). Group  $VI_B$  has Se and Te with the structure of Fig. 5, in which the atoms are linked in chains with each atom having two neighbors. There is only one nearest neighbor to each atom in solid iodine, Fig. 6, for which  $8 - N = 1$ . The pairs of iodine atoms

<sup>1</sup> Neither of these common ways of drawing crystal structures shows the effective size of the atoms in relation to their distance apart, for they are usually spheres in contact with the nearest neighbors. Only the positions of the atom centers are indicated.

correspond to the diatomic molecules of the other elements of this group. The  $8 - N$  rule does not apply to Group III<sub>B</sub> (B, Al, Ga, In, Tl), but there seems to be some effect of the rule in Group II<sub>B</sub>. In this group, Hg crystallizes in a simple rhombohedral lattice, equivalent to a distorted simple cubic, in which there are six nearest neighbors for each atom.

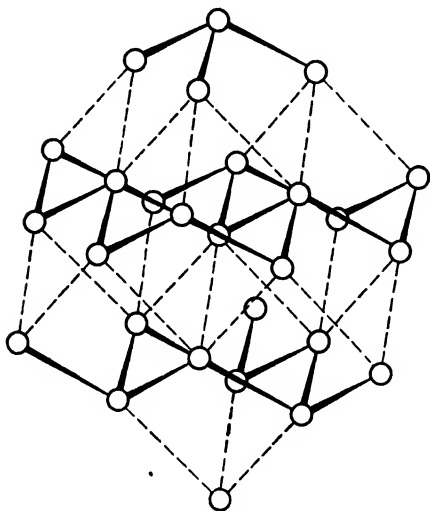


FIG. 4.—The structure of antimony. Each atom has three nearest neighbors, as indicated by the connecting lines.

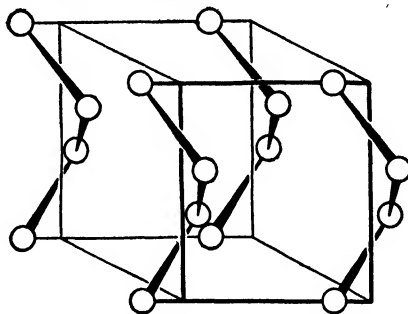


FIG. 5.—The structure of tellurium. Atoms are arranged in spiral chains in which each atom has two nearest neighbors.

Also in this group are h.c.p. Zn and Cd, but the unit cells of these metals are not the normal shape expected of close-packed spheres ( $c/a = 1.633$ )

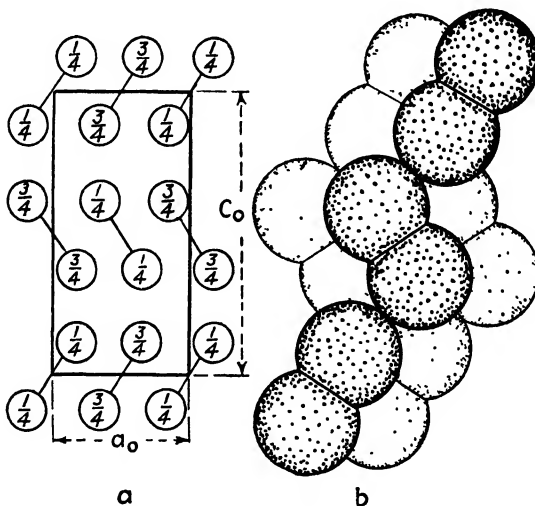


FIG. 6.—The structure of iodine. (a) Projection on (010) plane. Fractions indicate distances below the plane of the paper. (b) Drawing showing the packing of iodine atoms in the structure. (Wyckoff.)

but are stretched along the  $c$ -axis to axial ratios of approximately 1.9. Consequently, each atom has six nearest neighbors in the (0001) plane



in which it lies, while the atoms in the planes next above and below this are more distant.

**Allotropy.**—Many of the elements exist in more than one form (see Appendix VII).<sup>1</sup> The low-temperature b.c.c. structure of iron ( $\alpha$ -Fe) changes to f.c.c. at 910° ( $\gamma$ -Fe) and reverts to b.c.c. again at about 1400° ( $\delta$ -Fe). A similar reversion seems to occur in cobalt where a f.c.c. phase divides two h.c.p. ranges. Usually, however, the various modifications are different, as in manganese where the  $\alpha$ ,  $\beta$ , and  $\gamma$  forms have 58, 20, and 2 atoms per unit cell, respectively. The familiar white form of tin ( $\beta$ ) is tetragonal, while the gray form ( $\alpha$ ) is stable below 18°C. and has the diamond cubic structure. This low-temperature form is the “tin pest” to which tinned articles are sometimes subject when exposed to cold weather. Some of the reported allotropic changes are based on inadequate experimental data—for example, heats of recrystallization may be mistaken for latent heats of transformation. Some polymorphic modifications have been found in electrolytic deposits that are not seen under ordinary conditions.

Bridgman<sup>2</sup> has shown that many unusual allotropic forms of the elements appear at high pressures. The transformations with increasing pressures are always to more dense modifications, an expression of Le Châtelier's principle.

## SOLID SOLUTIONS

**Types of Solid Solution.**—The lattice of nickel can accommodate atoms of copper without losing its f.c.c. structure. Substitution of copper atoms for nickel atoms on the f.c.c. lattice points is an example of the formation of a **substitutional solid solution**. In the Cu-Ni system the two elements can be substituted in all proportions and are said to form a continuous series of solid solutions. All alloys of the system consist of a f.c.c. lattice with copper and nickel atoms distributed at random on the lattice points. A continuous series of solid solutions is found only between elements of the same crystal structure and only when the sizes of the solute and solvent atoms are not too different.

Addition of an element in substitutional solid solution may either increase or decrease the lattice parameter, as shown by examples in Fig. 7. Usually the unit cell is enlarged by dissolving atoms larger than those of the solvent and contracted by dissolving atoms smaller than the solvent atoms. This is not always true, however; for example, some Ag-Au alloys have a smaller unit cell than either silver or gold (see Fig. 8). To a rough approximation the lattice parameters in substitutional solutions

<sup>1</sup> Polymorphism among the elements is termed **allotropy**.

<sup>2</sup> P. W. BRIDGMAN, *Phys. Rev.*, vol. 48, p. 893, 1935; *Proc. Natl. Acad. Sci.*, vol. 23, p. 202, 1937.

vary linearly with composition expressed in atomic percent. This rule, **Vegard's law**, is indicated by dot-dash lines in Figs. 7 and 8, and the deviations from it are seen to be marked.<sup>1</sup> Lattice constants may be smaller than, equal to, or greater than those predicted by Vegard's law. The law holds for Au-Pt, Au-Pd, Mo-W, Pt-Ir, Pt-Rh, Pb- $\beta$ -Tl, and possibly Sb-Bi; but negative deviations (smaller lattice constants) are found in the systems Cu-Ni, Au-Ag, Ag-Pd, Ag-Pt, Co-Ni, and Cr-Fe and presumably indicate a specific attraction for the unlike atoms. Positive deviations are found in Cu-Au, Cu-Pd, Fe-Cr (at the Fe end) and at both

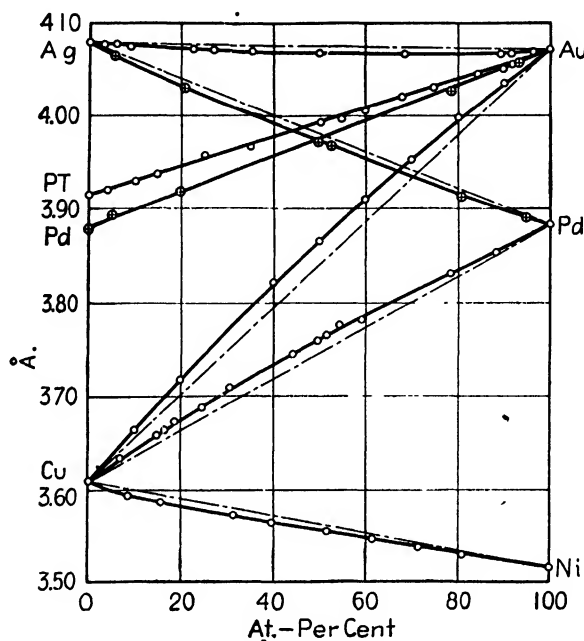


FIG. 7.—Lattice constants in systems exhibiting a continuous series of solid solutions. Dot-dash lines indicate Vegard's law.

ends of the eutectic system Cu-Ag. Atoms of very similar size and electronic structure tend to form systems in which Vegard's law is followed, while negative deviations tend to occur in those systems in which intermetallic compounds are formed.<sup>2</sup>

<sup>1</sup> R. F. Mehl points out that the cube of the lattice parameter rather than the parameter itself is a more logical quantity to plot when considering deviations from the rule of mixtures in atomic percent. (*Trans. A.I.M.E.*, vol. 111, p. 91, 1934; R. F. Mehl and B. J. Mair, *J. Am. Chem. Soc.*, vol. 50, p. 55, 1928.) The effect of plotting the parameter cubed or the volume per atom against atomic percent is to lower the curves, making positive deviations from the rule of mixtures less marked, making "ideal" Vegard's law curves show negative deviations, and increasing the magnitude of negative deviations from the rule of mixtures. When atoms are nearly the same in size, the methods of plotting differ but slightly.

<sup>2</sup> A. WESTGREN and A. ALMIN, *Z. physik. Chem.*, vol. B5, p. 14, 1929. E. R. JETTE, *Trans. A.I.M.E.*, vol. 111, p. 75, 1934.

As a rule, alloy systems in which the liquidus is convex, *i.e.*, bulges upward, give negative deviations, while the opposite is true for systems with a concave liquidus.<sup>1</sup> Atomic radii are altered by changes in coordination number; decreasing the coordination number from 12 to 8 decreases radii 2 to 3 percent. This alters the predicted "rule of mixtures" curve slightly for systems in which the elements crystallize in different structures.<sup>2</sup>

**Interstitial solid solutions** are formed when light atoms with small radii are accommodated in the interstices of the lattice of a solvent. The solid solution of carbon in  $\gamma$ -Fe (austenite) is an example of this type; the iron atoms are on f.c.c. lattice points, and the carbon atoms occupy interstitial positions. The largest "holes" in the lattice are at the points

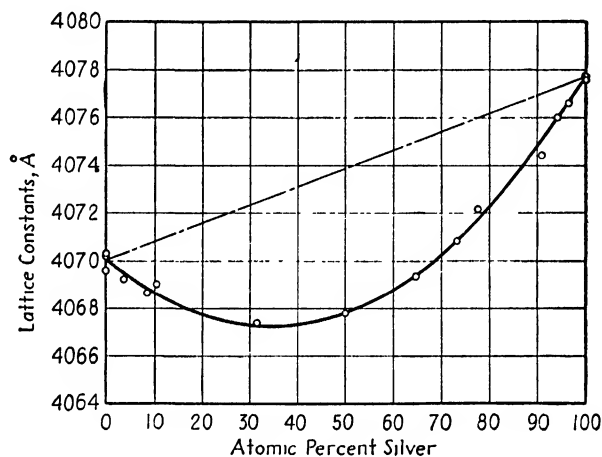


Fig. 8.—Lattice constants in the silver-gold system, showing negative deviations from Vegard's law.

$\frac{1}{2}00$  and  $\frac{1}{2}\frac{1}{2}\frac{1}{2}$ , Fig. 9, and here the small carbon atom is able to fit in with only a slight expansion of the unit cell.<sup>4</sup> The elements H, B, C, and N tend to take up interstitial positions in alloys; all have radii less than  $1.0\text{\AA}$ . When a solvent lattice accepts one of these interstitially, there is always an expansion of the unit cell.

In multicomponent systems some atoms may be dissolved interstitially and others substitutionally. For example, in a manganese steel the manganese atoms are on lattice points, replacing iron atoms, and the carbon atoms are interstitial.

<sup>1</sup> F. HALLA, "Kristallchemie und Kristallphysik metallischer Werkstoffe," Barth, Leipzig, 1939.

<sup>2</sup> E. R. JETTE, *Trans. A.I.M.E.*, vol. 111, p. 75, 1934.

<sup>3</sup> In a b.c.c. lattice like  $\alpha$ -Fe there are "holes" at positions of the type  $\frac{1}{2}00$  and  $\frac{1}{2}\frac{1}{2}0$  and others at positions of the type  $\frac{1}{2}\frac{1}{2}\frac{1}{2}$ ; of the former type there are three holes per Fe atom and of the latter six per Fe atom (*cf.* C. H. Johansson, *Arch. Eisenhüttenw.*, vol. 11, p. 241, 1937; see also discussion of austenite, Chap. XXII).

A type of solid solution in which not all the lattice points of the structure are occupied is called a **subtraction solid solution** or a **defect lattice**. An example is the  $\beta$  phase in the system Ni-Al,<sup>1</sup> in which adding aluminum results in removing some nickel atoms from lattice points without aluminum atoms' having taken their place.<sup>2</sup> Another example is the phase "FeO," in which there are vacant points on the lattice of iron atoms.<sup>3</sup> In some instances, a pair or a group of atoms may replace a single atom of an intermediate phase.<sup>4</sup>

A solid solution at an extremity of a binary-alloy diagram is referred to as a **terminal solid solution**. There are also intermediate phases that are true solid solutions. These **intermediate solid solutions** may have

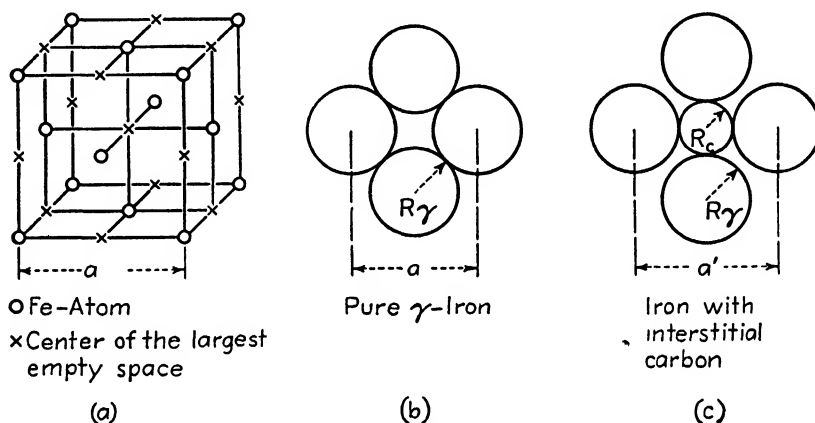


FIG. 9. -Holes in the  $\gamma$ -iron structure. (a) Location of the largest holes in the b.c.c. unit cell are indicated by crosses. (b) Atomic packing in  $\gamma$ -iron. Atomic radius is  $R_\gamma$ . (c) Atomic packing in austenite, with carbon atom of radius  $R_c$  dissolved interstitially, expanding the lattice.

either narrow or wide ranges of homogeneity and may or may not include a composition having a simple chemical formula. One is justified in classifying intermediate phases as **intermetallic compounds** only if they have a narrow range of homogeneity and simple stoichiometrical proportions and if atoms of identical kinds occupy identical points on the lattice. In general, the term "compound" is inappropriate. The homogeneity range may not actually include a composition having a simple chemical formula—the phase "CuAl," for example, exists in a homogeneity range that does not include the composition CuAl. In systems such as Ag-Cd the  $\epsilon$  phase corresponds to the composition  $\text{AgCd}_3$ , but the structure is h.c.p., and it is impossible to place the Ag atoms on one set of equivalent points and the Cd atoms solely on another set; in fact, the two kinds of

<sup>1</sup> A. J. BRADLEY and A. TAYLOR, *Proc. Roy. Soc. (London)*, vol. A159, p. 56, 1937.

<sup>2</sup> It is curious that when *nickel* is added, it replaces *aluminum* atom by atom.

<sup>3</sup> E. R. JETTE and F. FOOTE, *J. Chem. Phys.*, vol. 1, p. 29, 1933.

<sup>4</sup> M. VON STACKELBERG, *Z. physik. Chem.*, vol. B9, p. 437, 1930.

atoms are distributed at random on the atom positions, just as in a solid solution. Intermediate phases may be of any type between the ideal solid solution on the one hand and the ideal chemical compound on the other. Even a single alloy may be a true solid solution at high temperatures and yet resemble a compound at low temperatures if it becomes an ordered superlattice as is discussed later.

**Determination of the Type of Solid Solution.**—The types of solid solutions are distinguished from each other by density comparisons. The density of an alloy computed from an x-ray measurement of the unit-cell size will agree with the observed density if the correct type of solution is assumed. For a substitutional solid solution the calculated density  $\rho_c$  is given by the relation

$$\rho_c = \frac{n\bar{A}}{VN}$$

where  $n$  is the number of atoms contained in the unit cell of volume  $V$ ,  $N$  is Avogadro's number, and  $\bar{A}$  is the mean atomic weight of the atoms.<sup>1</sup>

For an interstitial solid solution there is a contribution to the density by the interstitial atoms in addition to the contribution from the lattice-point atoms given by the above formula. There is usually a fraction of an interstitial atom, on the average, in each cell. If we call this  $n^*$  and let  $n$  be the number of lattice-point atoms per cell, then we may determine  $n^*$  from the relation  $n^*:n = \text{atomic percent interstitial atoms:atomic percent lattice-point atoms}$ . If the interstitial atoms have a mean atomic weight  $\bar{A}^*$ , their contribution to the density, to be added to the above  $\rho_c$ , amounts to  $n^*\bar{A}^*/VN$ .

**Generalizations Concerning Solubility.**—Several factors are now known that control the ranges of solubility in alloy systems: the type of crystal structure of the alloying elements, the relative sizes of the atoms (the "size factor"), the electronegativity of one element with respect to the other, and the concentration of valence electrons in the alloys. These factors are understood largely through the work of Hume-Rothery at Oxford University.<sup>2</sup>

<sup>1</sup> The mean atomic weight is computed from the atomic percentages  $p_1$ ,  $p_2$ , etc., of the elements comprising the alloy and the atomic weights  $A_1$ ,  $A_2$ , etc., with the formula

$$\bar{A} = \frac{p_1 A_1}{100} + \frac{p_2 A_2}{100} + \dots$$

The atomic percentages are obtained from weight percentages  $w_1$ ,  $w_2$ , etc., by the relation

$$p_1 = \frac{w_1/A_1}{w_1/A_1 + w_2/A_2 + \dots} \cdot 100.$$

<sup>2</sup> W. HUME-ROTHERY, "The Structure of Metals and Alloys," Institute of Metals, London, 1936.

Complete solid solubility of two elements in all proportions is never encountered unless the elements have the same crystal structure and similar atomic radii. Silver and gold, which form a continuous series of solid solutions, are both f.c.c. and the atoms differ only 0.2 percent in size. Molybdenum, which is b.c.c. in structure, is completely soluble in tungsten, which is also b.c.c. with similar atomic radius. However, molybdenum has only limited solubility in silver, which differs only 6 percent in atomic radius but is f.c.c.

When atomic radii differ less than about 15 percent, the **size factor** is favorable to solid-solution formation. The size factor must be favorable if a complete series of solid solutions is to occur; an unfavorable size factor (radii differing more than 15 percent) restricts solubility. In fact, the greater the difference in size, the more limited the solubility, other things being equal. If the sizes differ by 8 percent or more but are still in the favorable range, there is usually a continuous series of solutions but a minimum in the liquidus curve; this represents a tendency toward the formation of a eutectic.<sup>1</sup>

Another factor controlling solubility is the **chemical-affinity effect**.<sup>2</sup> The more electronegative the solute element and the more electropositive the solvent, or vice versa, the greater is the tendency to restrict solid-solution ranges and to form intermetallic compounds. The electronegativity of elements in the periodic table increases from left to right in any period and from the bottom to the top in any group. Thus elements of Group VI<sub>B</sub> (S, Se, Te) form stable sulphides, selenides, and tellurides with the electropositive metals, and solid solutions of these elements in normal metals are usually very limited. Group V<sub>B</sub> (P, As, Sb, Bi) with somewhat less pronounced electronegative character usually dissolve up to a few atomic percent in the electropositive metals, and as the metals approach each other in the electrochemical series the solid solutions tend to become more extensive.

The **relative valency effect** also governs solubility. It may be described by saying that a metal of lower valency tends to dissolve a metal of higher valency more readily than vice versa. Silicon, which crystallizes according to the 8 - *N* rule, has a structure that depends on each atom's having four neighbors. Each atom shares an electron with each of the four neighbors so that an octet of electrons is built up. If an atom of

<sup>1</sup> For detailed discussions of the effect of size and polarizability on solubility, see papers by W. Hume-Rothery and G. V. Raynor, *Phil. Mag.*, vol. 26, pp. 129, 143, 152, 1938.

<sup>2</sup> Hume-Rothery calls this the "electronegative valency effect" since it depends on the separation of the elements in the electromotive series. It seems more appropriate to give it a name that emphasizes the role of affinity between the unlike atoms and that avoids confusion with the relative valency effect.

copper is substituted for a silicon atom there will be insufficient electrons to form the covalent bonds, and it is therefore understandable that solubility is very restricted—silicon dissolves less than 2.0 atomic percent copper. On the other hand, copper dissolves 14 atomic percent of the higher valence silicon. Magnesium (valence 2) dissolves less than 0.2 atomic percent gold (valence 1), but gold dissolves magnesium to the extent of 20 or 30 atomic percent. Removal of valence electrons from a structure is more serious than the addition of a limited number of electrons above the fundamental electron-atom ratio for the structure.

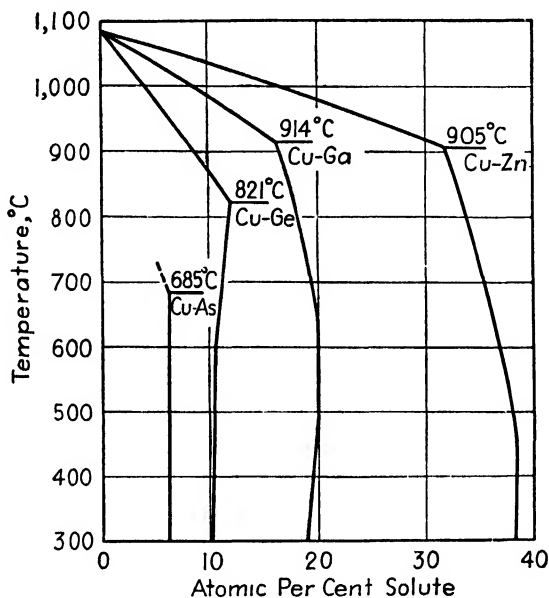


FIG. 10.—Solidus and solid solubility curves for some copper-alloy systems.

A solvent possesses a definite capacity to absorb the valence electrons of the solute. Copper can dissolve another univalent element in unlimited amounts (with a favorable size factor) and forms a continuous series of solutions with nickel, for example. But copper dissolves decreasing amounts as the valency of the solute increases, as illustrated in Fig. 10. Each atom of zinc contributes one additional electron to the solution, each atom of gallium contributes two, germanium three, and arsenic four. The corresponding maximum solubilities in copper (and silver) are approximately 40 atomic percent for one additional electron, 20 percent for two, and 13 percent for three. Thus the total number of valence electrons that can be accommodated per atom of the alloy is about the same for all these alloys, in which the size factor is favorable. The maximum solubility corresponds to a valence electron to atom ratio of 1.4:1—an **electron concentration** of 1.4.

Electron concentration is a factor in ternary alloys (but probably a less decisive one).<sup>1</sup> It is often possible, for example, to dissolve two solute metals in copper in any proportion so long as their combined effect does not increase the electron concentration beyond the critical value for the lattice of the solvent.

The expansion of the lattice of silver for dilute solutions of Cd, In, Sn, or Sb has likewise been correlated with electron concentration.<sup>2</sup> The expansion produced by one atom of solute is proportional to the valence of the solute. This is a quantitative result supporting the principle frequently stated in a qualitative way, that the solubility of a metal is inversely proportional to the amount of alteration it causes in the lattice constant of the solvent.

Hume-Rothery has also pointed out that the liquidus temperatures and likewise the solidus temperatures of various copper alloys are almost identical at identical electron concentrations, and the same is true of silver alloys.

It is a general rule (to which there are exceptions) that in a binary system the solubility in the high-melting metal is greater than in the low-melting metal.

### INTERMEDIATE PHASES

It is rare to find alloy systems in which intermediate phases obey the normal valencies of the elements. This is a consequence of the fact that the phases have *metallic* binding, which means that valence electrons are free to move about in the lattice, as contrasted with inorganic or organic compounds in which the electrons are tightly bound into stable groups of atoms. Attempts at first were made to define an intermetallic compound and to distinguish it from an intermediate solid solution, but the attempts were a source of confusion rather than of clarification. It was later realized that some phases had chemical formulas that followed valence rules and yet had the metallic conductivity and reflectivity characteristic of metallic binding, consequently that the compounds possessed an intermediate type of binding between covalent and metallic, resulting from a partial breakdown of covalent bonds. Intermediate types of binding can exist, in fact, between all the ideal types of binding, ionic, homopolar, molecular, and metallic.

**Structures of Compounds with Normal Valency.**—From the early work of Goldschmidt<sup>3</sup> and others it was found that the simple structures

<sup>1</sup> See W. HUME-ROTHERY, G. W. MABBOTT, and K. M. CHANNEL-EVANS, *Trans. Roy. Soc. (London)*, vol. A233, p. 40, 1934; A. J. BRADLEY, W. L. BRAGG, and C. SYKES, *J. Iron Steel Inst.*, vol. 141, p. 63, 1940.

<sup>2</sup> W. HUME-ROTHERY, *Nature*, vol. 135, p. 1038, 1935.

<sup>3</sup> V. M. GOLDSCHMIDT, *Trans. Faraday Soc.*, vol. 25, p. 253, 1929.



illustrated in Figs. 11 and 12 are common to a great number of compounds, including many intermetallic phases that obey normal valency laws.

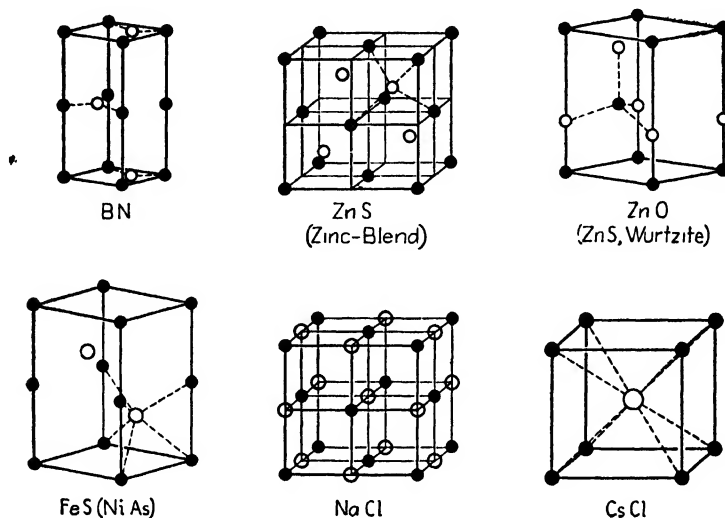


FIG. 11.—Typical crystal structures of compounds of type  $AX$ . (Goldschmidt.)

The structure of **rock salt** ( $\text{NaCl}$ ) may be considered as two interpenetrating f.c.c. lattices of the two types of atoms, with the corner

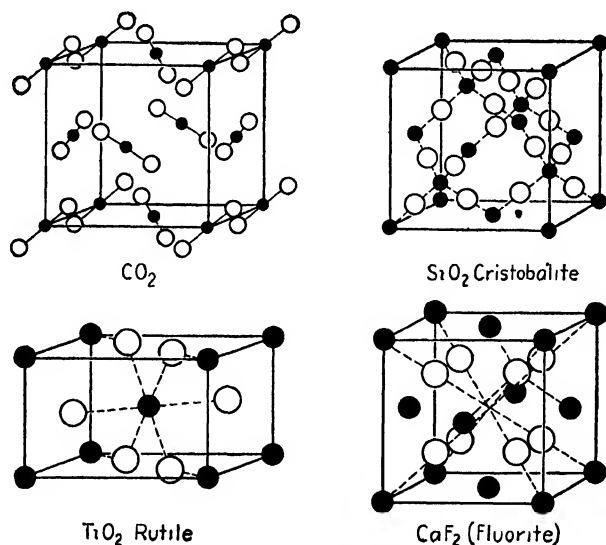


FIG. 12.—Typical crystal structures of compounds of type  $AX_2$ . (Goldschmidt.)

of one located at the point  $\frac{1}{2}00$  of the other. The **fluorite** structure ( $\text{CaF}_2$ ) is also cubic, with Ca atoms at cube corners and face centers and with F atoms at all quarter-way positions along the cube diagonal ( $\frac{1}{4}\frac{1}{4}\frac{1}{4}$ ,

$\frac{1}{4}\frac{3}{4}\frac{3}{4}$ , etc.). These typically ionic structures are found among alloys of metals with elements of Groups IV<sub>B</sub>, V<sub>B</sub>, and VI<sub>B</sub>:<sup>1</sup>

NaCl Structure		CaF <sub>2</sub> Structure
MgSe	BaTe	Mg <sub>2</sub> Si
CaSe	MnTe	Mg <sub>2</sub> Ge
SrSe	SnTe	Mg <sub>2</sub> Sn
CaTe	PbTe	Mg <sub>2</sub> Pb
SrTe	PbSe	Cu <sub>2</sub> Se

The **diamond** structure is formed by elements having a ratio of 4 electrons to 1 atom (C, Si, Ge, Sn). Among alloys we also find closely related structures when the electron-atom ratio is 4. The **zinc blende structure** (ZnS) may be regarded as two interpenetrating face-centered lattices of the elements, with the corner of one located at the position  $\frac{1}{4}\frac{1}{4}\frac{1}{4}$  of the other, as in the diamond structure. Figures 11 and 12 show the close similarity between ZnS and CaF<sub>2</sub> structures. The **wurtzite structure** (ZnS, ZnO) has one kind of atom on h.c.p. positions and the other at intermediate points, where each atom is surrounded symmetrically by four atoms of the other kind.<sup>2</sup> Normal valency rules hold for these so-called **adamantine compounds**, for their binding is covalent. They are formed between an element that is a certain number of places to the left of the column containing C, Si, Ge, Sn and an element an equal number of places to the right in the periodic table:<sup>3</sup>

Zinc Blende Structure			Wurtzite Structure
BeS	BeSe	BeTe	MgTe
AlP	AlAs	AlSb	CdSe
GaP	GaAs	GaSb	$\alpha$ -AgI
$\alpha$ -CdS	CdSe	CdTe	$\beta$ -ZnS
$\alpha$ -ZnS	ZnSe	ZnTe	$\beta$ -CdS
HgS	HgSe	HgTe	MgTe
$\beta$ -AgI	CuI	CuBr	
InP	InSb	GeSb	

The **nickel arsenide structure** (NiAs) is frequently formed by the transition metals Cr, Mn, Fe, Co, Ni, Cu, Pd, and Pt alloyed with the metalloids S, Se, Te, As, Sb, and Bi. The structure is composed of alternating layers of metal and metalloid atoms, each layer being a h.c.p. (0001) plane. The alloys have metallic conductivity and there can be more than 50 atomic percent of the metal present; so for these reasons they are more metallic than ionic. The following examples are known:<sup>3</sup>

<sup>1</sup> W. HUME-ROTHERY, "The Structure of Metals and Alloys," Institute of Metals, London, 1936.

<sup>2</sup> Coordinates are Zn: 000;  $\frac{1}{3}, \frac{2}{3}, \frac{1}{2}$ ; and O: 00u,  $\frac{1}{3}, \frac{2}{3}, u + \frac{1}{2}$ ; where u is approximately  $\frac{2}{3}$ , *c/a* is roughly 1.63.

<sup>3</sup> W. HUME-ROTHERY, "The Structure of Metals and Alloys," Institute of Metals, London, 1936. These structures are discussed in the section on Norbury's electron-atom ratios.

## Nickel Arsenide Structure

CrS	CoTe	AuSn	MnSb
CoS	FeTe	CuSn	PdSb
FeS	NiTe	PtSn	PtSb
NiS	CrTe	NiSn	MnAs
CoSe	MnTe	CoSb	NiAs
FeSe	PdTe	FeSb	NiBi
NiSe	PtTe	NiSb	
CrSe	FeSn	CrSb	

Hume-Rothery<sup>1</sup> has shown that two generalizations are possible regarding normal valency compounds: (1) There is a general tendency for all metals to form normal valency compounds with elements of Groups IV<sub>B</sub>, V<sub>B</sub>, and VI<sub>B</sub>. (2) This tendency and the stability of the compound are greater the more electropositive the metal and the more electronegative the *B* subgroup element.

Electronegativity increases in one period in passing toward higher atomic numbers and in one group in passing upward (toward lower atomic numbers). Thus, for example, Mg<sub>2</sub>Si, Mg<sub>2</sub>Sn, and Mg<sub>2</sub>Pb are listed in what one would expect to be the order of decreasing stability, for in the electrochemical series Si is more electronegative than Sn, and the latter is more electronegative than Pb. The melting points of these normal valency compounds serve as a rough indication of stability and they bear out this principle, for they are, respectively, 1102, 780, and 553°C.

**Structurally Analogous Phases and Hume-Rothery's Rule.**—It has long been noted that equilibrium diagrams for alloys of Cu, Ag, and Au with metals of the *B* subgroups show remarkable similarities. When the structures of the intermediate phases were determined by x-rays, largely by Westgren and Phragmén in Sweden, the similarities became even more impressive.

The system Ag-Cd is typical. As indicated in the diagram, Fig. 13, any alloy containing less than about 42 atomic percent Cd is homogeneous  $\alpha$ , which is a f.c.c. phase. Near 50 atomic percent there is a  $\beta$  phase (AgCd), which has the CsCl type structure, with the Ag and Cd atoms at cube corners and centers, respectively. Throughout a homogeneity range near 60 percent, there is a complex phase,  $\gamma$ , with 52 atoms in a large unit cell. The  $\epsilon$ -phase and the  $\eta$ -phase are h.c.p.

In the Cu-Sn system a  $\beta$  phase with a structure analogous to  $\beta$ -AgCd is found at 17 atomic percent (Cu<sub>5</sub>Sn = 16.7 percent), and in Cu-Al alloys one occurs at 25 atomic percent (Cu<sub>3</sub>Al). In 1926, Hume-Rothery<sup>2</sup> pointed out that the formulas for the  $\beta$  phases fall on or near compositions giving a ratio of 3 valence electrons to 2 atoms. Thus, in AgCd, 1 elec-

<sup>1</sup> W. HUME-ROTHERY, "The Structure of Metals and Alloys," Institute of Metals, London, 1936.

<sup>2</sup> W. HUME-ROTHERY, *J. Inst. Metals*, vol. 35, pp. 295, 307, 1926.

tron is contributed by an atom of Ag and 2 by an atom of Cd, making 3 electrons for the two atoms. In  $\text{Cu}_3\text{Al}$  there are 4 atoms and 6 valence electrons (3 from the Al and 1 from each Cu atom). In  $\text{Cu}_5\text{Sn}$  there are 6 atoms and 9 valence electrons (4 from Sn, 1 from each Cu).

Thus, the key to all structurally analogous phases in these systems is electron concentration; similar structures occur at similar electron-atom ratios. The phases can well be called **electron compounds** because of

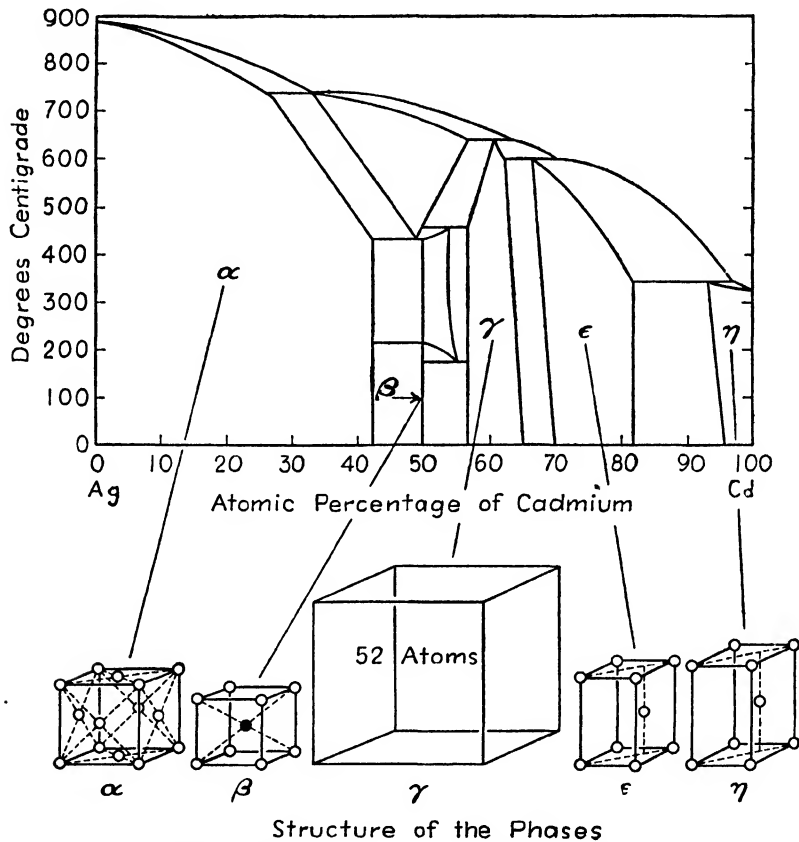


FIG. 13.—Crystal structures of the phases in the Ag-Cd system, a structurally analogous system.

this. The  $\beta$  phases occur at electron-atom ratios of 3:2,  $\gamma$  phases at 21:13, and  $\epsilon$  phases at 7:4 (also at some other ratios, as we shall see later), when the number of valence electrons is taken as the number of electrons in excess of the last completed shell, as follows:

Valence	Element
1	Cu, Ag, Au (Group I)
2	Be, Mg, Zn, Cd, Hg (Group II)
3	Ga, Al, In (Group III)
4	Si, Ge, Sn, Pb (Group IV)
5	P, As, Sb, Bi (Group V)
0	Fe, Co, Ni, Ru, Rh, Pd, Pt, Ir, Os (Group VIII)

It is found that in some systems at the electron-atom ratio of 3:2 a phase appears that is isomorphous with the complicated structure of  $\beta$ -manganese. This is a cubic crystal with 20 atoms per unit cell.<sup>1</sup>

The structures of the  $\gamma$  phases are not all identical but are strikingly similar, and all have large unit cells. The unit cell of  $\gamma$ -brass ( $\text{Cu}_5\text{Zn}_8$ ) contains 52 atoms and may be considered as made up of 27 unit cells of  $\beta$  brass (which would amount to 54 atoms) with two atoms removed and

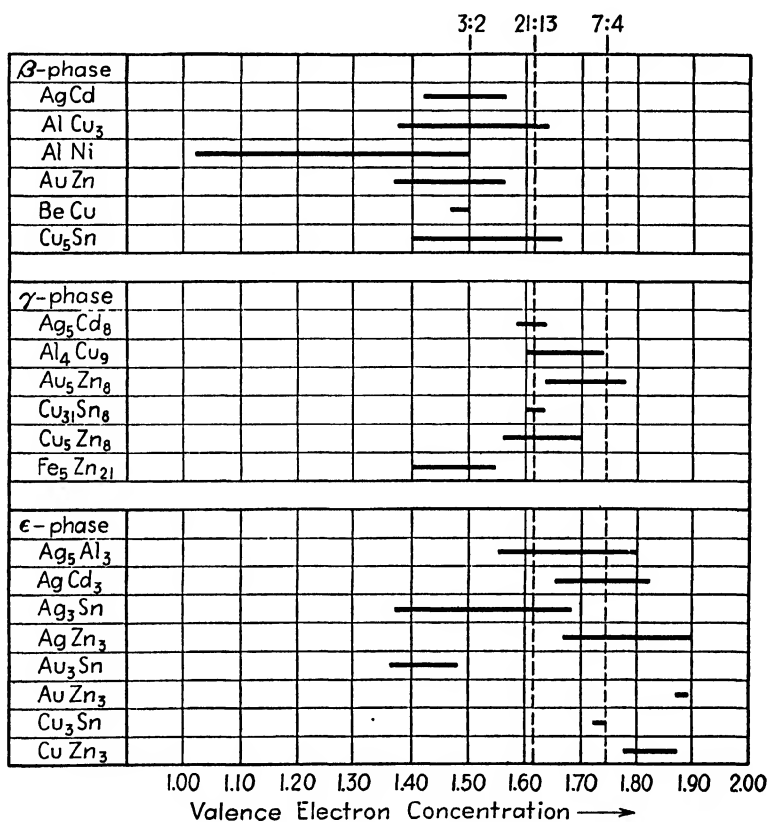


FIG. 14.—Valence electron concentrations for several typical  $\beta$ ,  $\gamma$ , and  $\epsilon$  phases, compared with Hume-Rothery's ratios.

the rest shifted somewhat in position. The phase  $\text{Cu}_5\text{Zn}_8$  has a b.c.c. space-lattice;  $\text{Cu}_9\text{Al}_4$  has a simple cubic space-lattice with 49 to 52 atoms in the unit cell;  $\text{Cu}_{31}\text{Sn}_8$  (cr  $\text{Cu}_{41}\text{Sn}_{11}$ ) has a cubic space-lattice with 416 atoms per unit cell.<sup>2</sup> The ternary alloys of Cu-Zn-Al have a  $\gamma$  structure when the electron ratio is 21:13.

Table XI lists the approximate formulas of a number of electron compounds.<sup>3</sup>

<sup>1</sup> G. D. PRESTON, *Phil. Mag.*, vol. 5, p. 1207, 1928.

<sup>2</sup> A. WESTGREN and G. PHRAGMÉN, *Z. anorg. allgem. Chem.*, vol. 175, p. 80, 1928.

<sup>3</sup> W. HUME-ROTHERY, "The Structure of Crystals," Institute of Metals, London, 1936. H. WITTE, *Metallwirtschaft*, vol. 16, p. 237, 1937.

It must be realized that these phases exist over composition ranges of varying widths (often 10 or 20 atomic percent), and the ratios 3:2, 21:13, 7:4 are not always included within the ranges. A better understanding of the actual correlation with valence-electron concentration may be had from Fig. 14, where some of these phases are plotted on an electron-concentration scale. There are many exceptions to these rules that are not shown. Wide homogeneity ranges are usually associated with a favorable size factor.

TABLE XI.—STRUCTURALLY ANALOGOUS PHASES

Electron-atom ratio 3:2		Electron-atom ratio 21:13	Electron-atom ratio 7:4
$\beta$ Structure (b.c.c.)	$\beta$ -Manganese structure (cubic, complex)	$\gamma$ -Brass structure (cubic, complex)	Structure (h.c.p.)
AgCd	Ag <sub>3</sub> Al	Ag <sub>5</sub> Cd <sub>3</sub>	AgCd <sub>3</sub>
AgMg	Au <sub>3</sub> Al	Ag <sub>5</sub> Hg <sub>3</sub>	Ag <sub>3</sub> Sn
AgZn	Cu <sub>3</sub> Si	Ag <sub>5</sub> Zn <sub>3</sub>	Ag <sub>5</sub> Al <sub>3</sub>
AuCd	CoZn <sub>3</sub>	Au <sub>5</sub> Cd <sub>3</sub>	Ag <sub>5</sub> In
AuMg		Au <sub>5</sub> Zn <sub>3</sub>	AgZn <sub>3</sub>
AuZn		Cu <sub>5</sub> Cd <sub>3</sub>	AuCd <sub>3</sub>
CuBe		Cu <sub>5</sub> Hg <sub>3</sub>	AuZn <sub>3</sub>
CuZn		Cu <sub>5</sub> Zn <sub>3</sub>	Au <sub>3</sub> Sn
Cu <sub>3</sub> Al		Cu <sub>9</sub> Al <sub>4</sub>	Au <sub>3</sub> Hg
Cu <sub>3</sub> Ga		Cu <sub>9</sub> Ga <sub>4</sub>	Au <sub>5</sub> Al <sub>3</sub>
Cu <sub>3</sub> Sn		Cu <sub>9</sub> In <sub>4</sub>	CuCd <sub>3</sub>
CoAl		Cu <sub>31</sub> Si <sub>8</sub>	CuZn <sub>3</sub>
FeAl		Cu <sub>31</sub> Sn <sub>8</sub>	Cu <sub>3</sub> Ge
NiAl		Co <sub>5</sub> Zn <sub>21</sub>	Cu <sub>3</sub> Si
		Fe <sub>5</sub> Zn <sub>21</sub>	Cu <sub>3</sub> Sn
		Ni <sub>5</sub> Zn <sub>21</sub>	FeZn <sub>7</sub>
		Pd <sub>5</sub> Zn <sub>21</sub>	
		Rh <sub>5</sub> Zn <sub>21</sub>	
		Pt <sub>5</sub> Zn <sub>21</sub>	
		Ni <sub>5</sub> Cd <sub>21</sub>	
		Na <sub>31</sub> Pb <sub>8</sub>	
		Cu <sub>7</sub> Zn <sub>4</sub> Al <sub>2</sub>	

The mean **volume per atom** in intermediate phases is nearly always less than in the pure metals. This is especially true for the  $\beta$  phases containing aluminum (FeAl, CoAl, NiAl, Cu<sub>3</sub>Al), in which the contraction may amount to as much as 15 percent<sup>1</sup> and is probably associated chiefly

<sup>1</sup> A. WESTGREN, *Z. angew. Chem.*, vol. 45, p. 33, 1932. A. WESTGREN and A. ALMIN, *Z. physik. Chem.*, vol. B5, p. 14, 1929. E. ZINTL and G. BRAUER, *Z. physik. Chem.*, vol. B20, p. 245, 1933.

with the aluminum atom. Pronounced contraction also occurs in the  $\gamma$ -phase alloys ( $\text{Cu}_9\text{Al}_4$ ,  $\text{Ni}_5\text{Cd}_{21}$ ,  $\text{Ag}_3\text{Li}_{10}$ , and  $\text{Na}_{31}\text{Pb}_8$ ).<sup>1</sup> Bernal<sup>2</sup> has pointed out that contraction increases as the structure departs more and more from the metallic, and Zintl<sup>3</sup> concluded that the Hume-Rothery electron-concentration rules should not necessarily apply when the contractions are large.

**Norbury's Electron-atom Ratios.**—Norbury has suggested<sup>4</sup> that the unit cell of each of the  $\gamma$  phases can be viewed as constructed from a set of 27 b.c.c. unit cells of fundamental ratio 3:2 by replacing two atoms

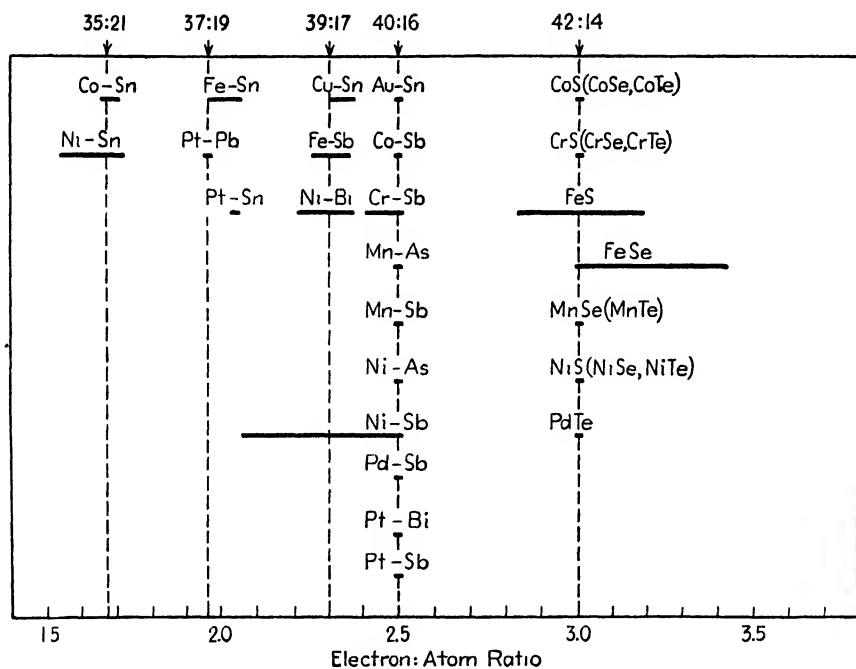


FIG. 15.—Valence electron: atom ratios of phases having a nickel arsenide structure. Norbury's ratios indicated.

of the set by two electrons. The unit cell would then contain the correct number of atoms ( $2 \times 27 - 2 = 52$ ) and would have an electron-atom ratio of 83:52 instead of Hume-Rothery's 21:13, the corresponding formula for  $\gamma$ -brass being  $\text{Cu}_{21}\text{Zn}_{31}$  instead of  $\text{Cu}_5\text{Zn}_8$ . A comprehensive investigation by thermal analysis<sup>5</sup> has, in fact, given exactly the formula  $\text{Cu}_{21}\text{Zn}_{31}$ . The  $\gamma$  structure in Cu-Cd, Cu-In, Na-Pb, Fe-Zn, and other

<sup>1</sup> CHARLES W. STILLWELL, "Crystal Chemistry," McGraw-Hill, New York, 1938.

<sup>2</sup> J. D. BERNAL, *Trans. Faraday Soc.*, vol. 25, p. 367, 1929.

<sup>3</sup> A. WESTGREN, *Z. angew. Chem.*, vol. 45, p. 33, 1932. A. WESTGREN and A. ALMIN, *Z. physik. Chem.*, vol. B5, p. 14, 1929. E. ZINTL and G. BRAUER, *Z. physik. Chem.*, vol. B20, p. 245, 1933.

<sup>4</sup> A. L. NORBURY, *J. Inst. Metals*, vol. 65, p. 355, 1939.

<sup>5</sup> R. RUER and K. KREMERS, *Z. anorg. Chem.*, vol. 184, p. 193, 1929.

systems<sup>1</sup> also agrees as well with the 83:52 ratio as with the 21:13 ratio—in some cases, better.

To account for the fact that only about half the h.c.p. phases ( $\epsilon$  type) occur at the 7:4 ratio, Norbury suggests that the electron-atom replacement principle holds here also. Taking 14:8 (= 7:4) as the basic ratio, he obtains 13:9 by replacing one electron by an atom and 15:7 by the reverse process. The three concentrations 14:8, 13:9, and 15:7 together account quite well for the known phases, particularly the invariant phases in the systems Ag-Hg, Ag-As, Cu-Si, Cu-Ge, and Cu-Sn.

Carrying the electron-atom replacement over to the hexagonal nickel arsenide structures (*cf.* page 210), Norbury suggests that the basic lattice forms at an electron-atom ratio 5:2, as it does in Au-Sn, Co-Sb, Cr-Sb, Ni-Sb, and Pd-Sb alloys. If this ratio is written 40:16 and modified by atom-electron replacement to the subsidiary ratios 39:17, 37:19, 35:21 and 42:14, it will be found to account satisfactorily for these structures. Figure 15 summarizes observed and theoretical ratios. The ratios may give either the actual number of atoms in the cell or a simple fraction of that number. The validity of these rather arbitrary assumptions will doubtless remain uncertain until quantum mechanical calculations have been made.

**Interstitial Compounds.**—The transition metals alloy with H, B, C, and N to produce compounds that are metallic, have high melting points, and are extremely hard. Dispersed in steel they harden it, or cemented together they form high-speed long-life cutting tools.

Gunnar Hägg has been largely responsible for systematizing these structures, appropriately called interstitial compounds.<sup>2</sup> He has shown that they may be classified according to the relative sizes of the transition metal and metalloid atoms, *i.e.*, the radius ratio  $R_X/R_M$ , where  $R_X$  is the radius of the small nonmetallic atom H, B, C, or N and  $R_M$  is the atomic radius of the transition metal. When  $R_X/R_M$  is less than 0.59, the structures are simple; when the ratio is more than 0.59, they are complex.

1. When the radius ratio is under 0.59, the metal atoms are nearly always on a lattice that is f.c.c., h.c.p., or in a few instances b.c.c.; occasionally, they are on a lattice that is a slightly distorted form of one of these. The small metalloid atoms are located interstitially, as in interstitial terminal solid solutions. Nitrides, carbides, and hydrides with the formula  $MX$  are generally cubic with the metal atoms at f.c.c. positions and with the metalloids at interstitial positions in a structure of the NaCl type or the zinc blende type (positions indicated by open

<sup>1</sup> H. WITTE, *Metallwirtschaft*, vol. 16, p. 237, 1937.

<sup>2</sup> G. HÄGG, *Z. physik. Chem.*, vol. B12, p. 33, 1931; vol. B11, p. 433, 1930. A. WESTGREN, *J. Franklin Inst.*, vol. 212, p. 577, 1931.



circles in Fig. 11). Examples are the nitrides ZrN, ScN, TiN, VN, CrN; the carbides ZrC, TiC, TaC, VC; and the hydrides ZrH and TiH. An exception is TaH, which is based on a b.c.c. lattice. ✓

The compounds  $M_2X$  generally have the metal atoms arranged in hexagonal close packing ( $Fe_2N$ ,  $Cr_2N$ ,  $Mn_2N$ ;  $W_2C$ ,  $Mo_2C$ ,  $Ta_2C$ ;  $Zr_2H$ ,  $Ta_2H$ ,  $Ti_2H$ ), but sometimes they are cubic ( $Pd_2H$ ,  $W_2N$ ,  $Mo_2N$ ).

In the system Ti-H the compound TiH has the zinc blende structure, and  $TiH_2$  has the fluorite ( $CaF_2$ ) structure; the difference between these is merely that half the interstices are filled in the former, and all are filled in the latter (see Fig. 12). To be sure, the position of the H atoms cannot be detected with certainty by x-rays, but the probable positions can be inferred from the radius of the H atom and the dimensions of the holes into which it might fit. The H atoms probably go into the largest interstices in TaH and the next largest in  $Ti_2H$ , TiH,  $TiH_2$ ,  $Zr_2H$ , and  $Ta_2H$ .

2. Large radius ratios ( $R_X/R_M > 0.59$ ) nearly always go with complex crystal structures. In this class are the carbides of Cr, Mn, Fe, Co, and Ni ( $R_X/R_M = 0.60 - 0.61$ ) and the borides of Fe and N.

In dicarbides the  $C_2$  groups may enter as parallel units into interstices of the metal lattice instead of entering as individual atoms.<sup>1</sup> This results in tetragonal rather than cubic cells for the isomorphous phases  $CaC_2$ ,  $SrC_2$ ,  $BaC_2$ ,  $LaC_2$ ,  $CeC_2$ ,  $PrC_2$ , and  $NdC_2$ .

**Phases Containing Alkali and Alkaline-earth Elements.**—Zintl and his collaborators<sup>2</sup> have surveyed a large number of systems of the alkali and alkaline-earth elements for examples of  $\beta$  phases at 50 atomic percent composition. Because the CsCl structure of the  $\beta$  phases is stable only when the radius ratio is greater than 0.73, the investigations were confined to examples in this range. A caesium chloride structure occurs in many systems: LiAg, LiTl, LiHg, LiZn, LiCd, LiGa, LiIn; MgTl, CaTl, SrTl; NaIn, NaBi. In others a structure occurs (NaTl type) that consists of two interpenetrating diamond lattices each containing atoms of a single element, one lattice being displaced half of a body diagonal with respect to the other; atomic radii are nearly equal in this structure. Examples are known as follows: LiZn, LiCd, LiGa, LiIn; NaSn, NaTl.

From a study of atomic radii in these compounds it was found that there is nearly always a contraction which seems to be the result of polarization of the large alkali atoms by neighboring small atoms. Thus the greater the contraction, the more the interatomic bonds differ from the truly metallic. There are many exceptions to Hume-Rothery's rule in these compounds, particularly in phases where contraction is large, presumably because of their nonmetallic character.

<sup>1</sup> M. VON STACKELBERG, *Z. physik. Chem.*, vol. B9, p. 437, 1930.

<sup>2</sup> E. ZINTL and B. BRAUER, *Z. physik. Chem.*, vol. B20, p. 245, 1933.

Another set of analogous phases has the formula  $AX_3$ . The  $A$  atoms are at the corners of a cubic lattice, the  $X$  at face centers. Examples are  $\text{NaPb}_3$ ,  $\text{CaPb}_3$ ,  $\text{SrPb}_3$ ,  $\text{CePb}_3$ ,  $\text{CaTl}_3$ ,  $\text{CaSn}_3$ ,  $\text{CeSn}_3$ ,  $\text{LaSn}_3$ ,  $\text{LaPb}_3$ ,

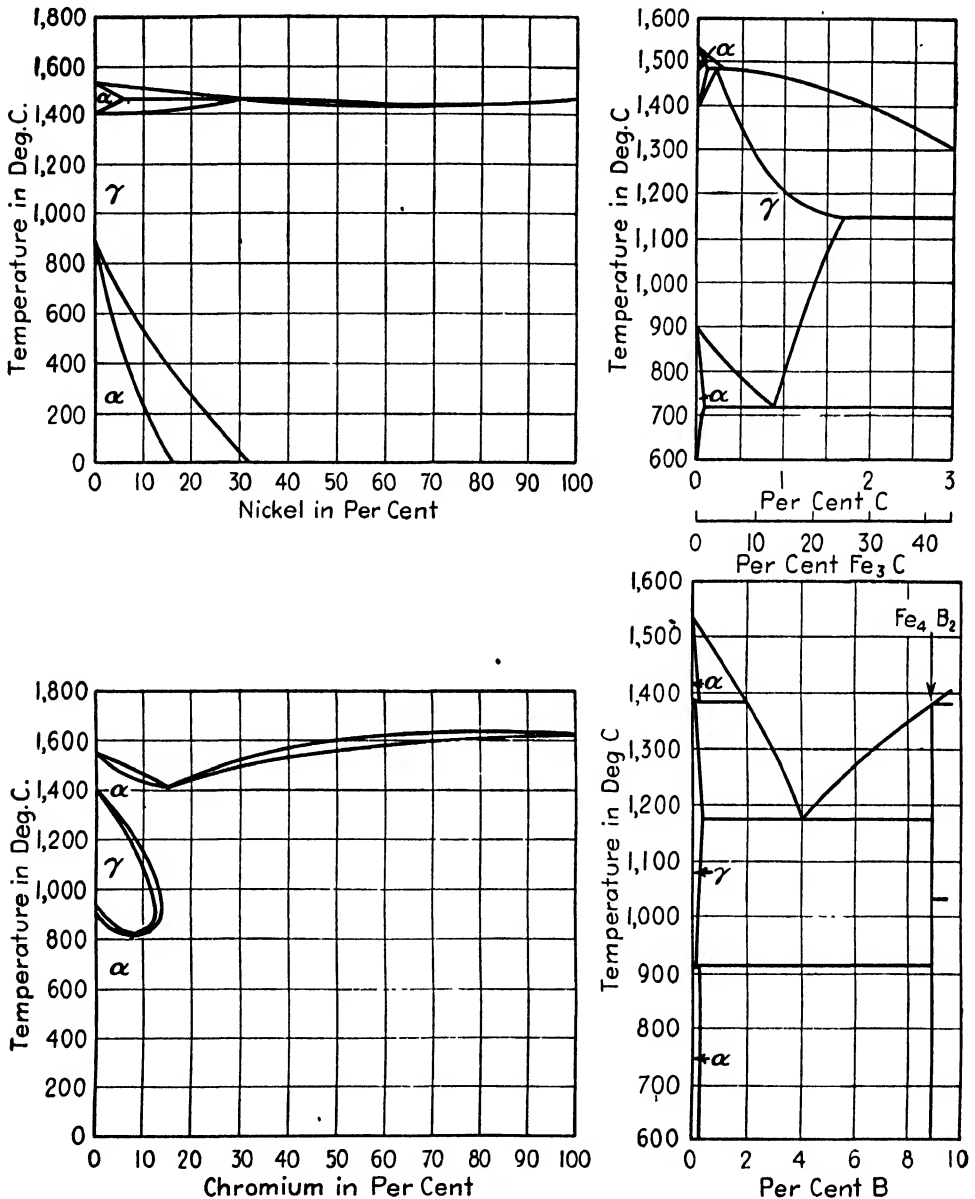


FIG. 16.—Classification of binary iron alloys as to extent of the gamma field.

$\text{PrSn}_3$ , and  $\text{PrPb}_3$ . This structure requires the ratio  $R_A/R_X$  in the range 1.0 to 2.4, as shown by Goldschmidt, and actually all the known phases do lie in this range.

**Periodic Relations in Iron Alloys.**<sup>1</sup>—Wever<sup>2</sup> has pointed out a close correlation between the position of an element in the periodic table and its effect on the range of the  $\gamma$  phase when alloyed with iron. The iron alloys may be grouped into four classes exemplified by Fig. 16, with (1) an open  $\gamma$  field as in Fe-Ni, (2) a closed  $\gamma$  field as in Fe-Cr, (3) an expanded field (Fe-C), and (4) a narrowed field (Fe-B). When these types are compared with the positions of the alloying elements in the periodic table, as in Fig. 17, the regularities are very striking. Group VIII metals open the  $\gamma$  field; the alkali and alkaline-earth metals (Groups I and II)

	a I b		a II b		a III b		a IV b		a V b		a VI b		a VII b		a VIII b		b
I													1H				2He
II	3Li ▲		4Be ●		5B ○		6C □		7N □		8O		9F				10Ne
III	11Na ▲		12Mg ▲		13Al ●		14Si ●		15P ●		16S ○		17Cl				18Ar
IV	19K ▲		20Ca ▲		21Sc		22Ti ●		23V ●		24Cr ●		25Mn ■		26Fe ■	27Co ■	28Ni ■
		29Cu □		30Zn □		31Ga		32Ge ●		33As ●		34Se		35Br			36Kr
V	37Rb ▲		38Sr ▲		39Yt		40Zr ○		41Nb ●		42Mo ●		43Tc		44Ru ■	45Rh ■	46Pd ■
		47Ag ▲		48Cd ▲		49In		50Sn ●		51Sb ●		52Te		53I			54Xe
VI	55Cs ▲		56Ba ▲		58Ce ○		72Hf		73Ta ●		74W ●		75Re		76Os ■	77Ir ■	78Pt ■
		79Au □		80Hg ▲		81Tl ▲		82Pb ▲		83Bi ▲		84Po		85At			86Rn
VII	87Fr ▲		88Ra ▲		89Ac		90Th		91Pa		92U						

■ Open  $\gamma$ -field      □ Expanded  $\gamma$ -field      ▲ Insoluble  
● Closed  $\gamma$ -field      ○ Contracted  $\gamma$ -field

FIG. 17.—Periodic table showing behavior of elements in binary iron alloys.

are insoluble; while most of the intermediate metals produce closed  $\gamma$  fields.

When these types are plotted on a curve of atomic radii (Fig. 18), it is apparent that atomic size correlates with this behavior, for all the larger atoms in each period are insoluble and the smallest produce open fields. But it is equally apparent that a complete systematization is not possible on the basis of size alone. Crystal structure or electron configuration may also be determinative factors.

**Imperfections in Crystals.**—Countless experiments have shown that crystals contain many flaws and irregularities, a detailed knowledge of which is much to be desired because of their effect on the physical

<sup>1</sup> The structures in Fe-C alloys are covered in Chap. XXII.

<sup>2</sup> F. WEVER, "Ergebnisse der technische Röntgenkunde," vol. II, p. 240, Akademische Verlagsgesellschaft m.b.H., Leipzig, 1931; *Proc. World Eng. Cong., Tokyo*, vol. 34, p. 239, 1931.

properties. For extensive bibliographies the reader is referred to the various reviews and symposia.<sup>1</sup>

A study of their x-ray-reflecting power led Darwin to conclude that actual crystals diffract as if they are composed of small blocks  $10^{-4}$  to  $10^{-6}$  cm. on an edge, each block being a perfect crystal but neighboring blocks being tilted out of registry.<sup>2</sup> The widths of reflected x-ray beams

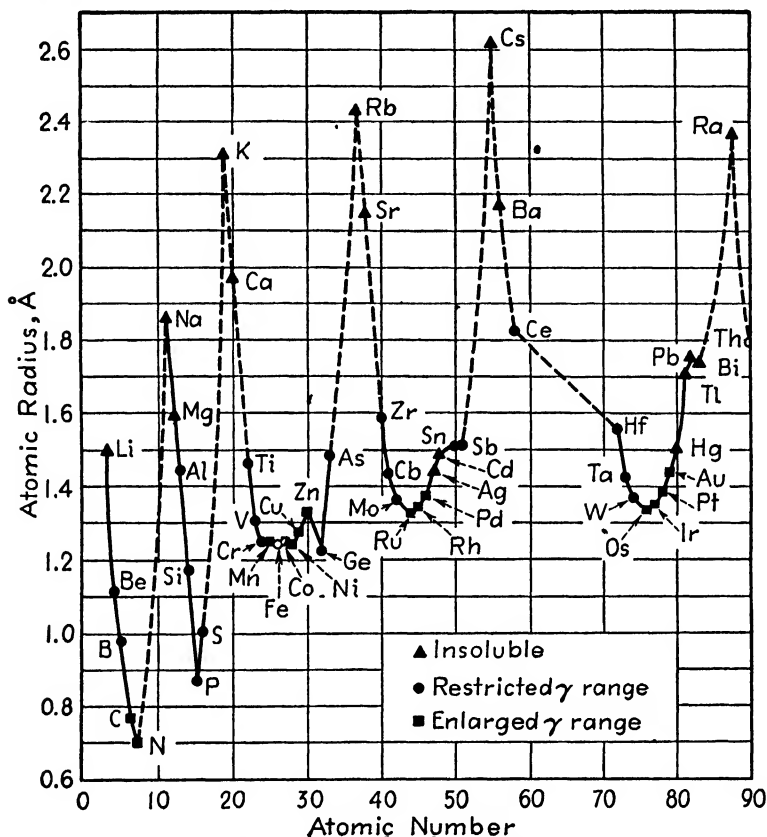


FIG. 18.—Relation of atomic radius to behavior of elements in binary iron alloys. (Wever.)

from single crystals give concrete evidence for imperfection.<sup>3</sup> An ideal crystal produces a diffracted line 3 to 6 sec. of arc in width; selected

<sup>1</sup> "International Conference on Physics, vol. II, The Solid State of Matter," Physical Society, London, 1935. *Z. Krist.*, Vol. 89, 1934, Sonderheft: "Ideal- und Realkristall." W. HUME-ROTHERY, "The Structure of Metals and Alloys," Institute of Metals, London, 1936. C. A. ZAPFFE and C. E. SIMS, *Trans. A.I.M.E.*, vol. 145, p. 225, 1941. Internal Strains in Solids, *Proc. Phys. Soc. (London)*, vol. 52, p. 1, 1940.

<sup>2</sup> C. G. DARWIN, *Phil. Mag.*, vol. 27, pp. 315, 675, 1914; vol. 43, p. 800, 1922.

<sup>3</sup> "International Conference on Physics, vol. II, The Solid State of Matter," Physical Society, London, 1935. *Z. Krist.*, vol. 89, 1934, Sonderheft: "Ideal- und Realkristall." A. H. COMPTON and S. K. ALLISON, "X-rays in Theory and Experiment," D. Van Nostrand, New York, 1935. R. M. BOZORTH and F. E. HAWORTH, *Phys. Rev.*, vol. 45, p. 821, 1934.

samples of diamond, calcite, quartz, and rochelle salt give reflections of this type.

Most crystals, however, give diffracted lines several hundred seconds in width. Metals appear to be particularly imperfect, as indicated by the following measurements of widths by Bozorth and Haworth,<sup>1</sup> (measured at half maximum intensity) W, 360 sec.; Fe, 840 sec.; Ni, 1500 sec.; Al, 1500 sec. The degree of imperfection is governed largely by conditions existing during growth, and it varies widely in different samples of a given crystal.

Griffith<sup>2</sup> found that freshly prepared glass fibers, free from cracks, had tensile strengths of a million pounds per square inch, greatly exceeding the normal value. Experiments on rock salt and mica<sup>3</sup> also confirmed the weakening effect of surface cracks. Extending this view, Smekal<sup>3</sup> postulated that solid metals are weakened by internal cracks and flaws, some arising during growth and others during subsequent handling.

Buerger<sup>4</sup> and Davey<sup>5</sup> have emphasized the effect of dendritic and branching growth from a nucleus in developing imperfections. As errors in alignment tend to be cumulative during the growth of a dendritic arm or branch, the resulting structure may resemble a columnar grain structure and has been called a *lineage structure* by Buerger. The nature of lineage imperfection is illustrated in Fig. 19, in which the growth from a central nucleus and the flaws at the lineage boundaries are exaggerated.

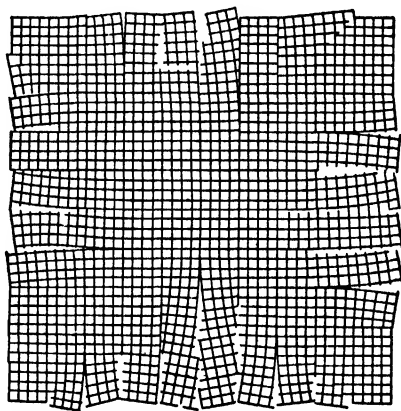


FIG. 19.—Sketch illustrating lineage structure. (Buerger.)

The freezing of drops of liquid that are entirely enclosed by dendrite arms is certainly a fruitful source of imperfection, as are also segregation and coring in the freezing of an alloy. Not infrequently the imperfection is so great that Laue spots are badly distorted, and the solid is better described as a polycrystalline aggregate with a preferred orientation than as a single crystal.

Many studies of crystalline imperfection have attempted to show that crystals are composed of a mosaic of uniformly sized blocks  $10^{-4}$  or

<sup>1</sup> R. M. BOZORTH and F. E. HAWORTH, *Phys. Rev.*, vol. 45, p. 821, 1934.

<sup>2</sup> A. A. GRIFFITH, *Trans. Roy. Soc. (London)*, vol. A221, p. 180, 1921.

<sup>3</sup> "International Conference on Physics, vol. II, The Solid State of Matter," Physical Society, London, 1935.

<sup>4</sup> M. J. BUERGER, *Z. Krist.*, vol. 89, pp. 195, 242, 1934.

<sup>5</sup> W. P. DAVEY, *Trans. A.S.S.T.*, vol. 21, p. 965, 1933.

$10^{-5}$  cm. on an edge. Goetz pointed out<sup>1</sup> that etch pits on the cleavage surfaces of bismuth appear to have certain regularities in size and spacing. However, Buerger<sup>2</sup> is confident that these regularities are illusory. A similar observation on regularities in Widmanstätten figures<sup>3</sup> likewise has been strongly objected to.<sup>4</sup> The semiregularity in the spacing of slip lines, while much discussed in this connection, may be a reflection of microscopic segregation during growth or a result of local stresses around the slipped surfaces and is inconclusive evidence for a regular mosaic. Much of the reasoning from microstructural observations overlooks the fact that one set of planes, say (100), is supposed to bound the blocks of the mosaic while a set of planes with entirely different indices causes the markings. The magnetic domains that become visible when magnetic powders are allowed to settle on surfaces of magnetic crystals<sup>5</sup> are intensely interesting but involve laws of interaction of elementary magnets upon one another, which scarcely can be analogous to the laws of group phenomena among nonmagnetic atoms. Why, then, should it be argued<sup>6</sup> that the scale of magnitude of magnetic powder patterns and their regularity implies imperfections of the same scale and regularity in all crystals? Recent studies of the shape of the magnetic domains indicate that they are far from the equiaxed shape that is generally assumed for blocks in a mosaic crystal. The segregation of polonium in bismuth crystals takes place on (111) planes  $0.54 \times 10^{-4}$  cm. apart.<sup>7</sup> The stratifications obtained by Straumanis<sup>8</sup> in crystals of zinc and cadmium, which have spacings of  $0.8 \times 10^{-4}$  cm., appear to be responsible for regularities in etching characteristics and in slip lines.

Theoretical understanding of the subject has been hindered by incorrect calculations, lack of carefully planned and executed experiments, biased conclusions, and inconsequential debate—in short, all that which scientists have learned must be avoided if science is to progress without painful detours. Attempts by Zwicky<sup>9</sup> to prove that a regular secondary

<sup>1</sup> A. GOETZ, *Proc. Nat. Acad. Sci.*, vol. 16, p. 99, 1930.

<sup>2</sup> M. J. BUEGER, *Z. Krist.*, vol. 89, p. 195, 242, 1934.

<sup>3</sup> W. P. DAVEY, *Trans. A.S.S.T.*, vol. 21, p. 965, 1933.

<sup>4</sup> R. F. MEHL, *Trans. A.S.S.T.*, vol. 21, p. 998, 1933.

<sup>5</sup> F. BITTER, *Phys. Rev.*, vol. 38, p. 1903, 1931; vol. 41, p. 507, 1932. W. C. ELMORE and L. W. MCKEEHAN, *Trans. A.I.M.E.*, vol. 120, p. 236, 1936. W. C. ELMORE, *Phys. Rev.*, vol. 56, p. 210, 1939.

<sup>6</sup> C. A. ZAPFFE and C. E. SIMS, *Trans. A.I.M.E.*, vol. 145, p. 225, 1941. N. P. GOSS, *Trans. A.I.M.E.*, vol. 145, p. 265, 1941.

<sup>7</sup> A. B. FOCKE, *Phys. Rev.*, vol. 45, p. 219, 1934; vol. 46, p. 623, 1934.

<sup>8</sup> M. STRAUMANIS, *Z. physik. Chem.*, vol. B13, p. 316, 1931.

<sup>9</sup> For bibliography, see M. J. BUEGER, *Z. Krist.*, vol. 89, pp. 195, 242, 1934. "International Conference on Physics, vol. II, The Solid State of Matter," Physical Society, London, 1935.

structure is a more stable structure than an ideally perfect crystal structure have not been successful, and most investigators believe that a perfect crystal is in the lowest energy state.

It appears likely that the electron microscope will soon do much to clarify these matters. The detail that is brought out on the surface of a metal by etching is remarkable. Figure 20 is an electron-microscope photograph of the etched surface of annealed high-purity copper. The dark lines are depressions in the surface, where the acid has attacked more rapidly. Pictures of this type from grains of various orientations have led the author to the following conclusions, which must be regarded

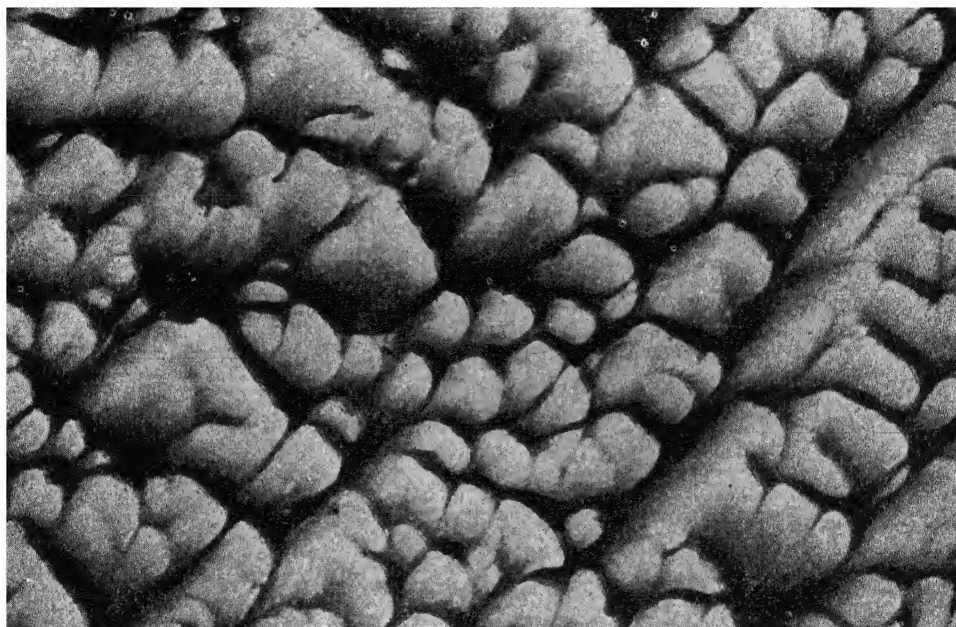


FIG. 20.—Portion of a grain of annealed high purity copper, etched with ferric chloride reagent,  $\times 20,000$  (1 mm. = 500A; 20 mm. = 1 micron). A transmission electron-microscope photograph of a replica of the surface prepared by the method of R. D. Heidenreich and V. G. Peck, *J. App. Phys.*, vol. 14, p. 23, 1943.

as tentative until further research is completed: the areas outlined by the etchant appear to be rod-shaped, a few tenths of a micron in diameter and several microns in length. In Fig. 20 the cross sections of these rods are seen; the rods extend upward and to the right. It is possible that these are mosaic blocks that are tilted slightly with respect to each other and separated by boundaries that etch more rapidly than the blocks. No evidence for a regular spacing of mosaic blocks can be found, but the average dimension of the etched blocks is about what has been expected from the researches mentioned above. Similar structures are being found in certain other metals and in alloys.

## THE STRUCTURE OF LIQUID METALS

The structure of the liquid state is intermediate between the structures of the solid and gaseous states. In a crystalline solid there is an arrangement of atoms that repeats itself identically at regular intervals in three dimensions. In gases, on the other hand, the arrangement of atoms is completely chaotic. X-ray diffraction has shown that the arrangement of atoms in a liquid is neither so random as in gases nor so regular as in crystals; there is a definite preference for certain interatomic distances, and this statistical distribution causes characteristic diffraction effects. There are no atoms closer than a certain minimum distance from any other atom, but at this minimum distance there are, on the average, several atoms. In the language of the crystallographer, there is coordination in the liquid. The structure has been described as somewhat analogous to the arrangement of ball bearings in a box continuously shaken. At any instant, a number of balls will be in contact with any given ball, or nearly in contact with it, and this ever-changing group will prevent others from forming a group at slightly greater distances. There is, however, no regularly repeating structure, close-packed or otherwise, as there is in crystals.

**Earlier Methods of Analysis.**—The diffraction pattern from a liquid consists of a few diffuse bands—seldom more than two—and at first sight appears to offer a discouragingly small amount of information from which to deduce the “structure” of the liquid. The first attempts to analyze patterns of this sort consisted simply in applying Bragg’s law to the diffraction angles of the maximum intensity in the bands. It was later recognized that since there is no regularly repeating lattice in the liquid the ordinary Bragg’s law cannot apply directly, and a corrected form must be used:  $\lambda = 2(0.815r) \sin \theta$ , where  $r$  is the distance between the centers of two atoms adjacent to each other in the liquid and  $\theta$  is half the angle of deviation of the beam.<sup>1</sup>

**The Radial-distribution Method.**—In recent years it has become recognized that if the analysis of liquid structure is to be put on a rigorous basis the experimenter must use *all* the information in the diffraction pattern, not merely the position of the one or two peaks. Fortunately, there is now available a method for doing this. The method was suggested by Zernike and Prins<sup>2</sup> and was first successfully used in a study

<sup>1</sup> This is Ehrenfest’s formula. A discussion of it will be found in A. H. Compton and S. K. Allison, “X-rays in Theory and Experiment,” p. 172, Van Nostrand, New York, 1935. In comparing the work of different laboratories it is necessary and sometimes difficult to determine whether they used the ordinary Bragg’s law or the Ehrenfest formula.

<sup>2</sup> F. ZERNIKE and J. A. PRINS, *Z. Physik*, vol. 41, p. 184, 1927.



of liquid mercury by Debye and Menke.<sup>1</sup> In this method a monochromatic beam of x-rays is diffracted from a small capillary tube or from a stream of the liquid, and the intensity diffracted at different angles is measured by an ionization chamber or by a microphotometer record of a photographic film. The measured intensities are corrected for absorption in the sample, for polarization in the beam, and for the presence of incoherent radiation and are placed on an absolute-intensity scale so that the intensity is known relative to the intensity of scattering of a single electron. The curve is then analyzed by a Fourier method, yielding a curve that gives the average number of atoms between  $r$  and  $r + dr$  from any atom in the liquid.<sup>2</sup>

The formulas for analyzing liquids with a single kind of atom are derived from the **Debye equation**<sup>3</sup>

$$I = Nf^2 \sum_n \frac{\sin sr_n}{sr_n}$$

where  $I$  is the intensity of the coherent scattered radiation,  $s = 4\pi(\sin \theta)/\lambda$ ,  $\theta$  is half the angle of scattering,  $\lambda$  is the wavelength,  $f$  is the structure factor,  $r$  is the separation between the  $n$ th pair of atoms in the liquid, and  $N$  is the effective number of atoms in the sample. The sum is taken over all pairings of atoms (*i.e.*, for a group of three atoms there would be three pairings of atoms to compute). The formula supposes that on the average the surroundings of all atoms are identical and are oriented at random in space. By introducing a radial distribution function such that  $4\pi r^2\rho(r)$  is the number of atoms between  $r$  and  $r + dr$  from any atom, the equation leads by the use of the Fourier integral theorem to the **Zernike-Prins formula** for a monatomic liquid:

$$4\pi r^2\rho(r) = 4\pi r^2\rho_0 + \frac{2r}{\pi} \int_0^\infty s \left( \frac{I}{Nf^2} - 1 \right) \sin rs \, ds$$

<sup>1</sup> P. DEBYE and H. MENKE, *Physik. Z.*, vol. 31, p. 797, 1930.

<sup>2</sup> The beam should be monochromatized by reflection from a crystal. If the monochromator is set at the Bragg angle  $\theta_c$  and the beam is diffracted by the liquid through an angle of deviation  $2\theta_1$ , the polarization factor is  $\frac{1}{2}(1 + \cos^2 \theta_c \cos^2 \theta_1)$ , which for molybdenum radiation reflected from rock salt reduces to very nearly the same polarization factor ordinarily used in crystal-structure analysis. Curves are available giving the values for all the elements and giving also the amount of incoherent scattering that will be obtained at various angles. The corrected intensity curve is made to fit the sum of the coherent ( $f^2$ ) and incoherent curves at high  $\theta$  values by multiplying the corrected intensities by a suitable factor, and when this is accomplished the corrected intensities have been reduced to absolute units; *i.e.*, the intensities are then known in terms of the scattering from a single electron, since the atoms can be assumed to scatter independently at large angles.

<sup>3</sup> P. DEBYE, *Ann. Physik*, vol. 46, p. 809, 1915.

where  $s = 4\pi(\sin \theta)/\lambda$ ,  $\rho_0$  is the average density of the liquid in atoms per unit volume, and  $I/N$  is the coherent scattered intensity in electron units.

The quantity  $s[(I/Nf^2) - 1]$  is taken from the corrected intensity curve obtained experimentally, and the integration involved in the equation is carried out graphically or by the use of a harmonic analyzer for a number of different values of  $r$ . An example of the type of radial-distribution curve derived in this way is shown in Fig. 21, which was obtained for liquid sodium at 103°C. by Tarasov and Warren<sup>1</sup> and confirmed by Trimble and Gingrich.<sup>2</sup>

The density at any distance,  $r$ , from an atom is plotted as ordinate against  $r$  as abscissa in curve (a), which may be compared with curve

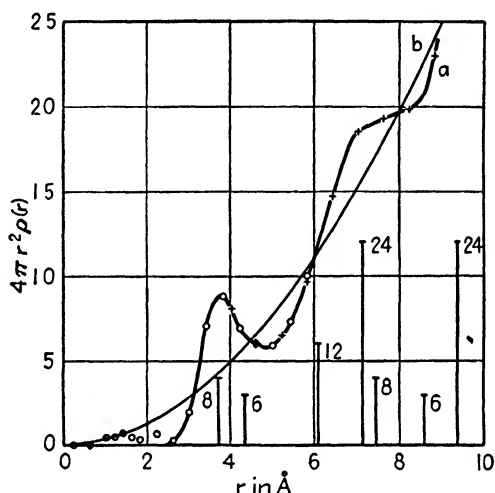


FIG. 21.—Structure of liquid sodium. (a) Radial distribution of atoms,  $4\pi r^2 \rho(r)$ . (b) Curve for radial distribution  $4\pi r^2 \rho_{av}$ , if density were constant. (c) Distribution of neighbors in crystalline sodium. The numbers of atoms at the various distances are indicated by the numbers.

(b), the curve for the radial distribution if the density were constant, and with the distribution of atoms in crystalline sodium, plotted as vertical lines in the lower portion of the diagram. The distance from  $r = 0$  to the position of the first peak in curve (a) represents the most probable distance to nearest neighbors. The area under the curve between any value  $r$  and  $r + dr$  gives the average atomic population between the distances  $r$  and  $r + dr$  from any atom in the liquid. The deviations from the uniform-density curve (b) show that there is a definite tendency for close-packing arrangements in the liquid, with a concentration at 3.73 Å comparable with the distance 3.72 Å for nearest atoms in the solid (at room temperature). A similar curve for sodium at 400°C. has less pronounced peaks and indicates that the close-packed

<sup>1</sup> L. TARASOV and B. WARREN, *J. Chem. Phys.*, vol. 4, p. 236, 1936.

<sup>2</sup> F. H. TRIMBLE and N. S. GINGRICH, *Phys. Rev.*, vol. 53, p. 278, 1938.

arrangements become less marked as the temperature is increased. The structure thus approaches somewhat nearer the randomness characteristic of a gas, as a result of the more violent thermal motions.

**Liquid Metals.**—A number of studies on liquid metals have been made in addition to those on sodium summarized in the preceding paragraph.<sup>1</sup> The **close-packed metals** as well as the less closely packed **b.c.c. metals** melt to form liquids in which the close-packed distances are prominent. The structure has been described as the set of distances present in the crystal "blurred" by the violent kinetic motions of the liquid atoms (a concept embodied in the equations by Prins and Petersen),<sup>2</sup> but statements of this kind frequently have been made without consideration of other kinds of atom distribution that might be equally capable of explaining the patterns.

The results for **tin** and **bismuth**, metals which do not possess close-packed structures in the solid state, would be particularly interesting if different experimenters had agreed in their findings. At present it seems uncertain whether the liquids are best considered as "close-packed" like the liquids of b.c.c. metals or, on the other hand, as blurred derivatives of their solid crystal structures, or whether some other type of "complex" exists in the liquid. The difficulty in drawing conclusions from the literature on this subject is that none of the experimenters on the European continent used the careful technique that is necessary for a rigorous investigation, *viz.*, Fourier analysis and crystal monochromatized x-rays. Radiation direct from the x-ray tube or even filtered radiation gives untrustworthy patterns because of the large amount of white radiation present. Also, analysis by Bragg's law or the Prins-Petersen formula leads to incomplete and uncertain conclusions.

**Mercury** has been assigned to the close-packed type of liquids, with a predominant spacing of  $3.2\text{\AA}$ ,\* but this metal is extremely difficult to work with because of the high absorption correction needed. Furthermore, oxide films are likely to form and cause diffraction, and the fluorescent radiation that is emitted by the sample tends to obscure the diffraction pattern. There apparently has been no determination using the best technique. The same can be said of liquid **gallium**, which present results seem to indicate is not a close-packed liquid.<sup>3</sup>

<sup>1</sup> For reviews, see J. T. RANDALL, "The Diffraction of X-rays by Amorphous Solids, Liquids, and Gases," Chap. V, Wiley, New York, 1934; A. LATIN, *J. Inst. Metals*, vol. 66, p. 177, 1940.

<sup>2</sup> J. A. PRINS and H. PETERSEN, *Physica*, vol. 3, p. 147, 1936.

\* H. MENKE, *Physik. Z.*, vol. 33, p. 593, 1932. F. SAUERWALD and W. TESKE, *Z. anorg. Chem.*, vol. 210, p. 247, 1933. O. KRATKY, *Physik. Z.*, vol. 34, p. 482, 1933. J. A. PRINS, *Trans. Faraday Soc.*, vol. 33, p. 110, 1937.

<sup>3</sup> P. DEBYE and H. MENKE, *Physik. Z.*, vol. 31, p. 797, 1930. F. SAUERWALD and W. TESKE, *Z. anorg. Chem.*, vol. 210, p. 247, 1933.

**Liquid Alloys.**—Liquid hydrocarbons when completely miscible give patterns different from the patterns of either constituent. The principal peak is at a position intermediate between the peaks for the constituents; thus the situation is analogous to that in solid solutions. On the other hand, immiscible hydrocarbons give patterns in which the two individual patterns are superimposed.<sup>1</sup> Similar principles might be expected to govern miscible and immiscible alloys.

There have been no rigorous analyses of liquid alloys. Eutectic alloys of **Bi-Sn**, **Sn-Pb**, **Pb-Bi**, and **Sn-Zn** have been photographed with unfiltered radiation by Danilov and Radtchenko,<sup>2</sup> and each photograph showed a band whose peak was intermediate between the peaks for each of the constituent metals of the eutectic. From the fact that the intensity curve for the eutectic was like an average of the curves for the two pure components they concluded that the melt consisted of small separate regions of the pure metals—that the structure of the eutectic is “fore-shadowed” in the liquid state. Few will agree that the data warrant such conclusions, and the work is reviewed here as an example of a problem requiring more than a superficial treatment to distinguish among several possible explanations. The same can be said of some studies of liquid alloys of the composition  $\text{Na}_2\text{K}$ ,\*  $\text{Hg}_5\text{Tl}_2$ , and  $\text{KHg}_2$ .† Investigators concluded that the compounds of these compositions existing in the solid state persist to some degree in the liquid state. This concept has been used in much of the work of G. W. Stewart<sup>3</sup> on liquid hydrocarbons and has been given the name “cybotaxis” by him. Certain special types of aggregations in liquids (“mesomorphic states”) such as the “smectic” and “nematic” have been discussed in connection with long-chain compounds<sup>4</sup> but do not occur in metals and alloys. Here again, as Warren has emphasized,<sup>5</sup> a critical attitude toward the data is more fruitful (and, of course, more scientific) than loose speculation. One may well ask several questions in such experiments. Is the liquid a single homogeneous phase? Is the liquid homogeneous, or do residual nuclei remain from the incompletely melted solid? Are the coordination number and spacings approximately the same as in the solid,

<sup>1</sup> A summary of this work will be found in J. T. Randall, “The Diffraction of X-rays by Amorphous Solids, Liquids, and Gases,” Wiley, New York, 1934, and G. W. Stewart, *Phys. Rev.*, vol. 35, p. 726, 1930.

<sup>2</sup> V. J. DANILOV and I. V. RADTCHENKO, *Physik. Z. Sowjetunion*, vol. 12, p. 756, 1937.

\* K. BANERJEE, *Indian J. Phys.*, vol. 3, p. 399, 1929.

† F. SAUERWALD and W. TESKE, *Z. anorg. Chem.*, vol. 210, p. 247, 1933.

<sup>3</sup> G. W. STEWART, *Rev. Modern Phys.*, vol. 2, p. 116, 1930.

<sup>4</sup> Symposium on Structure and Intermolecular Forces in Liquids and Solutions, *Trans. Faraday Soc.*, vol. 33, p. 1, 1937. GEORGE L. CLARK, “Applied X-rays,” 3d ed., Chap. XX, McGraw-Hill, New York, 1940.

<sup>5</sup> B. E. WARREN, *J. Applied Phys.*, vol. 8, p. 645, 1937.

or are they characteristic of a different sort of complex tending to form only in the liquid and not properly described as nuclei of the solid? In short, precisely what are the differences between solid and liquid?

When the density of a liquid differs but little from the density of the corresponding solid, it follows that there can be no marked change in coordination or spacing of nearest neighbors, and so density measurements are nearly as revealing as all but the best x-ray measurements. Nevertheless, careful x-ray work can yield distribution curves that serve as useful bases for theoretical calculations. Entropy, heat of fusion, and heat of vaporization are quantities which have been calculated recently with considerable success for sodium<sup>1</sup> and potassium<sup>2</sup> from such curves.

**The Amorphous State.**—Vitreous and amorphous materials are like liquids in that they possess no regular crystalline structure. Amorphous ("explosive") **antimony**, for example, deposited electrolytically or by evaporation in vacuum gives the broad halo pattern characteristic of a glass<sup>3</sup> as does **arsenic** deposited from the vapor phase.<sup>4</sup> In one respect, the structure of an amorphous substance differs from that of a liquid: in the solid each atom has permanent neighbors at fairly definite distances, while in the liquid the neighbors about any atom are continuously changing. A glass is thus properly called an undercooled liquid, a liquid in which atomic mobility has been reduced to an almost negligible amount. When mobility is induced by heat-treatment, a vitreous product "devitrifies" into a product that is definitely crystalline.

It is typical of diffraction patterns from liquids and glasses that there is no scattering at very small angles; this means that there are no large-scale inhomogeneities in the sample, no "crystallites" separated by voids. In silica gel, on the other hand, there is very strong small-angle scattering as a result of the existence in the gel of colloidal particles 10 to 100Å in size with voids between them. In the colloidal state it is possible to have all sizes of crystallites. As the particles become smaller, the diffraction lines broaden continuously and merge until at crystallite sizes of about 10Å there remain only the typical halos of the amorphous state.

It is commonly stated that metals cannot be reduced to an amorphous state by cold work. This appears to be true with regard to cold rolling, but with extremely severe shearing strains under high compressive stress Bridgman<sup>5</sup> has reduced crystalline fragments to a state giving typical amorphous patterns.

<sup>1</sup> C. N. WALL, *Phys. Rev.*, vol. 54, p. 1062, 1938.

<sup>2</sup> N. S. GINGRICH and C. N. WALL, *Phys. Rev.*, vol. 56, p. 336, 1939.

<sup>3</sup> J. A. PRINS, *Trans. Faraday Soc.*, vol. 33, p. 110, 1937.

<sup>4</sup> W. E. MCCORMICK and W. P. DAVEY, *Phys. Rev.*, vol. 47, p. 330, 1935.

<sup>5</sup> P. W. BRIDGMAN, *Phys. Rev.*, vol. 48, p. 825, 1935.

## CHAPTER XII

### SUPERLATTICES

In an ordinary solid solution the different species of atoms are arranged at random on the atomic positions of the lattice. At the composition  $AB$ , for example, any given lattice point is occupied indifferently by either  $A$  or  $B$  atoms, and there is a constant interchange of atoms of both species at each lattice point. There are many solid solutions, however, in which a different atom distribution can be induced. Atoms of one kind can be made to segregate more or less completely on one set of atomic positions, leaving atoms of the other kind to the remaining positions. The resulting arrangement can be described as a lattice of  $A$  atoms interpenetrating a lattice of  $B$  atoms. The segregation of atoms to particular atom sites takes place with little or no deformation of the lattice, creating an ordered solid solution, or **superlattice**, out of a random solid solution, but not a new phase in the usual sense of this term.

In a disordered solid solution every plane of atoms is identical (statistically) with every other, but in an ordered superlattice this is no longer true. For example, alternate planes of a set may become  $A$ -rich and  $B$ -rich planes, respectively, and the distance between identical planes may become twice the distance between identical planes of the disordered alloy (or some other multiple of this distance). Diffraction patterns of the alloy will then contain reflections ("superlattice lines") from the new and larger spacings which are not present in patterns of the disordered alloy. An example is reproduced in Fig. 1. Bain<sup>1</sup> in 1923, and Johansson and Linde<sup>2</sup> in 1925 were the first to observe these lines with x-ray diffraction, though the possibility of ordering had been considered some years earlier by Tammann.<sup>3</sup>

The formation of superlattices takes place at relatively low temperatures and at compositions expressed by a simple formula like  $AB$  or  $AB_3$ , or at compositions near these. At all temperatures above a certain critical temperature the usual randomness persists; when the temperature is lowered through the critical point, order sets in and increases as the temperature drops, approaching perfection only at low temperatures.

<sup>1</sup> E. C. BAIN, *Chem. & Met. Eng.*, vol. 28, pp. 21, 65, 1923; *Trans. A.I.M.E.*, vol. 68, p. 625, 1923.

<sup>2</sup> G. H. JOHANSSON and J. O. LINDE, *Ann. Physik*, vol. 78, p. 439, 1925.

<sup>3</sup> G. TAMMANN, *Z. anorg. Chem.*, vol. 107, p. 1, 1919.

The intensive study of superlattices that followed their discovery has provided a remarkably clear view of the dynamic conditions within metallic crystals, the balance between the tendency of the atoms to take up regular positions and the opposing tendency of thermal agitation to maintain a chaotic arrangement. The main features of the order-disorder

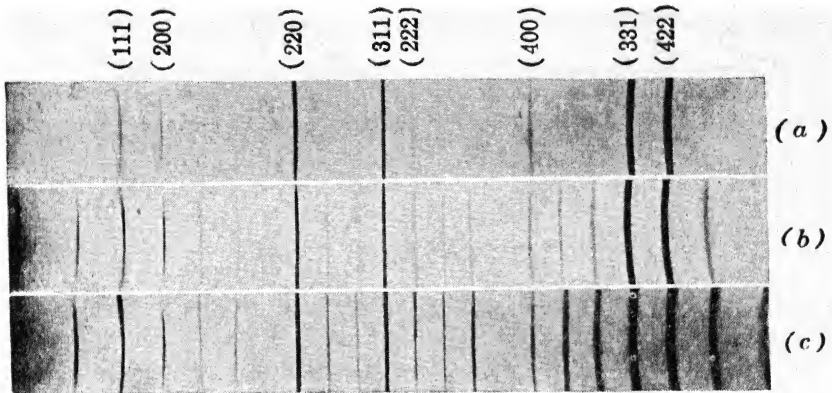


FIG. 1.—Powder-diffraction patterns of the superlattice  $\text{AuCu}_3$ . (a) Disordered, (b) partially ordered, (c) highly ordered. (From C. Sykes and H. Evans, *J. Inst. Metals*, vol. 58, p. 255, 1936.)

transformation have been worked out theoretically with marked success and confirmed by experiment.<sup>1</sup>

**Common Types of Superlattices.**—Copper-gold alloys of about 25 atomic percent gold ( $\text{AuCu}_3$ ) were among the first investigated. In the disordered state, which exists at high temperatures,  $\text{AuCu}_3$  has a random array of Au and Cu atoms on a face-centered cubic (f.c.c.) lattice (Fig.

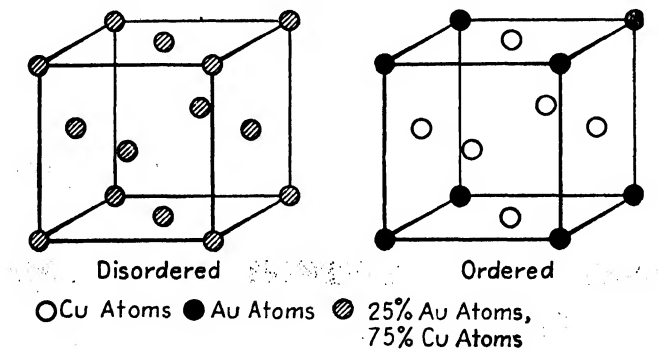


FIG. 2.—The superlattice of  $\text{AuCu}_3$  (cubic).

2). If the alloy is annealed below a critical temperature, about  $400^\circ\text{C}$ . ( $750^\circ\text{F}$ .), the atoms segregate as shown in the drawing of the ordered

<sup>1</sup> An extensive review has been published by F. C. Nix and W. Shockley, *Rev. Modern Phys.*, vol. 10, p. 1, 1938, and shorter ones by F. C. Nix, *J. Applied Phys.*, vol. 8, p. 783, 1937, C. S. Barrett, *Metals & Alloys*, vol. 8, p. 251, 1937, and F. Seitz, "The Modern Theory of Solids," McGraw-Hill, New York, 1940.

structure, Au atoms going to the cube corners and Cu atoms to the face centers. This represents the condition when ordering is complete, the equilibrium condition at low temperatures.

This structure has been observed in the following alloys:  $\text{AuCu}_3$ ,  $\text{PtCu}_3$ ,  $\text{PdCu}_3$ ,\*  $\text{FeNi}_3$ ,  $\text{MnNi}_3$ ,  $(\text{MnFe})\text{Ni}_3$ .

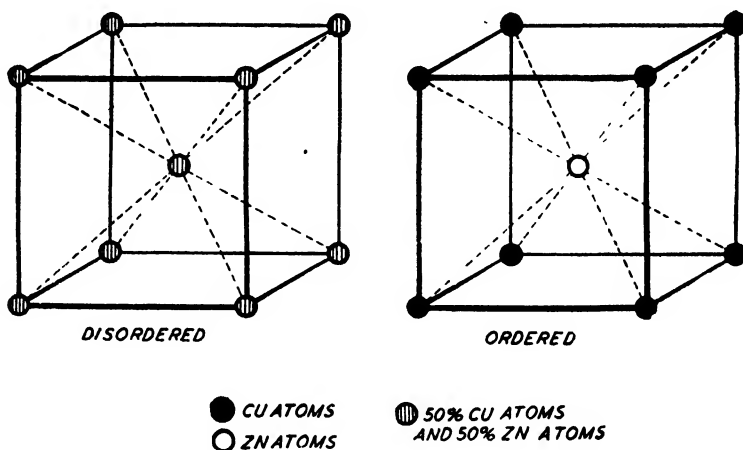


FIG. 3.—The superlattice of  $\beta$ -brass (cubic, CsCl type).

The superlattice in  $\beta$ -brass is illustrated in Fig. 3. The disordered crystal is body-centered cubic (b.c.c.) with equal probabilities of having Cu and Zn atoms at each lattice point; the ordered structure has Cu atoms and Zn atoms segregated to cube corners and centers, respectively, in a structure of the CsCl type. This type of superlattice is characteristic of the following alloys of formula  $AB$ :  $\text{CuZn}$ ,  $\text{CuBe}$ ,  $\text{CuPd}$ ;  $\text{AgMg}$ ,  $\text{AgZn}$ ,  $\text{AgCd}$ ;  $\text{AuNi}$ ,  $\text{NiAl}$ ,  $\text{FeCo}$ .

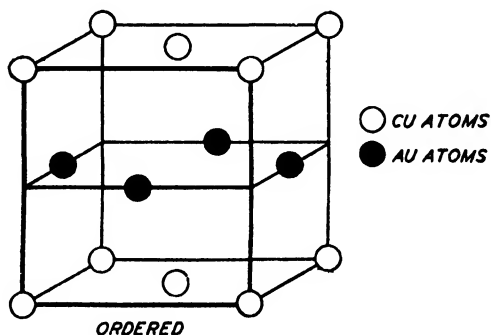


FIG. 4.—The tetragonal superlattice of  $\text{AuCu}$ .

In the Cu-Au system, from 47 to 53 atomic percent a superlattice forms in which alternate layers of Cu and Au atoms form on (001) planes

\*  $\text{PdCu}_3$  has been shown to be actually tetragonal, slightly distorted from cubic [W. L. Bragg, C. Sykes, and A. J. Bradley, *Proc. Phys. Soc. (London)* vol. 49, p. E96, 1937].



of the f.c.c. solid-solution lattice, distorting it into a tetragonal structure, illustrated in Fig. 4. The fourfold axis is normal to the alternating planes of Cu and Au atoms, and the axial ratio is approximately  $c/a = 0.93$ .\*

Another superlattice in this composition range of the system Cu-Au has a surprising unit cell formed out of 10 cells of the disordered lattice,<sup>1</sup> as shown in Fig. 5. The structure is orthorhombic, with two axes nearly equal ( $b/a = 1.003$  to  $1.031$  in different samples) and the third ten times

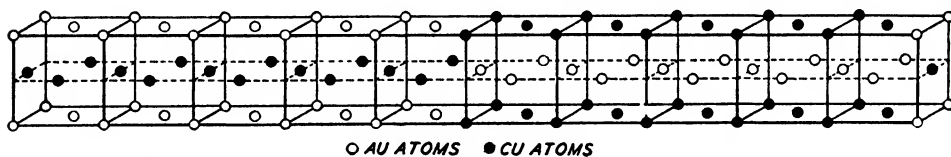


FIG. 5.—One unit cell of the orthorhombic superlattice of AuCu.

as long. It is found when a 50 atomic percent alloy is quenched from about  $420^{\circ}\text{C}$ . or when 36 to 65 atomic percent alloys are annealed and quenched from somewhat lower temperatures.<sup>2</sup>

In the Cu-Pt system near 50 atomic percent the f.c.c. disordered lattice takes up the ordered structure shown in Fig. 6a, consisting of alternating layers of Cu and Pt atoms on (111) planes. This form of

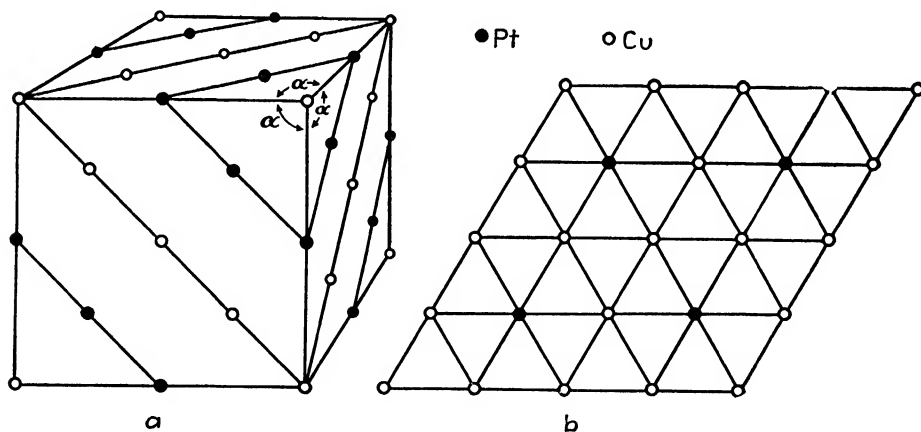


FIG. 6.—The rhombohedral superlattice of CuPt. (a) Distribution of atoms at the composition CuPt. Alternate (111) planes are occupied by Cu and Pt atoms. (b) Distribution of atoms on a single (111) plane, at the composition  $\text{Cu}_3\text{Pt}_3$ .

ordering produces a lattice distortion from cubic to rhombohedral.<sup>3</sup> Copper atoms in excess of the 50-50 composition displace Pt atoms at

\* C. H. JOHANSSON and J. O. LINDE, *Ann. Physik*, vol. 82, p. 449, 1927; vol. 25, p. 1, 1936. R. HULTGREN and L. TARNOPOL, *Trans. A.I.M.E.*, vol. 133, p. 228, 1939.

<sup>1</sup> C. H. JOHANSSON and J. O. LINDE, *Ann. Physik*, vol. 78, p. 439, 1925.

<sup>2</sup> After quenching to room temperature the atomic structure undergoes a curious alteration: the ratio  $b/a$  increases, sometimes changing as much as from 1.018 to 1.031.

<sup>3</sup> J. O. LINDE, *Ann. Physik*, vol. 30, p. 151, 1937.

random on the Pt (111) planes, but in alloys with Pt atoms in excess of the 50-50 ratio there is an interesting tendency for them to displace certain atoms in the Cu (111) planes in the manner illustrated by the sketch of the (111) plane in Fig. 6b. Each Pt atom tends to be surrounded by Cu atoms; this arrangement would be complete in a  $\text{Cu}_3\text{Pt}_5$  alloy.

In the Cu-Pd system one of the ordered structures (37 to 48 atomic percent Pd) has the CsCl structure, although it forms from a f.c.c. disordered state. In spite of this change of lattice, however, it is probably a superlattice transformation, since the physical properties vary with temperature in a way similar to typical superlattices and since it can be shown that a relatively small adjustment of lattice dimensions is required in the transformation instead of an extensive rearrangement of atoms.<sup>1</sup>

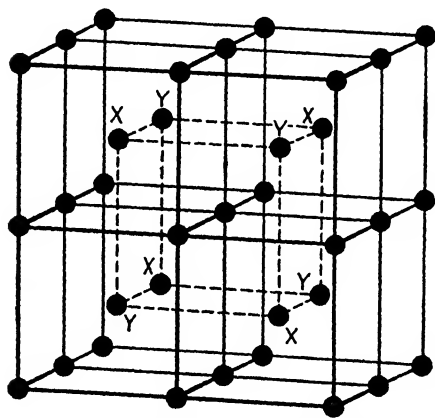


FIG. 7.—The structure of  $\text{Fe}_3\text{Al}$  and  $\text{FeAl}$ . Al atoms fill the X positions in  $\text{Fe}_3\text{Al}$  and the X and Y positions in  $\text{FeAl}$ .

Bradley and Jay<sup>2</sup> have determined the superlattices in the system Fe-Al in detail. As Al is added to the body-centered lattice of Fe, at first the Al atoms replace Fe atoms at random, but beyond 18 atomic percent they concentrate in certain positions and desert others. From 18 to 25 atomic percent the Al atoms concentrate more and more in the positions labeled X in Fig. 7, this process being completed at the composition  $\text{Fe}_3\text{Al}$ . From 25 to 50 atomic percent, increasing numbers of Al atoms go to Y positions until both X and Y positions are

filled with Al atoms at the composition  $\text{FeAl}$ . The structure is then similar to the ordered structure in  $\beta$ -brass. In both  $\text{Fe}_3\text{Al}$  and  $\text{FeAl}$  the atom is surrounded by the maximum number of unlike atoms. A structure similar to  $\text{Fe}_3\text{Al}$  is found in  $\text{Fe}_3\text{Si}$ .<sup>\*</sup> The Heusler alloy  $\text{Cu}_2\text{MnAl}$  is ordered when in the ferromagnetic condition; the atoms are in a b.c.c. cell like that of Fig. 7, with the Al atoms in Y positions, the Mn atoms in X positions, and the Cu atoms at the remaining points.<sup>3</sup>

<sup>1</sup> C. H. JOHANSSON and J. O. LINDE, *Ann. Physik*, vol. 78, p. 439, 1925; vol. 82, p. 449, 1927.

<sup>2</sup> A. J. BRADLEY and A. H. JAY, *Proc. Roy. Soc. (London)*, vol. A136, p. 210, 1932; *J. Iron Steel Inst.*, vol. 125, p. 339, 1932.

<sup>\*</sup> G. PHRAGMÉN, *Stahl u. Eisen*, vol. 45, p. 299, 1925.

<sup>3</sup> A. J. BRADLEY and J. W. RODGERS, *Proc. Roy. Soc. (London)*, vol. A144, p. 340, 1934.

Hexagonal close-packed structures exist in superlattices of  $\text{Mg}_3\text{Cd}$ ,<sup>\*</sup>  $\text{MgCd}_3$ ,<sup>†</sup>  $\text{Ni}_3\text{Sn}$ ,<sup>‡</sup> and in the quasi-binary system  $\text{Mg-AgCd}_3$ ,<sup>§</sup> in the range from 37 to 70 atomic percent Mg.||

The ternary phases  $\text{Ag}_2\text{HgI}$  and  $\text{Cu}_2\text{HgI}$  show complex order-disorder changes resembling somewhat those in  $\text{AuCu}_3$ ,<sup>¶</sup> but involving ordered and disordered arrangements of both metal atoms and vacant lattice points.

**Elements of Superlattice Theory.**—Theoretical treatments of superlattices have been given by Borelius,<sup>1</sup> Johansson and Linde,<sup>2</sup> Gorsky,<sup>3</sup> Dehlinger,<sup>4</sup> and Dehlinger and Graf,<sup>5</sup> chiefly on the basis of formal thermodynamic relations. It was considered anew by Bragg and Williams,<sup>6</sup> Williams,<sup>7</sup> Bethe,<sup>8</sup> and Peierls,<sup>9</sup> who as a group started with simple assumptions about atomic forces and calculated quantitative results that compared very favorably with experiment. The point of view of this second series of papers is outlined here.

In a fully ordered alloy there are great distances within a crystal through which there is a perfect arrangement of *A* atoms on one set of lattice points and *B* atoms on another set. The ordering is consistent, "in step," through long distances. This long-distance order may be defined as to degree by a fraction, *S*, which varies from zero at complete disorder up to unity at complete order. The **degree of long-distance order** *S* is the fraction of the atoms that are in their right positions minus the fraction that are in wrong positions. As a simple illustration, consider an alloy *AB* in which 100 *A* atoms and 100 *B* atoms are randomly arranged; just half of the *A* atoms are in the places they would occupy in the ordered structure, and the other half are in wrong positions; and the same would be true of the *B* atoms, giving *S* = 0. If 75 *A* atoms were right and 25 wrong, the order would be  $0.75 - 0.25 = 0.50$ .

\* U. DEHLINGER, *Z. anorg. allgem. Chem.*, vol. 194, p. 223, 1930.

† K. RIEDERER, *Z. Metallkunde*, vol. 29, p. 423, 1937.

‡ P. RAHLFS, *Metallwirtschaft*, vol. 16, p. 640, 1937.

§ F. LAVES and K. MOELLER, *Z. Metallkunde*, vol. 29, p. 185, 1937.

|| Atom positions in  $\text{Mg}_3\text{Cd}$  and similar structures are as follows: Mg: 000,  $\frac{1}{2}$ 00,  $0\frac{1}{2}$ 0,  $\frac{1}{6}\frac{1}{6}\frac{1}{6}$ ,  $\frac{2}{3}\frac{1}{3}\frac{1}{3}$ ,  $\frac{2}{3}\frac{2}{3}\frac{1}{3}$ ; Cd:  $\frac{1}{2}\frac{1}{2}$ 0,  $\frac{1}{6}\frac{1}{6}\frac{1}{6}$ .

¶ J. A. KETELAAR, *Z. physik. Chem.*, vol. B26, p. 327, 1934; vol. B30, p. 53, 1935; *Z. Krist.*, vol. 87, p. 436, 1934.

<sup>1</sup> G. BORELIUS, *Ann. Physik*, vol. 20, pp. 57, 650, 1934.

<sup>2</sup> C. H. JOHANSSON and J. O. LINDE, *Ann. Physik*, vol. 78, p. 439, 1925.

<sup>3</sup> W. GORSKY, *Z. Physik*, vol. 50, p. 64, 1928.

<sup>4</sup> U. DEHLINGER, *Z. physik. Chem.*, vol. B26, p. 343, 1934.

<sup>5</sup> U. DEHLINGER and L. GRAF, *Z. Physik*, vol. 64, p. 359, 1930.

<sup>6</sup> W. L. BRAGG and E. J. WILLIAMS, *Proc. Roy. Soc. (London)*, vol. A145, p. 699, 1934; vol. A151, p. 540, 1935.

<sup>7</sup> E. J. WILLIAMS, *Proc. Roy. Soc. (London)*, vol. A152, p. 231, 1935.

<sup>8</sup> H. A. BETHE, *Proc. Roy. Soc. (London)*, vol. A150, p. 552, 1935.

<sup>9</sup> R. PEIERLS, *Proc. Roy. Soc. (London)*, vol. A154, p. 207, 1936.

This definition may be generalized to cover the condition in which  $n$  atomic positions of a total number  $N$  can be occupied by either kind of atom.<sup>1</sup> In the structure  $\text{Fe}_3\text{Al}$  the fraction  $n/N = \frac{1}{2}$ , since even in the completely disordered state one-half of the atom positions are still occupied exclusively by one kind of atom. Suppose a fraction  $r$  of the  $n$  sites is occupied by  $A$  atoms in the state of perfect order; these  $rn$  sites are right positions for  $A$  atoms. In a partially ordered alloy, some of these positions are filled by  $A$  and some by  $B$  atoms. If  $p$  is the probability

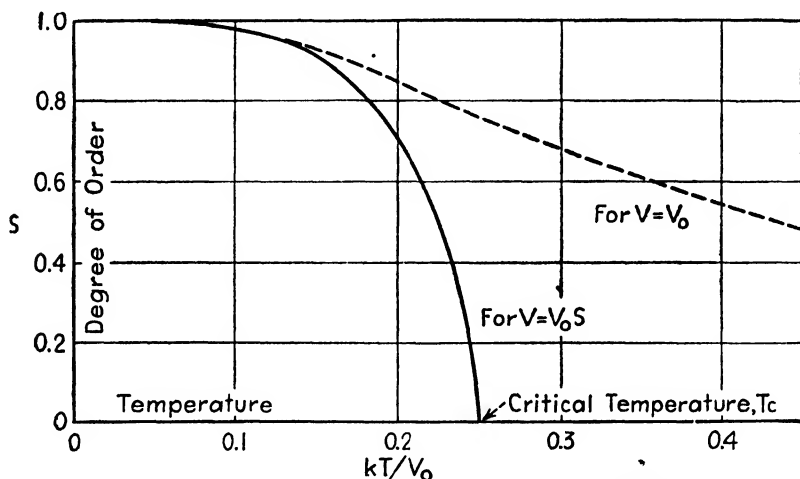


FIG. 8.—Dependence of order on temperature according to the Bragg and Williams theory for long-distance order at equilibrium.

that a right position for an  $A$  atom is filled by an  $A$  atom, then the long-distance order is defined by the relation

$$S = \frac{p - r}{1 - r}$$

which varies from 0 to 1 as order increases.

In an alloy of  $A$  and  $B$  atoms the energy of the crystals will be a minimum when order is complete and will be increased an amount  $V$  if a pair of atoms is interchanged so that an  $A$  atom takes a place that should be occupied by a  $B$  atom, and a  $B$  atom moves to a position that should be occupied by an  $A$  atom. In other words,  $V$  is the net amount of work required to effect this interchange. Under thermal agitation an equilibrium will be reached such that the ratio of the number of atoms in the right positions to the number in wrong positions is equal to Boltzmann's factor  $e^{-V/kT}$ , where  $k$  is Boltzmann's constant, and  $T$  is the absolute temperature.

<sup>1</sup> W. L. BRAGG and E. J. WILLIAMS, *Proc. Roy. Soc. (London)*, vol. A145, p. 699, 1934.

If  $V$  were a constant, say  $V_0$ , independent of the degree of order in the alloy, there would be a gradual increase in disorder with rising temperature along a curve plotted in Fig. 8 as a dashed line. This cannot be the case, however, for a decrease in order results in a decrease in the forces that tend to maintain order. The distinction between right and wrong positions for an atom, in fact, vanishes when disorder is complete, and the energy  $V$  to effect an interchange then drops to zero. This dependence of  $V$  on order is responsible for the decrease of order at an accelerating rate as the temperature is raised. As Bragg puts it, demoralization sets in, and there is a complete collapse of the ordered state.

To make a theoretical calculation of the degree of order in equilibrium at each temperature it is therefore necessary to assume a particular relation between  $V$  and the degree of order. For simplicity, Bragg and

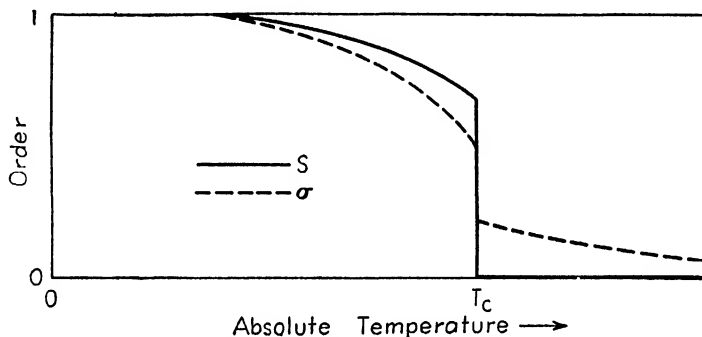


FIG. 9.—Dependence of long-range order  $S$  and short-range order  $\sigma$  on temperature in an  $AB_3$  superlattice.

Williams<sup>1</sup> assumed that  $V$  is proportional to the degree of long-distance order,  $S$ , according to the relation  $V = V_0 S$ , where  $V_0$  is a constant representing the interchange energy when the order is complete. The curve for equilibrium order vs. temperature is shown in Fig. 8 by the solid line. The curve is computed for a superlattice of composition  $AB$ , such as  $\beta$ -brass and  $AuCu$ ; it also holds for  $Fe_3Al$ . Long-distance order decreases to zero at a critical temperature  $T_c$  that is directly analogous to the Curie temperature at which a ferromagnetic material loses its ferromagnetism.<sup>2</sup>

<sup>1</sup> W. L. BRAGG and E. J. WILLIAMS, *Proc. Roy. Soc. (London)*, vol. A145, p. 699, 1934.

<sup>2</sup> Each point on the curve of equilibrium order satisfies two conditions that can be stated as follows: (1) The dependence of  $V$  upon  $S$  is assumed to be  $V = V_0 S$  and it is assumed to be practically independent of temperature. (2) The dependence of equilibrium order upon  $V$  is dependent upon the Boltzmann factor  $e^{-V/kt}$  in a way that leads to the relation  $S = \tanh(V/4kt)$  when applied to a superlattice where  $r = \frac{1}{2}$  (e.g.,  $CuZn$ ,  $Fe_3Al$ ). Plotting  $S$  against  $T$ , the equilibrium degree of order is found at the intersection of the straight line of relation (1) with the curve of relation (2). At this intersection the interchange energy  $V$  caused by the amount of

The critical temperature  $T_c$  is directly related to the ordering energy  $V_0$ ; in a 50 atomic percent alloy the relation is approximately  $V_0 = 4kT_c$ , where  $k$  is Boltzmann's constant.

A similar calculation for a composition like  $\text{AuCu}_3$  gives a similar curve up to a certain temperature and then an abrupt drop to zero order, as indicated by the solid curve in Fig. 9.

**Short-range Order.**—In Bragg and Williams's theory discussed above it is assumed that the ordering energy is proportional to the long-distance order in a crystal, yet it seems certain that the principal interactions in crystals are between very close neighbors. A logical development of superlattice theory is therefore to consider a concept of order that concerns only nearest neighbors, and to compute ordering energies based on nearest neighbor interactions. Theories based on this point of view have been worked out by Bethe<sup>1</sup> and extended by Williams,<sup>2</sup> Peierls,<sup>3</sup> Easthope,<sup>4</sup> and Kirkwood.<sup>5</sup>

Short-range order is defined in terms of the number of "right pairs" of atoms, just as long-distance order is defined in terms of the number of right atoms. A right pair is a pair of unlike atoms, an  $AB$  pair. At increasing temperatures the number of  $AB$  pairs diminishes and the number of  $AA$  and  $BB$  pairs (wrong pairs) increases until a disordered state is reached in which half the pairs are right and half are wrong. The local, or short-range, order  $\sigma$  may be defined as the probability of finding an unlike atom beside a given atom minus the probability of finding a like atom there. Considering a certain  $A$  atom, the probability that a nearest neighbor is a  $B$  atom is  $\frac{1}{2}(1 + \sigma)$ , while the probability that it is an  $A$  atom is  $\frac{1}{2}(1 - \sigma)$ . The Boltzmann factor gives the ratio of these two when equilibrium is reached at a temperature  $T$ :

$$\frac{\frac{1}{2}(1 - \sigma)}{\frac{1}{2}(1 + \sigma)} = e^{-v/kT}$$

where  $v$  is the change in energy of the crystal when one pair is changed from an  $AB$  to an  $AA$  pair. This energy  $v$  must be positive if a superlattice is to form; if it is negative, there will be a tendency for like atoms

order present just balances the shuffling tendency of thermal agitation. As the temperature is raised, the intersection of (1) and (2) occurs at lower and lower  $S$  values until the intersection occurs at  $S = 0$  at the critical temperature. Here  $S = \tanh(V/4kT)$  approximates  $S = V/4kT$ , and by substituting relation (1) for this temperature,  $T_c$ , one obtains  $V_0 = 4kT_c$ .

<sup>1</sup> H. A. BETHE, *Proc. Roy. Soc. (London)*, vol. A150, p. 552, 1935.

<sup>2</sup> E. J. WILLIAMS, *Proc. Roy. Soc. (London)*, vol. A152, p. 231, 1935.

<sup>3</sup> R. PEIERLS, *Proc. Roy. Soc. (London)*, vol. A154, p. 207, 1936.

<sup>4</sup> C. E. EASTHOPE, *Proc. Cambridge Phil. Soc.*, vol. 33, p. 502, 1937.

<sup>5</sup> J. G. KIRKWOOD, *J. Chem. Phys.*, vol. 6, p. 70, 1938.

to cluster together and precipitate from solid solution.<sup>1</sup> If  $v_{AA}$ ,  $v_{BB}$ , and  $v_{AB}$  are the energies associated with the pairs  $AA$ ,  $BB$ , and  $AB$ , respectively, then

$$v = \frac{1}{2}(v_{AA} + v_{BB}) - v_{AB}.$$

If  $v$  were a constant independent of the degree of order, we should find  $\sigma$  decreasing slowly toward zero at high temperatures and there would be no critical point. In Bethe's theory  $v$  is assumed to depend upon order in a manner he computes from the long-distance order that exists in the crystal, and this accounts for the accelerated decline toward zero as the temperature is raised toward the critical point.

The curve resembles the curve for Bragg and Williams's theory at low temperatures, as will be seen from Fig. 9, but at the critical temperature Bethe's theory predicts that  $\sigma$  does not fall entirely to zero but to a

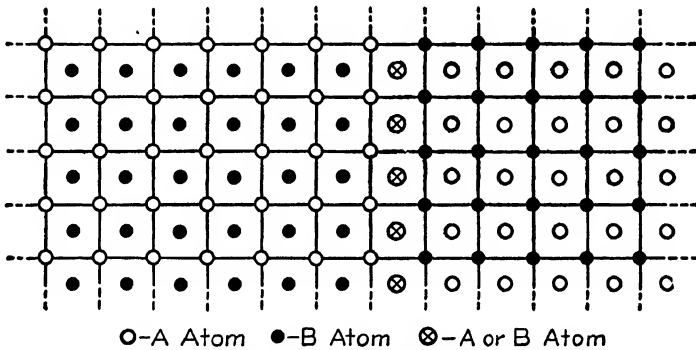


FIG. 10.—Out-of-step domains in a superlattice.

residual value greater than zero, a value which in turn gradually decreases as the temperature is still further increased. Thus even at high temperatures there are more than the random number of  $AB$  atom pairs; and while they are unable to link up together into a constant long-distance order in the crystal, they are able to form small domains within which there is order. At  $T_c$  the domains begin to hook together into long-distance order, and as the temperature is lowered the long-distance order increases toward perfection. Even at low temperatures, however, a crystal may be divided into domains "out of step" with each other in the manner indicated in Fig. 10. The energy for each degree of order may be computed by statistical mechanics from the number of different arrangements of atoms that will have that degree of order.

The existence of local order above the critical temperature has been confirmed by observations on specific heats of superlattices, as will be

<sup>1</sup> The theory of precipitation from a simple binary eutectic system has been discussed by R. Becker, *Z. Metallkunde*, vol. 29, p. 245, 1937. See R. F. Mehl and L. K. Jetter, *The Mechanism of Precipitation from Solid Solution*, *The Theory of Age Hardening*, "Symposium on Age Hardening," A.S.M., Cleveland, Ohio, 1940.

discussed later; it has also been shown by certain diffuse rings in electron diffraction patterns.<sup>1</sup> Bethe's first treatment of the local-order problem was limited to simple structures of composition  $AB$ ; this was extended to composition  $AB_3$  by Peierls<sup>2</sup> and generalized to compositions other than stoichiometric ratios by Kirkwood,<sup>3</sup> Easthope,<sup>4</sup> and others.

**Dependence of  $T_c$  on Composition.**—Easthope's theory<sup>4</sup> for the variation of the critical temperature with composition indicates that  $T_c$  is a maximum at 50 atomic percent for structures like the simple cubic or b.c.c. in which each atom has unlike atoms for nearest neighbors when fully ordered. His predictions for  $T_c$  vs. composition are plotted in Fig.

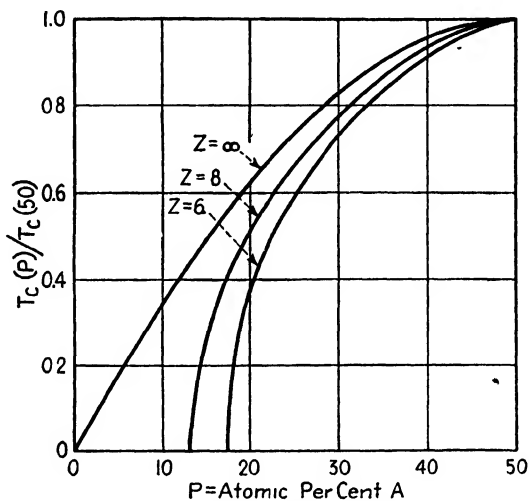


FIG. 11.—Easthope's theoretical curves for critical temperature vs. composition for structures with coordination numbers 6, 8 and  $\infty$  (the latter corresponding to the Bragg-Williams theory).

11 on a temperature scale expressed as fractions of  $T_c$  at 50 atomic percent. The curve is symmetrical about this composition. He does not predict a maximum in  $T_c$  for f.c.c. lattices at the stoichiometric ratio  $AB_3$ .

Shockley<sup>5</sup> treats the f.c.c. lattice as four interpenetrating lattices of the simple cubic type and notes that in ordered  $AuCu$  two of these are pure Cu and two are pure Au, while in ordered  $AuCu_3$  three of these are Cu and one is pure Au. By considering the degree of order on each of these interpenetrating lattices separately he is able to treat intermediate compositions and to compute the free energy as a function

<sup>1</sup> L. H. GERMER, F. E. HAWORTH, and J. J. LANDER, *Phys. Rev.*, vol. 61, p. 93, 1942.

<sup>2</sup> R. PEIERLS, *Proc. Roy. Soc. (London)*, vol. A154, p. 207, 1936.

J. G. KIRKWOOD, *J. Chem. Phys.*, vol. 6, p. 70, 1938.

<sup>4</sup> C. E. EASTHOPE, *Proc. Cambridge Phil. Soc.*, vol. 33, p. 502, 1937.

<sup>5</sup> W. SHOCKLEY, *J. Chem. Phys.*, vol. 6, p. 130, 1938. F. C. NIX and W. SHOCKLEY, *Rev. Modern Phys.*, vol. 10, p. 1, 1938.



of composition for all alloys of the system. His theory predicts a phase diagram in which the ordered tetragonal phase ( $\text{AuCu}$ ), the ordered cubic phase ( $\text{AuCu}_3$ ), and the disordered phase are separated by two-phase regions (Fig. 12). Both ordered structures have a maximum  $T_c$  at 50 atomic percent, and there is symmetry around this composition. Modification of the theory will be necessary to account for the lack of symmetry that actually exists in the  $\text{AuCu}$  system and to account for the fact that an orthorhombic rather than a cubic structure forms; yet the prediction of

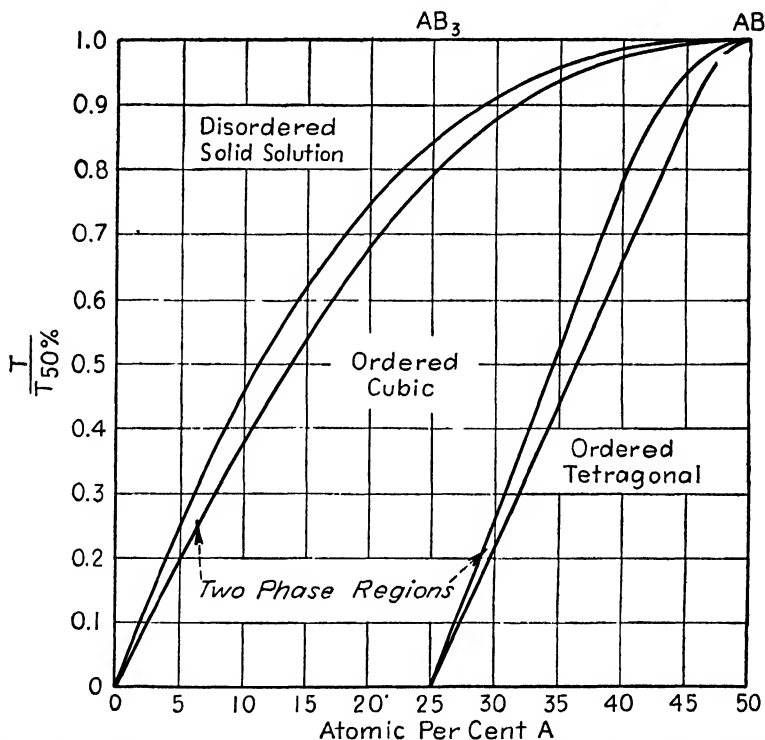


FIG. 12.—Shockley's theoretical phase diagram for f.c.c. superlattices.

two phase changes in some of the alloys (an example has been observed<sup>1</sup>) and the prediction of two-phase regions (not yet observed) are most interesting.

**Phenomena Related to Superlattices.**—Superlattices have a close parallel in ferromagnetism. Bragg and Williams's treatment of long-distance order  $S$  is analogous to Weiss's theory of ferromagnetism,  $S$  corresponding to the magnetization and  $V$  to the difference in potential energy for the parallel and antiparallel electron spins. Similarly, the theory of local order parallels the modern theory of ferromagnetism, with interaction assumed only between neighboring electron spins (except that quantum mechanics is not involved in calculations of order as it is in

<sup>1</sup> C. H. JOHANSSON and J. O. LINDE, *Ann. Physik*, vol. 25, p. 1, 1936.

magnetism).<sup>1</sup> Another close analogy is the vibration and rotation of molecules in crystals such as the ammonium halides where there is a critical temperature above which all the ammonium radicals rotate and below which the rotation is gradually replaced by oscillation. Fowler has presented the theory of these transitions<sup>2</sup> in each of which there is a critical temperature, properly called a Curie temperature, resulting from an ordering force that decreases with order.

**Specific Heats of Superlattices.**—The order-disorder transformation has a marked effect on the specific heat of an alloy. Energy must be supplied to interchange atoms from right to wrong positions, for the fully ordered state is the one of lowest energy. The specific heat during dis-

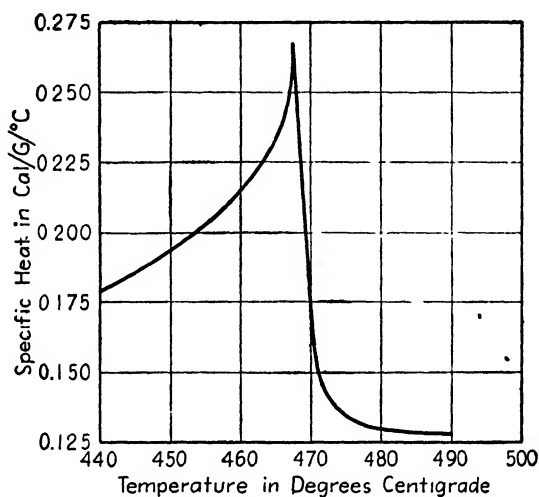


FIG. 13.—Specific heat vs. temperature in  $\beta$ -brass (50.4 % Zn).

ordering is greater than the normal value that is given approximately by the law of Dulong and Petit; the value at each temperature depends upon the rate of decrease of order with temperature. Just below the critical temperature the order drops most rapidly and the specific heat rises to a maximum and then drops precipitously, as shown in Fig. 13. However, the specific heat does not become infinite—*i.e.*, there is no latent heat—unless there is an infinitely sharp drop in order at the critical temperature  $T_c$ . The transformation in superlattices at 50 atomic percent should not show a latent heat, for theory predicts a steady decrease in order with increase in temperature, as in Fig. 8. On the other hand, at all compositions other than 50 atomic percent (for example,  $AB_3$ ), a

<sup>1</sup> F. BLOCH, *Z. Physik*, vol. 61, p. 206, 1930. A. SOMMERFELD and H. A. BETHE, "Handbuch der Physik," vol. XXIV, pt. 2, p. 607, Springer, Berlin. N. F. MOTT and H. JONES, "The Theory of the Properties of Metals and Alloys," Oxford, New York, 1936.

<sup>2</sup> R. H. FOWLER, *Proc. Roy. Soc. (London)*, vol. A149, p. 1, 1935.

latent heat is predicted from the abrupt drop in order at  $T_c$  (cf. Fig. 9). Cu-Zn and Cu-Au alloys confirm these predictions, but  $\text{Cu}_3\text{Pd}$  and  $\text{MgCd}$  apparently do not, and some modifications of the theory are required.<sup>1</sup> Theory and experiment are in reasonable agreement for the total energy change from order to disorder but are divergent in predicting the maximum specific heat just below  $T_c$ .\*

In all specific-heat curves for superlattices there is evidence for the existence of local order above the critical temperature—the curves continue to fall as the local order is further destroyed by thermal agitation. Sykes and Wilkinson's measurements<sup>2</sup> (Fig. 13) show this prominently for  $\beta$ -brass. The long-distance order breaks up into small partially ordered domains that are out of step with one another, and at still higher temperatures the order approaches zero in each of these. Since the interactions among atoms are largely between nearest neighbors, energies and specific heats are determined by the degree of local order.

**Electrical Resistivity of Superlattices.**—Electrical resistivity, like x-ray diffraction, reveals long-distance order but is insensitive to local order. When the disordered state is retained at room temperature by quenching from above the critical temperature, the strains from the irregularity of the distribution are superimposed upon the distortions from thermal agitation, both contributing to the electrical resistance. Annealing below  $T_c$  induces order and removes the disordered component of resistance, sometimes lowering the resistivity of the alloy by as much as a factor of 3. Measurements on Cu-Au alloys, reproduced in Fig. 14, show the maximum effect of ordering at compositions  $\text{AuCu}_3$  and  $\text{AuCu}$ , where ordering is most complete. In the Cu-Pt system (Fig. 15) it will be recalled that the CuPt structure distributes excess Pt atoms differently

<sup>1</sup> F. C. NIX and W. SHOCKLEY, *Rev. Modern Phys.*, vol. 10, p. 1, 1938.

\* In Bragg and Williams's theory, the notation of the preceding pages being used, an increase in order from  $S$  to  $S + dS$ , which accompanies a fall of temperature  $-dT$ , involves an increase in the number of atoms in right positions from  $rn(p + dp)$ ; and since  $S = (p - r)/(1 - r)$ , we have  $dp = (1 - r) dS$ . With the potential energy decreasing by  $V = V_0 S$  at each atom interchange, the crystal gives off energy  $dE = Vrn(1 - r) = V_0 nr(1 - r)S dS$ . This integrated between any limits  $S_1$  and  $S_2$  gives the evolution of energy from ordering ("configurational energy"), which for the total change  $S = 0$  to  $S = 1$  is  $V_0 nr(1 - r)/2$ . For a superlattice of the  $AB$  type with  $n = N$  and  $r = \frac{1}{2}$ , the equation reduces to  $NV_0/8$  per mol. On Bethe's theory and Kirkwood's theory this energy of transformation from  $\sigma = 1$  to  $\sigma = 0$  is  $3Nv/2$  for simple cubic  $AB$  structures and  $2Nv$  for b.c.c. structures. The configurational specific heat is a maximum just below  $T_c$ ; the predicted values on the different theories are as follows for b.c.c.  $AB$  superlattices: Bragg and Williams,  $1.50R$ ; Bethe  $1.78R$ ; Kirkwood  $2.20R$ . The observed value for  $\beta$ -brass is  $5.1R$ , and so all theories are too low in this very sensitive and critical test. Mott [*Proc. Phys. Soc. (London)*, vol. 49, p. 258, 1937] predicts higher theoretical values from a quantum mechanical computation of the energy in  $\beta$ -brass.

<sup>2</sup> C. SYKES and H. WILKINSON, *J. Inst. Metals*, vol. 61, p. 223, 1937.

from excess Cu atoms, the former taking ordered positions on (111) Cu planes of the face-centered lattice, the latter taking random positions.

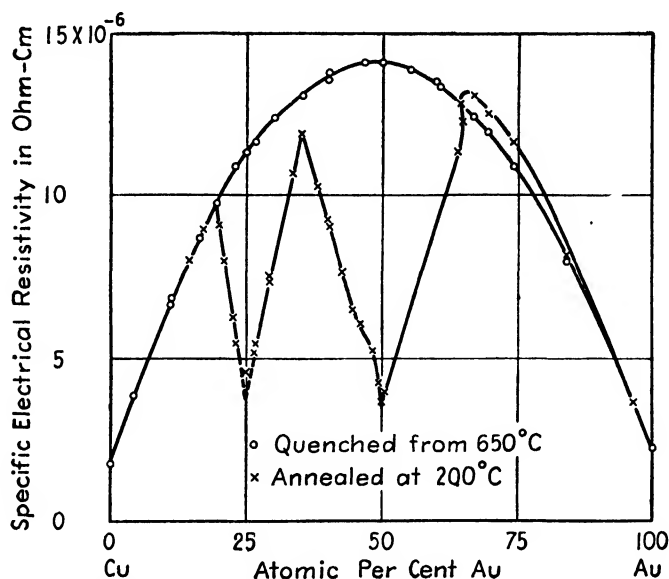


FIG. 14.—Electrical resistivity vs. composition for the Cu-Au system. (o) Alloys quenched from 650°C. (disordered), (x) alloys annealed at 200°C. (ordered).

This doubtless accounts for the low resistivity of the ordered alloys above 50 atomic percent compared with those below.

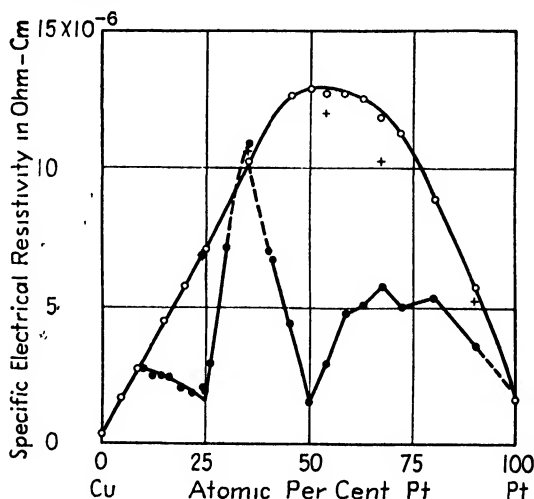


FIG. 15.—Electrical resistivity vs. composition for the Cu-Pt system. (o) Alloys quenched and cold-worked (disordered), (+) alloys quenched from 900°C. (nearly disordered), (●) alloys annealed at 300°C. (ordered).

Disorder makes a large contribution to the electrical resistance, superimposed upon the resistance due to thermal vibrations. Bragg and Williams's calculated curve of resistivity vs. temperature for AuCu in

equilibrium is reproduced in Fig. 16 and compared with measured values obtained during a slow rate of cooling.<sup>1</sup> The experimental curve deviates from the theoretical because of the increasing sluggishness of diffusion at the lower temperatures, the alloy finally "freezing" into a state of partial order when atomic interchange becomes negligible.

There is an abrupt change in resistance at the critical temperature in  $\text{AuCu}_3$ , corresponding to the abrupt change in long-distance order from 0 to about 0.4. The abruptness is partly obscured, however, by sluggish

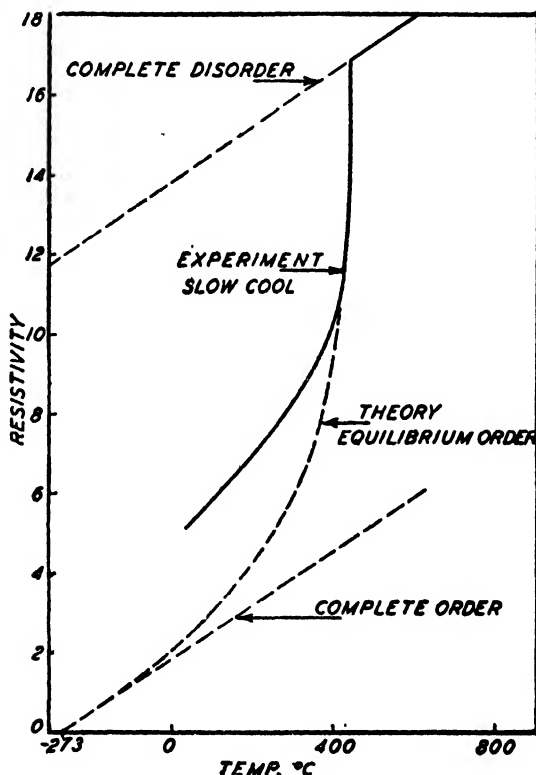


FIG. 16.—Electrical resistivity of Au-Cu alloys during slow cooling from above the critical temperature.

diffusion, by the limited size of the domains in which order is coherent, and by strains introduced during the change from a cubic to a tetragonal lattice. These factors produce a hysteresis effect, making  $T_c$  appear at different temperatures on heating and on cooling.

Plastic deformation tends to destroy long-distance order. It will be seen from Fig. 17 that an annealed  $\text{AuCu}_3$  alloy reverted to the resistance of a fully disordered alloy when reduced 60 percent in cross section by drawing through a die.<sup>2</sup> The disordered (quenched) alloy remained

<sup>1</sup> N. S. KURNAKOW and N. W. AGEW, *J. Inst. Metals*, vol. 46, p. 481, 1931.

<sup>2</sup> O. DAHL, *w. Metallkunde*, vol. 28, p. 133, 1936.

relatively unchanged, thus resembling pure metals and random solid solutions, most of which are increased only about 2 percent in resistivity.

**Other Physical Properties of Superlattices.**—Mechanical properties are altered when ordering takes place. Hardness, tensile strength, and elastic limit generally increase.<sup>1</sup> For example, if the alloy AuCu is quenched to retain disorder and is then annealed at 150 to 300°C., the hardness increases with time much as in a precipitation hardening alloy (Fig. 18).<sup>2</sup> The microstructure is acicular,<sup>3</sup> resembling martensite. Doubtless the formation of many nuclei of the ordered tetragonal phase induces severe strains which are responsible for much of the hardening. In  $\beta$ -brass the ordering process takes place almost instantly. It cannot

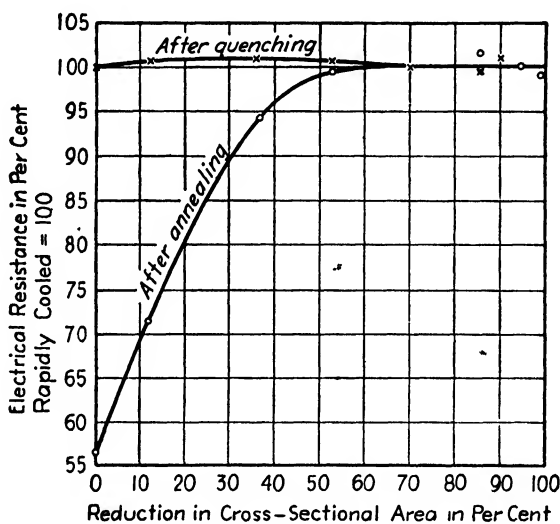


FIG. 17.—Effect of cold work (wire drawing) on the electrical resistivity of AuCu<sub>3</sub>.

be prevented or even retarded by quenching, and it cannot be destroyed by cold work. As expected of a superlattice having this rapid ordering, it is found that the conductivity of  $\beta$ -brass is unaffected (within 1.5 percent) by the rate of cooling from above the critical temperature (450 to 470°C.) and by cold work. In spite of this, the hardness of a sample quenched from above the critical temperature is greater than the hardness of one that has been slowly cooled.<sup>4</sup> The additional hardness must have its origin in out-of-step domains. Hardness changes in  $\beta$ -brass during aging<sup>4</sup> (Fig. 19) are also understandable on this basis. An alloy

<sup>1</sup> G. SACHS, "Praktische Metallkunde," vol. III, pp. 68–81, Springer, Berlin, 1935.

<sup>2</sup> L. NOWACK, *Z. Metallkunde*, vol. 22, p. 94, 1930.

<sup>3</sup> N. KURNAKOW, S. ZEMCZUZYNY, and M. ZASEDATELEV, *J. Inst. Metals*, vol. 15, p. 305, 1916. W. GORSKY, *Z. Physik*, vol. 50, p. 64, 1928. J. L. HAUGHTON and R. J. M. PAYNE, *J. Inst. Metals*, vol. 46, p. 457, 1931.

<sup>4</sup> C. S. SMITH, *Metals Tech., Tech. Pub.* 1517, October, 1942.

quenched from 500°C. presumably has many small out-of-step domains which rapidly coalesce during aging, quickly lowering the hardness. An alloy quenched from a temperature where ordering is about half complete

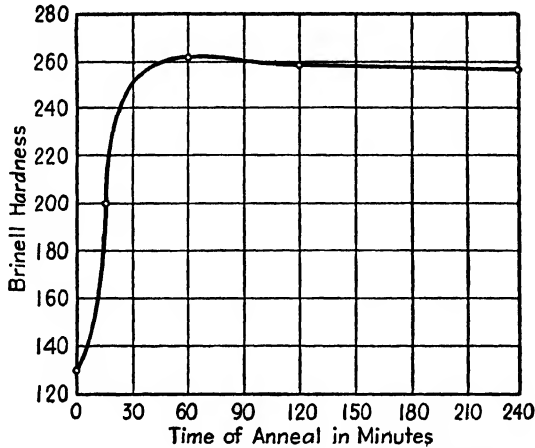


FIG. 18.—Hardening of CuPt by annealing a quenched alloy under the critical temperature. (Annealing temperature 500°C.)

(425°C.) probably contains domains of larger size, which grow more slowly, and hence hardness decreases more slowly.

Dilatometric changes occur during ordering, for lattice constants are altered. Young's modulus increases with ordering in  $\text{Cu}_3\text{Pd}$  and

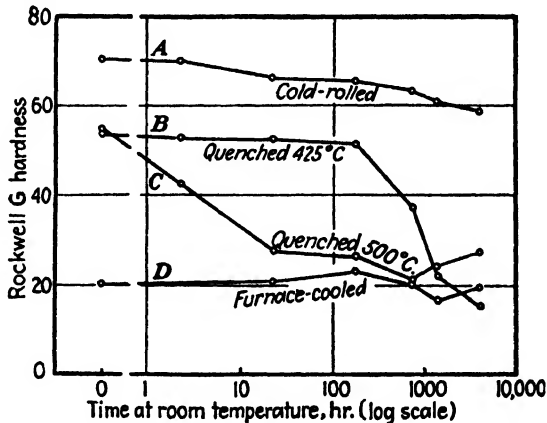


FIG. 19.—Hardness of  $\beta$ -brass aged at room temperatures. A, samples annealed at 425°C., slowly cooled to room temperature, and cold-rolled 15 percent reduction. B, annealed 1 hr. at 500°C., furnace-cooled to 425°C., held 1 hr. at 425°C., and quenched. C, annealed 1 hr. at 500°C. and quenched. D, annealed 1 hr. at 425°C. and furnace-cooled. (C. S. Smith.)

$\text{AuCu}_3$  but decreases in  $\text{AuCu}$  and  $\text{CuPd}$ . Siegel<sup>1</sup> has shown that the elastic constants are sensitive to *local* order.

<sup>1</sup> S. SIEGEL, *Phys. Rev.*, vol. 57, p. 537, 1940.

Diamagnetic susceptibility increases when  $\text{AuCu}_3$ ,  $\text{Cu}_3\text{Pd}$ , and  $\text{CuPd}$  become ordered but decreases for  $\text{AuCu}$ .<sup>\*</sup>  $\text{Ni}_3\text{Mn}$  is ferromagnetic in the annealed state and nonferromagnetic when cold-worked; resistance changes resemble those in  $\text{Cu}_3\text{Au}$  and suggest that ordering is responsible.<sup>1</sup>

The Heusler alloys are known to be ordered in the ferromagnetic state.<sup>2</sup> Pt-Cr alloys containing 20 to 50 atomic percent chromium are also ferromagnetic, but the composition with highest saturation magnetization (about 30 percent) is not that for which the strongest and sharpest superlattice lines are seen in x-ray patterns.<sup>3</sup> The relation of ferromagnetism to superstructures becomes still more uncertain when it is noted that the ferromagnetic nonferrous alloys  $\text{SnMn}_2$ ,  $\text{SnMn}_3$ ,  $\text{MnSb}_2$ , and  $\text{Mn}_2\text{Sb}$  have not been identified with superstructures. While some permanent-magnet alloys show superlattice lines when treated to give high coercive force, the intensity of the lines is not proportional to the coercive force, and so the correlation is doubtful.<sup>4</sup>

**The Rate of Approach to Equilibrium.**—Bragg and Williams have made some interesting calculations of the rate at which an alloy will approach its equilibrium degree of order at any temperature. They assumed that the rate of approach is directly proportional to the discrepancy between the actual and the equilibrium order. The constant of proportionality was taken as  $1/\tau$ , where  $\tau$  is the "time of relaxation" of the alloy, the time required for the departure from equilibrium to be reduced to  $1/e$  or (0.368) of its initial amount. A reasonable expression for  $\tau$  is then  $\tau = Ae^{W/kT}$ , where  $A$  is roughly of the order of  $10^{-12}$  and  $W$  is the "activation energy" that a pair of neighboring dissimilar atoms must have in order to surmount their potential barrier and exchange positions.

This expression for the relaxation time permits an estimate of the range of states that can be produced in an alloy by different heat-treatments. Rapid quenching will retain a degree of order characteristic of a high temperature, and annealing for several days will produce a degree of order characteristic of a lower temperature; but the calculations indicate that these two temperatures will differ by only about 30 percent (on the absolute-temperature scale) because of the rapid change of  $\tau$  with  $T$ . Bragg and Williams estimate from resistance curves that, for  $\text{AuCu}_3$ ,  $\tau$  is 1 sec. at about  $550^\circ\text{C}$ . (a temperature above the transition point), which accounts for the fact that complete disorder can be main-

\* H. J. SEEMANN and E. VOGT, *Ann. Physik*, vol. 2, p. 976, 1929. B. SVENSSON, *Ann. Physik*, vol. 14, p. 699, 1932.

<sup>1</sup> F. C. NIX and W. SHOCKLEY, *Rev. Modern Phys.*, vol. 10, p. 1, 1938.

<sup>2</sup> A. J. BRADLEY and J. W. RODGERS, *Proc. Roy. Soc. (London)*, vol. A144, p. 340, 1934. O. HEUSLER, *Ann. Physik*, vol. 19, p. 155, 1934.

<sup>3</sup> E. FRIEDERICH and A. KAUSMANN, *Physik. Z.*, vol. 36, p. 185, 1935.

<sup>4</sup> F. C. NIX and W. SHOCKLEY, *Rev. Modern Phys.*, vol. 10, p. 1, 1938.



tained by quenching. Because of sluggish diffusion, prolonged annealing at temperatures below  $270^{\circ}\text{C}.$ , on the other hand, could not be expected to produce degrees of order corresponding to temperatures much below  $270^{\circ}\text{C}.$  where the equilibrium order  $S$  is approximately 0.75. In the case of Cu-Zn the rate of diffusion is so fast ( $\tau$  so small) that it is impossible to retain the disordered structure by quenching, and the alloy at room temperature is always highly ordered.

It appears likely, however, that this treatment of the problem overlooks some important complications. There is much reason to believe that as an alloy is cooled below  $T_c$  a number of nuclei start to grow independently of one another and with a noncoherent relation to one another. Their growth must continue until they touch, and then they must coalesce until the whole of a grain—or the whole of some natural subdivision of a grain—contains a coherent array with no out-of-phase regions remaining unabsorbed. Experiments of Sykes and Evans<sup>1</sup> have suggested that the rate of ordering within each nucleus may be as much as a thousand times faster than the rate of growth and coalescence of the nuclei. Once the coalescence has been completed, subsequent alterations in order seem to be at the rapid rate characteristic of a nucleus.

**Compounds, Superlattices, and Solid Solutions Compared.**—The interactions among atoms may be so strong ( $V$  so great) as to cause the virtual value of the critical temperature  $T_c$  to lie above the melting point. Such is the case in phases that are ordered at all temperatures in the solid state. An example seems to be  $\text{Cu}_3\text{Sb}$  (with  $\text{Fe}_3\text{Al}$  structure), and  $\text{AuZn}$  is another (with the  $\text{CsCl}$  structure). Alloys with these characteristics closely resemble true chemical compounds.

It will be seen that the whole range of intermetallic structures can be considered from this point of view. When atomic interactions are strong, they may retain order, as in a compound, up to a temperature at which another phase has a lower free energy and begins to form; taking as an example  $\text{AgZn}$ , the new phase is another solid of different crystal structure, while in  $\text{AuZn}$  the new configuration is the liquid phase. With less intense ordering forces between the atoms the ordered arrangement may decrease gradually to a low value or to zero at the critical temperature. Finally, if  $V$  is very small—and this must be true at low concentrations in terminal solid solutions, since any ordered array would put the solute atoms far apart on the lattice—the critical temperature will be below room temperature, or at least so low that the atoms will not diffuse appreciably into their ordered positions.

The behavior of an alloy will thus be governed largely by two constants, the interaction energy  $V_0$ , which is the net amount of work necessary to switch a pair of atoms into disordered positions in the fully

<sup>1</sup> C. SYKES and H. EVANS, *J. Inst. Metals*, vol. 58, p. 255, 1936.

ordered alloy, and the activation energy  $W$  that the atoms must acquire in order to make the exchange. Approximate values<sup>1</sup> for these in AuCu, expressed in electron volts, are  $V_0 = 0.3$ ,  $W = 1.85$ . The value  $W$  may also be converted to calories,  $Q$  ( $Q = 23,066W$ ), and will then be seen to be of the same order as the heats of activation for diffusion in solid solution.<sup>2</sup> It is also of the same order of magnitude as the heats of activation for recovery from cold work; for example, in experiments<sup>3</sup> on permalloy the rate of sharpening of broadened x-ray diffraction lines has yielded the value  $W = 1.7$  electron volts.

<sup>1</sup> W. L. BRAGG and E. J. WILLIAMS, *Proc. Roy. Soc. (London)*, vol. A145, p. 699, 1934.

<sup>2</sup> R. F. MEHL, *Trans. A.I.M.E.*, vol. 122, p. 11, 1936.

<sup>3</sup> J. F. DILLINGER, *Phys. Rev.*, vol. 49, p. 863, 1936.

## CHAPTER XIII

### THE ELECTRON THEORY OF METALS AND ALLOYS

The physicists who in recent years have applied the mathematics of quantum mechanics to the problems of the metallic state have greatly increased our understanding of the phenomena of physical metallurgy, including conductivity, magnetism, specific heat, lattice energy, and alloy structure. The details of the theories they have developed are often of great complexity and are presented in a mathematical language to which most people are allergic, but the results can be presented in a simple manner. A summary of certain results of general interest is given below, with a minimum outline of the reasoning by which they were derived. For details and comprehensive treatments the reader is referred to the books of Mott and Jones<sup>1</sup> and Seitz<sup>2</sup>, and to the review articles.<sup>3</sup>

**Metallic Binding.**—It is now well established that the atoms in metal crystals are ionized and that a metal should be thought of as an assemblage of positive ions immersed in a cloud of electrons. The electrons of this cloud are relatively “free”: they are not bound to any particular ion but move rapidly through the metal in such a way that there is always an approximately uniform density of them throughout the interior between the ions. Metal crystals are held together by the electrostatic attraction between this “gas” of negative electrons and the positively charged ions. The binding forces in metals are thus in sharp contrast to those in nonmetallic substances, where the predominating forces are from one atom to another or from positive to negative ions.

**Cohesive and Repulsive Forces in Metals.**—Wigner and Seitz<sup>4</sup> have shown a convenient way to calculate the attractive forces between the positive ions and the electrons of a metal. Planes are drawn bisecting the lines joining an atom to each of its neighbors; these planes then form polyhedra surrounding each atom of the crystal. The polyhedra are

<sup>1</sup> N. F. MOTT and H. JONES, “The Theory of the Properties of Metals and Alloys,” Oxford, New York, 1936.

<sup>2</sup> F. SEITZ, “The Modern Theory of Solids,” McGraw-Hill, New York, 1940; “The Physics of Metals,” McGraw-Hill, New York, 1943.

<sup>3</sup> J. C. SLATER, *Rev. Modern Phys.*, vol. 6, p. 209, 1934. N. F. MOTT, *Science Progress*, vol. 31, p. 414, 1937. F. SEITZ and R. P. JOHNSON, *J. Applied Phys.*, vol. 8, pp. 84, 186, 246, 1937. W. SHOCKLEY, *Bell System Tech. J.*, vol. 18, p. 645, 1939.

<sup>4</sup> E. WIGNER and F. SEITZ, *Phys. Rev.*, vol. 43, p. 804, 1933; vol. 46, p. 509, 1934. E. WIGNER, *Phys. Rev.*, vol. 46, p. 1002, 1934.

convenient units for the calculation of the energy of the lattice, for each polyhedral cell contains one ion and, on the average, one free electron (in monovalent metals). The potential energy of the lattice consists of (1) the energy arising from the positive and negative charge in each polyhedron and (2) the energy of the interaction of each polyhedron with its neighbors. The second of these two energies is very small, since each cell is electrically neutral and is nearly the shape of a sphere; this term can therefore be treated as a small correction—amounting to 1 percent or less—to the calculation of the energy of interaction between the positive and negative charges in one cell. The polyhedra, which are rhombic dodecahedra in face-centered cubic lattices, can be replaced by spheres for approximate calculations since they are nearly spherically symmetrical.

Balanced against the attraction of each positive ion for the negative electrons that happen to be within its electrostatic field are two principal repulsive forces: (1) the mutual repulsion of the electrons in the electron gas (this may be termed the “pressure” of the gas) and (2) the repulsion between ions that are in contact. Calculations show that the pressure of the gas is not inversely proportional to its volume  $V$ , as with an ordinary gas, but is proportional to  $1/V^{\frac{1}{3}}$ .

The free electrons thus contribute two opposing terms to the potential energy of the lattice. The attractive force is furnished by the potential energy of the electrons in the electric field of the ions; this energy varies inversely as the mean distance between ions, therefore as  $-1/V^{\frac{1}{3}}$ . The repulsive force derives from the kinetic energy of the electron gas; this energy varies as  $1/V^{\frac{1}{3}}$ . Summing these two terms gives

$$E = \frac{A}{V^{\frac{1}{3}}} - \frac{B}{V^{\frac{1}{3}}} \quad (1)$$

where  $A$  and  $B$  are constants and  $V$  is the volume of the metal.

It has been shown<sup>1</sup> that for monovalent crystals this energy  $E$  is approximately equal to the total energy of the crystal, other terms being negligible. If computations are carried out for various assumed values of the lattice constant of a metal,  $E$  is found to vary in the manner illustrated in Fig. 1 (a plot for sodium). The minimum on a curve of this type gives the theoretical prediction of the lattice constant. The difference in energy between this minimum and the value of  $E$  for an infinitely large lattice constant is the energy that would be required to remove the atoms from the crystal and scatter them to infinity; this is the heat of sublimation. The curvature of the curve at the minimum

<sup>1</sup> For details, see N. F. MOTT and H. JONES, “The Theory of the Properties of Metals and Alloys,” Chap. IV, Oxford, New York, 1936; FREDERICK SEITZ, “The Modern Theory of Solids,” Chap. X, McGraw-Hill, New York, 1940.

is directly related to the compressibility of the crystal. Bardeen's<sup>1</sup> theoretical values of lattice constant, heat of sublimation, and compressibility are compared with observed values in Table XII.

TABLE XII

Physical property	Lithium	Sodium
Lattice constant, (Å):		
Observed.....	3.46	4.25
Calculated.....	3.49	4.53
Heat of sublimation, k-cal. per gram atom:		
Observed.....	39	26
Calculated.....	34	23
Compressibility, sq. cm. per dyne:		
Observed.....	$7.4 \times 10^{-12}$	$12.3 \times 10^{-12}$
Calculated.....	$8.4 \times 10^{-12}$	$12.0 \times 10^{-12}$

For the noble metals the atom cores as well as the valence electrons must be taken into account, or otherwise the predicted compressibility would be too high. It appears that with the metals Cu, Ag, and Au—and probably many others—the inner shells of the atoms come into

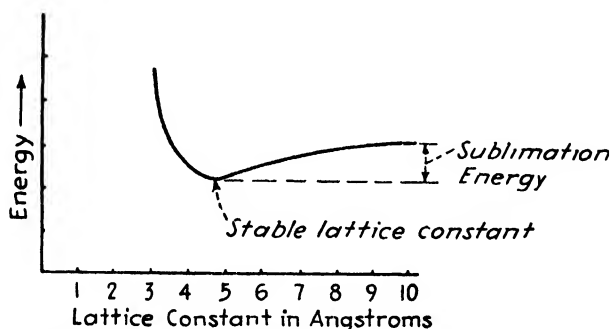


FIG. 1.—Variation of energy with lattice constant. Computed for sodium.

contact and begin to overlap before the lattice constant is reduced to the minimum point on the curve corresponding to Fig. 1. A strong repulsion then sets in, and the energy curve turns upward more steeply than in Fig. 1; therefore, the compressibility is lower. One may properly think of these metals as composed of hard spheres in contact. The spherical ions are held in their tight-packed array by the attraction between them and the electron gas in which they are immersed.

The theoretical prediction of what type of crystal structure will be the most stable for any element is a task too difficult for quantum mechanics in its present state. In the first place, its proper method of attack would be to calculate the energy of every possible crystalline

<sup>1</sup> J. BARDEEN, *J. Chem. Phys.*, vol. 6, pp. 367, 372, 1938.

arrangement of atoms to see which has the lowest energy. But even if this infinitely laborious task were possible, the results would be unreliable, for the best of the present methods of calculation can yield an accuracy of only about 5 k. cal. per mol, and the difference between a stable structure and an unstable one may be much less than this. Some theories have succeeded, however, in bringing out *differences* in energies between different structures in such a way as to give useful results in spite of the uncertainties about the total energies; these are discussed in a subsequent section (page 265).

The resistance of metals to cleavage may be understood as arising from electrostatic attraction, since any force tending to pull the ions apart also tends to increase the average distance between ions and their neighboring electrons. Cleavage at grain boundaries is resisted by the same attractive force, since the electron gas is presumed to be substantially the same at a boundary as elsewhere. Most of the energy of the lattice arises from the interactions within each polyhedron; *i.e.*, it depends on electrostatic attraction over very short distances, a fact which suggests that disarranged atoms at a grain boundary should not appreciably reduce cohesion across the boundary. This point of view also provides an answer to the question, "Why does a metal not fall apart when slip is occurring?" For even if there is a high state of disorder possibly approximating a molten condition at the slipping surface, there still remains the electrostatic attraction holding the crystal together.

**Electron Energies in a Metal.**—Many important advances in the theory of metals have been made by studying the movement of valence electrons in metals. In the first important theory of electrical conduction, the Drude-Lorentz theory, it was assumed that in the interior of a metal the electric field is uniform. The conduction electrons in this uniform field were believed to be a sort of gas that is free to drift about whenever an electric field is applied externally, as, for example, when wires from a battery touch the metal. The drift of electrons creates an electric current, and the collisions of the electrons with the ions of the metal interfere with the flow and cause electrical resistance.

The general outlines of this theory are still valid, but it has been so elaborated from its early form as to be almost unrecognizable. The modern theories are based on the fact that a moving electron does not act as if it were a small hard particle but behaves as if it were a system of waves. These waves that constitute the electron (or, better, that describe the motion of the electron) have a definite wavelength that depends upon the velocity of the electron according to the relation

$$\lambda = \frac{h}{mv} \quad (2)$$

where  $\lambda$  is the wavelength,  $v$  is the velocity of the electron,  $m$  is the mass of the electron, and  $h$  is a constant known as Planck's constant.

The problem was undertaken of calculating the velocities that a wavelike electron could have as it moved around in a metal within which the electric field was assumed to be uniform. The problem is analogous to that of calculating what various modes of elastic vibration are possible for the solid block of metal, *i.e.* its natural frequencies. In both the sound-wave problem and the electron-wave problem a series of modes of vibration are found with different wavelengths, like the fundamental tone and the overtones of a vibrating string. Each mode of vibration corresponds to a definite wavelength according to the relation given in Eq. (2). As a consequence of this, the electron is permitted to have only certain discrete velocities in the metal. If an electron were made to go faster and faster through a crystal, it would increase its velocity by jumps, not continuously, and if we could hear the waves belonging to this electron we should hear a scale composed only of the harmonics of some fundamental tone, not the continuously ascending wail of a siren. The kinetic energies of the electrons are related to their velocities by the equation

$$E_{\text{kin}} = \frac{1}{2}mv^2 \quad (3)$$

and by Eq. (2) this may be written in terms of electron wavelengths:

$$E_{\text{kin}} = \frac{h^2}{2m\lambda^2} \quad (4)$$

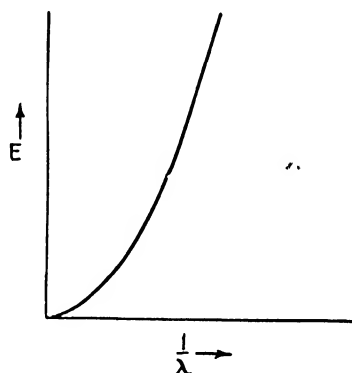


FIG. 2.—Energy of an electron moving in a uniform field of force.

The energy thus varies with wavelength as in Fig. 2, along a parabolic curve. This curve could be properly drawn as a string of closely spaced dots representing the closely spaced energy values that are permitted an electron in a crystal.

There are a great many energy values—**energy levels**, as they are called—that are permitted an electron in a crystal; in fact, there are more levels than there are electrons. To determine which of these possible energy levels will actually be occupied by electrons, it is necessary to make use of **Pauli's exclusion principle**, which states that only two electrons can exist in any one energy level in the entire crystal. The two electrons in one energy level must be spinning in opposite directions. Suppose we were to build a crystal by starting with a lattice of positive atom nuclei and adding the electrons one by one until the crystal became electrically neutral. The first electrons added would fill the lowest energy levels, where they would be tightly bound to the

individual nuclei. These would be the ones that would take part in the processes of x-ray emission, discussed in Chap. III. As these levels became filled, two electrons going to each level, succeeding additions would go to higher levels. When all the electrons had been placed, we should find all the lower levels up to some maximum energy completely filled and all the levels above this empty.

The theory just outlined is more successful than the earlier Drude-Lorentz theory in explaining certain physical properties of metals, particularly their specific heats. The earlier theory postulated a gas of free electrons in a metal; if each particle of this gas were to behave as a particle of an ordinary gas, it would have a heat capacity of  $\frac{3}{2}k$ , where  $k$  is the gas constant. But the total contribution to the specific heat of the metal from the conduction electrons when computed on this basis is

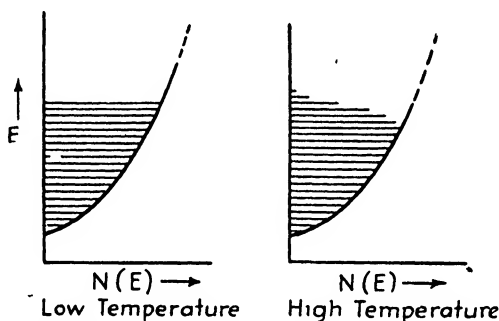


FIG. 3.—Effect of temperature on distribution of electron energies,  $E$ , in a metal. Curve gives allowed number of levels,  $N(E)$ , in each energy interval; horizontal lines give actual number (schematic).

much too great, about a hundred times greater than the observed value. The newer concept removes this discrepancy, for only a small proportion of the electrons contribute to the specific heat. When the temperature of a metal is raised, the electrons in the lower energy levels cannot accept any thermal energy because for them to do so would require that they move up to a level that is slightly higher than the one they are in and there are no available empty spaces in the tightly filled band of levels that would permit this. Only the electrons at or near the very top of the layer of filled levels are able to find vacant levels above them and are able, therefore, to accept additional energy. This may be represented schematically by the sketches in Fig. 3 for a crystal at a low temperature (Fig. 3a) and at a high temperature (Fig. 3b). The number,  $N(E)$ , of allowed energy levels in each interval on the energy scale is indicated by the horizontal distance out to the curve; the number of levels in each interval that are actually filled is indicated by the lengths of the horizontal lines. The electrons at the top of the filled region may be said to be “splashed” up to higher energies by the heat waves.



**The Zone Theory of Solids.**—An extremely important advance in this theory was made by discarding the assumption that the electrons move in a uniform electric field within a crystal and investigating the problem of electrons moving in a periodically varying field. The crystalline array of positive charges (the positive ions) produces a crystallographically varying field which interacts with the wave of the electron. Under these circumstances, the electrons can be diffracted by the lattice of ions just as x-rays are diffracted, and in fact the condition for diffraction is the same as the Bragg condition for reflection, *viz.*,  $n\lambda = 2d \sin \theta$ , where  $\lambda$  is now the electron wavelength. The reflection of electrons within the crystal changes the relation between wavelength and energy sketched in Fig. 2. There can be no electrons in the crystal that have an energy just correct for reflection (if they also have a direction of motion that is correct for reflection). In other words, there is a gap in the allowed energy levels, as indicated in Fig. 4. It will be seen from the figure that electrons having wavelengths slightly greater than the critical wavelength for Bragg reflection have their energies depressed below the value of the smooth parabolic curve, while those having wavelengths slightly less than the critical wavelength have their energies raised, leaving a gap in energy.

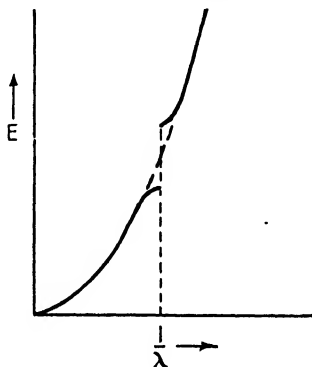


FIG. 4.—Energy of an electron moving in the periodic field of a crystal. Gap in curve results from diffraction of electrons with critical direction and velocity.

The gaps in the allowed energy levels depend upon reflection of the electrons and therefore upon the direction of motion of electrons, and they will occur at different energy values for electrons going in different directions. In some crystals the gaps for differently directed electrons happen to coincide and leave a range of energy that is forbidden to electrons whatever their velocity and direction of motion. In other crystals the gaps for one direction of electron motion overlap the curves for another direction, and the gaps are effectively closed. Davisson and Germer's electron-diffraction experiments which proved the wave nature of the electron also indicated the existence of these gaps, for when critically directed and accelerated electrons were directed at a nickel crystal the electrons did not penetrate the crystal but reflected from it. The gaps divide the spectrum of energies into **zones**, or **bands** (**Brillouin zones**).

The energy levels just discussed are represented mathematically by the various solutions of Shrödinger's wave equation.<sup>1</sup> If the equation is set up for a crystal conceived as a box, with abrupt boundaries on all

<sup>1</sup> Shrödinger's equation for an electron of mass  $m$  moving with constant total energy  $E$  in a potential field  $V(x, y, z)$  is

sides and a uniform potential everywhere within the box, the solutions of the wave equation lie along the curve of Fig. 2; this was the model on which Sommerfeld's theory of electrical conduction was based. Now if the wave equation is written for a periodic field, such as must exist in a crystal composed of a periodic array of atoms or ions, the solutions have the discontinuities shown by the full line in Fig. 4.

There is a strict analogy between x-ray and electron diffraction and the motion of valence electrons through the lattice. Atomic planes that have large values of the structure factor and thus reflect x-rays strongly give rise to large gaps in the allowed energy levels, while planes of small structure factor cause little deviation from the parabolic curve. Let us see how these zones and gaps are related to the energy levels of isolated atoms.

In an isolated atom the energy levels of an electron are relatively few and are represented on a diagram such as has been drawn to explain x-ray emission (page 50).<sup>1</sup> When a number,  $N$ , of atoms are brought together to form a solid, each individual level of the atom becomes spread

$$\frac{\partial^2 \psi}{\partial x^2} + \frac{\partial^2 \psi}{\partial y^2} + \frac{\partial^2 \psi}{\partial z^2} + \frac{8\pi m}{h^2} (E - V)\psi = 0$$

where  $h$  is Planck's constant and  $m$  is the electronic mass. To give physical significance to  $\psi$ , the wave function or amplitude, it was first assumed that  $\psi^2$  at any point is the electron density at that point; later,  $\psi^2$  was seen to be the *probability* of an electron being at a given point at a given instant. A "time exposure" of an electron in motion in an atom or a crystal would be a photograph of  $\psi^2$ .

Values of  $\psi$  that are finite, single valued, and continuous throughout space exist only for certain values of  $E$ . It is these values which are the allowed energies for electrons in an atom or a crystal.

<sup>1</sup> The energy states of an atom are defined in terms of four quantum numbers,  $n$ ,  $l$ ,  $m$ , and  $m_s$ . The energy level is fixed chiefly by the **principal quantum number**,  $n$ . The size of the orbit increases with  $n$ , which may have any positive integral value;  $n$  has the values 1, 2, 3 . . . for the  $K, L, M$  . . . electrons, respectively. The **angular momentum quantum number**,  $l$ , has a smaller effect on the energy levels; for those levels belonging to a given  $n$ , the number  $l$  may have any positive integral value from 0 to  $n - 1$ . Following the notation introduced by spectroscopists, the letters  $s, p, d, f, g, h, \dots$  are used to stand for  $l = 0, 1, 2, 3, 4, 5, \dots$ . A quantum state having  $n = 3$  and  $l = 2$  is known as a "3d" state and an electron occupying that state is a "3d electron." The **magnetic quantum number**,  $m$ , has a very small influence on energy levels. The **spin quantum number**,  $m_s$  (sometimes written  $S$ ), is related to the direction of rotation of the spinning electrons. This quantum number may be either  $+\frac{1}{2}$  or  $-\frac{1}{2}$ ; electrons occupying quantum states with  $m_s = +\frac{1}{2}$  are rotating oppositely to those with  $m_s = -\frac{1}{2}$ . The number of electrons in each state is commonly written as an exponent above the letter giving the angular-momentum quantum number. The electron configuration of helium, for example, is written  $1s^2$  since there are two electrons in the state  $n = 1, l = 0$ , while for lithium it is written  $1s^2 2s^1$  to indicate two additional electrons in the  $2s$  state for which  $n = 2, l = 0$ . Pauli's principle states that no two electrons in an isolated atom can have the same set of four quantum numbers.

into a series of  $N$  levels clustering in a band about the original level. Grains of ordinary size contain so many atoms (roughly  $10^{17}$ ) that the levels in the band form almost a continuum. The upper limit of a band is marked by a gap of the type illustrated in Fig. 4. Such bands of  $N$  levels into which the energy spectrum of a crystal is divided are called "zones" (Brillouin zones). The calculations of the distribution of levels in these zones, the extent to which they overlap or have gaps between them, and the extent to which they are filled with electrons are of first importance in predicting the physical properties of crystals.

**Zones in Conductors and Insulators.**—Figure 5a is a schematic plot of two zones in a crystal that is an insulator. The plot indicates the density of the levels, *i.e.*, the number of energy levels  $N(E)$  between

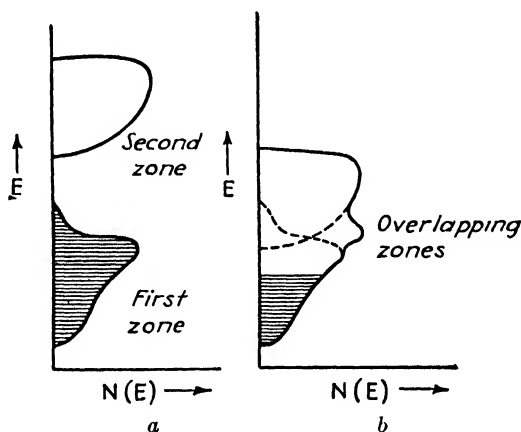


FIG. 5.—*a*, Illustrating gap between zones characteristic of an insulator; first zone filled. *b*, Possible zone configuration in a metal; partially filled and overlapping zones.

energy  $E$  and  $E + \Delta E$ , and shows two zones separated by an energy interval. The first zone is shaded to indicate that it is filled with electrons, while the second zone contains none. If an electric field is applied to this crystal, the field would tend to change the energy of the electrons by a small amount, causing the net drift in one direction that constitutes an electric current. But since every level in the zone is occupied, no electron can be transferred from one level to another in the zone. Furthermore, the electrons at the top of the first zone cannot move into the vacant levels of the second zone because the gap between the zones is large compared with the energy they can receive from the field. With all electrons anchored to their former energy states the application of an electric field is without effect, and the crystal is an insulator.

Consider now Fig. 5b, which represents a metal in which each atom supplies one valence electron. The first band is only half filled because the  $N$  atoms of the crystal have each contributed one valence electron to the zone of  $N$  levels and two electrons have gone into each level. An

electric field can now move any of the many electrons at the top of the filled portion of the band into one of the many vacant levels immediately above it in either band, and the electrons can have a net motion through the lattice in the direction of the field. The metal is therefore a conductor. Homopolar and ionic crystals possess narrow zones separated by gaps, and since there are an even number of valence electrons per atom all zones are completely filled. This is the condition for insulators.

Insulators may become conductors at elevated temperatures if the thermal agitation is sufficient to raise some electrons above the gap into the empty zone above. Or they may be made conducting by irradiation with light, provided that the energy transferred to some electrons by light quanta suffices to raise them into an unfilled zone. The so-called "semiconductors" appear to be made conducting by virtue of defects in the lattice (interstitial atoms, impurities, or vacant lattice points) which introduce additional energy levels into which the electrons can move.

The conception of filled or semifilled, overlapping or separated zones sketched above has been the first theory adequate to explain the tremendous range in electrical resistivities that are encountered among the elements, a range of  $10^{-6}$  for silver to  $10^{14}$  or so for diamond.

**Factors Affecting Electrical Resistance of Metals.**—The electron theory accounts for all the factors that alter the electrical resistance of metals.<sup>1</sup>

1. The resistance of metals increases with temperature. This is interpreted as the result of thermal vibrations of the atoms interfering with the motion of conduction electrons. Thermal motions of atoms in a crystal can be analyzed as the superposition of many sets of elastic waves of varying amplitude and wavelength. When an electron going in the right direction and with the right speed encounters one of these sets of waves, it is deflected (diffracted) from its normal path. As the number and amplitude of these elastic waves increase with temperature, scattering becomes more pronounced, the electron paths become more frequently interrupted, and the resistance increases.

2. Resistance increases with impurities and alloying. When atoms dissolve in a metal to form a random solid solution, the resistance is always increased. This is accounted for by the distortions produced in the lattice by the foreign atoms. The disturbances cause scattering of the conduction electrons, thereby hindering electron flow and increasing resistance, both at low temperatures and at elevated temperatures.<sup>2</sup>

<sup>1</sup> F. SERTZ, "The Modern Theory of Solids," McGraw-Hill, New York, 1940; "The Physics of Metals," McGraw-Hill, New York, 1943.

<sup>2</sup> Superconductivity, the abrupt drop in resistance to nearly zero which occurs in many metals at temperatures near absolute zero, is not covered by any well-developed theory at the present time.

3. Resistance increases with increasing randomness in a superlattice. A well-ordered superlattice possesses a low electrical resistance, but the irregularities introduced when disorder begins cause increased scattering of electrons.

4. Cold work increases electrical resistance. This may be attributed to the presence of locally distributed internal strains, including disturbances at boundaries between grain fragments, and disturbances around the imperfections or places of misfit in the lattice, the "dislocations." The local disturbances scatter the electrons and increase the resistance.

5. Precipitation from solid solution during aging is also believed to set up internal strains which scatter the electrons as well as harden the alloy. Another possible origin of resistance during age hardening is the scattering of electrons from precipitated crystals. It has been proposed that this becomes pronounced when the dimensions of the particles become approximately the same as the wavelength of the conduction electrons, a few atom diameters.<sup>1</sup>

**Energy Levels and Ferromagnetism.**—A metal that is strongly attracted by a magnet is "ferromagnetic." Slater<sup>2</sup> has advanced a theory of ferromagnetism in the elements near iron in the periodic table, based on a calculation of the zones in the element copper.<sup>3</sup>

In Fig. 6 the  $N(E)$  curves are plotted for two zones of Cu, those known<sup>4</sup> as 4s and 3d. Assuming that these  $N(E)$  curves do not change appreciably throughout the ferromagnetic elements, iron, cobalt, nickel, and their alloys, it is possible to indicate the top of the filled levels for the various metals on a single plot. This is done in Fig. 6 by dotted lines that are labeled with the number of 3d and 4s electrons per atom. The outer shell of electrons, 4s, which forms the "gas" of free electrons, is filled to the line numbered 11 in copper and to the lines numbered 10, 9, and 8, respectively, in nickel, cobalt, and iron. The next inner shell of electrons, 3d, is completely filled in copper but is only partly filled in the transition elements from nickel (line 10) to scandium (line 1). All these elements, therefore, have zones only partly filled with valence electrons and for this reason are conductors.

Figure 6 serves as a basis for an understanding of ferromagnetism. The elementary magnets of a ferromagnetic material are the electrons

<sup>1</sup> This theory does not appear to be confirmed by data on the precipitation from the solid solution of silver in aluminum, for maximum effect on resistance is found when the particles are much larger than conduction-electron wavelengths. (A. H. Geisler, C. S. Barrett, and R. F. Mehl, *Tech. Pub.* 1557, Metals Technology, February, 1943.) Aging is discussed further in Chap. XXI.

<sup>2</sup> J. C. SLATER, *J. Applied Phys.*, vol. 8, p. 385, 1937.

<sup>3</sup> H. M. KRUTTER, *Phys. Rev.*, vol. 48, p. 664, 1935.

<sup>4</sup> The nomenclature is given in the footnote, p. 258.

which are spinning about an axis through their center. In a magnetic field the electrons are limited to two orientations only: the magnetic moment caused by the spinning electricity must be directed either parallel to the field or opposite to the field, "antiparallel." When there are two oppositely directed electrons in a given shell, their moments cancel and there cannot be a large magnetic moment in one direction as is necessary

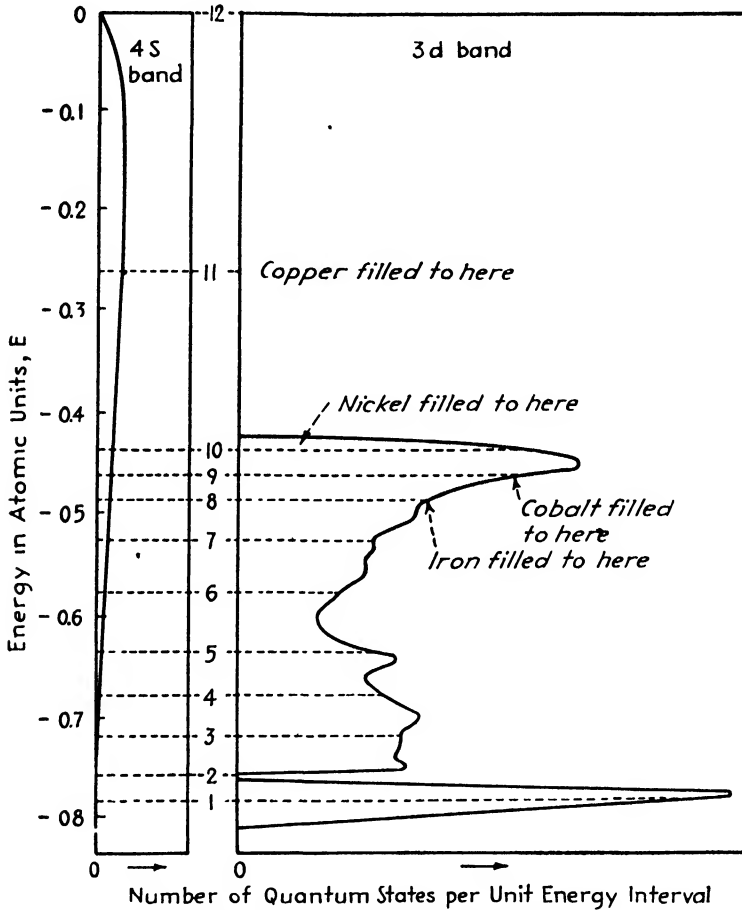


FIG. 6.—Zone configuration in copper and iron-group elements. (Krutter, Slater.)

for the material to be ferromagnetic. This condition of balanced spins prevails for most elements in the periodic table. The ferromagnetic elements, however, contain partly filled 3d shells as indicated by Fig. 6. Although the 3d band of levels is capable of holding 10 electrons per atom, 5 directed each way, there are believed to be in a crystal of iron an average of only 7.3 electrons in this shell per atom. A maximum number of these will be directed parallel to the field, but since there are spaces for only 5 directed this way there remain 2.3 electrons that must spin in the opposite direction. The net result is  $5 - 2.3 = 2.7$  unpaired

electrons to produce the ferromagnetism. The net magnetic moment is therefore equal to the number of empty spaces in the  $3d$  band. Similar calculations show that the unpaired  $3d$  electrons in cobalt, nickel, and copper are 1.7, 0.6, and 0 per atom, respectively. These net magnetic moments agree very well with the saturation magnetization for these elements.

The number of unpaired electrons in the  $3d$  band can be altered at will by forming a solid solution of a ferromagnetic element with an element having a different number of valence electrons. Thus if nickel is alloyed with increasing amounts of copper, the electron-atom ratio (the electron concentration) will gradually be increased and the vacancies in the  $3d$  band will be progressively filled. Measurements show that the ferromagnetism steadily decreases in this series of alloys and finally vanishes at almost exactly the composition where the band is completely filled. Many other series of alloys have been studied in which Cr, Mn, Fe, Co, Ni, and Cu are alloyed with one another, and it is well established that electron concentration, which fixes the number of unpaired electrons in the  $3d$  band, is the factor that governs the amount of ferromagnetism—the magnetic moment at saturation. Another condition that must be met if an atom is to be ferromagnetic is that the radius of the  $3d$  shell must bear a certain relation to the interatomic distance.<sup>1</sup> This is because the atoms must be the right distance apart in order that the electrons in one atom can align the spins in neighboring atoms.

The tendency to align the electron spins in neighboring atoms is opposed by the tendency of thermal agitation to induce disorder. It will be recalled that an analogous battle between opposing tendencies goes on in superlattices with regard to ordering and disordering of atoms. The balance between ordering and disordering forces produces a net magnetization that falls with increasing rapidity as the temperature is raised, along a curve very similar to a superlattice order curve, reaching zero at the critical temperature known as the Curie point.

The magnetic ordering force in ferromagnetic metals fails to align the electrons of all atoms in a crystal into a uniform “long-distance order.” The magnetic moments of atoms in a small portion of a grain are aligned one way and those in the adjoining portions are aligned in the opposite way, forming alternating bands across a crystal. These subdivisions, known as domains, are of varying sizes in the range  $10^{-13}$  to  $10^{-8}$  cc. or  $10^{10}$  to  $10^{15}$  atoms, as indicated by the magnitude of the magnetic impulse they cause when their direction of magnetization is reversed<sup>2</sup> (the Barkhausen effect). When one magnetizes a ferromagnetic

<sup>1</sup> J. C. SLATER, *Phys. Rev.*, vol. 36, p. 57, 1930. W. SHOCKLEY, *Bell System Tech. J.*, vol. 18, p. 645, 1939.

<sup>2</sup> R. BOZORTH and J. DILLINGER, *Phys. Rev.*, vol. 35, p. 733, 1930.

crystal, the properly oriented domains grow at the expense of the others until at saturation all are parallel to the applied field. There is much interest in the studies of Bitter, McKeehan, and Elmore,<sup>1</sup> who have deposited magnetic colloidal powers on a polished surface to show the pattern made by these domains and the alterations in the pattern caused by reversing the applied field. When viewed under a microscope, the patterns show remarkable complexity and many interesting crystallographic features.

**Paramagnetism and Diamagnetism.**—Substances that are very weakly attracted by a magnet are called paramagnetic and substances that are repelled, diamagnetic. Paramagnetism is dependent upon the tendency of a permanent magnet to align itself parallel to a magnetic field in which it is placed. The elementary magnets that undergo alignment are the individual spinning electrons. It will be recalled that in each energy level there are two electrons with oppositely directed spins. When a magnetic field is applied, there is a tendency for some of these to shift the direction of their spins into parallelism with the field. However, this shifting involves a slight change in energy and cannot take place unless there are vacant levels into which the shift can be made. Whenever there are bands that are only partly filled, such appropriately located levels will be found; this is the situation, we have seen, in all conductors. From this point of view all the common metals, which are good conductors, should be paramagnetic unless the conditions in their *3d* bands happen to be right for ferromagnetism. Furthermore, an insulator should be neither ferromagnetic nor paramagnetic, for the bands in an insulator are crowded to capacity and are separated by gaps from all unfilled bands.

It is, in fact, the rule for insulators to be diamagnetic, but the prediction that conductors should be paramagnetic breaks down about half the time. Diamagnetism in insulators and in conductors is due to the motion of the electrons in their orbits around the atom nuclei, this motion being altered by an applied field in a manner such as to set up a repulsive force. This closed-orbit magnetic effect sometimes overbalances the magnetic moment from reversed spins and makes a conductor diamagnetic instead

<sup>1</sup> E. BITTER, "Introduction to Ferromagnetism," McGraw-Hill, New York, 1937. *Phys. Rev.*, vol. 38, p. 1903, 1931; *Phys. Rev.*, vol. 41, p. 507, 1932. W. C. ELMORE and L. W. MCKEEHAN, *Phys. Rev.*, vol. 46, pp. 226, 529, 1934. W. C. ELMORE, *Phys. Rev.*, vol. 51, p. 982, 1937; *Phys. Rev.*, vol. 58, p. 640, 1940. F. W. CONSTANT and J. M. FORMVALT, *Phys. Rev.*, vol. 56, p. 373, 1939. W. C. ELMORE, *J. Applied Phys.*, vol. 10, p. 724, 1939; *Phys. Rev.*, vol. 53, p. 757, 1938. W. C. ELMORE and L. W. MCKEEHAN, *Trans. A.I.M.E.*, vol. 120, p. 236, 1936. W. C. ELMORE, *Phys. Rev.*, vol. 54, p. 389, 1938. H. S. AVERY, V. O. HOMERBERG, and E. COOK, *Metals & Alloys*, November, 1939, p. 353.



of paramagnetic, a situation most likely to happen when the 3d band is just filled.

**Zone Theory of Alloy Phases.**—There is considerable promise that the zone theory will afford an understanding of alloy phases and constitution diagrams. Much, in fact, has already been accomplished in this field. The zone theory of alloy structures can be summarized by saying that an alloy will assume that type of crystal structure in which there are enough *low-energy* states to accommodate all the electrons. Given the structure of a phase, it is possible to calculate at least approximately the zones and how they are filled. If the electrons fill the levels of one zone and must spill over into the lower levels of another zone which is separated from the first by a gap, they will have an abnormally high energy; the crystal as a whole may then have higher energy than some other structure in which this does not occur. When the ratio of valence electrons to atoms in an alloy is gradually increased by adding successive amounts of a higher valence metal, the upper limit of the filled levels moves up slowly until a zone is nearly filled. Further additions then result in a rapid increase in the energy (particularly if the next zone is separated from the first by a gap). Jones<sup>1</sup> has found that at this point a new phase begins to appear in the alloy. The predicted values for the electron-atom ratios in the structurally analogous phases (see Chap. XI, page 211) agree with the observed values remarkably well (Table XIII) in spite of the fact that the calculations were only approximate.

TABLE XIII

Phase	Hume-Rothery's value	Jones's value
$\alpha$	.	1.362
$\beta$	$\frac{3}{2} = 1.5$	1.480
$\gamma$	$\frac{21}{12} = 1.615$	1.538
$\eta$	$\frac{7}{4} = 1.75$	1.7

Jones's value for the limit of solubility of the  $\alpha$  phase, 1.362, is in satisfying agreement with the observed electron-atom ratios listed in Table XIV. The solubility of the  $\beta$  subgroup elements in magnesium, zinc, and cadmium has been discussed along similar lines.<sup>2</sup>

In general it can be said that the theory of zones in alloys should eventually lead to a unified theory for most of the equilibrium lines on

<sup>1</sup> H. JONES, *Proc. Roy. Soc. (London)*, vol. A144, p. 225, 1934; vol. A147, p. 396, 1934. N. F. MOTT and A. JONES, "The Theory of the Properties of Metals and Alloys," Oxford, New York, 1936.

<sup>2</sup> W. HUME-ROTHERY and G. V. RAYNOR, *J. Inst. Metals*, vol. 63, p. 227, 1938.

TABLE XIV

Alloy	Maximum Solubility
Cu-Zn	1.384
Cu-Al	1.408
Cu-Ga	1.406
Cu-Si	1.420
Cu-Ge	1.360
Cu-Sn	1.270
Ag-Cd	1.425
Ag-Zn	1.378
Ag-Hg	1.35
Ag-In	1.40
Ag-Al	1.408
Ag-Ga	1.380
Ag-Sn	1.366
Theoretical	1.362

phase diagrams. Even now we can see that when alloys have the same crystal structure and the same electron concentration they should have identical or very similar systems of zones, they should have these zones filled to nearly the same level, and consequently they should have very similar properties. Hume-Rothery's results on the liquidus and solidus curves for solid solutions of copper and silver, which showed similar temperatures for similar electron concentrations, are examples of this principle. The Hume-Rothery rules relating intermediate phases in structurally analogous systems to electron concentration are another example. Our understanding of phase transformations in metals and the effects of alloying on them will doubtless be greatly increased in the next few years as a result of the theories that have been briefly sketched in this chapter.

## CHAPTER XIV

### STRESS MEASUREMENT BY X-RAYS

X-ray diffraction as a means of determining stresses is finding increasing application. For some problems it offers definite advantages over all other types of strain gauges. It is the only method by which stresses can be determined without having measurements on the structure in the unstressed condition. Consequently it is the only method of determining residual, "locked-up" stresses in an object without cutting up the object so as to relieve the stresses—it is the only truly nondestructive test for residual stresses. The method detects elastic stresses only, while other strain gauges are affected by both elastic and plastic strains. This is a result of the fact that the x-ray method is fundamentally a measure of interatomic spacings, which are altered by elastic stresses but not by plastic flow. The x-ray beam that is employed strikes an area roughly  $\frac{1}{8}$  in. in diameter and determines the strain within this area as contrasted with the usual strain gauge, which employs a gauge length of 1 in. or more. This is a useful feature of the method in the study of localized stresses and steep stress gradients.

The peculiarities of the method are not all to its advantage. All recording is done photographically at the present time, and while the exposures may be reduced to a quarter of an hour or less it obviously cannot compete with mechanical or electrical gauges in speed. It requires equipment more costly and more cumbersome than the competitive devices. It registers only the stresses in the *surface* of a metallic object because the radiation does not penetrate appreciably into the interior; it therefore deals always with a biaxial stress since the stress component perpendicular to the surface is always zero. Perhaps the most unfortunate characteristic of the method is that it is satisfactory only for metals that yield reasonably sharp diffraction lines. With fine-grained annealed steel it is capable of the very satisfactory accuracy of 2000 or 3000 psi., but with cold-worked or quenched steels that give diffuse lines the error is four or five times this and the method (in its present state of development) is seldom of value.

The pioneer work on the method was done by Lester and Aborn<sup>1</sup> in 1925. It was shown that the spacing  $d$  of the atomic planes is altered by

<sup>1</sup> H. H. LESTER and R. H. ABORN, *Army Ordnance*, vol. 6, pp. 120, 200, 283, 364, 1925-1926.

applied stresses. The distance  $d$  acts as a gauge length, and changes in this length enable the elastic strains to be measured and the stresses to be computed. The strain can be determined by Bragg's law

$$n\lambda = 2d \sin \theta$$

from measured values of the diffraction angle  $\theta$ . When back-reflection cameras were applied to the problem in 1930,<sup>1</sup> it became apparent that under favorable conditions the x-ray strain gauge could compete in accuracy with other types of strain gauges.

In the first applications only the *sum* of the principal stresses existing at the surface was determined. Later it was shown that the principal stresses can be determined individually<sup>2</sup> and that an exposure of the material in the unstressed state was unnecessary<sup>3</sup> since the unstressed value of  $d$  can be computed from two measurements on the stressed metal. Numerous techniques and methods of computation have been proposed, but only the more satisfactory ones will be presented here. While the equations for some of these are complex, it should be understood that in routine work it is almost always possible to reduce the computations to simple slide-rule operations requiring but a minute or two. Some fundamental principles of stress and strain in elastic bodies will first be reviewed.

**Elastic Stress-Strain Relations.**—Strain,  $\epsilon$ , is defined by the relation

$$\epsilon = \frac{\Delta l}{l} \quad (1)$$

where  $\Delta l$  is the change in length of a line in a stressed body having the original length  $l$ . If this is produced by a stress  $\sigma$  (a force divided by the area over which it is applied) and if the stress acts in a single direction, Hooke's law states that the strain will be proportional to the stress,

$$\epsilon = \frac{\sigma}{E} \quad (2)$$

The constant of proportionality,  $E$ , is Young's modulus. Consider a rectangular coordinate system with tension  $\sigma_x$  applied in the  $X$  direction, and assume that the body is isotropic. That is, assume that the elastic properties are the same in all directions through the material. There will then be a contraction in all directions at right angles to  $X$ , and if strains parallel to  $Y$  and  $Z$  are  $\epsilon_y$  and  $\epsilon_z$ , respectively, then

<sup>1</sup> G. SACHS and J. WEERTS, *Z. Physik*, vol. 64, p. 344, 1930.

<sup>2</sup> C. S. BARRETT and M. GENSAMER, *Phys. Rev.*, vol. 45, p. 563, 1934 (abstract); *Physics*, vol. 7, p. 1, 1936. R. GLOCKER and E. OSSWALD, *Z. tech. Physik*, vol. 16, p. 237, 1935.

<sup>3</sup> F. GISEN, R. GLOCKER, and E. OSSWALD, *Z. tech. Physik*, vol. 17, p. 145, 1936.

$$-\epsilon_y = -\epsilon_z = \nu\epsilon_x = \frac{\nu\sigma_x}{E} \quad (3)$$

where  $\nu$  is Poisson's ratio and negative signs denote contraction.

In addition to the strains produced by stresses normal to a surface, the **normal strains** mentioned above, there are **shear strains**. The magnitude of a shear strain,  $\gamma$ , is defined by the lateral displacement of a plane relative to another parallel plane per unit distance separating the planes. Referring to Fig. 1,

$$\gamma = \frac{b}{h} = \tan \alpha.$$

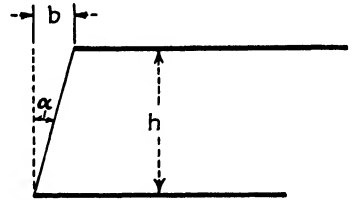


FIG. 1.—Diagram illustrating shear strain.

The proportionality between shear strain and the shear stress,  $\tau$ , that produces it may be written

$$\gamma = \frac{\tau}{G} \quad (4)$$

where the constant  $G$  is the modulus of elasticity in shear, the torsion modulus. In a rectangular coordinate system, shear stresses and shear strains require subscripts to designate their directions; a shear stress acting on a plane perpendicular to the  $X$  direction and along the  $Y$  direction is written  $\tau_{xy}$ , and a shear strain on a plane perpendicular to  $X$  and acting in the direction of  $Y$  is written  $\gamma_{xy}$ .

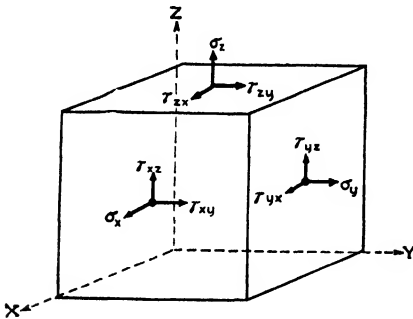


FIG. 2.—Diagram illustrating equilibrium of shear stresses,  $\tau$ , and normal stresses,  $\sigma$ , on an element of volume.

If an infinitesimal parallelepiped, say a cube, is inscribed in the stressed body and the cube edges are taken as coordinate axes, there will be in general three components of stress acting on each face, as in Fig. 2, but in ordinary conditions of equilibrium many of these are equal (for example,  $\tau_{yz} = \tau_{zy}$  and  $\sigma_x = \sigma_{-x}$ ). It requires, in fact, no more than six of these components of stress

to specify completely the state of stress at a point in an isotropic solid:  $\sigma_x$ ,  $\sigma_y$ ,  $\sigma_z$ ,  $\tau_{xy}$ ,  $\tau_{yz}$ , and  $\tau_{zx}$ .

A simplification results if the coordinate axes of Fig. 2 are directed in such a way that the shear stresses on all faces are zero. This is always possible, regardless of the complexity of the stress system. The stresses normal to the cube surfaces are then the **principal stresses**  $\sigma_1$ ,  $\sigma_2$ , and  $\sigma_3$ , and these are related to the principal strains in isotropic bodies by the equations

$$\left. \begin{aligned} \epsilon_1 &= \frac{1}{E} [\sigma_1 - \nu(\sigma_2 + \sigma_3)] \\ \epsilon_2 &= \frac{1}{E} [\sigma_2 - \nu(\sigma_1 + \sigma_3)] \\ \epsilon_3 &= \frac{1}{E} [\sigma_3 - \nu(\sigma_1 + \sigma_2)] \end{aligned} \right\} \quad (5)$$

Equations (2) and (3) are special cases of these relations. Individual grains of a polycrystalline material are usually anisotropic,  $E$  varying with crystallographic direction, but if there is no preferred orientation of the grains the material may still follow closely the laws for an isotropic medium.

**Method for Sum of Principal Stresses ( $\sigma_1 + \sigma_2$ ).**—An x-ray method of stress analysis suitable for determining uniaxial stresses and the sum of

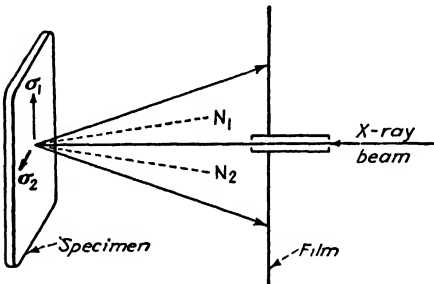


FIG. 3.—Back-reflection camera set up for stress determination with beam normal to surface. Reflecting plane normals are  $N_1$  and  $N_2$ .

the principal stresses in the plane of the surface requires one photograph of the stressed specimen and another of the same material in the stress-free state.<sup>1</sup> If we assume that the material is elastically isotropic and is subjected to principal stresses  $\sigma_1$  and  $\sigma_2$  lying in the plane of the surface, the normal strain perpendicular to the surface will be  $\epsilon_1 = -(\sigma_1 + \sigma_2)\nu/E$ , where  $\nu$  is Poisson's ratio and  $E$  is Young's modulus. (At a free surface

the stress normal to the surface is zero; thus  $\sigma_3 = 0$ .) For simple tension,  $\sigma_2 = 0$  and the sign of  $\sigma_1$  is positive; this produces a strain in the  $Z$  direction which is a contraction (indicated by the negative sign). The spacing of the atomic planes lying parallel to the surface will thereby be altered from  $d_0$  (the unstressed value) to  $d_\perp$ , so that  $\epsilon_1 = (d_\perp - d_0)/d_0$ . Therefore, measurements of  $d_\perp$  and  $d_0$  give the sum of the principal stresses,

$$\sigma_1 + \sigma_2 = -\frac{E}{\nu} \left( \frac{d_\perp - d_0}{d_0} \right). \quad (6)$$

Strain measurements by x-rays require precision technique, which means that back-reflection cameras must be employed. (These cameras have been discussed in Chap. VII, page 122.) Figure 3 illustrates a back-reflection camera set for determining stresses by this method. An x-ray beam passes through a pinhole placed at the focusing position, goes through a hole in the film, and strikes the specimen perpendicularly,

<sup>1</sup> G. SACHS and J. WEERTS, *Z. Physik*, vol. 64, p. 344, 1930. F. WEVER and H. MÖLLER, *Arch. Eisenhüttenw.*, vol. 5, p. 215, 1931–1932.

reflecting from planes that are nearly parallel to the surface ( $N_1$  and  $N_2$  are the reflecting-plane normals). Using cobalt  $K\alpha$  radiation for an iron or steel specimen, reflection will occur from (310) planes with  $\theta = 80^\circ 37.5'$ , and the strain measured along the (310) plane normals will closely approximate the desired strain  $\epsilon_\perp$  and can be used in the above equations. Copper  $K\alpha$  radiation is suitable for aluminum and duralumin since the (511) reflection occurs at about  $81^\circ$ . Cobalt reflects from copper at  $\theta = 81^\circ 46.5'$  (400 reflection) and from brass (68 percent copper) at  $75^\circ 30'$ . Nickel reflects from cartridge brass (331) planes at  $79^\circ$ , and iron reflects from magnesium (105) planes at  $83^\circ$ .

The best accuracy to be expected of this method is about  $\pm 1 \times 10^{-4} \text{\AA}$  for the spacing of atomic planes, corresponding to  $\pm 2$  kg. per sq. mm. or about 3000 psi. in stress for iron and steel specimens.<sup>1</sup> Owing to the fact that the reflecting planes are not exactly parallel to the surface, Eq. (6) is only an approximate expression; the computed stress ( $\sigma_1 + \sigma_2$ ) will be on the average about 7 percent too small.<sup>2</sup> The film is usually rotated about its center during the exposure to smooth out spottiness in the lines.

The distance between the film and the specimen surface can be determined by placing a powdered calibrating substance on the specimen. The lattice spacing of this substance is known, and so one can compute the specimen-to-film distance from a measurement of a Debye ring produced by it. Annealed gold or silver powder is suitable for iron, aluminum, duralumin, and brass samples.<sup>3</sup>

The distance from specimen to film can also be measured directly, permitting exposure times only half as long as those when calibration substances are used. The distance can be measured by inside micrometers or can be set at a predetermined value, say 5.00 cm., by a metal pointer attached to the hub of the camera.<sup>4</sup> A feeler gauge slipped between the end of the pointer and the specimen enables one to determine when the camera is adjusted to the proper distance. The pointer is then removed during the exposure. A suitably inscribed circle on the film, concentric with the axis of rotation of the film, facilitates accurate measurement. Thomas states that film shrinkage errors amount to about 1 part in 84,000 in lattice-constant measurement and may be neglected; in any event, a circle inscribed on the film before development can be used to calibrate for shrinkage, or photographic plates that have been drilled for the passage of the beam can be employed to eliminate shrinkage.

<sup>1</sup> H. MÖLLER and J. BARBERS, *Mitt. Kaiser-Wilhelm Inst. Eisenforsch. Düsseldorf*, vol. 16, p. 21, 1934. H. MÖLLER, *Mitt. Kaiser-Wilhelm Inst. Eisenforsch. Düsseldorf*, vol. 21, p. 295, 1939.

<sup>2</sup> R. GLOCKER, "Materialprüfung mit Röntgenstrahlen," Springer, Berlin, 1936.

<sup>3</sup> The Au 333 reflection with copper  $K\alpha_1$  is at  $\theta = 78^\circ 56'$  and with cobalt  $K\alpha_1$  the 420 reflection is at  $\theta = 78^\circ 46'$ ;  $a_0$  for Au is  $4.0700 \text{\AA}$ ;  $a_0$  for Ag is  $4.077 \text{\AA}$ .

<sup>4</sup> D. E. THOMAS, *J. Sci. Instruments*, vol. 18, p. 135, 1941.

At a standard distance the displacement of the diffracted line corresponds directly to a certain stress; for example, for a distance which gives a gold ring 50.0 mm. in diameter, a shift of  $\frac{1}{10}$  mm. in the position of one side of the 310 line from iron corresponds to  $(\sigma_1 + \sigma_2) = 9.2$  kg. per sq. mm. (13,000 psi.), assuming  $E = 21,000$  kg. per sq. mm. ( $30 \times 10^6$  psi.) and  $\nu = 0.28$ . With aluminum, assuming  $E = 7200$  kg. per sq. mm. ( $10.3 \times 10^6$  psi.) and  $\nu = 0.34$ , the same shift would indicate  $(\sigma_1 + \sigma_2) = 2.4$  kg. per sq. mm. (3420 psi.).

Since only  $(\sigma_1 + \sigma_2)$  is determined, this method gives a limited view of the stress situation, and in fact the method cannot detect torsional stresses in the surface since these have  $\sigma_1 = -\sigma_2$ . The unstressed reading can be obtained by removing the load, or in an internally stressed piece it sometimes can be had by cutting out a small piece of the specimen

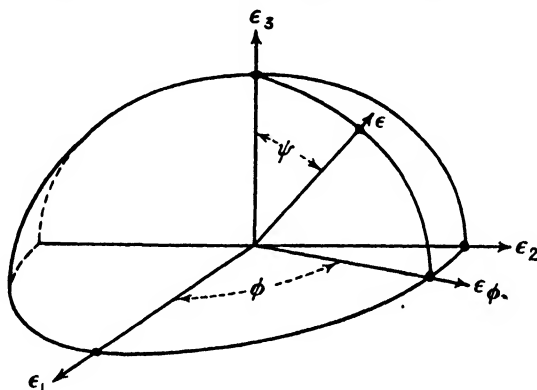


FIG. 4.—The ellipsoid of strain. Principal strains are  $\epsilon_1$ ,  $\epsilon_2$ , and  $\epsilon_3$ .

with saw cuts or with a hollow drill. Stress-relief annealing can also be resorted to, but at some risk of dissolving or precipitating some elements from the diffracting matrix, which would change the unstressed value of the lattice spacings.

**Equations for the Ellipsoid of Strain and of Stress.**—Before taking up other procedures for stress analysis the fundamental equations on which all are based will be presented.

Under homogeneous elastic deformation a spherical element of volume in an isotropic solid is deformed into an ellipsoid. The normal strain,  $\epsilon$ , in any chosen direction is given by the approximate equation for the ellipsoid of strain

$$\epsilon = a_1^2 \epsilon_1 + a_2^2 \epsilon_2 + a_3^2 \epsilon_3 \quad (7)$$

where  $\epsilon_1$ ,  $\epsilon_2$ , and  $\epsilon_3$  are the principal strains (Fig. 4) and  $a_1$ ,  $a_2$ , and  $a_3$  are the direction cosines of the chosen direction with respect to the directions of the principal strains.<sup>1</sup> In terms of the coordinates  $\phi$ ,  $\psi$  of Fig. 4,

<sup>1</sup> A derivation of elastic-theory formulas will be found in S. Timoshenko, "Theory of Elasticity," McGraw-Hill, New York, 1934.



the direction cosines may be written

$$\left. \begin{aligned} a_1 &= \sin \psi \cos \phi \\ a_2 &= \sin \psi \sin \phi \\ a_3 &= \cos \psi = \sqrt{1 - \sin^2 \psi} \end{aligned} \right\} \quad (8)$$

If the direction cosines are substituted in (7) together with the values of the principal stresses  $\epsilon_1$ ,  $\epsilon_2$  and  $\epsilon_3$  from (5) and if we set  $\sigma_3 = 0$  (since the stress normal to a free surface is zero), then Eq. (7) may be written

$$\epsilon - \epsilon_3 = \frac{1 + \nu}{E} (\sigma_1 \cos^2 \phi + \sigma_2 \sin^2 \phi) \sin^2 \chi. \quad (9)$$

Now the approximate equation for the stress ellipsoid is

$$\sigma = a_1^2 \sigma_1 + a_2^2 \sigma_2 + a_3^2 \sigma_3 \quad (10)$$

where  $a$ ,  $a_2$ , and  $a_3$  are the direction cosines of the stress  $\sigma$  with respect to the principal axes of stress. When  $\psi = 90^\circ$ , this becomes

$$\sigma_\phi = \sigma_1 \cos^2 \phi + \sigma_2 \sin^2 \phi \quad (11)$$

which gives the component of stress in the direction  $\phi$ . Substitution of (11) in (9) leads to the relation

$$\sigma_\phi = (\epsilon - \epsilon_3) \cdot \frac{E}{1 + \nu} \cdot \frac{1}{\sin^2 \psi}. \quad (12)$$

Let  $d_0$  be the spacing of atomic planes in the unstressed condition,  $d_\perp$  the spacing in the stressed metal perpendicular to the surface, and  $d_\psi$  the spacing in the direction  $\psi$ ,  $\phi$ ; then

$$\epsilon - \epsilon_3 = \frac{d_\psi - d_0}{d_0} - \frac{d_\perp - d_0}{d_0} = \frac{d_\psi - d_\perp}{d_0}. \quad (13)$$

To a close approximation this may be written

$$\epsilon - \epsilon_3 = \frac{d_\psi - d_\perp}{d_\perp}, \quad (14)$$

and Eq. (12) may be reduced to the convenient form

$$\sigma_\phi = \frac{d_\psi - d_\perp}{d_\perp} \cdot \frac{E}{1 + \nu} \cdot \frac{1}{\sin^2 \psi}. \quad (15)$$

**Two-exposure Method for  $\sigma_\phi$ .**—The component of stress in any desired direction in the surface can be determined from two exposures, one with the beam normal to the surface giving  $d_\perp$ , and one with the beam inclined in the plane of the normal and the component  $\sigma_\phi$ , giving  $\sigma_\phi$  in Eq. (15).<sup>1</sup> No exposure of the material in the unstressed state is neces-

<sup>1</sup> F. GISEN, R. GLOCKER, and E. OSSWALD, *Z. tech. Physik*, vol. 17, p. 145, 1936.

sary. The usual practice is to make the inclined exposure with the beam  $45^\circ$  from the perpendicular. It is necessary to use rings of a comparison substance (usually gold, silver, or brass) on the surface of the specimen to determine the effective distance from the irradiated spot to the film, as illustrated in Fig. 5 where  $r$  is the radius of a gold calibrating ring and  $r - s$  the radius of a specimen ring. Measurement of the distance  $s$  between the rings on the side nearest the specimen gives a calculation of  $d$  at the angle  $\psi = \psi_0 + \eta$ , which is different from the value of  $d$  on the other side of the rings at  $\psi = \psi_0 - \eta$ . Both measurements may be computed independently in Eq. (15), or the more sensitive one,  $(\psi_0 + \eta)$ , may be used. Direct measurement of the distance from specimen to film

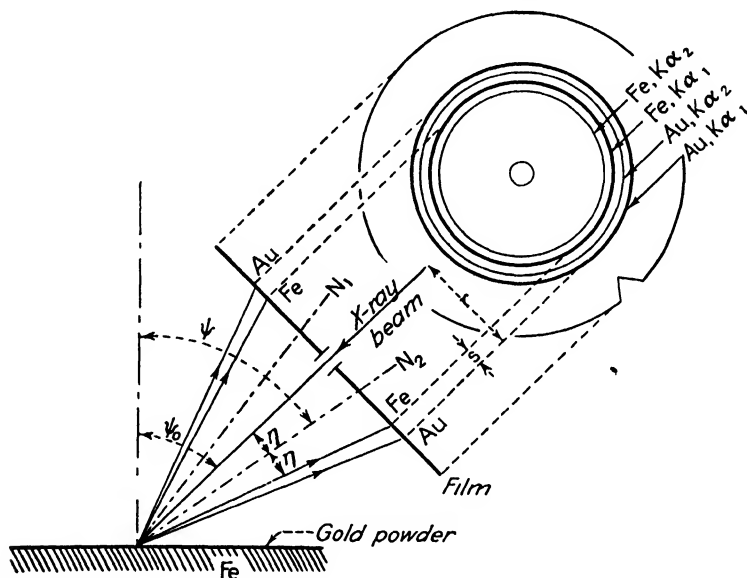


FIG. 5.—Back-reflection camera inclined at  $\psi_0 = 45^\circ$ , and type of film obtained with cobalt radiation, iron specimen, and gold calibrating powder on surface.

is possible if sufficient care is taken and if a circle is put on the film concentric with the axis.<sup>1</sup>

A convenient procedure is to calculate a relationship between stress and the ring displacement rather than to apply Eq. (15) to every reading. For this purpose one finds the multiplying factor that will bring the diameter of the calibration ring ( $2r$ ) to some standard value, say 50 mm., and the measured  $s$  is also multiplied by this factor. This value can then be compared with a prepared table or chart relating  $s$  to  $\sigma_\phi$  for the given experimental conditions.

Möller and Gisen<sup>2</sup> conclude that visual measurement of the films gives about the same accuracy as measurement with a recording micropho-

<sup>1</sup> D. E. THOMAS, *J. Sci. Instruments*, vol. 18, p. 135, 1941.

<sup>2</sup> H. MÖLLER and F. GISEN, *Mitt. Kaiser-Wilhelm Inst. Eisenforsch. Düsseldorf*, vol. 19, p. 57, 1937.

tometer, *viz.*,  $1 \times 10^{-4} \text{Å}$  in atomic spacings for photographs with sharp lines. This corresponds to about 1.7 kg. per sq. mm. (2400 psi.) in stress with a steel specimen when  $\psi_0 = 45^\circ$ . With diffuse lines the error is four or five times this, and a microphotometer can be used to advantage.

**Correction for Oscillation of Film (Two-exposure Method).**—The spottiness of rings from large-grained material should be removed by rotating the film in perpendicular exposures, but this is not advisable in inclined exposures where the rings deviate more from the circular. However, oscillation back and forth through a limited range of angles may be used to smooth out the lines. This decreases the average angle of inclination of the planes reflecting to the lower side of the film from  $\psi_0 + \eta$  to  $\psi_0 + \eta \div \Delta\psi$ , while on the upper side of the film  $\psi_0 - \eta$  is increased to  $\psi_0 - \eta + \Delta\psi$ ; the azimuthal position,  $\phi$ , also changes through a range. The errors in stress computations decrease with the range of oscillation and can be kept small enough to be neglected if oscillation is limited to  $\pm 30^\circ$  or less.<sup>1</sup>

**Single-exposure Method for  $\sigma_\phi$ .**—A stress component may be determined from a single inclined exposure if the diffraction rings are measured at two positions on their circumference.<sup>2</sup> The beam is inclined toward the direction in which the component  $\sigma_\phi$  is to be measured; that is, the beam lies in the plane containing the normal and the component to be measured, thus at the angle  $\phi$ , and is  $\psi_0$  from the normal. The ring from the specimen is measured with reference to the ring from the calibration substance, both at the top of the ring where  $\psi_1 = \psi_0 - \eta$  and at the bottom where  $\psi_2 = \psi_0 + \eta$ , giving spacings  $d_1$  and  $d_2$ , respectively. Equation (12) is written for each set of measurements, giving two simul-

<sup>1</sup> The value of  $\Delta\psi$  is small—for iron specimens with cobalt radiation  $\Delta\psi$  is only  $0.1^\circ$  for a range of oscillation  $\delta = \pm 10^\circ$ ,  $1.3^\circ$  for  $\delta = \pm 30^\circ$ , and  $2.8^\circ$  for  $\delta = \pm 45^\circ$ . Oscillation of the film also alters  $\phi$  through a range  $\pm \Delta\phi$ . In a photograph of iron with  $\psi_0 = 45^\circ$ ,  $\pm \Delta\phi = 2.0^\circ$  for  $\delta = \pm 10^\circ$ ,  $5.9^\circ$  for  $\delta = \pm 30^\circ$ , and  $8.5^\circ$  for  $\delta = \pm 45^\circ$ , provided that the diffraction lines are measured on the lower side where  $\psi = \psi_0 + \eta$ . On the upper side the range  $\pm \Delta\phi$  is larger, being  $2.8$ ,  $7.9$ , and  $10.8^\circ$  for  $\delta = \pm 10$ ,  $30$ , and  $45^\circ$ , respectively. (R. Glocker, B. Hess, and O. Schaaber, *Z. tech. Physik*, vol. 19, p. 194, 1938.) If a stress component,  $\sigma_\phi$ , is determined from a perpendicular and an inclined exposure (iron with cobalt radiation,  $\psi = 45^\circ + \eta$ ), an oscillation of  $\delta = \pm 30^\circ$  requires corrections that depend upon the stress ratio defined by the relation  $\sigma_{\phi+90} = k\sigma_\phi$ , the percentage correction being as follows:

$k$	-6	-3	0	+3	+6
Percentage	+3.4	+2.5	+1.4	+0.5	-0.5

<sup>2</sup> R. GLOCKER, B. HESS, and O. SCHAABER, *Z. tech. Physik*, vol. 19, p. 194, 1938. An alternate method of computation is given by D. E. Thomas, *J. Sci. Instruments*, vol. 18, p. 135, 1941.

taneous equations whose solution is

$$\sigma_{\phi} = \left( \frac{E}{1 + \nu} \right) \left( \frac{d_1 - d_2}{d_0} \right) \frac{1}{\sin 2\psi_0 \sin 2\eta}. \quad (16)$$

For the incident beam at  $\psi_0 = 45^\circ$ , this reduces to

$$\sigma_{\phi} = \left( \frac{E}{1 + \nu} \right) \left( \frac{d_1 - d_2}{d_0} \right) \frac{1}{\sin 2\eta}. \quad (17)$$

In this formula,  $d_0$  need not be determined accurately on each individual specimen for the normal lattice constant for unstressed metal may be used (2.8610 for steel). This is a rapid method but is less accurate than the method employing a perpendicular exposure in addition to the inclined one, for an error of  $\pm 1 \times 10^{-4} \text{ \AA}$  in  $d$  in Eq. (17) introduces an error of  $\pm 3.5 \text{ kg. per sq./mm. (5000 psi.)}$  for steel specimens, twice the error of the two-exposure method.<sup>1</sup>

**Methods for Determining  $\sigma_1$  and  $\sigma_2$  When Their Directions Are Known.**—When the directions of the principal stresses are known (for example, in a cylinder containing quenching stresses), Eq. (15) can be applied to give the principal stresses  $\sigma_1$  and  $\sigma_2$ . For this purpose the perpendicular exposure is combined with an inclined exposure in which the beam is tipped toward  $\sigma_1$  and also with an exposure in which the beam is tipped toward  $\sigma_2$ . Thus, three exposures, all of them on the stressed material, serve to determine completely the surface stresses.

If  $d_0$  is obtained by an exposure of the specimen in the stress-free state, then two inclined exposures of the stressed material will serve, one giving the spacing  $d_{\psi}$  at the angle  $\psi$  from the normal and at the azimuth  $\phi$ , the other giving  $d_{\psi'}$  at the same angle from the normal and at azimuth  $\phi + 90^\circ$ .<sup>\*</sup> Eqs. (2), (3), and (7) for these conditions lead to the relations

$$\left. \begin{aligned} \sigma_1 + \sigma_2 &= \left( \frac{d_{\psi} + d_{\psi'} - 2d_0}{d_0} \right) \left( \frac{E}{(1 + \nu) \sin^2 \psi - 2\nu} \right) \\ \sigma_1 - \sigma_2 &= \left( \frac{d_{\psi} - d_{\psi'}}{d_0} \right) \left( \frac{E}{(1 + \nu) \sin^2 \psi} \right) \end{aligned} \right\} \quad (18)$$

The sum of these equations gives  $\sigma_1$  while the difference gives  $\sigma_2$ .

If one uses the single inclined exposure method for  $\sigma_{\phi}$ , with the beam inclined toward  $\sigma_1$  and again with the beam tipped toward  $\sigma_2$ , the two principal stresses may be determined with only two exposures.<sup>2</sup> How-

<sup>1</sup> The correction to be introduced if the film is oscillated is small. For a photograph of iron with  $\psi_0 = 45^\circ$  and an oscillation of  $\pm 15^\circ$  the correction for  $\sigma_{\phi}$  is 1.1 percent; for  $\pm 30^\circ$  it is 4.5 percent.

<sup>\*</sup> C. S. BARRETT and M. GENSAMER, *Physics*, vol. 7, p. 1, 1936.

<sup>2</sup> R. GLOCKER, B. HESS, and O. SCHAABER, *Z. tech. Physik*, vol. 19, p. 194, 1938.

ever, this shorter method, based on Eqs. (16) or (17) has lower accuracy than three-exposure methods. A still less accurate method has been proposed<sup>1</sup> in which the diffraction ring of a single inclined photograph is measured in four places.

The various equations of this chapter can be solved to give the unstressed lattice spacing,  $d_0$ , from three or more measurements of the stressed state. For example, a perpendicular exposure combined with two inclined exposures at azimuths  $\phi$  and  $\phi + 90^\circ$  will give  $d_0$  by simultaneous equations of types (6) and (15).

**Method Giving Magnitude and Direction of Principal Stresses.**—Both the magnitudes and directions of  $\sigma_1$  and  $\sigma_2$  can be determined if the components of stress are computed for three directions in the surface. The maximum accuracy can be obtained if one uses a perpendicular expo-

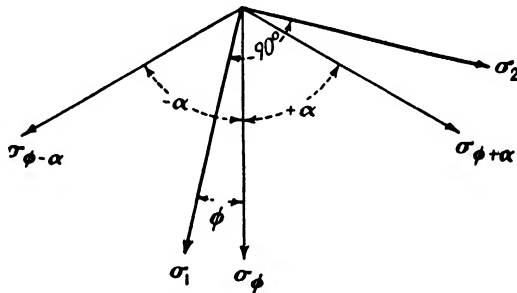


FIG. 6.—Arrangement of principal stresses ( $\sigma_1, \sigma_2$ ) and stress components in the specimen surface.

sure paired with three inclined exposures at azimuth angles  $\phi$ ,  $\phi + 60^\circ$ , and  $\phi - 60^\circ$ .<sup>\*</sup> An error of  $\pm 1 \times 10^{-4} \text{ \AA}$  in spacing then corresponds to  $\pm 2.3 \text{ kg. per sq. mm.}$  ( $\pm 3300 \text{ psi.}$ ) in the principal stresses in steel and an error in their direction that is given by the relation  $\pm 65^\circ/(\sigma_1 - \sigma_2)$  where the stresses  $\sigma_1$  and  $\sigma_2$  are given in kilograms per square millimeter. These figures are computed for beams at an angle of inclination of  $45^\circ$  and for stress directions that would give minimum accuracy.

The stress components in the plane of the surface at angles  $\phi$ ,  $\phi + \alpha$ ,  $\phi - \alpha$  (Fig. 6) are given by the relations<sup>2</sup>

$$\left. \begin{aligned} \sigma_\phi &= \frac{1}{2}(\sigma_1 + \sigma_2) + \frac{1}{2}(\sigma_1 - \sigma_2) \cos 2\phi \\ \sigma_{\phi+\alpha} &= \frac{1}{2}(\sigma_1 + \sigma_2) + \frac{1}{2}(\sigma_1 - \sigma_2) \cos 2(\phi + \alpha) \\ \sigma_{\phi-\alpha} &= \frac{1}{2}(\sigma_1 + \sigma_2) + \frac{1}{2}(\sigma_1 - \sigma_2) \cos 2(\phi - \alpha) \end{aligned} \right\} \quad (19)$$

<sup>1</sup> H. MÖLLER and H. NEERFELD, *Mitt. Kaiser-Wilhelm Inst. Eisenforsch. Dusseldorf*, vol. 21, p. 289, 1939.

<sup>\*</sup> H. MÖLLER, *Mitt. Kaiser-Wilhelm Inst. Eisenforsch. Dusseldorf*, vol. 21, p. 295, 1939.

<sup>2</sup> See for example C. E. FULLER and W. A. JOHNSTON, "Applied Mechanics," vol. II, art. 42, Wiley, New York, 1913.

Solving for  $\sigma_1$ ,  $\sigma_2$ , and  $\phi$  with  $\alpha = 60^\circ$ , we have

$$\begin{aligned}\sigma_1 &= \frac{1}{3} [\sigma_\phi + \sigma_{\phi-60} + \sigma_{\phi+60} + \sqrt{(2\sigma_\phi - \sigma_{\phi-60} - \sigma_{\phi+60})^2 + 3(\sigma_{\phi-60} - \sigma_{\phi+60})^2}] \\ \sigma_2 &= \frac{1}{3} [\sigma_\phi + \sigma_{\phi-60} + \sigma_{\phi+60} - \sqrt{(2\sigma_\phi - \sigma_{\phi-60} - \sigma_{\phi+60})^2 + 3(\sigma_{\phi-60} - \sigma_{\phi+60})^2}] \\ \tan 2\phi &= \frac{\sqrt{3} (\sigma_{\phi-60} - \sigma_{\phi+60})}{2\sigma_\phi - \sigma_{\phi-60} - \sigma_{\phi+60}}\end{aligned}\quad (20)$$

The components of stress  $\sigma_\phi$ ,  $\sigma_{\phi+60}$ , and  $\sigma_{\phi-60}$  are determined by inclined beam exposures at azimuth angles  $\phi$ ,  $\phi + 60$ ,  $\phi - 60$ , each exposure being combined with an exposure perpendicular to the surface, using Eq. (15). Alternatively, this four-exposure technique may be shortened by merely using three inclined exposures and Eq. (16), but the accuracy is then cut to about half. The simultaneous equations relating stress components to the principal stresses can be solved graphically if desired.<sup>1</sup>

**Values of the Elastic Constants. Anisotropy.**—The elastic constants that are measured mechanically do not necessarily apply accurately to x-ray determinations of stress. Each grain is anisotropic, and the strain is measured always along a certain crystallographic direction (along [310] for iron). Therefore, the grains that reflect have only certain orientations with respect to the axes of stress, and the effective values of  $E$  and  $\nu$  in these orientations may differ from the over-all average orientations, the latter being measured in a mechanical test.

The theoretical treatment of the problem has been carried out on the assumptions both that the grains are stressed equally and deform independently of one another and that they all are strained equally.<sup>2</sup> Comparison of the predictions of these theories with x-ray measurements of specimens subjected to known stresses led Möller and Martin<sup>3</sup> to conclude that neither of these two assumptions is correct. They suggest that effective elastic constants be determined empirically by x-raying a specimen with known stresses; for steel they obtained the values  $E = 22,030$  kg. per sq. mm. ( $31.5 \times 10^6$  psi.) and  $\nu = 0.374$  by the x-ray method in place of the mechanically measured values  $E = 21,000$  kg. per sq. mm. ( $30 \times 10^6$  psi) and  $\nu = 0.28$ . Glocker and Schaaber,<sup>4</sup> on the other hand, found

<sup>1</sup> W. R. OSGOOD and R. G. STURM, *Bur. Standards J. Research*, vol. 10, p. 685, 1933 (three components). W. R. OSGOOD, *Bur. Standards J. Research*, vol. 15, p. 579, 1935 (four components). A. H. STANG and M. GREENSPAN, *Bur. Standards J. Research*, vol. 19, p. 437, 1937 (four components).

<sup>2</sup> R. GLOCKER, *Z. tech. Physik*, vol. 19, p. 289, 1938. H. MÖLLER and G. MARTIN, *Mitt. Kaiser-Wilhelm Inst. Eisenforsch. Dusseldorf*, vol. 21, p. 261, 1939. H. MÖLLER and J. BARBERS, *Mitt. Kaiser-Wilhelm Inst. Eisenforsch. Dusseldorf*, vol. 17, p. 157, 1935. H. MÖLLER and G. STRUNK, *Mitt. Kaiser-Wilhelm Inst. Eisenforsch. Dusseldorf*, vol. 19, p. 305, 1937.

<sup>3</sup> H. MÖLLER and G. MARTIN, *Mitt. Kaiser-Wilhelm Inst. Eisenforsch. Dusseldorf*, vol. 21, p. 261, 1939.

<sup>4</sup> R. GLOCKER and O. SCHAABER, "Ergebnisse der technische Röntgenkunde," vol.

agreement between x-ray and mechanical values of the torsion modulus,  $G = E/2(\nu + 1)$ , obtaining the value 8200 kg. per sq. mm. ( $11.7 \times 10^6$  psi.). They concluded, as did Möller and Strunk,<sup>1</sup> that, in using a perpendicular and an inclined photograph to determine a stress component, it is permissible to use the mechanical value of the elastic constants and to omit an anisotropy correction. In practice, the experimental errors are usually much greater than any uncertainties from an incorrect choice of elastic constants.

**Equipment for Stress Measurement.**—Equipment for stress measurement usually consists of a portable x-ray tube mounted in a ray-proof and shockproof housing (the smaller the better) and supported on an adjustable stand, as, for example, in Fig. 7. The tube may be connected to the portable power source by an insulated cable. A back-reflection camera is essential and should be mounted on the x-ray tube itself, somewhat in the fashion sketched in Fig. 8. The film is mounted on a small film holder that can be rotated or oscillated in its own plane to remove spottiness from the rings, with the beam passing through an adjustable pinhole system at its center. The smallest pinhole should be placed at the focusing position, *viz.*, on the circumference of the circle that passes through the Debye ring on the film and is tangent to the irradiated spot on the surface of the specimen. The film is covered with black celluloid (black paper is likely to leave a radiograph of the paper fiber on the film).

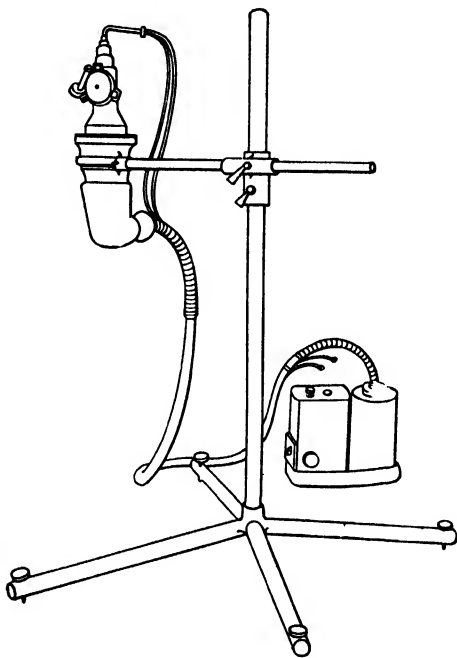


FIG. 7.—Portable x-ray stress-measuring apparatus.

Tests have indicated<sup>2</sup> that varying the distance from the film to the specimen makes no appreciable difference in the accuracy of measurements, but decreasing the pinhole size from 1 to 0.3 mm. decreases the error in a set of measurements from  $\pm 2.5 \times 10^{-4} \text{Å}$  to  $\pm 0.6 \times 10^{-4} \text{Å}$ .

VI, Spannungsmessung an Werkstücken, p. 34, Akademische Verlagsgesellschaft m.b.h., Leipzig, 1938.

<sup>1</sup> H. MÖLLER and G. STRUNK, *Mitt. Kaiser-Wilhelm Inst. Eisenforsch. Düsseldorf*, vol. 19, p. 305, 1937.

<sup>2</sup> F. WEVER and A. ROSE, *Mitt. Kaiser-Wilhelm Inst. Eisenforsch. Düsseldorf*, vol. 17, p. 33, 1935.

Exposure times vary from a few hours to a fraction of an hour, depending on pinholes, focal-spot size, and absorption in the window of the x-ray tube. Much time can be lost in adjusting the tube to the proper distance and angle with respect to the object unless one provides convenient distance and angle gauges. Some European equipment has been designed so that the tube and camera snap quickly from a perpendicular position to a position inclined at  $45^\circ$ .

To read the films it is necessary to employ a microphotometer only if the lines are broad. Tests in several laboratories have indicated that reasonably sharp lines can be read by eye with sufficient accuracy if reading conditions are good, but the cross hair that is moved over the film should be very fine if it is not to obscure the diffraction line. A fine needle

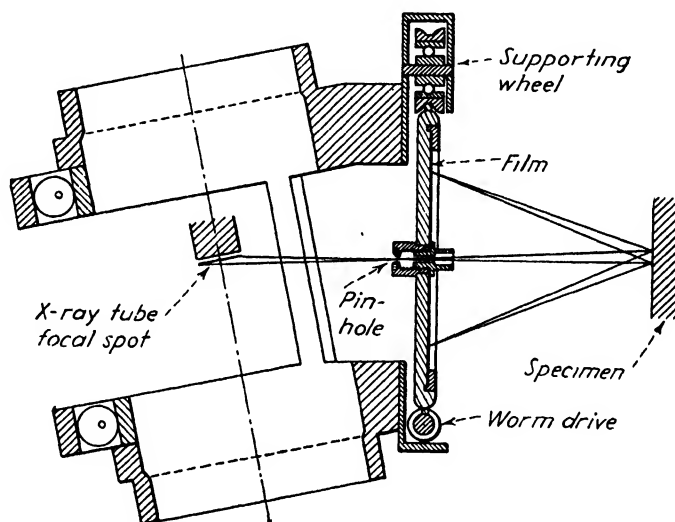


FIG. 8.—Back-reflection camera clamped to x-ray tube.

point is preferred by some as more of the diffraction line remains visible than when a cross hair is used. If the diameter of a ring is to be measured, it is important, of course, to see that the points measured are diametrically opposite each other.

**Applications.**—A review of the published applications of x-ray stress measurement will serve to illustrate the possibilities of the method as a research tool. The author is aware of no detailed publications on routine uses of the method in the field or shop, and such uses are likely to remain comparatively rare because of their cost. There seems to have been some use of the method in Germany for determining stresses in railroad bridges and there has been some use of it in this country for determining internal stresses in rails. It is particularly suited for following the changes in residual stresses of rails, car wheels, bridges, etc., when the x-ray is directed at a portion of the surface that is not subject to abra-



sion, a surface from which any superficial cold-worked layer has been removed by etching.

Early results with the x-ray method are illustrated in Fig. 9, where residual stresses in a welded steel plate around a fillet-welded reinforcing strap are plotted.<sup>1</sup> A hollow-core drill was used that removed a 0.16-in. core for measurement of the unstressed condition. It will be noted that the plate just beyond the patch had a high tensile stress,  $(\sigma_1 + \sigma_2) = 140,000$  psi., which was well beyond the yield point for uniaxial tension. The butt weld in the plate was in compression,  $(\sigma_1 + \sigma_2) = -64,000$  psi. A butt-welded plate analyzed by the same method showed the weld to be in tension,  $(\sigma_1 + \sigma_2) = 34,000$  psi., and the plate to vary from zero stress to 14,000 psi. in compression.

The fact that welding stresses vary abruptly over small distances in a structure lends added importance to the x-ray method in welding research. An example is shown<sup>2</sup> in a welded triangle of chrome-molybdenum steel tubing (Fig. 10). The tensile stresses in the welds are balanced by an irregular distribution of compressive stresses near by in the tubing. The stresses indicated are  $(\sigma_1 + \sigma_2)$ . Details of the welding technique and dimensions are not given, but it was stated that the irradiated spot on the specimen was 2 mm. wide by 6 mm. long and that the accuracy was  $\pm 1$  to  $3 \times 10^{-4} \text{Å}$ . A "carbon-steel" triangle of the same sort contained lower stresses (32,000 psi. maximum instead of 62,000).

The residual stresses around holes in fatigue specimens were measured by Gisen and Glocker.<sup>3</sup> The results of one experiment are summarized in Fig. 11 and Table XV. The carbon-steel specimen was first drilled, then thoroughly stress-relieved at  $650^\circ\text{C}$ . The rim of the hole was thrown into compression by local cold working, and the stresses were measured. The table gives these stresses in the

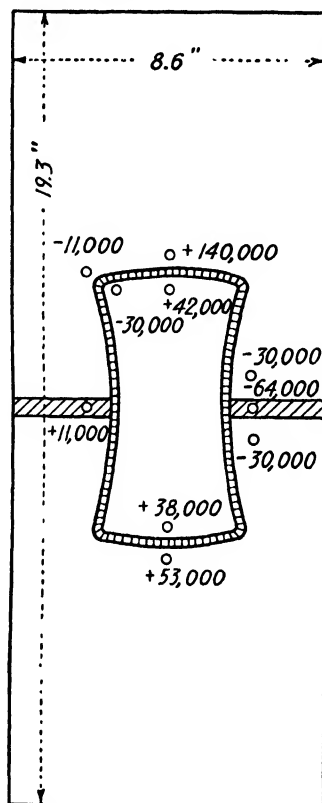


FIG. 9.—Stresses around a fillet-welded reinforcing strap;  $(\sigma_1 + \sigma_2)$  in psi.

<sup>1</sup> H. MÖLLER and J. BARBERS, *Mitt. Kaiser-Wilhelm Inst. Eisenforsch. Düsseldorf*, vol. 16, p. 21, 1934.

<sup>2</sup> H. MÖLLER and A. ROTH, *Mitt. Kaiser-Wilhelm Inst. Eisenforsch. Düsseldorf*, vol. 19, p. 127, 1937.

<sup>3</sup> F. GISEN and R. GLOCKER, *Z. Metallkunde*, vol. 30, p. 297, 1938.

transverse and longitudinal direction. The specimen was then put in a rotating-beam fatigue machine and run at 16.2 kg. per sq. mm. (23,000 psi.) for  $10^7$  cycles, after which the stresses were found to have been

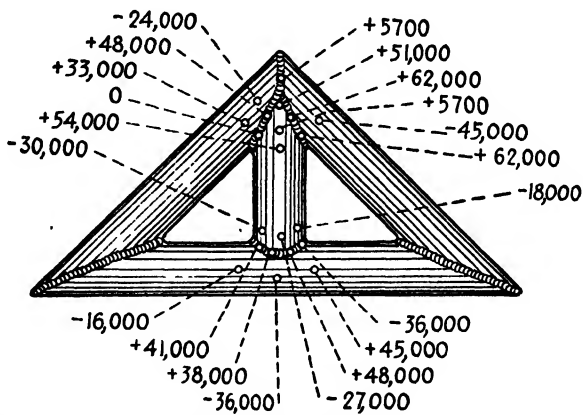


FIG. 10.—Stresses in a welded triangle of steel tubing. ( $\sigma_1 + \sigma_2$ ) in p.i. (Möller and Roth.)

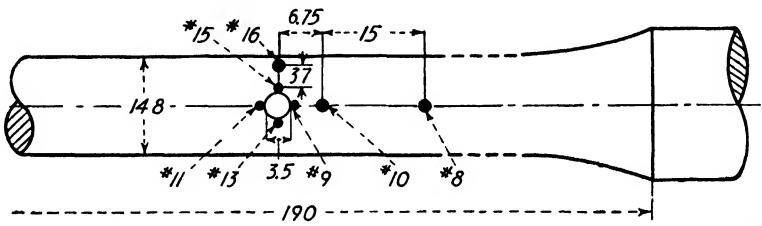


FIG. 11.—Stations at which stresses were measured on a fatigue specimen containing a hole. Dimensions are in millimeters; stresses are given in Table XV. (Gisen and Glocker.)

altered; a further stressing of  $2.8 \times 10^6$  cycles at 20 kg. per sq. mm. (28,400 psi.) altered the stresses to the values given in the last two columns.

TABLE XV.—STRESS MEASUREMENTS AT POSITIONS INDICATED IN FIG. 11

Position Number	Before fatiguing, psi.		After $10^7$ cycles at 23,000 psi.		After $2.8 \times 10^6$ more at 28,400 psi.	
	Longi-tudinal	Transverse	Longi-tudinal	Transverse	Longi-tudinal	Transverse
8	- 4,300	+ 5,700	- 1,400	0		
9	-12,800	+ 1,400	-21,300	-14,000	0	+10,000
10	-15,600	- 8,500	- 7,100	0	-22,800	+ 2,800
11	- 8,500	0	- 5,700	+ 7,100		+ 5,700
13	-18,500	-12,800	-35,600	-12,800	+18,500	- 8,500
15	-15,600	0	-35,600	-25,600	-22,800	- 4,300
16	- 8,500	-10,000	-17,100	-24,200	0	+12,800

The importance of surface conditions in x-ray stress research is illustrated by experiments by Wever and Möller,<sup>1</sup> who compared x-ray and mechanical measurements of stresses on the outer face of a quenched-steel shafting. After normalizing, annealing, and quenching, the outer surface was turned on a lathe. X-ray measurements indicated  $(\sigma_1 + \sigma_2) = -38,000$  psi., whereas mechanical measurements by the boring-out method of Sachs<sup>2</sup> showed  $-97,000$  psi. As more and more of the center was drilled out, the surface stresses  $(\sigma_1 + \sigma_2)$  steadily changed toward compression, but the x-ray always showed about 60,000 psi. greater tensional stress than the mechanical method. From additional experiments this was found to be the result of stresses in a thin surface layer about 0.01 in. deep originating when the surface was turned

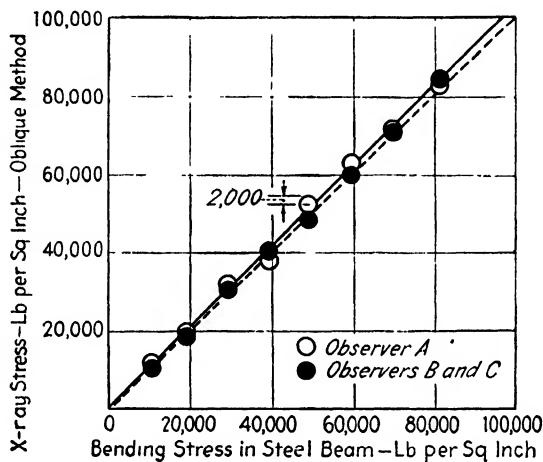


FIG. 12.—Comparison of stresses determined by x-rays (two-exposure method) and stresses computed from the curvature of a bent beam. Annealed mild steel. (Norton and Loring.)

on the lathe. Satisfactory agreement between the methods could be obtained when the surface was not machined, and fair agreement could be obtained when the machined surface was etched off.

Norton and Loring have applied the method to the residual stresses near a weld.<sup>3</sup> They first tested the reproducibility of the method by bending a small beam. The results are shown in Fig. 12 with calculated stresses on the surface of the beam plotted as abscissas and x-ray stresses (obtained with the two-exposure method) plotted as ordinates. The points for different observers who read the films agreed satisfactorily and fell close to the 45° dotted line. The ordinary values of the elastic constants were used in the computations. This experiment was followed by a determination of the biaxial stresses in an annealed mild-steel plate

<sup>1</sup> F. WEVER and H. MÖLLER, *Mitt. Kaiser-Wilhelm Inst. Eisenforsch. Düsseldorf*, vol. 18, p. 27, 1936.

<sup>2</sup> G. SACHS, *Z. Metallkunde*, vol. 19, p. 352, 1927.

<sup>3</sup> J. T. NORTON and B. M. LORING, *Welding J.*, research supplement, June, 1941.

along one edge of which had been placed a weld bead. Two components of stress were determined at a number of points on the specimen with the results shown in Fig. 13. The arrows and figures indicate the magnitude of the components parallel and perpendicular to the weld bead at each station (the direction and magnitude of the *principal stresses* were not determined). The distribution is complex; considering the stresses across the center from *A* to *B* it is seen that the components parallel to the bead vary from compression in the bead to tension near it, then back to compression near the center, and finally back to tension again at the edge farthest from the weld. It was shown that these stresses were not

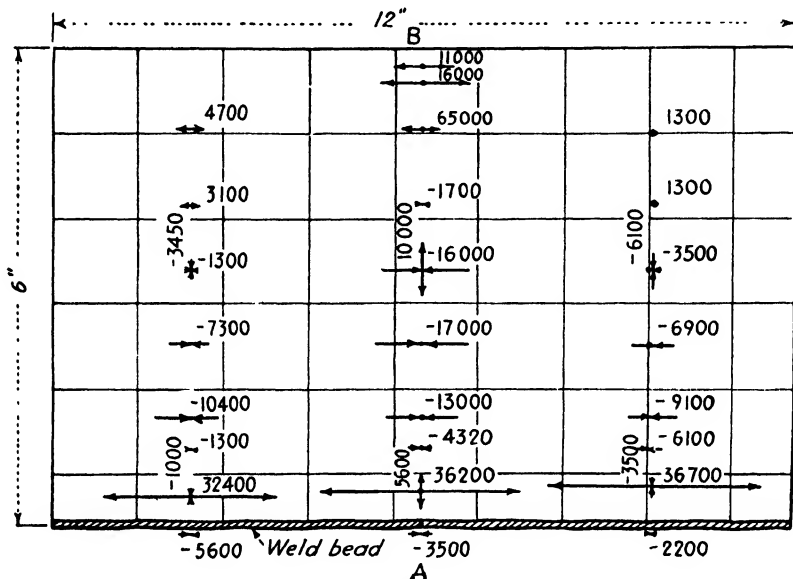


FIG. 13.—Residual stresses caused by welding a bead along one edge of an annealed-steel plate. (Norton and Loring.)

greatly altered by machining off the bead; hence, they resulted largely from plastic flow in the metal near the weld.

In a recent investigation Norton and Rosenthal reported x-ray measurements on the effect of external loading upon residual stresses.<sup>1</sup> A biaxial state of residual stress was introduced into mild-steel strips by squeezing them between two round electrodes of a butt-welding machine and heating locally with a current of 3000 amp. for a few seconds. The results on one of the plates are reproduced in Fig. 14, where the curves marked I show, respectively, the longitudinal and the transverse components of the stresses after the heating, measured along a line through the center of the electrodes. The electrodes contacted the strip from -0.5 to 0.25 on the scale of inches, and it will be noted that the heated

<sup>1</sup> J. T. NORTON and D. ROSENTHAL, *J. Am. Welding Soc.*, vol. 22, no. 2, p. 63S, 1943.

zone was left with stresses approximating the tensile yield point for the steel (which was 35,000 psi.). Curves II, III, IV, and V give the history of these residual stresses after loading and unloading the strip successively to 7200, 16,000, 29,500, and 38,300 psi. Loading to the yield point relieved all the stresses and replaced them with compressive stresses in the direction of the applied load. Since the stresses left after tensile loading were uniformly compressive over both front and back surfaces, the interior of the strip (which was 0.3 in. thick and 3 in. wide) must have been under residual tension. The relief of stresses by fatigue and by bending was also studied by these investigators. Plastic flow induced by applied loads always tends to reduce the residual stresses, and these stresses do not

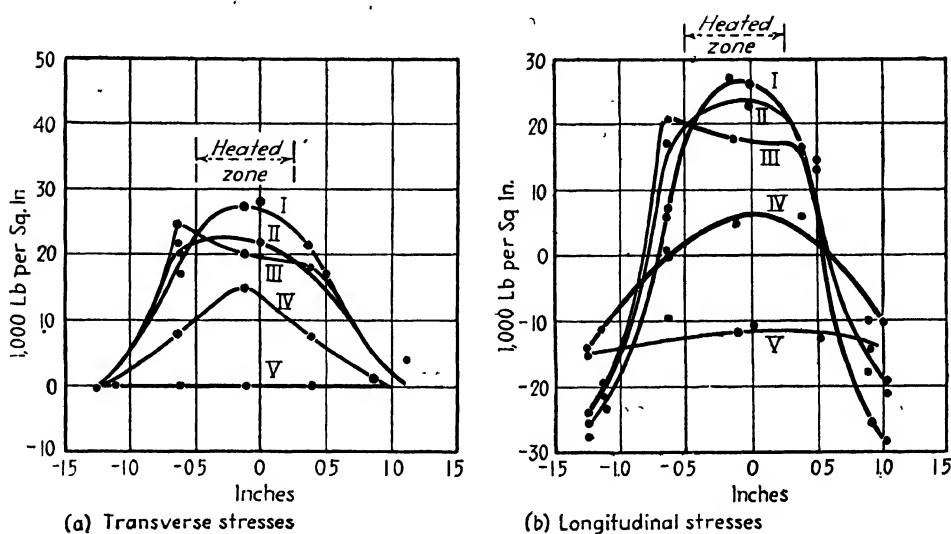


FIG. 14. Residual stresses in a mild-steel strip after local heating and after subsequent straining in tension. I. Directly after heating and cooling. II. After applying 7,200 psi. tensile stress. III. After applying 16,000 psi. tensile stress. IV. After applying 29,500 psi. tensile stress. V. After applying 38,300 psi. tensile stress. (Norton and Rosenthal.)

affect the safety of a structure provided that the material of which the structure is composed is ductile and that the ductility is not decreased by severe triaxial stresses (such as are introduced by notches).

The compressive stresses remaining on the surface after a tensile load, illustrated in Fig. 14, may account for some results of Smith and Wood,<sup>1</sup> who found abnormal values of the lattice constant in specimens that had been stressed beyond the yield point. The increase in the (310) plane spacings of iron amounted to as much as 0.04 percent. They interpreted

<sup>1</sup> W. A. Wood and S. L. Smith, *Nature*, vol. 146, p. 400, 1940. S. L. Smith and W. A. Wood, *Proc. Roy. Soc. (London)*, vol. A176, p. 398, 1940; vol. A178, p. 93, 1941; vol. A179, p. 450, 1942. W. A. Wood and S. L. Smith, *J. Inst. Metals*, vol. 67, p. 315, 1941.

the result as a volume expansion of the lattice, a dilation, which might be the same phenomenon as the change of density with cold work.<sup>1</sup> In any case, whether there are new values of the spacings of all planes or merely a residual surface stress in a specimen that has been plastically deformed, it appears advisable at present to determine the unstressed value of the lattice constant by the two-exposure technique rather than by preparing a stress-free sample. This is suggested because any surface stresses that may exist are difficult to remove by cutting out a sample, while if annealing is resorted to there is the possibility that the density and lattice constant of the material will be altered.

X-rays have been used to measure live loads such as surface stresses in tensile specimens,<sup>2</sup> but such tests are merely for developing technique, estimating accuracy, and testing the method. Modern mechanical and electrical strain gauges are to be preferred when they can be employed, and for determining stress distributions in complex shapes the well-developed methods of photoelasticity are extremely effective.

**X-ray vs. Other Methods of Residual-stress Analysis.**—Numerous reviews of the residual stresses determined by mechanical or sectioning methods are available.<sup>3</sup> The principal methods can be briefly listed as follows:

1. For cylindrical specimens, Sachs's method is best.<sup>4</sup> Successive layers are bored out of the inside of a cylinder, and precision measurements are made of outside diameter and length.

2. For thin-walled cylinders approximate results can be obtained by cutting strips longitudinally or circumferentially.<sup>5</sup>

3. Complete analysis of thin-walled cylinders requires measurements on both longitudinal slots and circumferential rings as the walls are thinned in successive steps.<sup>6</sup>

<sup>1</sup> For recent discussions of this loss of density with cold work, cf. C. Zener, *Trans. A.I.M.E.*, vol. 147, p. 361, 1942, and discussions of this paper.

<sup>2</sup> G. SACHS and J. WEERTS, *Z. Physik*, vol. 60, p. 481, 1930. H. MÖLLER and J. BARBERS, *Mitt. Kaiser-Wilhelm Inst. Eisenforsch. Düsseldorf*, vol. 16, p. 21, 1934. F. WEVER, *Stahl u. Eisen*, vol. 53, p. 497, 1933.

<sup>3</sup> G. SACHS and K. R. VAN HORN, "Practical Metallurgy," A.S.M., Cleveland, Ohio, 1940. W. SPRARAGEN and G. E. KLAUSSEN, "Shrinkage Stresses in Welding," report of Literature Division of the Engineering Foundation Welding Research Committee, New York, 1937. C. S. BARRETT, *Metals & Alloys*, vol. 5, pp. 131, 154, 170, 196, 224, 1934. L. REEVE, *Welding Ind.*, vol. 4, p. 344, 1936.

<sup>4</sup> G. SACHS, *Z. Metallkunde*, vol. 19, p. 352, 1927; G. SACHS and K. R. VAN HORN, "Practical Metallurgy," A.S.M., Cleveland, Ohio, 1940.

<sup>5</sup> W. H. HATFIELD and G. L. THIRKELL, *J. Inst. Metals*, vol. 22, p. 67, 1919. R. J. ANDERSON and E. G. FAHLMAN, *J. Inst. Metals*, vol. 32, p. 367, 1924. D. K. CRAMP-  
TON, *Trans. A.I.M.E.*, vol. 89, p. 233, 1930.

<sup>6</sup> N. DAWIDENKOW, *Z. Metallkunde*, vol. 24, p. 25, 1932. G. SACHS and G. ESPEY, *Metals Tech., Tech. Pub.* 1386, October, 1941.

4. For plate specimens, welds, etc., strain-gauge stations are put on the surface and the specimen is sawed into small pieces, thus releasing the macroscopic stresses. A strain-gauge rosette with gauge lengths in three or four directions at one point on the surface allows full determination of stresses. In these tests it is usually assumed that the stresses do not vary with depth below the surface.

5. Mathar's method<sup>1</sup> measures the strains released by drilling a hole about 0.5 in. in diameter through a plate. The strains are related to stresses by calibration experiments on strips stressed in a testing machine.

Several of these methods could be made to employ x-ray diffraction for strain measurement, but in most cases it would be inadvisable and uneconomical to do so. On the other hand, nondestructive measurement of residual stresses is a proper field for x-rays; changes resulting from stress-relieving treatments and from service conditions may be followed without the necessity of sectioning. If a strain gauge is rigidly attached to a structure to detect such changes, it will register both elastic and plastic strain while x-rays will register the elastic strain only.

<sup>1</sup> J. MATHAR, *Arch. Eisenhüttenw.*, vol. 6, p. 277, 1933; *Trans. A.S.M.E.*, vol. 56, pp. 249, 254, 1934. F. BOLLENRATH, *Stahl u. Eisen.*, vol. 54, pp. 630, 873, 1934; vol. 57, pp. 389, 419, 1937.

## CHAPTER XV

### THE PLASTIC DEFORMATION OF METALS

Plastic flow in crystals occurs by two fundamental mechanisms: slip and twinning. Accompanying the plastic flow are three important modes of lattice reorientation: uniform rotation of crystals, bending of the lattice between the planes of slip, and division of crystals into deformation bands within which the lattice rotates in different directions. Flow may be terminated by either brittle cleavage or ductile fracture. The present chapter concerns the crystallography of slip, twinning, and fracture, including the stresses necessary for these operations, and concludes with a discussion of how the laws of flow in single crystals are modified by conditions in polycrystalline metals.

Subsequent chapters take up current theories of plastic flow, the structure of deformed metal, the nature and theories of preferred orientations generated by plastic flow, and directional properties resulting from preferred orientations.

#### SLIP IN METAL CRYSTALS

**Slip Planes and Directions.**—Plastic deformation in a crystal occurs by the movement of lamellae of the crystal over one another. The

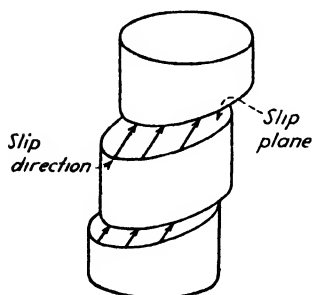


FIG. 1.—Sketch of movement on crystallographic slip planes.

movement is concentrated in a succession of planes, or at least in very thin sheets, as in Fig. 1, leaving the intervening blocks undeformed, like the movement of cards in a pack when the pile is distorted. The displacement takes place along a crystallographic plane, the **slip plane** or **glide plane**, and in a crystallographic direction, the **slip direction**. As details of this mechanism are fundamental to an understanding of plastic flow, strain hardening, cold work, and preferred orientations, a great amount of research has been devoted to the

subject in the last twenty years.<sup>1</sup> A summary of slip planes and slip directions is given in Table XVI.

<sup>1</sup> E. SCHMID and W. BOAS, "Kristallplastizität," J. Springer, Berlin, 1935. C. F. ELAM, "The Distortion of Metal Crystals," Oxford, New York, 1935. H. J. GOUGH, Edgar Marburg Lecture, *Proc. A.S.T.M.*, vol. 33, pt. 2, p. 3, 1933. Report of a Conference on Internal Strains in Solids, *Proc. Phys. Soc. (London)*, vol. 52, 1940. "International Conference on Physics, vol. II, The Solid State of Matter," Physical Society, London, 1935.



TABLE XVI.—SLIP IN METALS

Structure	Metal	Low temperatures		High temperatures	
		Plane	Direction	Plane	Direction
F.c.c.	Al	(111)	[10 $\bar{1}$ ]	(100)	[10 $\bar{1}$ ]
	Cu	(111)	[10 $\bar{1}$ ]		
	Ag	(111)	[10 $\bar{1}$ ]		
	Au	(111)	[10 $\bar{1}$ ]		
	Ni	(111)	[10 $\bar{1}$ ]		
	Cu-Au	(111)	[10 $\bar{1}$ ]		
	$\alpha$ -Cu-Zn	(111)	[10 $\bar{1}$ ]		
	$\alpha$ -Cu-Al	(111)	[10 $\bar{1}$ ]		
	Al-Cu	(111)	[10 $\bar{1}$ ]		
	Al-Zn	(111)	[10 $\bar{1}$ ]		
	Au-Ag	(111)	[10 $\bar{1}$ ]		
B.c.c.	$\alpha$ -Fe	(110)	[111]	(110)	[111]
		(112)	[111]		
		(123)	[111]		
	Mo	(112)	[111]		
	W	(112)	[111]		
	K	(123)	[111]		
	Na	(112)	[111]		
	$\beta$ -Cu-Zn	(110)	[111]		
		(112)(?)			
	$\alpha$ -Fe-Si; 5% Si	(110)			
H.c.p.	Mg	(0001)	[2 $\bar{1}$ 10]	(10 $\bar{1}$ 1) (10 $\bar{1}$ 2)(?) (0001)	[2 $\bar{1}$ 10] [2 $\bar{1}$ 10]
		(10 $\bar{1}$ 1)(?)			
	Cd	(0001)	[2 $\bar{1}$ 10]		
	Zn	(0001)	[2 $\bar{1}$ 10]		
	Be	(0001)	[2 $\bar{1}$ 10]		
	Zn-Cd	(0001)	[2 $\bar{1}$ 10]		
	Zn-Sn	(0001)	[2 $\bar{1}$ 10]		
	Te	(0001)			
Rhombohedral	Bi	(111)	[10 $\bar{1}$ ]		
	Hg	(100) and Complex			
Tetragonal	$\beta$ -Sn (white)	(110)	[001]	(110)	[111]
		(100)	[001]		
		(100)	[011](?)		
		(10 $\bar{1}$ )	[101]		
		(121)	[101]		

In face-centered cubic (f.c.c.) metals the slip plane is normally the plane in the lattice that is most densely packed with atoms, (111), and the same is true of the hexagonal close-packed (h.c.p.) metals, which have the basal plane (0001) as the slip plane. Other planes may become active at elevated temperatures, but these are also planes of relatively high atomic density. In the body-centered cubic (b.c.c.) and tetragonal lattices, slip can occur on several planes, most of which are among the most densely packed ones. Data are somewhat inconclusive for  $\beta$ -brass, Te, Hg, and Sn.<sup>1</sup> Investigation of Bi and Sb\* failed to reveal evidence of slip when deformed at room temperature in tension, for all the deformation was by the process of twinning. However, by compression or by elevating the temperature it is possible to produce slip.<sup>2</sup>

Many metals probably change their slip planes when deformed at unusually high or low temperatures. Examples that have been noted to date include Al,<sup>3</sup> Mg,<sup>4</sup>  $\beta$ -Sn,<sup>†</sup> Mo,<sup>†</sup> Na,<sup>‡</sup> K,<sup>‡</sup> and Fe-Si alloys.<sup>§</sup> Andrade<sup>5</sup> has correlated the operative slip planes in b.c.c. materials with the temperature relative to the melting point. If  $T$  is the absolute temperature at which slip takes place and  $T_m$  the melting point, then the results may be arranged as in Table XVII. This correlation does not seem to apply, however, to iron and Fe-Si alloys, for all three planes, (110), (112), and (123), are active at room temperature in iron<sup>6</sup> and in Fe-Si alloys<sup>§</sup> containing less than 4 percent silicon. At low temperatures or with silicon contents above 4 percent only (110) is an active slip plane in these silicon alloys,<sup>§</sup> whereas (112) would be expected from Table XVII.

It is evident that the slip plane chosen in any lattice is rather easily influenced by temperature and chemical composition and perhaps by the amount of previous deformation, but the slip direction is not so fickle.

<sup>1</sup> H. MARK and M. POLANYI, *Z. Physik*, vol. 18, p. 75, 1923. I. OBINATA and E. SCHMID, *Z. Physik*, vol. 82, p. 224, 1933. E. N. DA C. ANDRADE and P. J. HUTCHINGS, *Proc. Roy. Soc. (London)*, vol. A148, p. 120, 1935.

\* H. J. GOUGH, Edgar Marburg Lecture, *Proc. A.S.T.M.*, vol. 33, pt. 2, p. 3, 1933.

<sup>2</sup> E. N. DA C. ANDRADE, "International Conference on Physics, vol. II, The Solid State of Matter," p. 173, Physical Society, London, 1935. W. F. BERG, "International Conference on Physics, vol. II, The Solid State of Matter," p. 178, Physical Society, London, 1935.

<sup>3</sup> R. KARNOP and G. SACHS, *Z. Physik*, vol. 41, p. 116, 1927; vol. 42, p. 283, 1927. W. BOAS and E. SCHMID, *Z. Physik*, vol. 71, p. 703, 1931.

<sup>4</sup> E. SCHMID, *Z. Elektrochem.*, vol. 37, p. 447, 1931.

<sup>†</sup> E. SCHMID and W. BOAS, "Kristallplastizität," J. Springer, Berlin, 1935.

<sup>‡</sup> E. N. DA C. ANDRADE and L. C. TSIEN, *Proc. Roy. Soc. (London)*, vol. A163, p. 1, 1937.

<sup>§</sup> C. S. BARRETT, G. ANSEL, and R. F. MEHL, *Trans. A.S.M.*, vol. 25, p. 702, 1937.

<sup>5</sup> E. N. DA C. ANDRADE, Report of a Conference on Internal Strains in Solids, *Proc. Phys. Soc. (London)*, vol. 52, p. 1, 1940.

<sup>6</sup> H. J. GOUGH, *Proc. Roy. Soc. (London)*, vol. A118, p. 498, 1928.

TABLE XVII

Metals	$T/T_m$	Slip plane
W, Mo, Na	0.08–0.24	(112)
Mo, Na, $\beta$ -brass	0.26–0.50	(110)
Na, K	0.80	(123)

In f.c.c., b.c.c., rhombohedral, hexagonal, and tetragonal crystals the most closely spaced row of atoms in the lattice is always the direction of slip. In iron, where (110), (112), and (123) all function as slip planes, the direction of slip is always the close-packed direction, [111], which is common to all three sets of planes;<sup>1</sup> and the choice of slip direction is less sensitive to the amount of deformation, the temperature at which deformation is carried out, and the composition than is the slip plane. In ionic lattices of the sodium chloride type, slip is also along the lines of greatest atomic density,  $[1\bar{1}0]$ , although the slip plane, (110), is not the plane of greatest density.<sup>2</sup>

A plane of slip and a direction of slip lying in that plane constitute a **slip system**. Face-centered cubic metals, having four (111) planes and three [101] directions in each, possess 12 slip systems; body-centered iron has four [111] directions around each of which are arranged 12 slip planes having the slip direction as their zone axis, thus giving 48 slip systems.

**Slip Lines.**—Slip is an abrupt movement, sometimes accompanied by an audible tick when the total deformation is small, as was first observed by Joffé and Ehrenfest.<sup>3</sup> In transparent crystals the intermittent nature of the process is evident from observations with polarized light. When a crystal is placed between crossed nicols, individual slip movements cause streaks of light to appear along the slip planes, a result of double refraction from the strains left in the crystal along the slip plane after the slip has occurred.<sup>4</sup>

Slip is most commonly recognized by the presence of slip lines formed by the intersections of slip planes with the surface of a crystal. When the slip direction lies parallel to the surface, there is, of course, no upward displacement of one portion with respect to another, and the lines are nearly invisible. (This fact has been used to determine the slip directions in cylindrical specimens.<sup>5</sup>) Slip lines are distinguishable from other types

<sup>1</sup> H. J. GOUGH, *Proc. Roy. Soc. (London)*, vol. A118, p. 498, 1928.

<sup>2</sup> An extensive discussion of the geometry of slip and its relation to atomic configuration, particularly in minerals, has been published by M. J. Buerger, *Am. Mineral.*, vol. 15, pp. 45, 174, 226, 1930.

<sup>3</sup> ABRAM F. JOFFÉ, "The Physics of Crystals," McGraw-Hill, New York, 1928.

<sup>4</sup> J. W. OBREIMOW and L. W. SCHUBNICKOW, *Z. Physik*, vol. 41, p. 907, 1927. W. SCHÜTZE, *Z. Physik*, vol. 76, p.135, 1932.

<sup>5</sup> H. J. GOUGH, Edgar Marburgh Lecture, *Proc. A.S.T.M.*, vol. 33, pt. 2, p. 3, 1933.

of strain markings by the fact that they are not visible when a deformed metal is polished and etched after the slip has occurred. When slip is on a single set of planes, the slip lines can be very straight. Figure 2 is the appearance of a polished surface of an iron-silicon crystal deformed on two slip planes of the type (110), and Fig. 3 shows an iron crystal deformed on an indefinite number of slip planes. The wavy slip lines of iron are characteristic of slip in this material and were attributed at first to a glide process, "banal glide," in which the slip direction but not the slip planes was considered to be crystallographic, but later investigations showed that the waviness was merely the result of the many slip systems in iron and the ease with which the movement can shift from one to another.<sup>1</sup>

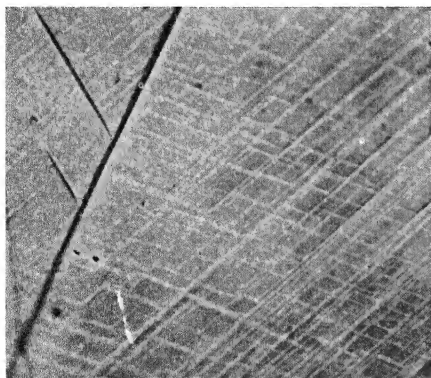


FIG. 2.—Slip lines from two sets of (110) slip planes in silicon ferrite. Black markings at upper left are twins.  $\times 250$ .

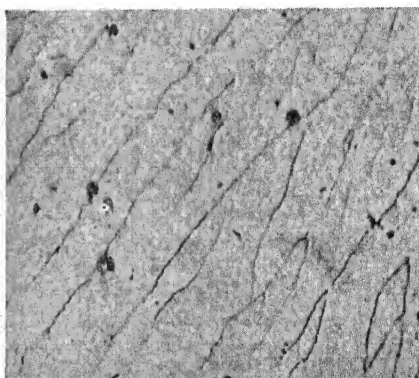


FIG. 3.—Wavy slip lines in  $\alpha$ -iron.  $\times 200$ .

If the movement along slip planes is concentrated on a single plane, the contour of the surface after deformation should appear as in Fig. 4a for compression or Fig. 4b for tension. By electroplating a layer of copper on an iron crystal and then cutting and polishing a section at right angles to the surface, Rosenhain found a saw-tooth contour, as expected from Fig. 4b. Greenland,<sup>2</sup> however, found that single crystals of mercury had contours like Fig. 4c or 4d at a slip line, suggesting that movement had occurred on a series of closely grouped planes rather than on a single one. Hoyt<sup>3</sup> has discussed similar features in the deformation of zinc. It is common to find that slip bands appearing as single lines at low magnification will resolve into groups of closely spaced lines at high magnification, while the regions between the bands, which appear undeformed at low magnification, may contain minute lines that become visible when the resolving power and magnification are increased. Clustering of slip

<sup>1</sup> H. J. GOUGH, Edgar Marburg Lecture, *Proc. A.S.T.M.*, vol. 33, pt. 2, p. 3, 1933.

<sup>2</sup> K. M. GREENLAND, *Proc. Roy. Soc. (London)*, vol. A163, p. 28, 1937.

<sup>3</sup> S. L. HOYT, *Trans. A.I.M.E.*, vol. 74, p. 116, 1927.

lines within a band that appears to be a single line at low magnifications is seen in Fig. 5.<sup>1</sup> In this sample of  $\alpha$ -brass the minimum distance between individual lines resolved by the microscope is approximately 2000 atom

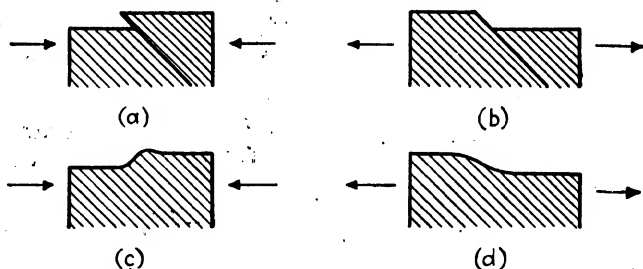


FIG. 4.—Sketches (a) and (b) represent contour expected of surface after slip from compressive and tension stresses, respectively; (c) and (d) illustrate contours found by Greenland on mercury.

diameters, and the displacement of the horizontal scratch indicates an average movement of about 700 atom diameters per visible slip plane.

The displacement at an individual slip line in iron is roughly  $5 \times 10^{-5}$  cm. according to measurements of Rosenhain.<sup>2</sup> In single

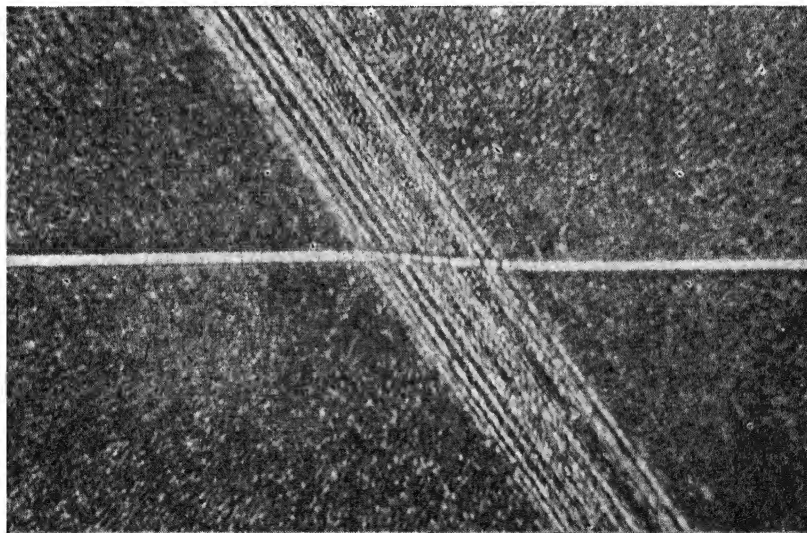


FIG. 5.—Cluster of slip lines in  $\alpha$ -brass cutting across a scratch.  $\times 800$ . (Treuting and Brick.)

crystals of aluminum, Yamaguchi<sup>3</sup> found an average displacement of  $7 \times 10^{-5}$  cm., while Andrade<sup>4</sup> states that the movement may amount to

<sup>1</sup> R. G. TREUTING and R. M. BRICK, *Trans. A.I.M.E.*, vol. 147, p. 128, 1942.

<sup>2</sup> W. ROSENHAIN, "Introduction to Physical Metallurgy," Van Nostrand, New York, 1916.

<sup>3</sup> K. YAMAGUCHI, *Sci. Papers Inst. Phys. Chem. Research (Tokyo)*, vol. 8, p. 289, 1928.

<sup>4</sup> Report of a Conference on Internal Strains in Solids, *Proc. Phys. Soc. (London)*, vol. 52, p. 1, 1940.

as much as 0.1 mm. in metals. It is clear then that, although a simple shift of one atom distance may occur at times, it is not these small displacements that produce the visible lines. The principal slip bands involve a much larger shift, amounting to hundreds or thousands of atom distances. Perhaps they are composed of a whole avalanche of small displacements.

Slip bands are frequently spaced about a micron apart ( $10^{-4}$  cm.) with considerable regularity, a fact that has led to much speculation. Andrade and Roscoe<sup>1</sup> found a probability distribution around a spacing of  $4.2 \times 10^{-4}$  cm., for parallel bands in lead and noted that the spacing was independent of temperature (between 0 and 100°C.), diameter of the crystal, and rate of stretch (varied by a factor of 3000). The spacing did not change with increasing deformation in crystals of lead, cadmium, or mercury for a considerable extension, which indicates that deformation proceeded on slip bands already formed. On the other hand, Yamaguchi<sup>2</sup> observed that the slip bands in aluminum crystals increased in number and became more closely spaced as deformation continued. The behavior of different metals in this respect may be presumed to be related to the amount of strain hardening that results within the slip band during the straining. If the material within a band hardens markedly, it must tend to divert subsequent slip to undeformed regions that are softer, while if the material deforms without appreciable strain hardening further slip can continue in the same band. Thus the stress-strain curve of aluminum shows marked strain hardening and this metal deforms by adding to the number of slip bands, while lead, cadmium, and mercury, when stretched at temperatures where little strain hardening results, deform on the previously existing bands in conformity with this principle.<sup>3</sup>

**Critical Resolved Shear Stress for Slip.**—There is a rather clearly defined stress at which a given crystal will begin to flow at an appreciable rate. Below this stress the rate of strain is so slow it requires long-time tests to measure it. In this range the flow is called **creep**. In the neighborhood of the critical stress the rate of strain increases rapidly and becomes easily measurable with comparatively crude equipment; it is this type of flow that is commonly referred to as **slip**. Many investigations have shown that differently oriented crystals of a given metal will begin to slip when different stresses are applied to their cross section but that *the stresses resolved on the slip plane and in the slip direction are always the*

<sup>1</sup> E. N. DA C. ANDRADE and R. ROSCOE, *Proc. Phys. Soc. (London)*, vol. 49, p. 152, 1937.

<sup>2</sup> K. YAMAGUCHI, *Sci. Papers Inst. Phys. Chem. Research (Tokyo)*, vol. 8, p. 289, 1928. C. F. ELAM, "The Distortion of Metal Crystals," Oxford, New York, 1935.

<sup>3</sup> Report of a Conference on Internal Strains in Solids, *Proc. Phys. Soc. (London)*, vol. 52, p. 1, 1940.

same, the critical resolved shear stress. This is readily computed from the applied load. Referring to Fig. 6, suppose a force  $F$  is applied to a crystal having a cross section of area  $A$ . If the slip plane is inclined at an angle  $\phi$  to the cross-section plane, its area will be  $A/\cos \phi$ , and consequently the stress per unit area acting on the slip plane will be  $F/(A/\cos \phi)$ . This stress is directed along the axis of the crystal, and to resolve this along the slip direction one must multiply by the cosine of

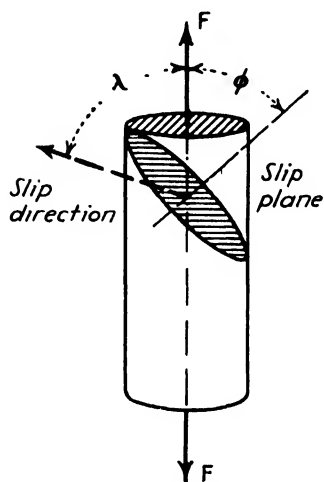


FIG. 6.—Coordinates for calculating resolved shear stresses.

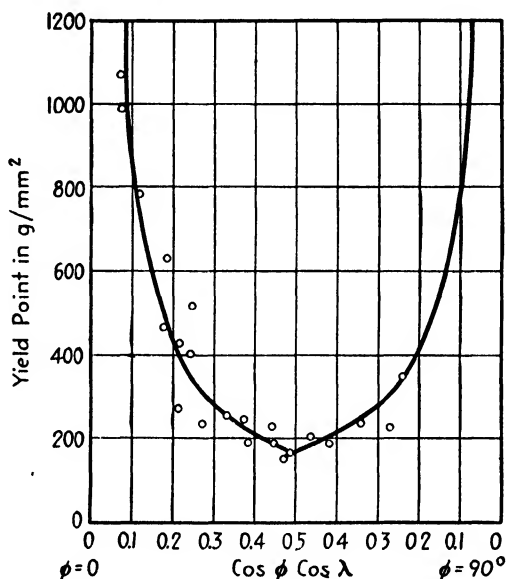


FIG. 7.—Illustrating variation of yield points with orientation of magnesium crystals. Solid curve follows constant resolved-shear-stress law. (Schmid.)

the angle  $\lambda$  between the axis and the direction of slip. The resolved shear stress is then

$$\tau = \frac{F}{A} \cos \phi \cos \lambda.$$

The loads that are required to stretch differently oriented crystals of magnesium are shown in Fig. 7 from the work of Schmid.<sup>1</sup> It will be seen that they vary by more than a factor of 5. The abscissa of this plot is the function  $\cos \phi \cos \lambda$  computed from the known orientations of the crystals, and the curve that is plotted is the variation in load that would be expected if a *constant resolved shear stress* were required for slip in the different crystals. The experimentally determined points follow the curve within the limit of error of the experiments and verify the law. There would have been a systematic trend in the observed values away from the curve if the component of stress *normal* to the slip plane influ-

<sup>1</sup> E. SCHMID, Z. *Elektrochem.*, vol. 37, p. 447, 1931.

enced the slip, and it will be seen that this is not the case. Hydrostatic tests up to 40 atm. have also failed to disclose any influence of normal stress on the resolved shear stress required for slip.<sup>1</sup> The constant-resolved-shear-stress law has been found not only with hexagonal crystals but with cubic and with lower symmetry crystals and appears to be generally applicable.

Hexagonal crystals usually have only one slip plane, the basal plane; the resolved shear stress for a given load is a maximum when this plane is not far from an inclination of  $45^\circ$  to the axis. When this plane is either flatly or steeply inclined to the axis, the resolved stress approaches zero (cf. equation above). Face-centered cubic crystals, on the other hand, have so many slip systems that the resolved shear stress in the most *highly*

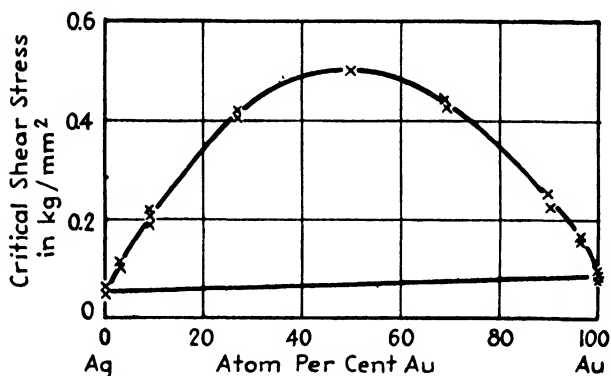


FIG. 8.—Variation in critical shear stress with composition in Ag-Au alloys. (*Sachs and Weerts.*)

stressed plane for a given load can vary only by a factor of 2, and with iron the variation is even less. The orientation dependence has been computed and plotted stereographically and otherwise.

Experiments have repeatedly shown that, when there are several crystallographically equivalent slip systems in a crystal, the one having the greatest resolved shear stress will become active; or if two are stressed equally, there will be slip on both. The critical shearing stress is different for different crystallographic planes of the same crystal, and it differs greatly with different metals, different degrees of purity of a given metal, different temperatures at which deformation is carried out, and different degrees of prior strain. A summary of measured values is given in Table XVIII. If it were possible to inhibit slip on all planes but one, this one could be made the active slip plane regardless of its indices or the density of atomic packing on the plane. It seems certain that planes of higher indices than those of Table XVIII are prevented from becoming active merely by the fact that the planes of easy slip operate and relieve the

<sup>1</sup> M. POLANYI and E. SCHMID, *Z. Physik*, vol. 16, p. 336, 1923.



applied stress before the critical value of the stress is reached on any other planes.

The critical shear stress in the Ag-Au alloys, which form a complete series of solid solutions, is plotted in Fig. 8. The maximum occurs at about the 50 atomic percent composition.<sup>1</sup> A very similar variation with composition is found with Cu-Ni alloys.<sup>2</sup>

TABLE XVIII.—CRITICAL RESOLVED SHEAR STRESS FOR SLIP IN CRYSTALS AT 20°C.

Metal	Impurity content percent	Slip plane	Direction	Critical stress, kg. per sq. mm.
Cu	0.1	(111)	[10 $\bar{1}$ ]	0.10
Ag	0.01	(111)	[10 $\bar{1}$ ]	0.060
Au	0.01	(111)	[10 $\bar{1}$ ]	0.092
Ni	0.2	(111)	[10 $\bar{1}$ ]	0.58
Mg	0.05	(0001)	[11 $\bar{2}$ 0]	0.083
Zn	0.04	(0001)	[11 $\bar{2}$ 0]	0.094
Cd	0.004	(0001)	[11 $\bar{2}$ 0]	0.058
	0.004	(11 $\bar{2}$ 0)		>0.03
$\beta$ -Sn	0.01	(100)	[001]	0.19
	0.01	(110)	[001]	0.13
	0.01	(101)	[10 $\bar{1}$ ]	0.16
	0.01	(121)	[10 $\bar{1}$ ]	0.17
Bi	$\sim 0.1$	(111)	[10 $\bar{1}$ ]	0.221
Hg	$\sim 10^{-6}$	(100)	....	0.007
NaCl		(110)	[1 $\bar{1}$ 0]	$\sim 0.2$
AgCl	... ..	(110)	[1 $\bar{1}$ 0]	$\sim 0.1$

<sup>1</sup> E. SCHMID, "International Conference on Physics, vol. II, The Solid State of Matter," Physical Society, London, 1935.

The critical shearing stress of Zn-Cd and Zn-Sn alloys, shown in Fig. 9,<sup>3</sup> illustrates the general rule that the hardening effect of a *soluble* impurity is greater than that of an *insoluble* one, for cadmium is soluble to the extent of roughly 1.5 percent in zinc (at 250°C.), whereas tin is soluble to less than 0.1 weight percent. Greenland's results<sup>4</sup> on crystals of high-purity distilled mercury are particularly interesting (Fig. 10). The presence of an impurity in concentrations of 1 part in 10<sup>6</sup> or 10<sup>7</sup> has an important effect on the critical shearing stress. (The tests were made at -60°C., about 23° below the melting point.)

<sup>1</sup> G. SACHS and J. WEERTS, *Z. Physik*, vol. 62, p. 473, 1930.

<sup>2</sup> E. OESWALD, *Z. Physik*, vol. 83, p. 55, 1933.

<sup>3</sup> P. RÖSBAUD and E. SCHMID, *Z. Physik*, vol. 32, p. 197, 1925.

<sup>4</sup> K. M. GREENLAND, *Proc. Roy. Soc. (London)*, vol. A163, p. 28, 1937.

Aging of an aluminum alloy containing 5 percent copper increased the critical stress from 1.9 up to 9.3 kg. per sq. mm. The former value was measured in a crystal slowly cooled from 525 to 300°C., the latter after quenching from 525°C. and aging at 100°C. for 1 hr.<sup>1</sup>

**Dependence on Temperature.**—The critical resolved shear stress for a metal decreases with increasing temperature and drops abruptly to zero at the melting point (at the solidus temperature in alloys). Experimental data for hexagonal metals (Fig. 11) indicate a rather small dependence on temperature, particularly in the neighborhood of the melting point.<sup>2</sup> This is also true of aluminum and tungsten.<sup>3</sup> The

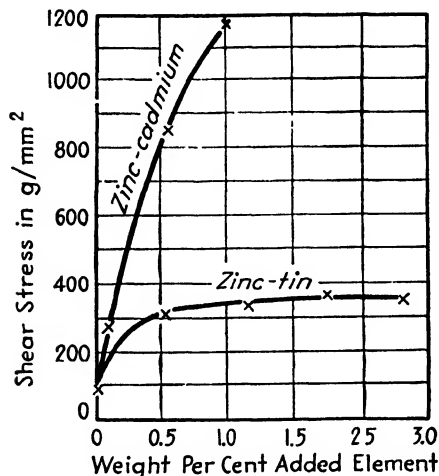


FIG. 9.—Critical shearing stress of Zn-Cd and Zn-Sn alloys. Cadmium is soluble, tin almost insoluble, in the concentrations shown. (Rosbaud and Schmid.)

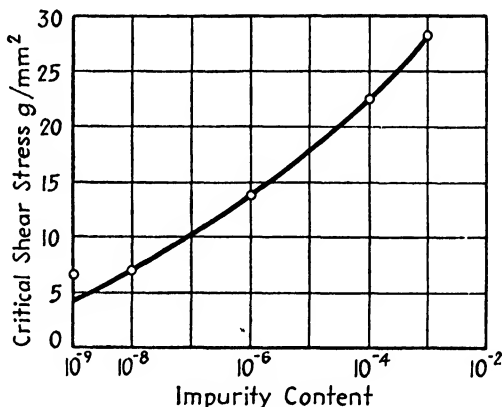


FIG. 10.—Critical shearing stress of single crystals of mercury containing silver as an impurity. Tested at -60°C. (Greenland.)

critical shear stress even near absolute zero is still of the same order of magnitude as at room temperature, and much ductility remains in crystals of cadmium, zinc, and many other metals at these low temperatures. The fact that different slip systems are observed at different temperatures (*e.g.*, aluminum and magnesium) indicates that the alteration in shear strength with temperature is not uniform on all planes of a lattice.

**Strain Hardening.**—The shear stress necessary to cause slip is always increased by prior deformation of the crystal. If a crystal of zinc is sheared as much as 500 percent, which is possible for suitably oriented crystals, the shear stress necessary to continue slip on the basal plane will

<sup>1</sup> R. KARNOP and G. SACHS, *Z. Physik*, vol. 49, p. 480, 1928.

<sup>2</sup> E. SCHMID and W. BOAS, "Kristallplastizität," J. Springer, Berlin, 1935.

<sup>3</sup> "International Conference on Physics," vol. II, The Solid State of Matter, Physical Society, London, 1935.

have increased by a factor of about 7. An even more rapid strain hardening is observed with f.c.c. metals than with hexagonal metals,

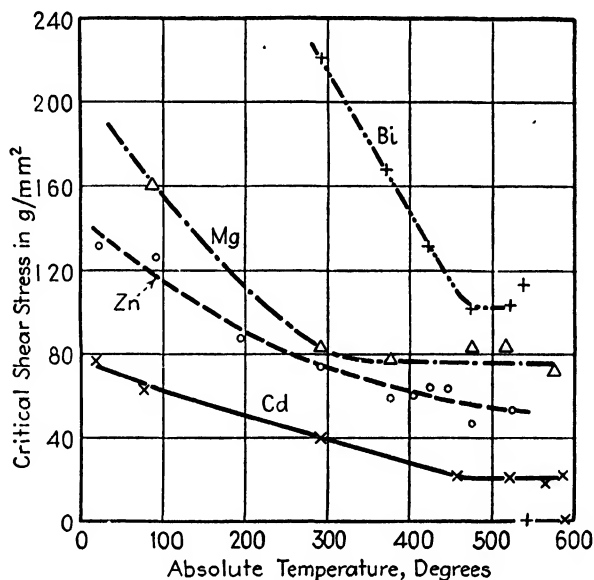


FIG. 11.—Effect of temperature on critical shear stress of metal crystals. (*Schmid and Boas.*)

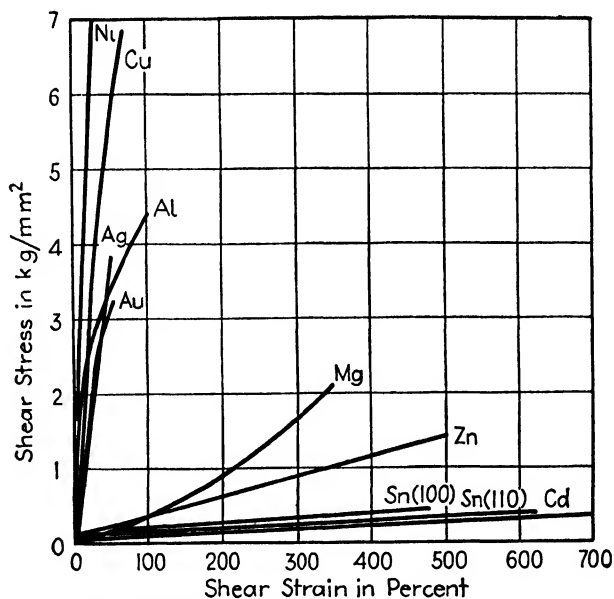


FIG. 12.—Shear-stress—shear-strain diagrams for single crystals. (*Schmid and Boas*)

as is seen in the curves of Fig. 12, where the resolved shear stress is plotted against the amount of shear strain for the f.c.c. metals Ni, Cu, Ag, Al, and Au, the hexagonal metals Mg, Zn, and Cd, and tetragonal

Sn.\* The data of Fig. 12 indicate that strain hardening in some crystals (*e.g.*, zinc) increases linearly with the amount of strain. According to Taylor's results, Fig. 13, aluminum hardens with a different curve. Both the tensile tests (dots) and the compression tests (crosses) follow the parabolic curve  $\sigma = c\sqrt{S}$ , where  $\sigma$  is the resolved shear stress,  $S$  is the shear strain on the slip plane, and  $c$  is a constant. Obviously, the normal stress, which is different in the two tests, does not affect the curve. The whole of the strain-hardening curve, including the initial critical stress, is a function of the rate of deformation. The shape of the curve can be dependent, for example, on whether the stress or the strain is increased uniformly with time,<sup>1</sup> and if the crystal is tested rapidly the stresses will always be higher than if the test is run slowly. The influence of time is further discussed in the following section.

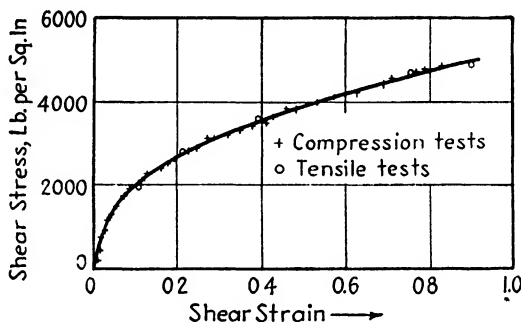


FIG. 13.—Strain hardening in aluminum compression specimens (+) and tensile specimens (O). (Taylor).

**Dependence of Strain Hardening on Temperature.**—Stress-strain curves for magnesium are reproduced in Fig. 14 to show the effect of the temperature at which the test is run.<sup>2</sup> The amount of strain hardening decreases markedly as the temperature is raised. The dashed curves marked  $100^{\circ}S$  and  $250^{\circ}S$  were for a rate of test about a hundredfold faster than the others. It will be noted that, while the rate was not an important factor at  $100^{\circ}C.$ , it exerted a profound effect at  $250^{\circ}$ . Other metals show a temperature dependence of strain hardening of much the same sort. Curves for aluminum are reproduced in Fig. 15.<sup>3</sup>

The effect of holding a metal at a given temperature for a length of time is to anneal the metal and bring about a softening, a **recovery** from the strain hardening. In this process a short time at a high temperature is equivalent to a long time at a low temperature. Stress-strain curves are often considered to be the result of a balance between two

\* E. SCHMID and W. BOAS, "Kristallplastizität," J. Springer, Berlin, 1935.

<sup>1</sup> R. HOUWINK, "Elasticity, Plasticity and Structure of Matter," University Press, Cambridge, Mass., 1937 (especially the chapter by W. G. Burgers).

<sup>2</sup> E. SCHMID, *Z. Elektrochem.*, vol. 37, p. 447, 1931.

<sup>3</sup> W. BOAS and E. SCHMID, *Z. Physik*, vol. 71, p. 703, 1931.

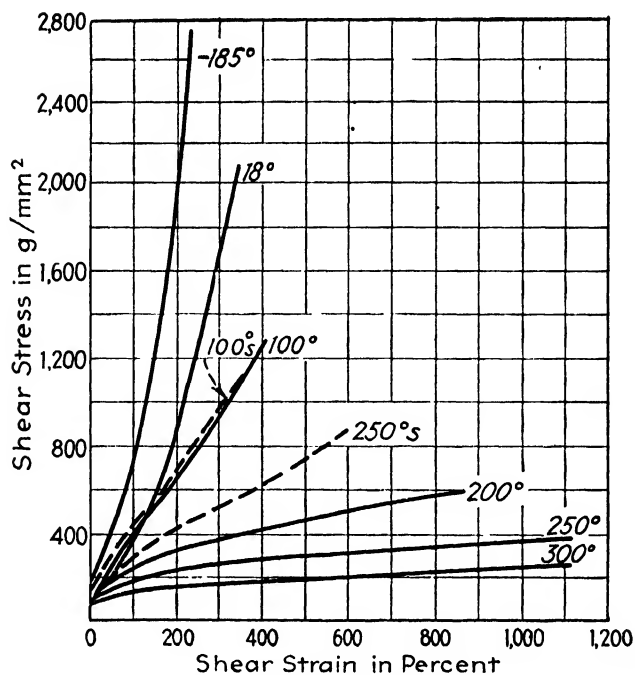


FIG. 14.—Strain hardening in magnesium crystals at different temperatures. Dashed curves 100°S and 250°S are for a rate of test a hundred-fold faster than the others. Temperatures in degrees centigrade. (Schmid and Siebel.)

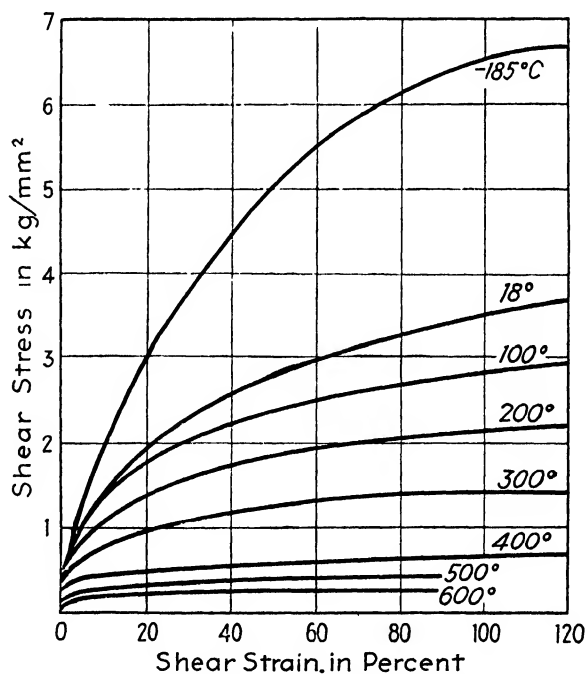


FIG. 15.—Strain hardening in aluminum crystals at different temperatures. (Boas and Schmid.)

opposing tendencies, strain hardening and recovery. At low temperatures, the hardening predominates and the stress-strain curve rises steeply. At elevated temperatures, recovery is proceeding at a rate comparable with the rate of strain hardening, and eventually a temperature is reached at which recovery almost wholly prevents strain hardening. The stress-strain curve is then horizontal (see Figs. 14 and 15).

The separate effects of hardening and recovery can be distinguished more easily if successive stress-strain curves are run with annealing treatments interposed. Figure 16 gives the result of such an experiment on zinc,<sup>1</sup> which partly recovers from the effects of cold work in a rest interval of  $\frac{1}{2}$  min. and completely recovers in an interval of a day. The yield strength is lowered from *A* to *B* (Fig. 16*a*) by a  $\frac{1}{2}$ -min. rest, whereas it

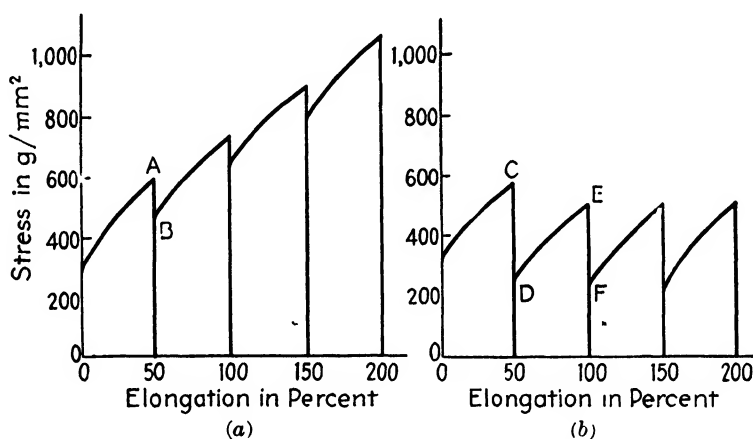


FIG. 16.—Partial recovery (a) and complete recovery (b) in zinc crystals at room temperature. Tests interrupted for  $\frac{1}{2}$  min. in (a) and for 1 day in (b). (Haase and Schmid.)

drops from *C* to *D* or from *E* to *F* (Fig. 16*b*) during a day's rest. It has been objected that the rate of recovery deduced from interrupted tests of this type is much less than the rate of recovery deduced from strain-hardening curves at elevated temperatures, such as those of Figs. 14 and 15. This may mean that the recovery theory is an incomplete or invalid explanation for the temperature dependence or that recovery rates are greater while deformation is proceeding than during a static condition. The critical stress for slip in *undeformed* crystals decreases with rising temperature, and it is reasonable to assume that the same effect also occurs in *work-hardened* material; so this is doubtless also an important factor in the temperature dependence of stress-strain curves.

**Lattice Rotation with Simple Slip.**—When a crystal slips on a single set of planes as in Fig. 17, it shears “sideways” without altering its orientation, but when it is strained in a tensile machine it is not free to do

<sup>1</sup> O. HAASE and E. SCHMID, *Z. Physik*, vol. 33, p. 413, 1925.

this. The constraints of the tensile grips keep the ends in line, and the crystal is forced to deform as in Fig. 18. The central necked-down portion is therefore altered in orientation in such a way that the slip direction becomes more nearly parallel to the axis of tension.

In the compression test another kind of rotation occurs which is easily understood with reference to Fig. 19. The slip planes, indicated by the diagonal lines, rotate toward a position parallel to the plane of the compression plates. The axis about which this rotation takes place is indicated by  $A_r$  and is obviously parallel to the intersection of the slip planes with the compression plates.

The amount of rotation increases as deformation

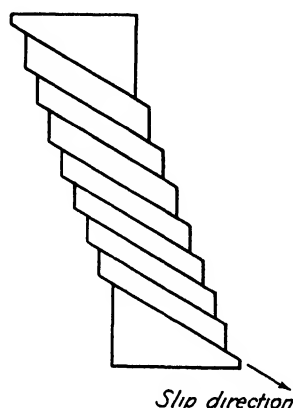


FIG. 17.

FIG. 17.—Deformation of a crystal by slip without constraint.

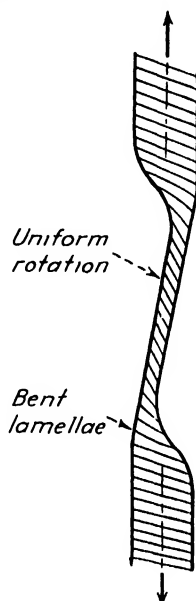


FIG. 18.

FIG. 18.—Rotation and bending in a single crystal elongated in a testing machine. Homogeneous rotation of the necked-down region ends in bend gliding near the grips. The slip direction approaches the tension axis.

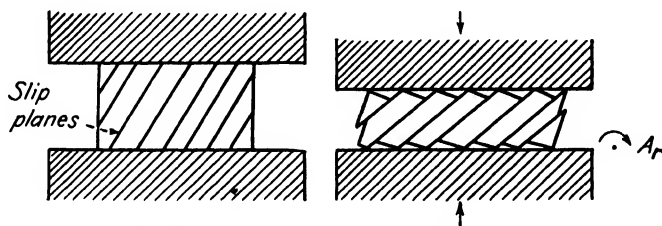


FIG. 19.—Homogeneous lattice rotation in compression. Rotation is around axis  $A_r$ . The slip plane approaches the compression plane.

proceeds and can be computed from simple formulas.<sup>1</sup> For tension the relation is

$$\sin \chi_1 = \frac{l_0}{l_1} \sin \chi_0$$

where  $\chi_0$  and  $\chi_1$  are the initial and final angles between the slip plane and

<sup>1</sup> E. SCHMID and W. BOAS, "Kristallplastizität," Springer, Berlin, 1935.

the tension axis, while  $l_0$  and  $l_1$  are the initial and final lengths of the specimen. By x-ray determination of the orientations before and after deformation it is thus possible to learn the type of rotation a crystal has undergone and thus to determine the indices of the slip system that operated. (This has been useful for hexagonal and f.c.c. crystal studies but is not reliable when many slip systems are active, as in b.c.c. metals or in grains of an aggregate.)

**Duplex Slip.**—As a slip plane rotates away from a position for maximum resolved shear stress (approximately  $45^\circ$  from the axis of tension), the resolved shear stress on the plane diminishes, whereas another potential slip plane in the same crystal—if one exists—is subjected to an increasing component of the stress. Ultimately, the two planes will receive equal components of shear stress, and there will be slip on both planes simultaneously or alternately (duplex slip).

It is found experimentally that crystals tend to rotate slightly past the orientation where duplex slip should start before the second slip plane begins to function. For reasons that are not understood, this is more pronounced in alloy crystals than in pure metals—for instance, it is prominent with crystals of  $\alpha$ -brass.\* A reasonable interpretation of this is that the critical resolved shear stress for slip becomes greater on the inactive plane than on the active one. Since there is strain hardening on the active one, this implies that there is even greater strain hardening on the latent slip planes. In seeking an understanding of this it should be remembered that slip on the second plane must *cut through* the active slip planes, whereas for slip to continue on a plane parallel to those that originally operated it is necessary merely to fit a new slip plane *between* the planes on which slip has previously occurred. If one assumes that strain hardening is localized largely in the vicinity of the slip planes, it would be expected that continued slip on the first set of planes would follow the relatively soft material between slip planes, whereas slip on the second set of planes would have to cut across the relatively harder material around the already existing slip planes.

**Rotation from Duplex Slip.**—Taylor and Elam\* showed that single crystals of aluminum when elongated in tension deform by slip on (111) planes in [110] directions, with an accompanying rotation of [110] toward the axis of tension, until duplex slip starts. The lattice then rotates so as to maintain the axis of tension in a plane symmetrical to the two acting slip planes—*i.e.*, so as to keep equal stresses on the two active systems. Duplex slip and its corresponding rotation continue until the two active slip directions lie in the same plane as the axis of tension and on opposite sides of it. Further elongation does not then cause rotation, and this

\* V. GÖLER and G. SACHS, *Z. Physik*, vol. 55, p. 581, 1929.

<sup>1</sup> G. I. TAYLOR and C. F. ELAM, *Proc. Roy. Soc. (London)*, vol. A102, p. 643, 1923



position is retained until fracture. The nature of these rotations is conveniently shown in stereographic projection, with the axis of tension indicated by a point which moves over a standard projection of the cubic lattice (Fig. 20). The rotation of the axis along the great circle toward  $[110]$  can be noted, as well as the rotation along the symmetrical plane between slip directions  $[011]$  and  $[110]$  to the stable end position, in which  $[121]$  is parallel to the axis.<sup>1</sup>

In deformation by compression, single slip in f.c.c. crystals brings the specimen axis into the plane symmetrical to the poles of the active slip planes; then double slip causes the specimen axis to move in this plane until it reaches the  $[110]$  position that lies in the plane containing the poles of the active slip planes and midway between them. This is a position which is stable throughout the remainder of the deformation.<sup>2</sup>

Hexagonal metals slipping only on the basal plane (0001) rotate so as to bring the basal plane toward the plane of compression or parallel with the axis of tension and cannot exhibit duplex slip. The rotation is eventually stopped, however, by the onset of slip on other planes or, more generally, by twinning.

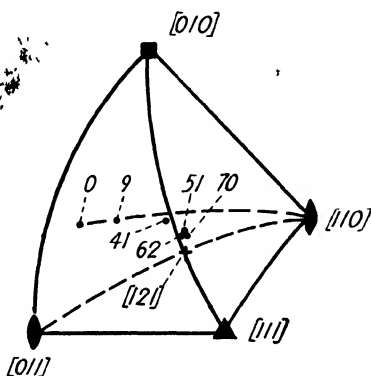


FIG. 20.—Rotation of axis of aluminum single crystal during elongations up to 70 percent. Initial rotation is along a great circle toward the active slip direction  $[110]$ ; then duplex slip moves the axis toward  $[121]$ . (Taylor and Elam.)

**Deformation Bands.**—A common feature of the structure of cold-worked metal is the banded appearance of individual grains. The bands are formed in both single crystals, where their widths may be a millimeter or more, and grains of an aggregate, where they have microscopic dimensions as in Fig. 21. They are visible on a polished and etched surface as twins are, but they differ from twins in that they appear with varying contrast after varying degrees of cold work. Rosenhain<sup>3</sup> believed them to be amorphous metal left on slip planes after slip had taken place. Howe was unsatisfied with this theory and devoted an entire chapter of his book<sup>4</sup> to the “X-bands,” as he called them. He regarded them as regions in which the lattice orientation had changed without reaching a twinned orientation but remarked that their nature had yet to be

<sup>1</sup> G. I. TAYLOR and C. F. ELAM, *Proc. Roy. Soc. (London)*, vol. A108, p. 28, 1925.

<sup>2</sup> G. I. TAYLOR and W. S. FARREN, *Proc. Roy. Soc. (London)*, vol. A111, p. 529, 1926. G. I. TAYLOR, *Proc. Roy. Soc. (London)*, vol. A116, p. 39, 1927.

<sup>3</sup> W. ROSENHAIN, *Engineering*, vol. 96, p. 39, 1913.

<sup>4</sup> H. M. HOWE, “The Metallography of Steel and Cast Iron,” McGraw-Hill, New York, 1916.

discovered. Pfeil<sup>1</sup> made a detailed study of them in iron and surmised that they consisted of lamellar regions within which differing orientations have arisen as a result of slip on different planes. We now know that this view is correct and that this progressively increasing contrast with increasing degrees of cold work is the result of a progressive growth of orientation differences between adjoining bands.<sup>2</sup> The rotation in individual bands creates new grain boundaries within crystals and must therefore contribute to work hardening; it is also an important factor in the development of preferred orientations<sup>3</sup> and will be discussed in later chapters in this connection.

Deformation bands occur in many metals. Mathewson and Phillips<sup>4</sup>

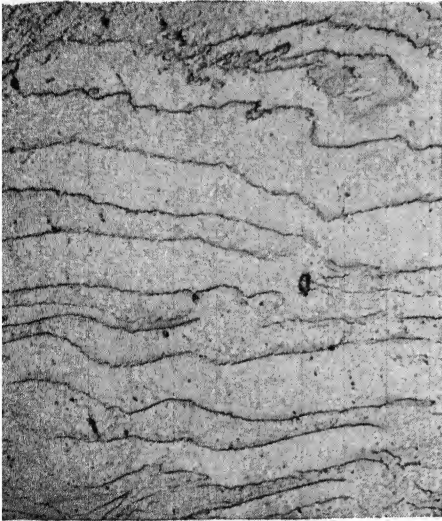


FIG. 21.—Deformation bands in a grain of iron. Section perpendicular to axis of compression, polished and etched after 68 percent reduction in thickness.  $\times 100$ .

observed strain markings in  $\alpha$ -brass that resemble the deformation bands of iron in that their prominence increases with increasing cold work. Probably all f.c.c. metals exhibit them. Johnson<sup>5</sup> has reported them in rolled copper and  $\alpha$ -brass, Adcock<sup>6</sup> in rolled cupronickel (80 percent copper, 20 percent nickel), Elam<sup>7</sup> in rolled silver, and Rosenhain<sup>8</sup> in cupronickel manganese. They make a striking appearance on the surface of large grains of copper after cold rolling (Fig. 22). Body-centered cubic iron exhibits deformation bands after all types of deformation and with both homogeneous and heterogeneous strain, and it is not unlikely that bands are produced in all other b.c.c. metals. The

tendency for a crystal or a grain to develop bands depends upon the orientation of the grain with respect to the direction of flow. For

<sup>1</sup> L. B. PFEIL, *J. Iron Steel Inst., Carnegie Scholarship Mem.*, vol. 15, p. 319, 1926; vol. 16, p. 153, 1927.

<sup>2</sup> C. S. BARRETT, *Trans. A.I.M.E.*, vol. 135, p. 296, 1939.

<sup>3</sup> C. S. BARRETT, *Trans. A.I.M.E.*, vol. 135, p. 296, 1939. C. S. BARRETT and L. H. LEVENSON, *Trans. A.I.M.E.*, vol. 135, p. 327, 1939; vol. 137, p. 112, 1940; vol. 147, p. 57, 1942.

<sup>4</sup> C. H. MATHEWSON and A. PHILLIPS, *Trans. A.I.M.E.*, vol. 54, p. 608, 1916.

<sup>5</sup> F. JOHNSON, *J. Inst. Metals*, vol. 21, p. 335, 1919; vol. 27, p. 93, 1922.

<sup>6</sup> F. ADCOCK, *J. Inst. Metals*, vol. 27, p. 73, 1922.

<sup>7</sup> C. F. ELAM, *J. Inst. Metals*, vol. 27, p. 94, 1922.

<sup>8</sup> W. ROSENHAIN, *J. Inst. Metals*, vol. 27, p. 96, 1922.

example, an iron crystal having a  $[100]$  axis parallel to the axis of compression will form no bands, and the same is true if  $[111]$  is parallel to the axis of compression; crystals of all other orientations become banded.

The crystallography of the bands has not been extensively studied. It is known, however, that in iron during elongation the boundaries first form on  $\{100\}$  and  $\{111\}$  planes, and in aluminum during compression they form on  $\{100\}$  planes and perhaps others in addition to these. Some "twinlike" bands reported by Elam<sup>1</sup> in  $\beta$ -brass, which formed on  $\{100\}$  and  $\{111\}$  planes, were probably deformation bands.

**Lattice Bending.**—Not all the distortion of the lattice in crystals is so regular as the type discussed in the preceding section. The lattice within a single deformation band often exhibits a large range of orientations from one side to another, and even in the absence of clearly defined bands there is usually a spread in orientation from point to point within a crystal or grain. Figure 18, page 303, illustrates a simple case of this in which the lamellae between slip planes have been bent by the constraints imposed by the grips of the tensile machine. In polycrystalline material the constraints of neighboring grains cause the inhomogeneities of stress that produce the bending. There is probably no crystallographic regularity to this type of distortion because of the random nature of the imposed stresses; nevertheless, it is an important characteristic of the structure of cold-worked metal and is discussed further in Chap. XVII.

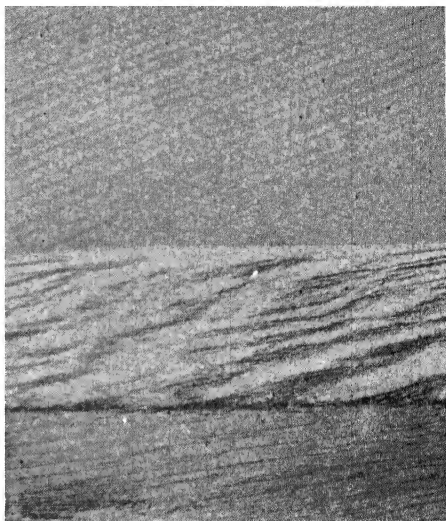


FIG. 22.—Deformation bands in large grains of copper after rolling.  $\times 1$ .

## TWINNING

Crystals may deform not only by slip but by twinning. Twinning results when a lamella within a crystal takes up a new orientation related to the rest of the crystal in a definite symmetrical fashion. The lattice within the twinned portion is a mirror image of the rest; the plane of symmetry relating the one portion to the other is called the *twinning plane*. During deformation the formation of twins takes place with a click, and a rapid succession of clicks is responsible for the "cry" that is heard when a bar of tin is bent. Twins also appear in some metals during

<sup>1</sup> C. F. ELAM, *Proc. Roy. Soc. (London)*, vol. A153, p. 273, 1936.

annealing, probably as the result of growth from minute twinned nuclei produced by straining. They are also found in some metals after a phase transformation has occurred.

The symmetrical relation between a twin and its parent crystal may be described by stating that rotation of  $180^\circ$  about a certain axis (the **twinning axis**) in the crystal would put the crystal into the twinned orientation, though this statement is not meant to imply that twinning actually occurs by lattice rotation. The atom movements that produce a deformation twin are *shearing* movements of the atomic planes over one another, not rotation of planes. This type of movement is usually one of simple shear, in which every plane of atoms shifts in the same direction

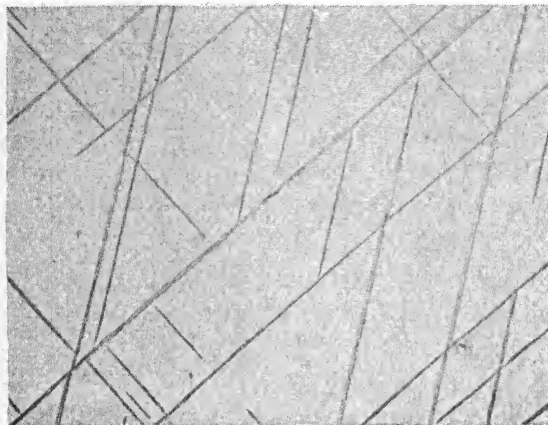


FIG. 23.—Twins (Neumann bands) in a crystal of ferrite. Photomicrograph of a polished and etched grain.  $\times 100$ .

and shifts an amount proportional to its distance from the twinning plane. When twins are produced by deformation, it is sometimes possible to see that shearing of this kind actually occurs.<sup>1</sup>

**Deformation Twins.**—Iron and alloyed ferrites are twinned by impact at room temperature and by slow deformation at lower temperatures to form the characteristic narrow lamellae known as **Neumann bands**, shown in Fig. 23. That these lamellae are actually twins was under dispute for many years but has now been proved by microscopic methods<sup>2</sup> and by x-ray reflections.<sup>3</sup>

<sup>1</sup> In some crystals (for example, Mg, Zn, white Sn, Bi, Sb) studies of atomic positions have shown that the individual atoms do not shift into their twinned positions by the operation of *homogeneous* shear such that each atom layer moves a distance proportional to its distance from the twinning plane. The macroscopic dimension changes even in these cases, however, do correspond to simple shear. [G. Kolesnikow, *Physik. Z. Sowjetunion*, vol. 4, p. 651, 1933; Bruce Chalmers, *Proc. Phys. Soc. (London)*, vol. 47, p. 733, 1935.]

<sup>2</sup> K. HARNECKER and E. RASSOW, *Z. Metallkunde*, vol. 16, p. 312, 1924.

<sup>3</sup> C. H. MATHEWSON and G. H. EDMUNDS, *Trans. A.I.M.E.*, vol. 80, p. 311, 1928.

Deformation twins are usually distinguishable from slip lines by the following characteristics: (1) Twins are visible after polishing and etching while slip lines are not. (2) Twins usually can be seen under high magnification to have a definite width so that two boundaries can be seen to each band, whereas slip produces a narrow *line* on the surface. These characteristics are illustrated in the twins of Fig. 23. These criteria are not always decisive, however. Markings found after polishing and etching may be deformation bands, but these can usually be distinguished from twins by the fact that they increase in visibility (contrast) with increasing deformation of the specimen. Again, in some alloys there may be a transition phase formed in thin lamellae which somewhat resemble twins. Metastable  $\beta$ -brass, for example, can undergo this martensite-like transformation and produce remarkably long straight and narrow striae of the transition structure;<sup>1</sup> so also can  $\beta$ -copper aluminum.<sup>2</sup> While slip lines themselves are invisible after polishing and etching, in a supersaturated solid solution there may be precipitation along the slipped surfaces which serves to delineate them. Careful microscopy then shows strings of tiny particles lying along the traces of the slip planes in the surface of polish, indicating a more rapid nucleation or growth (or both) in the highly strained material adjacent to the slipping surfaces.<sup>3</sup> Perhaps it is possible for the distortion along a slip plane to cause a local rotation or fragmentation of the lattice of a type that could be revealed by etching.

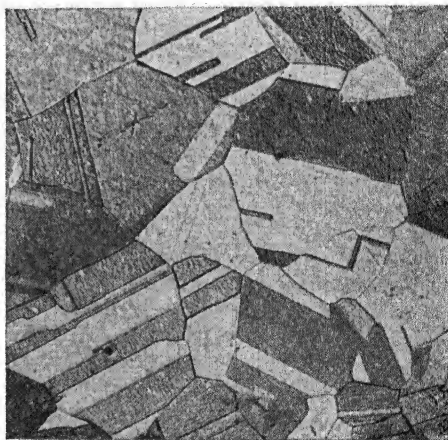


FIG. 24.—Annealing twins in brass, electrolytic polish.  $\times 100$ .

Copper and its solid solutions appear to be twinned by deformation under certain conditions, producing thin lamellae much like Neumann bands<sup>4</sup> which grow during annealing into longer and wider bands of the microstructure of Figs. 24 and 25, so characteristic of copper and brass. Twinning is a major factor in the deformation of some metals such as zinc, where a change of shape of a crystal sometimes occurs almost entirely by conversion of the crystal into one or more twinned orientations at early stages of deformation and where twinning may provide favorably

<sup>1</sup> A. B. GRENINGER and V. G. MOORADIAN, *Trans. A.I.M.E.*, vol. 128, p. 337, 1938.

<sup>2</sup> A. B. GRENINGER, *Trans. A.I.M.E.*, vol. 133, p. 204, 1939.

<sup>3</sup> See, for example, W. L. FINK and D. W. SMITH, *Trans. A.I.M.E.*, vol. 128, p. 223, 1938.

<sup>4</sup> C. H. MATHEWSON, *Trans. A.I.M.E.*, vol. 78, p. 7, 1928.

oriented slip planes for further deformation in the advanced stages of deformation.<sup>1</sup>

Bismuth and antimony (rhombohedral) are believed to deform at room temperature entirely by twinning.<sup>2</sup> The appearance of a polished surface of a single crystal of antimony after a stressing that produced abundant

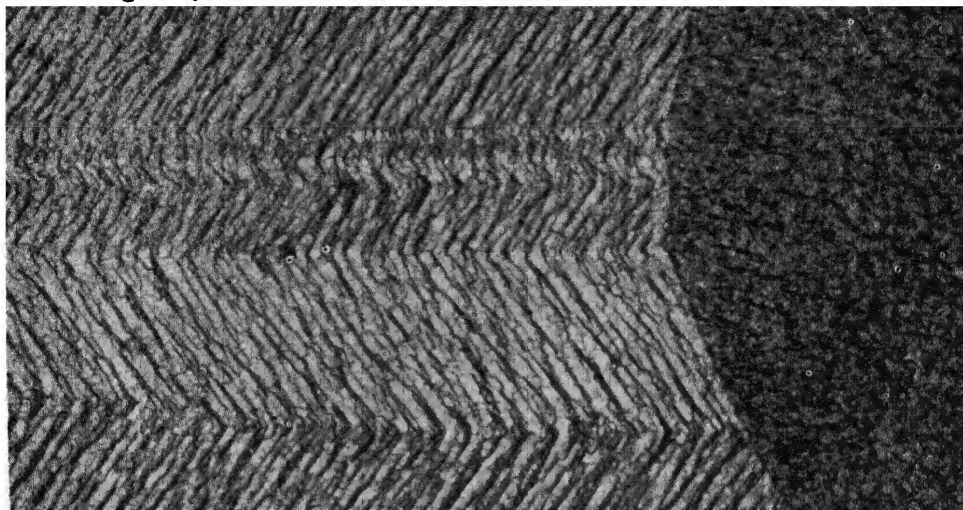


FIG. 25.—Annealing twins in brass, etched to develop facets revealing the orientations.  $\times 1000$ . (Lucas.)

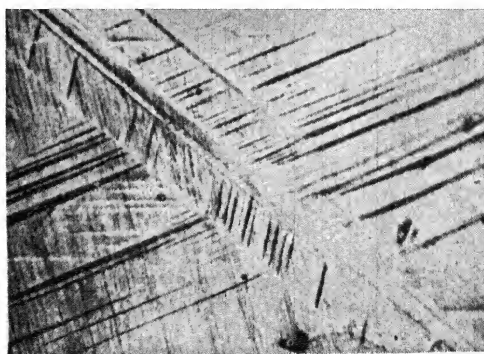


FIG. 26.—Single crystal of antimony after deformation, showing primary and secondary twins but no slip lines.  $\times 130$ . (Gough.)

slip lines in other crystals is illustrated in Fig. 26. It will be noted that secondary twins form abundantly within primary twins.

<sup>1</sup> C. H. MATHEWSON and A. J. PHILLIPS, *Trans. A.I.M.E.*, vol. 74, p. 143, 1927. G. EDMUNDS and M. L. FULLER, *Trans. A.I.M.E.*, vol. 99, p. 175, 1932. E. SCHMID and G. WASSERMANN, *Z. Physik*, vol. 48, p. 370, 1928. H. MARK, M. POLANYI, and E. SCHMID, *Z. Physik*, vol. 12, p. 58, 1922.

<sup>2</sup> H. J. GOUGH and H. L. COX, *Proc. Roy. Soc. (London)*, vol. A127, p. 431, 1930; *J. Inst. Metals*, vol. 48, p. 227, 1932.

Twinning during deformation is usually accompanied by a sharp click, which indicates that it is a very abrupt process. When twinning occurs during a tensile test of a single crystal, there are jagged irregularities in the stress-strain curve, as in the later stages of the curve for cadmium in Fig. 27.

Interesting experiments on twinning in tin have been reported by Chalmers,<sup>1</sup> who has found that large blocks of white tin (tetragonal  $\beta$ ) twin during impact at room temperature with the expenditure of a definite amount of energy per unit volume of the twinned material.\* This energy is  $8 \times 10^6$  ergs per cc. Since the potential energy of the lattice after twinning is the same as before, this twinning energy appears in the crystal after twinning as heat, save for slight losses. It corresponds to a rise in temperature of  $0.05^\circ\text{C}.$ , which was approximately what Chalmers observed. It is possible by subsequent impacts either to extend the twinned portion or to untwin the crystal.

**Crystallography of Twins.**—The observations of twinning in metals have been summarized by Mathewson,<sup>2</sup> by Schmid,<sup>3</sup> and by Gough<sup>4</sup> and are presented in Table XIV. It will be noticed that invariably the twinning plane in f.c.c. metals is  $\{111\}$ , in b.c.c. metals  $\{112\}$ , in h.c.p. metals  $\{10\bar{1}2\}$ , and in rhombohedral metals  $\{011\}$ .\*

**Orientations from Twinning.**—The symmetry relationships produced by twinning, which are important in connection with deformation and recrystallization studies, are best described by means of the stereographic

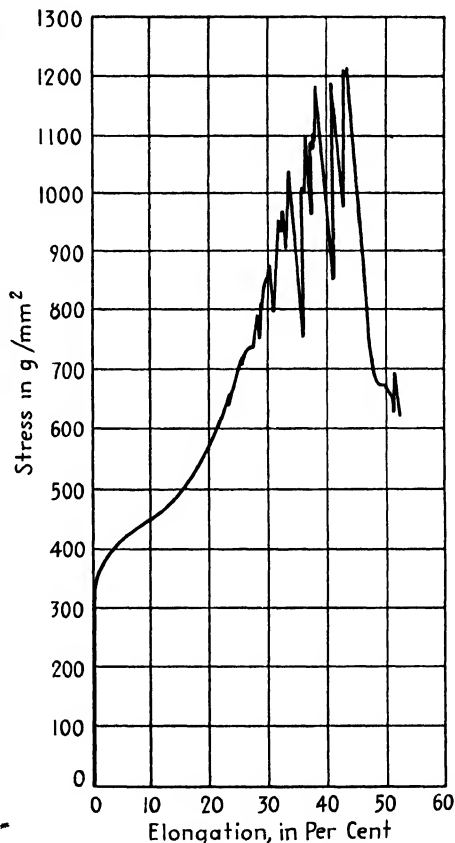


FIG. 27.—Stress-strain curve for a cadmium single crystal with irregularities due to twinning. (Boas and Schmid.)

<sup>1</sup> BRUCE CHALMERS, *Proc. Phys. Soc. (London)*, vol. 47, p. 733, 1935.

<sup>2</sup> C. H. MATHEWSON, *Trans. A.I.M.E.*, vol. 78, p. 7, 1928.

<sup>3</sup> E. SCHMID, *Z. Metallkunde*, vol. 20, p. 421, 1928.

<sup>4</sup> H. J. GOUGH, Edgar Marburg Lecture, *Proc. A.S.T.M.*, vol. 33, pt. 2, p. 3, 1933.

\* Referred to hexagonal axes, this is  $\{01\bar{1}2\}$ . Twinning on  $(10\bar{1}1)$  in Mg, reported by E. Schmid, *Z. Elektrochem.*, vol. 37, p. 447, 1931, has not been confirmed by the careful investigation conducted by P. W. Bakarian, *Tech. Pub.* 1561, *Metals Tech.*, 1943.

TABLE XIX.—CRYSTALLOGRAPHY OF TWINNING IN METALS

Lattice	Metal	Twinning plane ( $k_1$ )	Twinning direction ( $n_1$ )*
B.c.c.	$\alpha$ -Fe	(112)	[111]
	$\beta$ -Cu-Zn	(112)	[111]
	W	(112)	[111]
H.c.p.	Cd	(10 $\bar{1}$ 2)	
	Zn	(10 $\bar{1}$ 2)	
	Zn-Cd	(10 $\bar{1}$ 2)	
	Zn-Sn	(10 $\bar{1}$ 2)	
	Be	(10 $\bar{1}$ 2)	
	Mg	(10 $\bar{1}$ 2)	
F.c.c.	Al	(111)	[11 $\bar{2}$ ]
	Cu	(111)	[11 $\bar{2}$ ]
	Ag	(111)	[11 $\bar{2}$ ]
	Au	(111)	[11 $\bar{2}$ ]
	Cu-Zn	(111)	[11 $\bar{2}$ ]
	Cu-Al	(111)	[11 $\bar{2}$ ]
	Al-Cu	(111)	[11 $\bar{2}$ ]
	Al-Zn	(111)	[11 $\bar{2}$ ]
	Au-Ag	(111)	[11 $\bar{2}$ ]
	Cu-Au	(111)	[11 $\bar{2}$ ]
Rhombohedral	Bi	(011)	
	As	(011)	
	Sn	(011)	
Tetragonal	$\beta$ -Sn (white)	(331)	

\* See p. 316.

projection. The simplest case is illustrated in Fig. 28, the case of (111) twinning in a f.c.c. metal. The open squares are the  $\langle 100 \rangle$  directions of the original crystal, the black squares the  $\langle 100 \rangle$  directions formed from these by reflection across the indicated (111) twinning plane. The black squares AAA then represent the orientation of one of the twins that could form from the original crystal. It is interesting to note that the twinned orientation would also have been given by reflection across the (112) plane shown; this is always the case in cubic lattices and means that as far as *lattice orientations* are concerned the kind of twinning found in face-centered and in body-centered lattices is the same. (There is a difference between them in the distances between atoms, discussed in the following section.<sup>1</sup>)

<sup>1</sup> A. B. GRENINGER, *Trans. A.I.M.E.*, vol. 120, p. 293, 1936, has pointed out that



If twinning occurs on all  $\{111\}$  face-centered planes or on all  $\{112\}$  body-centered planes, there results in either case a total of four new orientations, whose cube poles are plotted as black squares in Fig. 28. If each of the twins of the "first order" is itself again twinned, a set of "second-order" twins is formed with 12 new orientations, etc.<sup>1</sup>

**Atom Movements in Twinning.**—In many lattices the movement required to produce a twin is a simple homogeneous shear, each plane moving a distance proportional to its distance from the twinning plane. An example of this type is sketched in Fig. 29, the b.c.c. lattice. In the unit cube drawn in the upper part of the figure the twinning plane,  $(211)$ , is indicated by dot-dash lines; this plane stands perpendicular to the paper in the lower part of the figure, and the atom movements to form a twin are indicated by arrows. The movement of an atomic layer to produce a twin is rather similar to the movement to produce slip. This is readily seen in the f.c.c. lattice, for which the twinning movements are shown in Fig. 30. The shear of one  $(111)$  layer, indicated by filled circles, over the underlying layer, indicated by open circles, is one-third the identity distance in the direction of motion, which is  $30^\circ$  from the closest packed direction that is the direction of motion in slip. (Two such motions along a zigzag path would give the type of movement that occurs in slip, as indicated by the dashed line in the lower right of the figure.)

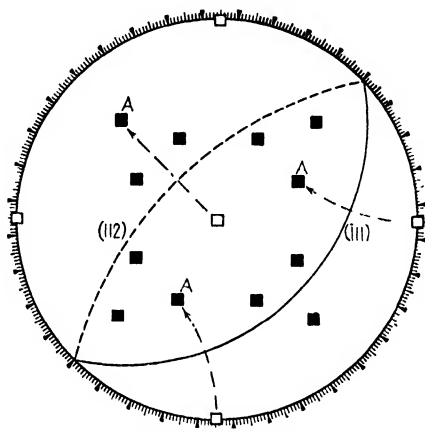


FIG. 28.—Orientations in twinned cubic crystals. Hollow squares are cube axes of original crystal; black squares are cube axes of first-order twins; twinning planes are indicated by full and dashed great circles.

The similarity between the fundamental movements in twinning and slip has led to suggestions that dislocations are responsible for twinning in much the same way that they are postulated for slip,<sup>3</sup> and it is hoped that a more thorough understanding of one process will give a better understanding of the other. However, it is not likely that the analogy between the two will be very complete, for the atomic motions in the

---

the two components of a  $(111)$  or  $(112)$  twin have in common the following: one  $\{111\}$  plane, three  $\{110\}$  planes, and three  $\{112\}$  planes, and many others.

<sup>1</sup> The orientations for two and three generations in cubic metals and in zinc are plotted in Mathewson's review.

<sup>3</sup> J. FRENKEL and T. KONTOROVA, *J. Phys. Chem. (U.S.S.R.)*, vol. 1, p. 137, 1939, F. SEITZ and T. A. READ, *J. Applied Phys.*, vol. 12, p. 470, 1941.

twinning of tin and some other metals are not so simple as the cases discussed here.<sup>1</sup>

In view of the fact that twinning on  $\{111\}$  planes and on  $\{112\}$  planes of cubic metals leads to the same orientation, one wonders why twins choose one plane in face-centered lattices and another in body-centered lattices. It has been suggested<sup>2</sup> that the components of a twin have in common at least one plane of atoms and that the reflecting plane (twin-

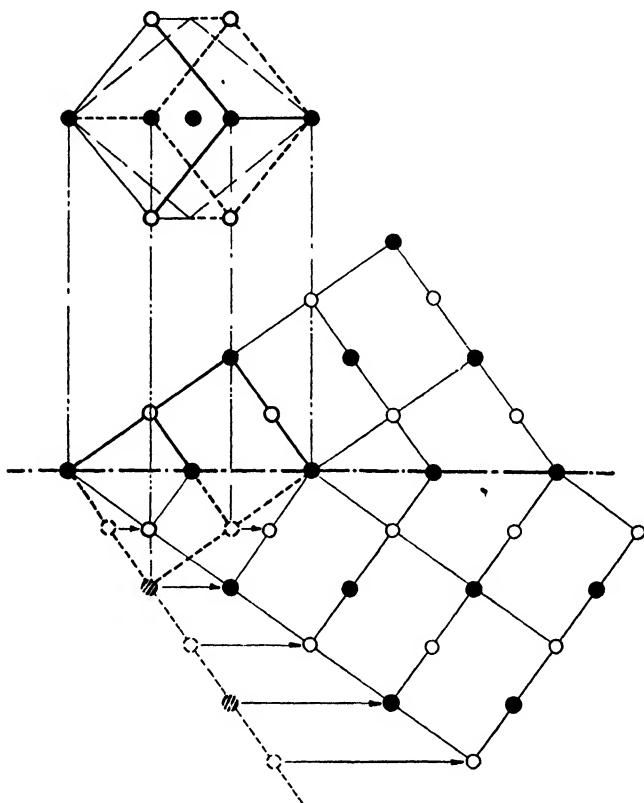


FIG. 29.—Shear movements for twinning a body-centered cubic crystal. Twinning plane is normal to the paper, intersecting it along the heavy dot-dash line in the lower drawing. Shear of atoms below this is indicated by arrows. Position of (211) plane in unit cell is indicated by dot-dash line in upper drawing.

ning plane) can only be one for which the operation of twinning does not bring atom centers closer together than the normal closest distance of approach in either component.

If the f.c.c. crystal is considered from this standpoint, it will be found that the distance between nearest atoms remains unchanged by  $\{111\}$

<sup>1</sup> BRUCE CHALMERS, *Proc. Phys. Soc. (London)*, vol. 47, p. 733, 1935. See first footnote on p. 308.

<sup>2</sup> L. W. MCKEEHAN, *Nature*, vol. 119, pp. 120, 392, 1927. G. D. PRESTON, *Nature*, vol. 119, p. 600, 1927.

twinning, but that  $\{112\}$  twinning would have placed certain neighboring atoms at  $a_0/\sqrt{6} = 0.408a_0$  instead of the normal  $a_0/\sqrt{2} = 0.707a_0$ , and thus only  $\{111\}$  twinning can occur without considerable distortion of atomic positions. On the other hand, b.c.c. crystals twinned on  $\{111\}$  would involve bringing atoms to  $a_0/\sqrt{3} = 0.577a_0$  in place of their normal  $a_0\sqrt{3}/2 = 0.866a_0$  (a decrease of 33 percent) and would therefore involve much distortion of atomic position, whereas  $\{112\}$  twinning would involve a decrease of only 5.8 percent, from  $0.866a_0$  to  $\frac{2}{3}\sqrt{\frac{3}{2}}a_0 = 0.816a_0$ .

**Critical Stress for Twinning.**—Experiments indicate, although not too conclusively, that there is a critical resolved shearing stress associated with the twinning process, just as there is with the process of slip, when twinning is caused by steady application of a load.<sup>1</sup> Davidson, Kolesnikov, and Fedorov reported an increase in the resistance to twinning with decreasing temperature, in the case of zinc, up to a value four to ten times the slip resistance. Practically nothing is known about the influence of composition on the stress to cause twinning, nor of the possible effect of normal stresses (although by analogy with slip resistance it appears likely that stresses normal to the twinning plane should have no effect). Miller found that the critical resolved shearing stress for twinning in 99.999 percent zinc was 300 to 600 g. per sq. mm. in single crystals that had immeasurably low critical stress for slip. The twinning stress decreased when the amount of preceding slip on the basal plane increased and when the speed of deformation increased.

**Deformation by Twinning.**—Schmid and Wassermann<sup>2</sup> have analyzed the change in shape that a crystal can undergo by twinning. Referring to Fig. 31, there are two important reference planes to be considered. These are the ones which remain undistorted by the shearing process—i.e., planes on which inscribed circles would remain unchanged. One of

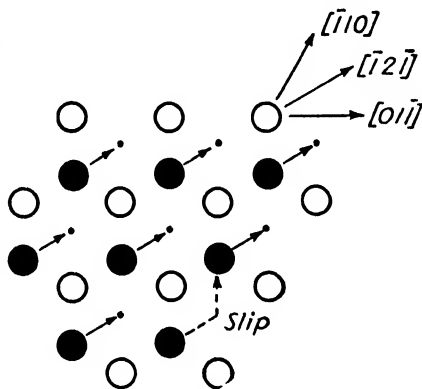


FIG. 30.—Movement of atoms in adjacent (111) layers of face-centered cubic lattice during twinning. Dashed arrow is corresponding movement in slip.

<sup>1</sup> N. DAVIDSON, A. F. KOLESNIKOV, and K. V. FEDOROV, *J. Exptl. Theoret. Phys.* (Russian), vol. 3, p. 350, 1933. R. F. MILLER, *Trans. A.I.M.E.*, vol. 122, p. 176, 1936. BRUCE CHALMERS, *Proc. Phys. Soc. (London)*, vol. 47, p. 733, 1935. H. J. GOUGH and H. L. COX, *Proc. Roy. Soc. (London)*, vol. A127, p. 431, 1930.

<sup>2</sup> E. SCHMID and G. WASSERMANN, *Z. Physik*, vol. 48, p. 370, 1928. For summaries of this treatment see E. Schmid and W. Boas, "Kristallplastizität," Springer, Berlin, 1935; C. F. Elam, "The Distortion of Metal Crystals," Oxford, New York, 1935.

the undistorted planes,  $K_1$ , is the twinning plane or glide plane and contains the glide direction  $n_1$ ; the second undistorted plane is  $K_2$ , located at an angle from the first that is determined by the magnitude of the shear. The shear is defined by the distance  $s$  through which a point moves that lies a unit distance from the plane  $K_1$  (see Fig. 31), and if  $2\phi$  is the acute angle between the planes  $K_1$  and  $K_2$  it follows that

$$\tan 2\phi = \frac{2}{s}.$$

The reference sphere on which the orientation of the axis of a crystal is plotted will be divided into four regions by these two undistorted planes  $K_1$  and  $K_2$ . A specimen whose longitudinal axis lies in one of the two regions in the *acute* angle between  $K_1$  and  $K_2$  will be shortened by the

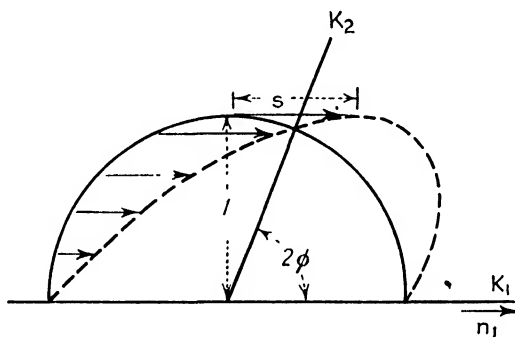


FIG. 31.—Homogeneous shear as in twinning. Undeformed planes  $K_1$  (the twinning plane) and  $K_2$  are normal to the paper.

formation of a twin, while a specimen in the *obtuse* angle between the undeformed planes  $K_1$  and  $K_2$  will be lengthened.<sup>1</sup> The actual magnitude of the dimension changes from twinning are by no means so great as those in slip; for example, the maximum extension possible by twinning a crystal of zinc amounts to only 7.39 percent when the crystal is entirely converted to a twin on the  $\{1012\}$  plane. But the role of twinning in the deformation of hexagonal metals is by no means unimportant, as has been mentioned earlier in this section, for twinning brings slip planes into positions favorable for further deformation.

<sup>1</sup> The new length  $l$  will be related to the length of the axis in the original untwinned crystal,  $l_0$ , by the formula

$$\frac{l}{l_0} = \sqrt{1 + 2s \sin \chi \cos \lambda + s^2 \sin^2 \chi}$$

where  $\chi$  and  $\lambda$  are the angles between the specimen axis and the glide plane  $K_1$  and the glide direction  $n_1$ , respectively, in the untwinned crystal. This is the same formula that applies to the elongation of a single crystal by shear during translation gliding (slip).

The deformation that accompanies twinning leads to intense local stresses in polycrystalline materials. The formation of a twin will be accompanied by slip lines in adjacent regions and sometimes will cause twins in neighboring grains (presumably when the shear stresses are appropriately directed). As a consequence of these local strains, the regions around twin bands are favored positions for nuclei of recrystallization. If a twin forms entirely across a single crystal, however, internal strains at its boundaries are small or absent and recrystallization is not promoted there—at least in tin.<sup>1</sup>

### FRACTURE

**Brittle Cleavage.**—Some metal crystals break without any previous deformation while others cleave only after considerable plastic flow has taken place. The brittleness or ductility of zinc and other hexagonal metals has been found to be related to the orientation of the lattice<sup>2</sup> in a way that can be understood if a certain stress resolved normal to a crystallographic cleavage plane is required for cleavage, just as a resolved shearing stress is required for slip. If  $\phi$  is the angle between the normal to the cleavage plane and the axis of tension (see Fig. 6, page 295), the component of the load  $F$  in the direction of the normal,  $F'$ , will be  $F \cos \phi$ . This will act over the area of the cleavage plane,  $A'$ , which is greater than the area of the cross section  $A$  according to the relation  $A' = A/\cos \phi$ . Thus the resolved normal stress acting normal to  $A'$  is

$$N = \frac{F'}{A'} = \frac{F}{A} \cos^2 \phi.$$

The load required to break a crystal may vary markedly with orientation, as shown by the experimental points in Fig. 32 for bismuth, for example; but when  $N$  is computed, it is found to be a constant. In this figure the curve is drawn to correspond with constant  $N$ . There is probably a particular value of  $N$  for cleavage on any plane of a crystal, but only the value for the one or two planes of lowest cleavage strength—the cleavage planes—can be measured, for critical values are never reached on the others.

Table XX gives cleavage planes and measured values of  $N$  for several crystals and several temperatures of test.<sup>3</sup> These apply to fractures that result in a flat, plane surface of cleavage, the type of cleavage for which the constant-normal-stress law holds (see Shearing Fracture below).

<sup>1</sup> BRUCE CHALMERS, *Proc. Phys. Soc. (London)*, vol. 47, p. 733, 1935.

<sup>2</sup> E. SCHMID and W. BOAS, "Kristallplastizität," Springer, Berlin, 1935. C. F. ELAM, "The Distortion of Metal Crystals," Oxford, New York, 1935.

<sup>3</sup> E. SCHMID and W. BOAS, "Kristallplastizität," Springer, Berlin, 1935. C. F. ELAM, "The Distortion of Metal Crystals," Oxford, New York, 1935. ABRAM F. JOFFÉ, "The Physics of Crystals," McGraw-Hill, New York, 1928.

There is an insignificant variation in  $N$  with temperature in the few cases that have been examined (for example, in crystals of bismuth tested at  $-80$  and  $20^\circ\text{C.}$  and in zinc at  $-80$  to  $-253^\circ\text{C.}$ ). Dissolved elements seem to increase  $N$ . The amount of previous deformation before fracture has surprisingly little effect on  $N$ ; in fact, if any effect is present it is scarcely as great as the scatter of the measured values of the cleavage stress. At liquid air temperature there seems to be a slight tendency for prior deformation to *lower* the cleavage strength of zinc crystals instead of increasing it as might be expected from strain hardening.<sup>1</sup> At somewhat

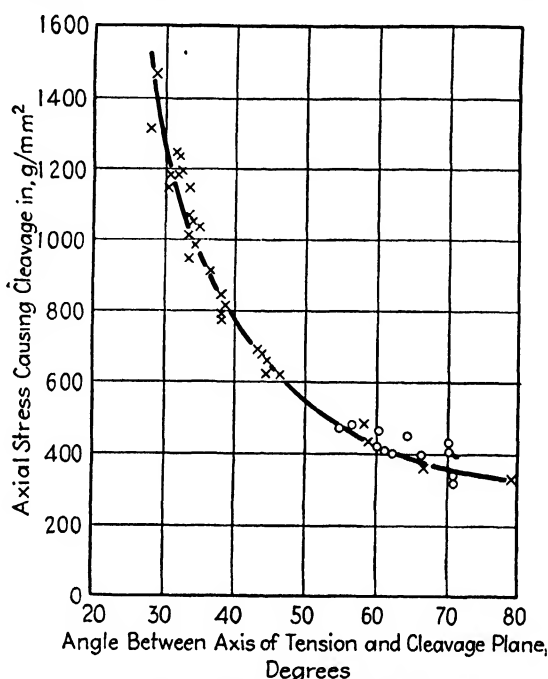


FIG. 32.—Dependence of stress causing brittle cleavage upon orientation for bismuth crystals. Testing temperatures  $-80^\circ\text{C.}$  (x) and  $20^\circ\text{C.}$  (o). (*M. Georgieff and E. Schmid, Z. Physik, vol. 36, p. 759, 1926.*)

higher temperatures the opposite tendency seems to hold, and the value of  $N$  decreases 30 to 40 percent when zinc is given an opportunity to recover (without recrystallizing) after being elongated.<sup>2</sup>

Cleavage can be induced in h.c.p. crystals, which are extremely ductile, if stress is applied almost perpendicularly to the basal plane. This plane is both the slip plane and the cleavage plane, and with tensile stress applied normal to it the component available for initiating slip is less than the critical stress for slip. Nothing then prevents the stress from increasing until cohesion between the basal planes is overcome. Cleavage in most crystals is facilitated by cooling to liquid air temperatures (which

<sup>1</sup> W. FAHRENHORST and E. SCHMID, *Z. Physik*, vol. 64, p. 845, 1930.

<sup>2</sup> See footnote 3 on p. 317.

increases the critical stress for slip more than the critical stress for cleavage) and by driving a sharp blade into the crystal along the cleavage plane (which produces a high ratio of normal stress to shearing stress under the edge of the blade).

TABLE XX.—CRITICAL NORMAL STRESS FOR BRITTLE CLEAVAGE OF SINGLE CRYSTALS

Metal	Cleavage plane	Temperature, °C.	Critical normal stress, kg. per sq. mm.
Zinc (0.03 percent cadmium)	(0001)	−185	0 18–0.20
	(1010)	−185	1 80
Zinc + 0.13 percent cadmium	(0001)	−185	0 30
Zinc + 0.53 percent cadmium	(0001)	−185	1 20
Bismuth	(111)	20	0 32
	(111)	− 80	0 32
	(11 $\bar{1}$ )	20	0 69
	(11 $\bar{1}$ )	20	0 66
Antimony	(10 $\bar{1}$ 0)	20	0.43
Tellurium	(10 $\bar{1}$ 2)		
Magnesium	(10 $\bar{1}$ 1)		
	(10 $\bar{1}$ 0)		
	(100)		0.44
Rock salt (dry)			

A few general rules<sup>1</sup> about cleavage in nonmetallic lattices may be mentioned here. It is always found that layer lattices (like graphite, MoS<sub>2</sub>, CdCl<sub>2</sub>, mica, CaSO<sub>4</sub>·2H<sub>2</sub>O, and CdI<sub>2</sub>) cleave parallel to the layers. In this group, Zn, Cd, As, Sb, and Bi can also be classed (although other cleavages are sometimes found in addition). Cleavages never break up radicals in ionic crystals or molecular complexes in homopolar crystals, but within the limits imposed by these two restrictions the cleavage planes are those most widely spaced. In ionic crystals which have no radicals, cleavage occurs so as to expose planes of anions, where such planes exist. Cubic crystals of the chemical formula AX cleave on {100} planes.

**Theoretical Calculations of Cleavage Strength.**—Polanyi suggested<sup>2</sup> that the tensile strength of an ideally perfect crystal could be calculated by considering the energy required to form the two new surfaces at the break. His estimates of tensile strength on this basis turned out to be 100 to 1000 times higher than the observed values. Zwicky,<sup>3</sup> on the basis of Born's proposed law of interatomic forces, made a more rigorous computation for cubic ionic crystals and obtained 200 kg. per sq. mm. for tensile strength, which is again more than 100 times the observed value. Born and Fürth<sup>4</sup> later tried a rigorous theoretical treatment for a cubic

<sup>1</sup> W. A. WOOSTER, "Crystal Physics," University Press, Cambridge, Mass., 1938.

<sup>2</sup> M. POLANYI, *Z. Physik*, vol. 7, p. 323, 1921.

<sup>3</sup> F. ZWICKY, *Physik. Z.*, vol. 24, p. 131, 1923.

<sup>4</sup> M. BORN and R. FÜRTH, *Proc. Cambridge Phil. Soc.*, vol. 36, p. 454, 1940.

crystal and still arrived at strengths nearly 100 times the normally observed ones. An approximate calculation from another point of view<sup>1</sup> leads to the conclusion that the breaking stress should be of the order of 0.1 to 0.5 Young's modulus, which is again a high value.

Much speculation has centered around the discrepancies between these theories and the observed strengths.<sup>1</sup> The low experimental values have frequently been attributed to stress concentrations at the base of small cracks. Experiments on mica by Orowan support this idea.<sup>2</sup> Mica may be cleaved so that the cleavage planes have the utmost perfection, but the edges of the sheets which have to be cut or ground contain many microscopic cracks. When the mica is tested in tension with wide grips that apply stress to the edges as well as to the middle of the sheet, a low strength is obtained. On the other hand, if narrow grips are used the edges are under very slight stress. With this arrangement the strengths are increased tenfold, indicating that stress concentrations at the cracks are an important factor and suggesting that cracks propagate from these highly stressed centers. Some tensile studies of rock salt that were made while specimens were immersed in water are also of interest in this connection. It was found that the salt acquired a much higher tensile stress when wet. While this was interpreted by some as evidence that the normal low value is the result of cracks and that the wetting serves to round off these cracks, others have maintained that the water dissolves in the lattice or is absorbed by it in such a way as to increase its strength.

Internal flaws resulting from accidents of growth (lineage structure, or mosaic structure) might be responsible for the difference between observed and computed values. But if these are to provide stress magnifications of 1000 and yet result in breaking stresses that are so nearly constant as they are found to be in metal crystals, the weakening from these flaws must be uniform from specimen to specimen to within a percent—a regularity that is somewhat difficult to imagine. On the other hand, the flaw theory does account for the fact that  $N$  is insensitive to temperature, at least below room temperature.<sup>3</sup>

The creation of transient cracks by thermal fluctuations has been considered, but a crack that would increase the stress a hundredfold seems to be very improbable from energy considerations.<sup>1</sup> Another suggestion, which has received little study, is that there may be tensile stresses

<sup>1</sup> F. SEITZ and T. A. READ, *J. Applied Phys.*, vol. 12, p. 470, 1941.

<sup>2</sup> E. OROWAN, "International Conference on Physics, vol. II, The Solid State of Matter," p. 89, Physical Society, London, 1935; *Z. Physik*, vol. 82, p. 235, 1933.

<sup>3</sup> If stress concentrations were involved in the rupture process, these could not also account for the low shearing stress for slip—unless supplemented by other mechanisms—for the stress concentration factors in the two processes are quite different in some cases, for example, in rock salt (F. Seitz and T. A. Read, *J. Applied Phys.*, vol. 12, pp. 470, 484, 1941).



of the order of the stress for cleavage existing in the vicinity of each dislocation of the type postulated to explain slip. (These are discussed on page 334.)

**Fürth's Theory.**—Born has proposed that melting is merely breaking due to the action of heat movement of the atoms and has obtained satisfactory results with this theory.<sup>1</sup> Fürth<sup>2</sup> has tried this point of view the other way around, *viz.*, that breaking is merely melting enforced by external stress. Considering the internal elastic energy resulting from the stress  $N$ , he derives the relation

$$N = \rho Q \frac{1 - \mu}{3 - 5\mu}$$

where  $Q$  is the melting energy per unit of mass,  $\rho$  is the density, and  $\mu$  is Poisson's ratio. The derivation assumes (1) freedom from imperfections, (2) isotropic material, (3) material behaving elastically up to the breaking point, and (4) testing at absolute zero. The formula was tested by comparison with tensile strengths of polycrystalline metals extrapolated to absolute zero. (Polycrystalline metals were believed by Fürth to fit the assumptions better than single crystals.) The average error between predicted and observed (extrapolated) values for 10 metals was only 27 percent, clearly of the right order of magnitude and as accurate as the extrapolated data. The success of the formula may be of considerable influence on theories of rupture and plasticity if it is successfully extended and if the mechanism by which heat originates and operates can be understood.

**Shearing Fracture.**—The fracture of magnesium crystals and tin crystals frequently occurs by the shearing of blocks past each other. This type of fracture produces not the flat, smooth surfaces characteristic of brittle cleavage but a rougher surface, usually slightly inclined to the slip plane. It is as if the slip process damaged a layer in the crystal where many slip planes were closely grouped, the final fracture following one after another of the damaged slip planes of the group. When this type of fracture brings ductile elongation to an end, it is found that the fracture occurs at a definite value of the resolved shear stress along the slip plane, a stress which is independent of the initial orientation.<sup>3</sup> In zinc and cadmium crystals the usual slip on the basal plane continues until deformation twins form. The reorientation of the lattice by twinning then brings new slip lines into favorable orientation, and slip is concen-

<sup>1</sup> M. BORN, *J. Chem. Phys.*, vol. 7, p. 591, 1939.

<sup>2</sup> R. FÜRTH, *Proc. Roy. Soc. (London)*, vol. A177, p. 217, 1941; *Proc. Cambridge Phil. Soc.*, vol. 37, p. 34, 1941.

<sup>3</sup> E. SCHMID and W. BOAS, "Kristallplastizität," pp. 133, 159, Springer, Berlin, 1935.

trated on these planes within the twins. The tensile specimen then immediately necks down and breaks. With zinc, cadmium, and magnesium crystals, in which the shearing type of fracture occurs, it is found that twinning and fracture begin at an approximately constant value of the resolved shearing stress on the basal plane,<sup>1</sup> provided that the basal plane is initially more than 15 to 20° from the axis of tension. There is no similar rule for cubic crystals, which neck down and break after double slip sets in. This limiting shear stress for the termination of basal slip decreases as the temperature of deformation increases. But at the same time the amount of elongation increases to an extent that makes the work of deformation (the area under the load-extension curve) practically a constant independent of initial orientation and of temperature.<sup>1</sup> Most of this work, of course, is dissipated as heat and is not retained in the crystal.

In polycrystalline tensile specimens that fail with a "cup-and-cone" type of fracture the center of the specimen fails first with a crack that is normal to the axis of tension. This appears to be a cleavage from normal stresses. Subsequently, the metal of the outer rim flows until a conical fracture develops, which is presumably a shearing fracture. The conical surface surrounding the central cup is a surface on which shear stresses are a maximum, or nearly so.

**Relative Stresses for Slip, Twinning, and Cleavage.**—It is useful to assume that the amount of deformation that can occur before twinning or fracture sets in is dictated by the relative values of the stresses required for slip, twinning, and cleavage. It will be recalled that there is a critical shearing stress for slip (which is increased by alloying, by decreasing temperature, and by plastic deformation). A similar critical shearing stress seems to exist for twinning and is decreased by plastic deformation. There is also a definite normal stress required to cleave crystals, which is little influenced by plastic flow and temperature. When a stress is applied to a crystal, it should cause slip, twinning, or cleavage, depending on whether the resolved stress on the slip plane in the slip direction, or on the twinning plane in the twinning direction, or normal to the cleavage plane exceeds the critical value for the process concerned.

Maurer and Mailänder<sup>2</sup> showed, for example, that the low-temperature brittleness of iron is best explained by considering the ratio of the cohesion across cleavage planes to the slip resistance. This ratio decreases with decreasing temperature and eventually reaches a value that results in a brittle failure by cleavage in preference to a ductile failure by slip, the ductile failure having a fibrous or a silky appearance,

<sup>1</sup> E. SCHMID and W. BOAS, "Kristallplastizität," pp. 133, 159, Springer, Berlin, 1935.

<sup>2</sup> E. MAURER and R. MAILÄNDER, *Stahl u. Eisen*, vol. 45, p. 409, 1925.

the brittle fracture a granular appearance. In the vicinity of the critical temperature there is a transition region where the ductility is falling rapidly. The width of this transition region will depend on the angle at which the slip resistance and cohesion curves approach each other, *i.e.*, the rapidity with which the ratio of cohesion to slip resistance varies with temperature. Notch-bend tests of alloy steels, for example, show a drop in energy absorption that is gradual over a considerable temperature range and thus indicate a slow rate of change of the ratio of cohesion to slip resistance. Heindlhofer<sup>1</sup> used these concepts to correlate temperatures of cold brittleness found in different types of test—notched bar,

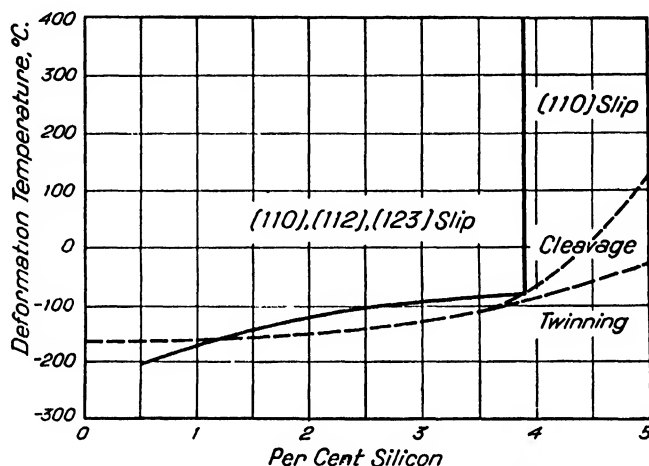


FIG. 33.—Dependence of slip on different planes, twinning, and brittle cleavage on temperature and composition of silicon-ferrite. Solid line separates region of (110) slip from region of (110) + (112) + (123) slip. Dashed lines give upper limits of regions where cleavage and twinning are produced in slow deformation by torsion.

tensile, and torsion. The ratio of the greatest normal stress to the greatest shearing stress in a notched bar "impact" specimen is considerably greater than 2:1 (but is somewhat indefinite); in a tensile specimen it is 2:1, and in a torsion specimen it is 1:1. Therefore, lowered plasticity occurs in the tensile test at a temperature where the ratio of cohesion to slip resistance is 2:1 (at about  $-155^{\circ}\text{C.}$  in iron) and where the ratio is 1:1 in the torsion test (below  $-185^{\circ}\text{C.}$  in iron). In the notched bar test the ratio exceeds 2:1 and induces brittleness at still higher temperatures (in the neighborhood of  $-20^{\circ}\text{C.}$  in iron). Since the cohesion of iron depends but little on the temperature, the resistance to flow must depend strongly on it.<sup>2</sup> A similar argument may be used to explain the relative prominence of twinning and slip.<sup>3</sup>

<sup>1</sup> K. HEINDLHOFER, *Trans. A.I.M.E.*, vol. 116, p. 232, 1935.

<sup>2</sup> F. SAUERWALD, B. SCHMIDT, and G. KRÄMER, *Z. Physik*, vol. 67, p. 179, 1931.

<sup>3</sup> C. H. MATHEWSON, *Trans. A.I.M.E.*, vol. 78, p. 7, 1928.

Slip, twinning, and cleavage in silicon-ferrite as a function of the temperature of deformation and the composition can be interpreted along these lines (Fig. 33).<sup>1</sup> The resistance to slip increases with silicon content more on the (112) and (123) planes than on the (110) planes, and so only (110) slip remains when the composition includes 4 percent or more of silicon. A similar effect is obtained with decreasing temperature (note the solid line in the figure). Brittle cleavage occurs below a certain temperature which increases with the silicon content, as shown by the upper dashed line, and twinning during slow deformation behaves simi-

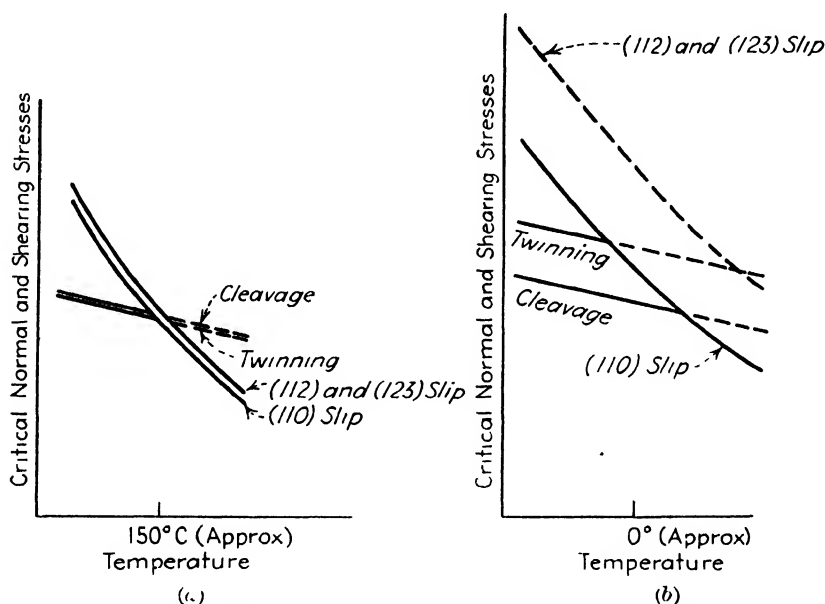


FIG. 34.—Schematic diagrams of critical stresses for slip, twinning, and cleavage to account for Fig. 35. Inhibited processes are indicated by dashed lines. (a) Low-silicon alloys, (b) high-silicon alloys (4 percent Si or more).

larly (lower dashed line). It appears, therefore, that the relative values of the critical stresses for these processes must vary with temperature, as shown in Fig. 34a for low-silicon alloys and Fig. 34b for alloys of more than 4 percent silicon. The dashed lines in these schematic diagrams represent processes that are prevented from happening because other processes prevent the stress from attaining the required magnitude.

Similar considerations explain why the ductility of hexagonal crystals is so markedly dependent on orientation.<sup>2</sup> From the measured values of critical stresses for slip, twinning, and cleavage [the latter both on (0001) and (10 $\bar{1}$ 0) planes], it is possible to predict which processes will occur in a crystal of any given orientation.

<sup>1</sup> C. S. BARRETT, G. ANSEL, and R. F. MEHL, *Trans. A.S.M.*, vol. 25, p. 702, 1937.

<sup>2</sup> E. SCHMID and W. BOAS, "Kristallplastizität," Springer, Berlin, 1935.

## PLASTIC FLOW IN POLYCRYSTALLINE METAL

The purpose of much of the experimental work on single crystals has been to understand the mechanism of flow in a polycrystalline metal. When the data from single crystals are applied to the polycrystalline case, however, many new complicating factors enter. The most important of these are the grain boundaries and the constraints imposed on the flow of a grain by the flow of the aggregate and by the variously oriented neighboring grains. The homogeneous strain of the single crystal is replaced by an inhomogeneous strain that varies from grain to grain and from point to point within a grain. Additional complexities arise from the different properties of the phases in polyphase alloys, and from their distribution. It is not surprising that investigators have reached a less satisfactory understanding of the conditions within the aggregate than within a single crystal.

**Grain Boundaries and Their Effect on Plastic Flow.**—Aston<sup>1</sup> measured the amount of strain at various distances from the grain boundary in large-grained tensile specimens and found that near a boundary there is less deformation than in the center of a grain. Similar observations of the effect of boundaries in restraining plastic flow have been made by others.<sup>2</sup> Chalmers<sup>3</sup> conducted an interesting experiment with tensile specimens composed of two crystals of tin in which the boundary between the pair of crystals extended longitudinally throughout the specimen. His results show that the critical stress depends upon the difference in orientation between the two crystals, being a minimum when the lattices in the two crystals are similarly oriented and a maximum when the orientations differ the most. This indicates that when slip planes in two adjacent grains are not parallel it is difficult for the block movement in one grain to cross the boundary into the next grain.

There seems no need to assume that there exists an amorphous cement along the boundaries which imparts additional strength to the whole, although this was a favored theory of early investigators, notably Rosenhain. It now appears more likely that there is merely a transition region at the boundary, where the atom positions represent a compromise between the crystalline arrangements in the two adjoining grains. The thickness of this layer of disturbed crystallinity can be roughly estimated. Various theories indicate that the preponderant forces between atoms in solids extend only between nearest neighbors or at most only a few atom

<sup>1</sup> R. L. ASTON, *Proc. Cambridge Phil. Soc.*, vol. 23, p. 549, 1927.

<sup>2</sup> D. HANSON and M. A. WHEELER, *J. Inst. Metals*, vol. 45, p. 229, 1931. H. C. H. CARPENTER, *J. Iron Steel Inst.*, vol. 107, p. 175, 1923. R. F. MILLER, *Trans. A.I.M.E.*, vol. 111, p. 135, 1934. G. SEUMEL, *Z. Krist.*, vol. 93, p. 249, 1936

<sup>3</sup> BRUCE CHALMERS, *Proc. Roy. Soc. (London)*, vol. A162, p. 120, 1937.

diameters. Because of this localization of forces the transition layer at a boundary must be exceedingly thin. One estimate puts the upper limit for the thickness of the layer at five interatomic distances,<sup>1</sup> too narrow to be seen on photomicrographs made with optical or electron microscopes.

The irregular atomic array at the boundary appears to be less stable than grain interiors. Chalmers<sup>2</sup> showed that in tin of high purity the grain-boundary material has a melting point about 0.14°C. below the melting point of the bulk material. Additional evidence for lattice imperfection at the boundary is obtained from numerous observations that atoms diffuse into many polycrystalline metals more rapidly along grain boundaries, where the potential barriers that must be overcome during diffusion are lower than those in the interior of grains. In many practical instances the properties of the boundaries are influenced by impurities that segregate at these places during freezing and by the penetration of oxygen and corrosive elements along the boundaries.

**The Effect of Grain Size on Plastic Flow and Hardness.**—Polycrystalline metal generally offers more resistance to deformation than single crystals. This is particularly true of zinc, as the stress-strain curve of Fig. 35 shows, and of magnesium.<sup>3</sup> Contrasted with this are the results<sup>4</sup> with aluminum, a f.c.c. metal with four slip planes in contrast to the single slip plane in hexagonal metals. In aluminum the curve for the aggregate is similar to some of the single crystal curves.

Indentation hardness increases with increasing fineness of the grains in polycrystalline metals.<sup>5</sup> Figure 36 illustrates the effect in copper. If the hardness is plotted against the amount of grain-boundary area per cubic millimeter of the sample, the relationship is linear. Hardness and resistance to deformation in iron likewise increase as grain size is reduced.<sup>6</sup> However, in most experiments on this subject there is an uncertainty as to whether the various treatments used to produce the different grain sizes have left the metal in comparable condition.

**The Hardness of Solid Solutions.**—Norbury<sup>7</sup> found that the indentation hardness of copper increased linearly with the atomic percent of any metal dissolved in it. He also compared the hardening effects of different solutes and found that the hardening effect of 0.1 atomic percent of an

<sup>1</sup> F. SEITZ and T. A. READ, *J. Applied Phys.*, vol. 12, p. 538, 1941.

<sup>2</sup> BRUCE CHALMERS, *Proc. Roy. Soc. (London)*, vol. A175, p. 100, 1940.

<sup>3</sup> C. F. ELAM, "The Distortion of Metal Crystals," Oxford, New York, 1935.  
E. SCHMID and W. BOAS, "Kristallplastizität," Springer, Berlin, 1935.

<sup>4</sup> R. KARNOP and G. SACHS, *Z. Physik*, vol. 41, p. 116, 1927.

<sup>5</sup> W. H. BASSETT and C. H. DAVIS, *Trans. A.I.M.E.*, vol. 60, p. 428, 1919. H. T. ANGUS and P. F. SUMMERS, *J. Inst. Metals*, vol. 33, p. 115, 1925.

<sup>6</sup> C. A. EDWARDS and L. B. PFEIL, *J. Iron Steel Inst.*, vol. 112, p. 79, 1925.  
T. ISHIGAKI, *Science Repts. Tôhoku Imp. Univ.*, vol. 16, p. 285, 1927.

<sup>7</sup> A. L. NORBURY, *Trans. Faraday Soc.*, vol. 19, p. 586, 1924.

alloying element added to copper or to lead was in almost direct proportion to the difference in atomic radii of the solute and solvent atoms. This relationship may also be expressed in terms of hardening vs. change of lattice parameter or vs. the extent of solid solubility, since these char-

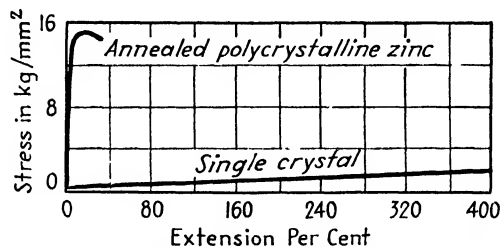


FIG. 35.—Stress-strain curves for zinc. (*Elam*)

acteristics are all interrelated. Figure 37 illustrates the relationship in copper alloys of controlled grain size.<sup>1</sup> Nickel has nearly the same atomic radius as copper, expands the copper lattice only slightly, is soluble up to 100 percent, and hardens it the least of any of the elements plotted in the figure. Antimony and tin differ the most in atomic radii, expand

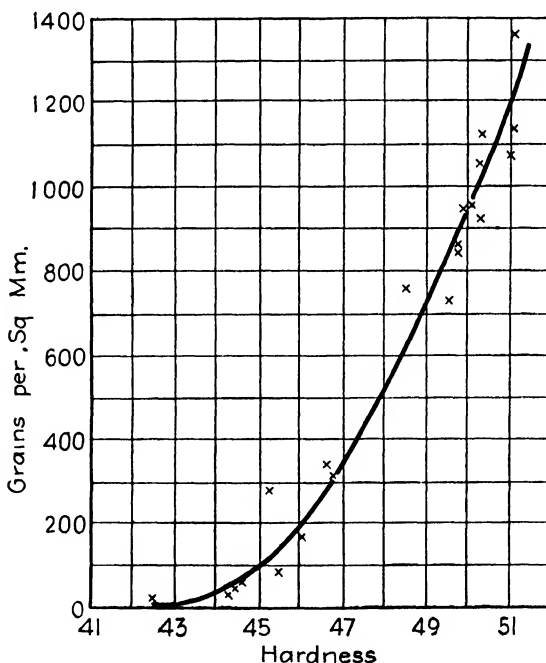


FIG. 36.—Variation of hardness with grain size in copper. (*Angus and Summers.*)

the copper lattice the most per atom dissolved, have the most restricted solubility (0.6 and 1.0 atomic percent, respectively), and exert the greatest hardening effects. The capacity of any of these alloys to be hardened by

<sup>1</sup> R. M. BRICK, D. L. MARTIN, and R. P. ANGIER,<sup>1</sup>Preprint 37, A.S.M., Cleveland, Ohio, 1942.

cold work is linearly proportional to its hardening by solution; an element that confers great solution hardening to the matrix also confers correspondingly great work-hardening properties.

Indentation hardness is itself largely a measure of work hardening for it is effectively a weighted average of the stress-strain curve from zero strain up to the maximum value encountered under the penetrator. This is recognized in Meyer's analysis of the Brinell impressions made with penetrator balls of various sizes and loads. If  $L$  is the load on a ball of diameter  $d$ , then  $L = ad^n$  where the constant  $n$  is an index of the work-hardening capacity of the metal.

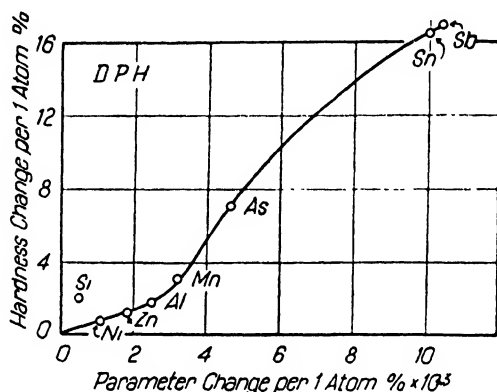


FIG. 37.—Comparative solid-solution hardening of copper alloys as related to alteration of lattice parameter. (Brick, Martin, and Angier.)

**The Effect of Fineness of Microstructure in Steels.**—Gensamer and his collaborators<sup>1</sup> studied the quantitative relation between the fineness of the microstructures in steel and the tensile properties. By causing the steel to react at different temperatures in the subcritical range they produced pearlite and spheroidite of varying fineness. Plotting the resistance to deformation at a constant value of strain against a measure of the fineness gave the linear relation shown in Fig. 38. The measure of fineness used was the logarithm of the mean straight path through the continuous phase (ferrite) from one hard cementite particle or lamella to another. It was found that a given value of mean path, along which slip occurs, corresponds to the same flow resistance regardless of the shape of the carbide particles—whether they are lamellae as in pearlite or globules as in spheroidite.

Determinations of the resistance to deformation are made at a controlled rate of straining, for the rate varies the resistance. The effect of

<sup>1</sup> M. GENSAMER, E. B. PEARSALL, W. S. PELLINI, and J. R. LOW, JR., The Tensile Properties of Pearlite, Bainite and Spheroidite, *Trans. A.S.M.*, vol. 30, p. 983, 1942. M. GENSAMER, E. B. PEARSALL, and G. V. SMITH, *Trans. A.S.M.*, vol. 28, p. 380, 1940.



rate is slight, however, at ordinary rates.<sup>1</sup> For example, as the rate is increased, Nadai has found a 10,000-fold increase in rate merely doubles the flow resistance in 0.35 percent carbon steel at 455°C. The resistance increases in proportion to the logarithm of the rate of straining, and there is a greater increase in the soft metals than in the hard ones.

**The Bauschinger Effect and the Elastic Aftereffect.**—A stress-strain curve is strongly influenced by any previous compression or extension the specimen has undergone. Prior compression raises the yield strength for further compression but lowers it for tension, as will be seen from Fig. 39.

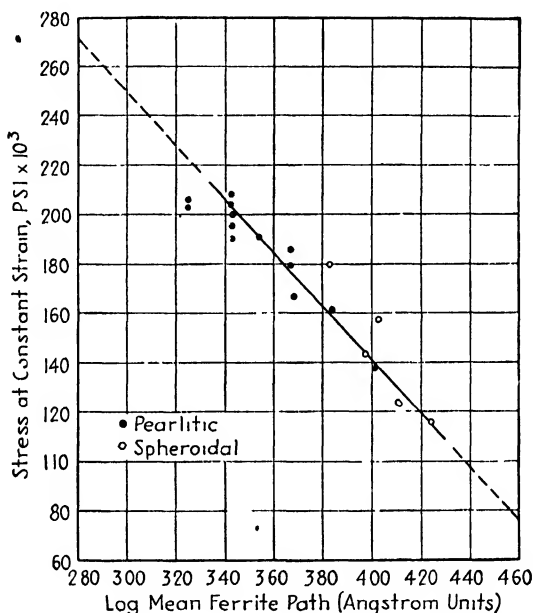


FIG. 38.—Stress at a constant amount of elongation as related to mean straight path through ferrite in steel of 0.80 per cent C, 0.74 per cent Mn with both pearlitic and spheroidal microstructures. (Gensamer, Pearsall, Pellini, and Low.)

Straining of either kind, in fact, raises the ability of the metal to withstand further stressing of the same kind and lowers its strength to stresses of the opposite kind.

This Bauschinger effect in polycrystalline material can be ascribed to the state of stress existing within the metal after the first deformation.<sup>2</sup> If some grains of the aggregate have an orientation such that they have a high yield strength to an applied tensile load while others have a low yield strength, then when the load is removed the latter will be brought into a compressive strain by the tensile stresses in the former and the final state is an equilibrium between compressive and tensile stresses in many small

<sup>1</sup> For a review of this subject see M. Gensamer, "Strength of Metals under Combined Loads," A.S.M., Cleveland, Ohio, 1941.

<sup>2</sup> G. MASING, *Wiss. Siemens Konzern*, vol. 3, p. 231, 1924; vol. 4, pp. 74, 244, 1925; vol. 5, pp. 135, 142, 1926.

regions. Consider now the state of stress upon reapplication of the tensile load to the grains that were originally the weak ones and that are now the compressed ones. They must first be reduced to zero stress from their elastically compressed state, then raised to their yield strength in tension, before flow can begin. The material has consequently been work-hardened for stresses in this direction. But if a *compressional* stress is applied, the grains that were left in a state of residual compression are already part way to their yield point in compression and slight additional stresses in this direction will start plastic flow. In fact, the compressional stress already existing is sufficient to cause a limited amount of

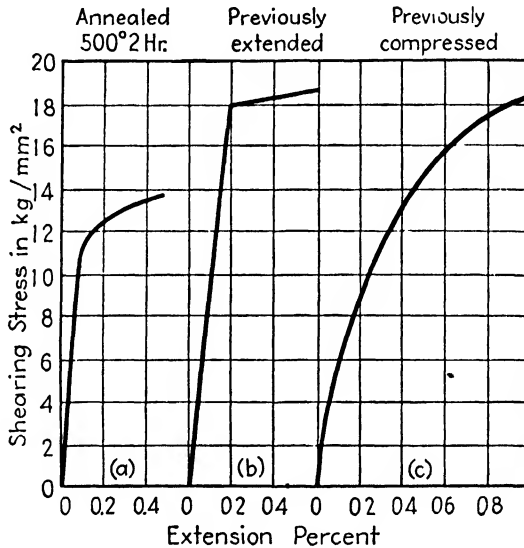


FIG. 39.—The Bauschinger effect in polycrystalline brass. Resistance to elongation is increased by prior elongation, from curve (a) to curve (b), and is lowered to curve (c) by prior compression. (*Sachs and Shoji.*)

flow, for after the tensile load is released there is a small additional contraction that takes place rather slowly (the elastic aftereffect). This contraction diminishes in rate in the way that the stresses in a bent beam diminish when they are relaxed by annealing. The flow is sufficiently rapid so that it is observed during a tensile test, where it causes the stress-strain curve during unloading to differ from the curve for reapplication of the load (at a given value of the load the strain is greater during the unloading than during the subsequent reloading).

**Taylor's Theory of Flow in Aggregates.**—When a single crystal is elongated in a tensile test, the central portion of the crystal remote from the influence of the grips is subjected to a uniform stress and is free to deform on a single slip plane, altering its shape in accord with this mechanism. A grain in an aggregate, on the other hand, is constrained on all sides by neighboring grains and cannot change its shape in an

arbitrary manner since the grain boundaries do not pull apart during the deformation. Each grain undergoes approximately the same strain as the aggregate; *i.e.*, it tends to elongate in proportion to the elongation of the bulk material and to contract laterally in proportion to the lateral contraction of the aggregate. An arbitrary change of shape of this type requires a minimum of five different slip systems to operate continually. Taylor,<sup>1</sup> has shown that the principle of least work limits the number to five and has computed which five will operate for a f.c.c. crystal of given orientation. Then, assuming that the shear-hardening curve for each of the five is similar to that for a slip plane in a single crystal he has computed the stress-strain curve for polycrystalline aluminum from the curve for a single crystal. The computed curve agrees well with the observed. Taylor's theory also predicts the direction of rotation of the grains during deformation. However, actual experimental determination of the direction of rotation has shown that about one-third of the grains rotate in ways not predicted by the theory.<sup>2</sup> This is attributed to the fact that each grain and each fragment of a grain deform inhomogeneously in a manner influenced by ever-changing flow of its neighbors, whereas Taylor's theory assumes uniform strain in all the grains. The theory does not predict a grain-size effect in tensile properties or hardness when there are many grains in the cross section of the specimen under test.

<sup>1</sup> G. I. TAYLOR, *J. Inst. Metals*, vol. 62, p. 307, 1938; "Stephen Timoshenko 60th Anniversary Volume," Macmillan, New York, 1938.

<sup>2</sup> C. S. BARRETT and L. H. LEVENSON, *Trans. A.I.M.E.*, vol. 137, p. 112, 1940.

## CHAPTER XVI

### THEORIES OF SLIP

The data reviewed in the preceding chapter characterized the process of slip in crystals as a gliding of blocks over one another along slip planes and in slip directions. This, to be sure, explains the visible results of plastic flow, but as a model of the slipping process it is far from adequate to account for the stresses that are required to make metals flow. Suppose, for example, an ideal crystal containing no imperfections were to slip with a uniform movement of all the atoms in a plane, each atom being pushed over the atom beneath at the same time. The shear stress necessary to cause this to happen should be the stress required to cause an elastic shear that would move the plane half an atomic distance parallel to the underlying plane; having reached this halfway point, the plane would then snap the rest of the way to the next position of equilibrium. The stress required for this amount of elastic displacement can be estimated by multiplying the shear by the shear modulus, and the result is about 1000 or 10,000 times the *observed* critical resolved shear stress for slip in single crystals. This discrepancy between calculated and observed yield strengths of crystals has stimulated much thought and has led to the development of a number of important theories of the plastic properties of crystalline materials.<sup>1</sup>

**Stress Concentrations.**—The earlier theories attempted to resolve the discrepancy between ideal and observed yield strengths by postulating that crystals contain cracks or other kinds of lattice flaws that set up local concentrations of stresses. Theories of this nature stemmed from the work of Griffith,<sup>2</sup> who showed the importance of cracks and other inhomogeneities in causing premature rupture of test specimens. Griffith calculated the stress at the edge of a thin transverse crack in a tensile specimen and found it many times larger than the average stress on the cross section. Smekal<sup>3</sup> suggested that stress concentrations of this sort

<sup>1</sup> For detailed summaries of this field see R. HOUWINK, "Elasticity, Plasticity and Structure of Matter," chapter by W. G. Burgers, University Press, Cambridge, Mass., 1937. F. SEITZ and T. A. READ, *J. Applied Phys.*, vol. 12, p. 107, 1941.

<sup>2</sup> A. A. GRIFFITH, *Proc. Intern. Congr. Applied Mechanics*, p. 55, Delft, 1924; *Trans. Roy. Soc. (London)*, vol. A221, p. 163, 1920.

<sup>3</sup> A. SMEKAL, "Report of the International Conference on Physics, vol. II, The Solid State of Matter," University Press, Cambridge, 1935; "Handbuch der Physik," vol. XXIV, p. 2, Springer, Berlin, 1933; *Z. Krist.*, vol. 89, p. 193, 1934, vol. 93, p. 161, 1936.

around flaws in a crystal start plastic flow at stresses far below the stresses that would be required in perfect crystals. Smekal attributed many of the flaws, particularly places of misfit at the boundaries of mosaic blocks, to accidents of growth. He believed the approximate regularity in the spacings of slip planes was evidence of regularity in the arrangement of flaws and listed as possible flaws the following: gaps, variation in orientation, incorporated foreign atoms, inclusions, twins, and mosaic-block boundaries.

**Becker-Orowan Theory.**—Becker extended this line of thought by pointing out the role of thermal motions of the atoms in initiating slip.<sup>1</sup> Thermal vibrations help the applied stress overcome the resistance to flow, giving the effect of adding to the applied stress a stress sufficient to reach the value of the critical shear stress for slip at a temperature of absolute zero,  $\tau_0$ . If the applied stress is  $\tau$ , the amount added is then  $(\tau_0 - \tau)$ . This added stress increases the energy of the crystal by the amount  $E$  given by the equation

$$E = \frac{V(\tau_0 - \tau)^2}{2G}$$

where  $V$  is the volume subjected to the stress and  $G$  is the shear modulus. The probability that a region in the crystal will acquire the energy  $E$  as a result of thermal fluctuations is given by the Boltzmann function

$$\text{Probability} = e^{-E/kT}$$

where  $k$  is Boltzmann's constant and  $T$  is the absolute temperature.

It is assumed that the velocity  $D$  of the deformation process is proportional to this probability; hence

$$D = c e^{-V(\tau_0 - \tau)^2/2GkT}$$

where  $c$  is a constant of proportionality. For a constant rate of flow this predicts that the critical shearing stress will vary so that  $(\tau_0 - \tau)^2/T$  is a constant, or, stated differently,

$$\tau = \tau_0 - aT^{1/2}$$

where  $a$  is a constant. The theory in this form is in qualitative accord with the dependence of critical shear stress on temperature. However, it does not account for the very low value of the shearing strength compared with that expected for the simple model of the ideal crystal.

Orowan<sup>2</sup> has extended this concept to include the effect of flaws acting as stress raisers, by substituting  $q\tau$  for the applied stress  $\tau$ , where  $q$  is the

<sup>1</sup> R. BECKER, *Physik. Z.*, vol. 26, p. 919, 1925.

<sup>2</sup> E. OROWAN, *Z. Physik*, vol. 89, pp. 605, 614, 634, 1934; summarized by W. G. Burgers and J. M. Burgers, First Report on Viscosity and Plasticity, *Proc. Roy. Acad.*

stress concentration factor. His formula for rate of flow is

$$D = ce^{-V(\tau_0 - q\tau)^2/2qkT}$$

and for the critical shear stress is

$$\tau = \frac{1}{q}(\tau_0 - aT^{\frac{1}{2}}).$$

The formulas developed in this way as a blending of the Smekal, Becker, and Orowan theories are successful in accounting for many characteristics of plastic flow in crystals but not for the relative effects of soluble and insoluble impurities, nor do they specify a mechanism by which the flow can leave a point of stress concentration and cross a region of average stress.

### THE THEORY OF DISLOCATIONS

The most successful theory to date for the mechanism of slip is the theory of dislocations, which postulates a movement by which the atomic forces are overcome one at a time. The concept was first applied to slip by Orowan,<sup>1</sup> Polanyi,<sup>2</sup> and Taylor<sup>3</sup> and is currently receiving so much attention in many laboratories that it will be presented here in some detail.

**Nature of a Dislocation.**—The type of dislocation treated at length by Taylor and others is illustrated in Fig. 1.<sup>4</sup> The upper side of the slip plane is compressed so that  $n + 1$  atoms on this side are opposite  $n$  atoms on the lower side. Alternately, the compressed region may be on the lower side so that  $n + 1$  atoms below are opposite  $n$  above. The former arrangement is designated as a *positive* dislocation and the latter as a *negative* one. If the dislocation starts at one side and runs through the crystal to the other side, it produces a shift of one portion with respect to the other a distance of one atomic spacing. The resulting displacement is the same whether a positive dislocation moves across a crystal toward the right or a negative dislocation moves across it toward the left.

Figure 1 is intended to represent a cross section of a three-dimensional crystal in which the dislocation is assumed to extend as a long line perpendicular to the plane of the drawing and the whole linear dislocation is assumed to move as a unit. The energy required to form a dislocation

*Sci. Amsterdam*, vol. 15, p. 205, 1935; see also G. Masing, *Z. Metallkunde*, vol. 31, p. 235, 1939.

<sup>1</sup> E. OROWAN, *Z. Physik*, vol. 89, p. 634, 1934.

<sup>2</sup> M. POLANYI, *Z. Physik*, vol. 89, p. 660, 1934.

<sup>3</sup> G. I. TAYLOR, *Proc. Roy. Soc. (London)*, vol. A145, p. 362, 1934.

<sup>4</sup> The dislocation pictured in Fig. 1 is but one of several possible ones; others have been discussed by J. M. Burgers, *Proc. Phys. Soc. (London)*, vol. 52, p. 23, 1940, and in references given in his article.

at a surface or at a flaw is about the same as that needed to form a lattice-point vacancy, an energy of the order of 1 electron volt ( $1.60 \times 10^{-12}$  erg)

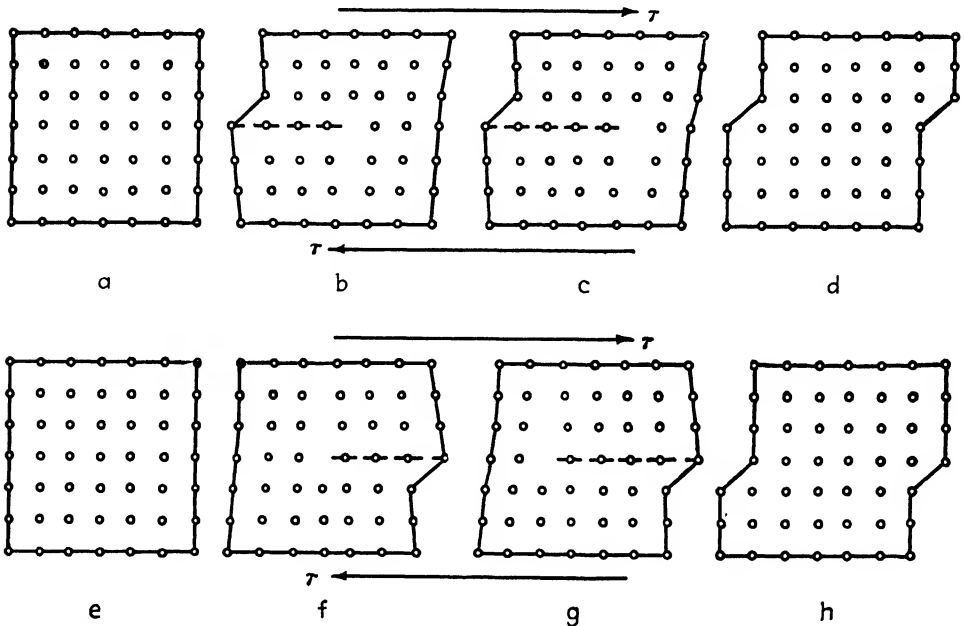


FIG. 1.—Generation and movement of a dislocation. In sketches *a*, *b*, *c*, and *d* a positive dislocation moves to the right; in *e*, *f*, *g*, and *h* a negative one moves to the left; the resulting deformation is identical. (Taylor.)

for a dislocation one atomic spacing in length. In the absence of other dislocations or of flaws it appears that a dislocation will move under the action of an almost infinitesimally small applied stress, unless it is required to change its length. But if a dislocation is generated as a short nucleus at a stress raiser and then grows in length as it enters a crystal, as postulated by Seitz and Read<sup>1</sup> and indicated in Fig. 2, there will then be an activation energy required for extending the length of the dislocation as well as one for its formation. Thermal fluctuations will aid both in formation and movement, but stress raisers will aid only in the formation; applied stresses guide the movement and extension of the dislocation and supply the free energy required for the process.

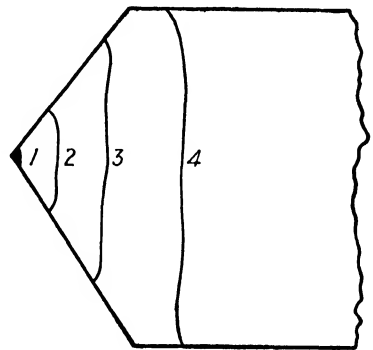


FIG. 2.—Suggested mechanism for nucleation and growth of a dislocation. Starting as a nucleus at 1, it grows in successive stages 2, 3, 4. (Seitz and Read.)

**Strain Hardening.**—Each dislocation is surrounded by a stress field, which plays an important role in all dislocation theories. A succession

<sup>1</sup> F. SEITZ and T. A. READ, *J. Applied Phys.*, vol. 12, pp. 100, 170, 470, 538, 1941.

of dislocations may be generated at a flaw and follow each other along a slip plane until they encounter some imperfection or boundary where they become stuck. The stress field that they set up at this point opposes the approach of additional dislocations and therefore hardens the metal.

Another way in which the stress field operates, according to Taylor, is to build up a superlattice of dislocations, which acts to raise the critical shearing stress in the following way: Suppose there are parallel linear dislocations on parallel slip planes of a crystal. The stresses around them will be such that like dislocations repel each other and unlike ones attract. Therefore the dislocations tend to form a superlattice in which there is a checkerboard arrangement of positives and negatives throughout the crystal. From elastic theory it is possible to compute the effect of one dislocation on another by the approximate formula

$$F_x = \pm \frac{A_r}{x^2 + y^2}$$

where  $F_x$  is the force acting in the slip direction (assumed to be the  $x$  direction) on a dislocation at the point  $xy$ , arising from a dislocation at the origin of coordinates when both dislocations extend in the  $z$  direction;  $A$  is a constant; the positive sign indicates repulsion of two like dislocations, and the negative sign is used if the dislocations are unlike and attract. Summing up terms of this sort for all neighboring dislocations in a superlattice of alternate layers of positive and negative dislocations, an approximate formula for the maximum force required to push the positive lattice through the negative lattice is<sup>1</sup>

$$F_x = - \frac{2\pi A}{b \sinh (2\pi a/b)}$$

where  $a$  is the distance from a layer of positive dislocations to the adjoining layer of negatives and  $b$  is the distance between dislocations on a given layer.<sup>2</sup> If this force is supplied by a shear stress  $\tau_{xy}$  applied externally, then

$$F_x = B\tau_{xy}$$

<sup>1</sup> Koehler has derived this formula by an approximate method that is equivalent to Taylor's. This approximation involves considering the force on one row of dislocations produced by the two neighboring rows of dislocations. For a more detailed treatment see J. S. Koehler, *Am. J. Phys.*, vol. 10, p. 275, 1942.

<sup>2</sup> Another treatment of the problem, with a more general system of coordinates, has been published by W. F. Brown, *Phys. Rev.*, vol. 60, p. 139, 1941, who pointed out that Taylor's original formulas were incorrect—as had also been noted by J. M. Burgers, *Proc. Roy. Acad. Sci. Amsterdam*, vol. 42, p. 293, 1939.



where  $B$  is a constant. Now if the block being deformed is of length  $L$  in the slip direction (the  $x$  direction) and  $h$  in the  $y$  and  $z$  directions and if the passage of a dislocation across the block from one side to the other moves the top of the block through a distance  $\lambda$  with respect to the bottom, then the movement of a dislocation  $1/n$ th of the way across the block will move the top  $\lambda/n$  with respect to the bottom. If we assume that all the dislocations entering the block are trapped within it, forming a checker-board pattern, then on the average each dislocation will have traveled halfway across the block and will have contributed a displacement of the top amounting to  $\lambda/2$ ; the total displacement will be this average multiplied by the total number of dislocations in the block, giving

$$\frac{\lambda Lh}{2ab},$$

which is a shear strain  $s$  amounting to

$$s = \frac{\lambda L}{2ab}.$$

Taylor assumed that the dislocations were distributed so that  $a = b$ , for which the above equation gives

$$a^2 = \frac{\lambda L}{2s}.$$

Substituting in the previous equations gives a formula in which the resolved shear stress necessary to produce plastic flow is proportional to the square root of the strain<sup>1</sup>

$$\tau_{xy} = \frac{2^{\frac{1}{2}}\pi A}{B \sqrt{\lambda L} \cosh 2\pi} \cdot \sqrt{s}.$$

The value of  $L$  can be found by fitting the theoretical stress-strain curve to the experimental one. For aluminum at very low temperatures,  $L = 1.8 \times 10^{-4}$  cm., which is in agreement with the dimensions of mosaic

<sup>1</sup>Seitz and Read have pointed out that the parabolic stress-strain relation of Taylor's theory follows from the assumption that the dislocation spacings parallel and perpendicular to the slip plane remain in a fixed ratio during deformation. If, on the other hand, the spacing normal to the slip plane decreased more rapidly than the spacing parallel to the slip plane, the strain hardening would be more rapid than Taylor postulated; stress-strain curves of various shapes might be accounted for by a proper assumption as to the dislocation arrangement. If the dislocations were concentrated into bands of the same order of width as the slip bands (presumably in the range between  $0.1 \mu$  and one atomic distance) with the bands spaced roughly  $1 \mu$  apart, this also would alter some of the quantitative conclusions of Taylor's paper.

blocks as estimated from other methods.<sup>1</sup> At room temperature Koehler concludes that  $L = 2.8 \times 10^{-4}$  cm. in aluminum.<sup>2</sup>

Taylor proposed that the dislocations originate in the boundary regions between the mosaic blocks and travel across a block to the opposite boundary, where they may be trapped by unfavorable stresses surrounding points of misfit. He suggested that a certain fraction succeeds in penetrating this barrier and that the fraction increases with increasing temperature, thermal agitation helping them through. Using Taylor's values of  $L$  and the relations discussed above, the dimension  $a$  in cold-worked aluminum ( $s = 1.2$ ) is computed to be  $1.46 \times 10^{-6}$  cm. at  $-185^\circ\text{C}$ . and increases with temperature to  $21.8 \times 10^{-6}$  cm. at  $600^\circ\text{C}$ .

**Slip Lines.**—The passage of a single dislocation would not produce a visible slip line, but if a stress-raising flaw generated a whole succession of dislocations the total displacement produced could amount to as much as the observed displacement at a slip line. A set of flaws located near a single slip plane could give rise to a succession of dislocations of this sort, and the spacing between slip lines according to this view would correspond to the distribution of flaws where dislocations are generated.

Another possible reason for the concentration of slip in narrow bands is the heat that is generated at a slip plane during plastic flow. Most of the energy to which a metal is subjected during cold work does not remain in the lattice but appears as heat, and the total amount would be sufficient to melt several percent of the total mass if it were concentrated. Accordingly, it has been postulated<sup>3</sup> that local melting occurs at slip bands during slip. This extreme view has been criticized on the basis that if the slip bands were  $500\text{\AA}$  wide the time required for thermal equilibrium would be only of the order of  $10^{-10}$  sec.\* Others have postulated that, without actually melting any locality, the temperature would nevertheless be sufficiently increased so that one dislocation would make others easier to start, etc., until a whole avalanche of dislocations moved across the crystal in a narrow band. It has been suggested that the jumps observed in the plastic extension of single crystals could be related to these heating effects accompanying the motion of dislocations. These jumps, accompanied by audible clicks, have been observed in NaCl,† Al,  $\alpha$ -brass,‡ and Zn,§ at low temperatures.

<sup>1</sup> G. I. TAYLOR, *Proc. Roy. Soc. (London)* vol. A145, p. 362, 1934 (see also W. F. Brown, *Phys. Rev.*, vol. 60, p. 139, 1941).

<sup>2</sup> J. S. KOEHLER, *Am. J. Phys.*, vol. 10, p. 275, 1942.

<sup>3</sup> A. W. STEPANOW, *Z. Physik*, vol. 81, p. 560, 1933.

\* F. SEITZ and T. A. READ, *J. Applied Phys.*, vol. 12, pp. 100, 170, 470, 538, 1941.

† ABRAHAM F. JOFFÉ, "The Physics of Crystals," McGraw-Hill, New York, 1928.

‡ M. CLASSEN-NEKLUDOWA, *Z. Physik*, vol. 55, p. 555, 1929.

§ E. SCHMID and M. A. VALOUCH, *Z. Physik*, vol. 75, p. 531, 1932.

**Temperature Effects.**—It has been calculated that stress concentrations unaided would be unable to form a dislocation unless they increased the average stress by a factor of about 1000 and that thermal fluctuations are chiefly responsible for the formation of dislocations. Thus physical tests at low temperatures reveal the behavior of a crystal when almost no new dislocations are being formed. It is surprising, then, to note that single crystals have been extended as much as 100 percent even at liquid air temperatures. Apparently this is made possible by the motion of the dislocations already present in the crystals when they are cooled.

Once fully formed, dislocations probably diffuse readily at ordinary temperatures, and a superimposed stress field causes them to drift in one direction more than another, thus producing a macroscopic strain. They are presumed to diffuse even in the absence of applied stress. Since the elastic energy of the stress field around a dislocation is lower when it is near a surface,<sup>1</sup> there is a continual diffusion out to the surface. This loss of dislocations through diffusion may constitute recovery. It is increased, just as atomic-interchange diffusion is, by increased temperature. While it seems necessary to postulate that the whole length of a dislocation moves as a unit during diffusion, this is probably not a serious difficulty for the theory, as one atom in a dislocation should be able to pull the others along with it to the next equilibrium position for some distance along the dislocation line. Recrystallization would be expected to reduce drastically the dislocation content of the metal and also to remove the dislocations left by cold work.

**Residual Energy from Cold Work.**—Koehler<sup>2</sup> has computed the energy required to produce a dislocation in work-hardened metals. The energy required to produce an isolated dislocation in copper is found to be about 3.16 electron volts per atomic distance along its length. If the dislocation is one of a regular two-dimensional superlattice, as assumed by Taylor, and if there are  $10^{12}$  lines of dislocation per square centimeter normal to their length, as is indicated by certain magnetic measurements,<sup>3</sup> then the binding energy of a dislocation in the superlattice is 0.43 electron volt per atomic distance. The energy associated with a dislocation in worked metal is then the difference between these two values, and the total strain energy is 0.42 cal. per g. This is in satisfying agreement with Taylor and Quinney's experimental value for copper, which is 0.5 cal. per g. Conversely, the measured values of strain energy can be used in a calculation of the distance between dislocations. Computations yield spacings,

<sup>1</sup> F. SEITZ and T. A. READ, *J. Applied Phys.*, vol. 12, pp. 100, 170, 470, 538, 1941.  
J. S. KOEHLER, *Phys. Rev.*, vol. 60, p. 397, 1941.

<sup>2</sup> J. S. KOEHLER, *Phys. Rev.*, vol. 59, p. 943(A), 1941; vol. 60, p. 397, 1941.

<sup>3</sup> W. F. BROWN, JR., *Phys. Rev.*, vol. 59, p. 528, 1941; vol. 60, p. 139, 1941.

$a$ , that are nearly the same in several metals—approximately 30 atomic spacings, in agreement with the results of magnetic measurements.

Peierls<sup>1</sup> has made an approximate computation of the distribution of strain around a dislocation and has concluded that the strain is appreciable only a very few atom distances from the center line of a dislocation. This result is consistent with the results of x-ray studies of cold-worked metals, for the x-ray results also require that the disturbance extend over regions much smaller than the dimensions of a mosaic block.

**Solid-solution Hardening.**—Since soluble impurities increase slip resistance more than insoluble ones, the hardening effect can be sought within the lattice rather than at the surface or on block boundaries. It can be ascribed to stresses centered around the dissolved atoms, which impede the movement of dislocations. A radially symmetrical tensile or compressive stress about the dissolved atom would be expected to vary with distance according to the formulas<sup>2</sup>

$$\sigma_r = \frac{4Gfa^3}{r^3}, \quad \sigma_\theta = \frac{-4Gfa^3}{r^3}$$

where  $\sigma_r$  is the stress in the radial direction and  $\sigma_\theta$  is the stress in the tangential direction,  $G$  is the shear modulus (of the order of  $10^{11}$  dynes per cc.),  $a$  is the atomic radius (about  $1.5 \times 10^{-8}$ ), and  $f$  is the relative difference in size of the solute and solvent atoms.

This view is in accord with the fact that in a system exhibiting complete miscibility the maximum hardness is found near the 50 atomic percent composition. It also accounts for the observation that hardening is proportional to the difference in size between solute and solvent atoms.

**Age Hardening.**—Age hardening can be understood qualitatively on the same basis as the solid-solution hardening discussed in the preceding section. The precipitate particles that form in a supersaturated matrix are too large or too small for the space they must occupy and consequently strain the matrix in their neighborhood. When a dislocation encounters a shearing stress unfavorable to its passage, as some of the stresses around these particles will be, the dislocation is stopped until a stress is applied that is capable of overcoming the local stress obstruction.<sup>3</sup> Some

<sup>1</sup> R. PEIERLS, *Proc. Phys. Soc. (London)*, vol. 52, p. 34, 1940.

<sup>2</sup> F. SEITZ and T. A. READ, *J. Applied Phys.*, vol. 12, pp. 100, 170, 470, 1941; the formula is derived from an elastic-theory expression given, for example, in A. E. H. LOVE, "The Mathematical Theory of Elasticity," p. 142, University Press, Cambridge, England, 1927.

<sup>3</sup> The coherence between transition lattices and the matrix from which they precipitate and the accompanying stresses are discussed more fully in another chapter. N. F. MOTT and F. R. N. NABARRO [*Proc. Phys. Soc. (London)*, vol. 52, p. 86, 1940] have made some preliminary computations of these stresses, assuming spherical particles, and have concluded that when the particles have grown beyond a certain minimum

hindrance to the motion of dislocations would also be expected at matrix-precipitate interfaces; this would be somewhat like the increase in hardness that accompanies decreasing grain size in a polycrystalline aggregate.

**Internal Friction.**—The term internal friction means the capacity of a solid to damp out elastic vibrations. If a bar is struck by a hammer, it will “ring” for a length of time that depends upon the magnitude of the internal friction; its vibrational energy will be dissipated quickly if the internal friction is high and slowly if the internal friction is low. The magnitude of the internal friction can be determined by the decrease in vibrational energy per cycle in the specimen when vibrating freely and may be stated in terms of the **decrement**, which is the energy dissipated per cycle divided by the total energy of vibration during the cycle. Several other indices of internal friction are also in common use.<sup>1</sup>

There are several processes contributing to the total internal friction of metals. Some are found only in ferromagnetic materials and as they are concerned only with magnetic-elastic theory will be disregarded here. Others are the results of heat flowing back and forth from point to point in the specimen during stressing.<sup>2</sup> The source of internal friction that is of interest in the present discussion is related to localized plastic flow in the crystal, for this may be interpreted in terms of the dislocation theory.

size their effect is no longer dependent on the size of the particles. This implies that overaging is a result of relief of stress rather than growth beyond a critical dispersion.

<sup>1</sup> The **logarithmic decrement** is often used. This is the natural logarithm of the ratio of the amplitude of vibration for two successive cycles:

$$\text{Logarithmic decrement} = \ln \frac{A_1}{A_0}.$$

Zener prefers the quantity  $1/Q$ , which is equal to the logarithmic decrement divided by  $\pi$ . It can be determined not only from the rate of decay of vibrations, but from the width of the “resonance curve” for forced vibrations—the curve of amplitude of vibration vs. the frequency of the driving force that induces the vibrations.

<sup>2</sup> Portions of the metal that are subjected to elastic compression are raised in temperature while portions that are stretched are lowered in temperature. Heat will flow from the warmer to the cooler regions and will dissipate energy unless the vibrations are so rapid that this cannot occur (in which case the process is “adiabatic”) or so slow that equilibrium is maintained at all times (in which case the process is “isothermal”). Zener and his coworkers have analyzed several sources of these thermal currents and conclude that they arise from macroscopic internal stresses, from stress inhomogeneities due to the variation of Young’s modulus from grain to grain in the differently orientated grains of an aggregate, and from local stresses at grain boundaries and at lattice imperfections resulting from cold work. A summary is given by C. Zener in *Proc. Phys. Soc. (London)*, vol. 52, p. 152, 1940, and bibliographies are given in recent papers. Cf. C. Zener, H. Clarke, and C. S. Smith, *Trans. A.I.M.E.*, vol. 147, p. 90, 1942; C. Zener, D. van Winkle, and H. Nielsen, *Trans. A.I.M.E.*, vol. 147, p. 98, 1942.

Read<sup>1</sup> has measured internal friction under conditions that should eliminate thermal currents and effects due to cold work, *viz.*, in single crystals vibrating at a frequency of several thousand cycles per second at strain amplitudes below  $10^{-5}$ . His measurements on a single crystal of copper as grown from the melt and the same crystal after annealing are reproduced in Fig. 3, which shows a very striking reduction in internal friction resulting from the annealing. Figure 3 is in accord with the idea that internal friction arises from pushing back and forth the dislocations that are present in the crystal, for if these dislocations are made to diffuse out of a crystal by annealing the internal friction of the crystal should then be lowered, as is found to be the case. It will be noted from Fig. 3

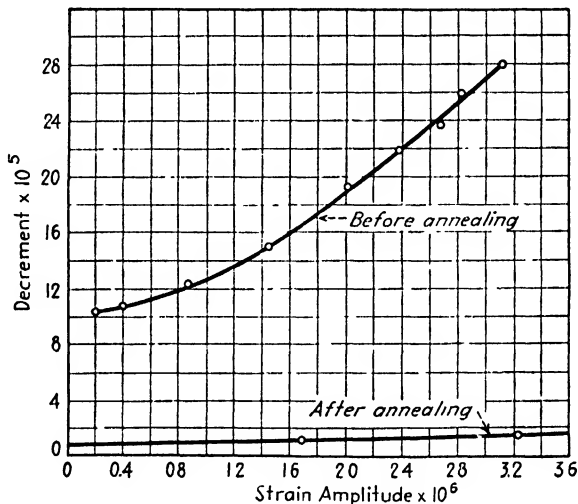


FIG. 3.—Internal friction of copper single crystal as prepared (upper curve) and after annealing 2 hr. at 500°C. (Read.)

that internal friction in the unannealed crystal increases with increasing amplitude. This is accounted for if one assumes that some of the dislocations are mobile when very low stresses are applied but that others are trapped by residual stresses in the crystal (such as the stresses around close-packed dislocations). The entrapped dislocations require comparatively large applied stresses to put them into motion and contribute to the internal friction only at the larger amplitudes.

Internal friction is increased by applying small loads to a crystal. Figure 4 shows the effect of applying 60, 120 and 150 psi. to a crystal of copper for 1 min. These loads caused no detectable permanent elongation of the crystal, and yet they appear to be responsible for generating many new dislocations (aided, of course, by thermal vibrations of the atoms).

<sup>1</sup> T. A. READ, *Trans. A.I.M.E.*, vol. 143, p. 30, 1941.

Internal friction in zinc crystals differs from that in copper in ways that can be accounted for by noting that zinc, unlike copper, is self-annealing at room temperature. In "dislocation language," the atomic mobility at room temperature permits dislocations already present in the crystal to diffuse out and lower the internal friction. Another interesting property of zinc is its single slip plane (the basal plane), which affords an excellent opportunity to test whether internal friction can actually be

correlated with plastic flow on slip planes as the theory would imply. The results plotted in Fig. 5 show a very marked dependence of internal friction upon the angle between the

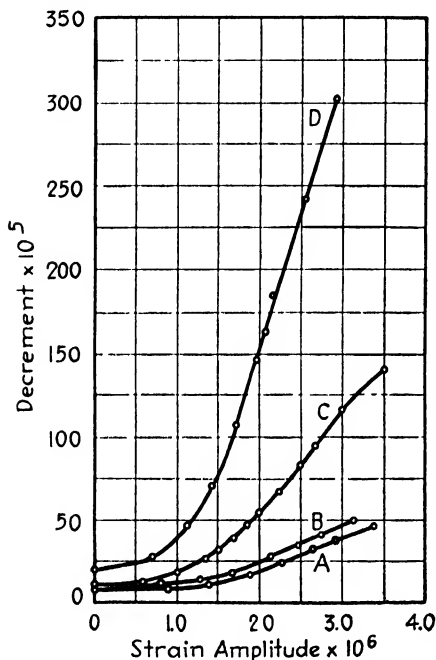


FIG. 4.

FIG. 4.—Internal friction of copper crystal increased by applying small stress for 1 min. Curve A was obtained before stressing; curve B, after applying 60 lb. per sq. in.; curve C, after applying 120 lb. per sq. in.; and curve D, after applying 150 lb. per sq. in. (*Read.*)

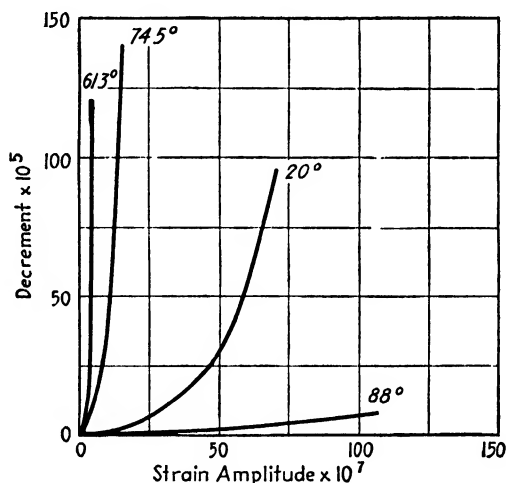


FIG. 5.

FIG. 5.—Variation of decrement with strain amplitude in zinc crystals the hexagonal axes of which make various angles with the axis of stress. (*Read.*)

basal plane and the axis of applied stress, increasing as this angle approaches the position for the maximum resolved shear stress ( $45^\circ$ ). Fig. 5 is therefore in qualitative agreement with the theory.

Zener finds that the internal friction in an  $\alpha$ -brass crystal (after thermal currents have been corrected for) depends upon temperature in the following way:

$$\text{Internal friction} = Ae^{-H/RT}$$

where  $A$  is a term that is inversely proportional to the frequency of vibration,  $R$  is the gas constant (1.986 cal. per mol), and  $H$  is a heat of activation associated with the process, which has the value  $H = 33,000$  cal.

per mol in 70-30  $\alpha$ -brass. This equation is also in accord with the concept that the fundamental mechanism for this type of internal friction is the motion of dislocations, an event occurring when the applied stress aided by thermal vibration overcomes the barriers to motion. Internal friction is less for stressing at high frequencies because the number of these events in the shorter time interval of one cycle is less than at low frequencies.

In polycrystalline metals internal friction is increased by cold work and is reduced by annealing below the recrystallization temperature<sup>1</sup> at temperatures that do not remove strain hardening or sharpen the diffuse lines in x-ray diffraction patterns. This may be taken to mean that the dislocations that are mobile enough to cause the internal friction in strain-hardened material increase in number with strain hardening but are not the ones responsible for the hardening or for the x-ray line broadening. Dislocations that find themselves moving in relatively unstressed regions are perhaps the source of the internal friction, while those entrapped in the intense stress fields closely surrounding other dislocations or surrounding lattice imperfections are perhaps the source of the strain hardening.

**Creep.**—A full interpretation of creep results in terms of dislocation theory would be welcome but has not yet been achieved. Nevertheless, the dislocation point of view is of considerable value in understanding many phases of the subject and merits a brief survey here.

Creep is a term applied to flow at rates slower than slip. The fundamental process of slip on crystallographic slip planes is probably responsible for the internal deformation of crystals during creep in spite of the fact that creep may occur without the formation of visible slip lines,<sup>2</sup> the slip being spread over more planes with less movement on each than is the case with slip at ordinary rates. At elevated temperatures this mechanism is supplemented by flow that appears to be concentrated at the crystal boundaries, producing the appearance of crystals "swimming" in their boundaries,<sup>3</sup> and if recrystallization is occurring it also contributes to the flow.<sup>4</sup> The discussion will be limited to conditions in which the latter two causes are believed to be inoperative.

The rate of strain at constant load vs. time is normally a curve in which there is a preliminary stage, "primary creep," in which the metal seems to be adjusting itself to the load, followed by a steady state,

<sup>1</sup> R. H. CANFIELD, *Trans. A.I.M.E.*, vol. 20, p. 549, 1932. F. FÖSTER and W. KÖSTER, *Z. Metallkunde*, vol. 29, p. 116, 1937. J. T. NORTON, *Trans. A.I.M.E.*, vol. 137, p. 49, 1940. A. W. LAWSON, *Phys. Rev.*, vol. 60, p. 330, 1941. C. ZENER, H. CLARKE, and C. S. SMITH, *Trans. A.I.M.E.*, vol. 147, p. 90, 1942.

<sup>2</sup> D. HANSON, *Trans. A.I.M.E.*, vol. 133, p. 15, 1939.

<sup>3</sup> H. F. MOORE, B. B. BETTY, and C. W. DOLLINS, *Univ. Illinois, Bull.* 272, 1935.

<sup>4</sup> K. VON HANFFSTENGEL and H. HANEMANN, *Z. Metallkunde*, vol. 29, p. 50, 1937. A. A. SMITH, *Trans. A.I.M.E.*, vol. 143, p. 165, 1941.



"secondary creep," in which the elongation is at a constant rate. These are illustrated in Fig. 6. If the stress is sufficiently high, the steady-state creep is followed by a third stage, which seems to be associated with the beginning of failure of the specimen (necking down). Extensive discussions of these stages and their characteristics will be found in reviews of creep by Hanson,<sup>1</sup> Kanter,<sup>2</sup> Kauzmann,<sup>3</sup> and others.

A series of experiments on single crystals of tin has been made by Chalmers,<sup>4</sup> which because of their apparent simplicity and fundamental significance make a good starting point for speculation. Chalmers found that by using strain gauges reading to  $10^{-7}$  cm. per cm. he could detect plastic flow at stresses less than 100 g. per sq. mm. In this range, creep produces a total extension that is practically independent of the stress and is limited to about  $10^{-5}$ . The rate of strain for this so-called "microcreep" when the load is first applied is proportional to the stress. As the load is increased, a stress is finally reached at which a much more rapid flow starts and a second mechanism of flow becomes operative.

Microcreep appears to be caused by the flow of dislocations already present in the metal. As these are limited in number, only a definite amount of extension can result from their movement. The applied stresses are presumably too low to generate more dislocations.

Chalmers detected a very small residual creep at low stresses after microcreep had been exhausted that could be ascribed to the spontaneous generation of dislocations by thermal fluctuations; it was approximately independent of stress, as might be expected at these low stress levels.

Following Seitz and Read, the initial rate of strain  $dS/dt$  in this range of stressing can be derived by assuming

$$\frac{dS}{dt} = N\bar{v}\lambda \quad (1)$$

in which  $N$  is the density of dislocations cutting across a plane normal to their length,  $\bar{v}$  is the mean velocity with which they move, and  $\lambda$  is the slip distance associated with the passage of one dislocation, presumably one

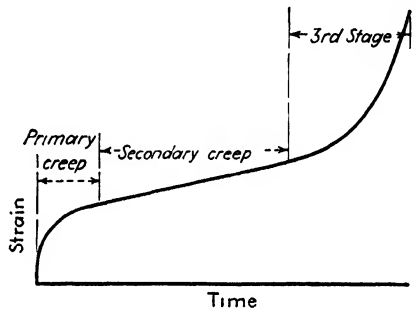


FIG. 6.—First, second, and third stages of creep.

<sup>1</sup> D. HANSON, *Trans. A.I.M.E.*, vol. 133, p. 15, 1939.

<sup>2</sup> J. J. KANTER, *Trans. A.S.M.*, vol. 24, p. 870, 1936; *Trans. A.I.M.E.*, vol. 131, p. 385, 1938.

<sup>3</sup> W. KAUFMANN, *Trans. A.I.M.E.*, vol. 143, p. 57, 1941.

<sup>4</sup> BRUCE CHALMERS, *Proc. Roy. Soc. (London)*, vol. A156, p. 427, 1936; *J. Inst. Metals*, vol. 61, p. 103, 1937.

atomic spacing in the slip direction. The velocity  $\bar{v}$  is the mean velocity with which the dislocations drift in the direction of the applied resolved shear stress as they wander about under the action of thermal fluctuations. Assuming that the potential barrier which must be surmounted to permit motion of dislocations is lowered in the direction of the resolved shear stress  $\tau$  by an amount  $-a\tau$  and is raised in the opposite direction by an amount  $a\tau$ , where  $a$  is a positive constant, the probability per unit time that a dislocation will jump in the forward direction is

$$p_+ = \frac{1}{t_1} e^{-(\epsilon_0 - a\tau)/kT}$$

where  $t_1$  is the time required for the jump to be completed from one equilibrium position to the next after it has acquired the necessary activation energy  $(\epsilon_0 - a\tau)$ . Similarly, the probability for a jump in the backward direction is

$$p_- = \frac{1}{t_1} e^{-(\epsilon_0 + a\tau)/kT}.$$

The mean velocity with which a dislocation drifts in the forward direction is then

$$\bar{v} = \lambda(p_+ - p_-) = \frac{\lambda}{t_1} \cdot e^{-\epsilon_0/kT} \sinh\left(\frac{a\tau}{kT}\right),$$

and by substitution in Eq. (1) this gives a rate of flow that is proportional to  $\sinh(a\tau/kT)$ . For small values of  $a\tau/kT$ , the equation for the rate of strain reduces to

$$\frac{dS}{dt} = \tau \cdot \frac{N\lambda^2 a}{t_1 k T} \cdot e^{-\epsilon_0/kT},$$

which predicts that the rate should increase linearly with  $\tau$ , and this is found to be so.

The relation of microcreep to primary creep in polycrystalline metals is obscure. Microcreep is not recoverable, whereas primary creep is recovered when the load is removed. Moreover, microcreep was not observed in bicrystal specimens having a longitudinal boundary. Creep experiments on single crystals of iron,<sup>1</sup>  $\alpha$ -brass,<sup>2</sup> zinc,<sup>3</sup> and cadmium<sup>4</sup> show preliminary stages in which the rate increases or decreases with time. Perhaps this is associated with alterations in the density of dislocations toward the equilibrium value from an initial density which may be either higher or lower.

<sup>1</sup> M. GENSAMER and R. F. MEHL, *Trans. A.I.M.E.*, vol. 131, p. 372, 1938.

<sup>2</sup> H. BURGHOFF and C. MATHEWSON, *Trans. A.I.M.E.*, vol. 143, p. 45, 1941.

<sup>3</sup> R. F. MILLER, *Trans. A.I.M.E.*, vol. 122, p. 176, 1936.

<sup>4</sup> W. BOAS and E. SCHMID, *Z. Physik*, vol. 100, p. 463, 1936.

Turning now to **steady-state**, or **secondary creep**, which occurs at higher stresses, we find that the constant rate in this range of stresses can be explained by the generation of new dislocations through applied stresses acting with thermal vibrations. The steady state may be thought of as an equilibrium condition in which the rate of generation is equal to the rate of loss and in which the creep rate is governed not by the rate of movement of the dislocations but by their rate of formation.

Steady-state creep varies with temperature, generally according to the relation<sup>1</sup>

$$\frac{dS}{dt} = A e^{-\epsilon/kT}$$

where  $A$  and  $\epsilon$  are constants characteristic of the metal. This relation can also be interpreted readily in terms of the generation of dislocations.

Kauzmann holds that the *length* of dislocations is a key factor in explaining many facts of creep and plastic flow. He concludes from the temperature dependence of creep rates that the length of dislocations is strongly temperature dependent. He also ascribes the variation in hardness from one metal to another, the variation in hardness with grain size, and the increase in hardness with solid-solution formation to differences in the length of dislocations.

Assuming that creep and internal friction are both evidences of dislocation behavior, it is pertinent to inquire to what extent they are correlated. Comparable data are meager and show poor correlation.<sup>2</sup> Seitz and Read conclude that the mechanisms responsible for microcreep and for internal friction at low stresses are different in an essential way that is undetermined at present. Possibly there is a characteristic difference in length between the dislocations that move in internal friction and those responsible for creep.

**Summary.**—The current, rapidly changing theory of dislocations may be summarized as follows: Thermal vibrations cause the generation of dislocations; they form chiefly at surfaces and at the boundaries of mosaic blocks and flaws, at places where the activation energy for their formation is lowered by a concentration of stress. Thermal fluctuations permit

<sup>1</sup> W. BOAS and E. SCHMID, *Z. Physik*, vol. 100, p. 463, 1935. Other expressions for the rate of creep in polycrystalline metals will be found in the summaries of Kanter and others (page 345).

<sup>2</sup> At low stresses Read finds that internal friction in tin is sensitive to annealing, whereas Chalmers finds that microcreep in tin is not affected by the thermal history of the specimen. The linear dependence of microcreep rate on stress should correspond to internal friction that is independent of amplitude and has about  $10^{-4}$  of the magnitude of the internal friction actually observed by Read. Actually, Read found a rapid increase in decrement with amplitude. A similar discrepancy is apparent in comparing the creep rates observed by Miller (*Trans. A.I.M.E.*, vol. 122, p. 176, 1936) for single crystals of zinc with the internal-friction measurements of Read.

them to move readily through the lattice until they encounter stress barriers at imperfections or at other dislocations. As the density of dislocations increases, an increasing stress is required to move them against their mutual interaction; this accounts for strain hardening. Dislocations near the surface have a smaller energy than have interior ones, and so there is a tendency for them to drift to the surface and effect a recovery from strain hardening. It seems likely that dislocations form as short nuclei and gain in length as they move into the interior of the crystal, perhaps extending throughout only one mosaic block or perhaps running through many. Some evidence indicates that local heating accompanies this movement and generates an avalanche of dislocations close together.

Internal friction for frequencies in the kilocycle range can be understood in terms of the generation and motion of dislocations; it decreases with annealing (and with self-annealing for zinc), and it increases with cold work, as if directly related to the number of dislocations present. Age hardening is ascribed to the hindrance of the passage of dislocations by stress fields surrounding precipitated particles. Solid-solution hardening may have a similar explanation, or possibly it results from shortening the average length of a dislocation.

The residual energy in a severely cold-worked metal can be accounted for if about  $10^{12}$  dislocation lines cross 1 sq. cm., a number that is in agreement with determinations based on magnetic measurements.

Microcreep in single crystals of tin may be attributed to the dislocations initially present; primary creep in polycrystalline metals probably reflects the approach to an equilibrium number of dislocations. In steady-state creep, dislocations are generated at a constant rate during loading. The relation between creep and internal friction is still ambiguous.

## CHAPTER XVII

### THE STRUCTURE OF COLD-WORKED METAL

The principal methods by which the structure of cold-worked metal is deduced are microscopic observations, studies of the alterations in mechanical and physical properties during deformation and annealing, and x-ray diffraction. Much can be inferred about the complexities of the structure from the microscopic and mechanical observations mentioned in the preceding chapters and from the preferred orientations and directional properties outlined in the following chapter, but the most direct evidence is obtained by diffraction. This chapter is a review of x-ray diffraction investigations of cold-worked metal. Researches in this field have been numerous, and it may be of service to include references to several studies that have only transient value in the development of our understanding of the subject, along with the more significant ones.

We shall first take up the **Laue method** and show that it reveals the range of orientation that exists within a small area. Other causes of streaks in Laue photographs will also be mentioned, and the fact emphasized that internal stresses cannot be deduced from the photographs. The second portion of the treatment covers investigations of the **widths of lines** in Debye photographs. Line widths are increased by internal stresses that are constant over distances of the order of thousands of angstroms, but not those that are distributed more locally. Unfortunately, lines are also widened by diffraction from small particles or small blocks of a mosaic lattice, and it is difficult to disentangle the two sources of widening. The **intensities of lines** are next discussed; intensities are decreased by local stresses, those varying over distances of a few angstroms. Thus the distortions that exist around imperfections and dislocations alter line intensities rather than line widths. It is now known that most of the energy left in a metal after cold work resides in these local stresses rather than in stresses distributed more uniformly. When a metal is **annealed** at or below the recrystallization temperature, the diffraction patterns undergo changes. Line widths are decreased, usually at the same time that the metal recovers from strain hardening. Softening and line sharpening are not always simultaneous, however, probably because dislocations and boundaries between grain "fragments" contribute to strain hardening but not to line widths. When a metal is subjected to **fatigue stressing**, it may become cold-worked and

alter its diffraction pattern. But since cold work during fatigue may be either beneficial or damaging and may take place in varying degrees in different metals or at different spots on a given object, x-rays do not appear to provide a useful criterion of impending failure.

### ASTERISM

**The Optical Analogy for Asterism.**—The well-known analogy pointed out by W. L. Bragg between diffraction of x-rays by atomic planes and the reflection of light by plane mirrors extends also to the diffraction by *bent* planes of atoms and the corresponding optical reflection from curved

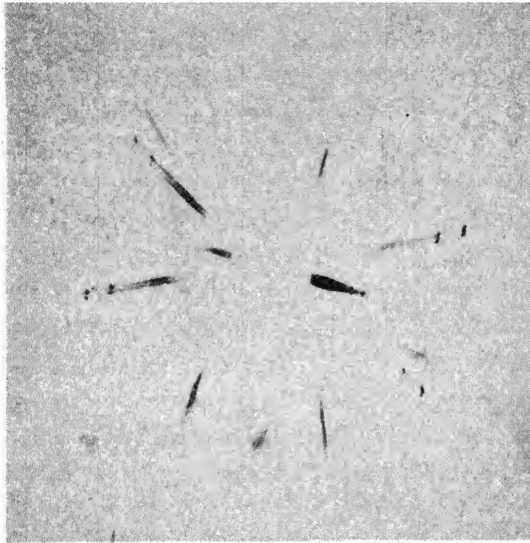


FIG. 1.—Asterism from bending a thin crystal of ferrite cylindrically (molybdenum radiation, unfiltered).

mirrors. It also applies to the reflection from crystal fragments arranged on a curved surface, corresponding to reflection from small mirrors arranged on a curved surface.

The optical analogy thus provides a convenient way of interpreting Laue patterns of deformed metals. Visualizing the atomic planes as mirrors, one sees at once that the Laue spots from a perfect crystal should be sharp, their size determined by the size and divergence of the x-ray beam and the dimensions of the camera, whereas Laue spots from bent planes should be elongated. The direction and amount of the elongation would depend on the position of the axis of bending with respect to the x-ray beam and the film, and also on the range of orientation of the planes within the area struck by the beam. Figure 1 is a typical example of the phenomenon. The spots elongate chiefly in radial or nearly radial directions, giving rise to the appearance known as "asterism."

It is also clear from the optical analogy that asterism could be produced by a preferred orientation of small crystallites, as in Fig. 2. If the crystallites were sufficiently small or the beam insufficiently collimated, the individual reflections would overlap, and the asterism streaks would resemble those from a bent crystal; there is thus an uncertainty as to whether in any particular case asterism is caused by bending of crystals or by grouping of small crystallites, or by both.

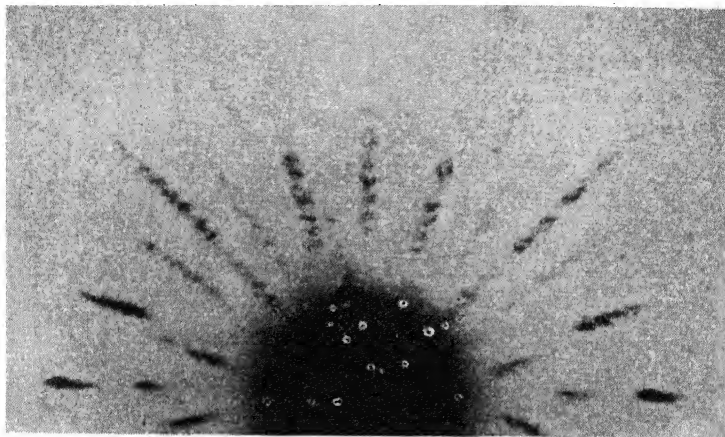


FIG. 2.—Pseudo asterism from preferred orientation in recrystallized rock salt. (S. Konobjewski and J. Mirer, *Z. Krist.*, vol. 81, p. 69, 1932.)

**Interpretation of Asterism in Terms of Range of Orientation.**—If a small crystal is placed in a beam of white radiation and rotated about an axis, the Laue spots will trace out curves on the film. When the axis of rotation coincides with the axis of the primary beam, these curves will simply be arcs of circles concentric with the primary beam, but with all other orientations of the axis of rotation the Laue spots will follow curves having a complex form expressed by equations of the fourth degree. A number of charts giving these curves for special arrangements of axis and film have been published, a very complete collection appearing in the "International Tables for Crystal Structure Determination."<sup>1</sup> A more generally useful method is to plot the streaks on a stereographic projection.

From the lengths of asterism streaks one can determine the range of orientation within that portion of the material that lies in the primary beam. In practice, there are certain limitations that often prevent a streak from developing to the full length required by this orientation range. These result from the fact that each streak (unless it is an arc of a circle concentric with the primary beam) is a spectrum of the primary x-rays; *i.e.*, each part is formed by x-rays of different wavelength. For

<sup>1</sup> "Internationale Tabellen zur Bestimmung von Kristallstrukturen," vol. II, p. 631, Bornträger, Berlin, 1935.

a streak formed by the  $(hkl)$  plane the wavelength of the ray forming any portion is given by Bragg's law  $n\lambda = 2d_{hkl} \sin \theta$ , and the streak must terminate abruptly at the short-wavelength limit of the spectrum (at  $\theta$  corresponding to  $\lambda_{\min}$ ), irrespective of any additional length that would have been permitted by the orientation range. On the long-wavelength end a streak may be prevented from developing to its true length by the lack of intensity in the long-wavelength components of the general radiation. The intensity distribution along a streak is the combined result of the distribution in orientation of the diffracting material, the wavelength-intensity distribution of the primary beam, the efficiency of the photographic emulsion, and the absorption characteristics of the crystal.<sup>1</sup> Abrupt changes in darkening will be found at  $\lambda$  values corresponding to the silver  $K$  absorption limit ( $\lambda = 0.485\text{\AA}$ ), the bromine  $K$  absorption limit ( $\lambda = 0.918\text{\AA}$ ), and critical-absorption limits of the elements in the crystal; and lines of intense blackening in the streaks will be found where characteristic radiation from the target is reflected. In the Laue pattern of Fig. 1 these points are illustrated. The thin crystal of  $\alpha$ -iron was uniformly bent into a cylinder and mounted with the cylindrical axis vertical, normal to the primary beam; there was an approximately uniform distribution of material throughout the orientation range. The  $K\alpha$  and  $K\beta$  lines from the molybdenum target as well as sharp edges at the silver and bromine absorption limits are visible on some of the striae. The factors just enumerated have led many investigators to use methods based on monochromatic rays in preference to the Laue method to determine the distribution in orientation of deformed crystals.

The construction of a stereographic projection of a Laue spot or streak is very simple. If the projection plane is taken normal to the incident beam and parallel to the photographic film, the rules for its construction are as follows:<sup>2</sup>

1. The x-ray beam, the Laue spot, and its projection all lie in a plane. Therefore, the spot itself and the projection of the spot have the same angular position about the beam as an axis.

2. The value of the Bragg angle  $\theta$  for a spot or portion of a streak is determined by the relation  $r = R \tan 2\theta$ , where  $r$  is the distance from the spot to the center of the film, and  $R$  is the distance from crystal to film. The angle  $\theta$  can be read directly from a chart of concentric circles spaced according to this relation. The spot is then plotted at a distance of  $\theta$  stereographic degrees measured inward from the outer circle of a stereographic net. (A polar net is most convenient for this purpose; but the equator of a Wulff net may be used as a scale.)

<sup>1</sup> Cf. p. 93 for a discussion of these factors.

<sup>2</sup> See Chap. IX, p. 154, for a more detailed discussion.



The streaks of Fig. 1 thus projected become the arcs of Fig. 3; these are shown superimposed on a stereographic net turned so that their differences in longitude can be read, giving the amount of rotation about the axis of the net. Many streaks are limited in length by the factors discussed above. If the projected striae cannot be made to coincide with the latitude circles on the net, a stereographic rotation of the arcs may be necessary in order to bring their axis of rotation into the plane of projection. The distribution of orientation may be shown, however, even if multiple axes operate, for the poles then are plotted as areas having definite shapes and sizes. Back-reflection Laue photographs

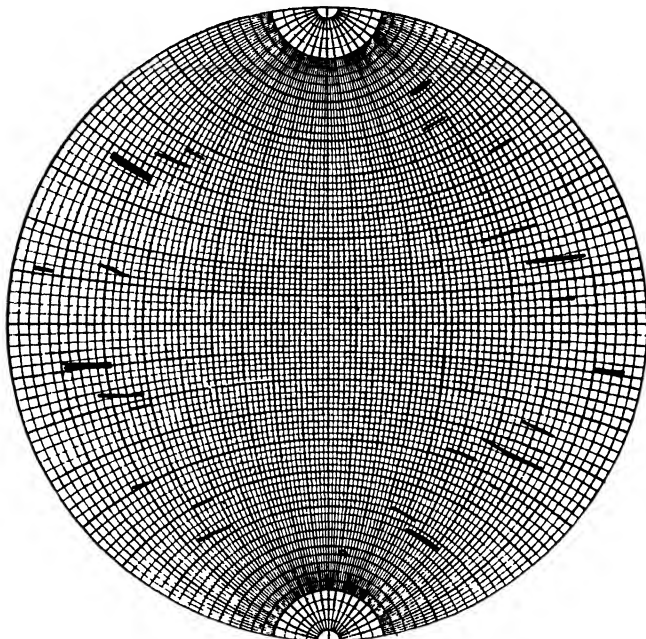


FIG. 3.—Stereographic projection of principal streaks of Fig. 1.

may also be plotted stereographically to show the extent and type of orientation divergence; the elongation of spots on these photographs is not predominantly radial as it is in the forward-reflection arrangement.

The predominantly radial direction of the streaks in forward-reflection Laue patterns is a direct consequence of the distorted angle relationships in the reflection projection. This will be understood if one considers the movement of a spot formed by reflection of a beam of light from a mirror that is rocked so that its normal moves within a small cone.<sup>1</sup> If the semivertical angle of this cone is  $e$ , the angle of incidence of a beam on a reflecting plane will vary through an angle  $2e$ , and the reflected beam through  $4e$  (Fig. 4). This will elongate the reflected spot radially to a

<sup>1</sup> W. L. BRAGG, "The Crystalline State," vol. I, General Survey, Macmillan, New York, 1934.

length  $4eR$ , where  $R$  is the distance from crystal to film. If the reflecting plane rocks around the beam as an axis, however, the reflected spot will move around the central beam through an angle  $2e$ . If the reflected beam is at an angle  $2\theta$  from the direct beam and the spot is at a distance  $r$  from the image of the direct beam, its lateral movement will be approximately  $2er = 2e \times 2\theta R$ . The ratio of major to minor axes of the elliptical spot will therefore be  $4eR/4e\theta R = 1/\theta$ . In the range of reflection of white radiation from the planes of greatest spacing, with  $\theta$  values roughly 5 to 10° (0.08 to 0.17 radian), the major axis is six to twelve times the minor axis.

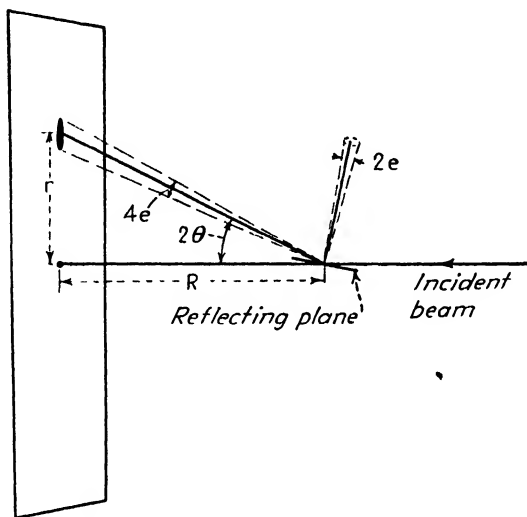


FIG. 4.—Illustrating the radial character of asterism.

**Asterism and Internal Stresses.**—The Laue method with its asterism streaks is definitely unsuited to the detection and measurement of internal stresses in metallurgical materials. The elastic distortions caused by internal stresses are negligible in comparison with the changes in orientation that result from plastic flow and are submerged by the latter. Numerous experiments have shown that Laue patterns from stressed and unstressed material are similar: single crystals loaded in tension give Laue patterns identical with the unstressed crystals as long as the load does not exceed the elastic range,<sup>1</sup> and photograms of deformed metals before and after a stress-relieving anneal are the same, provided that no recrystallization has occurred. Karnop and Sachs's<sup>2</sup> photograms of a stretched

<sup>1</sup> ABRAM F. JOFFÉ, "The Physics of Crystals," McGraw-Hill, New York, 1928. H. L. COX and I. BACKHURST, *Phil. Mag.*, vol. 7, p. 981, 1929. G. L. CLARK and M. M. BECKWITH, *Trans. A.S.M.*, vol. 25, p. 1207, 1937.

<sup>2</sup> R. KARNOP and G. SACHS, *Z. Physik*, vol. 42, p. 283, 1927. G. SACHS, *Plastische Verformung in "Handbuch der Experimental Physik,"* vol. V, Akademische Verlagsgesellschaft m.b.H., Leipzig, 1930.

aluminum crystal before and after annealing for  $\frac{1}{2}$  hr. at 400°C. show the point clearly (Fig. 5). The patterns are practically identical in appearance and indicate that the lattice orientations were not perceptibly altered; yet any internal stresses that may have resulted from the deformation were relieved by the anneal. Observations on small-grained material loaded below the proportional limit are less conclusive, for there is always uncertainty as to whether an occasional grain has been plastically deformed. Under special circumstances purely elastic deformation can be made to distort a crystal sufficiently to produce asterism; it is possible with mica crystals and with metals in thin sheet form,<sup>1</sup> where stresses introduced by bending remain small even with considerable curvature of the sheet.

In plastically deformed material the minor degree of asterism from elastic distortion is submerged by the distortions accompanying plastic

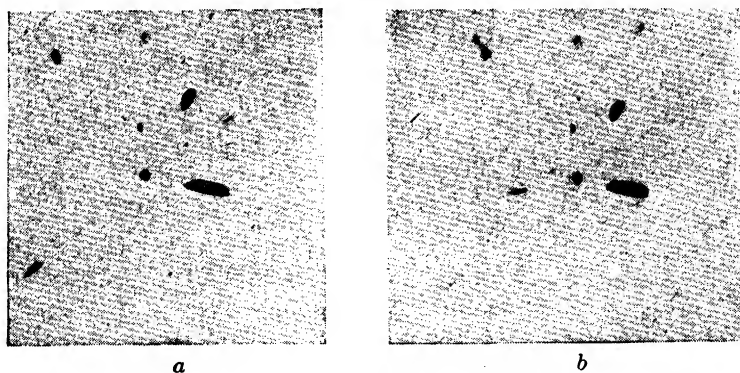


FIG. 5.— Laue photographs of aluminum crystal showing asterism. *a*, after 15 per cent elongation; *b*, same crystal after  $\frac{1}{2}$  hr. stress-relieving anneal at 400°C.

flow and cannot be separated from them. But even if it could be detected and separately identified, there would still be great difficulty in interpreting it in terms of the magnitude of internal stresses, for this requires the use of bent-beam formulas and therefore the knowledge of the radius of curvature and the thickness of the elastically bent elements within the crystals. The difficulties appear to be insurmountable for polycrystalline metals. Attempts have been made to solve the problem in nonmetallic single crystals, but the divergent conclusions that have been reached indicate the complexities involved: Konobejewski and Mirer<sup>2</sup> looked for a type of deviation of the Laue streaks from the directions corresponding to pure rotation, a deviation that could be attributed to elastically bent lamellae in plastically deformed sodium chloride; it was concluded that they were present. Seljakow<sup>3</sup> looked for evidence of elastic shear that

<sup>1</sup> G. L. CLARK and W. M. SHAFER, *Trans. A.S.M.*, vol. 28, p. 853, 1940.

<sup>2</sup> S. KONOBEJEWSKI and I. MIRER, *Z. Krist.*, vol. 81, p. 69, 1932.

<sup>3</sup> N. J. SELJAKOW, *Z. Krist.*, vol. 83, p. 426, 1932.

would reduce the symmetry of crystals and found an effect he ascribed to this. Yamaguchi<sup>1</sup> considered that his Laue patterns of deformed aluminum single crystals indicated "local curvature" at the boundaries of slip planes; the curvature was believed to be in the nature of elastic bending, since there was little spottiness in the Laue streaks. Manteuffel<sup>2</sup> and Komar,<sup>3</sup> having seen cases of pronounced spottiness, concluded the opposite—that fragmentation, not elastic bending, was the mechanism. Other related experiments in asterism have been made, but the above serve to emphasize the unsuitability of the method for internal-stress investigations.

Asterism accompanying a transformation of phase is illustrated in Fig. 6. This is a transmission photogram of a piece of steel that was

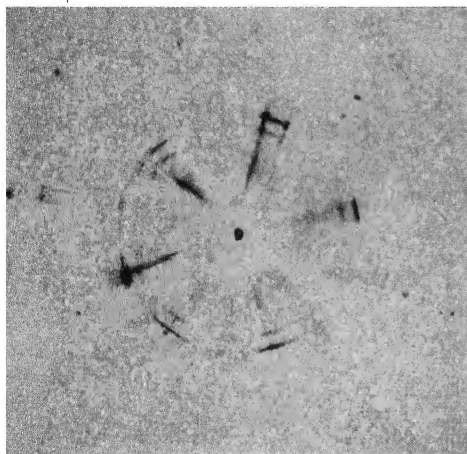


FIG. 6.—Asterism in cast hypoeutectoid steel, originally a single austenite grain (Mo radiation, transmission pattern).

originally a single grain of austenite; on cooling it has decomposed into ferrite grains with many orientations. The range of orientations has also been increased by the strains accompanying the transformation and possibly also by strains from thermal gradients that existed during cooling from the austenitic range.

**Crossed-grating Theory for Cold-worked Metals.**—Asterism has been interpreted as the result of relaxation of the third Laue condition, leaving only a two dimensional cross-grating interference pattern.<sup>4</sup> This point of view is

important in electron-diffraction work<sup>5</sup> and in some phases of x-ray work, but it is probably not important in considering cold-worked metals. As Bragg points out, the cross-grating pattern will appear with x-rays only if the crystal is thinner than two or three atom layers, because only then will the few atoms in each row parallel to the beam scatter in phase and act as one point of a cross grating. Thus cross-grating effects

<sup>1</sup> K. YAMAGUCHI, *Sci. Papers Inst. Phys. Chem. Research (Tokyo)*, vol. 11, pp. 151, 223, 1929.

<sup>2</sup> I. MANTEUFFEL, *Z. Physik*, vol. 70, p. 109, 1931.

<sup>3</sup> A. P. KOMAR, *Physik. Z. Sowjetunion*, vol. 9, p. 413, 1936.

<sup>4</sup> W. LINNIK, *Nature*, vol. 123, p. 604, 1929. W. L. BRAGG, *Nature*, vol. 124, p. 125, 1929. W. BERG, *Z. Krist.*, vol. 83, p. 318, 1932; vol. 89, p. 587, 1934. W. H. ZACHARIASEN, *Phys. Rev.*, vol. 53, p. 844, 1938.

<sup>5</sup> W. L. BRAGG and F. KIRCHNER, *Nature*, vol. 127, p. 738, 1931. G. P. THOMSON and W. COCHRANE, "Theory and Practice of Electron Diffraction," Macmillan & Company, Ltd., London, 1939.

would be expected only with plate-shaped crystallites which are extremely thin in the direction of the beam and are several hundred angstroms in diameter or with a lattice in which there is some lack of periodicity in one dimension. There has as yet been no proof that this condition exists in cold-worked metals. However, any crystal thinner than about  $100\text{\AA}$  will act as a two-dimensional grating for electrons. Consequently, an aggregate of equiaxed crystals each less than  $100\text{\AA}$  on a side will yield cross-grating electron diffraction patterns. Cross-grating diffraction may be distinguished from asterism arising from a range of orientation by analyzing the directions of the streaks or by preparing certain photographs with monochromatic radiation.

#### Asterism from Thermal Vibration.

—It has recently been demonstrated,<sup>1</sup> that a variety of asterism can be observed with undeformed crystals, as shown in Fig. 7. While this somewhat resembles the effect to be expected from either a crossed grating or from a preferred orientation, it actually arises from thermal agitation.<sup>2</sup> When the heat motion of the atoms of the lattice is analyzed as elastic waves of various frequencies and amplitudes,<sup>3</sup> it turns out that reflections are possible when Bragg's law is not fulfilled. In terms of the reciprocal-lattice concept the reciprocal lattice points are each surrounded by a "cloud" in reciprocal space, and reflection occurs whenever the reflection sphere touches one of these clouds. This asterism from thermal elastic vibrations can usually be seen only on overexposed Laue films at room temperature, but it becomes increasingly prominent as the temperature is raised. It is superimposed upon the normal spot pattern and consists of streaks that are always radial, as shown in Fig. 7. When monochromatic rays are used, diffuse maxima similar to Laue spots are seen.

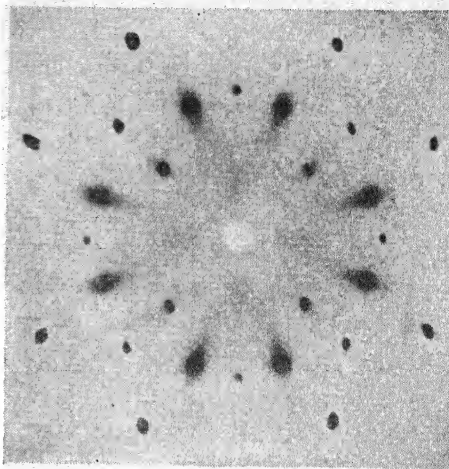


FIG. 7.—Thermal asterism in a Laue photograph of a single crystal of aluminum. X-ray beam along  $[100]$  with  $[001]$  vertical.

<sup>1</sup> A. P. R. WADLUND, *Phys. Rev.*, vol. 53, p. 843, 1938. G. D. PRESTON, *Proc. Roy. Soc. (London)*, vol. A172, p. 116, 1939; *Nature*, vol. 147, p. 467, 1941.

<sup>2</sup> G. D. PRESTON, *Proc. Roy. Soc. (London)*, vol. A172, p. 116, 1939; *Nature*, vol. 147, p. 467, 1941.

<sup>3</sup> M. BORN and T. v. KÁRMÁN, *Physik. Z.*, vol. 13, p. 297, 1912; vol. 14, pp. 15, 65, 1913. H. FAXÉN, *Ann. Physik*, vol. 54, p. 615, 1917; *Z. Physik*, vol. 17, p. 266, 1923. W. H. ZACHARIASEN, *Phys. Rev.*, vol. 57, p. 597, 1940; vol. 59, p. 860, 1941. W. H. ZACHARIASEN and S. SIEGEL, *Phys. Rev.*, vol. 57, p. 795, 1940. J. WEIGLE and CHARLES S. SMITH, *Phys. Rev.*, vol. 61, p. 23, 1942.

A variety of explanations has been advanced for the manner in which the thermal vibrations give rise to the streaks and monochromatic maxima, but both the position and intensity distribution of the maxima confirm the theory that elastic thermal waves are responsible.<sup>1</sup> These small-amplitude waves have such low frequencies compared with x-rays that they can be considered as "frozen-in" periodic disturbances, and they can be represented as additional terms in the Fourier series representing the distribution of matter in the crystal.

**Asterism from Structural Irregularity.**—Hendricks<sup>2</sup> has shown that asterism in crystals of mica arises from a lack of periodicity normal to the cleavage plane. The streaks, which are most clearly seen on Weissenberg photographs, follow zone lines; they are therefore not radial in ordinary Laue photographs, as they would be if they were of thermal origin (cf. previous section, page 357). A related phenomenon is reported by Bradley, Bragg, and Sykes,<sup>3</sup> who observed somewhat similar effects from submicroscopic lamellar arrangements of phases in Fe-Cu-Ni alloys after cooling at certain rates. Thomson and Cochrane<sup>4</sup> have suggested this explanation—a destruction of regular lattice periodicity normal to a set of planes—for some anomalous effects in electron diffraction patterns from hexagonal close-packed metals that are transforming to their face-centered cubic modification.

Carbon black can give two-dimensional diffraction. It is a material built of individual layers that are parallel and equidistant, but the distribution of particles with regard to translation parallel to the layers and rotation about the normal to the layers is completely random. The general theory has been worked out by Warren.<sup>5</sup> If the coordinate axes are chosen so that the crystal axes in the layer are  $a$  and  $b$  and the axis normal to the layer is  $c$ , there will be sharp reflections of the type  $(00l)$  and diffuse two-dimensional diffraction of type  $(hk)$ ; reflections of type  $(hkl)$  will be absent. The size of the two-dimensional layer in the plane of the layer,  $L$ , can be determined from the breadth of the two-dimensional reflection at half-maximum intensity,  $B$ , by the relation

$$L = \frac{1.84\lambda}{B \cos \theta}.$$

<sup>1</sup> S. SIEGEL and W. H. ZACHARIASEN, *Phys. Rev.*, vol. 57, p. 795, 1940. S. SIEGEL, *Phys. Rev.*, vol. 59, p. 371, 1941. R. Q. GREGG and N. S. GINGRICH, *Phys. Rev.*, vol. 59, p. 619, 1941. W. H. ZACHARIASEN, *Phys. Rev.*, vol. 59, p. 207, 1941.

<sup>2</sup> S. B. HENDRICKS, *Phys. Rev.*, vol. 57, p. 448, 1940.

<sup>3</sup> A. J. BRADLEY, W. L. BRAGG, and C. S. SYKES, *Researches into the Structure of Alloys*, *J. Iron Steel Inst.*, vol. 141, No. 1, p. 63, 1940.

<sup>4</sup> G. P. THOMSON and W. COCHRANE, "Theory and Practice of Electron Diffraction," p. 135, Macmillan, New York, 1939.

<sup>5</sup> B. E. WARREN, *Phys. Rev.*, vol. 59, p. 693, 1941.

In a powder diffraction pattern of a substance of this type, when  $L$  is small there is a displacement of the peak intensity of the two-dimensional reflections by the amount

$$\Delta (\sin \theta) = \frac{0.16\lambda}{L}$$

Thus if the two-dimensional character of the reflection were not realized and the pattern were analyzed in the ordinary way, it is likely that erroneous conclusions would be drawn.

**Local Curvature.**—Homogeneous rotation of the lattice in a single crystal during either compression or tension is unusual. The constraints imposed by the grips of the testing machine or by the friction of the specimen on the compression plates cause bending of the glide layers in the lattice, the so-called "bend gliding."<sup>1</sup> In polycrystalline material the interference of neighboring grains having differently oriented slip systems gives rise to much of this bend gliding.<sup>2</sup> It is possible, however, to deform a single crystal so as to minimize all such bending moments.<sup>3</sup> This has been done in both tension and compression. If, for example, carefully prepared single crystals are squeezed between polished and greased compression plates, the slip planes rotate toward a position parallel to the plane of the compression plate; it would then be expected that the lattice would rotate homogeneously. Yet a considerable range of orientation is found in a crystal deformed in this way,<sup>3</sup> as is shown by asterism in Laue photograms and by reflections of monochromatic rays.

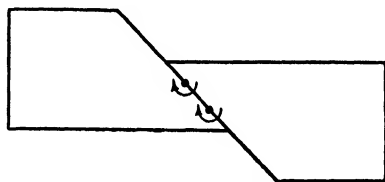


FIG. 8.—Sketch illustrating local curvature at a slip plane.

The inhomogeneous character of deformed single crystals led Taylor, Yamaguchi, and Burgers to postulate distortions of a local character, "local curvature," arising from disturbances at the slipping surfaces and consisting of rotation of portions of the lattice about an axis lying in the glide plane and perpendicular to the glide direction, as shown in Fig. 8. The rotation is the same, in both direction and sense, as would be experienced by detached portions of the lattice acting as rollers lying between the slipping surfaces and amounts to as much as 10, 20, or even 50° with severe deformation.

Another method of obtaining homogeneous deformation consists in pulling a long single crystal specimen in tension. In the center portion

<sup>1</sup> H. MARK, M. POLANYI, and E. SCHMID, *Z. Physik*, vol. 12, pp. 58, 78, 111, 1922.

<sup>2</sup> F. WEVER and W. E. SCHMID, *Mitt. Kaiser Wilhelm Inst. Eisenforsch. Düsseldorf*, vol. 11, p. 109, 1929.

<sup>3</sup> G. I. TAYLOR and W. S. FARREN, *Proc. Roy. Soc. (London)*, vol. A111, p. 520, 1926; vol. A116, p. 16, 1927.

of the specimen at sufficient distances from the grips there should be no bending moments or bendgliding. The presence of asterism in photographs of this region has also been interpreted in terms of local curvature.<sup>1</sup>

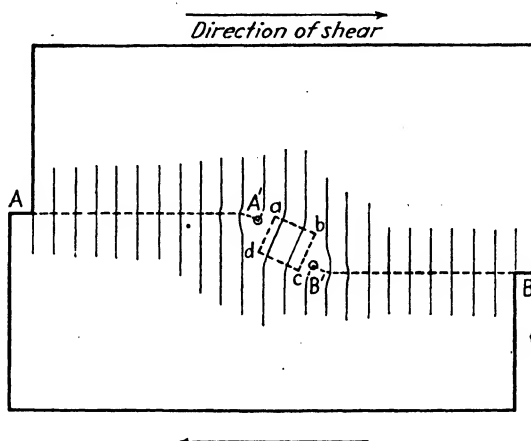


FIG. 9.—Burgers's suggested mechanism for producing local curvature.

There is a spread in orientation that increases approximately linearly with increasing deformation, as in compression.

Various suggestions have been made to account for these local rotations.

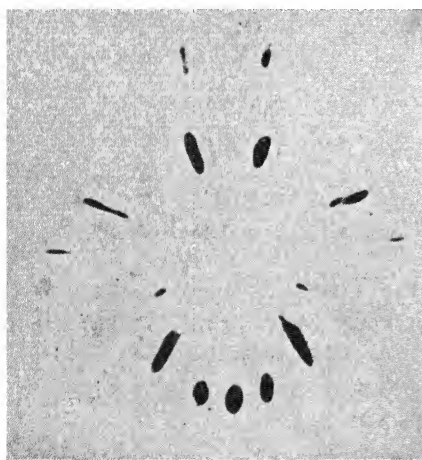


FIG. 10.—Laue photograph showing asterism from deformation bands in a single crystal of aluminum compressed 28 per cent.

Burgers, for example, has suggested that dislocations or slip movements approach each other, reaching the points  $A'$  and  $B'$  and creating local curvature in the region  $abcd$  in the manner indicated in Fig. 9.<sup>2</sup>

It cannot be safely concluded at the present time that the local curvatures postulated by Taylor, Yamaguchi, and Burgers actually exist. Most of the experimental evidence for them would be equally well explained by macroscopic variations in orientation, and it is questionable whether the latter have been eliminated in their experiments. In fact, a series of recent studies<sup>3</sup> has shown that it is the rule, rather than the exception, for different portions of the crystal to rotate in different

<sup>1</sup> K. YAMAGUCHI, *Sci. Papers Inst. Phys. Chem. Research (Tokyo)*, vol. 11, p. 223, 1929.

<sup>2</sup> J. M. BURGERS, *Proc. Phys. Soc. (London)*, vol. 52, p. 23, 1940.

<sup>3</sup> C. S. BARRETT, *Trans. A.I.M.E.*, vol. 135, p. 296, 1939. C. S. BARRETT and L. H. LEVENSON, *Trans. A.I.M.E.*, vol. 135, p. 327, 1939; vol. 137, p. 112, 1940.



directions, forming deformation bands of differing orientation (see page 305). These bands are found even when great care is taken to provide homogeneous compression. They produce asterism much like that attributed to local distortion, as illustrated in Fig. 10.

**Tests of the Local-curvature Theory.**—When an aluminum crystal is compressed in such a way as to avoid deformation bands, there is a spread in orientation of the order of  $\pm 10^\circ$ , but when plotted in a stereographic projection the directions of rotation does not coincide with

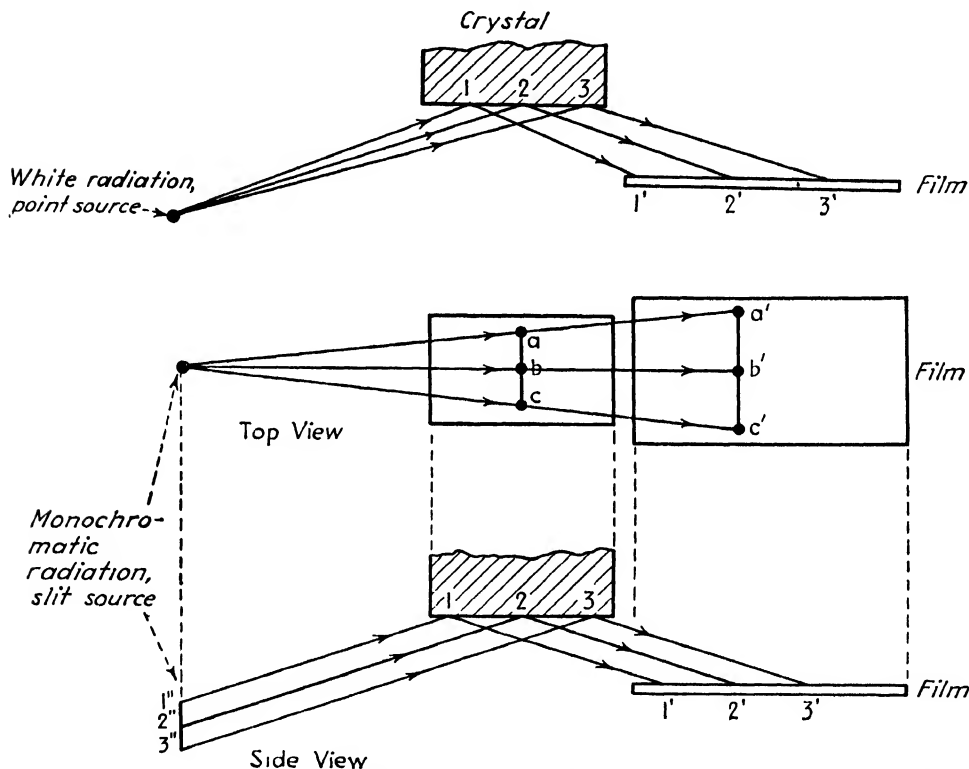


FIG. 11.—Berg's two arrangements for studying the fine structure of Laue spots. Points on crystal surface 1, 2, 3, *a*, *b*, *c* reflect to corresponding points on film, 1', 2', 3', *a'*, *b'*, *c'*.

the predictions of the local-curvature theory.<sup>1</sup> Komar and Mochalov<sup>2</sup> have criticized the theory also on the basis of their results on magnesium crystals etched to various thicknesses; these indicated macroscopic rather than microscopic rotations.

The theory derives support, however, from the x-ray experiments of Berg,<sup>3</sup> who shows that Laue spots made by reflection from the surface of deformed rock salt have a fine structure. When a crystal is arranged as

<sup>1</sup> C. S. BARRETT, *Trans. A.I.M.E.*, vol. 137, p. 128, 1940.

<sup>2</sup> A. KOMAR and M. MOCHALOV, *Physik. Z. Sowjetunion*, vol. 9, p. 613, 1936.

<sup>3</sup> W. BERG, *Z. Krist.*, vol. 89, p. 286, 1934.

in Fig. 11, each point in a Laue spot is made by rays from a single spot on the crystal face, provided that the crystal has a uniform orientation. If, however, there is local rotation at a slip plane, this transfers the

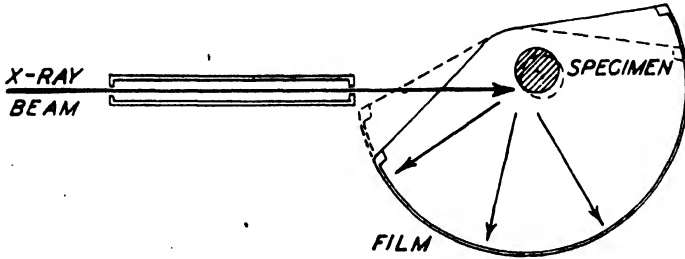


FIG. 12.—X-ray camera in which film and specimen are mounted on an oscillating carriage. Characteristic radiation is used.

reflected x-rays from one strip of the image to another, leaving an unexposed line through the image. Berg observes such lines, and the directions of rotation required to explain them are in accord with the local-curvature theory.

**Inhomogeneous Distortion in Polycrystalline Aggregates.**—In the deformation of grains of an aggregate it is difficult to separate the various

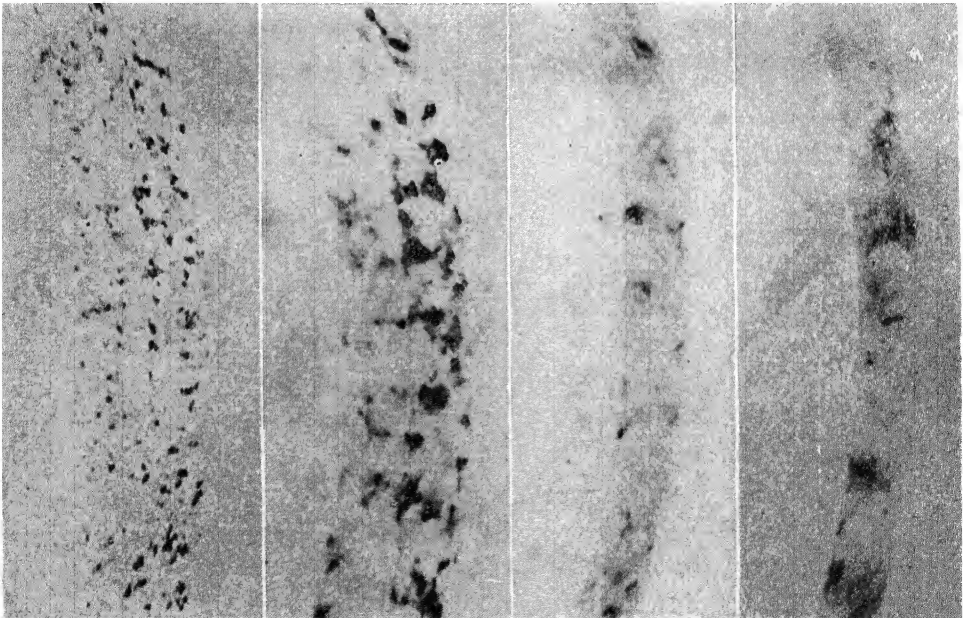


FIG. 13.—Photographs of polycrystalline iron after increasing amounts of elongation in tension. Made with camera of Fig. 12 ( $\text{FeK}\alpha$  (110) reflections).

factors causing spreading orientations in the grains, which produce asterism in Laue photograms. It is obvious that slip cannot proceed far without encountering interference from neighboring grains; severe bend-

ing and warping of the lattice then ensue; deformation bands form in many grains, and local curvature may also contribute to the inhomogeneity. Inasmuch as the average grain deforms by slip on several slip systems and is itself surrounded by several grains slipping in various ways, the average grain undergoes complex distortion. That this occurs can be shown clearly by plotting pole figures or by using an **oscillating-film technique**,<sup>1</sup> as illustrated in Fig. 12. In this camera the film and specimen are attached to the same carriage and rotate together; this permits the spreading of a Laue spot in all directions without altering the wavelength of the reflected beam. Figure 13 illustrates the results obtained in this camera and shows the gradually increasing complex spreading of spots from polycrystalline iron strained increasing amounts in tension.

The alterations in Laue photographs accompanying deformation are as follows: As deformation increases, there is first an elongation of spots chiefly in the radial direction, then an increase in the number of striae and a decrease in their sharpness, leading to an almost uniform blackening of Debye rings, and finally a grouping of the striae into intense spots, indicating a preferred orientation of steadily increasing perfection.

#### DIFFRACTION-LINE WIDTHS AND INTENSITIES

When stresses are distributed uniformly throughout *macroscopic* regions in a metal, they alter the interplanar distances in a homogeneous fashion and cause the reflected lines of a Debye pattern to shift without widening or loss of intensity. From an analysis of the shift a direct determination of the principal stresses is possible, as is discussed in Chap. XIV (page 267).

On the other hand, when stresses are distributed *microscopically* and vary from grain to grain or from region to region within one grain or even from point to point within a single region, the analysis of the strain becomes more uncertain. A complete analysis of this distribution is much to be desired for a better understanding of the conditions within metals after elastic and plastic deformation, and much effort has been directed to this end, but the complexities are great, and the available data meager. Although the general outlines of the subject are becoming clear, our knowledge at present is mainly qualitative.

For purposes of analysis it is convenient to consider a metal crystal as a mosaic of small regions within which the lattice is effectively perfect, a concept originally employed by C. G. Darwin in his analysis of x-ray diffraction. Each mosaic "block," or "domain," is considered to act as a coherent three-dimensional grating in diffracting the x-rays, with adjacent blocks out of registry enough to destroy this coherent diffrac-

<sup>1</sup> C. S. BARRETT, *Metals & Alloys*, vol. 8, p. 13, 1937.

tion and to cause each one to diffract independently. On the basis of this concept it is necessary to consider the following factors influencing diffraction: variation of lattice constants in different blocks, displacements of atoms within each block from the ideal positions, the size of the blocks, and other factors yielding effects similar to any of these, such as variations in composition.

**Lattice Constants Varying from Block to Block.**—The simplest model of a cold-worked metal is one in which the coherent blocks are strained homogeneously so that interplanar distances vary from block to block but are constant within each one. The domains are also assumed to be large enough so that no "particle-size widening" occurs; *i.e.*, their minimum dimension must exceed about  $10^{-5}$  cm. Each block according to this model will diffract independently at an angle corresponding to its state of strain. A diffracted line from the metal as a whole will then be the sum of the many individual components which deviate slightly from one another; the line thus will be abnormally wide.

A number of investigators have used this picture of the cause of line widening in cold-worked metals and have calculated from measurements of line widths the internal energy left in the metal. This has been compared with the calorimetrically measured values, which are in the neighborhood of 1 cal. per g. From calorimetric measurements, Taylor and Quinney<sup>1</sup> found 0.5 cal. per g. in cold-worked copper, 1.2 in iron, 0.78 in nickel, and 1.1 in aluminum; Farren and Taylor<sup>2</sup> found 0.38 cal. per g. in copper and 0.33 in aluminum after stretching; Rosenhain and Stott<sup>3</sup> found 0.23 cal. per g. in cold-worked aluminum.

Caglioti and Sachs<sup>4</sup> estimated the internal energy in copper after cold work using the expression  $\frac{3}{4}(\Delta a/a)^2(1/X)$  kg.-mm. per cu. mm., where  $X$  is the compressibility ( $0.74 \times 10^{-4}$  sq. mm. per kg. for copper), and  $(\Delta a/a)$  is the fractional change in lattice constant corresponding to the widening observed; the values obtained were only one-thousandth of the measured values of Farren and Taylor and of Taylor and Quinney. A similar result was found by Boas,<sup>5</sup> who assumed a stress distribution in the metal such that the energy would be  $\frac{3}{2}(\Delta a/a)^2(1/X)$  and obtained for copper, nickel, and gold residual strain energies of the order of  $10^{-3}$  cal. per g. after rolling and drawing, again about one-thousandth of the measured values.

<sup>1</sup> G. I. TAYLOR and H. QUINNEY, *Proc. Roy. Soc. (London)*, vol. A143, p. 307, 1934.  
H. QUINNEY and G. I. TAYLOR, *Proc. Roy. Soc. (London)*, vol. A163, p. 157, 1937.

<sup>2</sup> W. S. FARREN and G. I. TAYLOR, *Proc. Roy. Soc. (London)*, vol. A107, p. 422, 1925.

<sup>3</sup> W. ROSENHAIN and V. H. STOTT, *Proc. Roy. Soc. (London)*, vol. A140, p. 9, 1933.

<sup>4</sup> V. CAGLIOTI and G. SACHS, *Z. Physik*, vol. 74, p. 647, 1932.

<sup>5</sup> W. BOAS, *Z. Krist.*, vol. 96, p. 214, 1937.

Later investigators attempted a more precise specification of the distribution curve for the strains. Haworth<sup>1</sup> set up an empirical expression which gave the distribution of intensity in the lines from the annealed specimen, and from the difference between the lines from the cold-worked and annealed samples derived a distribution curve for interplanar spacing,  $\Delta d/d$ , reproduced in Fig. 14, and from this derived the mean square strain  $(\Delta d/d)_{av}^2$ .

Stibitz<sup>2</sup> has calculated the internal energy  $V$  stored in a metal by residual stress, in terms of the mean square strains,<sup>3</sup> and Haworth, using Stibitz's formula, obtained  $V = 0.065$  cal. per g. for permalloy (70

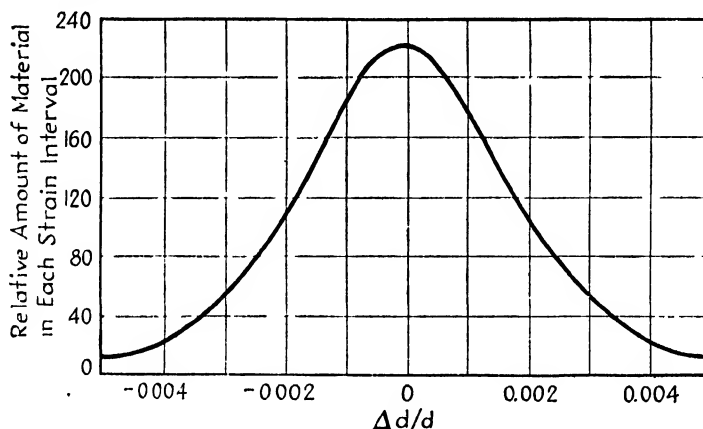


FIG. 14.—Frequency curve of strain  $\Delta d/d$  in hard-rolled permalloy. (Haworth.)

percent nickel, 30 percent iron) cold-rolled 96 percent. Brindley and Ridley,<sup>4</sup> assuming a Gaussian distribution of  $(\Delta d/d)$  and fixing the single adjustable parameter of this distribution so as to agree with the ratio of the peak intensity to the total energy of the diffracted lines, concluded

<sup>1</sup> F. E. HAWORTH, *Phys. Rev.*, vol. 52, p. 613, 1937.

<sup>2</sup> G. R. STIBITZ, *Phys. Rev.*, vol. 49, p. 862, 1936 (abstract); *Phys. Rev.*, vol. 52, p. 619, 1937.

<sup>3</sup> Assuming a statistical random distribution of the directions of the principal stresses,  $\sigma_x$ ,  $\sigma_y$ ,  $\sigma_z$ , and assuming that, for the average values,  $\sigma_x^2 = \sigma_y^2 = \sigma_z^2 = \sigma^2$  and  $\sigma_x\sigma_y = \sigma_y\sigma_z = \sigma_z\sigma_x = 0$ , the expression for the internal energy

$$V = \left(\frac{1}{2E}\right)(\sigma_x^2 + \sigma_y^2 + \sigma_z^2) - \left(\frac{\nu}{E}\right)(\sigma_x\sigma_y + \sigma_y\sigma_z + \sigma_z\sigma_x)$$

becomes

$$V = \frac{3(\sigma^2)_{av}}{2E}$$

which, with the value for  $(\Delta d/d)_{av}^2$ , may be written

$$V = \frac{3E}{2(1 + 2\nu^2)} \left(\frac{\Delta d}{d}\right)_{av}^2$$

where  $E$  is Young's modulus and  $\nu$  is Poisson's ratio.

<sup>4</sup> G. W. BRINDLEY and P. RIDLEY, *Proc. Phys. Soc. (London)*, vol. 51, p. 432, 1939.

that  $V = 0.0169$  cal. per g. for copper after cold work by filing, 0.034 for nickel, and 0.0834 for rhodium. They employed Stibitz's formula for the calculation.

Thus, while different investigators have arrived at the mean square value of the residual strains in different ways and have calculated the internal strain energy from this value with different mathematical expressions, all are in agreement that line widths interpreted in terms of variations of stresses from block to block can account for only an insignificant fraction of the maximum values found calorimetrically.

It must be concluded, therefore, that the principal part of the residual energy is in the form of distortions that are uniform over volumes too small to cause broadening of the diffraction lines.

**Atomic Displacements within a Block.**—It is possible that diffraction lines from cold-worked metals are widened by some sort of regular or irregular displacements of atoms from ideal lattice positions within the domains. Thus, even if there were no variation in the average spacing among different domains, there might be strains of a more local distribution. In this class would be found many types of defects that have been discussed in connection with crystalline imperfections (*Versetzung*, *Lockerstellen*, and "dislocations"). Here, also, belong the random displacements of thermal agitation and the strains around the dislocations that are currently believed to account for plastic flow in crystals. Calculations indicate that displacements within a block may alter either the width or the intensity of reflected lines, depending on the distribution of the displacements throughout the volume of the region. •

Dehlinger<sup>1</sup> made the *ad hoc* assumption that the displacements of the atoms vary periodically like the errors in a ruled grating. Assuming a sinusoidal variation of displacements, he predicted diffraction "ghosts" analogous to those obtained with an imperfect optical grating. If the periods of these displacements in the crystal were long, these ghosts would lie close to the normal lines, and blend with them. On the other hand, if the distortions were distributed with a short period in the crystal—a few interatomic distances—the ghosts would fall some distance from the normal diffraction lines and contribute to the background of the pattern. Boas<sup>2</sup> has applied Fourier analysis to the problem, treating distortions of a more general type, and his work has been neatly correlated by Brill and Renninger,<sup>3</sup> though the mathematics has been criticized in some particulars by Dehlinger and Kochendörfer.<sup>4</sup> Long-period

<sup>1</sup> U. DEHLINGER, *Z. Krist.*, vol. 65, p. 615, 1927.

<sup>2</sup> W. BOAS, *Z. Krist.*, vol. 97, p. 354, 1937.

<sup>3</sup> R. BRILL and M. RENNINGER, "Ergebnisse der technische Röntgenkunde," vol. VI, p. 141, Akademische Verlagsgesellschaft m.b.H., Leipzig, 1938.

<sup>4</sup> U. DEHLINGER and A. KOCHENDÖRFER, *Z. Krist.*, vol. 101, p. 134, 1939.

components in the disturbances, which would produce ghosts close to the normal lines and widen them, would not reduce the total diffracted energy (the "integrated intensity" of the lines), since the energy in the ghost lines would appear to belong to the principal lines. Short-period distortions, corresponding to the higher terms of a Fourier analysis of the atom displacements, would produce ghosts distributed through the interval between the principal lines; these would be lost in the background and would merely effect a transfer of intensity from the principal line to the background. This type of displacement approaches the type caused by thermal agitation as the number of periods increases.

Atomic displacements within individual domains due to any cause, according to these theories, should cause predominantly either a widening or a reduction of line intensity, depending upon whether they are spread out or localized. When highly localized they resemble somewhat the thermal displacements of atoms and have been appropriately called "frozen heat motion."<sup>1</sup>

**Measurements of Line Broadening.**—According to Ludwik and Scheu<sup>2</sup> there is no increase in line width when tensile loads are applied that are less than the elastic limit of the material. If this observation could be given full weight, it would indicate that polycrystalline grains were equally and uniformly strained by the elastic load, but this seems unlikely in view of the anisotropy of Young's modulus. It is more probable that widening is present but is too small to be easily observed.

The manner in which line width increases with plastic deformation has received extensive study.<sup>3</sup> Most observers find that plastic deformation widens the diffraction lines up to a limiting value that is essentially unchanged by further deformation of the same type. A typical curve, showing the usual leveling off at the limiting value, is reproduced in Fig. 15. It has been suggested that a definite limit of widening exists that is characteristic of the material,<sup>4</sup> but if a limiting value does exist it must certainly depend on the conditions of loading, the temperature of deformation, and the previous thermal and mechanical history of the specimen,<sup>5</sup> and it cannot be an invariant characteristic of a metal or alloy. Ludwik and Scheu,<sup>2</sup> in fact, have shown that line width at fracture depends upon the type of loading and heat-treatment and that the width at a brittle fracture is less than at a ductile fracture; others

<sup>1</sup> G. W. BRINDLEY, *Proc. Phys. Soc. (London)*, vol. 52, p. 117, 1940.

<sup>2</sup> P. LUDWIK and L. SCHEU, *Metallwirtschaft*, vol. 13, pp. 257, 429, 1934.

<sup>3</sup> For an earlier review of the subject see C. S. Barrett, *Metals & Alloys*, vol. 5, pp. 131, 154, 170, 196, 224, 1934.

<sup>4</sup> H. J. GOUGH and W. A. WOOD, *Proc. Roy. Soc. (London)*, vol. A154, p. 510, 1936; summarized in lecture to Royal Aeronautical Society, Apr. 20, 1936, and in *Metal Progress*, vol. 30, p. 91, 1936.

<sup>5</sup> C. S. BARRETT, *Metals & Alloys*, vol. 8, p. 13, 1937.

have shown a difference in maximum width from different kinds of deformation.<sup>1</sup>

Wood<sup>2</sup> has proposed that, for electrodeposited metals, the effects of particle-size and lattice-distortion widening can be separated. Assuming that lattice-distortion widening cannot surpass the limit found in cold work by rolling, he ascribes all widening in excess of this to the particle-size effect of small grains in the electrodeposit. Conversely, if cold-working a deposit leads to an increased widening equivalent in amount to the lattice-distortion limit, he concludes that the original deposit is free from distortion. He obtained evidence of both types of broadening with various nickel and chromium deposits.

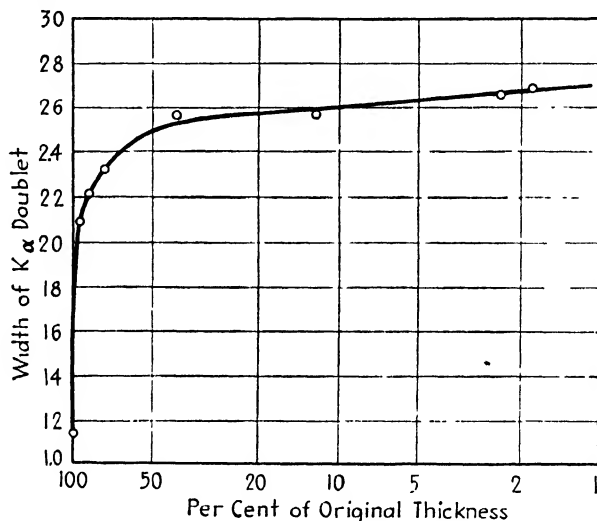


FIG. 15.—Breadth at half-minimum intensity of the reflected  $K\alpha$  doublet for permalloy reduced various amounts by cold rolling. (Haworth.)

Wood<sup>3</sup> contends that cold rolling cannot fragment metal grains below about  $10^{-5}$  cm. ( $1000\text{\AA}$ ) or that, if smaller fragment sizes are reached, they immediately recrystallize into regions of  $10^{-5}$  cm. or larger. However, his data for cold-rolled nickel actually would require a particle size of about  $3 \times 10^{-6}$  cm. if particle size were the sole cause of widening;<sup>4</sup> comparable figures for cold-worked brass and tungsten obtained by Stickley<sup>5</sup> with monochromatic radiation are  $10^{-6}$  cm.

Wood<sup>3</sup> set the lower limit for the particle size (the size if this were the only cause of widening) in copper, silver, and nickel at about  $1 \times 10^{-5}$

<sup>1</sup> F. E. HAWORTH, *Phys. Rev.*, vol. 52, pp. 613–620, 1937. U. DEHLINGER and A. KOCHENDÖRFER, *Z. Metallkunde*, vol. 31, p. 231, 1939.

<sup>2</sup> W. A. WOOD, *Phil. Mag.*, vol. 15, p. 553, 1933; vol. 20, p. 964, 1935.

<sup>3</sup> W. A. WOOD, *Proc. Phys. Soc. (London)*, vol. 52, p. 110, 1940.

<sup>4</sup> W. A. WOOD, *Phil. Mag.*, vol. 20, p. 964, 1935.

<sup>5</sup> E. E. STICKLEY, Doctoral dissertation, University of Pittsburgh, 1942; abstracted in *Univ. Pittsburgh Bull.*, vol. 39, No. 2, Jan. 10, 1943.



cm., in iron and molybdenum at about three times this amount, and in aluminum at  $10^{-4}$  cm. (no appreciable widening) and concluded that it goes through cyclic changes during progressive passes through the rolls.<sup>1</sup> Brindley and Ridley<sup>2</sup> obtained line widths from filed rhodium that would indicate a crystallite size of  $10^{-6}$  cm. if it were the only cause of the widening, but the line widths did not vary with  $\theta$  and  $\lambda$  as they should if particle size were the cause. Furthermore, there would be almost no primary extinction if the particles were small enough to explain the entire broadening; yet there is considerable extinction, and an estimate of crystallite size in rhodium from the extinction gives  $6.5 \times 10^{-5}$

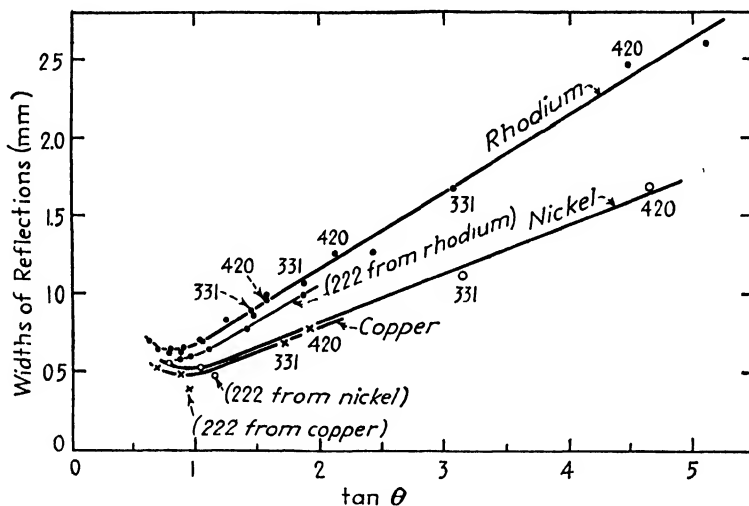


FIG. 16.- Widths of reflections from filed powders of copper, nickel, and rhodium as functions of  $\tan \theta$ . (Brindley and Ridley.)

cm. The line broadening with filed copper and nickel is less than with rhodium (Fig. 16); so here, also, crystallites must be at least  $10^{-6}$  cm. and may be much larger.

It must be remembered, however, that a large range of crystallite sizes is to be expected in a deformed grain. The crystallites smaller than  $10^{-6}$  cm. would contribute very diffuse reflections that might be submerged in the background of the lines and might effectively decrease the line intensity. The following experiment is important in this connection, for it suggests that deformation of the utmost severity can reduce all crystallites to a uniformly small size in some metals.

<sup>1</sup> He also reports that fatigue stressing is much less likely to cause grain fragmentation than static stressing of the same intensity and that single crystals stressed in fatigue in such a way that only one set of slip lines form show much less x-ray evidence of fragmentation than those in which duplex slip occurs.

<sup>2</sup> G. W. BRINDLEY and P. RIDLEY, *Proc. Phys. Soc. (London)*, vol. 50, p. 501, 1938.

Bridgman<sup>1</sup> has shown that severe shearing under tremendous pressure can widen diffraction lines beyond the amounts possible by rolling. He finds that in copper the lattice can be fragmented to such a degree that only a single diffuse Debye line can be seen. He estimates the grain diameter to be 10Å or less—practically amorphous. The lower melting metals like bismuth, while producing widened x-ray lines, retain a grain size large enough to give recognizable patterns, presumably because the rate of recrystallization overtakes the rate of fragmentation in these metals. Permalloy when deformed in the Bridgman apparatus gives wider lines than when rolled but does not reach—or at any rate does not retain—the amorphous state.<sup>2</sup>

An unsymmetrical widening of lines, which corresponds to a shift in the mean lattice constant, has been observed in rolled metals.<sup>3</sup> Since small particle size can lead only to symmetrical broadening, the asymmetry of lines has been suggested as a criterion of lattice distortion. However, asymmetry or line shifting can be accounted for merely by assuming an average stress different from zero in the portion of the metal contributing to the diffraction pattern, *i.e.*, by assuming that the residual stresses have a macroscopic distribution. This type of stress is to be expected in forming processes in which the flow is inhomogeneous.<sup>4</sup>

In a recent study of the subject Dehlinger and Kochendörfer<sup>5</sup> undertook a separation of particle-size widening and internal-stress widening by considering how the two effects varied with the angle of diffraction. The relation of Scherrer and von Laue for particle size was assumed,

$$b = \frac{0.9R\lambda}{L \cos \theta},$$

in which the width  $b$  in radians is related to the camera radius  $R$ , the wavelength  $\lambda$ , the crystal size  $L$ , and the Bragg angle  $\theta$ .

The variation of widening with angle when caused by variations of lattice constant from region to region was determined by taking the

<sup>1</sup> P. W. BRIDGMAN, *J. Applied Phys.*, vol. 8, p. 328, 1937.

<sup>2</sup> F. E. HAWORTH, *Phys. Rev.*, vol. 52, p. 613, 1937.

<sup>3</sup> W. A. WOOD, *Phil. Mag.* vol. 18, p. 495, 1934; *Proc. Phys. Soc. (London)*, vol. 52, p. 110, 1940.

<sup>4</sup> Some instances of preferential widening of certain lines have been reported, but the meaning of this phenomenon is obscure (see, for example, W. A. Wood, *Nature*, vol. 129, p. 760, 1932, for widening from cold work; and O. Dahl, E. Holm, and G. Masing, *Z. Metallkunde*, vol. 20, p. 431, 1928, for preferential widening of certain lines during age hardening). An amount of widening that varies continuously with angle is to be expected, however (see the discussion of Dehlinger and Kochendörfer's papers in the preceding section).

<sup>5</sup> U. DEHLINGER and A. KOCHENDÖRFER, *Z. Krist.*, vol. 101, p. 134, 1939; *Z. Metallkunde*, vol. 31, p. 231, 1939. A. KOCHENDÖRFER, *Z. Krist.*, vol. 101, 149, 1939.

logarithmic derivative of Bragg's law  $n\lambda = 2d \sin \theta$

$$\frac{\delta d}{d} = -\frac{\cos \theta}{\sin \theta} \delta \theta.$$

Since the line width  $S$  in radians is given by  $S/2 = 2R \delta \theta$  and assuming  $\delta d/d = \delta a/a$ ,

$$S = 4R \frac{\delta a}{a} \tan \theta.$$

Therefore the line widening caused by strains should be proportional to  $\tan \theta$ , and the widening from particle size should be proportional to  $\lambda \sec \theta$ . Dehlinger and Kochendörfer used this difference in angle dependence to make an estimate of the strain in cold-rolled copper as a function of the amount of rolling. The results, reproduced in Fig. 17, cannot be considered as showing more than qualitative trends, because of the assumptions involved in the calculations, but they seem to indicate a value for the strain  $\delta a/a$  that rises rapidly to a limiting value in the early stages of rolling. The cross in Fig. 17 is the value obtained from a broken surface of a tensile specimen.

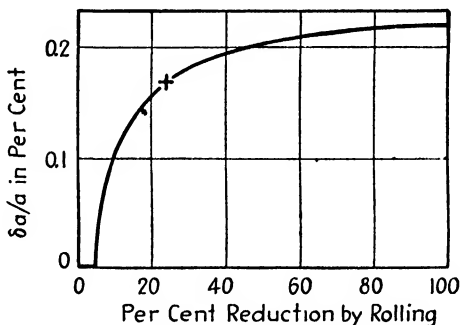


FIG. 17.—Line widening in copper, caused by cold rolling. Cross is value at broken surface of tensile specimen. (Dehlinger and Kochendörfer.)

Stickley<sup>1</sup> has conducted related experiments on brass and tungsten, seeking to differentiate strain widening from particle-size widening by plotting measured line widths against  $\tan \theta$ , as in Fig. 16, and against  $\lambda \sec \theta$  and by noting which plot most nearly approaches a straight line through the origin. The experiments were conducted using a curved crystal monochromator, a focusing camera, and careful corrections for overlapping  $K\alpha$  doublet lines and for slit width. Lines having indices  $h00$  were found to be wider than those having indices  $hhh$  when a brass sample was used, indicating anisotropy in the grains of brass. If the same average stress is assumed to be acting in the two directions  $[100]$  and  $[111]$  in the grains, and if the widening is caused by these stresses, the known anisotropy of Young's modulus in brass would account for this result. Anisotropic effects of this type are absent in tungsten, which is isotropic, and the  $\tan \theta$  plot (not the  $\lambda \sec \theta$  plot) approximates a straight line through the origin, in accordance with the strain hypothesis. How-

<sup>1</sup> E. E. STICKLEY, Doctor's dissertation, University of Pittsburgh, 1942; CHARLES S. SMITH and E. E. STICKLEY, *Phys. Rev.*, vol. 64, p. 191, 1943.

ever, Stickley adds, "It is not concluded, and indeed it can probably never be concluded, that particle size broadening is absent."

**Intensities of Diffraction Lines from Cold-worked Metals.**—The atomic scattering factor  $f$  decreases when a metal is strained by cold work. All reflections decrease in intensity, the higher order lines decreasing more than the lower orders. This was observed by Hengstenberg and Mark<sup>1</sup> some years ago, and recently Brindley and his collaborators have made a series of studies of the effect<sup>2</sup> in an attempt to determine the internal latent energy of cold work.

It is convenient to compare<sup>3</sup> the  $f$  factors from cold-worked metals with the  $f$  values from the same metals at elevated temperatures, making

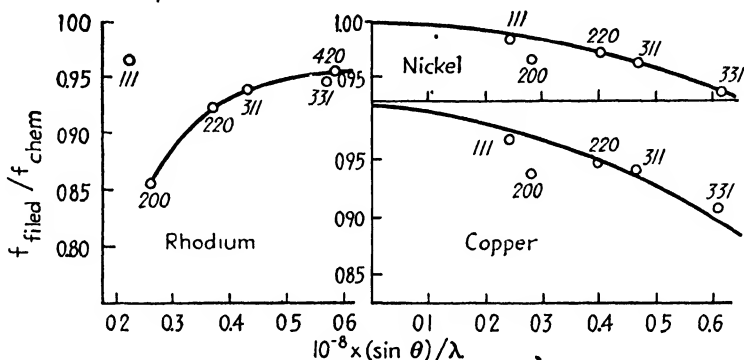


FIG. 18.—Scattering power of filed and of strain-free chemically prepared powders of rhodium, copper, and nickel. Ratio ( $f_{\text{filed}}/f_{\text{chem}}$ ) is square-root-of-intensity ratio. Curves are calculated values assuming randomly displaced atoms. Extinction corrections were applied only for rhodium. (Brindley and Spears.)

the assumption that in each case there are the same sorts of displacements of atoms from the positions of the undistorted lattice. In thermal agitation the displacements reduce the scattering power by a factor  $e^{-M}$ , and this factor has also been employed with cold work,

$$f_{cw} = f e^{-M}$$

where  $f_{cw}$  is the scattering factor for the cold-worked metal,  $f$  for the strain-free metal at the same temperature, and

$$M = \frac{8\pi^2}{3} \left( \frac{\sin \theta}{\lambda} \right)^2 \bar{u}^2$$

as for thermal agitation,  $\bar{u}^2$  being the mean square displacement of atoms from positions on the strain-free lattice.

<sup>1</sup> H. HENGSTENBERG and H. MARK, *Z. Physik*, vol. 61, p. 435, 1930; *Z. Elektrochem.*, vol. 37, p. 524, 1931.

<sup>2</sup> G. W. BRINDLEY and F. W. SPIERS, *Phil. Mag.*, vol. 20, pp. 882, 893; 1935. G. W. BRINDLEY and P. RIDLEY, *Proc. Phys. Soc. (London)*, vol. 50, p. 501, 1938; vol. 51, p. 432, 1939. G. W. BRINDLEY, *Proc. Phys. Soc. (London)*, vol. 52, p. 117, 1940.

<sup>3</sup> G. W. BRINDLEY and F. W. SPIERS, *Phil. Mag.*, vol. 20, pp. 882, 893; 1935.

Brindley and Spiers,<sup>1</sup> using this equation and the measured intensities of reflections from filed and from strain-free powders plotted in Fig. 18, obtained the values  $\sqrt{\bar{u}^2} = 0.083\text{\AA}$  and  $0.106\text{\AA}$  for filed nickel and copper, respectively, and  $0.090\text{\AA}$  for a Cu-Be alloy of 47 atomic percent beryllium, and found the variation of  $f$  vs.  $(\sin \theta)/\lambda$  in reasonable agreement with the above expressions. The calculated curves are drawn as full lines in Fig. 18.

Boas<sup>2</sup> calculated the latent energy content equivalent to this amount of average atomic displacement and obtained 7.4 cal. per g. for copper, 6.4 cal. per g. for nickel, and 3.5 cal. per g. from his measurements on gold. Haworth,<sup>3</sup> using the same displacements in a different formula, obtained 3.0 cal. per g. for copper and 3.7 cal. per g. for nickel.

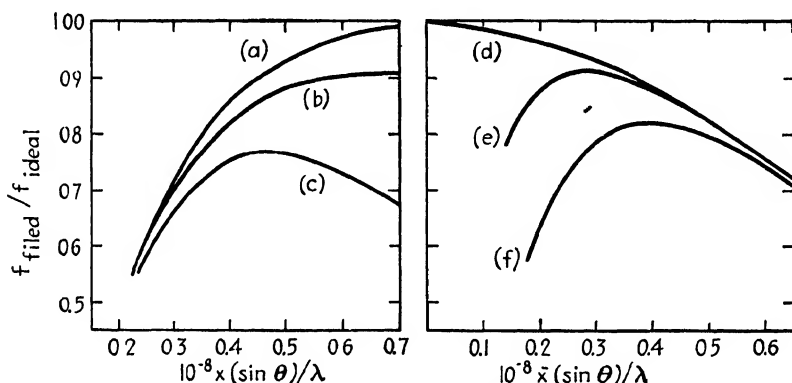


FIG. 19.—Effect of extinction and distortion on ratio of  $f$  for filed powder to  $f$  for ideal powder free from extinction and distortion. (a) Extinction alone, (b) extinction with small distortion, (c) extinction with larger distortion, (d) distortion alone, (e) distortion with small extinction, (f) distortion with larger extinction. (Brindley and Ridley.)

These values are larger than Taylor and Quinney's measured values<sup>4</sup> of the latent energy for cold-worked metals (0.5 to 1.2 cal. per g.) but are of the same order of magnitude (not an entirely different order of magnitude as in the case of line broadening).

Boas<sup>2</sup> suggests that, if atoms are displaced from true lattice points in *groups* instead of being displaced in a random fashion, smaller latent energies will be obtained; this emphasizes the fact that the results in this field are considerably dependent on the assumptions made (*cf.* Brill and Renninger's comments,<sup>5</sup> mentioned in a preceding section, page 366, on the role of ghosts in widening or in reducing the intensity of lines,

<sup>1</sup> G. W. BRINDLEY and F. W. SPIERS, *Phil. Mag.*, vol. 20, pp. 882, 893; 1935.

<sup>2</sup> W. BOAS, *Z. Krist.*, vol. 96, p. 214, 1937.

<sup>3</sup> F. E. HAWORTH, *Phys. Rev.*, vol. 52, p. 613, 1937.

<sup>4</sup> G. I. TAYLOR and H. QUINNEY, *Proc. Roy. Soc. (London)*, vol. A143, p. 307, 1934.  
H. QUINNEY and G. I. TAYLOR, vol. A163, p. 157, 1937.

<sup>5</sup> R. BRILL and M. RENNINGER, "Ergebnisse der technische Röntgenkunde," vol. VI, p. 141, Akademische Verlagsgesellschaft, m.b.H. Leipzig, 1938.

according to their proximity to the principal lines). **Extinction** is another variable that must be taken into account in interpreting the measurements, since it may be altered by cold work. Brindley and Ridley<sup>1</sup> point out that extinction plays the principal role at the small values of  $(\sin \theta)/\lambda$ , while distortion predominates at the large values, as indicated in Fig. 19. Thus the two effects should be separable, but the correction introduces additional complexity in the analysis. For cold-worked rhodium the extinction effect seems to predominate (*cf.* Figs. 18 and 19) and corresponds to a crystallite size of about  $6 \times 10^{-5}$  cm.\*

An interesting series of experiments by Fricke and his coworkers<sup>2</sup>

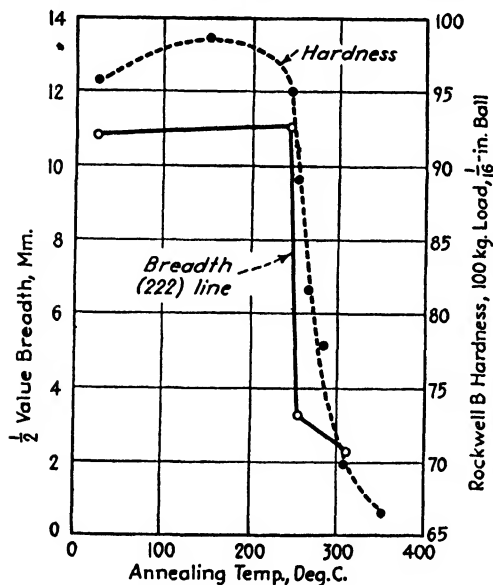


FIG. 20.—Recovery of cold-worked 70-30 brass with 1-hr. anneals. (Cold work was by forging to reduction of 85 to 90 percent.) (Wilson and Thomassen.)

determination, while for iron the figures obtained were 1.4 and 1.43, respectively.

The results in this field may be summarized by saying that the internal disturbances in cold-worked grains appear to be highly localized, extend-

<sup>1</sup> G. W. BRINDLEY and P. RIDLEY, *Proc. Phys. Soc. (London)*, vol. 51, p. 432, 1939.

\* When lattice distortion is calculated from reflected intensities, it increases through the series Rh, Ni, Cu (from the hardest to the softest), but line widths increase in the reverse order, paralleling hardness (Fig. 16).

<sup>2</sup> R. FRICKE and P. ACKERMANN, *Z. anorg. allgem. Chem.*, vol. 214, p. 177, 1933; *Z. Elektrochem.*, vol. 40, p. 630, 1934. R. FRICKE and J. LÜCKE, *Z. physik. Chem.*, vol. B23, p. 329, 1933; R. FRICKE and K. MEYRING, *Z. anorg. allgem. Chem.*, vol. 230, p. 366, 1937; R. FRICKE, *Z. Elektrochem.*, vol. 44, p. 291, 1938.

<sup>3</sup> R. FRICKE, O. LOHRMANN, and W. WOLF, *Z. physik. Chem.*, vol. B37, p. 60, 1937.

has a close connection with this problem: the energy content (heat of solution) of oxides (for example, ZnO, BeO, Fe<sub>2</sub>O<sub>3</sub>) increases when they are prepared by chemical reduction at lower and lower temperatures, and coincident with this increase in energy of the oxide powders is a greater loss in intensity of x-ray reflection. There is thus a direct correlation between the energy and the intensities of the lines. A similar correlation was found for iron reduced at different temperatures;<sup>3</sup> the excess energy of copper reduced at low temperatures over that reduced at high temperatures was 3.1 kcal. per gram atom by calorimetric measurement and 3.24 by x-ray

ing principally over regions of the order of  $10^{-7}$  or  $10^{-8}$  cm. rather than throughout a mosaic block  $10^{-4}$  cm. in diameter. They are thus similar to the distortions that are believed to surround the dislocations in the lattice; these are discussed in Chap. XVI.

**Recovery of Line Sharpness during Annealing.**—Diffraction lines from cold-worked metals return to normal sharpness during annealing. The sharpening results from the process of *recovery*, which may or may not proceed concurrently with *recrystallization* (formation and growth of visible strain-free grains).

Practical applications of line-width photographs have been made to detect incomplete or uneven stress-relief annealing. However, the test must be used with caution, for the surface layers of an object are frequently the most severely cold-worked and consequently recrystallize at temperatures lower than the bulk of the material.

As a rule, line width and hardness follow parallel curves during annealing,<sup>1</sup> just as they do during progressively increasing degrees of cold work,<sup>2</sup> but in the reverse direction. Wilson and Thomassen's<sup>3</sup> comprehensive study of line widths vs. annealing times and temperatures showed that copper, nickel, various  $\alpha$ -brasses, and several steels all lost their hardness simultaneously with their line broadening. Examples from this investigation are reproduced in Figs. 20 and 21.

Recovery of line sharpness begins in brass at temperatures below the recrystallization range<sup>4</sup> although it is not completed before the sharp diffraction spots from recrystallized grains appear in photographs. The

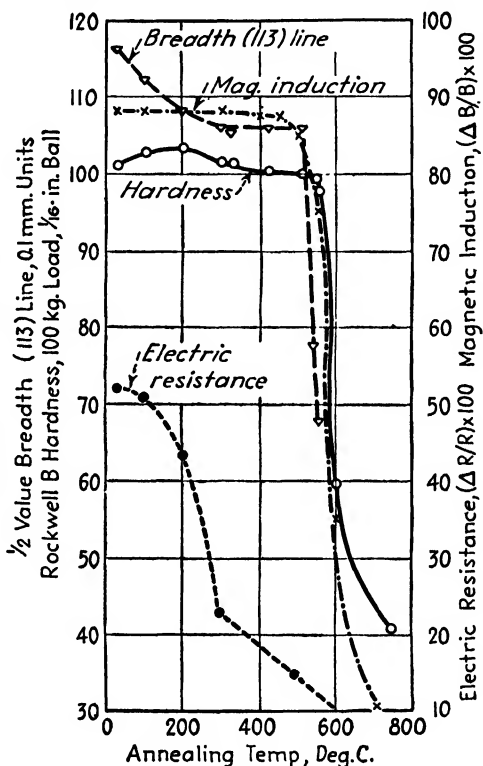


FIG. 21.—Recovery of cold-worked nickel with 1-hr. anneals (forged 75 percent). (Wilson and Thomassen.)

<sup>1</sup> W. A. WOOD, *Phil. Mag.*, vol. 19, p. 219, 1935 ( $\alpha$ -brass). J. E. WILSON and L. THOMASSEN, *Trans. A.S.M.*, vol. 22, p. 769, 1934.

<sup>2</sup> W. A. WOOD, *Phil. Mag.*, vol. 19, p. 219, 1935 ( $\alpha$ -brass); *Proc. Phys. Soc. (London)*, vol. 44, p. 67, 1932 (constantan).

<sup>3</sup> J. E. WILSON and L. THOMASSEN, *Trans. A.S.M.*, vol. 22, p. 769, 1934.

<sup>4</sup> J. E. WILSON and L. THOMASSEN, *Trans. A.S.M.*, vol. 22, p. 769, 1934. J. T. NORTON, *Trans. A.I.M.E.*, vol. 137, p. 49, 1940.

same is true of nickel<sup>1</sup> and iron.<sup>2</sup> In tungsten the lines sharpen at temperatures of 600 to 1500°C. (depending on the purity) while recrystallization begins at a higher temperature (800 to 2000°C.)—sometimes as much as 1000°C. above the recovery temperature.<sup>3</sup>

Tammann<sup>4</sup> found that in some instances different physical properties recovered at different temperatures. An example is given in Fig. 22.<sup>1</sup> Electrical resistance recovers at much lower temperatures than hardness and line width in iron and also in nickel, and yet in copper the curves are parallel.

The relative effects of time and temperature on line sharpening are seen in Fig. 23. There appears to be a close relation among hardness,

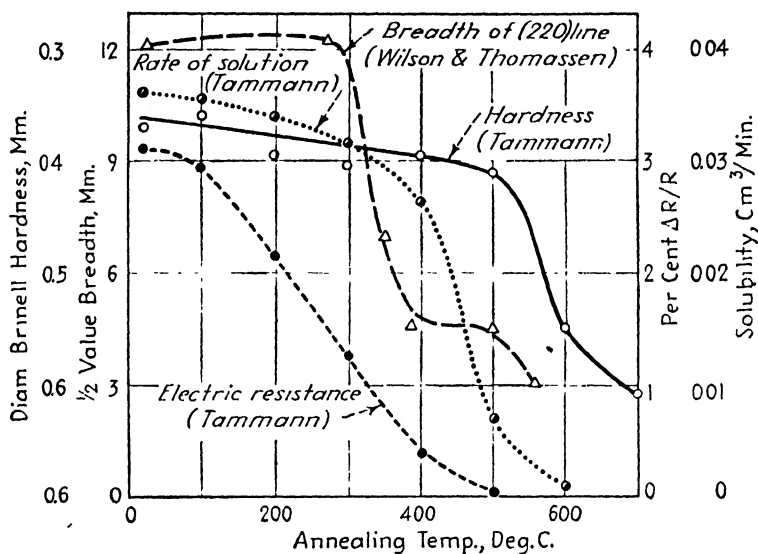


FIG. 22.—Recovery of cold-worked iron.

line width, and the tendency toward season cracking in brass (as indicated by the widely used mercurous nitrate test). It is also of interest that Wilson and Thomassen found maximum creep resistance in the same alloys that required the highest temperatures for line sharpening.

We have seen that in many cases the recovery of line sharpness is simultaneous with the recovery of hardness and the loss of the tendency to season-crack, and one is tempted to jump to the conclusion that the microscopic internal stresses that are presumably responsible for these

<sup>1</sup> J. E. WILSON and L. THOMASSEN, *Trans. A.S.M.*, vol. 22, p. 769, 1934.

<sup>2</sup> F. WEVER and B. PFARR, *Mitt. Kaiser-Wilhelm Inst. Eisenforsch. Düsseldorf*, vol. 15, p. 137, 1933. F. WEVER, *Stahl u. Eisen*, vol. 53, p. 497, 1933.

<sup>3</sup> A. E. VAN ARKEL and W. G. BURGERS, *Z. Physik*, vol. 48, p. 690, 1928. For other references see C. S. Barrett, *Metals & Alloys*, vol. 5, pp. 131, 154, 170, 196, 224, 1934.

<sup>4</sup> For a bibliography of Tammann's extensive research on this subject, see "Die Heraeus-Vacuumschmelze," pp. 86-108, Hanau, 1933.



effects and for the Bauschinger effect are the sole cause of strain hardening. However, other considerations make this conclusion unsafe. Hardness is increased when grain size is reduced, and it seems certain that the distortion and "fragmentation" of grains during cold work has the effect of reducing the effective grain size—i.e., the size of the regions through which slip progresses without encountering a boundary that acts as a barrier. It has also been pointed out that highly localized stresses which do not affect line width may nevertheless hinder plastic flow. Dislocations have a local stress field of this type. It appears, then, that several factors contribute to strain hardening and not all these produce line widening. In this way we may account for the observa-

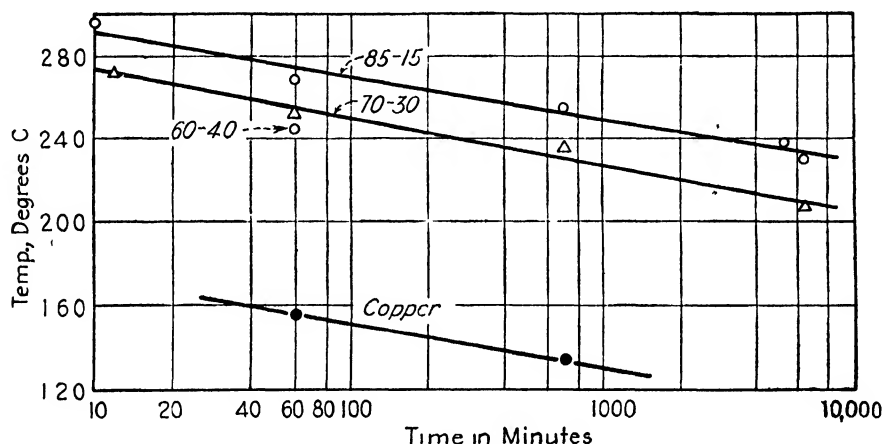


FIG. 23.—Relative effects of time and temperature of anneal for recovery of line sharpness in 60-40, 70-30, and 85-15 brass and in copper. (Wilson and Thomassen.)

tion<sup>1</sup> that in tungsten it is possible to bring about a complete recovery of line sharpness without appreciably reducing the tensile strength of the metal. Since the intensities of lines relative to the background are capable of revealing distortions more local in character than the distortions that widen lines, we might anticipate a somewhat better correlation of strain hardening with intensities than with line widths. It is uncertain whether any x-ray indication can be had of the contribution of internal boundaries to the hardness. However, we might anticipate that increasing amounts of disorganized boundary material would reduce the line intensities rather than widen the lines, unless the boundaries are so numerous that particle-size widening occurs.

**X-ray Studies of Fatigue.**—A reliable means of forestalling breakage of machines and structures from fatigue under repeated stresses would be of immense importance to engineers and metallurgists. For many years there has been a search for some nondestructive test that would reveal the extent of damage caused by repeated stresses and thus predict

<sup>1</sup> F. VON GÖLER and G. SACHS, *Z. Metallkunde*, vol. 19, p. 410, 1927.

whether or not the stresses will lead to fracture. Since x-ray methods have been most effective in revealing the internal structure of metals it is natural that they have been investigated hopefully for this purpose, and numerous tests have been reported, both here and abroad. It seems to the author that these methods must be regarded at present as unreliable for practical use; yet papers continue to appear expressing a favorable attitude toward the x-ray methods.

The publications of Gough and Wood,<sup>1</sup> for example, imply that progressive damage can be identified by x-ray diffraction patterns. Gough concludes that patterns will remain unchanged during stressing—or will change only at the first application of the load and will not alter their character after this—if stresses are within the *safe* range, whereas patterns will change progressively if stresses are employed that are unsafe and that will eventually cause fracture. Some experimenters have drawn similar conclusions<sup>2</sup> while others find no such correlation,<sup>3</sup> and it may be some years before there is full agreement on the exact value of the x-ray method in the fatigue field.

Results of tests conducted in cooperation with the Fatigue Committee of the A.S.T.M.<sup>4</sup> indicated that changes in x-ray diffraction patterns reveal cold work from fatigue, not damage. Cold work may occur in the safe range of stress as well as in the unsafe and may, in fact, be beneficial; so a test that reveals cold work obviously does not afford a direct diagnosis of ultimate failure from fatigue. The point is illustrated for 2S-O aluminum by Fig. 24, where spots that are sharp in the unstressed material (Fig. 24a) are seen to be extensively blurred by 505 million cycles in the safe range of stresses (Fig. 24b).

Gough has concluded that unsafe stressing can be detected by noticing whether diffraction spots continue to change as stressing continues. This cannot be accepted as a safe principle, for too many experiments indicate that cold work in the safe range may continue for millions of cycles. Kommers, for example, has reported<sup>5</sup> experiments in which cold work at stresses below the endurance limit must have continued for 15 million cycles or more, since there was an increase in the endurance limit through-

<sup>1</sup> H. J. GOUGH and W. A. WOOD, A New Attack upon the Problem of Fatigue of Metals, Using X-ray Methods of Precision, *Proc. Roy. Soc. (London)*, vol. A154, pp. 510–539, 1936; summarized in lecture to Royal Aeronautical Society, Apr. 20, 1936, by Gough and Wood, and in *Metal Progress*, vol. 30, p. 91, July, 1936.

<sup>2</sup> E. B. MARTIN, *Arch. Eisenhüttenw.*, vol. 10, p. 415, 1937. F. WEVER and H. MÖLLER, *Naturwissenschaften*, vol. 25, p. 449, 1937.

<sup>3</sup> C. S. BARRETT, *Metals & Alloys*, vol. 8, p. 13, January, 1937; *Metal Progress*, vol. 32, p. 677, 1937; *Trans. A.S.M.*, vol. 25, p. 1115, 1937. J. A. KIES and G. W. QUICK, N.A.C.A. Rept. 659, 1939.

<sup>4</sup> C. S. BARRETT, *Metals & Alloys*, vol. 8, p. 13, January, 1937.

<sup>5</sup> J. B. KOMMERS, *Proc. A.S.T.M.*, vol. 30, pt. 2, p. 368, 1930.

out this period. A number of investigators have studied also the temperature of fatigue specimens during stressing and have found heating, which is evidence for plastic flow; this is very marked at the beginning of the stressing and continues in lesser degree for many thousands of cycles. X-ray experiments of Wever and Möller indicate that flow may occur irregularly, with a sudden local deformation appearing after some millions of cycles of stressing during which flow is negligible. Spencer and Marshall<sup>1</sup> find that in 17S-T aluminum there is rarely any change in the sharpness of diffracted spots until the very last stages of fatigue;

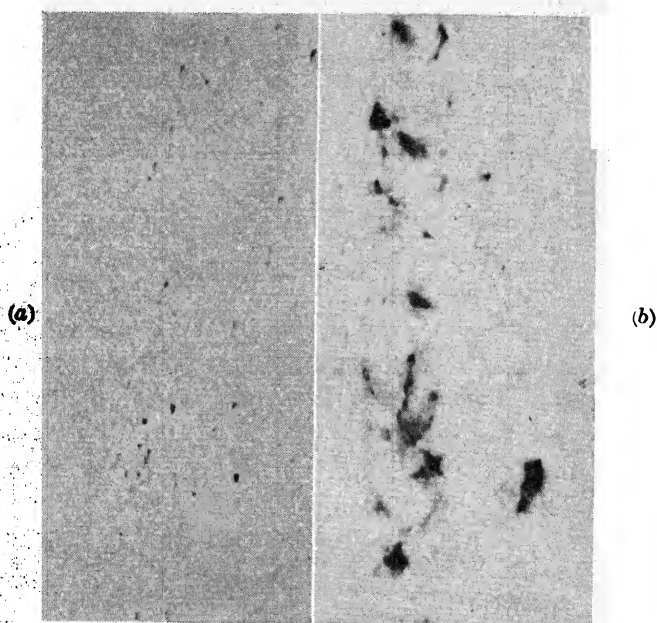


FIG. 24.—Spot sharpness in 2S-O aluminum after specimen had withstood 505,000,000 cycles in fatigue stressing. Made with camera of Fig. 12. (a) Unstressed area, (b) area stressed at 4000 psi. (below the endurance limit).

in fact, they usually find blurring of spots only in specimens that have already been broken, where the distortion could have occurred at the time of breaking. Their results, therefore, seem not at variance with the conclusions of Kies and Quick<sup>2</sup> and of the author<sup>3</sup> that the progress of fatigue damage does not correlate with blurring of spots.

Apparently the amount of blurring in x-ray patterns cannot serve to indicate whether a specimen is being stressed above or below the fatigue limit. For some metals and for some types of stressing there is very little alteration of the pattern caused by stressing below the endurance

<sup>1</sup> R. G. SPENCER and J. W. MARSHALL, *J. Applied Phys.*, vol. 12, p. 191, 1941.

<sup>2</sup> J. A. KIES and G. W. QUICK, N.A.C.A. Rept. 659, 1939.

<sup>3</sup> C. S. BARRETT, *Trans. A.S.M.*, vol. 25, p. 1115, 1937; *Metals & Alloys*, vol. 8, p. 13, January, 1937; *Metal Progress*, vol. 32, p. 677, 1937.

limit, even with the most prolonged tests, and yet other specimens will show drastic changes. Above the fatigue limit, stressing may or may not blur the diffraction spots prior to fracture; in fact, different areas on a specimen at the same stress level may show different behavior. This situation must be expected if x-ray patterns reveal cold work, for it is generally recognized that pronounced cold work sometimes occurs below the endurance limit, while under other conditions fatigue fracture may occur with little or no plastic flow. Nor is the amount of plastic flow necessarily uniform over the surface of the metal; those spots where cracks are eventually to occur are doubtless the most highly deformed spots on the surface and probably yield quite different diffraction patterns from neighboring areas where there is less flow. Unfortunately, in most of the practical cases and in many laboratory experiments the exact place where a crack is about to form is unknown, and perhaps only a few grains are so damaged that they start cracks. The experimenter therefore lacks information that is vital in the interpretation of his patterns, for he does not know whether his x-ray beam has happened to fall on a spot of maximum distortion or not.

In general, there is no assurance that a dangerous state of stressing will be detected, or that what appears dangerous is actually so. If any circumstances exist in which x-ray tests can be relied upon in practice, they can be discovered only by exhaustive laboratory tests using materials, stress distributions, and numbers of cycles that will actually be encountered.<sup>1</sup> At the present time, no conditions have been found for which x-ray tests or any other nondestructive test<sup>2</sup> has proved a reliable predictor of fatigue failure.

<sup>1</sup> The use of brittle lacquers, such as Stress Coat, is sometimes useful in locating the portions of an object where a fatigue crack is most likely to start.

<sup>2</sup> "Prevention of the Failure of Metals under Repeated Stress," Battelle Memorial Institute Staff, Wiley, New York, 1941.

## CHAPTER XVIII

### PREFERRED ORIENTATIONS RESULTING FROM COLD WORK

When a polycrystalline metal is plastically deformed, the lattice orientation in individual grains is altered toward a preferred orientation in which certain lattice directions are aligned with the principal directions of flow in the metal. The progress of reorientation is gradual; it is usually noticed on x-ray films only after the cross section of the metal has been reduced by a third or a half but is not completed until the metal has received reductions of 90 percent or more. The nature of the preferred orientation, or "deformation texture," that is finally reached and the manner in which it is reached are characteristic of the metal and of the nature of the flow (the magnitude of the three principal strains).

Much attention has been given to the subject because of its relation to the properties of commercial products. A fine-grained metal in which the grains are oriented at random will possess identical properties in all directions (provided that there are no elongated inclusions, segregations, or boundaries), but a metal with a preferred orientation of grains will have directional properties, "anisotropy," which may be troublesome, as, for example, in the deep drawing of sheet material. Orientations that are generated by the forming process are not returned to a random state by the recrystallization and grain growth accompanying subsequent annealing, as a rule, but are altered to new orientations known as "recrystallization textures," which are treated in the following chapter. It is usually necessary to maintain careful control of both rolling and annealing operations in order to produce a sheet that flows uniformly in all directions during subsequent deep drawing. Preferred orientations are also of prime importance in the manufacture of steel for electrical instruments, for magnetic anisotropy may be very desirable in some applications and a serious disadvantage in others. Anisotropy is discussed in Chap. XXI.

The first part of this chapter summarizes the deformation textures produced by wire drawing, swaging, extrusion, and compression—*i.e.*, by uniaxial strains—and discusses the theories that have been advanced to account for them. The second part deals with the textures produced by rolling and related forming processes.

The texture of a wire is frequently described as a "fiber texture" because it resembles the arrangement in natural fibrous materials. In the ideal case it consists simply of orientations having a definite crystallo-

graphic direction parallel to the wire axis. The texture is symmetrical around the wire axis, which is known as the "fiber axis." Deviations from an ideal texture are common and may have the nature of (1) a scatter about the ideal position or a random orientation superimposed upon the ideal texture; (2) a "double fiber texture," in which two different crystal directions are found in the axial position; and (3) a structure in which surface layers are disturbed by friction or other external factors.

**Textures of Polycrystalline Wires.**—In **face-centered cubic (f.c.c.) metals** the wire texture is usually a double fiber texture with [111] and [100] parallel to the axis; *i.e.*, the crystallites have either [111] or [100] parallel to the axis of the wire and have random orientations around the axis. The percentages of crystals in these two positions differ from metal to metal, as shown by the measurements of Schmid and Wassermann,<sup>1</sup> summarized in Table XXI. Lead resembles aluminum,

TABLE XXI

Metal	Percentage of crystals	
	With [100] parallel to the wire axis	With [111] parallel to the wire axis
Aluminum	0	100
Copper	10	60
Gold	50	50
Silver	75	25

with a single [111] texture,<sup>2</sup> while nickel has a double texture resembling copper.<sup>3</sup> Brass containing more than 10 percent zinc resembles silver, as does also bronze containing 5 percent tin and copper containing 30 percent silver.<sup>4</sup>

**Body-centered cubic (b.c.c.) metals** have a simple [110] texture. This was discovered for iron by Ettish, Polanyi, and Weissenberg<sup>3</sup> and has been confirmed many times. There appear to be no minor components in this texture, and it is not altered by elements in solid solution, such as vanadium and silicon.<sup>5</sup> Tungsten and molybdenum also are known to have a simple [110] texture.<sup>6</sup>

<sup>1</sup> E. SCHMID and G. WASSERMANN, *Z. Physik*, vol. 42, p. 779, 1927.

<sup>2</sup> W. HOFMANN, *Z. Metallkunde*, vol. 29, p. 266, 1937.

<sup>3</sup> M. ETTISCH, M. POLANYI, and K. WEISSENBERG, *Z. Physik*, vol. 7, p. 181, 1921, *Z. physik. Chem.*, vol. A99, p. 332, 1921.

<sup>4</sup> G. v. GOLER and G. SACHS, *Z. Physik*, vol. 41, pp. 873, 889, 1927.

<sup>5</sup> C. S. BARRETT and L. H. LEVENSON, *Trans. A.I.M.E.*, vol. 135, p. 327, 1939.

<sup>6</sup> M. ETTISCH, M. POLANYI, and K. WEISSENBERG, *Z. Physik*, vol. 7, p. 181, 1921; *Z. physik. Chem.*, vol. A99, p. 332, 1921. H. C. BURGER, *Physik. Z.*, vol. 23, p. 14, 1922. Z. JEFFRIES, *Trans. A.I.M.E.*, vol. 70, p. 303, 1924. H. B. DeVORE and W.

**Hexagonal metals** have wire textures that are less easily interpreted. Magnesium wire was first thought to have all directions in the basal plane parallel to the wire axis (owing to a scatter from the ideal orientation).<sup>1</sup> However, later work on drawn and on extruded Dowmetal (magnesium alloyed with aluminum, manganese, and zinc) indicates that only one set of directions in the basal plane has this position,<sup>2</sup> viz., the direction [210], in wire that has been formed at low temperatures.<sup>3</sup> At a working temperature of 450°C. the fiber axis shifts to [110]. The temperature at which the slip mechanism changes to (101) planes and [110] close-packed directions is 225° and does not correlate with this change in texture or explain it. Morell and Hanawalt suggest that duplex slip in [110] directions seems required to explain the low-temperature texture, while single slip suffices to explain the high-temperature texture. Zinc wires have the hexagonal axis about 70° from the wire axis with uniform distribution about the wire axis. This texture is obtained only after severe drawing; smaller reductions give a texture in which the hexagonal axis lies along the wire. Zirconium has a texture like magnesium, with the [210] direction in the basal plane parallel to the wire axis and with close-packed rows of atoms 30° to the axis.<sup>4</sup>

Twinning is responsible for producing those hexagonal textures in which the basal plane is not parallel to the wire axis. Studies of single crystals have shown that twinning becomes frequent, particularly in zinc, when the basal plane rotates into a position nearly parallel to the wire axis, and as a result the basal plane is suddenly reoriented to a position far removed from the original (a shift of 85°55' in zinc).

**Extruded rods** usually have the same textures as drawn wires. This is true of magnesium<sup>5</sup> and cubic metals<sup>6</sup> but is not true of zinc. Extruded rods of alloyed zinc (10% Al, 2.0% Cu, 0.03% Mg) have a texture with

---

P. DAVEY, *Phys. Rev.*, vol. 31, p. 160, 1928. W. G. BURGERS, *Z. Physik*, vol. 58, p. 11, 1929. T. FUJIWARA and Y. SEIKI, *Hiroshima J. Sci.*, vol. 6, p. 307, 1936 (cf. *Met. Abstracts*, vol. 3, p. 664, 1936). T. FUJIWARA, *Proc. World Eng. Congr., Tokyo*, pt. 4, vol. 36, p. 171, 1931. H. C. BURGER, *Physica*, vol. 1, p. 214, 1921.

<sup>1</sup> E. SCHMID and G. WASSERMANN, *Naturwissenschaften*, vol. 17, p. 312, 1929.

<sup>2</sup> L. G. MORELL and J. D. HANAWALT, *J. Applied Phys.*, vol. 3, p. 161, 1932.

<sup>3</sup> This direction is expressed in the three-indices system and is equivalent to [1010] in the four-indices notation. The indices mean a diagonal axis of type II, a direction midway between two close-packed rows of atoms in the basal plane. The close-packed rows are directions of the form [110] = [100] = [2 $\bar{1}$ 10].

<sup>4</sup> W. G. BURGERS, J. D. FAST, and F. M. JACOBS, *Z. Metallkunde*, vol. 29, p. 410, 1937.

<sup>5</sup> L. G. MORELL and J. D. HANAWALT, *J. Applied Phys.*, vol. 3, p. 161, 1932. E. SCHIEBOLD and G. SIEBEL, *Z. Physik*, vol. 69, p. 458, 1931.

<sup>6</sup> W. HOFMANN, *Naturwissenschaften*, vol. 24, p. 507, 1936; *Z. Metallkunde*, vol. 29, p. 266, 1937. G. WASSERMANN, *Z. Metallkunde*, vol. 30, Vorträge der Hauptverslg., p. 53, 1938.

the basal plane parallel to the axis of extrusion; extruded pure zinc has basal planes in both the parallel and perpendicular positions.<sup>1</sup> Drawing through a die, after extrusion, alters this texture by twinning and rotation until the normal drawing texture is obtained, with reductions of 50 per cent or more.

Wires formed by **rolling** and by **swaging** have the same textures at their centers as those formed by drawing through a die.<sup>2</sup> The **outer layers**, however, with almost any type of forming operation, contain orientations not found in the center.<sup>3</sup> The scatter about the mean orientation is greatest in the outer layers and decreases as successive layers are etched away. The metal at the center of a thin wire has a larger scatter than that at the center of a thick one. Schmid and Wassermann have shown that in hard-drawn copper wire the fiber axis is inclined to the axis of the wire in these outer layers in the manner

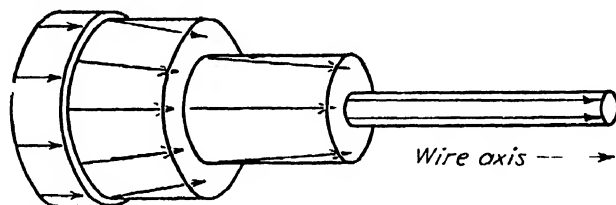


FIG. 1.—Zonal texture of drawn wires of cubic metals. Arrows show directions of fiber axes. (Schmid and Wassermann.)

indicated by the arrows in Fig. 1. The directions of the arrows in the different concentric zones of this figure indicate the directions of the fiber axes of the crystallites (the [111] and [100] directions in copper, for instance). The angle of inclination reaches 8 to 10° in some cubic metals. The length of the arrows indicates the sharpness of the orientation in each zone. Their conical arrangement has led some to use the term "conical fiber texture." This zonal structure originates in the conical (or irregular) flow of metal in the forming process and is therefore altered to some extent by variables in the forming process such as unidirectional vs. forward-and-backward drawing, die design, drawing vs. rolling, etc.<sup>4</sup>

<sup>1</sup> F. WOLBANK, *Z. Metallkunde*, vol. 31, p. 249, 1939.

<sup>2</sup> J. T. NORTON and R. E. HILLER, *Trans. A.I.M.E.*, vol. 99, p. 190, 1932. G. V. VARGHA and G. WASSERMANN, *Z. Metallkunde*, vol. 25, p. 310, 1933. J. THEWLIS, *Phil. Mag.*, vol. 10, p. 953, 1930. C. S. BARRETT and L. H. LEVENSON, *Trans. A.I.M.E.*, vol. 135, p. 327, 1939.

<sup>3</sup> E. SCHMID and G. WASSERMANN, *Z. Metallkunde*, vol. 19, p. 325, 1927; *Z. Physik*, vol. 42, p. 779, 1927. R. W. DRIER and C. T. EDDY, *Trans. A.I.M.E.*, vol. 89, p. 140, 1930. W. A. WOOD, *Phil. Mag.*, vol. 11, p. 610, 1931. G. GREENWOOD, *Z. Krist.*, vol. 78, p. 242, 1931; vol. 72, p. 309, 1929.

<sup>4</sup> E. SCHMID and G. WASSERMANN, *Z. Metallkunde*, vol. 19, p. 325, 1927. T. FUJIWARA, *Mem. Coll. Sci., Kyoto Imp. Univ.*, vol. A15, p. 35, 1932. G. WASSERMANN, "Texturen metallischer Werkstoffe," Springer, Berlin, 1939; *Z. Metallkunde*, vol. 30, Vorträge der Hauptverslg., p. 53, 1938.



With hexagonal metals, also, there is a zonal structure. Magnesium and zirconium wires, for instance, have the hexagonal axis  $90^\circ$  from the wire axis only in the core; in the outer zones this angle is about  $75^\circ$ .<sup>1</sup>

**Textures of Eutectic Wires.**—When the two phases of a binary eutectic are both deformed about equally by the wire-drawing operation, each phase takes up the texture it would exhibit in a single-phase wire. This is the case in Ag-Cu (72 per cent Ag) and Cd-Zn (83 percent Cd).<sup>2</sup> On the other hand, if one phase is practically undeformed during drawing it disturbs the flow in the other and distorts the texture, or it may even produce a random one, as in Al-Si alloys (12 percent silicon).<sup>3</sup>

**Compression Textures.**—**Face-centered cubic metals** after uniaxial compression have a fiber texture that is most simply described as [110] texture, *i.e.*, a face diagonal is parallel to the axis of compression and normal to the plane of compression.<sup>4</sup> However, this description is only a first approximation to a rather complex orientation; in the case of aluminum, half the crystallites are more than  $10^\circ$  from this orientation, regardless of the amount of compression.<sup>5</sup> Although there is a marked concentration near this [110] orientation, all possible orientations are found except those having [111] within about  $20^\circ$  of the compression axis. Crystallites in any one of these secondary orientations are less numerous than those near the [110] position, and only a very small number are found with [100] within  $15^\circ$  of the compression axis. The range of orientations found can be presented best on a unit triangle of a standard stereographic projection, as in Fig. 2. Each point on this plot shows the orientation of the compression axis in an area about 1 mm. in diameter on an inner surface of a compression block. The orientations were determined by an optical goniometer with a compression of 84 percent. The distribution determined by x-rays after "compression rolling"—rolling with many passes, each pass in a different direction—is shown in Fig. 3 and illustrates again the absence of orientations around [111], the near absence around [100], the concentration around [110], and the spread from [110] to [311]. It is concluded that the wide scatter

<sup>1</sup> E. SCHMID and G. WASSERMANN, *Naturwissenschaften*, vol. 17, p. 312, 1929. W. G. BURGERS and F. M. JACOBS, *Metallwirtschaft*, vol. 11, p. 285, 1935. E. SCHIEBOLD and G. SIEBEL, *Z. Physik*, vol. 69, p. 458, 1931.

<sup>2</sup> G. WASSERMANN, "Texturen metallischer Werkstoffe," p. 71, Springer, Berlin, 1939.

<sup>3</sup> E. SCHMID and G. WASSERMANN, *Z. tech. Physik*, vol. 9, p. 106, 1928.

<sup>4</sup> A. ONO, *Mem. Coll. Eng. Kyushu Imp. Univ.*, vol. 3, p. 195, 1925. G. SACHS and E. SCHIEBOLD, *Z. Ver. deut. Ing.*, vol. 69, pp. 1557, 1601, 1925; *Naturwissenschaften*, vol. 13, p. 964, 1925. F. WEVER, *Z. tech. Physik*, vol. 8, p. 404, 1927. G. I. TAYLOR, *Trans. Faraday Soc.*, vol. 24, p. 121, 1928. W. G. BURGERS and P. C. LOUWERSE, *Z. Physik*, vol. 67, p. 605, 1931.

<sup>5</sup> C. S. BARRETT and L. H. LEVENSON, *Trans. A.I.M.E.*, vol. 137, p. 112, 1940.

would exist with any amount of reduction, for it was found after 99.9 percent reduction nearly as in Fig. 3.

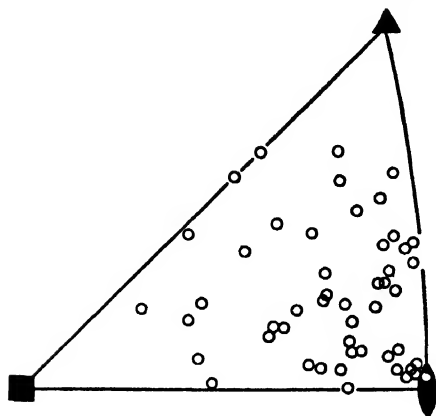


FIG. 2.

FIG. 2.—Orientations on inner faces of aluminum blocks after 84 percent compression. Optical determination, the orientations of the compression axis of randomly chosen areas, about 1 mm. in diameter, are indicated by small circles in the standard stereographic projection triangle bounded by the directions  $\blacksquare$  [001],  $\blacktriangle$  [111], and  $\bullet$  [011]. Note absence around [100] and [111] and wide, unsymmetrical scatter around [110].

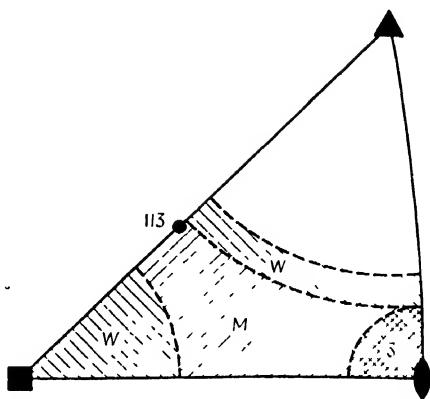


FIG. 3

FIG. 3.—Orientations in aluminum compressed 98 percent by compression rolling. Shaded areas on the projection indicate concentrations of orientations, deduced from x-ray line intensities (*S*, strong; *M*, medium; *W*, weak). Copper and nickel give similar plots.

The compression textures of nickel and copper are almost identical with the texture shown in Fig. 3, according to experiments by E. L.

Layland and the author,<sup>1</sup> but the texture of 70–30 brass is different, as shown in Fig. 4. No crystallites of  $\alpha$ -brass have [100] directions near the axis of compression, while a fair number have [111] in this region; the concentration around the [110] position is still predominant, and the range from [110] to [311] still persists.<sup>2</sup>

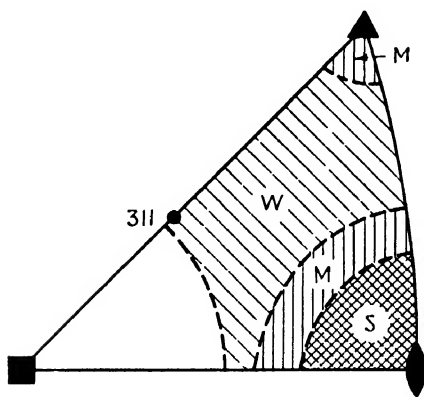


FIG. 4.—Orientations in 70–30 brass compressed 97 percent by compression rolling (x-ray results).

The weaker [100] component of this texture was not observed by some experimenters but is now well established (see Fig. 5, in which the spot at the top center is

<sup>1</sup> E. L. LAYLAND, unpublished senior thesis at Carnegie Institute of Technology, 1941.

<sup>2</sup> Unpublished results by the author.

caused by this component).<sup>1</sup> Experiments of J. J. Heger and the author<sup>2</sup> show that an Fe-Si alloy containing 4.6 percent silicon also has the double texture.

The hexagonal metal magnesium has a compression texture with the hexagonal axis parallel to the axis of compression.<sup>3</sup> The magnesium alloy Dowmetal has the same orientation after forging, although modifications can be produced.<sup>4</sup>

**Theories of Tension and Compression Textures.**—It is not possible to account for the textures of polycrystalline metals by assuming that each grain rotates in the way a single crystal does. Not merely one or two, but several, sets of slip planes are active in each grain, because the grains are required to fit together without voids after the deformation. The more successful theories of deformation textures have differed chiefly in the number of slip systems that are assumed to operate. Boas and Schmid<sup>5</sup> proposed that the three most highly stressed slip systems are active and the deformation texture is composed of orientations which are stable under the action of slip of this kind. That is, the rotations due to slip on these systems cancel one another when the stable position is reached. Boas and Schmid were able in this way to account for both the [100] and the [111] components of the tension texture and for the [110] compression texture of f.c.c. metals.

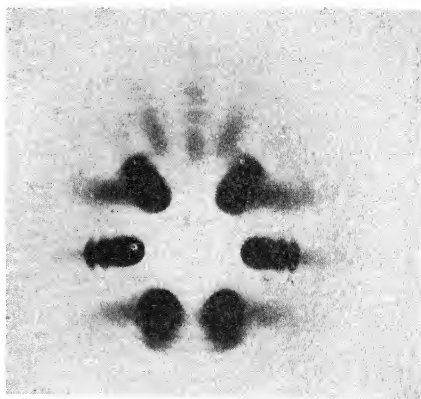


FIG. 5.—Diffraction pattern for iron after compression. X-ray beam directed at  $14^\circ$  to compressed sheet to show reflection from (100) planes lying in compression plane, which give spot at top center. Other prominent spots are from [111] texture.

When applied to b.c.c. metals Boas and Schmid's theory predicts a [111] compression texture when (110) planes are the only slip planes, and a double texture, [111] + [100], when additional slip planes of the type (112) are assumed. The same double texture would be expected on the basis of this theory if the slip systems are [110] + [112] + [123].\*

<sup>1</sup> A. ONO, *Mem. Coll. Eng., Kyushu Imp. Univ.*, vol. 3, p. 267, 1925. C. S. BARRETT, *Trans. A.I.M.E.*, vol. 135, p. 296, 1939.

<sup>2</sup> J. J. HEGER, unpublished senior thesis, Carnegie Institute of Technology, 1941.

<sup>3</sup> S. TSUBOI, *Mem. Coll. Sci., Kyoto Imp. Univ.*, vol. A11, p. 375, 1928.

<sup>4</sup> L. G. MORELL and J. D. HANAWALT, *J. Applied Phys.*, vol. 3, p. 161, 1932. J. T. NORTON, "Symposium on Radiography and X-ray Diffraction," p. 302, A.S.T.M., Philadelphia, Pa., 1936.

<sup>5</sup> W. BOAS and E. SCHMID, *Z. tech. Physik*, vol. 12, p. 71, 1931.

\* C. S. BARRETT, *Trans. A.I.M.E.*, vol. 135, p. 296, 1939.

The tension texture is predicted to be  $[110]$ . The theory is thus in satisfactory agreement with the principal textures that are observed but does not agree with some of the minor textures. For example, the compression texture of an Fe-Si alloy (4.6 percent silicon), in which slip is found to be only on  $(110)$  planes, has  $[111] + [100]$  textures while only  $[111]$  is predicted.<sup>1</sup> Face-centered cubic metals have many crystallites in minor orientations not accounted for by the theory. Pickus and Mathewson<sup>2</sup> suggested that three or more slip systems operate leading to end positions in which the functioning slip directions are symmetrically disposed about the direction of flow so that the lattice rotations cancel one another and the resolved shear stresses are equal on each plane. The probability of occurrence of each of the end positions is assumed to be proportional to the cosine of the angle between the direction of flow and the active slip directions—a factor suggested in order to take account of the component of the movement on slip planes that is effective in producing the required flow. It has been suggested that a minimum of two slip systems contributes to the dynamic equilibrium of deformation textures,<sup>3</sup> that all systems do,<sup>4</sup> and that an indefinite number do,<sup>5</sup> but theories along these lines have not been fully developed.

G. I. Taylor has worked out a theory of deformation textures that has a more rigorous basis than any previous one.<sup>6</sup> To permit any desired change of shape—such as will let grains fit together after deformation and will produce the same change of shape in the grains as in the aggregate as a whole—there must be at least five slip systems operating.<sup>7</sup> The “principle of least work” governs the choice of systems that must operate. This principle states that the *minimum* number will function which can produce the required change in shape. This number is five, except for special orientations. Furthermore, that group of five will be chosen for which the total work of deformation will be less than for any other group. Taylor computed the work that would be required on every group of five slip systems that could be chosen from the 12 possible systems in aluminum. There are 792 groups to be computed or ruled out by symmetry considerations of one kind or another, and Taylor considered all of these for each of 44 different orientations of aluminum single crystals. Having computed what groups of systems would operate at each orientation, he predicted in what direction the

<sup>1</sup> J. J. HEGER, unpublished senior thesis, Carnegie Institute of Technology, 1941.

<sup>2</sup> M. R. PICKUS and C. H. MATHEWSON, *J. Inst. Metals*, vol. 5, p. 555, 1938.

<sup>3</sup> F. WEVER, *Trans. A.I.M.E.*, vol. 93, p. 51, 1931.

<sup>4</sup> M. POLANYI, *Z. Physik*, vol. 17, p. 42, 1923.

<sup>5</sup> C. S. BARRETT, *Trans. A.I.M.E.*, vol. 135, p. 296, 1939.

<sup>6</sup> G. I. TAYLOR, *J. Inst. Metals*, vol. 62, p. 307, 1938; “Stephen Timoshenko 60th Anniversary Volume,” p. 218, Macmillan, New York, 1938

<sup>7</sup> R. v. MISES, *Z. angew. Math. Mech.*, vol. 8, p. 161, 1928

lattice would rotate. Some ambiguity arose when two groups gave the same minimum values of total work; a grain having an orientation in which this occurs will have a tendency to rotate in two or more directions. Taylor remarked that in this case the direction of rotation can be a result of any combination of the two groups and thus can be any direction within a considerable range.

Taylor's computed rotations for grains of f.c.c. metals during compression are plotted in Fig. 6.<sup>1</sup> The rotation of the axis of compression is indicated by vectors originating at the orientation considered and extending in the direction of the calculated rotation. The length of the arrows corresponds to the rotation that should accompany a compression of 2.37 percent. Double arrows indicate equally favored sets of five slip systems; any direction that lies between them could equally well occur. The predicted rotations of Taylor have been tested<sup>2</sup> in individual grains of aluminum with an optical goniometer; the results are

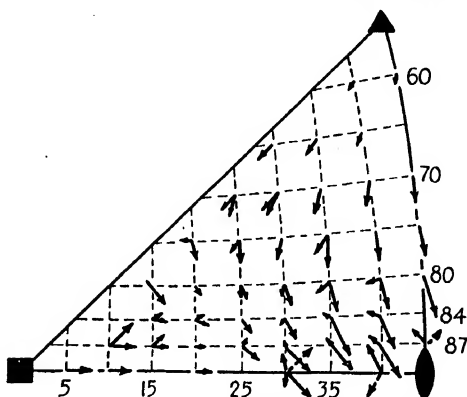


FIG. 6.—Taylor's calculated rotations of crystal axes in grains of a face-centered cubic polycrystalline aggregate during compression of 2.37 percent.

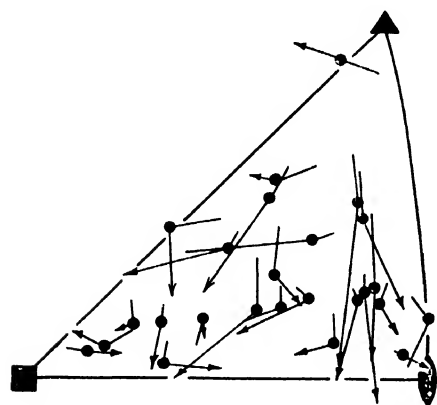


FIG. 7.—Observed rotations of crystal axes in grains of aluminum during compression. Arrows connect initial orientations with those after 11 percent (dots) and 31 percent (arrow heads) compression.

plotted in Fig. 7. In this figure the tails of the arrows are the initial orientations, the dots on the arrows are the orientations after 11 percent compression, and the heads of the arrows those after 31 percent compression. When Figs. 6 and 7 are compared, it is found that about half the grains rotate as predicted by the theory, about a third do not, and the rest are uncertain.

It is possible to explain the discrepancies between Figs. 6 and 7 by considering that there are nonuniform constraints on all sides of each grain affecting its strain and resulting in an irregular strain throughout the

material. That this occurs cannot be questioned, for it is the origin

<sup>1</sup> This figure is derived from the published chart that applies to tension, which is reproduced in Fig. 9.

<sup>2</sup> C. S. BARRETT and L. H. LEVENSON, *Trans. A.I.M.E.*, vol. 137, p. 112, 1940.

of the "orange-peel" surface sometimes encountered in deep-drawing operations, and it can readily be seen if a pair of polycrystalline blocks are placed together and compressed.

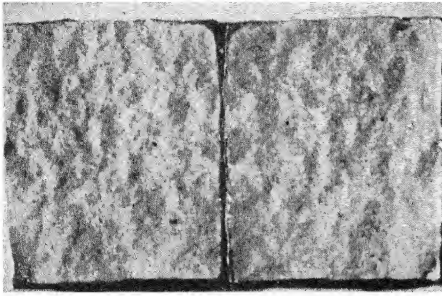


FIG. 8.—Polycrystalline blocks of aluminum with coarse grains compressed 22 percent. Rumpled surfaces show inhomogeneity of the deformation.

After deformation the inner surfaces are roughened (Fig. 8), clearly showing that each grain deforms in a manner influenced by the flow of its neighbors and not in the simple homogeneous manner that can be computed from the change of shape of the blocks. Consequently the rotation in an individual grain is not solely a function of the orientation of the grain.

The theoretical predictions, on the other hand, were based on the assumption that every grain changes its shape exactly as does the whole. If one considers Fig. 6 as

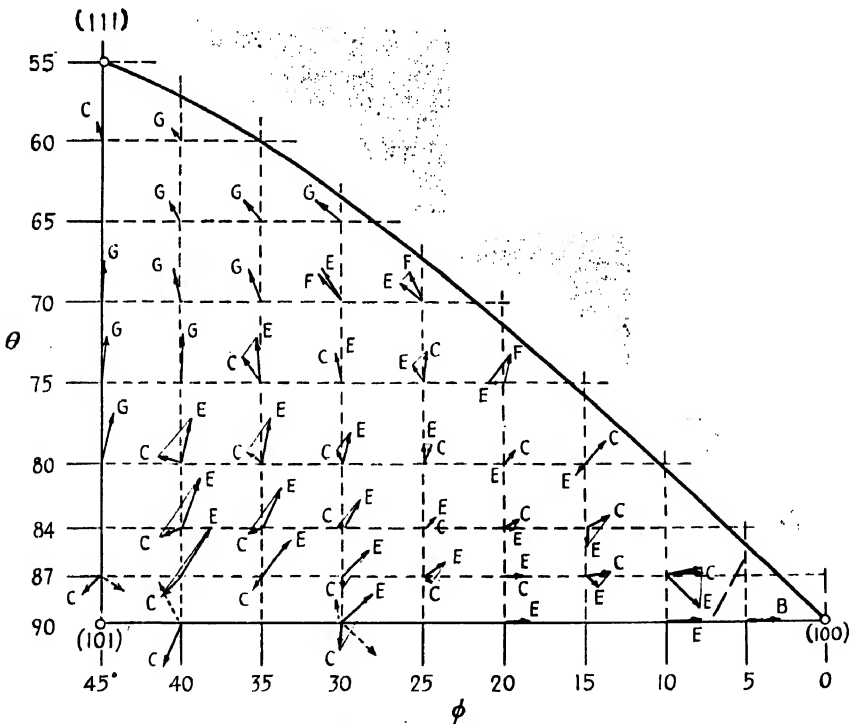


FIG. 9.—Taylor's calculated rotations for face-centered cubic polycrystalline grains during elongation of 2.37 percent.  $\theta$  and  $\phi$  are angles of the specimen axes from [010] and [100] respectively.

merely indicating the general trends of lattice rotations, it is seen that the trends are downward and to the right, in qualitative agree-

ment with the observed rotations. This accounts for the observed compression texture,  $[110]$ . Furthermore, if one notes the regions in which the direction of rotation is uncertain, it will be seen that these correspond to the lower intensity regions of the pole figure (Fig. 3).

The corresponding plot for tensional deformation is reproduced in Fig. 9. The arrows here are the reverse of those for the compression case, and their trend predicts a tension texture with  $[111]$  and  $[100]$  components, in agreement with experimental data.

Unfortunately, Taylor's mathematical solution of deformation textures is highly complex and unwieldy. To apply it to iron, which has slip on 48 slip systems, it would be necessary to consider all ways of choosing 5 from the 48, and there are no less than 1,712,304 ways of doing this. Even if considerations of symmetry and geometry should

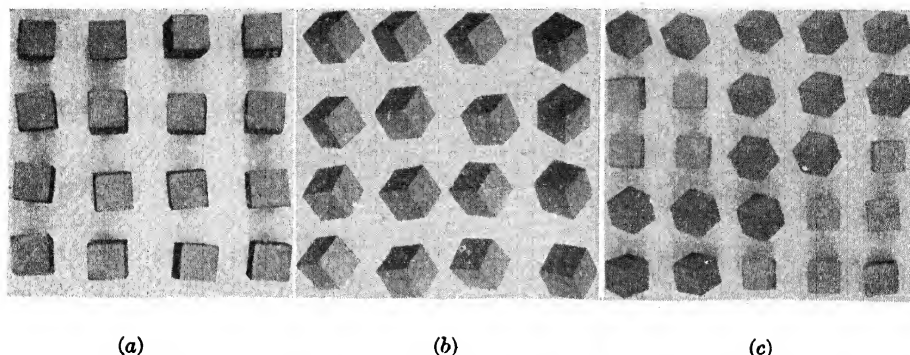


FIG. 10.—Models of orientations assumed by grains of iron after compression, viewed from a point on the axis of compression. (a)  $[100]$  texture, (b)  $[111]$  texture, (c) deformation bands,  $[100]$  and  $[111]$ .

reduce the number of calculations that must be made to less than one-thirtieth of this number, as the f.c.c. problem, the problem is still prohibitive in its rigorous form.<sup>1</sup> Neither Taylor's theory nor the ones that preceded it predicted deformation bands and the role they play in deformation textures. No theory has yet been advanced to account for the variation in tension textures with the different f.c.c. metals.

**Deformation Bands in the Compression of Iron.**—A micrographic and x-ray study of the structure of iron after compression has shown how the individual grains contribute to the preferred orientations of the aggregate.<sup>2</sup> The rotation of a grain is conditioned by its original orientation as follows: If it initially has  $[100]$  nearly parallel to the axis of compression, it will seek the  $[100]$  position and retain it. If it initially has

<sup>1</sup> A vector plot can be made of the resolved shear stresses on each system and of the rotation direction that each would cause if acting alone (C. S. Barrett, *Trans. A.I.M.E.*, vol. 135, p. 296, 1939), but this does not assist in applying the principle of least work.

<sup>2</sup> C. S. BARRETT, *Trans. A.I.M.E.*, vol. 135, p. 296, 1939.

[111] near the axis of compression, it will seek and retain the [111] position. But if the initial orientation is removed from either of these two stable positions, the grain will subdivide into deformation bands and alternate bands will rotate to the [111] and [100] positions.

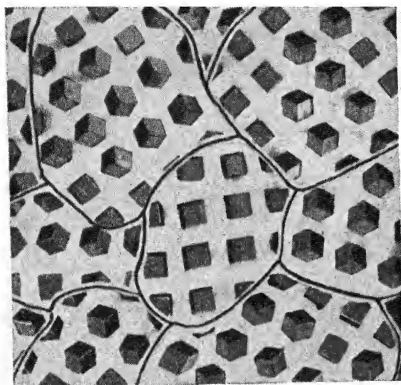


FIG. 11.

FIG. 11.—Model of polycrystalline iron after compression.

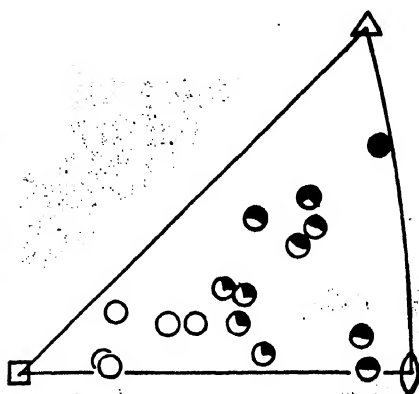


FIG. 12.

FIG. 12.—Projection showing relative prominence of [100] texture (white segments of circles) and [111] texture (black segments) after compression, as a function of initial orientation of iron crystals.

These three types of behavior are illustrated by models of compressed grains in which the orientations of unit cells are represented by blocks, Fig. 10. The structure of the aggregate, similarly illustrated in Fig. 11,

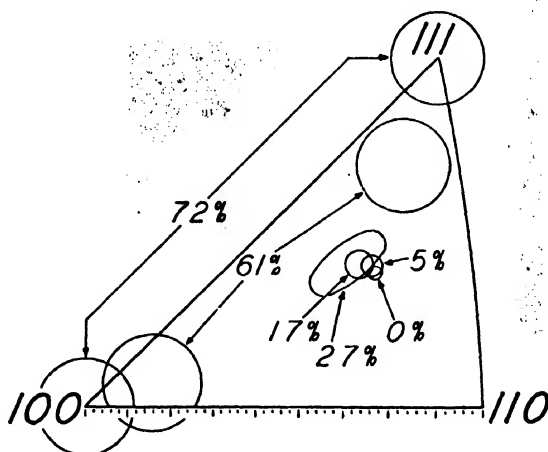


FIG. 13.—Rotation of a crystal of iron during successive stages of compression up to 72 percent.

is merely the sum of grains of all types. The contribution of a grain to each of the two final positions can be judged from its initial orientation and is indicated in Fig. 12, where the initial position of the compression axis for a number of crystals is plotted in a unit stereographic triangle



and the white and black segments of the circles show the relative prominence of the [100] and [111] components found after compression. X-ray measurements showing the rotation of the alternate bands in a crystal are plotted in Fig. 13, where the circular regions indicate the positions of the compression axis after various compressive deformations up to 72 per cent reduction in thickness, at which point the final texture was reached.<sup>1</sup>

**Deformation Bands in the Compression of Aluminum.**—Individual grains of aluminum appear to undergo a more haphazard distortion during compression than do grains of iron.<sup>2</sup> Typical grains contain a spread in orientation as high as  $10^\circ$  after a 10 percent reduction in thickness. This

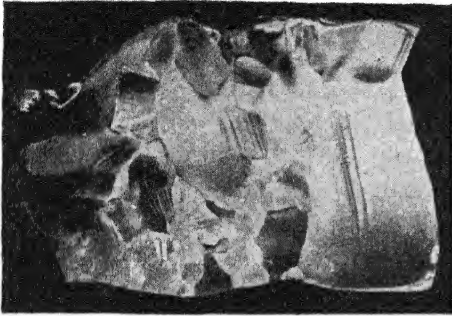


FIG. 14.

FIG. 14.—Large-grained aluminum compressed 44 percent, etched to reveal deformation bands and inhomogeneous orientations.  $\times 1$ .

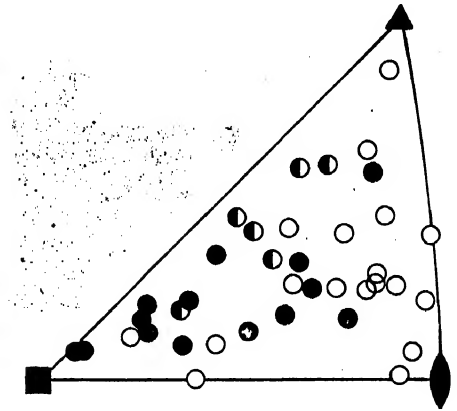


FIG. 15.

FIG. 15.—Dependence of banding tendency, during compression, on initial orientation of grains of aluminum. (●) grains forming bands; (○) no bands; (◐) uncertain, irregular orientations.

is increased to a maximum of about  $30^\circ$  after 30 percent reduction and a maximum of about  $50^\circ$  after 60 percent reduction. The spread in orientation is usually much greater than the average rotation of the material in the grain and is of a random nature that follows no simple rules; grains of identical orientation rotate and spread in different directions, presumably owing to perturbations in the direction of flow caused by neighboring grains.<sup>2</sup> As will be noted in Fig. 14, deformation bands are especially prominent in grains of certain orientations. The orientation dependence of the banding tendency is plotted in Fig. 15, where filled and partly filled circles indicate the initial orientations of grains which subsequently formed bands or irregularities in orientation and open circles indicate the initial orientations of those which did not. Frequently the

<sup>1</sup> C. S. BARRETT, *Trans. A.I.M.E.*, vol. 135, p. 296, 1939.

<sup>2</sup> C. S. BARRETT and L. H. LEVENSON, *Trans. A.I.M.E.*, vol. 137, p. 112, 1940.

boundaries of the bands are initially along cube planes, but with further deformation they become curved.

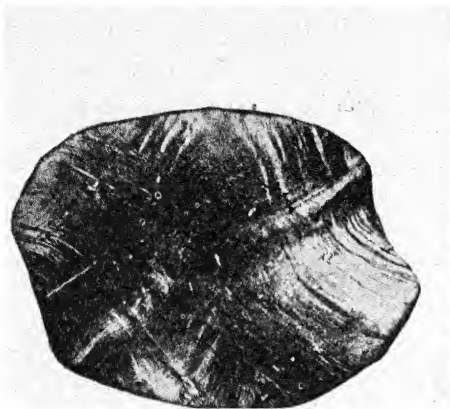


FIG. 16.—Transverse section of elongated iron crystal showing curved deformation bands.

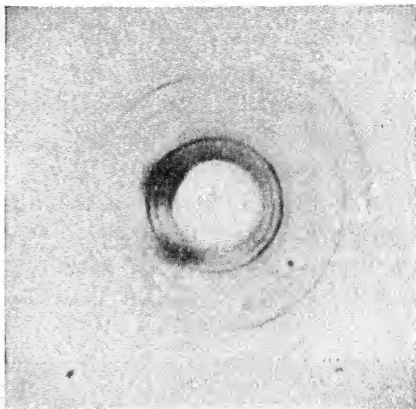


FIG. 17.—Diffraction pattern of a crystal similar to Fig. 16. X-ray beam parallel to axis of elongation.

The compression texture of aluminum is not a set of stable orientations retained by crystallites when once reached by them; instead, it is a large range of orientations within which the fragments are constantly moving during deformation. It seems to represent merely a statistical equilibrium between a tendency to rotate away from  $[111]$  and  $[100]$  directions toward  $[110]$  and an opposing tendency toward randomness.

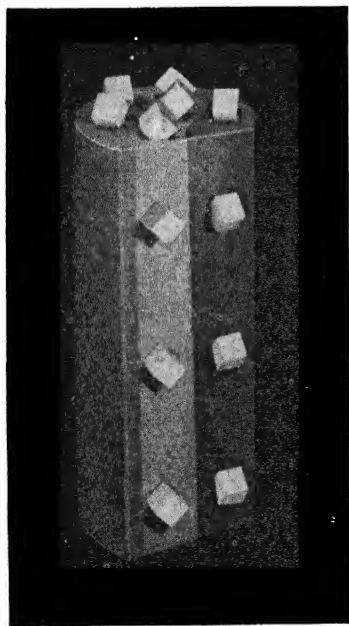


FIG. 18.—Model of deformation band in a crystal of iron drawn into a wire.

**Deformation Bands in the Elongation of Iron.**—During drawing, swaging, or elongating in tension individual grains of iron also take up increasingly wide ranges of orientation.<sup>1</sup> The spread is usually greatest in the azimuthal direction around the wire. Deformation bands form on crystallographic planes of the form  $[100]$  and  $[111]$  in the early stages of deformation, and the subsequent curving of these bands, their interpenetration, and the lattice rotation within them contribute to the scatter in orientation and sometimes produce a complete  $[110]$  fiber texture in a single grain. Figure 16 is a

photomicrograph of a single crystal deformed to simulate the deforma-

<sup>1</sup> C. S. BARRETT and L. H. LEVENSON, *Trans. A.I.M.E.*, vol. 135, p. 327, 1939.

tion of a grain in an aggregate during elongation. It exhibits marked bands. Figure 17 is the x-ray pattern for such a crystal, with the x-ray beam parallel to the axis of elongation, showing a large range of orientations around the axis. Wire forming processes force the deformation bands to swing into positions more and more closely parallel to the axis of the wire as the length of the wire increases and its diameter decreases. Such a structure may be represented by the model photographed in Fig. 18.

Textures produced in wires by recrystallization after cold drawing are discussed in the following chapter, together with other recrystallization textures.

### ROLLING TEXTURES

It was recognized by the early x-ray investigators of cold-rolled metal that preferred orientations must be specified in terms not only of the crystallographic directions parallel to the direction of rolling but also of the crystallographic planes parallel to the plane of the rolled sheet.<sup>1</sup> The orientations found in greatest frequency can be readily described by choosing one or two ideal orientations, but the details of the scatter about these ideal orientations can be specified only by listing a considerable number of less prominent orientations somewhat arbitrarily chosen. A less artificial description is possible by constructing a map of the orientation distribution—a pole figure (*cf.* Chap. IX). It has seemed advisable, therefore, to present much of the data of this chapter in the form of pole figures.

**Face-centered Cubic Rolling Textures.**—The principal orientation for all cold-rolled f.c.c. metals is one in which a plane of the form  $\{110\}$  is parallel to the rolling plane and a direction of the form  $\langle 112 \rangle$  is parallel to the rolling direction, which may be written  $(110)\parallel R.P.$   $[\bar{1}12]\parallel R.D.$  or simply  $(110)[\bar{1}12]$ . Metals having this principal texture are Cu,\* Al,† Ni,‡ Pt,§ Au,|| and Ag,¶ as well as face-centered alloys of Cu-Zn,\*\* Cu-Sn,¶

<sup>1</sup> H. MARK and K. WEISSENBERG, *Z. Physik*, vol. 14, p. 328, 1923; vol. 16, p. 314, 1923.

\* G. TAMMANN, *J. Inst. Metals*, vol. 44, p. 29, 1930. E. SCHMID and F. STAFFELBACH, *Schweiz. Arch. angew. Wiss. Tech.*, vol. 1, p. 221, 1935. W. IWERONOWA and G. SCHDANOW, *Tech. Phys. U.S.S.R.*, vol. 1, p. 64, 1934.

† E. A. OWEN and G. D. PRESTON, *Proc. Phys. Soc. (London)*, vol. 38, p. 132, 1925. G. V. VARGHA and G. WASSERMANN, *Metallwirtschaft*, vol. 12, p. 511, 1933.

‡ E. SCHMID and F. STAFFELBACH, *Schweiz. Arch. angew. Wiss. Tech.*, vol. 1, p. 221, 1935. S. T. KONOBEJEWSKI, *Z. Physik*, vol. 39, p. 415, 1926.

§ S. TANAKA, *Mem. Coll. Sci. Kyoto Imp. Univ. (A)*, vol. 8, p. 319, 1925; vol. 9, p. 197, 1925.

|| G. TAMMANN, *J. Inst. Metals*, vol. 44, p. 29, 1930.

¶ F. V. GOLER and G. SACHS, *Z. Physik*, vol. 41, p. 873, 1927; vol. 56, p. 477, 1929.

\*\* F. V. GOLER and G. SACHS, *Z. Physik*, vol. 41, p. 873, 1927; vol. 56, p. 477, 1929. W. IWERONOWA and G. SCHDANOW, *Tech. Phys. U.S.S.R.*, vol. 1, p. 64, 1934. A. BASS

Au-Ag,\* Fe-Ni,† Cu-Ni (40 percent nickel, constantan),\* and dilute lead alloys (for example, 0.26 percent calcium).‡ The only exception seems to be rolled lead,§ which probably recrystallizes during rolling and thus is not cold-rolled.

To describe the other orientations also present in many of these metals the indices  $(112)[11\bar{1}]$  are generally used;<sup>1</sup> so the rolled textures of aluminum, copper, gold, nickel, and the f.c.c. alloys of the Fe-Ni system can be listed as  $(110)[\bar{1}12]$  plus  $(112)[11\bar{1}]$ . The second of these two orientations is weak in silver\* and is absent in  $\alpha$ -brass containing 5 percent or more of zinc according to some investigators<sup>2</sup> but is present according to others.<sup>3</sup>

In addition to the two principal orientations listed above, traces of the orientation  $(100)[001]$  have been found in Fe-Ni (35.6 percent nickel),<sup>1</sup> in 70-30 brass,<sup>4</sup> and in copper;<sup>2</sup> weak orientations of the type  $(110)[001]$  have been noted in copper,<sup>2</sup> as well as an orientation near  $(124)[53\bar{3}]$  or  $(236)[53\bar{3}]$ . The indices  $(125)[53\bar{3}]$  have also been used for aluminum, copper, gold, and nickel,<sup>5</sup> and the indices  $(135)[21\bar{1}]$  for copper.<sup>6</sup> It must be pointed out that different observers will list different ideal orientations for textures that are fundamentally the same. This is the principal argument in favor of the use of pole figures to describe the experimental data. Even pole figures, as usually produced, are not free from subjective errors and are somewhat influenced by the nature of the radiation used (for example, white vs. characteristic), absorption effects, exposure times, etc. But they present a more complete and unbiased description of the texture than any other method in common use.

The pole figures for  $(111)$ ,  $(100)$ , and  $(110)$  poles in rolled aluminum, as plotted by Göler and Sachs,\* are given in Fig. 19. Pole figures for rolled copper and brass according to Iweronowa and Schdanow<sup>2</sup> are reproduced

and R. GLOCKER, *Z. Metallkunde*, vol. 20 p, 179, 1928. R. M. BRICK, *Trans. A.I.M.E.*, vol. 137, p. 193, 1940.

\* F. v. GÖLER and G. SACHS, *Z. Physik*, vol. 41, p. 873, 1927; vol. 56, p. 477, 1929.

† G. SACHS and J. SPRETNAK, *Metals Tech., Tech. Pub.* 1143, January, 1940. W. G. BURGERS and J. L. SNOEK, *Z. Metallkunde*, vol. 27, p. 158, 1935.

‡ H. HIRST, *J. Inst. Metals*, vol. 66, p. 39, 1940.

§ W. HOFFMANN, *Z. Metallkunde*, vol. 29, p. 266, 1937.

<sup>1</sup> G. SACHS and J. SPRETNAK, *Metals Tech., Tech. Pub.* 1143, January, 1940.

<sup>2</sup> W. IWERONOWA and G. SCHDANOW, *Tech. Phys. U.S.S.R.*, vol. 1, p. 64, 1934.

<sup>3</sup> O. DAHL and F. PAWLEK, *Z. Metallkunde*, vol. 28, p. 266, 1936. F. PAWLEK, *Z. Metallkunde*, vol. 27, p. 160, 1935. R. M. BRICK and M. A. WILLIAMSON, *Trans. A.I.M.E.*, vol. 143, p. 84, 1941.

<sup>4</sup> R. M. BRICK and M. A. WILLIAMSON, *Trans. A.I.M.E.*, vol. 143, p. 84, 1941.

<sup>5</sup> O. DAHL and F. PAWLEK, *Z. Metallkunde*, vol. 28, p. 266, 1936. F. PAWLEK, *Z. Metallkunde*, vol. 27, p. 160, 1935.

<sup>6</sup> C. S. BARRETT and F. W. STEADMAN, *Trans. A.I.M.E.*, vol. 147, p. 57, 1942.

in Figs. 20 to 22. Schmid and Staffelbach's pole figures<sup>1</sup> for copper and nickel differ from Fig. 20 only in a few details. Brick's results<sup>2</sup> on 70-30 brass rolled to a reduction of 99 percent and v. Goler and Sachs's pole figures for 85-15 brass rolled 98.8 percent agree in most respects with Figs. 21 and 22.<sup>3</sup> Hirst's results for rolled lead containing 0.26 percent calcium are similar to Fig. 20 but are not entirely similar to those obtained by Hoffmann<sup>4</sup> for lead plus 2 percent antimony.

In Fig. 23 are plotted several ideal textures falling within the intense areas of these pole figures. Brick concludes that a considerable part of the metal in rolled brass has (110) in the rolling plane and a spread of orientation from [113] to [117] in the rolling direction. From an analysis of rolled single crystals it appears that this entire spread from [113] to [117], together with "complementary orientations" symmetrical with these in the planes of symmetry of the rolling process, can be generated in a single brass crystal; identical results have been obtained with a copper crystal<sup>5</sup> having the initial orientation (110)[001]. Large ranges of orientation are, in fact, generated in most copper crystals during rolling,<sup>6</sup> and so it is probable that most of the ideal orientations of Fig. 23 are not truly stable—with the exception of (110)[ $\bar{1}12$ ], which remains a pseudo-single crystal even after 97.6 percent reduction.<sup>5</sup>

The presence of the  $\beta$  phase in 62-38 brass makes no detectable difference in the texture of the  $\alpha$  phase, but merely takes up its typical b.c.c. texture independently of the  $\alpha$  phase. The background intensity, corresponding to unoriented crystallites, increases with the percentage of zinc.<sup>7</sup>

A degree of correlation exists between rolling textures and the simple elongation and compression textures, as if the rolling process could be considered as the superposition of elongation in the rolling direction and compression normal to the rolling plane.<sup>8</sup> While the fundamental significance of this correlation may be problematical, it affords an interesting basis for comparing textures of f.c.c. materials. Thus the wire textures of silver and brass should resemble each other and differ from that of aluminum, which has no crystallites with [100] in the wire axis. This is in agreement with the observations on rolled textures. Similarly, the

<sup>1</sup> E. SCHMID and F. STAFFELBACH, *Schweiz. Arch. angew. Wiss. Tech.*, vol. 1, pp. 221, 1935.

<sup>2</sup> R. M. BRICK, *Trans. A.I.M.E.*, vol. 137, p. 193, 1940.

<sup>3</sup> For additional data on copper alloys see the recent results of Brick, Martin, and Angier reviewed on p. 430.

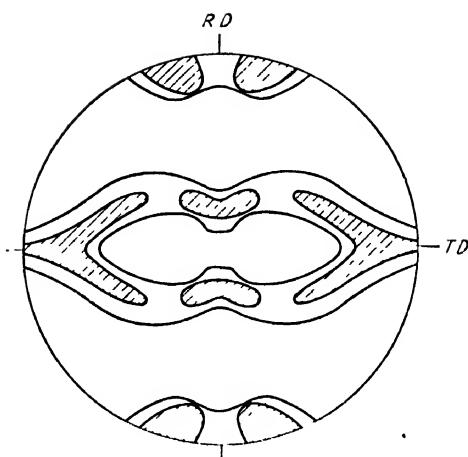
<sup>4</sup> W. HOFFMANN, *Z. Metallkunde*, vol. 29, p. 266, 1937.

<sup>5</sup> C. S. BARRETT and F. W. STEADMAN, *Trans. A.I.M.E.*, vol. 147, p. 57, 1942.

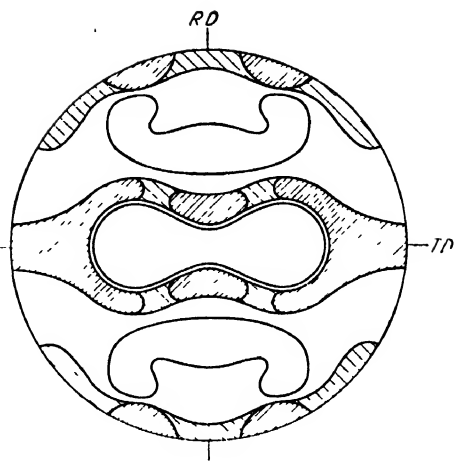
<sup>6</sup> H. C. VACHER, *J. Research Natl. Bur. Standards*, vol. 26, p. 385, 1941.

<sup>7</sup> W. IWERONOWA and G. SCHDANOW, *Tech. Phys. U.S.S.R.*, vol. 1, p. 64, 1934.

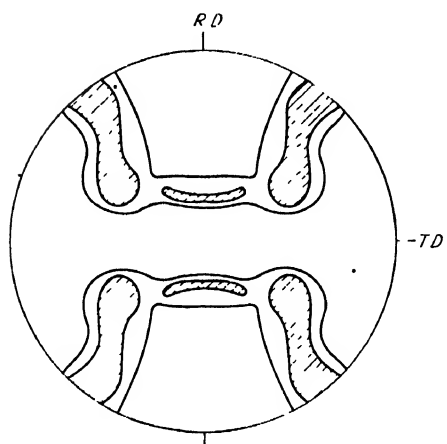
<sup>8</sup> F. WEYER, *Trans. A.I.M.E.*, vol. 93, p. 51, 1931.



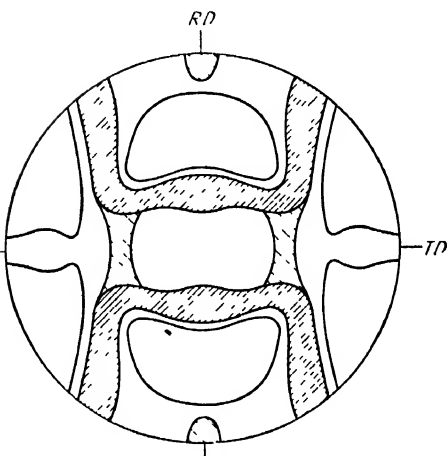
a, Octohedral planes, (111).



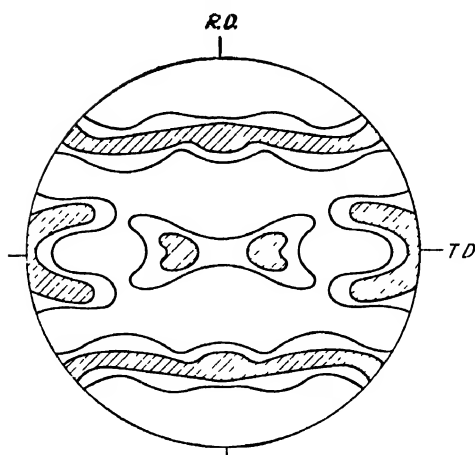
a (111).



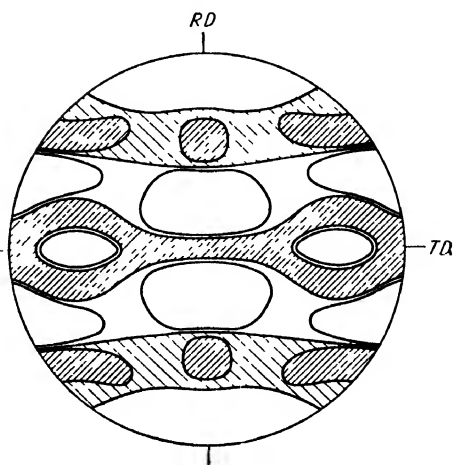
b, Cube planes, (100).



b (100).



c, Dodecahedral planes, (110).



c (110).

FIG. 19.—Pole figures for rolled aluminum, for 99.5 percent reduction in thickness. (v. Göler and Sachs.)

FIG. 20.—Pole figures for rolled copper, for a reduction of 97.7 percent. (Iwerson and Schdanow)

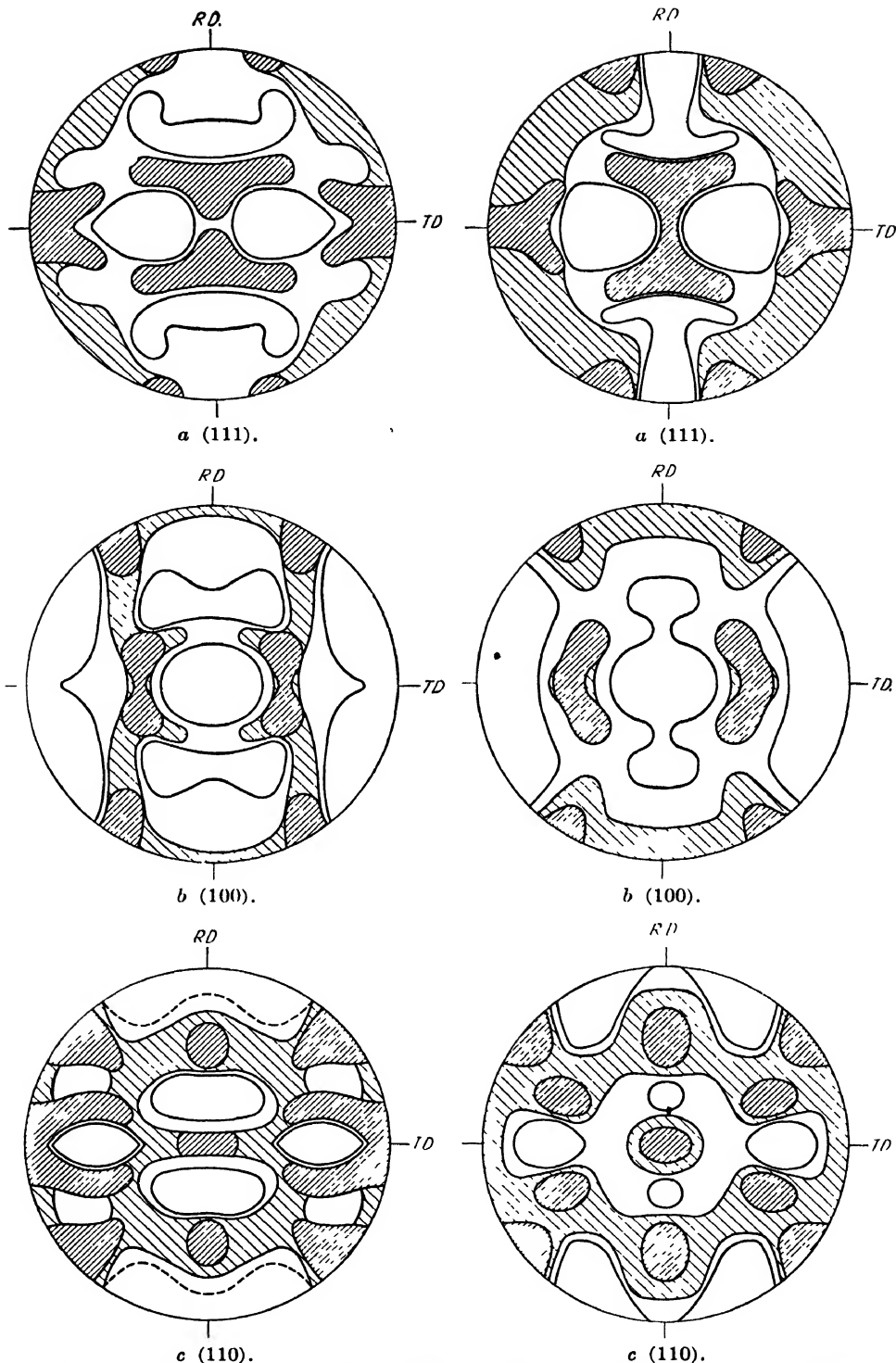


FIG. 21.—Pole figures for rolled brass (95 % Cu, 5 % Zn) for a reduction of 97.7 percent. (*Iweronowa and Schdanow.*)

FIG. 22.—Pole figures for  $\alpha$  phase in rolled brass of 62 % Cu, 38 % Zn (similar texture found in 80–20 brass). (*Iweronowa and Schdanow.*)

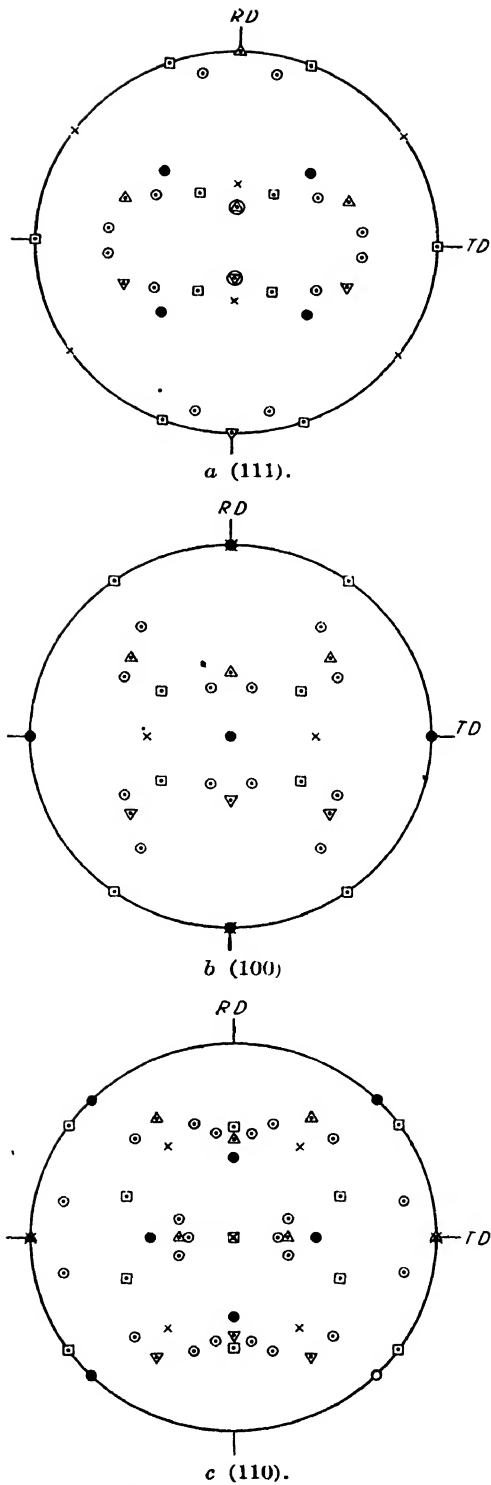


FIG. 23.—Pole figures for ideal orientations of face-centered cubic textures (compare with Figs. 19 to 22). Orientations indicated as follows:  $\square$  (110)[112],  $\triangle$  (112)[11 $\bar{1}$ ],  $\circ$  (236)[533],  $\times$  (110)[001],  $\bullet$  (100)[001].



compression texture of brass contains a  $[111]$  component that is missing from copper, and the corresponding differences will be noted in Figs. 20a and 22a at the center of the pole figures for the rolled material.

**Surface Textures in Face-centered Cubic Metals.**—Rolled sheets and foils less than about 1 mm. in thickness are homogeneous in texture throughout their thickness,<sup>1</sup> but thicker ones are likely to have a texture on the surface which differs from that in the interior. (This is analogous to the condition in drawn wires of small and of large diameter.<sup>2</sup>)

Vargha and Wassermann obtained the texture of Fig. 24 on the surface of an aluminum sheet 5 mm. in thickness. This orientation extended to a

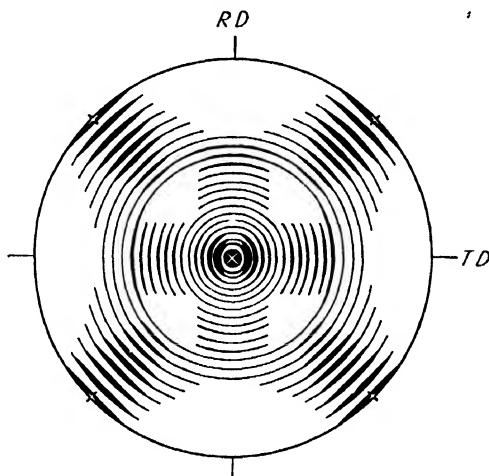


FIG. 24. (100) pole figure for the outer layers of rolled aluminum of 5 mm. thickness. Crosses give ideal (100)[011] position. (Vargha and Wassermann.)

depth of about 1.2 mm. and then gave way to an inner texture similar to that of Fig. 19. The surface orientation centers around the position (100)[011], as will be seen from the position of the crosses in Fig. 24. When several sheets of metal are rolled together, the inhomogeneity in texture is different for the outer and inner sheets of the pack.<sup>3</sup> There does not appear to be an explanation of the surface texture in terms of inclined flow of the sort that seems to account for the zonal texture of wires.<sup>4</sup> Straight and reversed rolling do not produce different textures, at least in copper strip,<sup>5</sup> but since the nature of flow at the surface is dependent upon roll diameter and reduction per pass it seems probable that surface textures are influenced by these variables.

<sup>1</sup> E. SCHMID and F. STAFFELBACH, *Schweiz. Arch. angew. Wiss. Tech.*, vol. 1, p. 221, 1935. W. G. BURGERS and F. L. SNOEK, *Z. Metallkunde*, vol. 27, p. 158, 1935. F. PAWLEK, *Z. Metallkunde*, vol. 27, p. 160, 1935.

<sup>2</sup> G. VARGHA and G. WASSERMANN, *Metallwirtschaft*, vol. 12, p. 511, 1933.

<sup>3</sup> S. T. KONOBEJEWSKI, *Z. Physik*, vol. 43, p. 741, 1927.

<sup>4</sup> G. WASSERMANN, "Texturen metallischer Werkstoffe," Springer, Berlin, 1939.

<sup>5</sup> H. V. ANDERSON and G. L. KEHL, *Metals & Alloys*, vol. 8, p. 73, 1937.

**Deformation Bands in Rolled Face-centered Cubic Metals.**—The optical goniometer shows the role of deformation bands in developing the rolling texture.<sup>1</sup> After high reductions each band has a mean orientation within the more intense regions of the polycrystalline pole figure. In many instances, the bands within a single grain are oriented symmetrically with respect to the rolling and normal directions of the sheet (*i.e.*, their orientations are mirror images of each other in the plane of the sheet or in the rolling direction–normal direction plane). Thus the development of “complementary” orientations in the sheet frequently occurs within individual grains as well as in the aggregate as a whole.

In photomicrographs of sections normal to the transverse direction, it has been noted that the deformation bands in the early stages of rolling lie at various angles to the surface and as rolling progresses are flattened into thin lamellae parallel to the surface, as a consequence of the elongation and thinning of the grains.

The microstructure of rolled copper and brass is complex, and doubtless it would be an oversimplification to say that all the markings are deformation bands of some simple type. However, Brick<sup>2</sup> notes that pronounced strain markings accompany the development of complementary orientations in a single crystal of brass. It is known also that macroscopic deformation bands in large-grained copper are often of complementary orientations.<sup>3</sup> X-ray experiments indicate that deformation bands, not deformation twins, constitute the principal mechanism of fragmentation by which complementary orientations are produced in the grains of cubic metals,<sup>4</sup> but the possibility that microscopic or sub-microscopic twins exist cannot be dismissed.

**Body-centered Cubic Rolling Textures.**—The numerous determinations of the texture of cold-rolled iron and steel have been in satisfactory agreement as to the principal features of the texture (with the exception of a few conclusions that apparently have been based on insufficient data). The texture is chiefly one in which [110] directions of the grains lie along the direction of rolling—with a deviation of a few degrees—and (001) planes lie in the plane of the rolled sheet, with a deviation from this position chiefly about the rolling direction as an axis.<sup>5</sup>

<sup>1</sup> C. S. BARRETT and F. W. STEADMAN, *Trans. A.I.M.E.*, vol. 147, p. 57, 1942.

<sup>2</sup> R. M. BRICK, *Trans. A.I.M.E.*, vol. 137, p. 193, 1940.

<sup>3</sup> C. S. BARRETT and F. W. STEADMAN, *Metals Tech.*, vol. 9, *Tech. Pub.* 1430, February, 1942. H. C. VACHER, *J. Research Natl. Bur. Standards*, vol. 26, p. 385, 1941.

<sup>4</sup> C. S. BARRETT and F. W. STEADMAN, *Metals Tech.*, *Tech. Pub.* 1430, February, 1942.

<sup>5</sup> Z. JEFFRIES, *Trans. A.I.M.E.*, vol. 70, p. 303, 1924. S. T. KONOBEJEWSKI, *Z. Physik*, vol. 39, p. 415, 1926. F. WEVER, *Mitt. Kaiser-Wilhelm Inst. Eisenforsch., Dusseldorf*, vol. 5, p. 69, 1924; *Z. Physik*, vol. 28, p. 69, 1924; *Trans. A.I.M.M.E.*, vol.

Orientations are found that are rotated about the rolling direction, [110], various amounts up to 45 or 55° each way from the ideal (001) position<sup>1</sup>—usually about 50° in mild steel.<sup>2</sup> The range of this deviation is a function of the percentage of total reduction.<sup>3</sup> Post<sup>4</sup> reported that it decreases with increasing reduction, but apparently he studied only the surface material, which Gensamer and Mehl<sup>5</sup> found to be somewhat differently oriented from the material in the inside of the sheet. McLachlan and Davey<sup>6</sup> found that the deviation also decreases with increasing percentage of total reduction for the material in the interior of the sheet and is independent of the reduction per pass.

The deviation about the cross direction as an axis (the direction in the plane of rolling 90° to the rolling direction) varies<sup>7</sup> under different conditions from about 20 to 6°, decreases with increasing percentage reduction,<sup>3</sup> and in the surface layers decreases with increasing roll diameter.<sup>4</sup> Exact comparison among the results of different observers is meaningless, for the crystallites decrease in number with increasing deviation from the ideal orientation,<sup>8</sup> and the limit that is observed depends greatly upon the x-ray technique, *e.g.*, length of exposure, use of white or characteristic radiation, reflection of the beam from the surface or transmission through the sheet, and grain size of the material.

93, p. 51, 1931. G. KURDJUMOW and G. SACHS, *Z. Physik*, vol. 62, p. 592, 1930. M. GENSAMER and R. F. MEHL, *Trans. A.I.M.E.*, vol. 120, p. 277, 1936. C. B. POST, *Trans. A.S.M.*, vol. 24, p. 679, 1936. R. M. BOZORTH, *Phys. Rev.*, vol. 50, p. 1076, 1936.

<sup>1</sup> F. WEVER, *Mitt. Kaiser-Wilhelm Inst. Eisenforsch. Dusseldorf*, vol. 5, p. 69, 1924; *Z. Physik*, vol. 28, p. 69, 1924; *Trans. A.I.M.E.*, vol. 93, p. 51, 1931. G. KURDJUMOW and G. SACHS, *Z. Physik*, vol. 62, p. 592, 1930. R. M. BOZORTH, *Phys. Rev.*, vol. 50, p. 1076, 1936.

<sup>2</sup> G. KURDJUMOW and G. SACHS, *Z. Physik*, vol. 62, p. 592, 1930. M. GENSAMER and R. F. MEHL, *Trans. A.I.M.E.*, vol. 120, p. 277, 1936. C. B. POST, *Trans. A.S.M.*, vol. 24, p. 679, 1936.

<sup>3</sup> C. B. POST, *Trans. A.S.M.*, vol. 24, p. 679, 1936. D. L. McLACHLAN and W. P. DAVEY, *Trans. A.S.M.*, vol. 25, p. 1084, 1937.

<sup>4</sup> C. B. POST, *Trans. A.S.M.*, vol. 24, p. 679, 1936.

<sup>5</sup> M. GENSAMER and R. F. MEHL, *Trans. A.I.M.E.*, vol. 120, p. 277, 1936.

<sup>6</sup> D. L. McLACHLAN and W. P. DAVEY, *Trans. A.S.M.*, vol. 25, p. 1084, 1937.

<sup>7</sup> F. WEVER, *Mitt. Kaiser-Wilhelm Inst. Eisenforsch. Dusseldorf*, vol. 5, p. 69, 1924; *Z. Physik*, vol. 28, p. 69, 1924; *Trans. A.I.M.E.*, vol. 93, p. 51, 1931. G. KURDJUMOW and G. SACHS, *Z. Physik*, vol. 62, p. 592, 1930. M. GENSAMER and R. F. MEHL, *Trans. A.I.M.E.*, vol. 120, p. 277, 1936. C. B. POST, *Trans. A.S.M.*, vol. 24, p. 679, 1936. R. M. BOZORTH, *Phys. Rev.*, vol. 50, p. 1076, 1936. D. L. McLACHLAN and W. P. DAVEY, *Trans. A.S.M.*, vol. 25, p. 1084, 1937.

<sup>8</sup> D. L. McLACHLAN and W. P. DAVEY, *Trans. A.S.M.*, vol. 25, p. 1084, 1937. R. M. BOZORTH, *Trans. A.S.M.*, vol. 23, p. 1107, 1935.

Typical pole figures for rolled iron are reproduced in Fig. 25, after Kurdjumow and Sachs.<sup>1</sup> The reduction was 98.5 percent from an initial thickness before cold rolling of about 0.8 mm. Certain of the less prominent orientations were described by Kurdjumow and Sachs with the ideal

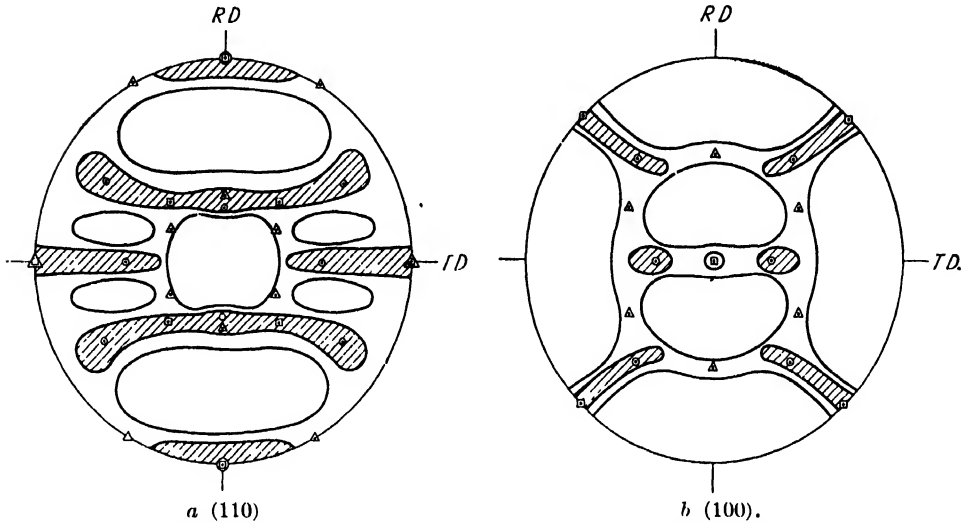


FIG. 25.—Pole figures for iron reduced 98.5 percent by cold rolling. Ideal orientations indicated as follows  $\square$  (100)[011],  $\circ$  (112)[ $\bar{1}\bar{1}0$ ],  $\triangle$  (111)[ $\bar{1}\bar{1}\bar{2}$ ]. (Kurdjumow and Sachs.)

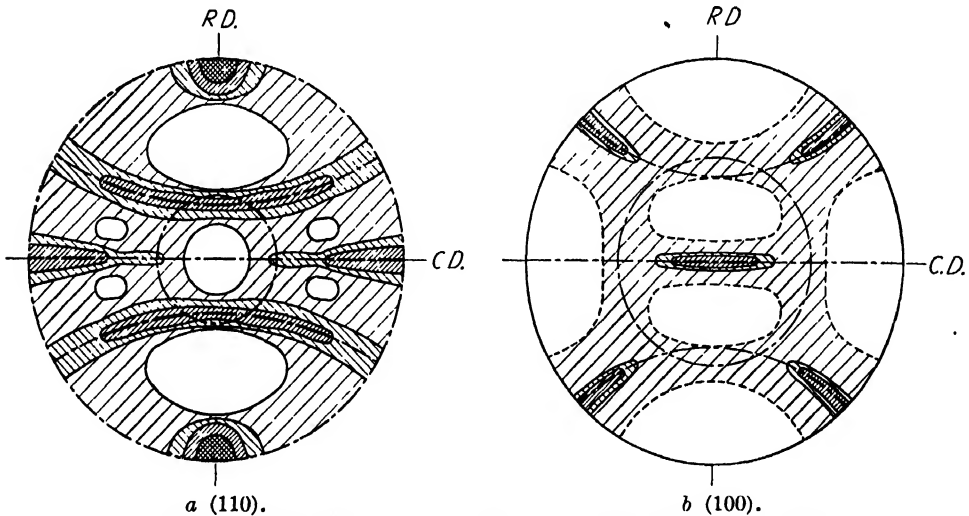


FIG. 26 — Pole figures for iron-silicon alloy (4.6 % Si) cold-rolled 95 percent.

orientations (112)[ $\bar{1}\bar{1}0$ ] and (111)[ $\bar{1}\bar{1}\bar{2}$ ], which are indicated in Fig. 25. Gensamer and Mehl<sup>2</sup> obtained a pole figure in mild steel (0.05 percent carbon) rolled 99 percent that was slightly sharper than that of Fig. 25 but was otherwise similar.

<sup>1</sup> G. KURDJUMOW and G. SACHS, *Z. Physik*, vol. 62, p. 592, 1930.

<sup>2</sup> M. GENSAMER and R. F. MEHL, *Trans. A.I.M.E.*, vol. 120, p. 277, 1936.

Pole figures for ferrite containing 4.6 percent silicon are practically identical with those for pure iron, as will be seen from Fig. 26, and the same is true of an alloy with a lower silicon content.<sup>1</sup> Nickel in solid solution in ferrite, judging by experiments of McLachlan and Davey,<sup>2</sup> seems to decrease merely the intensity of those orientations having (111) in the plane of the sheet (the orientations of the compression texture); the principal orientations, however, are similar to those in iron.

A more complete understanding of the rolling texture was obtained from a study of single crystals deformed to simulate the deformation of individual grains of an aggregate.<sup>3</sup> Depending on the initial orientation of both the normal and the rolling directions, certain crystals maintained a reasonably sharp single orientation during rolling; others rotated into

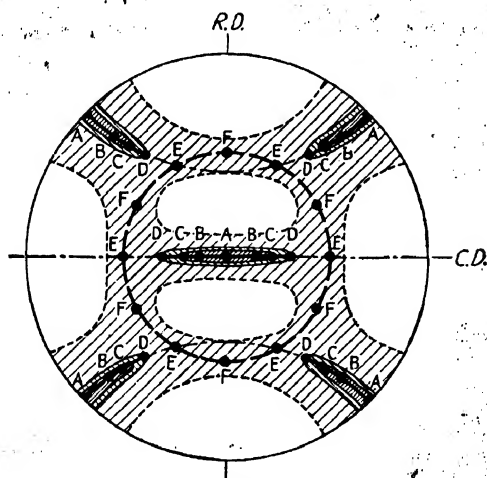


FIG. 27.

FIG. 27.—(100) pole figure for rolled iron with various ideal orientations shown as follows: A, (100)[011]; B, (115)[110]; C, ( $\bar{1}$ 13)[110]; D, (112)[ $\bar{1}$ 10]; E, ( $\bar{1}$ 11)[110]; F, (111)[112]. Heavy full lines represent a continuous set containing A to D. Dashed circle is a second continuous set containing E and F.

FIG. 28.—Model illustrating various ideal orientations stable in rolled iron. Reader is looking at rolling plane, with rolling direction vertical. Orientations are lettered to correspond to Fig. 27.



FIG. 28.

two or more such orientations, and some fragmented into a texture that resembled the polycrystalline texture. Rotation of crystals and frag-

<sup>1</sup> C. S. BARRETT, G. ANSEL, and R. F. MEHL, *Trans. A.I.M.E.*, vol. 125, p. 516, 1937.

<sup>2</sup> D. L. McLACHLAN and W. P. DAVEY, *Trans. A.S.M.*, vol. 25, p. 1084, 1937.

<sup>3</sup> C. S. BARRETT and L. H. LEVENSON, *Trans. A.I.M.E.*, vol. 145, p. 281, 1941.

ments occurred such that the final orientations of the crystals were within the shaded areas of the polycrystalline pole figure, which, of course, must represent the sum of the end positions sought by the individual grains.

In Fig. 27, which is a typical pole figure for (100) planes of ferrite, the rolling texture can be interpreted as the sum of the ideal positions *A* to *F*.<sup>1</sup> A model illustrating each of these orientations is shown in Fig. 28. The single-crystal studies show that these ideal positions have no special significance since the intermediate positions are equally numerous after rolling. It seems better, therefore, to say that there are two continuous sets of end positions: (1) a set including the orientations *A*, *B*, *C*, and *D*, having the [110] direction parallel to the rolling direction and the (001) plane at any angle up to 45 or 55° from the rolling plane; and (2) a set including the orientations *E* and *F*, having the (111) plane in the plane of the sheet and all possible positions of the rolling direction in this plane. The spread in orientation of a crystal that rotates into the first set is chiefly a spread about the rolling direction as an axis, while the spread for the second set is chiefly about the normal to the rolling plane.

The principal orientations in cold-rolled **molybdenum** are similar to those in iron, centering in the position (100)[011]. Jeffries<sup>2</sup> showed that the [011] directions deviated some 10° and the (100) about 13° from the ideal position, and Fujiwara<sup>3</sup> found a similar spread. Patterns made by Ransley and Rooksby<sup>4</sup> on molybdenum reduced 88 percent by straight rolling show a spread about the rolling direction as an axis that is of the same order as the spread with iron. Thus, in the absence of a complete pole-figure study of molybdenum, it may be assumed that the orientations are substantially the same as those in iron.

**Theories of the Rolling Textures.**—The flow of metal during rolling is such as to lengthen the rolled sheet at the expense of its thickness, leaving the width unchanged. If the sheet were appreciably widened, the flow would be equivalent to a superposition of elongation in the direction of rolling and compression in the direction normal to the sheet. This approximation to the flow is the basis for Wever's suggestion that cold-rolling textures are the superposition of tension and compression textures.<sup>5</sup> Let us see how this theory compares with the observed rolling texture of iron described in the preceding section. The first set of end positions, which corresponds to the tension texture, is composed of grains whose chief spread is around the tension axis, just like the grains in a drawn

<sup>1</sup> C. S. BARRETT, G. ANSEL, and R. F. MEHL, *Trans. A.I.M.E.*, vol. 125, p. 516, 1937.

<sup>2</sup> Z. JEFFRIES, *Trans. A.I.M.E.*, vol. 70, p. 303, 1924.

<sup>3</sup> T. FUJIWARA, *Proc. World Eng. Congr. Tokyo*, 1929, vol. 36, p. 179, 1931.

<sup>4</sup> C. E. RANSLEY and H. P. ROOKSBY, *J. Inst. Metals*, vol. 62, p. 205, 1938.

<sup>5</sup> F. WEVER, *Mitt. Kaiser Wilhelm Inst. Eisenforsch. Dusseldorf*, vol. 5, p. 69, 1924; *Z. Physik*, vol. 28, p. 69, 1924; *Trans. A.I.M.E.*, vol. 93, p. 51, 1931.

wire,<sup>1</sup> while the second set, corresponding to the compression texture, has large spreads around the compression axis, like the  $[111]$  component of the true compression texture.<sup>2</sup> Yet, as has been pointed out by Gensamer and Mehl,<sup>3</sup> the theory fails to explain why the complete tension texture does not appear; there is no material with  $[110]$  in the rolling direction having  $(001)$  at an angle to the rolling plane between  $55$  and  $90^\circ$ . Furthermore, only one orientation of the minor constituent of the compression texture<sup>2</sup> is present, *viz.*,  $(100)[011]$ . In fact, there are only two end positions consistent with the requirements of both tension and compression, *viz.*,  $A$  and  $E$  of Fig. 28.

The three "ideal" orientations used by Kurdjumow and Sachs to describe the texture,  $(100)[011]$ ,  $(112)[\bar{1}\bar{1}0]$ , and  $(111)[11\bar{2}]$ , have been found to be end orientations of single crystals, but the rest of the pole figure is not adequately explained as a spread about these three orientations alone, for there are, in fact, two continuous sets.

No theory has been worked out to date that will predict these end positions of the rolling texture on rigorous grounds. The complexity of the slip mechanism in iron makes Taylor's method<sup>4</sup> extremely laborious; it has not yet been applied to any rolling texture. Boas and Schmid extended their theory of tension and compression textures (page 387) to rolling textures by assuming that only those slip systems operate in rolling which lead to a thinning of the sheet. This excludes any slip system having a slip direction in the rolling plane or a slip plane perpendicular to the rolling plane. With these excluded, the three most highly stressed slip systems should rotate the grains of f.c.c. metals into the texture  $(110)[\bar{1}12]$ . This is the principal ideal texture of most face-centered cubic metals.

The theory advanced by Pickus and Mathewson (page 388) when applied to cold-rolled f.c.c. metals gives the following list of stable orientations in the order of decreasing frequency of their occurrence, with the most prominent first:  $(110)[\bar{1}12]$ ,  $(100)[001]$ ,  $(110)[001]$ ,  $(112)[11\bar{1}]$ ,  $(010)[101]$ ,  $(101)[10\bar{1}]$ . The list is in satisfying agreement with the ideal textures that have been listed by various experimenters.

**The Layer Structure of Rolled Steel.**—Preferred orientations in rolled sheets are not always homogeneous throughout the thickness. Gensamer and Mehl<sup>3</sup> found that the surface layers in a sheet of mild steel reduced 85 percent by cold rolling had the texture of Fig. 29*a*, whereas the interior had the texture of Fig. 29*b*. After a reduction of 99 percent, however, the

<sup>1</sup> C. S. BARRETT and L. H. LEVENSON, *Trans. A.I.M.E.*, vol. 135, p. 327, 1939.

<sup>2</sup> C. S. BARRETT, *Trans. A.I.M.E.*, vol. 135, p. 296, 1939.

<sup>3</sup> M. GENSAMER and R. F. MEHL, *Trans. A.I.M.E.*, vol. 120, p. 277, 1936.

<sup>4</sup> G. I. TAYLOR, *J. Inst. Metals*, vol. 62, p. 307, 1938; "Stephen Timoshenko, 60th Anniversary Volume," p. 218, Macmillan, New York, 1938.

layer effect was probably much less, for the over-all texture closely resembled that of Fig. 25.

The layer structure and its change with the degree of reduction may account, in part, for early observations<sup>1</sup> that the rolling texture changed in type during the rolling process. For example, an x-ray beam directed normal to the sheet would give a pattern in which the inner Debye ring would have six maxima if the texture in the sheet were that of Fig. 29*b*, but only four maxima if it were that of Fig. 29*a*. (This can be seen if one notes the number of places in which the reflection circle would cut the heavily shaded regions of the pole figures.) Consequently, what is merely a modification of the texture might appear, on the basis of a single x-ray pattern, to be a fundamental change in the texture.

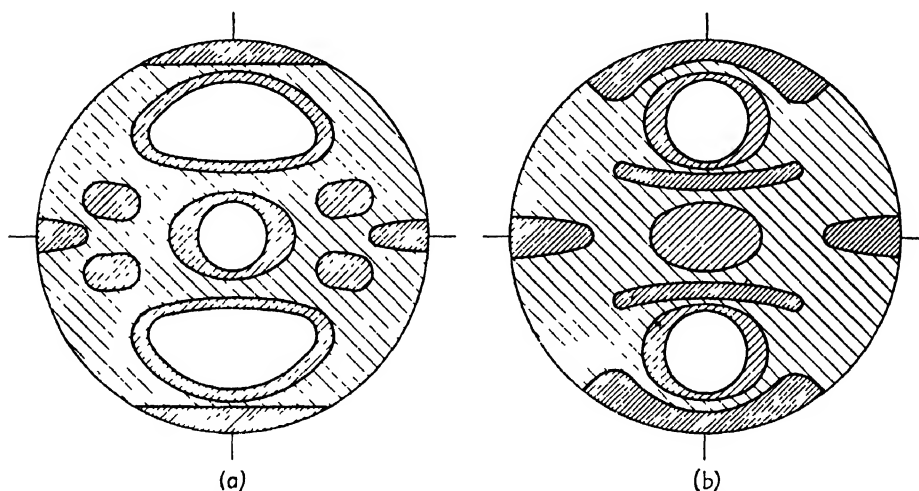


FIG. 29.—(110) pole figures for layers in a sheet of mild steel reduced 85 percent by cold rolling (a) outside layer of sheet, (b) inside of sheet (outer layers etched off). (*Gensamer and Mehl.*)

The origin of the surface texture is uncertain, but two possible explanations might be mentioned. (1) As is believed to be true in the zonal texture of wires, the flow of metal at the surface is different from the flow at the center; for example, the outer layers may shear over the inner ones. (2) The texture of the outside of the sheet may be produced by partial recrystallization of the outer layers, possibly caused by temperatures momentarily exceeding the recrystallization temperature of the severely worked metal.

**Variables Affecting the Texture of Steel.**—Preferred orientations develop gradually when a sheet is given increasing reductions. When x-ray patterns are made with the beam perpendicular to the sheet, the preferred orientation maxima on Debye rings first appear at reductions

<sup>1</sup> W. A. Sisson, *Metals & Alloys*, vol. 4, p. 193, 1933. G. TAMMANN and A. HEINZEL, *Arch. Eisenhüttenw.*, vol. 1, p. 663, 1928.



in the neighborhood of 30 to 60 percent. The first traces can be detected more easily with fine-grained sheets and by the use of an integrating camera that shifts the specimen under the beam during the exposure. The texture can be detected at earlier stages if the reflection circle is made to pass through the most intense maxima of the pole figure. Sisson<sup>1</sup> noted the beginnings of the texture with 10 to 30 percent reductions when the beam was directed along the transverse direction of the sheet (normal to the rolling direction and parallel to the plane of the sheet). Goss<sup>2</sup> gives 5 to 15 percent for this figure with commercial mild steel, but the effect of his small reduction may have been only to smear out the

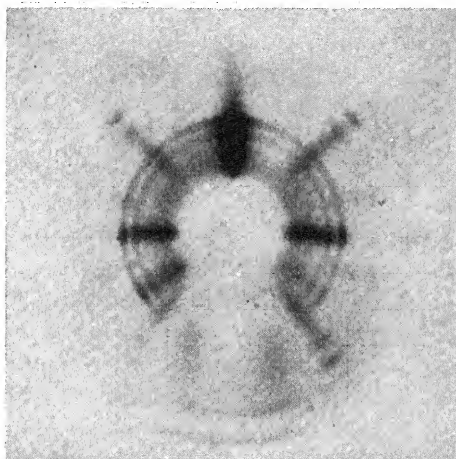


FIG. 30.—Pattern for rolled steel with intense spot (top center) from (110) planes normal to rolling direction (beam  $80^\circ$  from rolling direction,  $10^\circ$  from normal direction).

individual spots so as to render visible a texture present before rolling—a device that has been used as a substitute for an integrating camera.<sup>3</sup> Since more crystallites have their (110) planes normal to the rolling direction than in any other position, it follows that the most sensitive way to pick up faint orientations is to reflect from these. This may be done by directing the x-ray beam at an angle  $\theta$  to the sheet normal and along the plane containing the normal and the rolling direction, where  $\theta$ , the Bragg angle for the radiation used, is about  $7^\circ$  for the usual white radiation or  $10^\circ$  for molybdenum  $K\alpha$  radiation. This position puts the reflection circle through the rolling direction and yields the type of pattern shown in Fig. 30. Slightly better sensitivity should be obtained with the beam parallel to the plane of the sheet and  $\theta$  from the transverse direction, although this is less convenient.

<sup>1</sup> W. A. Sisson, *Metals & Alloys*, vol. 4, p. 193, 1933.

<sup>2</sup> N. P. Goss, *Metals & Alloys*, vol. 7, p. 131, 1936; *Trans. A.S.M.*, vol. 23, p. 511, 1935.

<sup>3</sup> G. SACHS and J. SPRETNAC, *Metals Tech., Tech. Pub.* 1143, January, 1940.

Sisson studied the effect of several variables on the texture of rolled steel and concluded that the nature and degree of preferred orientation are independent of roll diameter (at least from  $1\frac{1}{2}$  to 24 in.), reduction per pass (tested from 10 to 80 percent), and rolling speed (tested at 70 and 800 ft. per min.). Unidirectional rolling did not differ from reversed passes through the rolls. The application of tension to the strip as it passes through the rolls of a Steckel mill is without effect on the establishment or final degree of preferred orientation<sup>1</sup> (unless perhaps it lowers the relative amount of unoriented background material<sup>2</sup>), but smaller roll diameters give greater ranges of scattering about the transverse direction, according to Post.<sup>2</sup> Drawing sheets through a rectangular die gives textures equivalent to rolling a sheet the same amount<sup>3</sup> and again emphasizes the general principle that the direction of flow of the metal is the controlling factor in producing textures, rather than the details of the forming process.

The effect of increasing carbon content on the texture of steel is to increase the amount of randomness.<sup>4</sup> This arises from the fact that cementite is harder than ferrite. Because it deforms less, it forces the plastic ferrite to flow in irregular directions.

The degree to which preferred orientation has developed serves as a rough measure of the amount of reduction that has been given a strip, provided that this has been considerable. (Sisson remarks that the length of the arcs are related to the amount of reduction.<sup>5</sup>) This does not apply to reductions of some 15 percent or less, but in this range it is possible to distinguish between different amounts of cold work by noting to what extent the individual diffraction spots are blurred and by judging how clearly one can see the Debye rings. Commercial steel sheet of ordinary grain size changes progressively from a spotty pattern into a ring pattern with reductions between 5 and 30 percent,<sup>6</sup> the exact appearance at any stage depending on the initial grain size, specimen thickness, and camera design. Some blurring can be seen after the small amounts of cold work involved in roller leveling.

**Hexagonal Close-packed Rolling Textures.**—Rolling should tend to rotate the slip plane of hexagonal close-packed (h.c.p.) metals into the plane of the rolled sheet, and in accord with this tendency the predominating texture is one in which the basal plane, which is the slip plane, lies

<sup>1</sup> C. B. POST, *Trans. A.S.M.*, vol. 24, p. 679, 1936. A. HAYES and R. S. BURNS, *Trans. A.M.S.*, vol. 25, p. 129, 1937.

<sup>2</sup> C. B. POST, *Trans. A.S.M.*, vol. 24, p. 679, 1936.

<sup>3</sup> J. T. NORTON and R. E. HILLER, *Trans. A.I.M.E.*, vol. 99, p. 190, 1932.

<sup>4</sup> GEORGE L. CLARK, "Applied X-rays," pp. 532, 577, McGraw-Hill, New York, 1940.

<sup>5</sup> W. A. SISSON, *Metals & Alloys*, vol. 4, p. 193, 1933.

<sup>6</sup> GEORGE L. CLARK, "Applied X-rays," p. 574, McGraw-Hill, New York, 1940.

in or near the rolling plane, although modifications are found, as discussed below. This simple texture is most pronounced in metals with an axial ratio near that for the close packing of spheres ( $c/a = 1.633$ ), as in magnesium,<sup>1</sup> zirconium,<sup>2</sup> and hexagonal cobalt,<sup>3</sup> with  $c/a = 1.624$ , 1.589, and 1.624, respectively. Schmid and Wassermann<sup>4</sup> found nearly equal scattering in all directions from this position with magnesium, but Caglioti and Sachs,<sup>5</sup> as well as Bakarian,<sup>6</sup> found some directionality to the scatter, as indicated in Fig. 31a. The central shaded areas contain about 98 percent of the total material.<sup>6</sup> There is a tendency for the [100] direction to align with the rolling direction, as might be expected from the fact that this is the slip direction. This effect is to be seen in Fig. 31b,

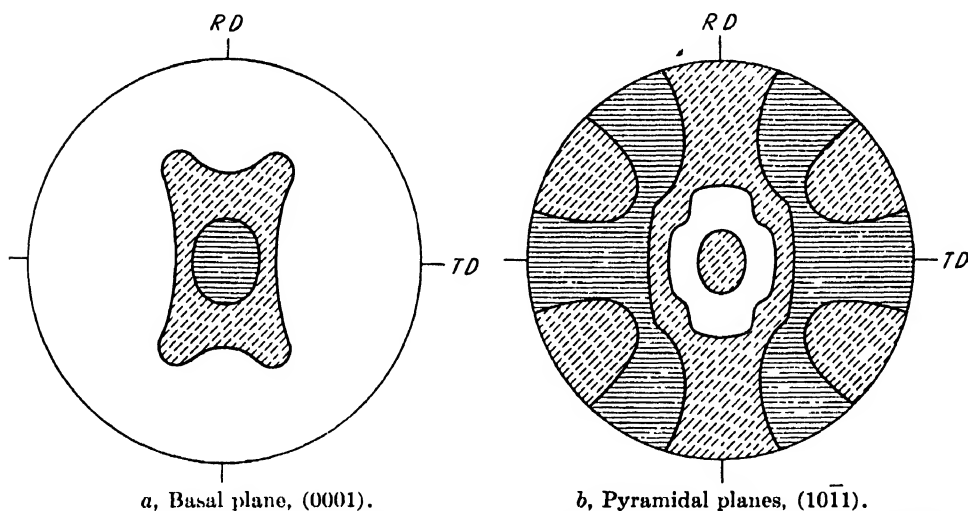


FIG. 31.—Pole figures for magnesium foil cold-rolled 97.5 percent. (Caglioti and Sachs.)

which is the pole figure for the pyramidal faces, but since a relatively small scatter will destroy this directionality in the basal plane it is not always found. Burgers and Jacobs's pole figures for zirconium are similar to these in most respects, but the principal deviation from the mean position is toward the transverse direction, rather than toward the rolling direction as in magnesium.

Zinc and cadmium (with axial ratios  $c/a = 1.856$  and 1.885, respectively) have rolling textures in which there is little material having

<sup>1</sup> E. SCHMID and G. WASSERMANN, *Metallwirtschaft*, vol. 9, p. 698, 1930. E. SCHIEBOLD and G. SIEBEL, *Z. Physik*, vol. 69, p. 458, 1931. V. CAGLIOTI and G. SACHS, *Metallwirtschaft*, vol. 11, p. 1, 1932. J. C. McDONALD, *Phys. Rev.*, vol. 52, p. 886, 1937. P. W. BAKARIAN, *Metals Tech.*, *Tech. Pub.* 1355, August, 1941.

<sup>2</sup> W. G. BURGERS and F. M. JACOBS, *Metallwirtschaft*, vol. 14, p. 285, 1935.

<sup>3</sup> G. WASSERMANN, *Metallwirtschaft*, vol. 11, p. 61, 1932.

<sup>4</sup> E. SCHMID and G. WASSERMANN, *Metallwirtschaft*, vol. 9, p. 698, 1930.

<sup>5</sup> V. CAGLIOTI and G. SACHS, *Metallwirtschaft*, vol. 11, p. 1, 1932.

<sup>6</sup> P. W. BAKARIAN, *Metals Tech.*, *Tech. Pub.* 1355, August, 1941.

the basal plane in the plane of the sheet. The hexagonal axis is found most frequently inclined 20 to 25° toward the rolling direction,<sup>1</sup> as shown in Fig. 32 for rolled zinc.

Another modification of this type of texture was found by Fuller and Edmunds<sup>2</sup> in a zinc alloy containing 1 percent copper and 0.01 percent

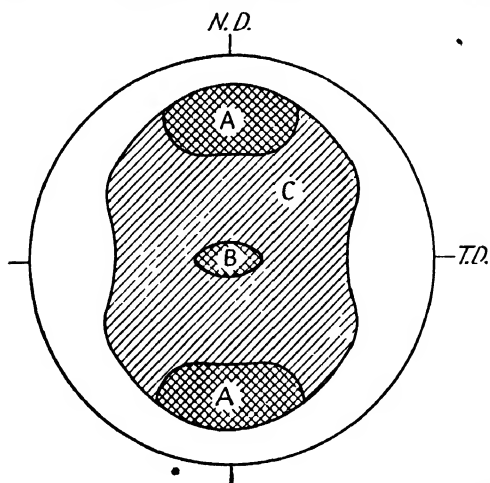
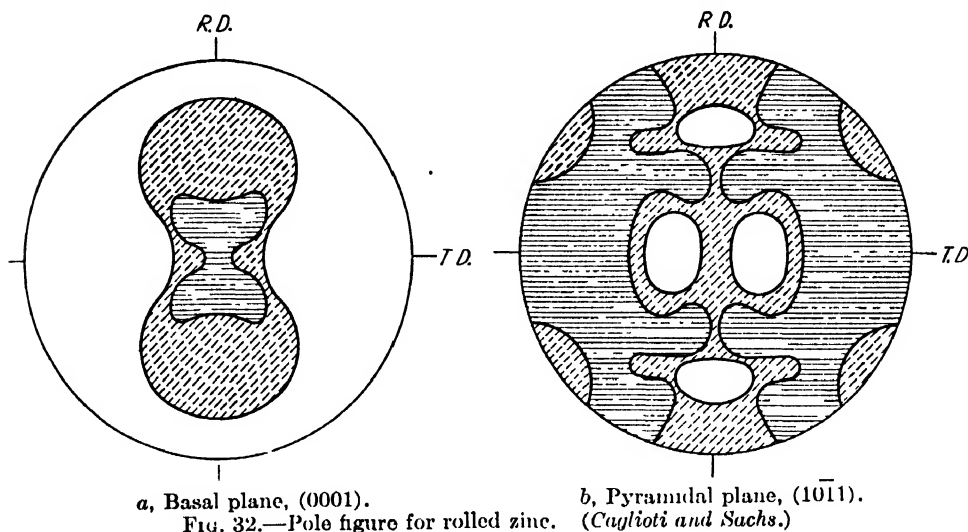


FIG. 33.—Pole figure for basal plane of a zinc alloy (1 % Cu, 0.01 % Mg). Rolling direction at center of plot. (Fuller and Edmunds.)

magnesium, Fig. 33. (In this pole figure the rolling direction appears at the center of the plot rather than the top.) A zinc alloy containing 10 percent aluminum and 0.3 percent copper gave similar results.<sup>3</sup> The

<sup>1</sup> V. CAGLIOTI and G. SACHS, *Metallwirtschaft*, vol. 11, p. 1, 1932. M. A. VALOUCH, *Metallwirtschaft*, vol. 11, p. 165, 1932.

<sup>2</sup> M. L. FULLER and G. EDMUNDS, *Trans. A.I.M.E.*, vol. 111, p. 146, 1934.

<sup>3</sup> E. SCHMID, *Z. Metallkunde*, vol. 31, p. 125, 1939. F. WOLBANK, *Z. Metallkunde*, vol. 31, p. 249, 1939.

orientations in the region *A* are developed by slip rotation; the region between *A* and *ND*, into which slip should also rotate crystals, is unpopulated. This is attributed to the action of twinning, which would carry the crystals out of this region into the equatorial zone between *B* and *TD*. Twinning into the area *B* of this zone is believed to be most frequent because this gives a reorientation conforming to the external change in dimensions of the strip during rolling. There can be no question that twinning is common during the rolling of zinc,<sup>1</sup> and the explanation of both the wire texture and the rolling texture on this basis is adequate; the dimensional changes are such as to tend to relieve the applied stresses.

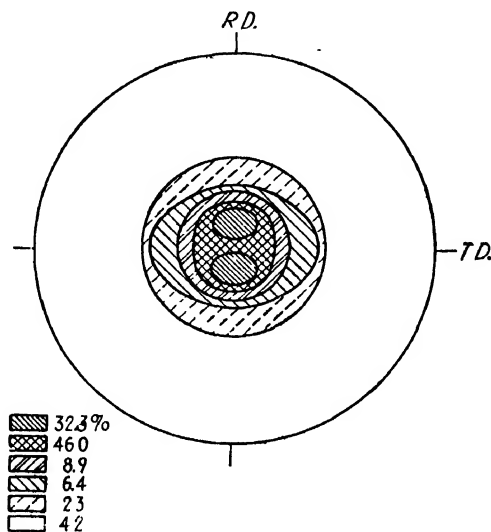


FIG. 34.—Basal-plane pole figure for rolled magnesium containing 0.20 percent calcium. Legend at left gives percentage of grains having orientations in the various shaded regions. (Bakarian.)

In extruded rods of zinc the axis of pressure is longitudinal and the effect of twinning would be to oppose this flow; accordingly, twinning is said to be absent.<sup>2</sup> Owing to the different axial ratio, twinning on (102) in magnesium leads to a lengthening in the direction of the hexagonal axis of the parent crystal. It would therefore oppose the flow in rolling and wire drawing and is not observed after these operations. However, it can be induced in sheets of rolled magnesium by bending the sheets.<sup>3</sup>

Twinning on (101) planes instead of the usual (102) has been observed in magnesium<sup>4</sup> and may possibly account for the peculiar effect of calcium

<sup>1</sup> C. H. MATHEWSON and A. J. PHILLIPS, *Trans. A.I.M.E.*, vol. 74, p. 143, 1927; vol. 78, p. 445, 1928.

<sup>2</sup> G. WASSERMANN, "Texturen metallischer Werkstoffe," Springer, Berlin, 1939.

<sup>3</sup> J. D. HANAWALT, paper presented before the A.S.T.M. meeting in Detroit, Mich., June, 1935.

<sup>4</sup> E. SCHMID, *Z. Elektrochem.*, vol. 37, p. 447, 1931.

on the pole figure of rolled magnesium.<sup>1</sup> The addition of 0.20 percent calcium to 99.98 percent magnesium breaks the central area into two maxima, Fig. 34. (This is one of the first pole figures that gives the percentage of material in each area.) A commercial alloy of 2.0 percent manganese and 0.15 percent calcium has a similar pole figure. The true cause of this double maximum will not be known until the effect of composition on twinning planes and slip planes is determined.

The rolling texture of magnesium and its alloys can be altered by changing the composition of the metal and the rolling technique, as shown by Hanawalt.<sup>2</sup> Under some conditions it is possible to produce a sheet

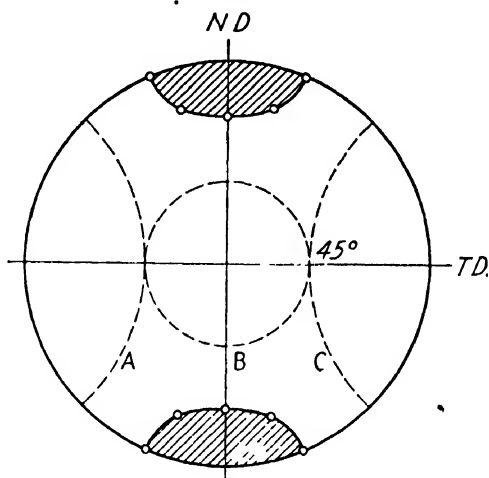


FIG. 35. Basal-plane pole figure for surface orientation of rolled zinc alloy (1 % Cu, 0.01 % Mg). Rolling direction at center of plot. Orientations having maximum shear stress for basal-plane slip are indicated by A and B for bending in two different directions in the sheet. (Fuller and Edmunds)

with almost random orientations, a condition favorable to formability. Rolling variables also alter the texture of rolled zinc and its alloys. There is a marked layer structure,<sup>3</sup> and the surface layers play an important role in determining the bending qualities of the sheet.<sup>4</sup> A typical pole figure of the surface material showing poor bending properties is shown in Fig. 35 (the rolling direction is at the center). When the texture of Fig. 35 extends to a depth of 0.0005 in. or more, strips cut in any direction in the sheet tend to fracture easily on a bend test; it is believed that this is related to the lack of material oriented so as to have the maximum resolved shear stress on the slip plane. The dashed circles A and B

<sup>1</sup> P. W. BAKARIAN, *Trans. A.I.M.E.*, vol. 147, p. 266, 1942.

<sup>2</sup> "Symposium on Radiography and X-ray Diffraction," A.S.T.M., Philadelphia, 1936.

<sup>3</sup> E. SCHMID and G. WASSERMAN, *Z. Metallkunde*, vol. 23, p. 87, 1931. G. EDMUNDS and M. L. FULLER, *Trans. A.I.M.E.*, vol. 99, p. 175, 1932.

<sup>4</sup> G. EDMUNDS and M. L. FULLER, *Trans. A.I.M.E.*, vol. 99, p. 175, 1932.

in the figure, which represent poles  $45^\circ$  to the axis of tension during bending and thus indicate planes of high shear stress, will be seen to avoid the dense areas of the pole figure.

**Cross Rolling.**—Important practical results are obtained by rolling a sheet in two directions  $90^\circ$  to each other, and various patents are concerned with the process. It will be remembered that b.c.c. metals have a rolling texture, after straight rolling, in which the cube plane is parallel to the surface and the face diagonal is in the direction of rolling,  $(100)[011]$ , with  $[01\bar{1}]$  in the cross direction, and that the scattering is almost entirely about the rolling direction. This scatter is remarkably reduced by rolling in the cross direction, leaving the orientation  $(100)[011]$  as the only important component of the texture.<sup>1</sup> The transverse direction

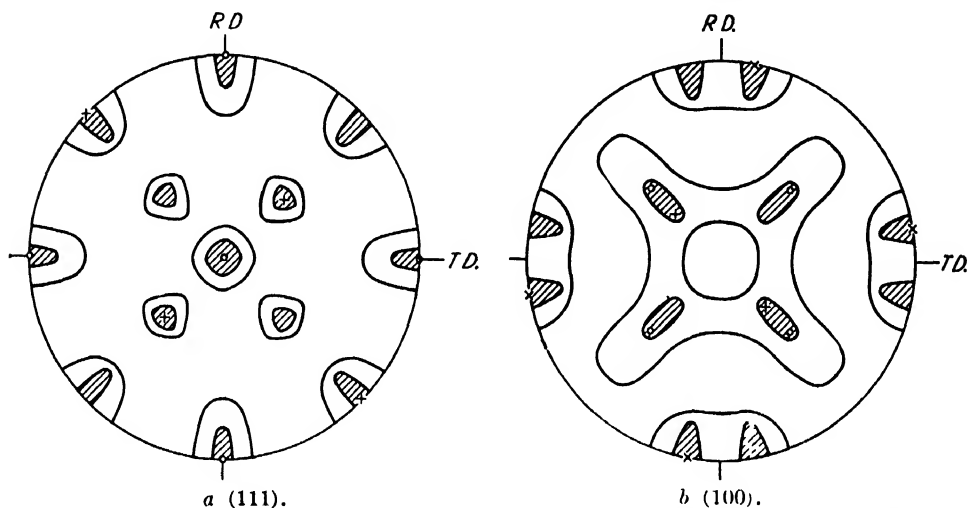


FIG. 36.—Pole figure for cross-rolled face-centered cubic non-nickel alloy. (Wassermann.)

in the sheet thus becomes similar to the longitudinal direction. The relative range of scatter around each of the two rolling directions (which are each  $[110]$  directions) is governed by the relative reductions by each kind of rolling. When only one change of rolling direction is used, the one used last has a somewhat greater influence on the texture if the percentage is more than three-fourths that of the first rolling, in which case the predominating range of scatter has the second rolling direction as the axis of scatter.<sup>2</sup> The highly preferred orientation produced by cross rolling molybdenum sheet causes marked brittleness along the cube planes, which stand  $45^\circ$  to the rolling direction.<sup>3</sup>

<sup>1</sup> C. J. SMITHELLS and C. E. RANSLEY, *J. Inst. Metals*, vol. 60, p. 172, 1937. C. E. RANSLEY and H. P. ROOKSBY, *J. Inst. Metals*, vol. 62, p. 205, 1938. G. WASSERMANN, *Z. Metallkunde*, vol. 30, Sonderheft Vorträge Hauptverslg., p. 53, 1938.

<sup>2</sup> G. WASSERMANN, *Z. Metallkunde*, vol. 30, Sonderheft Vorträge Hauptverslg., p. 53, 1938.

<sup>3</sup> C. E. RANSLEY and H. P. ROOKSBY, *J. Inst. Metals*, vol. 62, p. 205, 1938.

With f.c.c. metals, cross rolling is sometimes used commercially to reduce the directional dependence of the mechanical properties. Von Göler and Sachs<sup>1</sup> found the texture of cross-rolled copper more complex than the sum of two straight-rolling textures. Wassermann<sup>2</sup> obtained the texture of Fig. 36 by cross rolling face-centered cubic Fe-Ni sheet. The orientations in this texture are (a) (110) parallel to the sheet and  $[\bar{1}12]$   $10^\circ$  from each rolling direction, as indicated by crosses in the figure, and (b) (100)[001], indicated by small circles. The amount of strain hardening is less than with equal reductions in straight rolling, the recrystallization temperature is lower, and both deformation and recrystallization

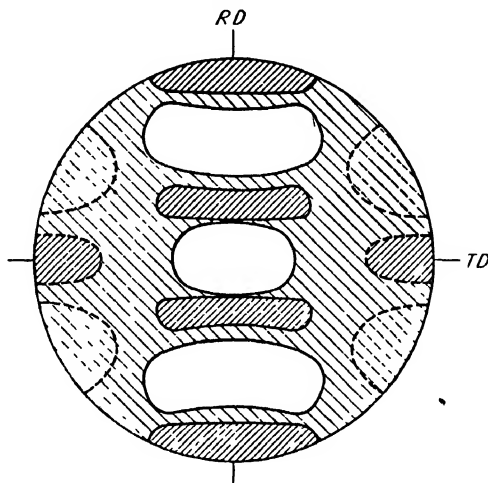


FIG. 37.—(110) pole figure for mild steel rolled 85 percent at  $780^\circ\text{C}$ . Maxima in dotted areas uncertain (Gensamer and Vukmanic.)

tallization textures are different from those encountered during straight rolling.<sup>3</sup>

**Hot Rolling.**—Hot-rolled steel is not free from preferred orientations;<sup>4</sup> in some cases, the texture is nearly the same as in cold-rolled steel. An example is seen in Fig. 37, the (110) pole figure for low-carbon steel reduced 85 percent by rolling at  $780^\circ\text{C}$ .<sup>5</sup> Since the texture is unlike the recrystallization texture for steel, it is probable that recrystallization did not occur to any considerable extent, unless a different recrystallization texture occurs under these conditions. Rolling the same material near  $910^\circ$  produces a more nearly random texture; here the transformation from  $\gamma$  to  $\alpha$  also contributes to randomness.

<sup>1</sup> F. v. GÖLER and G. SACHS, *Z. Physik*, vol. 41, p. 889, 1927.

<sup>2</sup> G. WASSERMANN, "Texturen metallischer Werkstoffe," Springer, Berlin, 1939.

<sup>3</sup> R. M. BRICK and M. A. WILLIAMSON, *Trans. A.I.M.E.*, vol. 143, p. 84, 1941.

<sup>4</sup> K. J. SIXTUS, *Physics*, vol. 6, p. 105, 1935. N. P. GOSS, *Trans. A.S.M.*, vol. 24, p. 967, 1936; *Metals & Alloys*, vol. 7, p. 131, 1936. M. GENSAMER and P. A. VUKMANIC, *Trans. A.I.M.E.* vol. 125, p. 507, 1937.

<sup>5</sup> M. GENSAMER and P. A. VUKMANIC, *Trans. A.I.M.E.*, vol. 125, p. 507, 1937.



**Torsion Textures.**—Relatively little study has been devoted to textures developed by torsional deformation. From the principle that textures are determined by the principal strains, it is likely that torsion textures are intimately related to rolling textures in the following way: The maximum elongation at any point in the wall of a twisted cylindrical rod or tube is in a direction tangential to the surface and  $45^\circ$  to the axis. This should correspond to the rolling direction of a rolled sheet. The radial direction in the torsion specimen is practically unchanged by the strain and should correspond to the transverse direction of the rolled sheet. The orientations of the torsion specimen should thus be the sum of a series of rolling textures tipped in this way and arranged around the axis.<sup>1</sup>

Ono<sup>2</sup> concluded that aluminum and copper have [111] directions parallel to the longitudinal axis of torsion specimens and that  $\alpha$ -iron has both [110] and [121] parallel to the axis. Sachs and Schiebold<sup>3</sup> concluded that the torsion texture of aluminum is a double fiber texture with [111] and [110] in the longitudinal axis. These experiments do not afford an adequate test of the theory proposed above.

**Cold-drawn Tubes.**—Norton and Hiller<sup>4</sup> showed that in the cold reduction of seamless steel tubing the texture is determined by the relative reductions of wall thickness and circumference—thus again by the magnitude of the principal strains. When only the wall thickness is reduced, the structure is identical with that of a rolled sheet, while when the wall thickness and circumference are reduced equally the texture is that of a wire. Other variables in the commercial drawing operation are without effect on the principal orientations of the tubes.

**Textures in Deep Drawing.**—Textures in deep-drawn articles can be predicted from the nature of the flow of metal, which can be specified in terms of the magnitude of the three principal strains. Hermann and Sachs<sup>5</sup> found this to be the case in drawn-brass cups, where a pole-figure analysis showed that the texture varied from point to point in accordance with the varying nature of the deformation. At the center of the bottom of the cup the texture was identical with an ordinary compression texture and was caused by the thinning of the sheet and the radial flow outward in all directions, just as in a compression test. At the upper rim of the cup, on the other hand, there was a compression texture with the compression axis tangential. This texture was caused by the shortening of the

<sup>1</sup> Unpublished research by M. Gensamer and the author.

<sup>2</sup> A. ONO, *Mem. Coll. Eng., Kyushu Imp. Univ.*, vol. 2, pp. 241, 261, 1922.

<sup>3</sup> G. SACHS and E. SCHIEBOLD, *Z. Ver. deut. Ing.* vol. 9, pp. 1557, 1601, 1925; *Naturwissenschaften*, vol. 13, p. 964, 1925.

<sup>4</sup> J. T. NORTON and R. E. HILLER, *Trans. A.I.M.E.*, vol. 99, p. 190, 1932.

<sup>5</sup> L. HERMANN and G. SACHS, *Metallwirtschaft*, vol. 13, p. 745, 1934.

circumference and the thickening of the sheet at the rim during the drawing operation. The compression texture persisted throughout the upper part of the side wall, but in the lower portions it was superimposed on a tension texture having the tension axis vertical (parallel to the axis of the cup).

An analysis of the plastic flow and orientations in a steel water pail<sup>1</sup> disclosed different conditions of strain and, of course, different textures

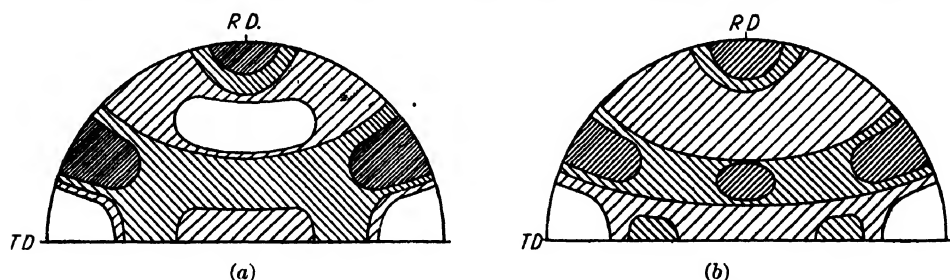


FIG. 38.—(110) pole figures for a deep-drawn steel water pail. Radial direction on the original blank is at R.D.; tangential at T.D. (a) Rim of the pail; deformation corresponds to 45 percent reduction by cold rolling. (b) Middle of wall; deformation corresponds to 30 percent reduction by cold rolling.

for the b.c.c. ferrite, but the same underlying correlation between the nature of the flow and the textures was found. Wall thicknesses were changed only a few percent by the draw. At the rim of the pail the circumference was reduced and the steel was elongated vertically along the wall of the pail (radially on the original blank) so that each element of volume was deformed as it would be in rolling a sheet, provided that one

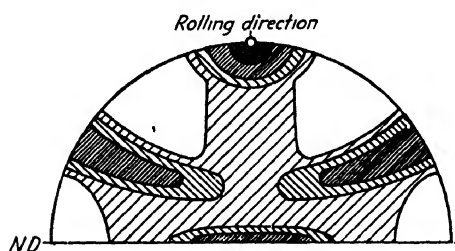


FIG. 39.—(110) pole figure for rolled steel, rotated 90° about the rolling direction for comparison with Fig. 38.

assumed the rolling direction to be radial in the blank and the rolling plane to be perpendicular to the plane of the blank. The deformation at the rim corresponded to a reduction of about 45 percent in rolling; at the middle of the wall the flow was similar and corresponded to about 30 percent reduction by rolling. Textures at these two points are shown in Fig. 38 and are, as expected, not very different from a rolling texture that has been rotated so that the transverse direction of the sheet is brought to the center of the projection, as in Fig. 39. It seems to be true generally in deep drawing that textures develop at smaller deformations than in rolling, perhaps because the flow is more homogeneous within the sheet.

**Textures from Machining and Polishing.**—The outermost layers of a steel block have a characteristic preferred orientation after machining

<sup>1</sup> Unpublished research by H. C. Arnold and the author.

in a shaper. A pole figure showing this has been plotted by Renninger<sup>1</sup> using data from back-reflection patterns. Polishing is also able to orient material near the surface. Lees,<sup>2</sup> using electron diffraction, found a very thin random layer at the surface of polished copper and gold and under this a layer in which the (110) planes were approximately parallel to the surface. The thickness of the oriented layer was of the order of 150 to 500 Å in copper, depending on the method of polishing, and was several thousand angstroms in gold.

**Summary.**—The predominant texture in cold-drawn wires of f.c.c. metals is a double fiber texture with [111] and [100] parallel to the wire axis; b.c.c. metals have a simple [110] fiber texture; hexagonal magnesium and zirconium have a [210] fiber texture, but zinc has a texture in which the hexagonal axis is about 70° from the axis of the wire.

The principal orientations after **compression** are [110] for f.c.c., [111] plus [100] for b.c.c., and [001] for hexagonal metals.

**Rolling textures** require pole figures for a full description. Principal "ideal" textures are as follows:

F.c.c., (110)[ $\bar{1}12$ ] + (112)[11 $\bar{1}$ ].

B.c.c., (100)[011].

H.c.p., (001)[100], modified in some instances by twinning.

Other kinds of deformation, as in tube drawing and deep drawing, produce orientations that depend upon the magnitude of the three principal strains during flow. Smearing of the surface of a metal during forming operations is responsible for producing orientations on the surface that differ from those in the interior.

It is thought that all textures of cubic metals can be accounted for on the basis of lattice rotation resulting from crystal slip, but the computation of what planes will slip is very difficult and has been attempted rigorously in only one instance. Simpler methods of computing these rotations have been employed with some success. Textures of the hexagonal metals are produced not only by rotation from slip but also by twinning, when twinning does not oppose the enforced change in dimensions.

Rotation of the lattice in grains of many metals is not a homogeneous rotation within each grain but is accompanied by the generation of deformation bands and less regular types of distortion so that some grains spread into the entire polycrystalline texture and only occasional ones have a small scatter in orientation.

<sup>1</sup> M. RENNINGER, *Metallwirtschaft.*, vol. 13, p. 889, 1934.

<sup>2</sup> C. S. LEES, *Trans. Faraday Soc.*, vol. 31, p. 1102, 1935.

## CHAPTER XIX

### PREFERRED ORIENTATIONS AFTER RECRYSTALLIZATION

The preferred orientations existing in deformed metals after recrystallization have been studied extensively not only because of their commercial importance but also because of the information they yield (or promise to yield) regarding the nature of the recrystallization process, particularly the laws governing the formation of submicroscopic recrystallization nuclei. Many perplexing results have come from these studies, and many results that are ambiguous when viewed in the light of later work. Our understanding of the fundamental relationships concerning these textures is fragmentary, and theories of the reasons for the results are still less satisfactory.

Three possibilities have been recognized for recrystallization textures: (1) The recrystallization texture is identical with the deformation texture (usually with a greater range of scatter). (2) The recrystallized grains have a random orientation. (3) The recrystallization texture is wholly different from the deformation texture. Most observers have concluded that a given metal can be made to recrystallize in two or three of these ways. When recrystallization occurs at a low temperature, the deformation texture is frequently retained, but an increasing tendency to become random is often noted with increasing temperatures. Unfortunately, the grain size is usually much larger with high-temperature annealing, and this makes it difficult to recognize the presence of a texture (an integrating camera is required). Some conclusions of randomness are thus uncertain; furthermore, it is possible that a texture may have existed when recrystallization was barely completed (the strained material just consumed), a texture which was subsequently modified or lost by coalescence of the new grains. Generally, a well-developed deformation texture must be obtained before a sharp recrystallization texture will develop.

It has been assumed frequently that when deformation and recrystallization textures agree each new grain has an orientation identical with the principal orientation of the strained grain in which it grows. This is not true in at least one instance, however, and perhaps is never true.<sup>1</sup>

When deformation and recrystallization textures do not agree, it is often possible to find minor amounts of material in the *strained* metal that

<sup>1</sup> C. S. BARRETT, *Trans. A.I.M.E.*, vol. 137, p. 128, 1940.

have the orientation of the *recrystallized* metal. From such experiments one would like to conclude that this deformed material furnishes the nuclei of the recrystallization texture. But the actual nuclei must constitute so small a portion ( $10^{-7}$  to  $10^{-10}$ ) of the total volume as to be invisible on any diffraction pattern; there must be ample material in any orientation whatever to provide these nuclei, and therefore such correlations between deformation and recrystallization textures are of doubtful significance.

Recrystallization textures are influenced to a greater or less extent by purity, alloy composition, degree of cold rolling preceding recrystallization, annealing temperature, original texture before cold rolling, intermediate anneals during cold rolling, rolling direction (straight vs. cross rolling), and initial grain size. Possibly these influences act in some way through their effect on the internal strain in the recrystallization nuclei, with the most severely strained points being the first to recrystallize, or possibly the rates of growth of these nuclei depend on the orientation and state of strain of the adjoining material. The shifting of atoms from the strained matrix to the new grain may proceed slowly if the new grain has the orientation of the matrix and most rapidly if the orientation differs in a certain way.

Owing to the uncertain state of recrystallization-texture theory at this time, the following summary deals mainly with experimental results.

**Recrystallized Face-centered Cubic Fiber Textures.**—Textures in **aluminum wires** after recrystallization have been found as follows:

1. No alteration of the deformation texture, which is [111], with recrystallization below  $500^{\circ}\text{C}.$ <sup>1</sup>
2. Increasing randomness with recrystallization above about  $500^{\circ}\text{C}.$ ,<sup>2</sup> particularly with wires of lower purity.<sup>3</sup>
3. A new texture, [112], in 99.95 percent aluminum recrystallized at  $600^{\circ}\text{C}.$ <sup>4</sup>
4. A sharpening of the old texture in 99.95 percent wire recrystallized at  $600^{\circ}\text{C}.$ <sup>5</sup> (perhaps merely a less pronounced zonal effect in the smaller diameter wire).

In **copper wires**, in which the deformation texture is [111] strong, [100] weak, various results have been reported as follows:

<sup>1</sup> E. SCHMID and G. WASSERMANN, *Z. tech. Physik*, vol. 9, p. 106, 1928. G. GREENWOOD, *Z. Krist.*, vol. 80, p. 481, 1931. G. SACHS and E. SCHIEBOLD, *Z. Metallkunde*, vol. 17, p. 400, 1925. F. V. GOLER and G. SACHS, *Z. Metallkunde*, vol. 19, p. 90, 1927. Unpublished experiments in the author's laboratory.

<sup>2</sup> G. SACHS and E. SCHIEBOLD, *Z. Metallkunde*, vol. 17, p. 400, 1925.

<sup>3</sup> E. SCHMID and G. WASSERMANN, *Z. tech. Physik*, vol. 9, p. 106, 1928. F. V. GOLER and G. SACHS, *Z. Metallkunde*, vol. 19, p. 90, 1927.

<sup>4</sup> E. SCHMID and G. WASSERMANN, *Z. Physik*, vol. 40, p. 451, 1926.

<sup>5</sup> E. SCHMID and G. WASSERMANN, *Z. tech. Physik*, vol. 9, p. 106, 1928.

1. No change in texture with recrystallization at or below 1000°C.<sup>1</sup>
2. A new texture, [112], after recrystallization at 1000°C.<sup>1</sup>
3. Retention of old texture in oxygen-free high-conductivity copper (99.996 percent) recrystallized at 300 and 500°C.; retention of [111] component, with [100] component uncertain or absent, at 1000°C.<sup>2</sup>
4. Incompletely identified change in texture with recrystallization near 800°C.<sup>3</sup>
5. Increase of the [100] and random components at the expense of the [111] components with annealing at 130°C. (varied in degree by change in silver content and amount of reduction).<sup>4</sup>

In 70-30 **brass wires** having a deformation texture with a [111] component strong and a [100] component weak, the deformation texture is retained with recrystallization at 360 and 800°C. (but the presence of the [100] component is uncertain at 800° owing to the large grains).<sup>2</sup> In wires of **lead** containing 2 percent antimony the deformation texture, [111], is retained upon recrystallization at room temperature.<sup>5</sup> In wires of an **Fe-Ni alloy** (53 atomic percent iron) a [100] texture resulted from annealing at 1100°C.<sup>6</sup>

**Compression** specimens of **aluminum** retain their deformation texture upon recrystallization at 400 to 440°C.<sup>7</sup> and at 600°C.<sup>8</sup> Pole figures showing the distribution of the axis of compression before and after recrystallization are shown in Figs. 1 and 2 for 99.97 percent aluminum compressed 98 percent by compression rolling.<sup>7</sup> Although the texture of the aggregate is almost unchanged, individual areas alter their orientation. This can be seen by partly recrystallizing large grains and etching to bring out the difference between the new grains and the strained matrix, as in Fig. 3. Figure 4 shows the orientation history of a crystal that started as a single crystal at the orientation marked by a cross. It was deformed with the production of deformation bands having orientations marked with open circles and finally was recrystallized into still other orientations, which are indicated with black circles tied to the deformation orientations of the corresponding areas.

The laws governing alterations in orientation of individual regions during recrystallization are not understood. Burgers and Louwerse<sup>8</sup> have proposed that the nuclei of recrystallization are tiny rotated fragments at the boundaries of slip planes, which are highly strained and unstable, and

<sup>1</sup> E. SCHMID and G. WASSERMANN, *Z. Physik*, vol. 40, p. 451, 1926.

<sup>2</sup> Unpublished work on experiments in the author's laboratory.

<sup>3</sup> G. TAMMANN and H. MEYER, *Z. Metallkunde*, vol. 18, p. 176, 1926.

<sup>4</sup> G. S. FARNAM and H. O'NEIL, *J. Inst. Metals*, vol. 55, p. 201, 1934.

<sup>5</sup> W. HOFFMANN, *Z. Metallkunde*, vol. 29, p. 266, 1937.

<sup>6</sup> W. G. BURGERS and F. M. JACOBS, *Metallwirtschaft.*, vol. 15, p. 1063, 1936.

<sup>7</sup> C. S. BARRETT, *Trans. A.I.M.E.*, vol. 137, p. 128, 1940.

<sup>8</sup> W. G. BURGERS and P. C. LOUWERSE, *Z. Physik*, vol. 67, p. 605, 1931.

have presented experimental data they thought supported this view. They were not able to find x-ray evidence of fragments actually having the required orientations, however, and were extrapolating a range that extended from the original orientation less than one-third of the way

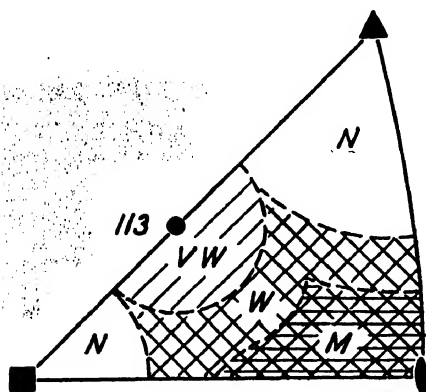


FIG. 1.

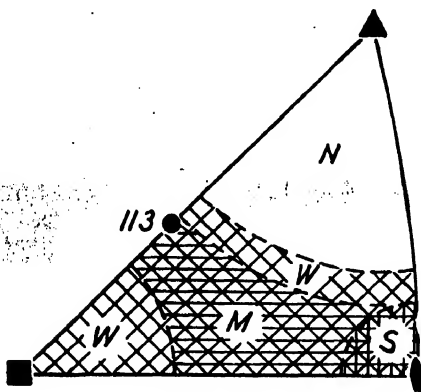


FIG. 2.

FIG. 1.—Orientations in aluminum compression-rolled 98 percent. Orientations of compression axis indicated by shading within a standard stereographic-projection triangle. Concentrations of orientations, deduced from intensities of x-ray lines, are labeled strong, medium, weak, very weak, or none (*S*, *M*, *W*, *VW*, *N*).

FIG. 2.—Orientations after recrystallization at 400°C. in specimen of Fig. 1. X-ray determination; only minor differences exist between deformation and recrystallization textures.

to the recrystallized orientation. Furthermore, the extrapolation was based on the distribution of orientations postulated in the "local-curvature theory," which is open to question.<sup>1</sup> It does not appear possible to account for the recrystallization orientations in compressed aluminum by

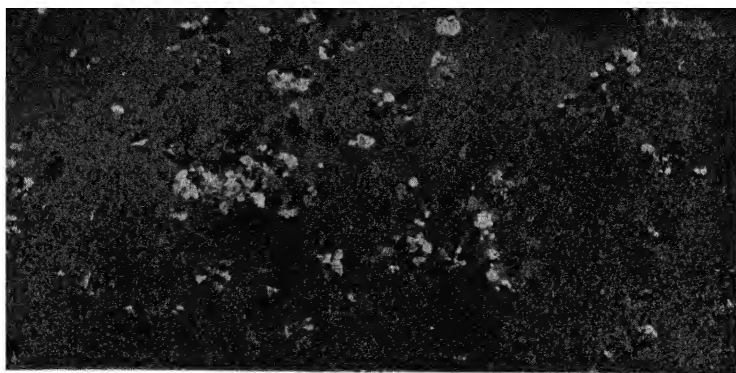


FIG. 3.—Partly recrystallized aluminum grain showing new orientations; etched to develop cubic etch pits.  $\times 6$ .

assuming that *twins* of the principal deformation texture form the nuclei for recrystallization.<sup>2</sup>

<sup>1</sup> See discussion of this theory on p. 359.

<sup>2</sup> C. S. BARRETT, *Trans. A.I.M.E.*, vol. 137, p. 128, 1940.

**Recrystallized Body-centered Cubic Fiber Textures.**—Wires of tungsten and molybdenum retain their deformation texture, [110], after recrystallization, at least when recrystallized at low temperatures;<sup>1</sup> a [100] texture has also been reported in molybdenum<sup>2</sup> and in Fe-Ni (53 atomic percent nickel).<sup>3</sup> Iron wires (hydrogen-purified low-carbon mild steel) as well as wires of ferrite containing 1.95 percent vanadium or 1.95 percent silicon retain their texture upon recrystallization at 580 and 800°C.<sup>4</sup> Steel wires behave in a similar fashion.<sup>5</sup>

Iron wires that have been swaged or rolled to an approximately square cross section have textures no different from round drawn wires either before or after recrystallization;<sup>4</sup> so presumably the symmetry of flow of the metal and not the manner of deformation governs recrystallization textures, just as it does deformation textures.

**Compression** specimens of iron (hydrogen-purified mild steel, also Armeo iron) retain the major component, [111], but appear to lose the minor component, [100], upon recrystallization at 580 and 850°C.<sup>4</sup>

**Face-centered Cubic Rolling Recrystallization Textures.**—Glocker made the first extended study of recrystallization textures when he studied rolled silver. The deformation texture, which could be described as one in which a (110) plane is parallel to the rolling plane, and a  $[\bar{1}12]$  direction is parallel to the rolling direction, i.e., (110)[ $\bar{1}12$ ], went over to the texture (113)[ $2\bar{1}1$ ] upon annealing at low temperatures but became random when annealed above 800°C.<sup>6</sup> The (113)[ $2\bar{1}1$ ] texture is obtained not only with silver but also with brass (33 to 39% Zn), bronze (5% Sn), 99% Ag-1% Zn, and Au-Ag alloys with

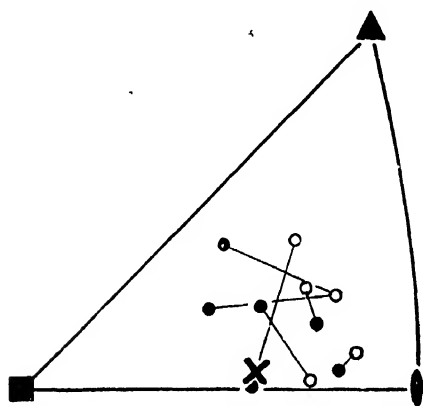


FIG. 4.—Orientations of individual areas of an aluminum crystal before and after recrystallization. Initial orientation shown by a cross, deformed areas by open circles, and recrystallized areas by black circles. Every area altered its orientation.

to the rolling plane, and a  $[\bar{1}12]$  direction is parallel to the rolling direction, i.e., (110)[ $\bar{1}12$ ], went over to the texture (113)[ $2\bar{1}1$ ] upon annealing at low temperatures but became random when annealed above 800°C.<sup>6</sup> The (113)[ $2\bar{1}1$ ] texture is obtained not only with silver but also with brass (33 to 39% Zn), bronze (5% Sn), 99% Ag-1% Zn, and Au-Ag alloys with

<sup>1</sup> Z. JEFFRIES, *Trans. A.I.M.E.*, vol. 70, p. 303, 1924. T. FUJIWARA, *Proc. World Eng. Congr., Tokyo, 1929*, pt. 4, vol. 36, p. 171, 1931.

<sup>2</sup> T. FUJIWARA, *Proc. World Eng. Congr., Tokyo, 1929*, pt. 4, vol. 36, p. 171, 1931.

<sup>3</sup> W. G. BURGERS and F. M. JACOBS, *Metallwirtschaft.*, vol. 15, p. 1063, 1936.

<sup>4</sup> Unpublished experiments in the author's laboratory.

<sup>5</sup> N. P. GOSS, *Trans. A.S.S.T.*, vol. 16, p. 405, 1929.

<sup>6</sup> R. GLOCKER, *Z. Physik*, vol. 31, p. 386, 1925. R. GLOCKER and E. KAUPP, *Z. Metallkunde*, vol. 16, p. 377, 1924. R. GLOCKER, E. KAUPP, and H. WIDMANN, *Z. Metallkunde*, vol. 17, p. 353, 1925. H. WIDMANN, *Z. Physik*, vol. 45, p. 200, 1927.



more than 70% Ag.<sup>1</sup> It also occurs in Cu-Be and Cu-Al alloys<sup>2</sup> (admixed with a (100)[001] texture in 99% Cu-1% Al).

The pole figures for this common texture, as it occurs in brass (15 percent zinc), have been plotted by v. Goler and Sachs and have been confirmed by Bass and Glocker<sup>3</sup> and by Brick, who obtained the results shown in Fig. 5 for 70-30 brass.<sup>4</sup> It will be noted that the (113)[ $\bar{2}11$ ] orientation, indicated by triangles and squares on these pole figures, is a close approximation to the maxima, when reproduced in all the symmetrical positions of the texture. According to v. Goler and Sachs, an

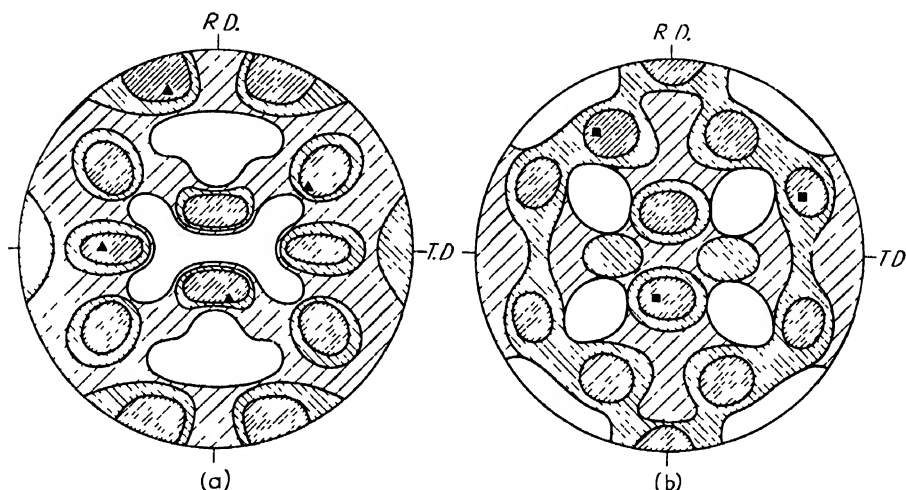


FIG. 5.—Recrystallization texture of brass reduced 99 percent by rolling, annealed at 400°C. (a) (111) pole figure; triangles show one (113)[ $\bar{2}11$ ] orientation. (b) (100) pole figure, squares show one (113)[ $\bar{2}11$ ] orientation.

orientation rotated 10° from this orientation is a somewhat more accurate description of the texture.<sup>1</sup>

**The Cube Texture.**—The most striking recrystallization texture known is the famous “cube texture,” (100)[001], which can be produced in many f.c.c. metals and alloys under certain conditions. In this texture the precision with which the cube axes are aligned with the rolling direction, the transverse direction, and the normal direction of the sheet is remarkable, as will be seen from Fig. 6. It is naturally of commercial importance, since it produces marked anisotropy in the physical properties, and it is a scientific curiosity of the first order. It is readily recognized even without x-rays, by the uniform sheen, resembling a single

<sup>1</sup> F. v. GOLER and G. SACHS, *Z. Physik*, vol. 56, p. 485, 1929.

<sup>2</sup> O. DAHL and F. PAWLEK, *Z. Metallkunde*, vol. 28, p. 266, 1936.

<sup>3</sup> A. BASS and R. GLOCKER, *Z. Metallkunde*, vol. 20, p. 179, 1928.

<sup>4</sup> R. M. BRICK, *Trans. A.I.M.E.*, vol. 137, p. 193, 1940. R. M. BRICK and M. A. WILLIAMSON, *Trans. A.I.M.E.*, vol. 143, p. 84, 1941.

crystal, that is seen after etching, or by an analysis of the direction of twin bands in the grains.

The cube texture has been obtained only in certain f.c.c. metals and alloys: Cu,\* Fe-Ni alloys containing 30 to 100 percent nickel,† Au,‡ Al,§ Cu-Zn containing up to 1 percent zinc,<sup>1</sup> Cu-Al with 0.2 percent aluminum,<sup>1</sup> Cu-Cd with 0.1 percent cadmium,<sup>1</sup> Cu containing 0.1 percent

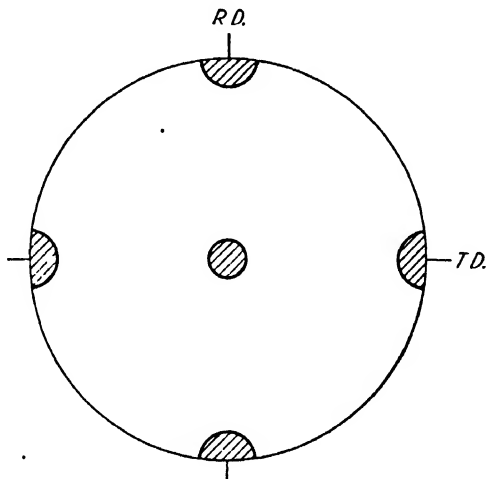


FIG. 6.—The cube texture in Fe-Ni sheet (50 % Ni); (100) pole figure. (Burgers and Snoek.)

oxygen,<sup>1</sup> Ni, Ni-Mn with 1 percent manganese,<sup>2</sup> and some ternary alloys of Fe, Ni, and Cu.<sup>3</sup> A well developed deformation texture must be obtained before recrystallization will give the cube texture; this requires

\* W. KÖSTER, *Z. Metallkunde*, vol. 18, p. 112, 1926. G. TAMMANN and H. MEYER, *Z. Metallkunde*, vol. 18, 176, 1926. G. SACHS, *Z. Ver. deut. Ing.*, vol. 70, p. 1634, 1926. F. v. GÖLER and G. SACHS, *Z. Physik*, vol. 41, p. 889, 1927. R. GLOCKER and H. WIDMANN, *Z. Metallkunde*, vol. 19, p. 41, 1927. H. WIDMANN, *Z. Physik*, vol. 45, p. 200, 1927. W. FAHRENHORST, K. MATTHAES, and E. SCHMID, *Z. Ver. deut. Ing.*, vol. 76, p. 797, 1932. O. DAHL and F. PAWLEK, *Z. Metallkunde*, vol. 28, p. 266, 1936. M. COOK and T. L. RICHARDS, *J. Inst. Metals*, vol. 66, p. 1, 1940. W. H. BALDWIN, *Metals Tech., Tech. Pub.* 1455, April, 1942.

† O. DAHL and F. PAWLEK, *Z. Metallkunde*, vol. 28, pp. 266, 230, 1936. F. PAWLEK, *Z. Metallkunde*, vol. 27, p. 160, 1935. O. DAHL and F. PAWLEK, *Z. Physik*, vol. 94, p. 504, 1935. W. G. BURGERS and J. L. SNOEK, *Z. Metallkunde*, vol. 27, p. 158, 1935. G. SACHS and J. SPRETNAC, *Trans. A.I.M.E.*, vol. 140, p. 359, 1940. H. G. MÜLLER, *Z. Metallkunde*, vol. 31, p. 322, 1939. G. WASSERMANN, *Z. Metallkunde*, vol. 28, p. 262, 1936.

‡ F. v. GÖLER and G. SACHS, *Z. Physik*, vol. 56, p. 485, 1929.

§ E. SCHMID and G. WASSERMANN, *Metallwirtschaft.*, vol. 10, p. 409, 1931.

<sup>1</sup> O. DAHL and F. PAWLEK, *Z. Metallkunde*, vol. 28, p. 266, 1936.

<sup>2</sup> O. DAHL and F. PAWLEK, *Z. Physik*, vol. 94, p. 504, 1935. F. v. GÖLER and G. SACHS, *Z. Physik*, vol. 56, p. 485, 1929.

<sup>3</sup> W. G. BURGERS and J. L. SNOEK, *Z. Metallkunde*, vol. 27, p. 158, 1935. H. G. MÜLLER, *Z. Metallkunde*, vol. 31, p. 322, 1939.

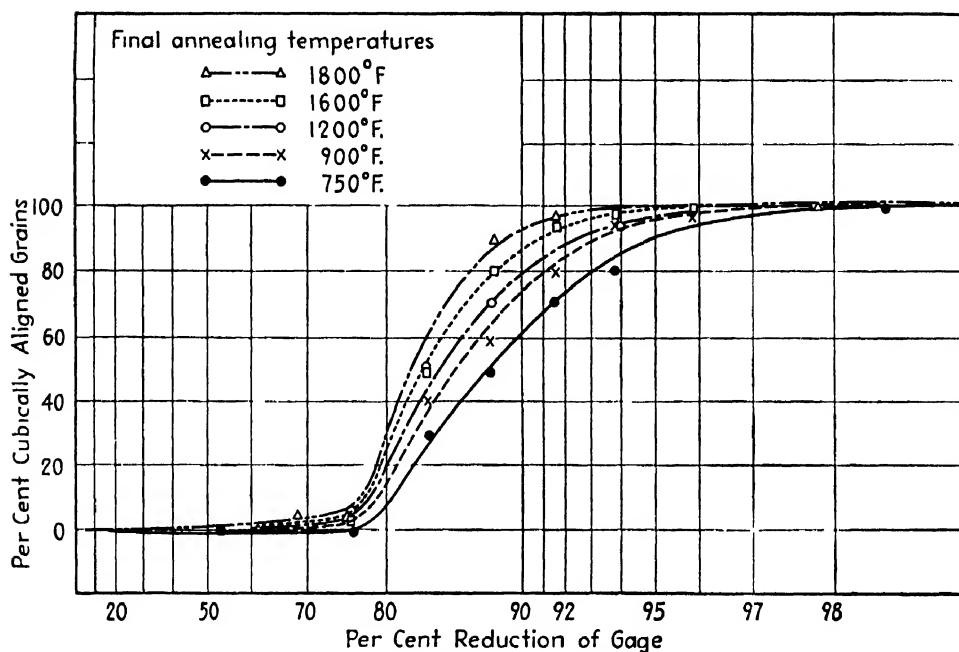


FIG. 7.—Variation of percentage of cubically aligned grains with amount of previous cold rolling. Starting material is hot-rolled copper (99.96 % Cu), 0.512-in. gauge. (Baldwin.)

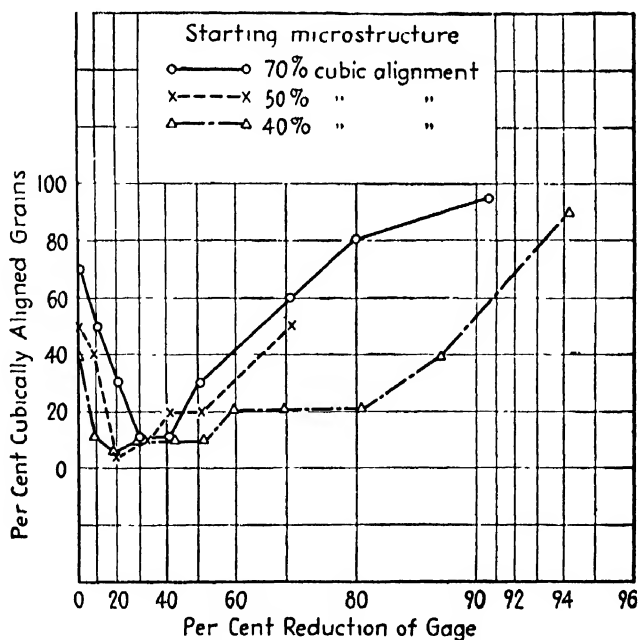


FIG. 8.—Percentage of cubically aligned grains after annealing versus cold reduction before annealing for copper having initially different percentages of grains in cubic alignment. Ready-to-finish anneal, 1200°F.; final anneal, 1200°F. (Baldwin.)

80 to 95 percent reduction. Baldwin<sup>1</sup> shows the relation between the percentage of reduction and the percentage of cubically aligned grains as in Fig. 7 for a strip that had been previously hot-rolled. Figure 8 illustrates the same relation for strips in which the cube texture had previously been developed. From the numerous studies of this texture it is clear that the following factors are effective in reducing and eliminating directionality caused by the presence of this texture:

1. Small cold reduction (roughly 50 percent or less) with intermediate anneals.
2. A final anneal at a low temperature.
3. Minor additions of certain alloying elements<sup>2</sup> (discussed below).

The cube texture is often, though not always, associated with a

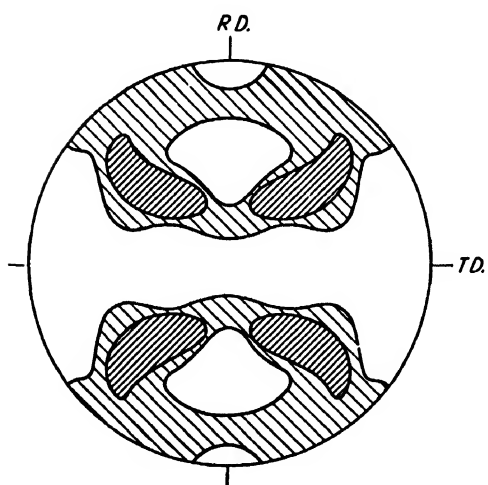


FIG. 9.—Octahedral pole figure for copper, initially having a complete cube texture, after 53.5 percent reduction. (Baldwin.)

tendency for the recrystallized grains to coalesce into extremely large grains. This is especially common when annealing temperatures are high<sup>3</sup> or when a sheet with a fully developed cube texture is reduced about 22 percent and again annealed.<sup>1</sup>

Extensive studies have been made of the effect of mill variables on the textures and grain sizes produced in copper and its alloys.<sup>4</sup> These are discussed further in Chap. XXI.

The transition from the cube texture to the ordinary deformation texture during rolling is worthy of study. A copper strip containing a fully developed cube texture acquired the texture of Fig. 9 after 53.5 percent reduction by cold rolling and acquired the normal rolling texture after 91 percent reduction.<sup>1</sup> Upon the final rolling texture, indicated in Fig. 10 by the outlined areas, is superimposed a set of paths along which Baldwin suggests that the individual poles have migrated from position

<sup>1</sup> W. H. BALDWIN, *Metals Tech., Tech. Pub.* 1455, April, 1942.

<sup>2</sup> H. WIDMANN, *Z. Physik*, vol. 45, p. 200, 1927.

<sup>3</sup> O. DAHL and F. PAWLEK, *Z. Metallkunde*, vol. 28, p. 266, 1936. F. PAWLEK, *Z. Metallkunde*, vol. 27, p. 160, 1935. M. COOK and C. MACQUARIE, *Trans. A.I.M.E.*, vol. 133, p. 142, 1939.

<sup>4</sup> O. DAHL and F. PAWLEK, *Z. Metallkunde*, vol. 28, p. 266, 1936. W. H. BALDWIN, *Metals Tech., Tech. Pub.* 1455, April, 1942.

1 to position 6.<sup>1</sup> (The path was drawn by Baldwin in accord with Boas and Schmid's theory of rotation during deformation by compression<sup>2</sup>.) It is interesting that when strips such as these are again annealed the resulting orientations appear to fall at points along these paths. For example, after the cube texture has been rolled 22 percent, recrystallization produces grains with an orientation between positions 3 and 4 on this path, as if those particles which have rotated to the most advanced positions along the path serve as recrystallization nuclei. Similarly, in the same strip rolled 91 percent the most advanced rotations have reached position 6 and the annealed metal is composed of grains of this orientation, which is (110)[ $\bar{1}12$ ].

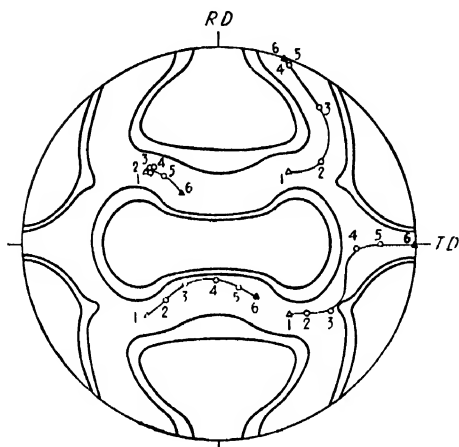


FIG. 10.—Suggested path of rotation of a cubically aligned grain during cold rolling, superimposed upon outline of final texture; (111) pole figure. (Baldwin.)

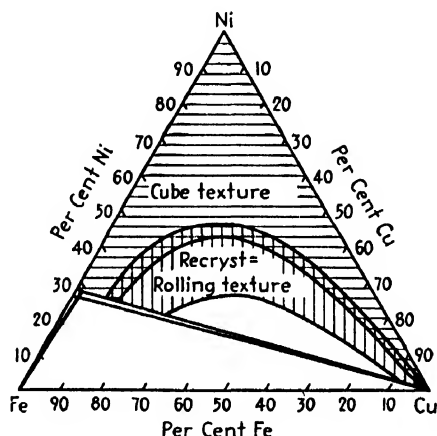


FIG. 11.—Recrystallization textures in Fe-Ni-Cu alloys. (Muller.)

Many **alloying additions** permit the cube texture to form (see list, page 426) but others inhibit it;<sup>3</sup> for instance, any of the following additions in weight percent to copper prevent the texture: 5% Zn, 1% Sn, 4% Al, 0.5% Be, 0.5% Cd, or 0.05% P. Arsenic added to copper also suppresses the texture.<sup>4</sup> These additions produce a (113)[ $\bar{2}11$ ] texture instead of the cube texture, with a few exceptions where the deformation texture is retained—for example, 0.5 percent cadmium—or produce a

<sup>1</sup> A single crystal of copper, initially in the (100)[001] position, when rolled 98.1 percent also spread into a nearly complete polycrystalline texture in which the most intense regions were complementary (135)[ $\bar{2}11$ ] positions, which were not far from position 6 of this figure. (C. S. Barrett and F. W. Steadman, *Metals Tech., Tech. Pub.* 1430, February, 1942.)

<sup>2</sup> W. BOAS and E. SCHMID, *Z. tech. Physik*, vol. 12, p. 71, 1931. See discussion on p. 387.

<sup>3</sup> O. DAHL and F. PAWLEK, *Z. Metallkunde*, vol. 28, p. 266, 1936.

<sup>4</sup> F. v. GÜLER and G. SACHS, *Z. Physik*, vol. 56, p. 485, 1929.

random texture when the reduction is by cold rolling and is less than about 90 percent.

Müller<sup>1</sup> found cube textures in Fe-Ni-Cu alloys at the compositions indicated in Fig. 11 by the horizontal shading. The compositions covered by the vertical shading retained the rolling texture during recrystallization, and the region of overlap could be made to produce either texture with proper control of temperature.

Brick, Martin, and Angier<sup>2</sup> have recently made a systematic study of the deformation and recrystallization textures in a series of copper alloys and have established two important generalizations applying to alloys that have been given high reductions and low-temperature anneals: (1)

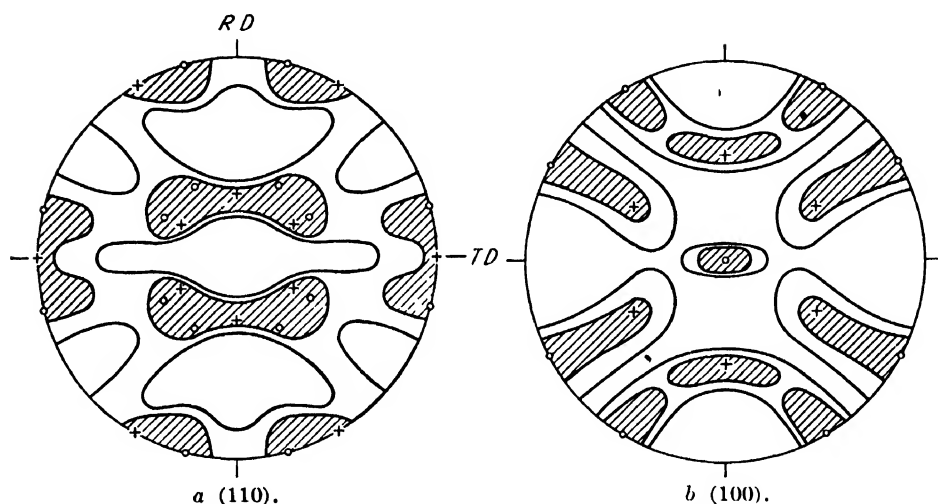


FIG. 12.—Recrystallization texture of rolled iron. (O) position near (100)[011], (+) (111) [112] position. (Kurdjumow and Sachs)

The *recrystallization texture* of copper is changed by smaller additions of alloying elements than the additions required to change the *deformation texture*. (2) Solute elements that have the more marked *solution-hardening effect* on copper seem to generate the more *complex recrystallization textures*—those more closely approximating a random distribution of orientations.

The results of this study show that in the Cu-Zn system the rolling texture changes from the copper to the brass type at about 5 atomic percent zinc, with a transition type appearing near 1 percent zinc. In alloys of copper with Mn, Al, As, Sb, Si, Mg, Sn, and Cu-Ni-Zn (“nickel silver”) the texture changes similarly to the rolling texture of brass; but in the systems Cu-Ni and Cu-Co only the copper rolling texture was observed. Upon recrystallization at temperatures between 425 and

<sup>1</sup> H. G. MÜLLER, *Z. Metallkunde*, vol. 31, p. 322, 1939.

<sup>2</sup> R. M. BRICK, D. L. MARTIN, and R. P. ANGIER, *A.S.M. Preprint* 37, 1942.

550°C. the recrystallization textures were found to have many variations. Complex textures approximating near randomness were induced by additions of 0.3 atomic percent Sb, 1.2 atomic percent Sn, 1.5 atomic percent Mg, and 4.2 and 5.4 atomic percent Ni. These elements (with the exception of nickel) are the ones that differ most markedly from copper in atomic radii and in the solution hardening effect in copper.<sup>1</sup> The nickel alloys, which had deformation textures like copper, took up a brasslike annealing texture at about 5 atomic percent. Other alloys also exhibited a change in the recrystallization texture at lower compositions than the change in deformation texture, *viz.*, the alloys containing Zn, Mn, and Al.

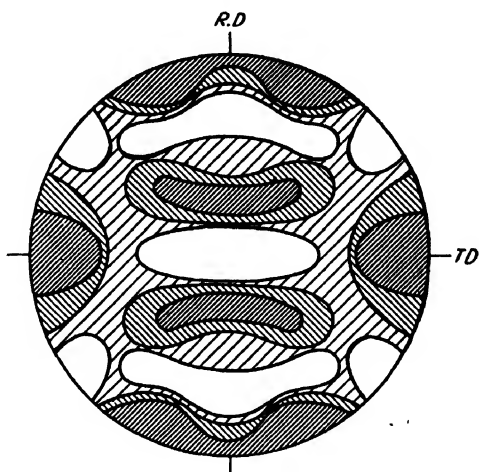


FIG. 13.—(110) pole figure for mild-steel sheet recrystallized at 580°C. (Gensamer and Lustman.)

**Body-centered Cubic Rolling Recrystallization Textures.**—The important texture in recrystallized iron and steel was first fully analyzed by Kurdjumow and Sachs.<sup>2</sup> Their pole figures are reproduced in Fig. 12. The principal orientations were identified as follows: (1) rolling plane (100), rolling direction 15° from [011]; (2) rolling plane (111), rolling direction [112]; and (3) rolling plane (112), rolling direction 15° from [110]. A comparison of other results with these is given in Table XXII. Pole figures for mild steel recrystallized at 580°C.<sup>3</sup> and for an Fe-Si alloy<sup>4</sup> are also shown (Figs. 13 and 14). The general features are similar; the recrystallization texture resembles the deformation texture rotated 15° in each direction around the sheet

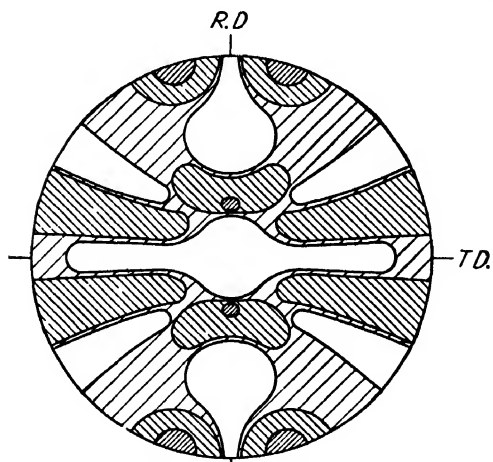


FIG. 14.—(110) pole figure for silicon-steel sheet (Fe-4.61% Si) recrystallized at 590°C. (originally cold-rolled 95 percent).

<sup>1</sup> The curve of relative hardening is given on p. 328.

<sup>2</sup> G. KURDJUMOW and G. SACHS, *Z. Physik*, vol. 62, p. 592, 1930.

<sup>3</sup> M. GENSAMER and B. LUSTMAN, *Trans. A.I.M.E.*, vol. 125, p. 501, 1937.

<sup>4</sup> C. S. BARRETT, G. ANSEL, and R. F. MEHL, *Trans. A.I.M.E.*, vol. 125, p. 516, 1937.

normal. The appearance of a diffraction pattern made with the beam perpendicular to a sheet having this texture is shown in Fig. 15.

TABLE XXII.—BODY-CENTERED CUBIC RECRYSTALLIZATION TEXTURES

Material	Recrys- tallization temper- ature, degrees centigrade	Recrystallization texture		Investigator	Method
		Roll- ing plane	Rolling direction		
Iron	Above 600	(100)	~15° from [011]	Glocker <sup>3</sup>	x-ray
Electrolytic iron and mild steel.	550 to 840	(100) (111) (112)	~15° from [011] [112] ~15° from [110]	Kurdjumow and Sachs <sup>1</sup>	x-ray, pole figure
Mild steel	650 580	Similar to ref. 1 Slightly different from ref. 1		Gensamer and Lustman <sup>2</sup>	x-ray, pole figure
Fe + 3.05% Si	1100*	(100) (110)	[001] [001]	Sixtus <sup>4</sup>	Optical (etch pits)
Fe + 3.50% Si. . .	1093*	(110)	[001]	Bozorth <sup>5</sup>	x-ray
Fe + 2.07% Si. . .	580	Similar to ref. 1		Barrett, Ansel, and Mehl <sup>6</sup>	x-ray, pole figure
Fe + 4.61% Si . .	590	Similar to ref. 1			
Fe + 4.61% Si . . .	860	Slightly different from refs. 1 and 2		Burwell <sup>7</sup>	x-ray, pole figure
Fe + 4.61% Si. . . .	1093				
Fe + 3.1% Si. . . . .	~1100*	(110)	[001]		

\* With intermediate anneal (see N. P. Goss, *Trans. A.S.M.*, vol. 23, p. 511, 1935; U.S. Patent 1965539.

<sup>1</sup> G. KURDJUMOW and G. SACHS, *Z. Physik*, vol. 62, p. 592, 1930.

<sup>2</sup> M. GENSAMER and B. LUSTMAN, *Trans. A.I.M.E.*, vol. 125, p. 501, 1937.

<sup>3</sup> R. GLOCKER, "Materialprüfung mit Röntgenstrahlen," p. 338, Springer, Berlin, 1927.

<sup>4</sup> K. J. SIXTUS, *Physics*, vol. 6, p. 105, 1935.

<sup>5</sup> R. M. BOZORTH, *Trans. A.S.M.*, vol. 23, p. 1107, 1935.

<sup>6</sup> C. S. BARRETT, G. ANSEL, and R. F. MEHL, *Trans. A.I.M.E.*, vol. 125, p. 516, 1937.

<sup>7</sup> J. T. BURWELL, *Trans. A.I.M.E.*, vol. 140, p. 353, 1940.

Recrystallization textures are sensitive to the schedule of rolling and intermediate annealing. The control of all such variables in the manufacture of steel sheet is of great importance, and much attention is devoted to the problem in plant laboratories. Published research represents but a fraction of the total knowledge of the subject. Goss,<sup>1</sup> using cycles of cold reduction followed by recrystallization, has produced a (110)[001] texture, which possesses high permeability in the rolling direction.<sup>2</sup> Frey and Bitter<sup>3</sup> find that each cycle of cold reduction followed by recrystallization

<sup>1</sup> N. P. Goss, *Trans. A.S.M.*, vol. 23, p. 511, 1935; U.S. Patent 1965539.

<sup>2</sup> R. M. BOZORTH, *Trans. A.S.M.*, vol. 23, p. 1107, 1935. J. T. BURWELL, *Trans. A.I.M.E.*, vol. 140, p. 353, 1940.

<sup>3</sup> A. A. FREY and F. BITTER, U.S. Patent 2112084.



serves to increase the percentage of crystals having the (110)[001] position and to decrease the percentage having the (100)[011] position. A marked improvement in silicon steel for transformer cores has been made in recent years by improving the magnetic permeability in the rolling direction through control of orientation.<sup>1</sup>

**Cross rolling** decreases the scatter in orientation about the rolling direction in the deformation texture of steel and other b.c.c. metals (see page 415). Use is made of this fact to produce desirable orientations in commercial sheet by a method due to Bitter.<sup>2</sup> By careful annealing following controlled rolling in both the longitudinal and transverse directions the deformation texture is maintained, giving a sheet in which the cube plane is parallel to the rolling plane and the [110] directions are

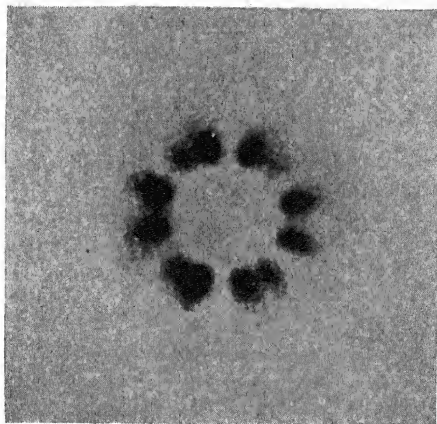


FIG. 15.—Pattern for recrystallized steel sheet, beam normal to the sheet (same sample as for Fig. 14).

parallel to each rolling direction. The direction of easiest magnetization, [100], is then at  $45^\circ$  to the rolling direction.

When steel is heated into the austenite range, the transformation to austenite and the reverse transformation to ferrite produce a random or nearly random texture, because of the multiplicity of orientations that results from a single orientation in the preceding phase.

**Hexagonal Close-packed Rolling Recrystallization Textures.**—Hexagonal metals seem to retain their rolling texture upon recrystallization. Straumann<sup>3</sup> found this with zinc and with Zn-Cd and Zn-Cu alloys, which showed uniform scattering of the hexagonal axis around the sheet normal, while Caglioti and Sachs<sup>4</sup> found the same with zinc and magnesium.

<sup>1</sup> Other U.S. Patents dealing with this subject are 2287466 and 2158065.

<sup>2</sup> F. BITTER, U.S. Patent 2046717.

<sup>3</sup> R. STRAUMANN, *Helv. Phys. Acta*, vol. 3, p. 463, 1930.

<sup>4</sup> V. CAGLIOTI and G. SACHS, *Metallwirtschaft*, vol. 11, p. 1, 1932.

**Summary.**—Some recrystallization textures resemble the deformation textures from which they grew, some are entirely different, and some are random. The control of preferred orientations is accomplished by control of hot-working, cold-working, and annealing schedules; metal purity; alloy composition; and amount of cross rolling. Commercial products having a well-developed orientation of a desirable type (as in transformer cores of high permeability in the rolling direction) or having a highly complex, near-random texture (as in sheet of deep-drawing quality) are usually developed by cut-and-try methods. Few fundamental principles are known.

A well-developed deformation texture is usually a prerequisite to a sharp recrystallization texture. Recrystallization textures of copper alloys are more sensitive to change by the addition of alloying elements than are deformation textures, and the alloying elements having the greatest solution-hardening effects on copper seem to generate the most nearly random recrystallization textures.

The sharply developed cube texture, (100)[001], which is common to many f.c.c. metals and alloys after rolling and recrystallization, becomes most pronounced with heavy cold reductions and high annealing temperatures. Many alloying additions prevent it; for example, any of the following additions, in weight percent, to copper, 5% Zn, 1% Sn, 4% Al, 0.5% Be, 0.5% Cd, 0.05% P.

Iron, steel, and alloyed ferrites have complex recrystallization textures in which the principal orientation is one having (100) in the rolling plane and [011] 15° from the rolling direction. By employing various cycles of cold reduction and intermediate annealing, sometimes with cross rolling, it has been found possible to develop pronounced textures of the types (100)[001], (110)[001], and (100)[011].

## CHAPTER XX

### ORIENTATIONS IN CASTINGS AND IN DEPOSITED FILMS

Metal castings frequently contain long columnar grains which extend from the surface inward in the direction of the greatest temperature gradient during freezing. The columnar structure is illustrated by a photograph of a copper ingot reproduced in Fig. 1. The long axis of the columnar grains tends to be an important crystal direction; *i.e.*, prominent crystal planes tend to be aligned parallel to the mold wall. The preferred

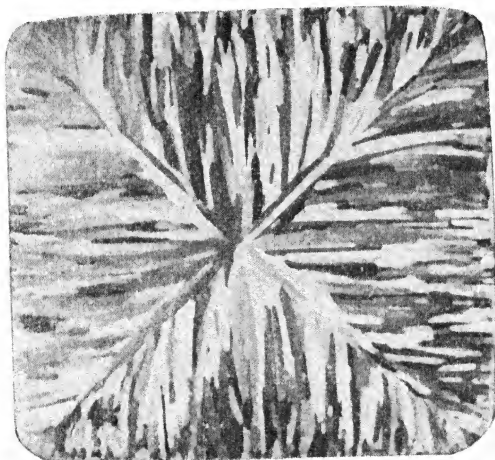


FIG. 1.—Columnar grains in cast copper.

orientations near the surface of a casting thus resemble the type of orientations found in a metal after compression, in that a crystal direction of low indices stands perpendicular to the surface and other crystal axes are oriented at random around this axis.

In electrodeposited films there is also a tendency for a texture, but the tendency is frequently overcome by conditions in the plating bath and in the underlying surface. Sometimes the orientations in the underlying metal are inherited in the deposit. Films deposited by sputtering during an electric discharge in a vacuum may be amorphous or crystalline, and when crystalline they also have a preferred orientation of the fiber-texture type unless conditions are such that they inherit an orientation from the material on which they are deposited.

**Textures in Cast Metal.**—A summary of textures in cast metal that have been found by x-rays is given in Table XXIII. All cubic metals have casting textures in which a cube axis is the fiber axis, which is normal to the cold surface of the mold. Textures in the hexagonal metals are complicated by the fact that the skin has orientations different from the underlying material and that there is sometimes an intermediate layer with yet another texture.<sup>1</sup> The orientation of the columnar grains of zinc was found by Nix and Schmid<sup>2</sup> to be a "ring fiber texture" with the basal plane parallel to the axis of the columnar grains but with no preferred direction in this plane. A careful investigation by Edmunds,<sup>1</sup> on the other hand, showed that columnar grains of zinc have a (100) prism plane approximately parallel to the surface. He noted that at the mold surface the grains have their basal plane parallel to the surface and that

TABLE XXIII.—TEXTURES OF CAST METALS

Structure	Metal	Normal to cold surface	Reference
B.c.c.	Fe-Si (4.3% Si) $\beta$ -Brass	[100] [100]	1
F.c.c.	Al Cu Ag Au Pb $\alpha$ -Brass	[100]	1
H.c.p.*	Cd ( $c/a = 1.885$ )	Columnar grains [210]; chilled surface [001]	2
		Columnar grains (001)	1
	Zn ( $c/a = 1.856$ )	Columnar grains, [210]; chilled surface, [001]	2
		Columnar grains (001)	1
	Mg ( $c/a = 1.624$ )	Columnar grains, (205)    surface	2
		Columnar grains [100]	1
Rhombohedral	Bi	[111]	1
Tetragonal	$\beta$ -Sn	[110]	1

\* Three-indices system, equivalent indices in four-indices systems are as follows (001) = (0001) = basal plane, [100] =  $[2\bar{1}\bar{1}0]$  = diagonal axis of type I = close-packed row of atoms in basal plane, [100] normal to the surface =  $(\bar{2}10)$  parallel to surface,  $[210]$  normal to surface = (100) parallel to surface.

<sup>1</sup> F. C. NIX and E. SCHMID, *Z. Metallkunde*, vol. 21, p. 286, 1929. E. SCHMID, *Z. Metallkunde*, vol. 20, p. 370, 1928.

<sup>2</sup> G. EDMUNDS, *Trans. A.I.M.E.*, vol. 143, p. 183, 1941.

<sup>1</sup> G. EDMUNDS, *Trans. A.I.M.E.*, vol. 143, p. 183, 1941.

<sup>2</sup> F. C. NIX and E. SCHMID, *Z. Metallkunde*, vol. 21, p. 286, 1929.

sometimes there is an intermediate layer with (101) parallel to the surface mixed with grains having the surface texture.

Northcott and Thomas confirmed that columnar grains of copper rich alloys are oriented with [100] parallel to the long dimension of the grains.<sup>1</sup> There are striations in the grains, presumably caused by coring in the dendrites, that are the intersections of {100} faces with the plane of polish, and these are parallel to the length of the grains. Equiaxed grains in the ingots are random in orientation.

Two binary eutectics have been studied.<sup>2</sup> In Zn-Cd (17 percent zinc) each of the two phases has the texture it has when alone, but in Al-Si (13 percent silicon) only the predominating phase is oriented. This phase (aluminum-rich) has its usual texture, with [100] as fiber axis, while the minor phase is randomly oriented.

To understand growth textures it is necessary to consider the anisotropy of the growth velocity of crystals.<sup>3</sup> When randomly oriented crystals start to grow from nuclei and grow with different velocities in different directions, they tend to block one another's progress. The only ones that find themselves able to continue growth unhindered are those having the direction of maximum growth velocity in the direction of the thermal gradient<sup>4</sup>—the direction of movement of the liquid-solid interface. These grains will become long columnar grains with their longitudinal axis parallel to the direction of greatest growth velocity.

**Orientations in Electrodeposits.**—The nature of the orientation in electrodeposited metal is of considerable technical importance and has been the object of much investigation with the microscope and with x-ray and electron diffraction. The subject is complex, for the deposit is affected by the nature of the electrolyte, its hydrogen ion concentration, the presence of addition agents, the temperature, the current density, the nature and condition of the base metal, stirring, rubbing, etc. There are also changes in texture as the deposited layer thickens, some of which have been ascribed directly to the thickness and others to changing conditions of temperature or concentration in the electrolyte.

Under some plating conditions the orientation of the base metal is copied by the deposit.<sup>5</sup> In fact, microscopic investigation of a cross

<sup>1</sup> L. NORTHCOTT and D. E. THOMAS, *J. Inst. Metals*, vol. 65, p. 205, 1939. The ingots studied were of Cu containing, respectively, 0.5% Mn, 1% P, 2% Al, 4% Sn, and 15, 33, and 47% Zn.

<sup>2</sup> F. C. NIX and E. SCHMID, *Z. Metallkunde*, vol. 21, p. 286, 1929.

<sup>3</sup> W. BOAS and E. SCHMID, *Z. Physik*, vol. 54, p. 16, 1929. A. G. HOYEM and E. P. T. TYNDALL, *Phys. Rev.*, vol. 33, p. 81, 1929. S. TSUBOI, *Mem. Coll. Sci., Kyoto Imp. Univ.*, vol. A12, p. 223, 1929. R. GROSS and H. MÖLLER, *Z. Physik*, vol. 19, p. 375, 1923.

<sup>4</sup> R. GROSS and H. MÖLLER, *Z. Physik*, vol. 19, p. 375, 1923.

<sup>5</sup> W. A. WOOD, *Proc. Phys. Soc. (London)*, vol. 43, p. 138, 1931. W. COCHRANE,

section through deposit and base metal shows that the grains in the deposit are frequently continuations of the grains in the base metal.<sup>1</sup> The conditions most favorable to the continuation of base-metal grains into the electrodeposit are the following: clean, freshly etched surfaces, small current densities, electrolytes without colloidal additions, and similarity in structure between base metal and deposit. When both metals are cubic, continuation is found only if the base metal has a parameter approximately equal to that of the deposit (2.4 percent smaller to 12.5 percent greater).<sup>2</sup> Exceptions to these rules have been observed, however. It is possible to have continuation when the two metals have different structures, presumably because of related atomic patterns at the interface, as in Widmanstätten structures. It is also possible to have continuation across a thin interposed layer of a second substance,<sup>3</sup> (perhaps through connecting pores or through orientations imparted to the layer). The continuity may occur only for certain grains of the base metal, as in rapidly applied industrial deposits, or it may be observed for all grains, for example, when the base metal itself is an electrodeposit.

The influence of the base metal does not extend very far into the deposited metal, and the outer layers are free to take up their characteristic orientation. Under some conditions the underlying layers are randomly oriented and succeeding layers become progressively more sharply oriented for some distance.<sup>4</sup> Current density and electrolyte composition may be such that the entire deposit is random,<sup>5</sup> or varying degrees of orientation can be produced, which Wood<sup>6</sup> suggests may correlate with the brightness of the deposit in the case of nickel and chromium. Not only the degree of orientation but even the nature of the texture can be altered by the plating conditions.<sup>7</sup> In every case where a deposit is free to assume its own texture the orientations are such that a crystal axis stands perpendicular to the surface or parallel to the direction of current flow, and there is rotational symmetry around

---

*Proc. Phys. Soc. (London)*, vol. 48, p. 723, 1936. G. P. THOMSON, *Proc. Roy. Soc. (London)*, vol. A133, p. 1, 1931.

<sup>1</sup> A. K. HUNTINGTON, *Trans. Faraday Soc.*, vol. 1, p. 324, 1905. A. K. GRAHAM, *Trans. Am. Electrochem. Soc.*, vol. 44, p. 427, 1923. A. W. HOTHERSALL, *Trans. Faraday Soc.*, vol. 31, p. 1242, 1935. W. BLUM and H. S. RAWDON, *Trans. Am. Electrochem. Soc.*, vol. 44, p. 305, 1923. G. TAMMANN and M. STRAUMANIS, *Z. anorg. allgem. Chem.*, vol. 175, p. 131, 1928.

<sup>2</sup> A. W. HOTHERSALL, *Trans. Faraday Soc.*, vol. 31, p. 1242, 1935.

<sup>3</sup> A. M. PORTEVIN and M. CYMBOLISTE, *Trans. Faraday Soc.*, vol. 31, p. 1211, 1935.

<sup>4</sup> W. G. BURGERS, *Phillips Tech. Rev.*, vol. 1, p. 95, 1936.

<sup>5</sup> R. GLOCKER and E. KAUPP, *Z. Physik*, vol. 24, p. 121, 1921.

<sup>6</sup> W. A. WOOD, *Phil. Mag.*, vol. 20, p. 964, 1935.

<sup>7</sup> R. GLOCKER and E. KAUPP, *Z. Physik*, vol. 24, p. 121, 1924. R. BOZORTH, *Phys. Rev.*, vol. 26, p. 390, 1925.

this axis. Thus the deposit has a fiber texture (or a double fiber texture) resembling the texture of a wire, the thickness direction of the deposit corresponding to the axial direction in the wire.

A brief summary of orientations that have been observed, assembled by Wassermann,<sup>1</sup> is given in Table XXIV.

TABLE XXIV.—TEXTURES IN ELECTRODEPOSITS

Metal	Fiber textures	Observers
Nickel . . . . .	[100], [100] + [110]; [112]	1, 5, 8, 9, 10, 11
Copper . . . . .	[110]; [100]	1, 6, 7
Silver . . . . .	[111] + [100]; [111]; [110]	1, 2, 3, 4, 5
Lead . . . . .	[112]	12
Gold . . . . .	[110]	5
Iron . . . . .	[111]; [112]	1, 5, 9, 11
Cobalt . . . . .	[110]	5
Chromium . . . . .	[100] + [111] (f.c.c.); [0001] (hexagonal)	1, 13, 14
Tin . . . . .	[111]; [001]	5, 16
Cadmium . . . . .	[1122]	17
Bismuth . . . . .	[211]; [100]	5, 15

<sup>1</sup> R. GLOCKER and E. KAUFF, *Z. Physik*, vol. 24, p. 121, 1924.

<sup>2</sup> S. TRUBOI, *Mem. Coll. Sci., Kyoto Imp. Univ.*, vol. A11, p. 271, 1928.

<sup>3</sup> G. R. LEVI and M. TABER, *Atti accad. Lincei*, vol. 18 (6), p. 463, 1934.

<sup>4</sup> H. HIRATA and H. KOMATSUHARA, *Mem. Coll. Sci., Kyoto Imp. Univ.*, vol. A10, p. 95, 1926.

<sup>5</sup> G. I. FINCH, A. G. QUARRELL, and H. WILMAN, *Trans. Faraday Soc.*, vol. 31, p. 1051, 1935.

<sup>6</sup> W. KOSTER, *Z. Metallkunde*, vol. 18, p. 219, 1926.

<sup>7</sup> H. HIRATA and Y. TANAKA, *Mem. Coll. Sci., Kyoto Imp. Univ.*, vol. A15, p. 9, 1932.

<sup>8</sup> G. L. CLARK and P. K. FROLICH, *Z. Elektrochem.*, vol. 31, p. 655, 1925.

<sup>9</sup> R. BOZORTH, *Phys. Rev.*, vol. 26, p. 390, 1925.

<sup>10</sup> W. G. BURGERS and W. ELENBAAS, *Naturwissenschaften*, vol. 21, p. 465, 1933.

<sup>11</sup> W. ELENBAAS, *Z. Physik*, vol. 76, p. 829, 1932.

<sup>12</sup> P. K. FROLICH, G. L. CLARK, and R. A. ABORN, *Z. Elektrochem.*, vol. 32, p. 295, 1926.

<sup>13</sup> W. ARKHAROW, *J. Tech. Phys., U.S.S.R.*, vol. 6, p. 1777, 1936 (*Metal Abstracts*, vol. 3, p. 665, 1936).

<sup>14</sup> W. A. WOOD, *Phil. Mag.*, vol. 24, p. 772, 1937.

<sup>15</sup> H. HIRATA, *Mem. Coll. Sci., Kyoto Imp. Univ.*, vol. A11, p. 429, 1928.

<sup>16</sup> H. HIRATA and Y. TANAKA, *Mem. Coll. Sci., Kyoto Imp. Univ.*, vol. A17, p. 143, 1934.

<sup>17</sup> A. RUBIO and J. GARCIA DE LA CUEVA, *Anales soc. españ. fis. quim.*, vol. 33, p. 521, 1935.

**Evaporated and Sputtered Metal Films.**—Thin layers of metals condensed from the vapor phase or deposited by cathodic sputtering have received extensive study by electron diffraction as well as by x-rays. They are of practical value; for instance, evaporated films of aluminum make very efficient mirror surfaces.<sup>2</sup> Orientations in the layers depend on the nature of the base and its temperature during deposition and are not necessarily the same with all metals of a given crystal structure. Orientations are generally altered when the layers are subsequently heated.

<sup>1</sup> G. WASSERMANN, "Texturen metallischer Werkstoffe," Springer, Berlin, 1939.

<sup>2</sup> J. STRONG, *Astrophys. J.*, vol. 83, p. 401, 1936.

Metals evaporated on amorphous, vitreous, or polished base material are likely to be oriented randomly if the base is at a low temperature and to be oriented in some fiber texture if the base is hot. In many cases, the low-temperature deposit is colloidal or even amorphous and gives very diffuse diffraction rings.<sup>1</sup> Although evaporated films are normally produced in a high vacuum, the presence of gas in the deposit may have much to do with the structure,<sup>2</sup> and the crystal lattice of sputtered films also seems to be definitely affected by the nature of the gas.<sup>3</sup>

When a deposited metal takes up a preferred orientation at the time of deposition or upon subsequent annealing, the texture is usually a fiber texture with the fiber axis normal to the surface. That is, there is a tendency for a certain crystallographic plane to lie parallel to the surface of the base material. There may be two such orientations coexisting, however, and they may form a double fiber texture. Exceptions have been noted when a stream of metal strikes a condensing surface obliquely. There is then a fiber texture with the fiber axis inclined both to the stream of metal and to the condensing surface.<sup>4</sup>

A summary of the fiber textures that have been observed with different temperatures of deposition and of annealing is given in Table XXV.<sup>5</sup> For a discussion of the conditions governing the choice of the different possible orientations the references cited in the table should be consulted.

Dixit<sup>4</sup> has observed three different orientations when an aluminum deposit  $10^{-5}$  or  $10^{-6}$  cm. thick is heated to various temperatures and has proposed that the transition  $[111] \rightarrow [100] \rightarrow [110]$  with increasing temperature is because the surface atoms behave as a two-dimensional gas. His theory is that with increasing temperature the area on the surface required for each atom increases and that this increase governs the crystal plane that can lie on the surface.

<sup>1</sup> F. KIRCHNER, *Z. Physik*, vol. 76, p. 576, 1932 (Sb, Se, Ag, Tl, Au, Bi). J. A. PRINS, *Nature*, vol. 131, p. 760, 1933. T. FUKUROI, *Sci. Papers Inst. Phys. Chem. Research (Tokyo)*, vol. 32, p. 196, 1937 (Cd, Zn). L. R. INGERSOLL and S. S. DE VINNEY, *Phys. Rev.*, vol. 26, p. 86, 1925 (Ni). L. R. INGERSOLL and J. D. HANAWALT, *Phys. Rev.*, vol. 34, p. 972, 1929 (Ni). M. GEN, J. ZELMANOFF, and A. SCHALNIKOFF, *Physik. Z. Sowjetunion*, vol. 4, p. 826, 1933 (Fe, Cd, Hg, Ni). G. HASS, *Naturwissenschaften*, vol. 25, p. 232, 1937; *Ann. Physik*, vol. 31, p. 245, 1938 (Sb, Ag). L. H. GERMER, *Phys. Rev.*, vol. 56, p. 58, 1939 (Au, Pd, Cu, Al, Mg).

<sup>2</sup> G. P. THOMSON and W. COCHRANE, "Theory and Practice of Electron Diffraction," p. 164, Macmillan, New York, 1939.

<sup>3</sup> S. OGAWA, *Sci. Repts. Tohoku Imp. Univ.*, vol. 26, p. 93, 1937. L. R. INGERSOLL and J. D. HANAWALT, *Phys. Rev.*, vol. 34, p. 972, 1929. L. R. INGERSOLL, *Phys. Rev.*, vol. 33, p. 1094, 1929. W. BUSSEN and F. GROSS, *Z. Physik*, vol. 86, p. 135, 1933; vol. 87, p. 778, 1934.

<sup>4</sup> K. R. DIXIT, *Phil. Mag.*, vol. 16, p. 1049, 1933.

<sup>5</sup> G. WASSERMANN, "Texturen metallischer Werkstoffe," Springer, Berlin, 1939.



TABLE XXV.—TEXTURES IN EVAPORATED AND SPUTTERED FILMS

Metal deposited	Texture	Technique	References
<b>F.c.c.:</b>			
Ag	[111]; [100]; [110]	Evaporated	1, 2
Al	[111]; [100]; [110]	Evaporated	1, 3, 4, 18
Au	[110]; [111]	Evaporated	3, 5, 6, 7
Pt	[100]; [111]	Spattered	5, 9
Pd, Cu, Ni	[111]	Evaporated	8, 9
<b>B.c.c.:</b>			
Fe	[111]	Evaporated	9
Mo	[110]	Evaporated	10
<b>Hexagonal:</b>			
Cd, Zn	[0001]	Evaporated	5, 11, 12, 13
<b>Rhombohedral:</b>			
Bi	[111], [110]	Evaporated	14, 15, 16, 17

<sup>1</sup> K. R. DIXIT, *Phil. Mag.*, vol. 16, p. 1049, 1933.

<sup>2</sup> H. MARK and R. WIERL, *Z. Physik*, vol. 60, p. 741, 1930

<sup>3</sup> L. BRÜCK, *Ann. Physik*, vol. 26, p. 233, 1936

<sup>4</sup> R. BEECHING, *Phil. Mag.*, vol. 22, p. 928, 1936.

<sup>5</sup> G. I. FINCH, A. G. QUARRELL, and H. WILMAN, *Trans. Faraday Soc.*, vol. 31, p. 1051, 1935.

<sup>6</sup> E. N. DA C. ANDRADE, *Trans. Faraday Soc.*, vol. 31, p. 1137, 1935

<sup>7</sup> S. R. SWAMY, *Proc. Phys. Soc. (London)*, vol. 46, p. 739, 1934.

<sup>8</sup> O. RÜDIGER, *Ann. Physik*, vol. 30, p. 505, 1937.

<sup>9</sup> S. DEMBINSKA, *Z. Physik*, vol. 54, p. 46, 1929

<sup>10</sup> I. R. LANDAU, *Metals & Alloys*, vol. 9, pp. 73, 100, 1938.

<sup>11</sup> M. VOLMER, *Z. Physik*, vol. 5, p. 31, 1921

<sup>12</sup> E. A. OWEN and E. W. ROBERTS, *Phil. Mag.*, vol. 22, p. 290, 1936.

<sup>13</sup> M. SFRAMANIS, *Z. Physik Chem.*, vol. B13, p. 316, 1931.

<sup>14</sup> F. KIRCHNER, *Z. Physik*, vol. 76, p. 576, 1932

<sup>15</sup> C. T. LANE, *Phys. Rev.*, vol. 48, p. 193, 1935.

<sup>16</sup> F. GROSS, *Z. Physik*, vol. 61, p. 520, 1930

<sup>17</sup> W. BUNSEN, F. GROSS, and K. HERRMANN, *Z. Physik*, vol. 64, p. 537, 1930.

<sup>18</sup> L. H. GERMER, *Phys. Rev.*, vol. 56, p. 58, 1939.

**Films Deposited on Single Crystals.**—Orientations in films deposited on single crystals are affected not only by the conditions mentioned above, but also by the atomic arrangement in the supporting crystal. The force fields around the atoms in the base material may be sufficient to produce a single orientation instead of a fiber texture, although at room temperature random deposits usually prevail. Gold, silver, nickel, and platinum deposited on the cleavage face (100) of rock salt take up the orientation of the underlying crystal<sup>1</sup> or an orientation related thereto<sup>2</sup> when the temperature is above a certain critical value. The body-centered cubic metals iron and chromium deposit with more than one

<sup>1</sup> H. LASSEN, *Physik. Z.*, vol. 35, p. 172, 1934. H. LASSEN and L. BRÜCK, *Ann. Physik*, vol. 22, p. 65, 1935. L. BRÜCK, *Ann. Physik*, vol. 26, p. 233, 1936.

<sup>2</sup> G. MENZER, *Z. Krist.*, vol. 99, p. 410, 1938. L. ROYER, *Ann. Physik*, vol. 23, p. 16, 1935.

orientation; some crystals in the layer take up the orientation of the rock salt and others have (110) parallel to the cube face and [110] parallel to the cube edge of the rock salt.

Gold, silver, and platinum on cleavage faces of calcite, mica, and quartz take up orientations that depend on the temperature and on the supporting crystal<sup>1</sup> presumably the factors governing orientations are closely related to those governing Widmanstätten structures, but the basic principles are sometimes complicated by the presence of twinning in the deposit.<sup>2</sup>

<sup>1</sup> O. RUDIGER, *Ann. Physik*, vol. 30, p. 505, 1937.

<sup>2</sup> F. KIRCHNER and H. CRAMER, *Ann. Physik*, vol. 33, p. 138, 1938. G. MENZER, *Naturwissenschaften*, vol. 26, p. 385, 1938.

## CHAPTER XXI

### ANISOTROPY

The practical importance of preferred orientations lies in the variation in properties with direction in commercial material, especially in rolled sheet. Directionality is usually undesirable in a product and is generally kept under strict control in the mills. Sheet used in deep drawing, for instance, must flow uniformly in all directions if a scalloped rim is to be avoided.

Anisotropy is responsible not only for this "earring" of deep-drawn objects, but also for uneven thinning, puckering, and splitting of the walls. Directionality in forgings may lead to insufficient ductility in some directions. Directionality in sheet steel for electrical uses may lead to undesirable electrical characteristics in one apparatus, but in another it may be exploited to give high permeability in an important direction (for example, parallel to the magnetic flux in a transformer core).

Owing to the interaction of each grain with the neighboring grains and with grain boundaries and imperfections, it is seldom possible to compute the anisotropy of a polycrystalline aggregate directly from the anisotropic properties of single crystals. Accordingly, the earlier sections of this chapter are devoted to the polycrystalline properties, which are of more general interest, and single crystal data are deferred to the later sections.

**Directionality in the Strength Properties.**—Directional properties in polycrystalline metals may arise from preferred orientations or from other causes, such as elongated inclusions, blowholes, cavities, segregation, nonmetallic inclusions, strings and layers of small grains, and the elongated shape of the grains themselves. Anisotropy caused by the preferred orientation of crystals is sometimes called "crystallographic fibering," and it is this with which we are chiefly concerned here, rather than with the so-called "mechanical fibering" from other causes. The properties of forgings in different directions depend more on mechanical than on crystallographic fibering<sup>1</sup> although in forgings of magnesium the reverse is true.<sup>2</sup> In many cases the causes are combined.

**Face-centered cubic metals** in the cold-rolled state are not highly anisotropic, but the tensile strength in the cross direction definitely

<sup>1</sup> G. SACHS and K. R. VAN HORN, "Practical Metallurgy," *A.S.M.*, Cleveland, Ohio, 1940.

<sup>2</sup> W. SCHMIDT, *Z. Metallkunde*, vol. 25, p. 229, 1933.

exceeds that in the longitudinal direction for copper and brass,\* nickel,† aluminum,‡ silver,§ Fe-Ni,|| and bronze¶ after severe cold rolling. High tensile and yield strengths and low ductility (elongation, reduction in area, ability to withstand bending) are usually found in the same directions. Anisotropy increases with the degree of reduction by rolling,\*\* as would be expected from the progressive development of rolling textures, but the anisotropy seldom amounts to as much as 10 percent in yield strength or tensile strength. Reduction of area in transverse specimens may be as low as half that in longitudinal specimens in brass and bronze.¶ Bend tests and notch-bend tests of all types are anisotropic,<sup>1</sup> owing to both crystallographic and mechanical fibering.<sup>2</sup> Test strips cut along the cross direction are least able to withstand bending, and the bending number increases as the rolling direction is approached in aluminum, copper, brass, and bronze.¶ Annealed sheets can be produced with varying degrees of anisotropy. An example of the degree of directionality encountered in brass is shown in Fig. 1, which gives the results of tensile tests on 65-35 brass strip that has had various annealing treatments.

\* W. B. PRICE and P. DAVIDSON, *Trans. Am. Inst. Metals*, vol. 10, p. 133, 1916. F. KORBER and P. WIELAND, *Mitt. Kaiser-Wilhelm Inst. Eisenforsch. Dusseldorf*, vol. 3, p. 57, 1921. F. KORBER and H. HOFF, *Mitt. Kaiser-Wilhelm Inst. Eisenforsch. Dusseldorf*, vol. 10, p. 175, 1928. E. SCHMID and G. WASSERMANN, *Metallwirtschaft*, vol. 10, p. 409, 1931. A. PHILLIPS and C. H. SAMANS, *Trans. A.I.M.E.*, vol. 104, p. 171, 1933. A. PHILLIPS and E. S. BUNN, *Trans. A.I.M.E.*, vol. 93, p. 353, 1931. F. v. GÖLER and G. SACHS, *Z. Physik*, vol. 56, p. 495, 1929. H. UNCKEL, *Z. Metallkunde*, vol. 31, p. 104, 1939. O. BAUER, F. v. GÖLER, and G. SACHS, *Z. Metallkunde*, vol. 20, p. 202, 1928. F. v. GÖLER and G. SACHS, *Z. Physik*, vol. 56, p. 495, 1929. M. COOK, *J. Inst. Metals*, vol. 60, p. 159, 1937; *Metal Ind. (London)*, vol. 50, pp. 337, 405, 1937.

† F. KORBER and H. HOFF, *Mitt. Kaiser-Wilhelm Inst. Eisenforsch. Dusseldorf*, vol. 10, p. 175, 1928.

‡ F. KORBER and H. HOFF, *Mitt. Kaiser-Wilhelm Inst. Eisenforsch. Dusseldorf*, vol. 10, p. 175, 1928. H. UNCKEL, *Z. Metallkunde*, vol. 31, p. 104, 1939.

§ E. SCHMID and G. WASSERMANN, *Metallwirtschaft*, vol. 10, p. 409, 1931. F. v. GÖLER and G. SACHS, *Z. Physik*, vol. 56, p. 495, 1929. E. RAUB, *Z. Metallkunde*, vol. 27, p. 77, 1935.

|| O. DAHL and F. PAWLEK, *Z. Metallkunde*, vol. 28, p. 230, 1936.

¶ H. UNCKEL, *Z. Metallkunde*, vol. 31, p. 104, 1939.

\*\* F. KORBER and H. HOFF, *Mitt. Kaiser-Wilhelm Inst. Eisenforsch. Dusseldorf*, vol. 10, p. 175, 1928. A. PHILLIPS and E. S. BUNN, *Trans. A.I.M.E.*, vol. 93, p. 353, 1931. H. UNCKEL, *Z. Metallkunde*, vol. 31, p. 104, 1939.

<sup>1</sup> G. TAMMANN and H. H. MEYER, *Z. Metallkunde*, vol. 18, p. 176, 1926; vol. 19, p. 82, 1927. H. UNCKEL, *Z. Metallkunde*, vol. 31, p. 104, 1939. W. A. STRAW, M. D. HELFRICK, and C. R. FISCHRUPE, *Trans. A.I.M.E.*, vol. 93, p. 317, 1931. F. KORBER and P. WIELAND, *Mitt. Kaiser-Wilhelm Inst. Eisenforsch. Dusseldorf*, vol. 3, p. 57, 1921. H. RÖHRIG and K. SCHÖNHERR, *Z. Metallkunde*, vol. 29, p. 337, 1937. E. MOHR, *Metallwirtschaft*, vol. 18, p. 405, 1939.

<sup>2</sup> G. SACHS and K. R. VAN HORN, "Practical Metallurgy," *A.S.M.*, Cleveland, Ohio, 1940.

Palmer and Smith<sup>1</sup> draw the following conclusions from many investigations of this type on brass.

1. If brass is fully recrystallized, the higher the final annealing temperature, the greater, invariably, is the directionality in the sheet, as revealed by the height of ears that form in drawing cups.

2. The lower the temperature of the anneal before the last rolling, the greater, invariably, is the degree of final directionality.

3. The lower the temperature of earlier anneals ("running-down" or "process" anneals), the greater the final directionality, unless very high reductions are used between anneals.

4. The degree of directionality is not significantly affected by the type or speed of the rolling mill, reduction per pass, lubrication of the strip

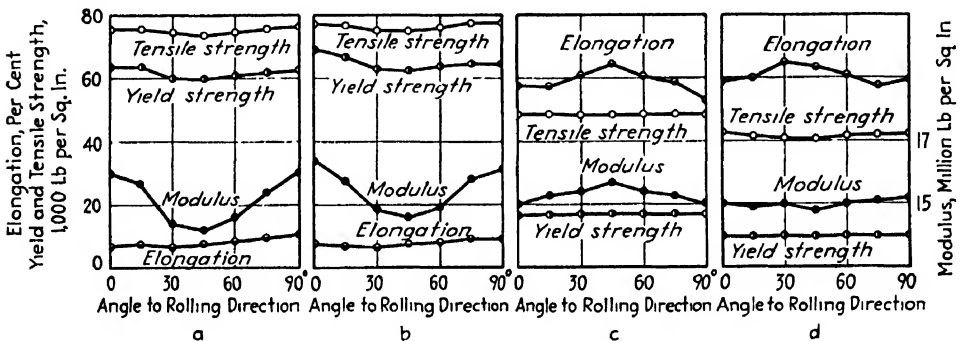


FIG. 1.—Directionality of physical properties in 65-35 brass strip. Normal reductions (four to six B. & S. numbers) and normal anneals (about 600°C.), followed by final treatments (a) hard rolled, (b) annealed 2 hr. at 200°C.; (c) annealed at 500°C. (produced no ears), (d) annealed at 700°C. (no ears). (Palmer and Smith.)

during rolling, size and orientation of grains in the casting, or impurities in the 65-35 brass (provided that they do not exceed 0.5% Pb, 0.05% Fe, 0.1% Si, 1% Mn, 1% Ni, 1% Al, 0.5% Cd, or small amounts of Li or Na added for deoxidation).

Burghoff and Bohlen<sup>2</sup> conclude that the directionality of 68-32 brass strip increases as follows:

1. As the penultimate reduction by rolling increases.
2. As the final reduction increases.
3. As the penultimate annealing temperature decreases.
4. As the final annealing temperature increases.

Sheets may be produced that form cups with four ears 45° to the rolling direction or six ears at 0 and 60° positions, depending upon the mill variables. Pole figures for samples giving four and six ears, respectively, are reproduced in Figs. 2a and 2b (the black triangles indicate the symmetrical positions (110)  $\bar{1}\bar{1}2$  which appeared to be somewhat more

<sup>1</sup> E. W. PALMER and C. S. SMITH, *Trans. A.I.M.E.*, vol. 147, p. 164, 1942.

<sup>2</sup> H. L. BURGHOFF and E. C. BOHLEN, *Trans. A.I.M.E.*, vol. 147, p. 144, 1942.

applicable than the usual (113)  $[\bar{2}11]$  positions). Four dense areas will be noted near the outside on one pole figure, six on the other; these correlate with the tendency to produce four and six ears, respectively. It will be seen further that, since the (111) planes are slip planes in this material, these (111) pole figures give directly the distribution of available slip planes and, to a first approximation, the distribution of slip systems. It would be expected that slip would be facilitated when a stress is applied to the sheet in directions that would cause the greatest resolved shear stress on the greatest number of grains. In Fig. 2a, this will be seen to correspond to directions  $45^\circ$  to the rolling direction, for then the concentrations in the rolling direction (at the top) and in the transverse

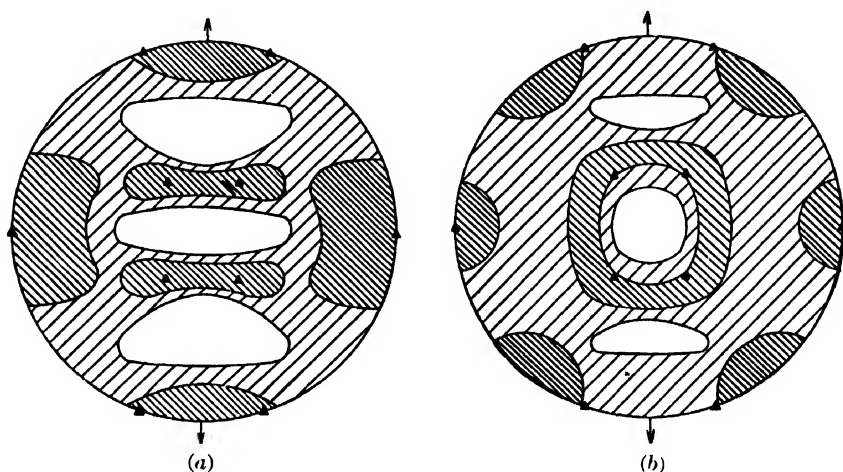


FIG. 2.- Pole figures for (111) poles in 68-32 brass strip. (a) Forms cups with four ears (rolled 84 percent, annealed  $425^\circ\text{C}.$ ; rolled 50 percent, annealed  $650^\circ\text{C}.$ ). (b) Forms cups with six ears, rolled 50 percent annealed  $565^\circ\text{C}.$ ; rolled 85 percent annealed  $650^\circ\text{C}.$  (Burghoff and Bohlen.)

direction (at the side) will lie  $45^\circ$  to the axis of tension and will receive large shear stress components. There is reason to expect, therefore, the observed behavior: in the drawing of a cup with symmetrical dies the metal would flow more easily in directions  $45^\circ$  to the rolling direction and produce ears at these positions. A similar argument applies—though less convincingly—to Fig. 2b.

When recrystallization produces a **cube texture**, (100)[001], the directionality of physical properties is extreme, as will be seen from the typical curves in Fig. 3 for copper.<sup>1</sup> There is a marked minimum in ductility at 0 and  $90^\circ$  positions and a peak at  $45^\circ$ . It is readily understandable that earing in the cup test is sensitive to the percentage of the grains that have this texture. Baldwin finds, in fact, a linear relation between ear height and this percentage. Ears occur at 0 and  $90^\circ$  to the rolling direction in sheets having 30 percent or more of the grains in cubic

<sup>1</sup> W. M. BALDWIN, *Metals Tech., Tech. Pub.* 1455, April, 1942.

alignment, whereas in the absence of this cube texture ears in face-centered cubic metals are usually at  $45^\circ$  to the rolling direction.<sup>1</sup>

Among **body-centered cubic metals**, cold-rolled iron has its highest tensile values in the transverse direction of the sheet.<sup>2</sup> Anisotropy in cold-rolled **low-carbon steel after annealing** at various temperatures is illustrated in Fig. 4.<sup>3</sup>

Ears on cups drawn from annealed sheet steel may be found at the  $45^\circ$  positions when the degree of reduction is low (about 40 percent) or at 0 and  $90^\circ$  to the rolling direction with higher reductions;<sup>4</sup> they increase

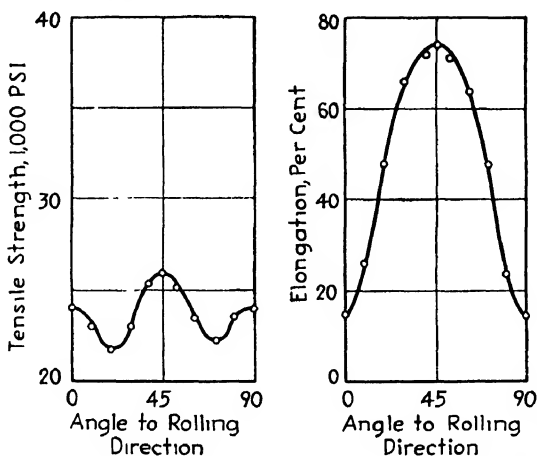


FIG. 3.—Directionality of tensile properties of copper strip having cube texture. (Bautwin.)

in height with the amount of rolling. Control of furnace practice, of hot- and cold-rolling schedules and of finishing and annealing temperatures in the modern mills yields a product that is effectively isotropic.

Anisotropy in **hot-rolled structural steel plate** is small<sup>5</sup> (carbon steel from 0.17 to 0.25% C, low-alloy steels containing up to 0.36% Si,

<sup>1</sup> K. KAISER, *Z. Metallkunde*, vol. 19, p. 435, 1927. W. H. BASSETT and J. C. BRADLEY, *Trans. A.I.M.E.*, vol. 104, p. 181, 1933. ARTHUR PHILLIPS and C. H. SAMANS, *Trans. A.I.M.E.*, vol. 104, p. 171, 1933. ARTHUR PHILLIPS and G. EDMUNDS, *Proc. A.S.T.M.*, vol. 29, pt. II, p. 438, 1929. E. RAUB, *Z. Metallkunde*, vol. 27, p. 77, 1935; *Mitt. Forsch.-Inst. Probiranst. Edelmetalle*, vol. 10, p. 53, 1936. M. COOK, *J. Inst. Metals*, vol. 60, p. 159, 1937, *Metal Ind. (London)*, vol. 50, p. 337, 1937. J. D. JEVONS, *J. Inst. Metals*, vol. 60, p. 174, 1937. Control of the cube texture is also treated in Chap. XX, p. 428, of the present book.

<sup>2</sup> J. WINLOCK and G. L. KELLEY, *Trans. A.S.S.T.*, vol. 12, p. 635, 1927. F. KÖRBER and H. HOFF, *Mitt. Kaiser-Wilhelm Inst. Eisenforsch. Dusseldorf*, vol. 10, p. 175, 1928. ARTHUR PHILLIPS and H. H. DUNKLE, *Trans. A.S.M.*, vol. 23, p. 398, 1935. C. A. EDWARDS, D. L. PHILLIPS, and C. R. PIPE, *J. Iron Steel Inst.*, vol. 133, p. 95, 1936.

<sup>3</sup> ARTHUR PHILLIPS and H. H. DUNKLE, *Trans. A.S.M.*, vol. 23, p. 398, 1935.

<sup>4</sup> ARTHUR PHILLIPS and H. H. DUNKLE, *Trans. A.S.M.*, vol. 23, p. 398, 1935. O. DAHL and J. PFAFFENBERGER, *Z. Physik*, vol. 71, p. 93, 1931.

<sup>5</sup> B. JOHNSTON and F. OPILA, *Trans. A.S.T.M.*, vol. 41, p. 552, 1941.

1.84% Ni, 1.14% Cu, 0.80% Cr). The elastic constants are isotropic ( $E = 29.54 \times 10^6$  psi.,  $\nu = 0.297$ ,  $G = 11.39 \times 10^6$  psi.), but ductility and strength vary with direction of testing. Average values for elongation in 2 in. for a series of carbon steels are 40.2 and 36.0 percent for longitudinal and transverse directions, respectively; the corresponding values for average true stress at fracture are 117,600 and 110,500 psi.<sup>1</sup>

Straight-rolled **molybdenum** has a minimum strength in bending when test strips are cut along the transverse direction of the sheet, but

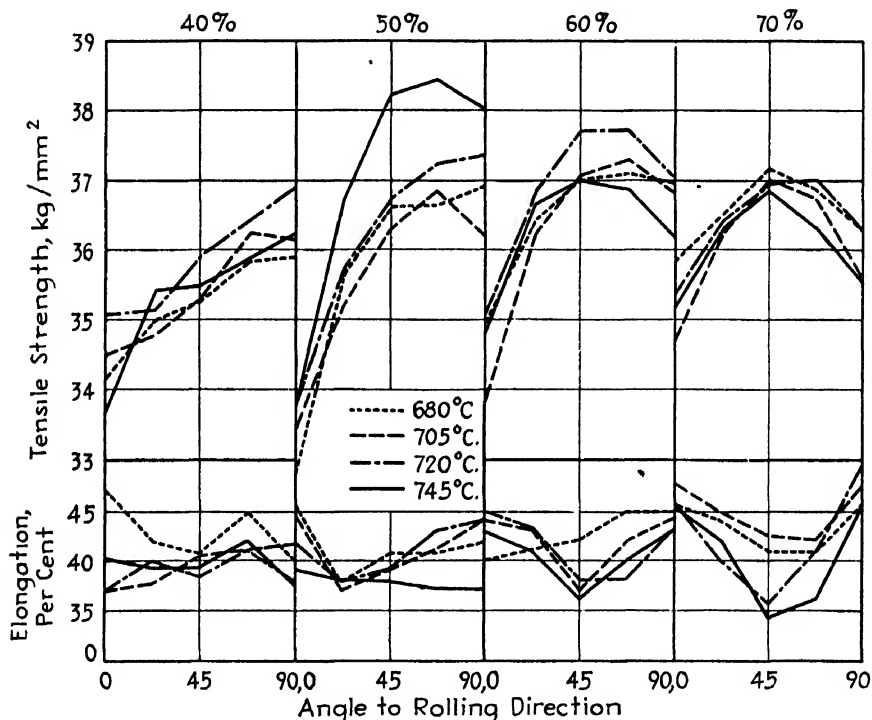


FIG. 4.—Directionality of tensile strength and elongation in annealed steel sheet with various reductions and annealing temperatures. (Phillips and Dunkle.)

the minimum shifts to the 45° position if the sheet is made by cross rolling and is annealed without recrystallization.<sup>2</sup> The cross-rolled sheet is extremely brittle, with cleavage along the cube planes that lie 45° from the rolling direction and normal to the sheet—the texture is (100)[011]. Similar brittleness has been observed in **tungsten** foil recrystallized at a high temperature.<sup>3</sup>

<sup>1</sup> True stress is the load divided by the area of the cross section at the necked-down section; tensile strength is the maximum load sustained by the specimen divided by the original area of the cross section.

<sup>2</sup> C. E. RANSLEY and H. P. ROOKSBY, *J. Inst. Metals*, vol. 62, p. 205, 1938. C. J. SMITHELLS, *J. Inst. Metals*, vol. 60, p. 172, 1937.

<sup>3</sup> W. G. BURGERS and J. J. A. PLOOS VAN AMSTEL, *Physica*, vol. 3, p. 1064, 1936.



**Hexagonal metals** with their distinctive and limited manner of crystallographic slip show a marked influence of texture on directionality of properties. The tensile strength and yield strength of rolled **zinc** is lower in the rolling direction than in the cross direction,<sup>1</sup> whereas the measures of ductility vary conversely. Bending properties are strongly influenced by the texture of surface layers (see page 414),<sup>2</sup> and these can be altered by mill practice. Directionality is not greatly altered by purity or rolling temperature,<sup>3</sup> but when the degree of working alters the nature of the preferred orientation there are marked alterations in the properties and their directionality which may be understood when the textures are compared with the properties of single crystals.<sup>4</sup>

Textures, directionality of physical properties, and formability are strongly correlated in the case of **magnesium** and its alloys.<sup>5</sup> It is possible to plan forming processes so that maximum yield and tensile strengths can be had in the direction of the maximum service stress or to increase greatly the elongation both in the cross direction and in the rolling direction by bending a sheet back and forth in straightening rolls, thus causing twinning and producing new possibilities for slip. Magnesium-alloy rods formed by cold drawing or cold extrusion (below 300°C.) possess a unique form of anisotropy: the yield strength in compression is only about half that in tension. This results from the fact that compression produces twinning, whereas tension does not. The effect is less in fine-grained alloys, which twin less readily. An extensive discussion of directionality in magnesium and its alloys will be found in Beck's "Technology of Magnesium and Its Alloys."<sup>6</sup>

**Miscellaneous Tests for Anisotropy.**—In addition to yield strength, tensile strength, elongation, reduction in area, elastic moduli, bend and

<sup>1</sup> E. SCHMID and G. WASSERMANN, *Z. Metallkunde*, vol. 23, p. 87, 1931. H. SIEGLERSCHMIDT, *Z. Metallkunde*, vol. 24, p. 55, 1932. C. H. MATHEWSON, C. S. TREWIN, and W. H. FINKELDEY, *Trans. A.I.M.E.*, vol. 64, p. 305, 1920. H. F. MOORE, *Univ. Illinois Bull. Eng. Expt. Sta.*, vol. 9, no. 52, 1911. O. BAUER, J. WEERTS, and F. BECK, *Metallwirtschaft*, vol. 12, p. 615, 1933. G. SACHS, *Z. Metallkunde*, vol. 17, p. 187, 1925.

<sup>2</sup> G. EDMUNDS and M. L. FULLER, *Trans. A.I.M.E.*, vol. 99, p. 175, 1932.

<sup>3</sup> O. BAUER, J. WEERTS, and F. BECK, *Metallwirtschaft*, vol. 12, p. 615, 1933. W. GUERTLER, F. KLEWETA, W. CLAUS, and E. RICKERTSEN, *Z. Metallkunde*, vol. 27, p. 1, 1935. G. WASSERMANN, "Texturen metallischer Werkstoffe," Springer, Berlin, 1939.

<sup>4</sup> E. SCHMID, *Z. Metallkunde*, vol. 31, p. 125, 1929; *Metallwirtschaft*, vol. 18, p. 524, 1939. F. WOLBANK, *Z. Metallkunde*, vol. 31, p. 249, 1939.

<sup>5</sup> "Symposium on Radiography and X-ray Diffraction," *A.S.T.M.*, Philadelphia, Pa., 1936. W. SCHMIDT, *Z. Metallkunde*, vol. 25, p. 229, 1933.

<sup>6</sup> A. BECK, "The Technology of Magnesium and Its Alloys," F. A. Hughes & Co. Ltd., London, 1940.

notch-bend tests, and the formation of ears on drawn cups, there are other tests that have been used occasionally to reveal anisotropy.

A **tear test** proposed by Brownsdon<sup>1</sup> and Jevons<sup>2</sup> is one of the simplest. Slots about 1 cm. wide are cut at different directions in a sheet, and by

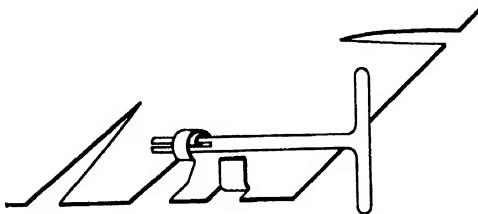


FIG. 5. Tear test for anisotropy in sheet metal. (Jevons.)

the use of a slotted key as shown in Fig. 5 strips are torn from the sheet in the way one opens a can of sardines. For reasons that are not understood, the relative lengths of the strips in different directions in the sheet seem to be indicative of the anisotropy.

**Cupping tests** frequently indicate directionality by the appearance of the metal around the deformed dome or cup and by the direction of splitting.<sup>3</sup> The Erickson cup test applied to copper, for example, results in characteristic breaks 0 and 90° to the direction of rolling if the specimen contains high percentages (60 to 100 percent) of grains aligned in the cube texture.<sup>4</sup> The breaks are at the positions where the true stress at fracture is a minimum.

The **vibrations in plates** form patterns of great variety, which can be seen if sand is scattered on the plate. If a plate is clamped at the center and stroked with a bow at the edge, the sand arranges itself along the nodal lines, forming Cladni figures. Tammann and his coworkers found that on round disks these figures, *Klangfiguren*, were sensitive to preferred orientations in the metal, and they correlated the figures for round disks with the rolling and annealing treatment.<sup>5</sup> No attempts were made to correlate them with x-ray determinations of the textures, with measurements of internal stresses (which were also thought to be a factor), or with direct measurements of the elastic constants; they were simply studied as a sensitive qualitative indication of internal changes.

**Magnetic-torque measurements** can be used to reveal anisotropy in ferromagnetic materials. In a torque magnetometer a disk-shaped sample is suspended on a wire in a magnetic field. In Williams's design of the instrument,<sup>6</sup> Fig. 6, the disk  $S_1$  is mounted on a vertical wire with

<sup>1</sup> H. W. BROWNSDON, *J. Inst. Metals*, vol. 60, p. 178, 1937.

<sup>2</sup> J. D. JEVONS, *J. Inst. Metals*, vol. 60, p. 174, 1937; *Metal Ind. (London)*, vol. 48, p. 607, 1936.

<sup>3</sup> J. D. JEVONS, *J. Inst. Metals*, vol. 60, p. 174, 1937; *Metal Ind. (London)*, vol. 48, p. 607, 1936. C. H. MARSHALL, *Proc. A.S.T.M.*, vol. 37, pt. 1, p. 518, 1937. J. D. JEVONS, *Metal Ind. (London)*, vol. 50, p. 405, 1937.

<sup>4</sup> W. M. BALDWIN, *Metals Tech.*, *Tech. Pub.* 1455, April, 1942.

<sup>5</sup> E. SCHRÖDER and G. TAMMANN, *Z. Metallkunde*, vol. 16, p. 201, 1924. G. TAMMANN and W. RIEDELSBERGER, *Z. Metallkunde*, vol. 18, p. 105, 1926.

<sup>6</sup> H. J. WILLIAMS, *Rev. Sci. Instruments*, vol. 8, p. 56, 1937.

bearings  $B_1$  and  $B_2$  and is located between the poles of an electromagnet, one-half of which is shown in the figure. Pointers are attached to the wire to indicate the angular position of the specimen and the torque exerted by the disk in twisting the supporting wire. The torque per unit volume is plotted against the azimuthal position of the disk, as shown in Fig. 7. Both single crystals and polycrystalline disks can be studied by instruments of this general type.<sup>1</sup> These instruments have

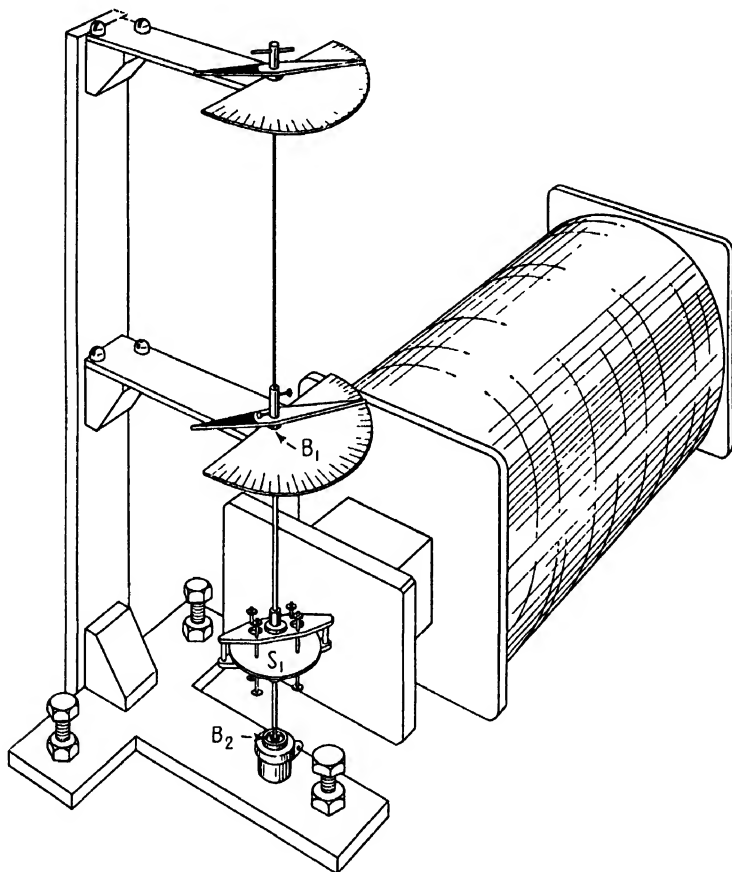


FIG. 6 Torque magnetometer for measuring magnetic anisotropy. Specimen  $S_1$  is between the poles of a magnet, one half of which is shown. (Williams.)

been used commercially to investigate and control manufacturing processes for producing steel for electrical purposes, since the torque curve is sensitive to changes caused by rolling and annealing procedures.<sup>2</sup>

<sup>1</sup> O. DAHL and J. PFAFFENBERGER, *Z. Physik*, vol. 71, p. 93, 1931. N. S. AKULOV and N. BRUCKATOV, *Ann. Physik*, (5), vol. 15, p. 741, 1932. N. P. GOSS, *Trans. A.S.M.*, vol. 23, p. 511, 1935. K. J. SIXTUS, *Physics*, vol. 6, p. 105, 1935. R. M. BOZORTH, *Phys. Rev.*, vol. 50, p. 1076, 1936. L. P. TARASOV and F. BITTER, *Phys. Rev.*, vol. 52, p. 353, 1937. L. P. TARASOV, *Trans. A.I.M.E.*, vol. 135, p. 353, 1939.

<sup>2</sup> H. J. WILLIAMS, *Rev. Sci. Instruments*, vol. 8, p. 56, 1937. N. P. GOSS, *Trans.*

Torque is exerted whenever the direction of the magnetic field does not coincide with a direction of easy magnetization in the material. A single crystal is saturated most easily when the magnetization is along a [100] direction; the ease of magnetization is intermediate along [110] and least along [111], as indicated in Fig. 8.<sup>1</sup> From equations giving the energy of the disk when magnetized in different directions the torque can be computed for all positions of a single crystal with any crystal plane in the plane of the disk.<sup>2</sup> The empirical torque curve for polycrystal-

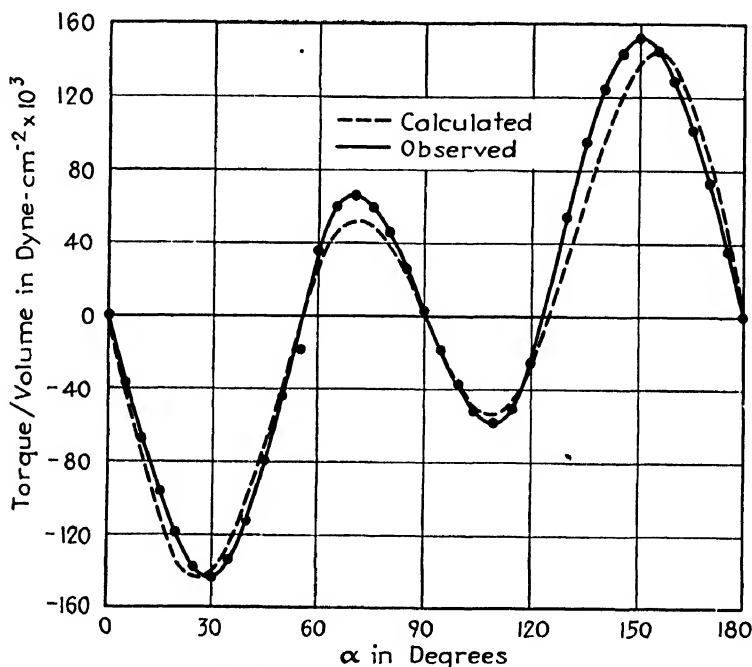


FIG. 7.—Magnetic-torque curve for a single crystal of silicon ferrite, with (110) in the plane of the disk. Field is parallel to [001] at the azimuthal position  $\alpha = 0$ . (Williams)

line material may then be compared with the curves computed for orientations that are assumed to be present in the disk.

As a means of determining unknown textures this method has serious disadvantages, for there seems to be no possibility of deriving rigorously the complete texture from an observed curve. Any texture or texture

*A.S.M.*, vol. 23, p. 511, 1935. K. J. SIXTUS, *Physics*, vol. 6, p. 105, 1935. I. P. TARASOV, *Trans. A.I.M.E.*, vol. 135, p. 353, 1939.

<sup>1</sup> Intensity of magnetization is  $I = (B - H)/4\pi$ , where  $H$  is the field strength and  $B$  is the magnetic induction.

<sup>2</sup> N. S. AKULOV and N. BRUCKATOV, *Ann. Physik*, vol. 15, p. 741, 1932. R. M. BOZORTH, *Phys. Rev.*, vol. 50, p. 1076, 1936. I. P. TARASOV and F. BITTER, *Phys. Rev.*, vol. 52, p. 353, 1937. R. M. BOZORTH and H. J. WILLIAMS, *Phys. Rev.*, vol. 59, p. 827, 1941.

component that is random around the normal to the disk gives no variation in torque, and the same is usually true for any material having (111) in the plane of the disk. However, simple textures, such as the cube texture, are readily recognized by comparison with observed or computed single-crystal curves, and reasonable agreement has been obtained by calculating torque curves from x-ray pole-figure data in highly cold rolled silicon steel.<sup>1</sup> When textures are less pronounced, as after smaller cold reductions, hot rolling, or recrystallization, there is less certainty in the interpretation. Nevertheless, the high sensitivity of torque curves and related methods of test to slight anisotropy and to variations in rolling and annealing schedules has made it of value in industrial laboratories.

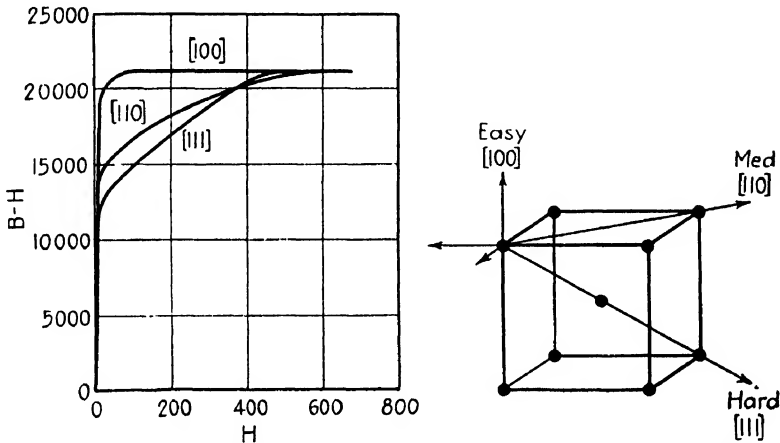


FIG. 8 -Ease of magnetization in the three principal directions of iron.

**Anisotropy of Elastic Properties of Crystals.**- Single crystals are generally anisotropic, and the formulas relating stress to strain must take account of the variation in "stiffness" of a crystal in different directions; many more constants of proportionality are required than for isotropic materials.<sup>2</sup> The relations between stress and strain are defined by the generalized Hooke's law, which is applicable to any homogeneous body, crystalline or not,

$$\left. \begin{aligned} \epsilon_x &= s_{11}\sigma_x + s_{12}\sigma_y + s_{13}\sigma_z + s_{14}\tau_{yz} + s_{15}\tau_{zx} + s_{16}\tau_{xy} \\ \epsilon_y &= s_{21}\sigma_x + s_{22}\sigma_y + s_{23}\sigma_z + s_{24}\tau_{yz} + s_{25}\tau_{zx} + s_{26}\tau_{xy} \\ \epsilon_z &= s_{31}\sigma_x + s_{32}\sigma_y + s_{33}\sigma_z + s_{34}\tau_{yz} + s_{35}\tau_{zx} + s_{36}\tau_{xy} \\ \gamma_{yz} &= s_{41}\sigma_x + s_{42}\sigma_y + s_{43}\sigma_z + s_{44}\tau_{yz} + s_{45}\tau_{zx} + s_{46}\tau_{xy} \\ \gamma_{zx} &= s_{51}\sigma_x + s_{52}\sigma_y + s_{53}\sigma_z + s_{54}\tau_{yz} + s_{55}\tau_{zx} + s_{56}\tau_{xy} \\ \gamma_{xy} &= s_{61}\sigma_x + s_{62}\sigma_y + s_{63}\sigma_z + s_{64}\tau_{yz} + s_{65}\tau_{zx} + s_{66}\tau_{xy} \end{aligned} \right\} \quad (1)$$

<sup>1</sup> R. M. BOZORTH, *Phys. Rev.*, vol. 50, p. 1076, 1936. L. P. TARASOV, *Trans. A I. M. E.*, vol. 135, p. 353, 1939.

<sup>2</sup> For the isotropic case, see p. 268.

and a corresponding set of relations

$$\left. \begin{aligned} \sigma_x &= c_{11}\epsilon_x + c_{12}\epsilon_y + c_{13}\epsilon_z + c_{14}\gamma_{yz} + c_{15}\gamma_{zx} + c_{16}\gamma_{xy} \\ \sigma_y &= c_{21}\epsilon_x + c_{22}\epsilon_y + c_{23}\epsilon_z + c_{24}\gamma_{yz} + c_{25}\gamma_{zx} + c_{26}\gamma_{xy} \\ \sigma_z &= c_{31}\epsilon_x + c_{32}\epsilon_y + c_{33}\epsilon_z + c_{34}\gamma_{yz} + c_{35}\gamma_{zx} + c_{36}\gamma_{xy} \\ \tau_{yz} &= c_{41}\epsilon_x + c_{42}\epsilon_y + c_{43}\epsilon_z + c_{44}\gamma_{yz} + c_{45}\gamma_{zx} + c_{46}\gamma_{xy} \\ \tau_{zx} &= c_{51}\epsilon_x + c_{52}\epsilon_y + c_{53}\epsilon_z + c_{54}\gamma_{yz} + c_{55}\gamma_{zx} + c_{56}\gamma_{xy} \\ \tau_{xy} &= c_{61}\epsilon_x + c_{62}\epsilon_y + c_{63}\epsilon_z + c_{64}\gamma_{yz} + c_{65}\gamma_{zx} + c_{66}\gamma_{xy} \end{aligned} \right\} \quad (2)$$

where the symbols  $\sigma$  and  $\tau$  represent normal and shear stresses and  $\epsilon$  and  $\gamma$  elongation and shear strains, respectively. In these equations the elastic constants  $s_{ij}$  and  $c_{ij}$  differ for each crystal and must be determined experimentally. Many of the coefficients are equal,<sup>1</sup> the number of independent constants decreasing as the symmetry of the crystal increases. In triclinic crystals, 21 are independent; in hexagonal crystals, 5; in cubic crystals, only 3. For example, in the cubic system the coefficients for Eqs. (1) are

$$\left. \begin{array}{cccccc} s_{11} & s_{12} & s_{12} & 0 & 0 & 0 \\ s_{12} & s_{11} & s_{12} & 0 & 0 & 0 \\ s_{12} & s_{12} & s_{11} & 0 & 0 & 0 \\ 0 & 0 & 0 & s_{44} & 0 & 0 \\ 0 & 0 & 0 & 0 & s_{44} & 0 \\ 0 & 0 & 0 & 0 & 0 & s_{44} \end{array} \right\} \quad (3)$$

When these are known, the strains along all axes of a cubic crystal can be computed from the stresses. Additional relations among the coefficients—the Cauchy-Poisson relations—should hold if all the forces in a crystal were acting between atom centers,<sup>2</sup> but measurements show that these relations rarely exist (*i.e.*, the early theories are inadequate). Recent theories are able to account remarkably well, usually to within 2 or 3 percent,<sup>3</sup> for the measured values of the elastic constants in some metals.

If a cylindrical crystal of a cubic metal is prepared with an orientation such that the direction cosines of the axis of the cylinder with respect to the crystal axes are  $\alpha$ ,  $\beta$ , and  $\gamma$ , then

<sup>1</sup> A. E. H. LOVE, "The Mathematical Theory of Elasticity," Cambridge, London, 1927. W. A. WOOSTER, "A Textbook on Crystal Physics," Cambridge, London, 1938.

<sup>2</sup> MAX BORN, Atomtheorie des festen Zustandes, "Encyklopadie der mathematischen Wissenschaften," vol. V pt. 3, 1926. P. P. EWALD, T. POSCHL, and L. PRANDTL, "The Physics of Solids and Fluids," Blackie, Glasgow, 1936. F. SEITZ—"The Modern Theory of Solids," McGraw-Hill, New York, 1940.

<sup>3</sup> F. SEITZ, "The Modern Theory of Solids," McGraw-Hill, New York, 1940.

$$\left. \begin{aligned} \frac{1}{E} &= s_{11} - 2 \left[ (s_{11} - s_{12}) - \frac{1}{2} s_{44} \right] (\alpha^2 \beta^2 + \beta^2 \gamma^2 + \gamma^2 \alpha^2) \\ \frac{1}{G} &= s_{44} + 4 \left[ (s_{11} - s_{12}) - \frac{1}{2} s_{44} \right] (\alpha^2 \beta^2 + \beta^2 \gamma^2 + \gamma^2 \alpha^2) \end{aligned} \right\} \quad (4)$$

For a hexagonal crystal, with  $\gamma$  the direction cosine of the specimen axis with respect to the hexagonal axis of the crystal,

$$\left. \begin{aligned} \frac{1}{E} &= s_{11}(1 - \gamma^2)^2 + s_{33}\gamma^4 + (2s_{13} + s_{44})\gamma^2(1 - \gamma^2) \\ \frac{1}{G} &= s_{44} + \left[ (s_{11} - s_{12}) - \frac{1}{2} s_{44} \right] (1 - \gamma^2) \\ &\quad + 2(s_{11} + s_{33} - 2s_{13} - s_{44})\gamma^2(1 - \gamma^2) \end{aligned} \right\} \quad (5)$$

The same arrangement of coefficients holds for an isotropic body, except that there are only two independent coefficients, since  $s_{44} = 2(s_{11} - s_{12})$  and  $c_{44} = \frac{1}{2}(c_{11} - c_{12})$ . The equations in scheme (3) are then identical

TABLE XXVI—MAXIMUM AND MINIMUM VALUES OF ELASTIC MODULI IN SINGLE CRYSTALS<sup>1</sup>

Metal	$E_{\max}$ kg / mm. <sup>2</sup>	Direction	$E_{\min}$ kg./ mm. <sup>2</sup>	Direction	$G_{\max}$ kg / mm. <sup>2</sup>	Direction	$G_{\min}$ kg / mm. <sup>2</sup>	Direction
Aluminum	7,700	[111]	6,400	[100]	2,900	[100]	2,500	[111]
Copper	19,400	[111]	6,800	[100]	7,700	[100]	3,100	[111]
Silver . . . . .	11,700	[111]	4,400	[100]	4,450	[100]	1,970	[111]
Gold . . .	11,400	[111]	4,200	[100]	4,100	[100]	1,800	[111]
$\alpha$ -Iron . . .	29,000	[111]	13,500	[100]	11,800	[100]	6,100	[111]
Tungsten . .	40,000	[111]	40,000	[100]	15,500	[100]	15,500	[111]
Magnesium	5,140	0°*	4,370	53 3°*	1,840	41 5°*	1,710	90°*
Zinc . . . .	12,630	70 2°	3,560	0°	4,970	90°	2,780	41 8°
Cadmium	8,300	90°	2,880	0°	2,510	90°	1,840	30°
$\beta$ -Tin . . . . .	8,640	[001]	2,680	[110]	1,820	45 7°†	1,060	[100]

\* Angle to the hexagonal axis

† In the plane (1120) at 45 7° to the hexagonal axis

<sup>1</sup> E. SCHMID and W. BOAS, "Kristallplastizität," Springer, Berlin, 1935.

with the equations between the principal stresses and strains previously given for an isotropic medium (page 270) where

$$E = \frac{1}{s_{11}} \quad G = \frac{1}{s_{44}} \quad \nu = -\frac{s_{12}}{s_{11}} = \frac{E}{2G} - 1. \quad (6)$$

Measured values of the elastic constants are summarized in Tables XXVI and XXVII.<sup>1</sup>

<sup>1</sup> For method of measurement using frequency of vibration of specimens, see W. F. Brown, *Phys. Rev.*, vol. 57, p. 558, 1940; vol. 58, p. 938, 1940. See also W. A. Good, *Phys. Rev.*, vol. 60, p. 605, 1941.

TABLE XXVII.—ELASTIC CONSTANTS OF CRYSTALS  
(Units are  $10^{-12}$  sq. cm. per dyne)<sup>1</sup>

Metal	$C_{11}$	$C_{12}$	$C_{44}$
Face-centered cubic:			
Aluminum . . . . .	1 59	— 0 58	3 52
Gold . . . . .	2 33	— 1 07	2 38
Silver . . . . .	2 32	— 0 993	2 29
Copper . . . . .	1 49	— 0 625	1 33
Lead . . . . .	9 30	— 4 26	6 94
Body-centered cubic:			
Iron . . . . .	0 757	— 0 282	0 862
Sodium . . . . .	48 3	—20 9	16 85
Potassium . . . . .	83 3	—37 0	38 0
Tungsten . . . . .	0 257	— 0 073	0 660

Metal	$C_{11}$	$C_{12}$	$C_{13}$	$C_{33}$	$C_{44}$
Hexagonal:					
Magnesium . .	2 23	—0 77	—0 45	1 98	5 95
Zinc	0 84	+0 11	—0 78	2 87	2 64
Cadmium	1 23	—0 15	—0 93	3 55	5 40

Metal	$C_{11}$	$C_{13}$	$C_{14}$	$C_{12}$	$C_{13}$	$C_{14}$	$C_{16}$
Lower symmetry:							
Antimony	1 77	3 38	1 10	—0 38	—0 85	—0 80	
Bismuth	2 69	2 87	10 48	—1 4	—0 62	+1 6	
Tin	1 85	1 18	5 70	—0 99	—0 25		13 5

Alloys, atomic percent	$C_{11}$	$C_{12}$	$C_{44}$
100Ag-0Au	2 32	—0 993	2 29
75Ag-25Au	2 07	—0 891	2 05
50Ag-50Au	1 97	—0 852	1 97
25Ag-75Au	2 05	—0 909	2 06
0Ag-100Au	2 29	—1 04	2 34
Cu <sub>3</sub> Au	1 34	—0 565	1 508
72Cu-28Zn	1 94	—0 84	1 39
50Cu-50Zn	3 88		
95Al-5Cu	1 5	—0 69	3 7

<sup>1</sup> F. SEITZ and T. A. READ, *J. Applied Phys.*, vol. 12, p. 100, 1941

**Elastic Moduli in Aggregates.**—The directional dependence of the elastic moduli in polycrystalline metal is dependent upon the orientations in the specimen and can be semiquantitatively predicted from the anisotropy of single crystals. The maximum value of Young's modulus,



$E$ , in face-centered cubic crystals is along the  $[111]$  direction, and the minimum is along  $[100]$ , the former about three times the latter in most face-centered cubic metals (aluminum is an exception and is nearly isotropic). In a direction  $\alpha$ ,  $\beta$ , and  $\gamma^\circ$  from the cube axes, respectively, the value is given by<sup>1</sup>

$$\frac{1}{E} = \frac{1}{E_{100}} - 3 \left( \frac{1}{E_{100}} - \frac{1}{E_{111}} \right) (\cos^2 \alpha \cos^2 \beta + \cos^2 \beta \cos^2 \gamma + \cos^2 \gamma \cos^2 \alpha)$$

When a double fiber texture is present or when a pole figure can be represented by two or more ideal orientations, it has been assumed that

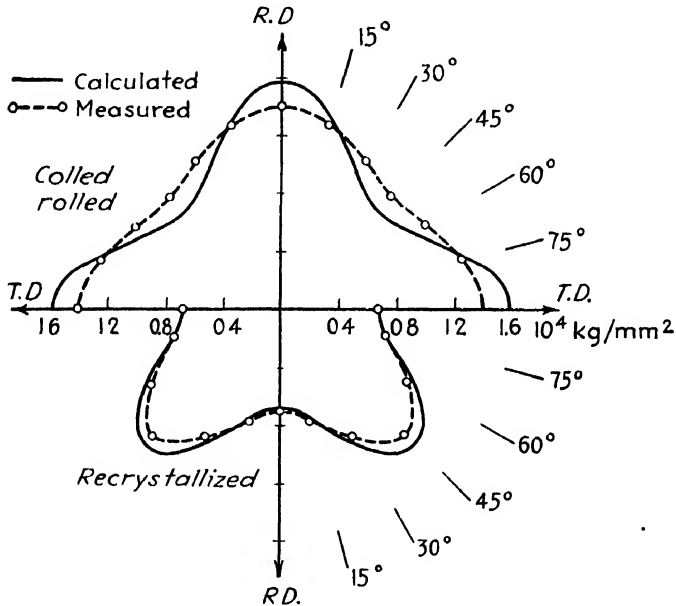


FIG. 9. Polar plot of Young's modulus in rolled and recrystallized copper sheet. Upper curves for rolled, lower for recrystallized. (Weerts.)

the quantity  $(1/E)$  for each orientation is additive and is weighted according to the amount of material in each orientation. Using this additivity principle, Weerts has computed  $(1/E)$  for rolled and for recrystallized copper sheet, with results agreeing satisfactorily with measured values, as shown in the polar plot of  $E$  in Fig. 9. The textures for these computations were assumed to be  $(110)[\bar{1}12]$  and  $(112)[11\bar{1}]$  in equal amounts for the rolled sheet and  $(100)[001]$  for the recrystallized material.

The large variation in elastic modulus of wires with annealing must arise from alterations in texture, since the elastic constants are almost unaffected by cold work and recovery. An example is the drop in  $E$  from

<sup>1</sup> J. WEERTS, *Z. Metallkunde*, vol. 25, p 101, 1933.

18,000,000 to 13,400,000 psi. when hard-drawn copper wire is annealed.<sup>1</sup> This is attributable to varying amounts of material in the two positions of the wire texture, [111] and [100], with annealing.<sup>2</sup>

The anisotropy of  $E$  in rolled iron has been computed<sup>3</sup> for an ideal texture composed of equal amounts of (100)[011] and (112)[ $\bar{1}\bar{1}$ 0] material with results that deviate in some directions as much as 40 percent from the measured values. Bruggeman<sup>4</sup> has made a more elaborate computation, using a closer representation of the actual pole figure. His results are within 10 percent of the measured values but are somewhat dependent upon assumed shapes of lamellar grains (the tangential deformation component and the normal stress component are assumed to be continuous across grain boundaries). Bruggeman<sup>5</sup> also has made computations of moduli for textures of many different metals, with fair agreement; random orientations have also been computed<sup>6</sup> using different methods of averaging, with and without considerations of grain-boundary conditions.

For hexagonal metals, anisotropy can be related to texture quite simply,<sup>7</sup> for properties vary only with angular distance from the hexagonal axis. The frequency with which the axis occurs at a given angle to the observation direction can be read from the pole figure. This frequency is used as the weight of the corresponding property value in the averaging process. Calculated values for an extruded zinc alloy (10% Al, 2% Cu, 0.03% Mg) were  $E = 11,200$  kg. per sq. mm.<sup>2</sup> and expansion coefficient  $= 19 \times 10^{-6}$ ; the observed values were 10,750 and  $21.4 \times 10^{-6}$ , respectively. For wire cold-drawn 80 percent the calculated values were  $E = 11,200$  and expansion coefficient  $= 23 \times 10^{-6}$ , while the observed values were 10,100 and  $22.3 \times 10^{-6}$ .

**Anisotropy of Physical Properties in Crystals.**—Specific electrical resistance does not vary with direction in crystals of the cubic metals,

<sup>1</sup> A. J. PHILLIPS and A. A. SMITH, *Proc. A.S.T.M.*, vol. 36, pt. 2, p. 263, 1936.

<sup>2</sup> With  $E_{111} = 27,600,000$  and  $E_{100} = 9,690,000$ , the principle of additivity of  $(1/E)$  would indicate that 73 percent of the cold-drawn wire was in the [111] position and 27 percent in the [100] position, whereas after recrystallization this is altered to 43 percent [111] and 57 percent [100], assuming for simplicity that there is no randomly oriented material in either sample.

<sup>3</sup> E. GOENS and E. SCHMID, *Naturwissenschaften*, vol. 19, p. 520, 1931.

<sup>4</sup> D. A. G. BRUGGEMAN, *Naturwissenschaften*, vol. 19, p. 811, 1931; *Z. Physik*, vol. 92, p. 561, 1934.

<sup>5</sup> D. A. G. BRUGGEMAN, *Z. Physik*, vol. 92, p. 561, 1934.

<sup>6</sup> D. A. G. BRUGGEMAN, *Z. Physik*, vol. 92, p. 561, 1934. A. HUBER and E. SCHMID, *Helv. Chim. Acta*, vol. 7, p. 620, 1934. W. BOAS and E. SCHMID, *Helv. Chim. Acta*, vol. 7, p. 628, 1934.

<sup>7</sup> W. BOAS, *Helv. Phys. Acta*, vol. 7, p. 878, 1934. E. SCHMID, *Z. Metallkunde*, vol. 30, Vorträge der Hauptverslg, p. 5, 1938. F. WOLBANK, *Z. Metallkunde*, vol. 31, p. 249, 1939.

but with crystals of lower symmetry it is anisotropic. The law of variation in hexagonal, rhombohedral, and tetragonal crystals depends on the angle,  $\phi$ , between the direction of measurement and the principal axis of the crystal (the hexagonal, trigonal, or tetragonal axis) according to the relation

$$\rho = \rho_{\perp} + (\rho_{\parallel} - \rho_{\perp}) \cos^2 \phi \quad (8)$$

where  $\rho_{\parallel}$  and  $\rho_{\perp}$  are the resistances parallel and perpendicular to the principal axis. The resistance has rotational symmetry around the principal axis.

TABLE XXVIII—ANISOTROPY OF PROPERTIES OF SINGLE CRYSTALS PARALLEL AND PERPENDICULAR TO THE PRINCIPAL AXIS<sup>1</sup>

Metal	Specific electrical resistance, $10^{-6}$ ohm-cm		Thermal expansion $\times 10^{-6}$			Thermoelectric force* $\times 10^{-6}$ volt/ $^{\circ}\text{C}$ .	
	$\parallel$	$\perp$	Temperature range, $^{\circ}\text{C}$	$\parallel$	$\perp$	$\parallel$	$\perp$
Magnesium	3.85	4.55	Near 20	26.4	25.6	1.87	1.66
Zinc	6.06	5.83	20–100	63.9	14.1	1.32	–0.50
Cadmium	8.36	6.87	20–100	52.6	21.4	1.60	–1.74
Mercury	0.0557	0.0737	–188–79	47.0	37.5	–17.9†	–15.1
Bismuth	138	109	Near 20	14.0	10.4		
Antimony	35.6	42.6	Near 20	15.6	8.0		
Tellurium	56000	154000	Near 20	–1.6	27.2		
$\beta$ -Tin	14.3	9.9	Near 20	30.5	15.5		

\* Comparison metal is copper. Minus sign indicates current flowing toward the copper at the cold junction.

† Measured against constantan.

<sup>1</sup> Data selected from the tabulation in E. Schmid and W. Boas, "Kristallplastizität," Springer, Berlin, 1935.

The same orientation dependence is obtained for other properties:<sup>1</sup> the specific resistance to heat flow; the coefficient of thermal expansion; the thermoelectric force (the e.m.f. against a comparison metal, say copper, with a  $1^{\circ}$  temperature difference); the constant in the Thomson effect (the quantity of heat generated in a unit length of wire having a temperature gradient of  $1^{\circ}$  per cm. and carrying a unit current of electricity); and the magnetic susceptibility (intensity of magnetization divided by the field strength). Each of these properties is isotropic for cubic crystals.

Representative values for some of these properties near room temperature in noncubic metals are given in Table XXVIII. Other ani-

<sup>1</sup> E. SCHMID and W. BOAS, "Kristallplastizität," Springer, Berlin, 1935.

sotropic properties include linear compressibility, temperature coefficient of thermal expansion, temperature coefficient of electrical conductivity, magnetic permeability, rates of diffusion and self-diffusion, and rates of chemical reactions such as oxidation and etching, etc. All these properties are altered when a metal is cold-worked. Electrode potential, thermal expansion, compressibility, coercive force, and electrical resistance are *increased* (the last usually about 2 percent, but 18 percent in molybdenum and 50 percent in tungsten); the temperature coefficient of electrical resistance, thermal conductivity, and maximum permeability are *decreased* when polycrystalline metal is cold-worked. Some of these changes may be due to changes in the physical properties of the individual grains, and some may be due to changes in texture or to the two causes combined.

## CHAPTER XXII

### AGE HARDENING AND TRANSFORMATIONS

The hardening of alloys by aging is of great industrial importance and unusual scientific interest. The changes of physical properties, which are exceedingly varied and complex, are worthy of much study and have been the subject of so many investigations it would not be possible adequately to summarize them here. The present discussion is limited to the more striking *crystallographic* features of the subject.<sup>1</sup>

Merica, Waltenberg, and Scott<sup>2</sup> were the first to point out that for an alloy to age-harden it must have a decreasing solubility with decreasing temperature, so that when the alloy is given a solution heat-treatment and then a quench it will be supersaturated with respect to one or more dissolved elements. Subsequent aging at a lower temperature is associated with changes in the supersaturated alloy.

**Theories of Age Hardening.**—Age hardening was first believed to be due to the keying of slip planes by particles that precipitated from the supersaturated matrix.<sup>3</sup> Many complexities were later discovered that made it necessary to modify this theory.

A major obstacle to the simple theory arose when various observers were unable to see any precipitate in Al-Cu alloys or in duralumin when aged to the maximum hardness at low temperatures. A number of theories were then proposed which associated the hardening with a preprecipitation process—some variety of association of solute atoms on the lattice of the matrix. These theories were not required, of course, for systems in which alterations in the microstructure could be detected during age hardening. It now appears from the work of Fink and Smith<sup>4</sup> that it is no longer necessary, even for Al-Cu alloys, to employ these theories of “knots,” “complexes,” or other invisible associations of atoms before precipitation, since microstructural alterations can be

<sup>1</sup> The reader is referred to the following reviews for extensive bibliographies and summaries wider in scope: “Symposium on the Age-hardening of Metals,” A.S.M., Cleveland, Ohio, 1940. W. L. Fink, *J. Applied Phys.*, vol. 13, p. 75, 1942

<sup>2</sup> P. D. MERICA, R. G. WALTEMBERG, and H. SCOTT, *Trans. A.I.M.E.*, vol. 64, p. 41, 1920.

<sup>3</sup> Z. JEFFRIES and R. S. ARCHER, “The Science of Metals,” p. 390, McGraw-Hill, New York, 1924.

<sup>4</sup> W. L. FINK and D. W. SMITH, *Mining and Met.*, vol. 16, pp. 228, 513, 1935, vol. 17, p. 101, 1936.

observed in Al-Cu as soon as hardness begins to increase, provided that the most careful metallographic technique is employed. Typical changes in properties with time are illustrated in Fig. 1 for Al-Cu (5.17 percent copper) aged at 160°C.<sup>1</sup>

The lattice-parameter curve in Fig. 1 illustrates another difficulty that was encountered in establishing aging theory. The first visible evidence of precipitation may occur, as it does here, long before there is any change in the lattice parameter of the matrix. This type of behavior at first was considered strong evidence that precipitation was

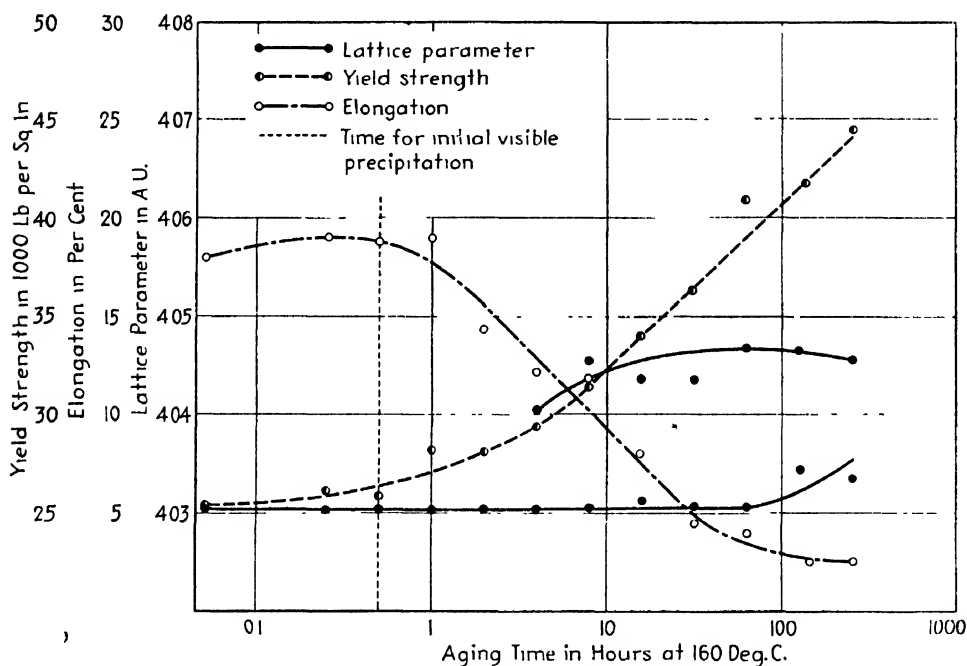


FIG. 1.—Aging curves for Al-Cu (5.17% Cu) aged at 160°C. (Fink and Smith.)

not responsible for hardening, since the precipitate, being richer in the dissolved element, on forming should deplete the matrix and thereby alter the matrix parameter.<sup>2</sup> Microstructural studies of Fink and Smith<sup>1</sup> have now provided a simple explanation. Precipitation occurs much more rapidly in certain restricted areas than in others and may be well advanced in these narrow bands when the bulk of the matrix is still unaltered. Slip lines and grain boundaries are favored regions for rapid precipitation in some alloys, as will be seen from Figs. 2 and 3. In the regions of rapid precipitation the lattice parameter alters to that of the depleted matrix (the upper branch of the parameter curve in

<sup>1</sup> W. L. FINK and D. W. SMITH, *Trans. A.I.M.E.*, vol. 122, p. 284, 1936.

<sup>2</sup> E. SCHMID and G. WASSERMANN, *Metallwirtschaft*, vol. 7, p. 1329, 1928. F. A. GÖLER and G. SACHS, *Z. Metallkunde*, vol. 22, p. 141, 1930.

Fig. 1) before the diffraction lines from other regions register any parameter change. Many examples can be listed in which there is a *uniform*

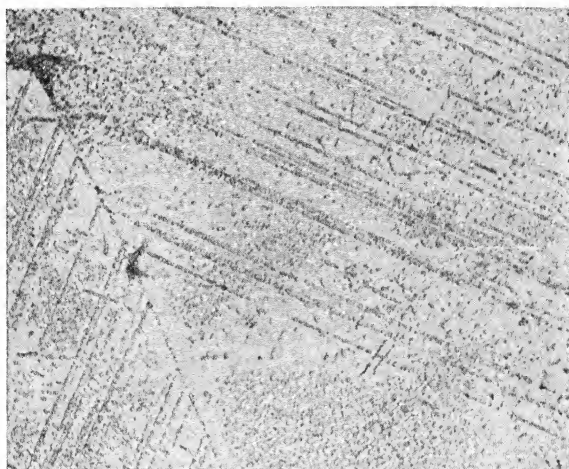


FIG. 2.—Microstructure of Al-Cu (5.17 % Cu) aged 4 hr. at 200°C. Precipitation is concentrated along slip planes and along grain boundary (at lower left).  $\times 500$ . (Fink and Smith.)

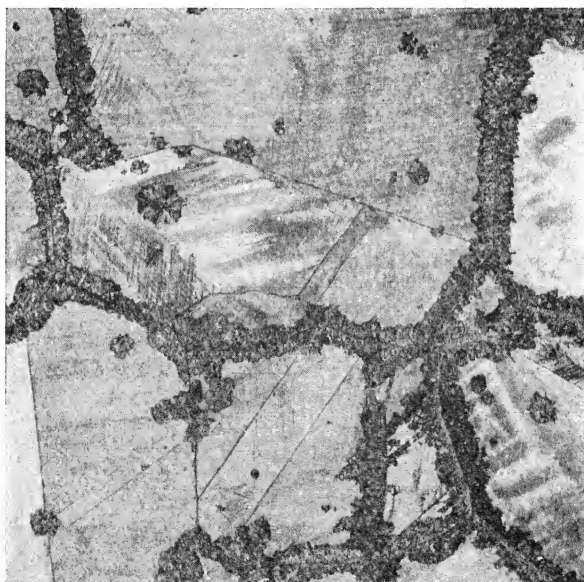


FIG. 3.—Microstructure of Cu-Be alloy (1.97 % Be, 0.03 % Fe, no Ni) showing band of rapid precipitation at grain boundaries. Quenched from 820°C., aged 2 hr. at 325°C.  $\times 75$ . (C. S. Smith.)

distribution of particles throughout the grains, and in these alloys the lattice constant of the matrix changes continuously during aging; other alloys show intermediate and mixed types.. Thus, x-ray investigations

must be accompanied by careful metallographic observations if the character of precipitation is to be understood. Some lattice-parameter anomalies have also been found that were traced to quenching stresses in the samples. This source of error is treated on page 184.

The present theory of aging includes the following steps in the precipitation process (at least in the systems Al-Cu, Al-Ag, and Al-Mg).

1. Statistical fluctuations of concentration in the matrix provide clusters of atoms of the correct composition to form nuclei.<sup>1</sup>

2. Thin platelike regions are produced which form two-dimensional diffraction gratings. These are presumably thin plates of a transition structure, and in systems having pronounced hardening they are probably coherent with the matrix, *i.e.*, there is a continuity across the matrix-precipitate interface. Strains accompanying this coherence induce hardening through interference with slip.<sup>2</sup>

3. The particles grow in thickness and in lateral dimensions, finally in some alloys attaining a size that yields three-dimensional diffraction; in other alloys the particles become only a few atom layers thick.

4. Upon reaching a certain size the transition structure transforms to the stable structure of the equilibrium precipitate. This appears to be associated with overaging and with the release of coherency stresses. There appear to be peculiar microstructural alterations associated with this stage in some alloys, such as recrystallization of the matrix or coalescence and realignment of the particles (Fig. 3).

Further details of steps 2, 3, and 4 are discussed in subsequent sections. It is believed that some of these steps are omitted in some alloys, and the relative importance of each step is a subject for research in each alloy system.

**Microstructures Resulting from Precipitation.**—The structures found during age hardening in fine-grained alloys are on a microscopic or a submicroscopic scale and are difficult to study in detail, but the structures formed in large grains and in single crystals during precipitation may be produced on a scale that is convenient for laboratory investigation. Detailed studies of these grosser structures have gone far in establishing a basis for the understanding of age hardening.

The beautifully regular markings on a polished and etched surface of an iron-nickel meteorite were first discovered by Widmanstätten early in the nineteenth century. It was nearly a century later that Osmond and Cartaud explained their origin, the precipitation of a new phase along certain crystallographic planes of the existing matrix crystal. It is a surprising fact that the study of meteorites has occupied an important

<sup>1</sup> W. L. FINK and D. W. SMITH, *Trans. A.I.M.E.*, vol. 137, p. 95, 1940.

<sup>2</sup> R. F. MEHL and L. K. JETTER, "Symposium on the Age-hardening of Metals," A.S.M., Cleveland, Ohio, 1940.



place in the development of physical metallurgy. The petrographer Sorby, who is recognized as the father of the metallurgical microscope, initiated metallography when he looked at steels under the microscope in a search for figures similar to the figures in meteorites. Osmond, Cortaud, and Roozeboom, inspired by an interest in meteorites, published the first phase diagram—one for the Fe-Ni system. Neumann bands were first found in meteorites and were eventually shown to be twins generated when the meteorites struck the earth. The study of meteorites has been continued to this day.

Networks of parallel lamellae similar to the meteoric structure have now been observed in artificially prepared Fe-Ni alloys (Fig. 4)

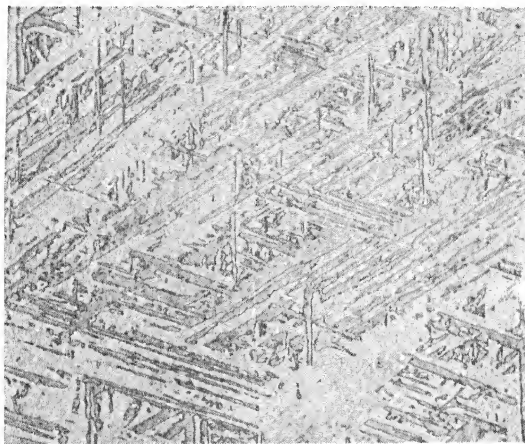


Fig. 4.—Widmanstätten pattern produced by slowly cooling an Fe-Ni alloy (27 % Ni).  $\times 50$ . (*Derge and Kommel.*)

and in a great number of other alloys and have come to be known as Widmanstätten structures. They are to be expected whenever a solid solution, homogeneous at one temperature, is made to become supersaturated at another temperature. In the majority of cases the precipitating crystals are thin plates forming on matrix planes of low indices, as shown in Figs. 4 and 5; occasionally, they form on planes of high indices or on irrational planes, and in some instances they form needles, geometrical shapes, rosettes, or irregular particles instead of plates. The orientation of the precipitate lattice is definitely related to the orientation of the matrix lattice. Because the crystallography of these structures and the orientation relationships involved are fundamental to the theory of age hardening, there has been continued interest in Widmanstätten figures in spite of their academic nature. Further interest derives from the fact that analogous relations between the lattices are found in all solid-solid reactions, whatever their type. A tabulation of the results of research in this field is given on page 486.

**Lattice Relationships in Widmanstätten Structures.**—Young<sup>1</sup> first showed by x-rays that the lamellae of meteorites were single crystals of definite orientation. The high-temperature face-centered cubic (f.c.c.) phase,  $\gamma$ , of the Fe-Ni alloy (roughly 8 percent nickel) precipitates body-centered cubic (b.c.c.)  $\alpha$  crystals as plates along the octahedral planes of the  $\gamma$  matrix. Within the  $\alpha$  plates the (110) planes are parallel to the plane of union with the matrix. The close similarity between the atomic array on the (110) plane in the plate and the (111) plane of the matrix, to which it is joined, suggests that atom movements during precipitation

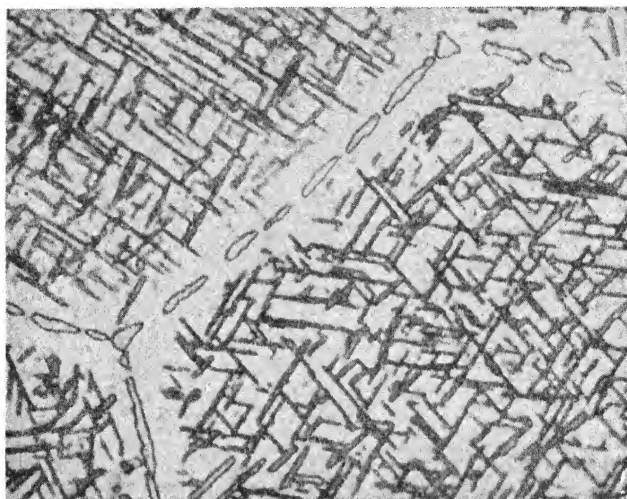


FIG. 5.—Widmanstätten pattern in Al-Ag (20.2 % Ag) aged 25 hr. at 387°C. Precipitation is  $\gamma'$  and  $\gamma$  in the form of plates on (111) planes of matrix.  $\times 2000$ .

are not extensive. This thought has been the keynote of nearly all theories in the field. A prime example of the simplicity in orientation that sometimes can be found and of the simplicity in atom movement that one feels sure must have produced it is offered by the system Al-Ag (aluminum-rich), one of the first Widmanstätten structures of microscopic dimensions to receive a thorough analysis (Fig. 5).<sup>2</sup>

It was found that in the Al-Ag system each plate of the precipitate, which is hexagonal close-packed (h.c.p.), forms along an octahedral plane of the f.c.c. matrix; the basal plane of the precipitate lies parallel to the octahedral plane of the matrix. Furthermore, the closest packed rows of atoms in matrix and precipitate are parallel. The two planes

<sup>1</sup> J. YOUNG, *Proc. Roy. Soc. (London)*, vol. A112, p. 630, 1926.

<sup>2</sup> R. F. MEHL and C. S. BARRETT, *Trans. A.I.M.E.*, vol. 93, p. 78, 1931.

that face each other across the interface between plate and matrix are both close-packed atom layers identical in pattern and almost identical in dimensions; the planes lying behind them are likewise similar. Merely the *sequence* of the layers undergoes a major alteration during precipitation. It was therefore concluded that precipitation takes place when certain close-packed layers of the matrix shift over one another so as to abandon the face-centered sequence of these layers,  $ABCABC \dots$ , and acquire the h.c.p. sequence  $ABAB \dots$ , in which every third layer, instead of every fourth, is above the first.

Further details of this process are now known<sup>1</sup> and may be presented with the aid of Fig. 6. The matrix structure (f.c.c.  $\delta$ ) is indicated in Fig. 6a with (111) as the base plane of the sketch. Figure 6b shows the

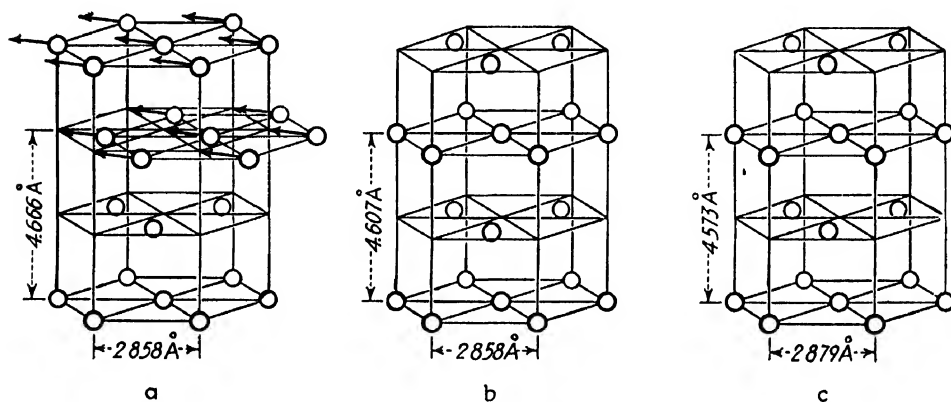


FIG. 6.—Crystal lattice of phases in Al-Ag alloys. *a*, matrix,  $\delta$  (face-centered cubic); *b*, transition phase  $\gamma'$  (hexagonal close-packed), *c*, equilibrium precipitate,  $\gamma$  (hexagonal close-packed).

transition structure that forms first during precipitation as the result of movements suggested by the arrows in Fig. 6a. This transitional structure ( $\gamma'$ ) is h.c.p. The atom spacings in the horizontal layers do not change during the  $\delta$  to  $\gamma'$  transition, though the vertical spacing decreases 1.4 percent. The basal plane of the new lattice maintains complete registry with the (111) plane of the matrix and continues to do so until the plate has grown to a thickness of many hundreds of angstroms. Finally, the stresses tending to tear the particle from registry become intolerable, and the transition to the stable structure of Fig. 6c occurs. The stable phase  $\gamma$  differs from the transition phase only in its dimensions *a* and *c*. Presumably the transition phase is merely a stressed form of the stable phase, the stresses arising from the coherency between precipitate and matrix.<sup>2</sup>

<sup>1</sup> C. S. BARRETT and A. H. GEISLER, *J. Applied Phys.*, vol. 11, p. 733, 1940. C. S. BARRETT, A. H. GEISLER, and R. F. MEHL, *Trans. A.I.M.E.*, vol. 143, p. 134, 1941.

<sup>2</sup> If  $\gamma'$  is considered as elastically strained  $\gamma$ , it has been estimated that the stresses

The sequence of events discussed above is in entire accord with the theory of Mott and Nabarro.<sup>1</sup> Assuming that the breaking away of a precipitated particle from the matrix plane on which it forms requires roughly the same energy as the melting of a monatomic layer of metal at the surface of the particle, Nabarro calculates that the particle will break away when its thickness equals

$$\frac{c_{11}\Lambda J\rho}{(c_{11} + 2c_{12})(c_{11} - c_{12})\delta^2}$$

where  $c_{11}$  and  $c_{12}$  are the elastic moduli,  $\Lambda$  is the latent heat of melting,  $J$  is the mechanical equivalent of heat,  $\rho$  is the density, and  $\delta$  is the misfit between the two lattices in the matched plane. If the constants for silver are inserted, the thickness for breaking away is roughly  $(107 \times 10^{-4})/\delta^2$ ; and for the reaction Nabarro considered, the precipitation of silver from copper, breaking away will occur when the particle is only two atoms thick and is incapable of giving sharp x-ray diffraction rings. In the present instance, the misfit between the unstrained (111) and (0001) planes is only  $(2.879 - 2.858)/2.858 = 0.0073$ , and the same constants would predict breaking away at about 320 atom layers, or 730 Å. The theory is thus in accord with the observed fact that sharp Debye rings can be obtained from  $\gamma'$  before it becomes large enough to break away and become  $\gamma$ .

The stresses in the matrix that keep the precipitate in the strained  $\gamma'$  condition are beyond much doubt an important contributor to the hardening.<sup>1</sup> It is an old idea that strains are set up during aging and that these are important in producing age hardening. The theories were based on the volume changes accompanying precipitation and more vaguely on precipitate-matrix interaction, but in recent years the importance of the effect of registry on strain has been pointed out,<sup>2</sup> and it now appears probable that strains accompanying coherence are the major factor. Strains arising from volume changes during precipitation exert a minor hardening effect, if any, and the transformations from  $\gamma'$  to  $\gamma$  in Al-Ag and from  $\theta'$  to  $\theta$  in Al-Cu, which are transformations that relieve the strains of registry, are accompanied by softening (overaging).

---

required are about 100,000 psi., compressional, in all directions parallel to the basal plane of the precipitate, and approximately zero along the  $c$  axis.

<sup>1</sup> N. F. MOTT and F. R. N. NABARRO, *Proc. Phys. Soc. (London)*, vol. 52, p. 86, 1940. F. R. N. NABARRO, *Proc. Phys. Soc. (London)*, vol. 52, p. 90, 1940; *Proc. Roy. Soc. (London)*, vol. A175, p. 519, 1940.

<sup>2</sup> R. F. MEHL and L. K. JETER, "Symposium on the Age-hardening of Metals," A.S.M., Cleveland, Ohio, 1940. W. L. FINK and D. W. SMITH, *Trans. A.I.M.E.*, vol. 122, p. 284, 1936; vol. 137, p. 95, 1940.

**Plane of Precipitation.**—Upon what crystallographic plane of the matrix will a plate of precipitate form? A review of some of the published data on various systems (Table XXIX, page 486) shows immediately that a plate will not necessarily grow on the plane of greatest atomic density, nor even on a plane containing one of the closest packed rows of atoms, nor on the cleavage, slip, or twinning planes. The plane chosen is the result of an interaction between matrix and precipitate structures, but thus far it has not been possible to state a crystallographic rule that applies to all systems. A rule that applies to most alloys is that the atomic planes facing each other across the matrix-precipitate interface have very similar atom patterns and atom spacings. This may be a manifestation of a more fundamental rule that the energy required to produce the interface must be a minimum. It appears that this energy

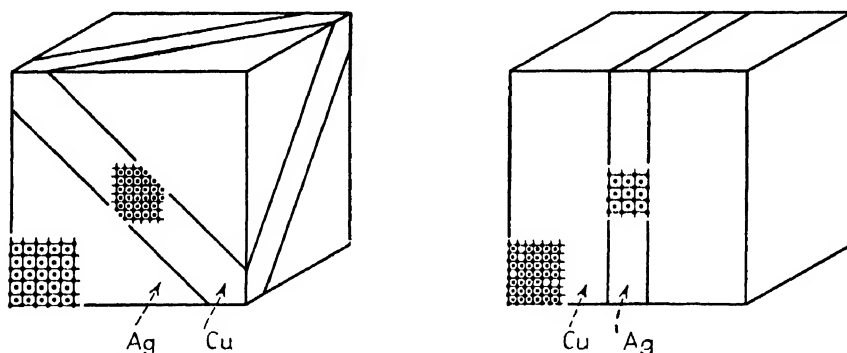


FIG. 7.—Lattice orientations and habit planes for precipitation in Ag-Cu alloys.

requirement will be met when the new crystal forms in such a way as to be as nearly as possible a continuation of the old; hence, one would expect matched planes at the interface.

A factor that may be determinative in some alloys is the activation energy that is required to shear or otherwise distort a matrix lattice so as to generate the new crystal within it. The Al-Ag example discussed earlier (Fig. 6) is consistent with this point of view, as well as with the preceding theory, for in this example the atom movements are almost identical with plastic deformation by slip. Unfortunately, this point of view is not applicable to many systems.

The data on Widmanstätten structures in the system Cu-Ag are interesting. This is a simple eutectic system, both lattices of which are f.c.c., in which a silver-rich precipitate can be grown in a copper-rich matrix, or vice versa. At one end of the system, plates of copper form on  $\{111\}$  planes of the silver matrix; at the other end, the plates of silver form on the  $\{100\}$  planes of the copper matrix. As indicated by the sketch in Fig. 7, all precipitated crystals have the same orientation as the

matrix.<sup>1</sup> Theories based on lattice continuity or on shearing movements appear not to apply to this system.

**Shape of Precipitated Particles.**—The external shape of precipitated crystals is platelike with a few exceptions, such as the  $\alpha$  needles that can be made to form in the  $\beta$  phase of Cu-Zn alloys<sup>2</sup> by suitable heat-treatment. Platelets and equiaxed polyhedra can also be formed in these alloys without altering the lattice orientation of the new crystals with respect to the old. It appears that external habit can be sensitive to conditions during growth somewhat as it is in the growth of crystals from liquid solution. It can be argued that if the original nucleus is platelike in shape the concentration gradients around the particle will tend to maintain this shape.<sup>3</sup>

A theoretical approach to the problem of shape has been made by Mott and Nabarro<sup>4</sup> by calculating the strain energy that will be developed when precipitate particles of various shapes form in a matrix. They have shown that the least strain energy is associated with particles having the form of a thin plate. This holds even after a particle has broken away from its registry with the matrix and in spite of the opposing tendency for the particle to become more spherical so as to minimize the surface energy. Since the tendency to spheroidization decreases with larger particles, the resulting form should be flatter the larger the particle. It may also be concluded that flatness is favored by a low rate of precipitation.

**Diffraction in the Early Stages of Aging.**—X-ray diffraction has recently furnished much information on the changes occurring in the early stages of the precipitation process during age hardening. The existence of transitional states, which precede the stable ones, was proved for the systems Al-Cu\* and Al-Ag.† Before transition structures become fully developed, however, x-ray diffraction effects can be obtained from the small platelike regions where the precipitation process is beginning. This

<sup>1</sup> C. S. BARRETT, H. F. KAISER, and R. F. MEHL, *Trans. A.I.M.E.*, vol. 117, p. 39, 1935.

<sup>2</sup> R. F. MEHL and O. T. MARZKE, *Trans. A.I.M.E.*, vol. 93, p. 123, 1931. J. WEERTS, *Z. Metallkunde*, vol. 24, p. 265, 1932. O. T. MARZKE, *Trans. A.I.M.E.*, vol. 104, p. 64, 1933.

<sup>3</sup> R. F. MEHL and C. S. BARRETT, *Trans. A.I.M.E.*, vol. 93, p. 78, 1931.

<sup>4</sup> N. F. MOTT and F. R. N. NABARRO, *Proc. Phys. Soc. (London)*, vol. 52, p. 86, 1940. F. R. N. NABARRO, *Proc. Phys. Soc. (London)*, vol. 52, p. 90, 1940; *Proc. Roy. Soc. (London)*, vol. A175, p. 519, 1940.

\* G. WASSERMANN and J. WEERTS, *Metallwirtschaft*, vol. 14, p. 605, 1935. W. L. FINK and D. W. SMITH, *Trans. A.I.M.E.*, vol. 122, p. 284, 1936; vol. 137, p. 95, 1940. G. D. PRESTON, *Proc. Roy. Soc. (London)*, vol. A167, p. 526, 1938, *Phil. Mag.*, vol. 26, p. 855, 1938.

† C. S. BARRETT, A. H. GEISLER, and R. F. MEHL, *Trans. A.I.M.E.*, vol. 143, p. 134, 1941.

was discovered in Al-Cu alloys by Guinier and his coworkers\* and independently by Preston.† The platelets produce streaks on Laue photographs such as would be caused by two-dimensional gratings located on {100} planes of the aluminum matrix. Guinier and Preston assumed that these platelets were clusters of copper atoms in the solid solution, but it now seems more probable that they are thin platelets of the transition phase ( $\theta'$ ), richer in copper than the matrix.<sup>1</sup> The dimensions of the platelets can be determined from the length and width of the diffraction streaks and average a few atomic layers in thickness by a few hundreds of angstroms in diameter; the dimensions increase as

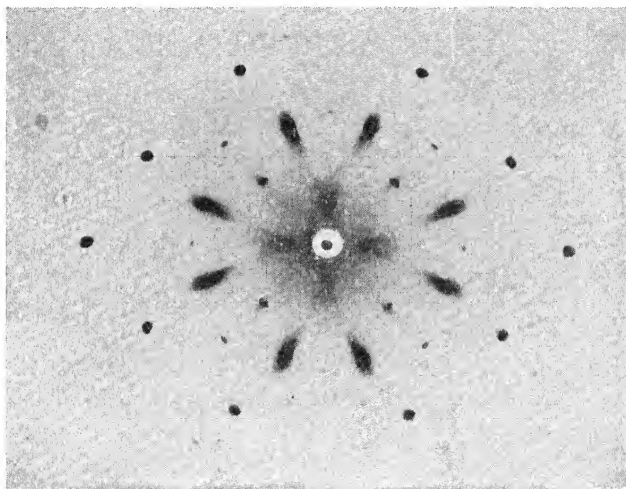


Fig. 8.—Laue photograph of single crystal of Al-Ag alloy (20.2 % Ag) in an early stage of aging (104 hr. at 150°C.). Shows prominent streaks.

aging is continued and eventually reach a value that gives three-dimensional diffraction. At a later stage the lattice transforms to the stable phase ( $\theta$ ).

Similar streaks in Laue photographs now have been observed and studied in detail in other age-hardening alloys. In aluminum-rich

\* A. GUINIER, *Compt. rend.*, vol. 204, p. 1115, 1937; vol. 206, p. 1641, 1938; *Nature*, vol. 142, p. 669, 1938. J. CALVET, P. JACQUET, and A. GUINIER, *J. Inst. Metals*, vol. 6, p. 177, 1939.

† G. D. PRESTON, *Nature*, vol. 142, p. 570, 1938; *Phil. Mag.*, vol. 26, p. 855, 1938; *Proc. Roy. Soc. (London)*, vol. A167, p. 526, 1938; *Proc. Phys. Soc. (London)*, vol. 52, p. 77, 1940. The platelets producing these diffraction effects have sometimes been called "Guinier-Preston zones" and "Guinier-Preston aggregates," after their discoverers.

<sup>1</sup> R. F. MEHL and L. K. JETTER, "Symposium on the Age-hardening of Metals," A.S.M., Cleveland, Ohio, 1940. C. S. BARRETT, A. H. GEISLER, and R. F. MEHL, *Trans. A.I.M.E.*, vol. 143, p. 134, 1941. A. H. GEISLER, dissertation, Carnegie Institute of Technology, Pittsburgh, Pa., 1942.

Al-Ag alloys, cross-grating diffraction is very evident.<sup>1</sup> Figure 8 is a pattern of a 20 percent silver alloy quenched and aged 104 hr. at 150°, showing sharply defined curved streaks. If the streaks are plotted on a stereographic projection, they follow great circles on the projection, as shown in Fig. 9, and the great circles are found to pass through  $[111]$  poles.

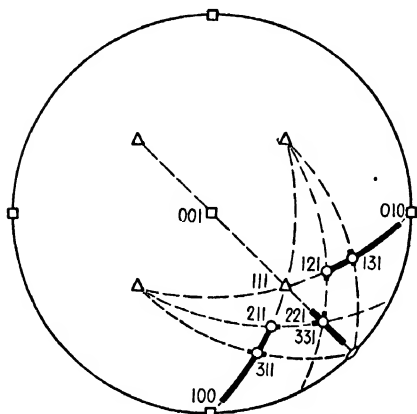


FIG. 9. Stereographic projection of one quadrant of Fig. 8. Streaks follow zone circles through  $(111)$  poles.

An interpretation of the pattern in terms of the reciprocal lattice may be seen by reference to Fig. 10. A reference sphere is centered at the origin,  $O$ , of the reciprocal lattice, and the points of the reciprocal lattice are projected radially upon the sphere. These points on the sphere may be shown, in turn, in a stereographic projection of the sphere. If there is a lack of periodicity of scattering power in the diffracting crystal such that one of the three Laue conditions is relaxed, causing diffraction as from a two-dimensional grating, then the reciprocal

lattice contains *lines* normal to the plane of the grating. In Fig. 10 this condition is indicated for a grating in the  $YZ$  plane. Heavy lines parallel to  $X$ , normal to the  $YZ$  plane, are drawn through the reciprocal lattice points. Projected on the reference sphere or on its stereographic projection, these lines are great circles that pass through the pole,  $P$ , of the two-dimensional grating responsible for the streaks.

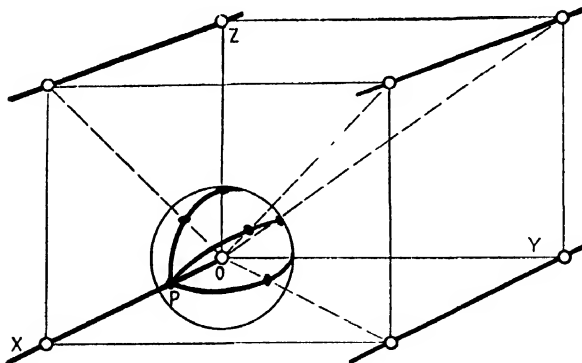


FIG. 10.—Reciprocal lattice points and lines projected on reference sphere.

Referring again to Fig. 9, it will be seen that the great-circle arcs converge to  $\{111\}$  poles. Thus the cross gratings are located on the  $\{111\}$  planes of the matrix. A similar analysis of the Al-Cu Laue patterns

<sup>1</sup> C. S. BARRETT and A. H. GEISLER, *J. Applied Phys.*, vol. 11, p. 733, 1940. C. S. BARRETT, A. H. GEISLER, and R. F. MEHL, *Trans. A.I.M.M.E.*, vol. 143, p. 134, 1941.



establishes cross gratings on  $\{100\}$  planes. Since the streaks of Fig. 8 run through the Laue spots of the matrix, the close-packed rows of atoms in the plane of the cross grating must lie parallel to the close-packed rows of the  $\{111\}$  matrix plane against which they lie. Later in the aging process the precipitating particles grow into three-dimensional particles of the transition phase  $\gamma'$  and finally transform to  $\gamma$ , without altering the orientation of the close-packed strings of atoms. Successive stages in the process are illustrated by the photographs in Figs. 11 and 12.

The length of a streak is governed by the thickness of the diffracting particle, the lateral width by the dimensions of the plate-shaped particle in its own plane. As the precipitate grows, the streaks condense into

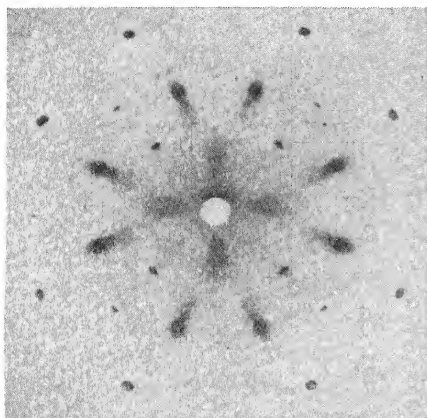


FIG. 11.—Advanced stage of aging in crystal of Fig. 8. Streaks are condensing into spots. (Aged  $2\frac{1}{2}$  hr. at  $200^{\circ}\text{C}$ .)

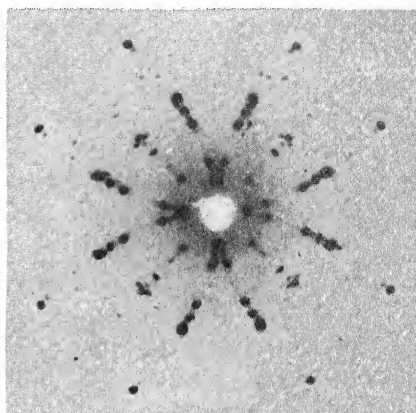


FIG. 12.—Fully developed precipitate in crystal of Figs. 8 and 11 gives sharp precipitate spots superimposed on streaks from smaller particles of precipitate. (Aged 1 hr. at  $320^{\circ}\text{C}$ .)

sharp spots (Fig. 12). The diffraction patterns thus serve to measure the variation of particle size with time and temperature of aging. Experiments confirm the theoretical prediction<sup>1</sup> that precipitating nuclei should be smaller with increasing supersaturation, for example, with low-temperature aging.

The two-dimensional gratings causing these effects could be thin clusters of silver atoms on  $\{111\}$  planes of the matrix, which later develop into nuclei of  $\gamma'$ , or they could be thin plates of the precipitate itself; metallurgists generally have preferred the latter supposition. The precipitate need not have reached full regularity of structure, however,

<sup>1</sup> R. BECKER, *Z. Metallkunde*, vol. 29, p. 245, 1937; *Ann. Physik.* vol. 32, p. 128, 1938; *Proc. Phys. Soc. (London)*, vol. 52, p. 71, 1940. Summarized by R. F. Mehl and L. K. Jetter, "Symposium on the Age-hardening of Metals," A.S.M., Cleveland, Ohio, 1940.

and the identity distance normal to the (111) plane may be  $n$  times the spacing of the (111) planes, where  $n = 2, 3, 4, 5$ , etc., at different places in the crystal.<sup>1</sup> The two-dimensional gratings in various alloys form along the same matrix planes that the final precipitated plates do. This suggests that the gratings are thin plates of the precipitate.

Experiments on Al-Mg alloys are particularly enlightening, for the scattering power of the aluminum and magnesium atoms is nearly identical. Thus any clustering of magnesium atoms on certain matrix planes could not lead to streaks. But streaks *are* observed, and so it must be concluded<sup>2</sup> that they are due to an alteration in the structure involving new atomic sites, not merely to a shifting of atoms to certain of the existing sites. The conclusion follows that in Al-Mg, and probably in other systems as well, the streaks on Laue patterns arise from platelets which properly can be called precipitate nuclei.<sup>3</sup>

**Phase Transformations in Pure Metals.**—There are many similarities between the lattice relationships in precipitation and those in all other solid-solid transformations in which a new phase grows within or upon the surface of an old phase. With the exception of the process of diffusion, which enters in some and not in others, much the same principles are found in all. The lattice in the new phase is crystallographically related in orientation to the lattice in the old phase, and in a great many instances the relationship is a simple one in which important rows and planes of atoms in the two phases are parallel. It has been mentioned how a h.c.p. precipitate forms in a f.c.c. matrix by a shearing process consisting of the slipping of close-packed layers over each other so as to produce the hexagonal sequence of the layers. The same alterations of lattice can be observed in the metal **cobalt**, which in cooling below 420°C. transforms from hexagonal to cubic close packing, and in the metal **thallium**, which has a similar transformation at 231°C.<sup>4</sup> Again the close-packed layers and rows of atoms in the old and new structures are parallel. The transformation in **pure iron** from f.c.c.  $\gamma$  to b.c.c.  $\alpha$  results in orientations that appear to follow this rule;<sup>5</sup> an exact determination of the relationship has been hampered by the wide scatter in orientation that accompanies it, but it is very similar to the relationship between austenite and ferrite in steels

<sup>1</sup> C. S. BARRETT and A. H. GEISLER, *J. Applied Phys.*, vol. 11, p. 733, 1940. C. S. BARRETT, A. H. GEISLER, and R. F. MEHL, *Trans. A.I.M.E.*, vol. 143, p. 134, 1941.

<sup>2</sup> A. H. GEISLER, dissertation, Carnegie Institute of Technology, Pittsburgh, Pa., 1942.

<sup>3</sup> The above reasoning assumes that the difference in size of segregated aluminum and magnesium atoms is not sufficient to distort the matrix lattice in a way that produces two-dimensional diffraction. Perhaps this assumption is not justified.

<sup>4</sup> G. WASSERMANN, *Metallwirtschaft*, vol. 11, p. 61, 1932. U. DEHLINGER, E. OSSWALD and H. BUMM, *Z. Metallkunde*, vol. 25, p. 62, 1933.

<sup>5</sup> R. F. MEHL and D. W. SMITH, *Trans. A.I.M.E.*, vol. 113, p. 203, 1934.

discussed in the following section.<sup>1</sup> The transformation from b.c.c. **zirconium** to the h.c.p. form below 862°C. involves complex lattice relationships.<sup>2</sup>

**Structures in Steel.**—Mutual orientation relationships are found not only in precipitation and in phase changes in pure metals, but also in other solid-solid transformations which are summarized in Table XXIX (page 486). The most important transformation is the eutectoid reaction

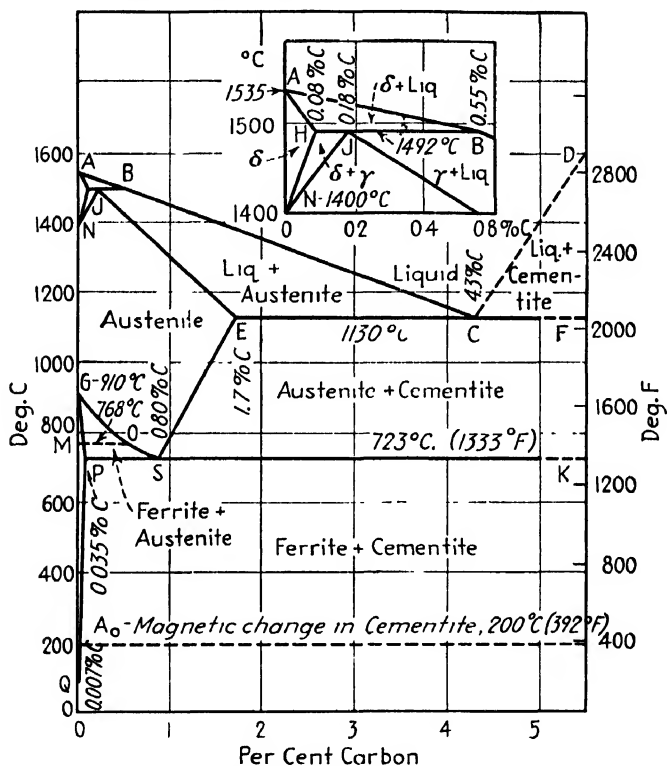


FIG. 13.—The iron-carbon constitution diagram (weight percent carbon). ("Metals Handbook.")

associated with the hardening of steel. More is known of the intricacies of this transformation than any other, though there may be many non-

<sup>1</sup> Arguing from the results of a double transformation in pure iron,  $\alpha$  to  $\gamma$  to  $\alpha$ , Wassermann (*Mitt. Kaiser-Wilhelm Inst. Eisenforsch. Dusseldorf*, vol. 17, p. 149, 1935) concluded erroneously that there was no crystallographic relationship. Since it is possible for one crystal of  $\alpha$  to form 24 different orientations of  $\gamma$  and, upon cooling, for each crystal of  $\gamma$  to form 24 orientations of  $\alpha$ , it follows that the total number of orientations possible after heating and cooling a single crystal is  $24 \times 24$  minus the number of duplications, actually 501 (J. Young, *Trans. Roy. Soc. (London)*, vol. A238, p. 393, 1939). Therefore, the double transformation experiment of Wassermann could have appeared to indicate randomness when true randomness did not exist.

<sup>2</sup> W. G. BURGERS, *Physica*, vol. 1, p. 561, 1934; *Metallwirtschaft*, vol. 13, p. 785, 1934.

ferrous eutectoid reactions of equal complexity. The following summary is limited to the crystallography of the transformation and does not cover the familiar and important aspects of the subject having to do with rates of reaction.<sup>1</sup>

The familiar iron-carbon diagram, Fig. 13, indicates that **austenite**, the interstitial solid solution of carbon in  $\gamma$ -iron, decomposes into ferrite and cementite. The solubility of carbon in  $\gamma$ -iron is much greater than in  $\alpha$ -iron (1.7 weight percent vs. 0.035 weight percent maximum). Seitz<sup>2</sup> has given the following explanation of this difference. The largest interstices in the b.c.c. arrangement of iron atoms are smaller than those of the f.c.c. structure; therefore, the carbon atoms can fit into the austenite interstices with less distortion than into ferrite.<sup>3</sup>

**Cementite** ( $\text{Fe}_3\text{C}$ ) is orthorhombic.<sup>4</sup> The unit cell contains 12 iron atoms and 4 carbon atoms and belongs to space group  $V_h^{16}\text{-Pbnm}$ ; the most precise values for the cell dimensions are<sup>5</sup>  $a = 4.5155$ ,  $b = 5.0773$ , and  $c = 6.7265\text{\AA}$ . The positions of the carbon atoms remained in doubt until Fourier synthesis<sup>6</sup> showed them to be at certain interstitial positions in the (nearly) close-packed structure of iron atoms.<sup>7</sup> Upon long-continued heating, cementite decomposes, the carbon forming graphite.

<sup>1</sup> For summaries of the kinetics see E. C. BAIN, *Trans. A.I.M.E.*, vol. 100, p. 13, 1932. E. C. BAIN, "Functions of the Alloying Elements in Steels," A.S.M., Cleveland, Ohio, 1941. R. F. MEHL, "Symposium on the Hardenability of Alloy Steels," p. 1, A.S.M., Cleveland, Ohio, 1938. E. S. DAVENPORT, *Trans. A.S.M.*, vol. 27, p. 837, 1939. R. F. MEHL, Campbell Memorial Lecture, A.S.M., Cleveland, Ohio, October, 1941.

<sup>2</sup> F. SEITZ, "The Physics of Metals," McGraw-Hill, New York, 1943.

<sup>3</sup> The distance between centers of a carbon atom and a neighboring iron atom in  $\alpha$ -iron is  $2.86 \sqrt{(\frac{1}{2})^2 + (\frac{1}{4})^2} = 1.59\text{\AA}$ , while in  $\gamma$ -iron it is  $3.56 \times 0.5 = 1.78\text{\AA}$ . The radius of an iron atom for a coordination number of 8 is 1.23 and for coordination number 12 is 1.26; in the undistorted lattices, this leaves spaces for an atom of  $0.36\text{\AA}$  radius in  $\alpha$ -iron and  $0.52\text{\AA}$  in  $\gamma$ -iron. The radius of carbon in diamond is  $0.77$ .

<sup>4</sup> A. WESTGREN and G. PHRAGMÉN, *J. Iron Steel Inst.*, vol. 105, p. 241, 1922. S. B. HENDRICKS, *Z. Krist.*, vol. 74, p. 534, 1930. A. WESTGREN, *Jernkontorets Ann.*, vol. 114, p. 457, 1932. H. LIPSON and N. J. PETCH, *J. Iron Steel Inst.*, vol. 142, p. 95, 1940. W. HUME-ROTHERY, G. V. RAYNOR, and A. T. LITTLE, *J. Iron Steel Inst.*, vol. 145, p. 143, 1942.

<sup>5</sup> W. HUME-ROTHERY, G. V. RAYNOR, and A. T. LITTLE, *J. Iron Steel Inst.*, vol. 145, p. 143, 1942.

<sup>6</sup> H. LIPSON and N. J. PETCH, *J. Iron Steel Inst.*, vol. 142, p. 95, 1940.

<sup>7</sup> The four carbon atoms are at  $uv\frac{1}{2}$ ;  $\frac{1}{2} - u, \frac{1}{2} + v, \frac{1}{4}$ ;  $uv\frac{1}{2}$ ;  $\frac{1}{2} + u, \frac{1}{2} - v, \frac{1}{4}$ , where  $u = 0.47$ ;  $v = -0.14$ ; four of the iron atoms are also on these equivalent points with  $u = -0.167$ ,  $v = 0.040$ ; and eight iron atoms are on the general positions

$$\begin{aligned}xyz; x, y, \frac{1}{2} - z; \frac{1}{2} - x, \frac{1}{2} + y, z; \frac{1}{2} - x, \frac{1}{2} + y, \frac{1}{2} - z \\ \bar{x}\bar{y}\bar{z}; \bar{x}, \bar{y}, \frac{1}{2} + z; \frac{1}{2} + x, \frac{1}{2} - y, \bar{z}; \frac{1}{2} + x, \frac{1}{2} - y, \frac{1}{2} + z\end{aligned}$$

with  $x = 0.333$ ,  $y = 0.183$ ,  $z = 0.065$ . The environment of each carbon atom consists of six iron atoms arranged at the corners of a triangular prism.

The equilibrium diagram indicates nothing about the mode of transformation or the distribution of the transformation products. In a steel

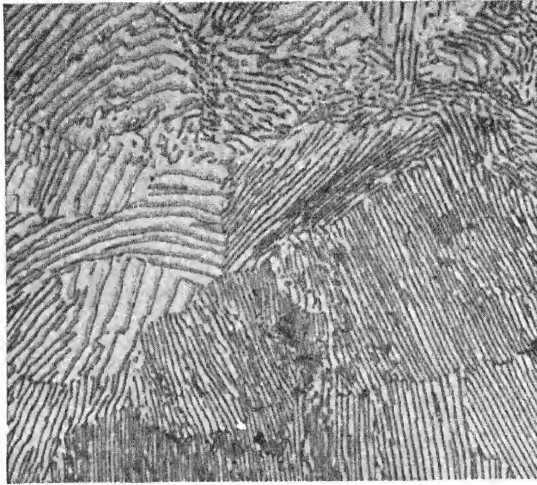


FIG. 14.—Pearlite formed in eutectoid simple carbon steel at 705°C.  $\times 1000$ . (*Vilella*.)

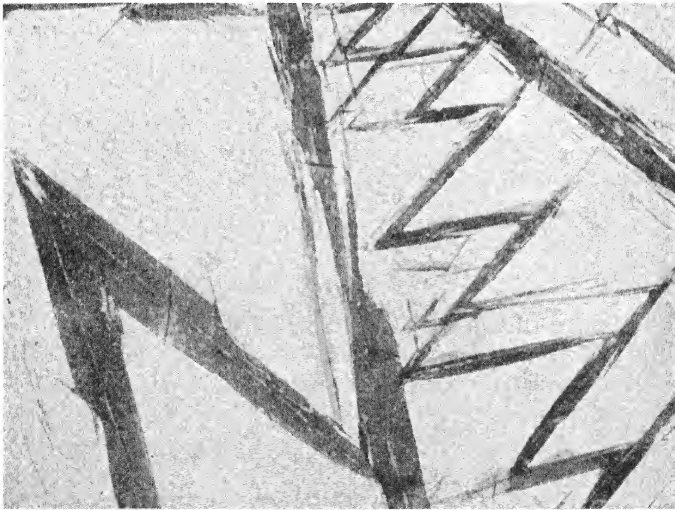


FIG. 15.—Martensite in 1.7 % C. steel quenched from 1150°C.  $\times 1000$ . (*Greninger*.)

of eutectoid composition (0.80 percent carbon in pure steels) slow cooling produces a lamellar structure of ferrite and cementite known as **pearlite** (Fig. 14). With faster rates of cooling these lamellae become finer and

more closely spaced, and at the same time the temperature at which pearlite forms from austenite decreases.

Upon exceeding a certain critical rate of cooling, a rate so fast that pearlite (which forms only at the high temperatures) is not given an opportunity to form, an acicular product—**martensite**—forms at a lower temperature. Martensite in a high-carbon steel is illustrated in Fig. 15. It is an unstable product having a body-centered tetragonal structure.<sup>1</sup> The axial ratio  $c/a$  depends on carbon content, as illustrated in Fig. 16.<sup>2</sup> It is instructive to note that austenite, martensite, and ferrite can all be considered as *body-centered tetragonal structures* differing only in axial ratio. Austenite has an axial ratio of  $c/a = \sqrt{2}/1 = 1.4$  referred

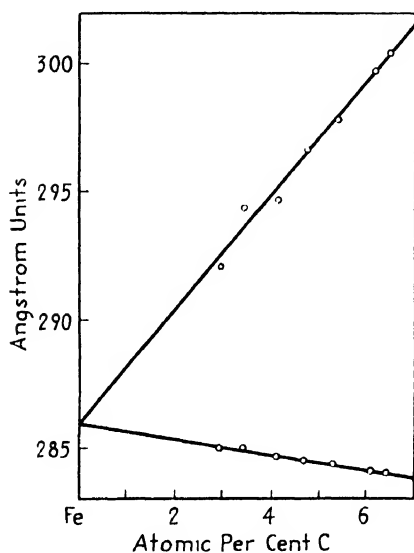


FIG. 16.—Variation in lattice constants  $a$  and  $c$  of martensite with carbon content of steel. (Seljakow, Kurdjumow, and Goodizow.)

to tetragonal axes, while martensite has  $c/a$  between 1.06 and 1.00, depending upon carbon content, and ferrite has  $c/a = 1$ . Martensite accordingly may be viewed as an intermediate step in the transformation from austenite to ferrite, a step in which the interstitially dissolved carbon atoms of austenite are retained in supersaturated solution in such a manner as to prevent for a time the completion of the transformation.<sup>3</sup> The simple concept of martensite formation as a compression of the  $c$  axis leads, however, to a prediction of orientations of martensite not in accord with those observed, which are discussed in a subsequent section, and a more likely theory of the transformation involves a shearing mechanism.

Martensite appears in the form of plates which spring full-formed from the matrix in a period of time of less than 0.002 sec.<sup>4</sup> when austenite is cooled through a certain temperature region<sup>5</sup> (below 240°C. in eutectoid steels)<sup>6</sup> and produces “needles”

<sup>1</sup> W. L. FINK and E. D. CAMPBELL, *Trans. A.S.S.T.*, vol. 9, p. 717, 1926. G. KURDJUMOW and E. KAMINSKY, *Z. Physik*, vol. 53, p. 696, 1929. E. ÖHMAN, *J. Iron Steel Inst.*, vol. 123, p. 445, 1931.

<sup>2</sup> G. KURDJUMOW and E. KAMINSKY, *Z. Physik*, vol. 53, p. 696, 1929.

<sup>3</sup> E. C. BAIN, *Trans. A.I.M.E.*, vol. 70, p. 25, 1924; *Trans. A.S.M.*, vol. 9, p. 752, 1926.

<sup>4</sup> H. J. WIESTER, *Z. Metallkunde*, vol. 24, p. 276, 1932. F. FORSTER and E. SCHEIL, *Z. Metallkunde*, vol. 28, p. 245, 1936.

<sup>5</sup> J. M. ROBERTSON, *Trans. A.I.M.E.* vol. 90, p. 117, 1930.

<sup>6</sup> A. B. GRENINGER and A. R. TROIANO, *Trans. A.S.M.*, vol. 28, p. 537, 1940. and discussions of this paper.

appearing in relief in a polished surface. Hence the shearing movements are more in the nature of the shearing movements characteristic of twinning and do not involve the slower mechanism of nucleation and growth. The rapidity of the transformation and the sluggishness of diffusion at low temperatures accounts for the retention of the carbon in solution; there is little or no diffusion of carbon into particles of cementite.

Martensite in rapidly quenched steels is a constituent that etches slowly and therefore appears white on photomicrographs. It is usually accompanied by residual untransformed austenite. Upon tempering at temperatures even as low as 100°C., martensite changes to a rapid etching

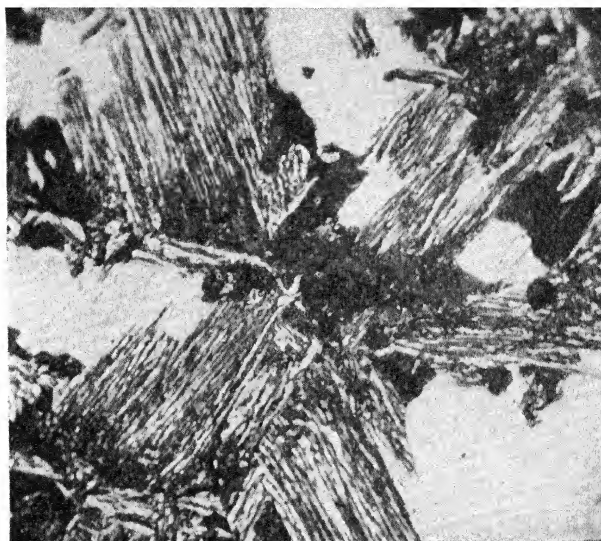


FIG. 17.—Bainite.  $\times 2000$ . (Vilella.)

constituent. The untempered form is often spoken of as **white** or  $\alpha$ -**martensite**; the tempered form has sometimes been called **black** or  $\beta$ -**martensite**, though it now seems better to drop this nomenclature. The tempering of martensite brings about a decrease in axial ratio of the tetragonal structure until it is replaced by a b.c.c. structure. This is doubtless because tempering permits carbon to diffuse into finely dispersed particles of cementite,<sup>1</sup> though tempering below 300°C. does not yield x-ray lines of cementite owing to the fineness of the particles of cementite or to the state of strain in them.

**Bainite** is the name given to the structure or structures that form on *isothermal* transformation at temperatures intermediate between those

<sup>1</sup> G. KURDJUMOW and E. KAMINSKY, *Z. Physik*, vol. 53, p. 696, 1929. G. KURDJUMOW, *Z. Physik*, vol. 55, p. 187, 1929. S. SEKITO, *Science Repts. Tōhoku Imp. Univ.*, Sendai, ser. 1, vol. 20, p. 313, 1931.

which produce pearlite and martensite (about 200 to 550°C. in carbon steels of eutectoid composition). At reaction temperatures just below those which produce the finest pearlite the characteristic appearance of bainite is that shown in Fig. 17, while at lower temperatures it is more pronouncedly acicular, as illustrated in Fig. 18.<sup>1</sup> Vilella, Guellich, and Bain<sup>2</sup> suggest that the reaction to the acicular product is "the successive, abrupt formation of plates of supersaturated ferrite along certain crystallographic planes of the austenite grains; this supersaturated ferrite begins at once to reject carbide *particles* (not lamellae) at a rate depending upon temperature."

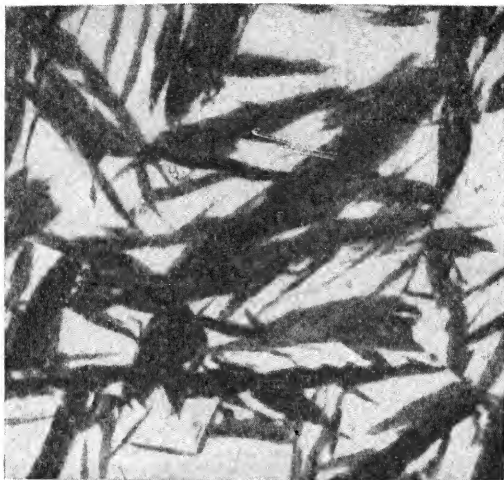


FIG. 18.—Bainite formed at a lower temperature than that of Fig. 17. (Vilella.)

Certain hypoeutectoid *alloy* steels when reacted in the neighborhood of 500°C. contain a reaction product that Davenport<sup>3</sup> calls the **X constituent**. Little is known about it at the present time; it may be a variety of acicular ferrite or bainite. It is most pronounced in steels rich in elements having strong carbide-forming tendencies, these alloying elements being Cb, Ti, V, W, Mo, Cr, and Mn.

**Orientations from the Decomposition of Austenite.**—Kurdjumow and Sachs<sup>4</sup> made the first study of lattice relationships in the austenite-martensite reaction. A large austenite grain with a carbon content of 1.4 percent was prepared by slow cooling from the melt. After homo-

<sup>1</sup> E. S. DAVENPORT and L. C. BAIN, *Trans. A.I.M.E.*, vol. 90, p. 117, 1930.

<sup>2</sup> J. R. VILELLA, G. E. GUELICH, and E. C. BAIN, *Trans. A.S.M.*, vol. 24, p. 225, 1936.

<sup>3</sup> E. S. DAVENPORT, *Trans. A.S.M.*, vol. 27, p. 837, 1939.

<sup>4</sup> G. KURDJUMOW and G. SACHS, *Z. Physik*, vol. 64, p. 325, 1930; *Mitt. deut. Materialprüfungsanstalt.*, vol. 13, p. 151, 1930.



genizing and quenching in water it was found that sufficient austenite had been retained to give the orientation of the original austenite crystal. Pole figures of the partly decomposed crystal indicated that a  $\{110\}$  plane and  $\langle 110 \rangle$  direction in this plane in a martensite crystal is parallel to a  $\{111\}$  plane and a  $\langle 111 \rangle$  direction in this plane in the austenite. This

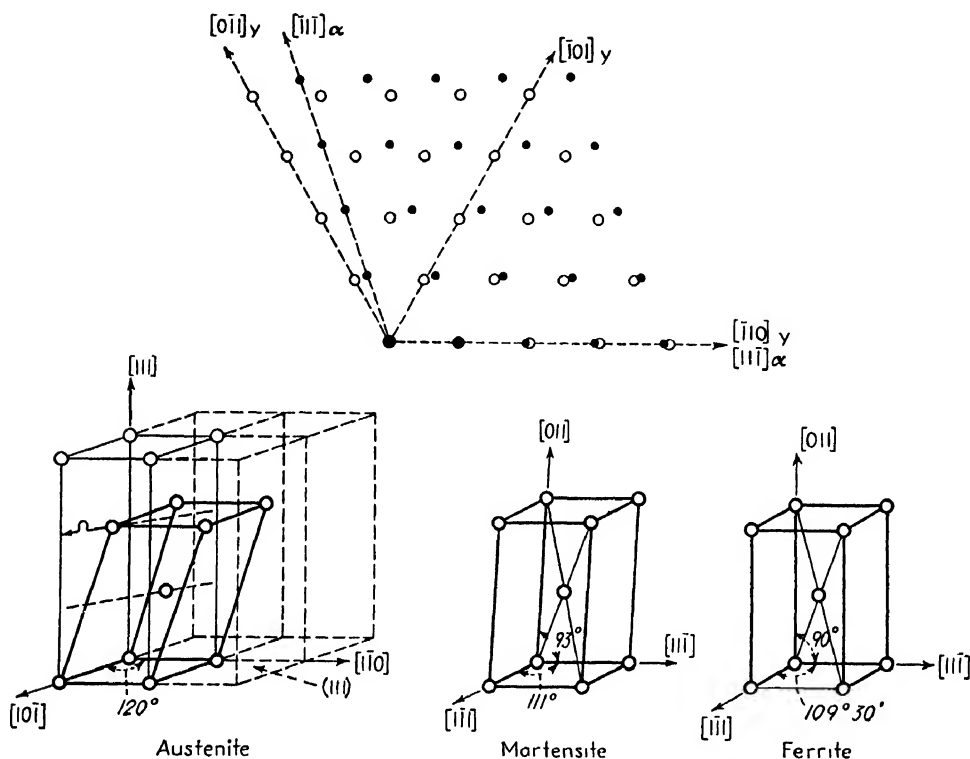


FIG. 19.—Possible atom movements in the formation of martensite from austenite. (Sachs.)

relationship, which we shall speak of as the **Kurdjumow-Sachs** relationship, may be written

$$\begin{array}{l} (111)\gamma' \parallel (110)\alpha \\ [\bar{1}\bar{1}0]\gamma \parallel [111]\alpha \end{array}$$

Tempering the tetragonal martensite to the  $\alpha$  phase produced no change in these orientations.

Six different orientations of  $\alpha$  can form on each  $(111)$  plane of the  $\gamma$  lattice, and since there are four equivalent planes of this type a total of 24 new orientations may form in the decomposition of a single  $\gamma$  crystal.

A set of atomic movements that could produce this result is sketched in Fig. 19.<sup>1</sup> At the top of the figure is an austenite  $(111)$  plane and the  $(011)$  ferrite plane that lies parallel to it, and at the bottom of the figure, from left to right, are sketches of austenite [with  $(111)$  as the base plane],

<sup>1</sup> G. SACHS, *Z. Metallkunde*, vol. 24, p. 241, 1932.

martensite, and ferrite. A shear that will transform a prism in austenite into the unit cell of martensite is indicated by an arrow; it is a shear on a slip plane of the austenite crystal, (111), and in a slip direction, which would make it seem a reasonable mechanism, but measurements of Greninger and Troiano on the actual shear and the habit plane in austenite, discussed below, make it appear unlikely—at least in high-carbon steels.

Nishiyami<sup>1</sup> analyzed by pole figures the orientations of  $\alpha$  that form from  $\gamma$  in the  $\gamma \rightarrow \alpha$  transformation in an Fe-Ni alloy of 30 percent nickel

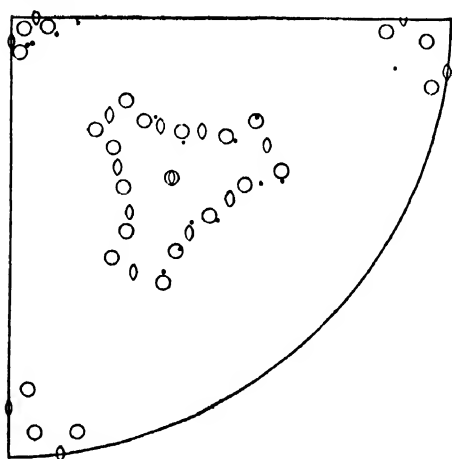


FIG. 20.

FIG. 20.—Stereographic projection of orientations of precipitate in Fe-Ni crystals (31 % Ni) transformed at 240°C. Circles are (110) $\alpha$  poles predicted by Kurdjumow and Sachs; ellipses are (110) $\alpha$  poles predicted by Nishiyama; dots are observed values. (Mehl and Derge.)

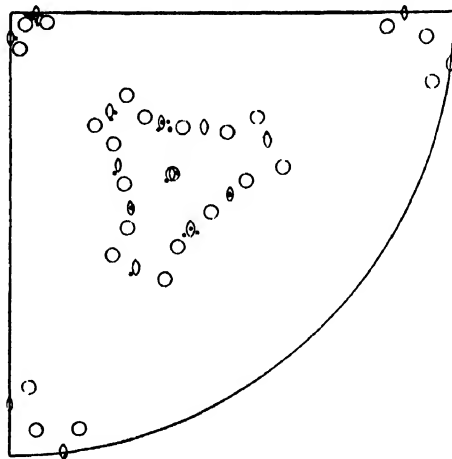


FIG. 21.

FIG. 21.—Same as Fig. 20 for transformation at -195°C. (Mehl and Derge.)

at the temperature of liquid nitrogen. The relationship that Nishiyami found gives 12 ferrite orientations in each crystal and may be written

$$\begin{aligned} (111)\gamma \parallel (110)\alpha \\ [\bar{2}11]\gamma \parallel [\bar{1}10]\alpha \end{aligned}$$

Nishiyami suggested that the atomic displacement during the transformation resembles twinning, and consists of a shear of  $19^\circ 28'$  on the (111) plane in the direction  $[\bar{2}11]$ , followed by certain expansions and contractions.

Mehl and Derge<sup>2</sup> pointed out that the Kurdjumow-Sachs relationship had been found when the  $\gamma \rightarrow \alpha$  transformation had occurred at a high temperature, while the Nishiyami relationship had been found when the transformation had occurred at a low temperature. Their proposal that temperature is a controlling factor was substantiated by an experiment on Fe-Ni alloys, the results of which are plotted as pole figures

<sup>1</sup> Z. NISHIYAMI, *Science Repts. Tohoku Imp. Univ.*, vol. 23, p. 637, 1934.

<sup>2</sup> R. F. MEHL and G. DERGE, *Trans. A.I.M.E.*, vol. 125, p. 482, 1937.

for [110] planes in Figs. 20 and 21. The corners of the stereographic triangles are cube axes of austenite, and within the triangles are plotted [110] poles for the Kurdjumow-Sachs relationship (open circles) and [110] poles for the Nishiyami relationship (open ellipses). Experimental results for a transformation at  $-195^{\circ}\text{C}.$ , shown as black dots in Fig. 21, indicate a Nishiyami mechanism, while results for a  $240^{\circ}\text{C}.$  transformation, Fig. 20, indicate a Kurdjumow-Sachs relationship. The products of a  $-70^{\circ}\text{C}.$  transformation seem to be of an intermediate type. Wassermann's experiments<sup>1</sup> on Fe-C and Fe-Ni alloys transformed at different temperatures also support these results. The transformation in a meteorite usually yields less perfect orientations,<sup>2</sup> though Young<sup>3</sup> found examples that were intermediate between the two types found in the artificial Fe-Ni alloys.

Orientation relationships accompanying the decomposition of austenite in an alloy of 22 percent nickel and 0.8 percent carbon were determined by Greninger and Troiano<sup>4</sup> using precision technique. Quenching to  $-77^{\circ}\text{C}.$  resulted in large martensite crystals in which (110) planes deviated from (111) austenite planes by an angle of about  $1^{\circ}$ . They stated that "except for the non-parallelism of these two closely-packed planes, the evaluated relationship may be described as about midway between the Kurdjumow and Sachs and the Nishiyami relationships." Upon tempering the tetragonal martensite to ferrite the close-packed planes became exactly parallel.

Greninger and Troiano advanced a theory for the atomic movements that occur during the formation of martensite, based on the shear distortion that may be seen on a polished surface when a plate of martensite intersects the surface, Fig. 22. They suggested that two shears, together with slight dimensional adjustments, would transform austenite to body-centered tetragonal martensite and that the first shear was responsible for the relief effect indicated in the figure. From goniometric measurements on the polished surface they determined this "first shear"

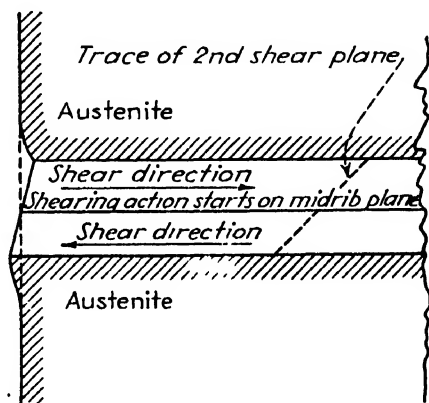


FIG. 22.—Shear movements in formation of a martensite crystal according to Greninger and Troiano.

<sup>1</sup> G. WASSERMANN, *Mitt. Kaiser-Wilhelm Inst. Eisenforsch. Dusseldorf*, vol. 17, p. 149, 1935.

<sup>2</sup> R. F. MEHL and G. DERGE, *Trans. A.I.M.E.*, vol. 125, p. 482, 1937.

<sup>3</sup> J. YOUNG, *Trans. Roy. Soc. (London)*, vol. A238, p. 393, 1939.

<sup>4</sup> A. B. GRENINGER and A. R. TROIANO, *Trans. A.I.M.E.*, vol. 145, p. 291, 1941.

(which was found to be on the irrational plane on which martensite forms), and knowing the total difference in orientation they deduced the "second shear" (which was on the (112) martensite plane in the  $[11\bar{1}]$  direction—the twinning elements for martensite crystals).<sup>1</sup> It was concluded that the midrib so frequently observed in martensite (Fig. 15), especially in hypereutectoid steels and in the martensite-like structure of Fe-Ni alloys, is the plane along which shear is initiated (Fig. 22).

Smith and Mehl<sup>2</sup> conducted a comprehensive investigation of the orientations of the various types of isothermal reaction products in plain carbon steel of eutectoid composition. Bainite formed at 450°C. and 350°C. displays the Nishiyami relationship; bainite formed at 250°C. and martensite displays the Kurdjumow-Sachs relationship. The habit plane changes continuously throughout this temperature range (see page 485).

Attempts to determine the orientations of ferrite lamellae in pearlite with respect to the parent austenite encounter difficulties due to the wide scatter<sup>3</sup> but nevertheless indicate rather conclusively that the orientations in fine pearlite are the same as those in coarse pearlite and are quite different from those in bainite, in martensite, in proeutectoid ferrite, or in pure iron.

Bainite formed at high temperature contains ferrite identical in orientation with ferrite that is formed by proeutectoid precipitation, a relationship which suggests that ferrite nucleates bainite. On the same basis, it may be concluded that ferrite alone does not nucleate the transformation to pearlite. There is reason to believe that, in bainite, ferrite precipitates first, as a supersaturated solid solution which later precipitates cementite.<sup>4</sup>

**Habit Planes for Austenite Decomposition Products.**—Although the habit planes of the various products of the  $\gamma \rightarrow \alpha$  transformation have been extensively studied, the meaning of the results is uncertain. When  $\gamma$ -iron is severely quenched and transforms to  $\alpha$ -iron, the relief effects on a polished surface indicate that  $\alpha$  forms as plates on  $\{111\}$  planes of

<sup>1</sup> The function of the first shear was conceived to be the production of a triclinic lattice "containing a unique set of parallel atomic planes whose interplanar spacings and atomic positions are the same as those of a set of parallel atomic planes in the martensite lattice; a second shear on this unique plane then generates the martensite lattice."

<sup>2</sup> G. V. SMITH and R. F. MEHL, *Trans. A.I.M.E.*, vol. 150, p. 211, 1942. G. V. SMITH, dissertation, Carnegie Institute of Technology, Pittsburgh, Pa., 1941.

<sup>3</sup> R. F. MEHL and D. W. SMITH, *Trans. A.I.M.E.*, vol. 116, p. 330, 1935. G. V. SMITH and R. F. MEHL, *Trans. A.I.M.E.*, vol. 150, p. 211, 1942.

<sup>4</sup> E. S. DAVENPORT and E. C. BAIN, *Trans. A.I.M.E.*, vol. 90, p. 117, 1930. G. V. SMITH and R. F. MEHL, *Metals Tech., Tech. Pub.* 1459, April, 1942.

$\gamma$ ;<sup>1</sup> a similar habit was generally thought to hold for the habit plane of martensite<sup>2</sup> until it was shown by thorough investigations<sup>3</sup> to be irrational in all steels except low-carbon steels, where it assumes a lathlike shape on  $\{111\}$  planes. No low-index plane is found in high-carbon steels for

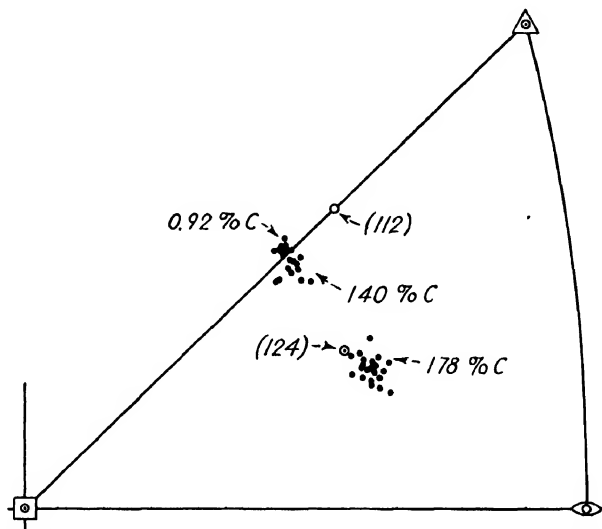


FIG. 23.—Variation of martensite habit plane with carbon content of steel shown by stereographic projection of pole of plane. (Greninger and Troiano.)

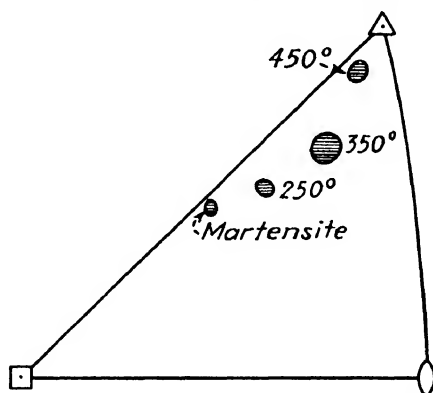


FIG. 24.—Stereographic projection of habit planes for martensite and for bainite formed at different temperatures in eutectoid carbon steel. (Smith and Mehl.)

martensite or for bainite formed at low temperatures, but nevertheless the habit planes are crystallographically determined. Variation of the

<sup>1</sup> A. SAUVEUR and C. H. CHOU, *Trans. A.I.M.E.*, vol. 84, p. 350, 1929. R. F. MEHL and D. W. SMITH, *Trans. A.I.M.E.*, vol. 113, p. 203, 1934.

<sup>2</sup> R. F. MEHL, C. S. BARRETT, and D. W. SMITH, *Trans. A.I.M.E.*, vol. 105, p. 215, 1933.

<sup>3</sup> A. B. GRENINGER and A. R. TROIANO, *Trans. A.I.M.E.*, vol. 140, p. 307, 1940. *Nature*, vol. 141, p. 38, 1938. G. V. SMITH and R. F. MEHL, *Metals Teach., Tech. Pub.* 1459, April, 1942.

TABLE XXIX.—CRYSTALLOGRAPHIC RELATIONSHIPS IN METALS AND ALLOYS\*

System	Type of change	High-temperature phase		Low-temperature phase		Crystallographic relations (high-temperature phase described first)	Reference
		Name	Lattice	Name	Lattice		
Fe	Transformation	$\gamma$ -Fe	F.c.c.	$\alpha$ -Fe	B.c.c.	$(111)\gamma \parallel (110)\alpha$ , $[110]\gamma \parallel [111]\alpha$	23
	Transformation	Taenite or $\gamma$ -Fe solid solution	F.c.c.	Kamagate or $\alpha$ -Fe solid solution	B.c.c.	$(111)\gamma \parallel (110)\alpha$ , $[111]\alpha$ rotated 2 to 4° from $[011]\gamma$ , about $[111]\gamma$	37, 38
Fe-Ni (28-34% Ni)	Transformation	$\gamma$ -Fe solid solution	F.c.c.	$(100)\gamma_1/(100)\alpha$ , $(011)\gamma_1 \parallel (010)\alpha$			3
				$(111)\gamma \parallel (110)\alpha$ , $[110]\gamma \parallel [111]\alpha$			21
				$(111)\gamma_1 \parallel (110)\alpha$ , $[211]\gamma_1 \parallel [110]\alpha$			25, 34
				$(111)\gamma_1 \parallel (110)\alpha$ , $[110]\gamma_1 \parallel [111]\alpha$ when transformed above room temperature			21
Fe-C	Precipitation (slowly cooled)	Austenite( $\gamma$ ) 0.4% C	F.c.c.	$(111)\gamma \parallel (110)\alpha$ , $[211]\gamma_1 \parallel [110]\alpha$ when transformed at -190°C.			21
				$(111)\gamma \parallel (110)\alpha$ , $[110]\gamma \parallel [111]\alpha$			18
	Martensitic transformation	Austenite( $\gamma$ ) 1.4% C	F.c.c.	$(111)\gamma \parallel (110)\alpha$ , $[110]\gamma \parallel [111]\alpha$			15, 34
				$(111)\gamma \parallel (011)$ , $[110]\gamma \parallel [111]$			15, 29
	Precipitation	Austenite( $\gamma$ ) 1.30% C	F.c.c.	Ferrite (proeutectoid)	B.c.c.	Plates which are not $(111)\gamma$ ; $(001)\text{Fe}_3\text{C}$ to plane of plate	18
Fe-C	Eutectoid decomposition	Austenite( $\gamma$ ) 0.80% C	F.c.c.	Martensite	B.c. tetragonal		
				Ferrite in pearlite	B.c.c.	$(110)\gamma \parallel (112)\alpha$ , $[112]\gamma \parallel [110]\alpha$ or possibly $(321)\gamma \parallel (331)\alpha$ , $[331]\gamma \parallel [321]\alpha$	24, 29

Fe-22%Ni-0.8%C; Martensitic transformation at -77°C.	Austenite	F.c.c.	Ferrite in 350 B.c.c. and 450° bainite	$(111)\gamma \parallel (110)\alpha, [211]\gamma \parallel [110]\alpha$	29
			Ferrite in 250° bainite	$(111)\gamma \parallel (110)\alpha, [110]\gamma \parallel [111]\alpha$	
	Martensite			$(111)\gamma 1^\circ \text{ from } (110)\alpha, [110]\gamma 2^\circ \text{ from } [111]\alpha$	12
Cu-Pd	Superlattice transformation	F.c.c.	Ordered $\beta$ solid solution	$(001)\alpha \parallel (113)\beta, [311]\alpha \parallel [100]\beta$	8
Cu-Zn	Pentectic reaction	F.c.c.	$\beta$ solid solution	$(111)\alpha \parallel (110)\beta, (\bar{1}\bar{1}0)\alpha \parallel (001)\beta$ $(111)\alpha, (110)\beta, (\bar{1}\bar{1}0)\alpha \parallel (111)\beta$ $(100)\alpha, (100)\beta, (010)\alpha \parallel (011)\beta$	9
Pb-Sb	Precipitation	F.c.c.	Sb solid solution	$(111)\text{Pb} \parallel (001)\text{Sb}, [110]\text{Pb} \parallel [100]\text{Sb}$	6
Co	Transformation	F.c.c.	$\beta$ -Co	$(111) \parallel (0001), [110] \parallel [11\bar{2}0]$	31
Tl	Transformation	F.c.c.	$\beta$ -Tl	$(111) \parallel (0001), [110] \parallel [11\bar{2}0]$	5
Al-Ag	Precipitation	F.c.c.	$\gamma$ phase (Ag-Al)	$(111) \parallel (0001), [110] \parallel [11\bar{2}0]$	17
			$\gamma'$ phase (transitional)	$(111) \parallel (0001), [110] \parallel [11\bar{2}0]$	1
Cu-Ag	Precipitation	F.c.c.	Cu solid solution	Plates on $\{100\}$ , all directions $\parallel$	2
			Cu solid solution	Plates on $\{111\}$ , all directions $\parallel$	
Al-Cu	Precipitation	F.c.c.	$\theta$ (CuAl <sub>2</sub> )	Plates on $(100)\text{Al}$ $(100) \parallel (100), [120] \parallel [011]^*$	20
			$\theta'$ (transitional)	$(100)\text{Al} \parallel (001)\theta', [110]\text{Al} \parallel [010]\theta'$	35, 27

\* Directions lie in plane of matching, unless noted otherwise.

TABLE XXIX.—CRYSTALLOGRAPHIC RELATIONSHIPS IN METALS AND ALLOYS\*—(Continued)

System	Type of change	High-temperature phase		Low-temperature phase		Crystallographic relations (high-temperature phase described first)	Reference
		Name	Lattice	Name	Lattice		
Au-Cu	Superlattice transformation	$\alpha$ solid solution	F c c.	AuCu	F c c. tetragonal	(100) $\parallel$ (100), [010] $\parallel$ [010]	26, 4
Cu-Zn	Precipitation	$\beta$ phase	B c c.	$\alpha$ solid solution	F c c.	(110) $\beta$ $\parallel$ (111) $\alpha$ , [111] $\beta$ $\parallel$ [110] $\alpha$ Variable habit, plates; needles $\parallel$ [556] $\beta$	36, 30, 16
Cu-Sn	Precipitation	$\beta$ phase	B c c	$\alpha$ solid solution	F c c.	(110) $\beta$ $\parallel$ (111) $\alpha$ , [111] $\beta$ $\parallel$ [110] $\alpha$	28
	Eutectoid decomposition	$\beta$ phase	B c c.	$\alpha$ solid solution	F c c.	(110) $\beta$ $\parallel$ (111) $\alpha$ , [111] $\beta$ $\parallel$ [110] $\alpha$	14
Ag-Zn	Precipitation	$\beta$ phase	B c c.	$\alpha$ solid solution	F c c.	(110) $\beta$ $\parallel$ (111) $\alpha$ , [111] $\beta$ $\parallel$ [110] $\alpha$	28
Fe-N	Precipitation	$\alpha$ solid solution	B c c.	Fe <sub>3</sub> N	F c c.	(210) $\alpha'$ (112)	19
Cu-Al	Eutectoid decomposition	$\beta$ phase	B c c.	$\alpha$ solid solution	F c c.	(110) $\beta$ $\parallel$ (100) $\alpha$	32
Cu-Zn	Transformation at low temperature	$\beta$ phase (supercooled)	B c c.	$\alpha$ solid solution	F c c	Thin plates on (155) $\beta$ or (166) $\beta$	11
Cu-Sn	Transformation at low temperature	$\beta$ phase (supercooled)	B c c.	$\alpha$ solid solution	F c c.	Thin plates on (133) $\beta$	11
Cu-Zn	Precipitation	$\beta$ phase	B c c.	$\gamma$ phase	$\gamma$ cubic	(100) $\beta$ $\parallel$ (100) $\gamma$ , [010] $\beta$ $\parallel$ [010] $\gamma$	36
Cu-Sn	Eutectoid decomposition	$\beta$ phase	B c c.	$\gamma$ phase	$\gamma$ cubic	(100) $\beta$ $\parallel$ (100) $\gamma$ , [010] $\beta$ $\parallel$ [010] $\gamma$	13, 14
				$\gamma'$ intermediate phase	Hex. $\sim \gamma$	Nearly like $\beta$ to $\gamma$	13, 14



Cu-Al	Eutectoid decomposition	$\beta$ phase	B.c.c.	$\gamma$ phase	$\gamma$ cubic	(100) $\beta$    (100) $\gamma$ , [010] $\beta$    [010] $\gamma$	33
	Low temperature decomposition	$\beta_1$ phase	B.c.c. (ordered)	$\gamma'$ phase (martensitic)	H.c.p. (ordered)	Thin plates $2^\circ$ from (133) $\beta_1$ (110) $\beta_1$    (00-1) $\gamma'$ , [111] $\beta_1$    [01 0] $\gamma'$ (011) $\beta_1$ , $4^\circ$ from (00-1) $\gamma'$ , [111] $\beta_1$    [01-0] $\gamma'$	10
		$\beta_1$ phase	B.c.c. (ordered)	$\beta'$ phase (martensitic)	Trigonal <sup>o</sup>	Thin plates $2^\circ$ from (133) $\beta_1$	
Ag-Zn	Transformation	$\beta$ phase	B.c.c.	$\epsilon$ phase	H.c.p.	(111) $\beta$    (0001), (110) $\beta$    (10 $\bar{1}$ 0)	36
						Nearly like $\beta \rightarrow \gamma$ in Cu-Sn	14
Ag-Zn	Precipitation	$\beta$ phase	B.c.c.	$\gamma$ phase	$\gamma$ cubic	(100) $\beta$    (100) $\gamma$ , [010] $\beta$    [010] $\gamma$	36
Fe-P	Precipitation	$\alpha$ solid solution	B.c.c.	Fe <sub>3</sub> P	B.c. tetragonal	Plates   (21 1 4) $\alpha$	18
Zn-Cu	Precipitation	$\epsilon$ phase (Zn)	H.c.p.	$\eta$ phase	H.c.p.	(10 $\bar{1}$ 4) $\epsilon$    (10 $\bar{1}$ 4) $\eta$ , [11 $\bar{2}$ 0] $\epsilon$    [11 $\bar{2}$ 0] $\eta$	7
Mg-Sn	Precipitation	Mg solid solution	H.c.p.	Mg <sub>2</sub> Sn	Cubic (CaF <sub>2</sub> type)	(00-1)Mg   (111), [10-0]   [110] (00-1)Mg   (110), [10-0]   [110] (00-1)Mg   (111), [11 0]   [110]	6

## REFERENCES

- <sup>1</sup> C. S. BARRETT, A. H. GEISLER, and R. F. MEHL, *Trans. A.I.M.E.*, vol. 143, p. 134, 1941.
- <sup>2</sup> C. S. BARRETT, H. F. KAISER, and R. F. MEHL, *Trans. A.I.M.E.*, vol. 117, p. 39, 1935 (Cu-Ag).
- <sup>3</sup> O. B. BØGGILD, *Sætertyk of Meddelelser om Grønland*, vol. 74, p. 1, 1927.
- <sup>4</sup> V. DEHLINGER and L. GRAF, *Z. Physik*, vol. 64, p. 339, 1930.
- <sup>5</sup> V. DEHLINGER, E. OSSWALD, and H. BUMM, *Z. Metallkunde*, vol. 25, p. 62, 1933.
- <sup>6</sup> G. DERGE, A. R. KOMMEL, and R. F. MEHL, *Trans. A.I.M.E.*, vol. 117, p. 39, 1935 (Mg-Sn)
- <sup>7</sup> M. L. FULLER and J. L. RODDA, *Trans. A.I.M.E.*, vol. 104, p. 116, 1933 (Cu-Zn).
- <sup>8</sup> L. GRAF, *Physik. Z.*, vol. 14, p. 489, 1935.
- <sup>9</sup> A. B. GRENINGER, *Trans. A.I.M.E.*, vol. 124, p. 379, 1937.
- <sup>10</sup> A. B. GRENINGER, *Trans. A.I.M.E.*, vol. 133, p. 204, 1939.
- <sup>11</sup> A. B. GRENINGER and G. MOORADIAN, *Trans. A.I.M.E.*, vol. 128, p. 337, 1938.
- <sup>12</sup> A. B. GRENINGER and A. R. TROLIANO, *Trans. A.I.M.E.*, vol. 145, p. 289, 1941.
- <sup>13</sup> J. ISAVTSCHEW and G. KURDUMOW, *Metallwirtschaft*, vol. 11, p. 554, 1932.

- 14 J. IALTSCHEW and G. KURJUMOV, *Physik. Z. Sowjetunion*, vol. 5, pp. 6, 22, 1934.
- 15 G. KURJUMOV and G. SACHS, *Z. Physik*, vol. 64, p. 325, 1930, *Mat. deut. Materialprüfungsanstalt*, vol. 13, p. 151, 1930.
- 16 O. T. MARKEE, *Trans. A.I.M.E.*, vol. 104, p. 64, 1933.
- 17 R. F. MEHL and C. S. BARRETT, *Trans. A.I.M.E.*, vol. 93, p. 78, 1931, (Al-Ag, Cu-Si).
- 18 R. F. MEHL, C. S. BARRETT and D. W. SMITH, *Trans. A.I.M.E.*, vol. 105, p. 215, 1933.
- 19 R. F. MEHL, C. S. BARRETT, and H. S. JERABEK, *Trans. A.I.M.E.*, vol. 113, p. 211, 1934 (Fe-N, Fe-P).
- 20 R. F. MEHL, C. S. BARRETT, and F. N. RHINES, *Trans. A.I.M.E.*, vol. 99, p. 203, 1932 (Al-Cu, Al-MgSi).
- 21 R. F. MEHL and G. DERGE, *Trans. A.I.M.E.*, vol. 125, p. 482, 1937.
- 22 R. F. MEHL and O. T. MARKEE, *Trans. A.I.M.E.*, vol. 93, p. 123, 1931 (Cu-Zn, Cu-Al).
- 23 R. F. MEHL and D. W. SMITH, *Trans. A.I.M.E.*, vol. 113, p. 203, 1934 (Fe-C).
- 24 R. F. MEHL and D. W. SMITH, *Trans. A.I.M.E.*, vol. 116, p. 330, 1935.
- 25 Z. NISHIYAMA, *Sci. Repts. Tohoku Imp. Univ.*, vol. 23, p. 637, 1934.
- 26 K. OSHIMA and G. SACHS, *Z. Physik*, vol. 63, p. 210, 1930.
- 27 G. D. PRESTON, *Phil. Mag.*, vol. 26, p. 855, 1938.
- 28 D. W. SMITH, *Trans. A.I.M.E.*, vol. 104, p. 48, 1933.
- 29 G. V. SMITH and R. F. MEHL, *Metals Tech. Publ.*, 1459, April, 1942.
- 30 M. STRAUJANIS and G. WEERTS, *Z. Physik*, vol. 78, p. 1, 1932.
- 31 G. WASSERMANN, *Metallwirtschaft*, vol. 11, p. 61, 1932.
- 32 G. WASSERMANN, *Metallwirtschaft*, vol. 13, p. 133, 1934.
- 33 G. WASSERMANN, *Z. Metallkunde*, vol. 26, p. 256, 1934.
- 34 G. WASSERMANN, *Mit. Kaiser-Wilhelm Inst. Eisenforsch. Dusseldorf*, vol. 17, p. 149, 1935.
- 35 G. WASSERMANN and J. WEERTS, *Metallwirtschaft*, vol. 14, p. 605, 1935.
- 36 J. WEERTS, *Z. Metallkunde*, vol. 24, p. 265, 1932.
- 37 J. YOUNG, *Proc. Roy. Soc. (London)*, vol. A112, p. 630, 1926.
- 38 J. YOUNG, *Phil. Trans. Roy. Soc.*, vol. A238, p. 393, 1939.

martensite habit plane in steels of various carbon contents is indicated on a stereographic projection of the austenite lattice in Fig. 23, and variation of the bainite habit plane with isothermal reaction temperature is plotted in Fig. 24.

Studies by Greninger<sup>1</sup> of the martensite-like reaction in certain non-ferrous alloys also revealed irrational (high indices) habit planes, as will be seen from Table XXIX, page 486. Thus the habit plane alters with the temperature of the reaction while the orientation relationships change but little.

Pearlite forms on one or more sets of planes of high indices,<sup>2</sup> and the same is true of proeutectoid cementite,<sup>3</sup> which supports the suggestion that cementite nucleates pearlite.

**Orientations in Other Reactions.**—To the list of reactions in which new phases are generated having their orientations crystallographically related to phases already present must be added **peritectic reactions**, as Greninger has shown,<sup>4</sup> **oxidation reactions**,<sup>5</sup> and alloy layers produced by **diffusion**.<sup>6</sup>

The orienting of **overgrowths** by substrates has been shown to depend upon a sufficient similarity in atomic positions in the matching planes;<sup>7</sup> if the atomic patterns are similar, as in alkali halides, the lattice parameters may differ as much as 25 or 30 percent without causing the deposited crystal to become randomly oriented. When the habit of crystals is altered by impurities in the liquids from which they crystallize, it is probable that oriented adsorbed layers of the *impurities* are responsible.<sup>8</sup> Oriented electrodeposits are common; these are treated in Chap. XX.

Orientation relationships are found in all types of transformations. When the two phases are of similar structure and approximately equal lattice dimensions, it can be predicted that the new will have an orienta-

<sup>1</sup> A. B. GRENINGER and V. G. MOORADIAN, *Trans. A.I.M.E.*, vol. 128, p. 337, 1938.

A. B. GRENINGER, *Trans. A.I.M.E.*, vol. 133, p. 204, 1939.

<sup>2</sup> G. V. SMITH and R. F. MEHL, *Metals Tech., Tech. Pub.* 1459, April, 1942.

<sup>3</sup> R. F. MEHL, C. S. BARRETT, and D. W. SMITH, *Trans. A.I.M.E.*, vol. 105, p. 215, 1933. A. B. GRENINGER and A. R. TROIANO, *Trans. A.I.M.E.*, vol. 140, p. 307, 1940.

<sup>4</sup> A. B. GRENINGER, *Trans. A.I.M.E.*, vol. 124, p. 379, 1937.

<sup>5</sup> MÜLLER and SCHWABE, *Z. Elektrochem.*, vol. 37, p. 185, 1931 (Cr<sub>2</sub>O<sub>3</sub>). H. C. H. CARPENTER and C. F. ELAM, *J. Iron Steel Inst.*, vol. 105, p. 83, 1922 (Fe-O). R. F. MEHL and E. L. MCCANDLESS, *Trans. A.I.M.E.*, vol. 125, p. 531, 1937 (Fe-O). R. F. MEHL, E. L. MCCANDLESS and F. N. RHINES, *Nature*, vol. 134, p. 1009, 1934 (Cu<sub>2</sub>O). K. H. MOORE, *Ann. Physik*, vol. 33, p. 133, 1938 (Cu<sub>2</sub>O).

<sup>6</sup> R. F. MEHL, discussion to A. B. GRENINGER, *Trans. A.I.M.E.*, vol. 124, p. 390, 1937 (Cu-Zn).

<sup>7</sup> L. ROGER, *Compt. rend.*, vol. 182, p. 326, 1926; vol. 179, p. 2050, 1925. C. A. SLOAT and A. W. C. MENZIES, *J. Phys. Chem.* vol. 35, p. 2005, 1931.

<sup>8</sup> P. GAUBERT, *Compt. rend.*, vol. 143, p. 776, 1906; vol. 167, p. 491, 1918; vol. 180, p. 378, 1925. C. W. BUNN, *Proc. Roy. Soc. (London)*, vol. A141, p. 567, 1933.

tion identical with the old. When the reaction is at a *surface*, the pattern of atoms in the two interfacial planes will be similar provided that similar planes exist in the phases. When the reaction generates a new phase *within* the old, there appear to be several factors that can influence the orientation. The most important among these are probably (1) close matching of atoms at the interface and close similarity in atomic distribution in the neighborhood of the interface, which means that little energy is required to create the interface; and (2) simple shearing processes that create the new lattice by overcoming a minimum shear resistance or activation energy. When the second factor is an important one, it seems likely that the nucleus always forms abruptly in the manner of motion characteristic of twinning or slip, which are closely analogous processes that require but little energy to create the interface. Whatever the underlying factors may be, it appears to be a general rule that when one given phase is generated from another it will have the same orientation with respect to the parent phase regardless of the type of reaction by which it is formed.<sup>1</sup>

<sup>1</sup> R. F. MEHL, *Trans. A.I.M.E.*, vol. 124, p. 390, 1937

## CHAPTER XXIII

### ELECTRON DIFFRACTION

The use of electrons for diffraction purposes dates from 1927, when Davisson and Germer<sup>1</sup> first showed that it was possible, following the prediction by De Broglie that material particles should act as waves. Following the lead of these experimenters in America and G. P. Thomson in England, the field has rapidly developed not only as a branch of physics research but as a practical diffraction method supplementing the x-ray. It is of particular value as a means of investigating extremely thin films and surface layers and has earned a place for itself in many industrial and academic laboratories on this account.

**Electron Waves.**—When a stream of electrons strikes a crystal, it behaves exactly as if it were a train of waves. It is not necessary to insist that the electrons actually consist of waves, but they do proceed in the directions that true waves of a certain wavelength would go. The electron wavelength  $\lambda$ —or, more precisely, the wavelength that accounts for the motion of the electrons—is given by the simple equation

$$\lambda = \frac{h}{mv}$$

where  $h$  is Planck's constant and  $mv$  is the momentum (mass times velocity) of the electron. The wavelength is therefore inversely proportional to the velocity, which in turn is directly related to the voltage applied to the vacuum tube in which the electron moves. If a potential,  $V$ , of a few thousand volts is applied, the kinetic energy of the electron is

$$\frac{1}{2} mV^2 = \frac{eV}{300}$$

where  $m$  is the mass of the electron and  $e$  is its charge in electrostatic units. From these equations it follows that

$$\lambda = \sqrt{\frac{150}{V}} \quad \text{angstroms.}^2$$

<sup>1</sup> C. J. DAVISSON and L. H. GERMER, *Phys. Rev.*, vol. 30, p. 705, 1927.

<sup>2</sup> For values of  $V$  above a few thousand volts, this formula requires correction (a 2.5 percent correction at 50,000 volts) because the mass of the electron varies with its velocity. Relativity theory gives the corrected form, which can be reduced to the

Table XXX illustrates the range of wavelengths that can be obtained readily in the laboratory.

TABLE XXX	
Voltage	Wavelength, Å
150	1 0
10,000	0 1227
30,000	0 0697
50,000	0 0536
70,000	0 0447

Since it is convenient to operate electron-diffraction equipment at potentials between 30,000 and 70,000 volts, it follows that the electrons ordinarily used in diffraction work have a wavelength between one-tenth and one-twentieth of the wavelength of x-rays used for similar work.

It might be mentioned that all other material particles as well as electrons have this property of acting as if they were waves. Physicists have succeeded in diffracting atoms and molecules from crystal surfaces; if it were not for certain technical difficulties, we might even be diffracting golf balls about the laboratory! The difficulties in experiments with particles heavier than electrons are considerable, however, and these experiments do not yield a proportionate amount of new information above that given by electron diffraction. The same can be said of experiments with slow electrons produced in apparatus operating at only a few hundred volts. Consequently, applications of interest to metallurgists have been made almost entirely with fast electrons in the range between 30,000 and 70,000 volts.

**Apparatus.**—Electron diffraction requires a highly evacuated container in which a collimated stream of electrons (from either a hot filament or a gas-discharge tube) falls on a specimen and then on a photographic plate within the container. The electrons are accelerated by a constant-potential direct-current source, which may be used also for x-ray diffraction. A hot-filament camera is shown in Fig. 1. From the filament at the left the electrons pass through the pinholes to the specimen (here a thin film) and on to a photographic plate. The plate is arranged to be moved so as to record several patterns side by side.

A more elaborate design is shown in Fig. 2. Electrons from a discharge tube at the top are controlled by passing between trapping plates in which the potential can be varied and through an electromagnet that serves to focus the beam. After diffracting from a specimen on an

approximate equation

$$\lambda = \frac{h \sqrt{150/eV m_0}}{(1 + eV/1200m_0c^2)}$$

where  $m_0$  is the mass of the electron at rest,  $h$  is Planck's constant, and  $c$  is the velocity of light (see Appendix IX for values).

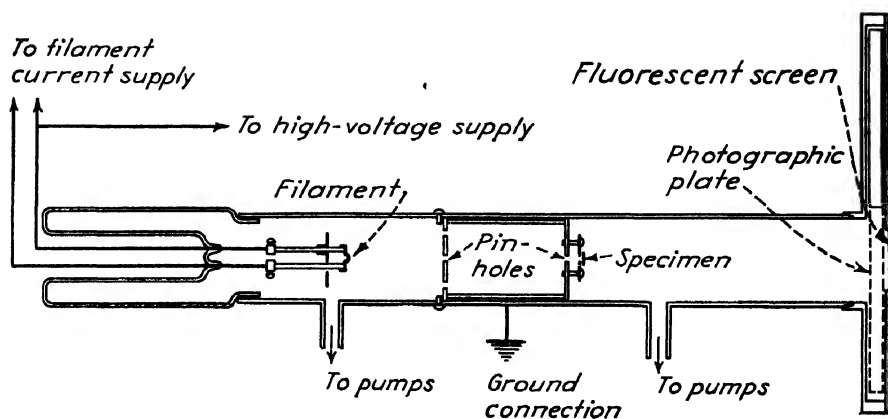


FIG. 1.—Electron-diffraction camera. Electrons from filament pass through pinholes and specimen and strike photographic plate.

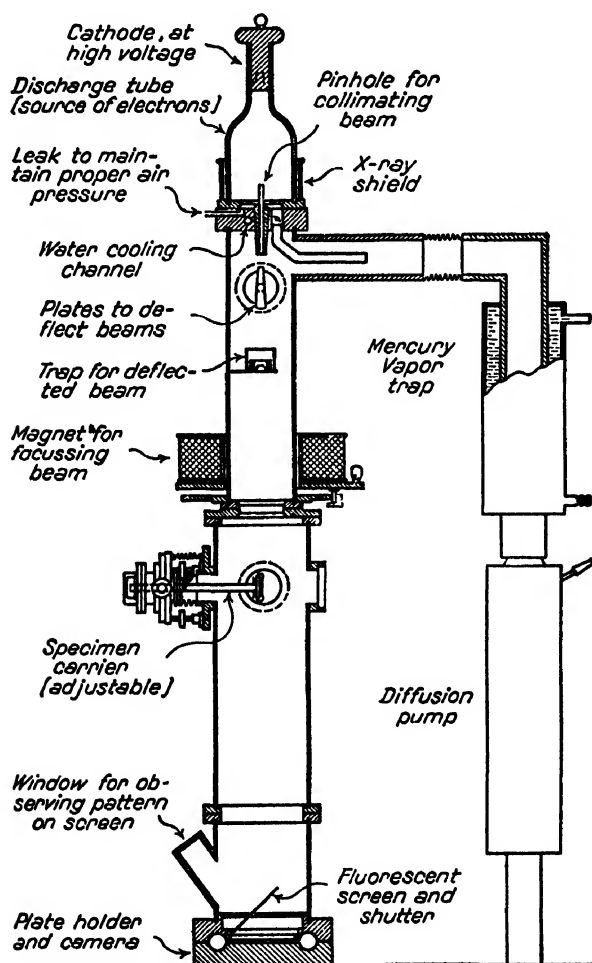


FIG. 2.—Electron-diffraction camera with gas discharge to furnish electrons. (Cambridge Instrument Company.)

adjustable specimen holder, the electrons strike a fluorescent screen or a photographic plate. Owing to the short wavelength of the electrons, the diffraction rings are confined to a very narrow range of angles around the primary beam, and the cameras are much larger than x-ray cameras. A distance of 50 cm. or more from specimen to plate is common.

Details of construction and operation need not concern us here, for they are adequately treated in books on the subject<sup>1</sup> and in numerous articles.<sup>2</sup> In constructing an apparatus—many investigators make their own—due attention should be given to means of obtaining a high vacuum free from contamination by vacuum-pump vapors, adjusting and interchanging of specimens without breaking the vacuum, and changing or removing photographic plates in such a way as to regain the vacuum quickly. A rectified and filtered high-voltage source is essential since a constant voltage is required to maintain a constant wavelength. When a hot filament is used, it should be provided with adjustments to focus the electron beam on the pinhole system. These requirements are met in electron microscopes, which are therefore convertible to diffraction cameras.<sup>3</sup> Since high-voltage electrons strike the metal around the pinhole, there are x-rays emitted that should be absorbed within the apparatus. With a satisfactory beam through the pinholes ( $10^{-8}$  or  $10^{-9}$  amp. through pinholes 0.1 to 0.2 mm. in diameter), the exposure times are much faster than x-ray exposures—a matter of seconds rather than hours. Slow fine-grained plates and films are used. A bar magnet or an electromagnet outside the camera may be used to direct the beam through the pinhole system and onto the specimen.

**Specimens.**—A metallic film so thin as to be translucent or transparent will diffract electrons very strongly; a layer of oxide thin enough to give temper colors likewise produces a good pattern, and in many cases even invisible films can be detected.

<sup>1</sup> "The Structure of Metallic Coatings, Films, and Surfaces," Faraday Society, London (reprinted from *Trans. Faraday Soc.*), 1935. "Theory and Practice of Electron Diffraction," G. P. THOMSON and W. COCHRANE, Macmillan Company, Ltd., London, 1939.

<sup>2</sup> G. I. FINCH, A. G. QUARRELL, and H. WILMAN, *Trans. Faraday Soc.*, vol. 31, p. 1051, 1935. L. H. GERMER, *Rev. Sci. Instruments*, vol. 6, p. 138, 1935. W. G. BURGERS and J. C. BASART, *Physica*, vol. 1, p. 543, 1934. G. P. THOMSON, *Trans. Faraday Soc.*, vol. 31, p. 1049, 1935. J. R. TILLMAN, *Phil. Mag.*, vol. 18, p. 656, 1934 (magnetic focusing). S. B. HENDRICKS, L. R. MAXWELL, V. L. MOSLEY, and M. E. JEFFERSON, *J. Chem. Phys.*, vol. 1, p. 549, 1933. R. JACKSON and A. G. QUARRELL, *Proc. Phys. Soc. (London)*, vol. 51, p. 237, 1939 (high-temperature specimen holder). H. J. YEARIAN and J. D. HOWE, *Rev. Sci. Instruments*, vol. 7, p. 26, 1936. R. MORGAN and N. SMITH, *Rev. Sci. Instruments*, vol. 6, p. 316, 1935. R. R. WILSON, *Rev. Sci. Instruments*, vol. 12, p. 91, 1941 (detail of vacuum joint).

<sup>3</sup> J. HILLIER, R. F. BAKER, and V. K. ZWORYKIN, *J. Applied Phys.*, vol. 13, p. 571, 1942.



It is somewhat difficult to prepare a film so thin that electrons can be transmitted through it, for this requires thicknesses of a few hundred angstroms or less (about a millionth of an inch). Nevertheless, thin **transmission specimens** are prepared in the following ways:

1. Etching a metal foil (usually by floating it on the etching bath).
2. Depositing a substance from the vapor state on a thin cellulose film (or equivalent).
3. Sputtering metal in a gas-discharge tube upon a cellulose film.
4. Precipitating a colloid on a film.
5. Electrodepositing on a substrate which is subsequently etched off.
6. Skimming an oxide layer from molten metal.
7. Oxidizing a thin film or etching an oxidized metal so as to leave the oxide layer.

There is frequently some uncertainty as to whether a film has undergone some change during the process of removal.

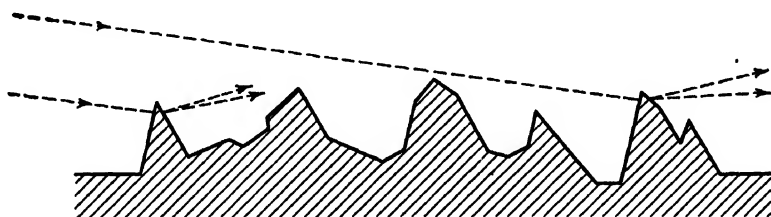


FIG. 3.—Diffraction of electrons from projecting points of a specimen.

**Reflection specimens** are more readily prepared and more widely applicable to metallurgical problems. A reflection specimen must have a surface that is rough on a microscopic scale, for the electrons must penetrate small projections, as in Fig. 3. The surface is slightly mat in appearance when properly prepared and must be as clean as the experimenter can make it. A light etch followed by washes in water, alcohol, and benzene serves for metals; oxides are often sufficiently rough when formed on polished surfaces. Electrodeposits and condensed or sputtered films are usually satisfactory without further treatment. The specimen is mounted nearly parallel to the beam and gradually moved into the beam until the spot on the fluorescent screen is just cut off.

**Identification of Polycrystalline Materials.**—Most applications of electron diffraction involve the identification of reaction products, particularly those formed on metal surfaces. In such studies the patterns are analogous to x-ray powder patterns, consisting of concentric Debye rings that are interpreted just as x-ray patterns are. Typical reflection patterns are reproduced in Fig. 4.

The patterns provide the same kind of information that x-ray diffraction provides for thicker layers, *viz.*, the identification of the phases in

the layer and their crystal structures, the approximate grain size in the layer, the state of strain in the layer, and the orientation of the grains.

The peculiar advantage of the use of electrons for work in this field lies in the fact that they are diffracted strongly by the outermost atoms of the specimen and convey information to the photographic plate concerning these atoms only, whereas x-rays penetrate more deeply and do not register the surface layers unless their thickness is measured in thousands of angstroms.

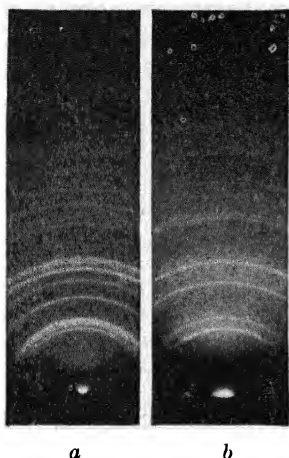


FIG. 4.—Electron diffraction patterns formed by reflection from surface of a specimen. All electron-diffraction patterns reproduced here are direct prints of the original plates, in conformity with the usual practice in papers on the subject, and to distinguish them from the x-ray patterns in this book, which are double printed so as to give diffraction spots that are black. (a) Zinc oxide, (b)  $\gamma$  Al-Zn. (Fuller.)

Identification is carried out by comparison with known materials or by computation of spacings; the card-index system<sup>1</sup> developed for x-rays is applicable here, although some difficulties may be encountered from the lower precision of the spacing measurements and the somewhat altered line intensities.

The extraordinary sensitivity of the electron-diffraction camera to thin layers of material can be a considerable nuisance when it comes to carrying out an experiment. It is a standard complaint that almost anything, if given a chance, will collect on the specimen in sufficient quantities to cause trouble. The thinnest invisible deposits of grease, for example, give excellent diffraction patterns, as many investigators have found to their sorrow, and a little mercury deposited from vapor that has worked back into the camera from the vacuum pump will quickly affect the patterns and introduce "extra rings." If a specimen is rubbed lightly with rubber, say during etching, the spectrum of rubber appears. With some metals it is almost impossible to avoid obtaining the spectrum of an oxide film that forms while the specimen is being prepared and loaded into the camera—a few minutes at room temperature will produce a detectable oxide film on copper. Perhaps some extra rings are also to be ascribed to refraction of the beam when it enters and leaves the same surface of a reflection specimen.<sup>2</sup>

Some extra rings from thin deposited films have been identified with an altered crystal structure in the deposit. When aluminum, for example, is deposited on platinum, the first layers of aluminum atoms

<sup>1</sup> See p. 139.

<sup>2</sup> K. LARK-HAROWITZ, H. J. YEARIAN, and J. D. HOWE, *Phys. Rev.*, vol. 48, p. 101, 1935.

are forced into a tetragonal structure with interatomic distances in the basal plane matching those of the platinum with which it was in contact.<sup>1</sup> Similarly, a thin layer of oxide on zinc matches the zinc in its basal plane dimensions, in spite of the fact that the oxide does not normally have a hexagonal structure. Quarrell<sup>2</sup> found, in fact, that all the face-centered metals he examined (Co, Ni, Cu, Pt, Pd, Au, Ag) when evaporated onto cellulose films or deposited electrolytically showed extra rings. A normal film of silver  $4 \times 10^{-6}$  cm. thick yields a face-centered cubic pattern as in Fig. 5, whereas Quarrell's thin films produced the pattern of Fig. 6, which contains a weak line just within the innermost 111 line of the

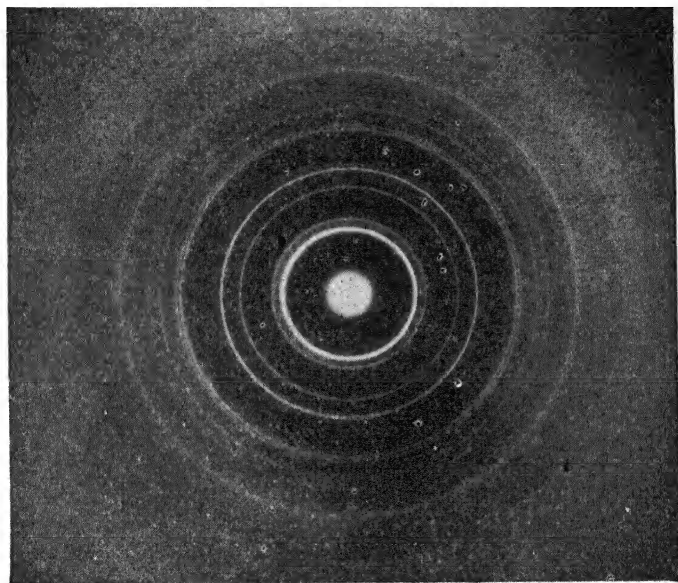


FIG. 5.—Pattern from transmission through silver film  $4 \times 10^{-6}$  cm. in thickness. Electron wavelength 0.051 angstrom. (Germer.)

f.c.c. pattern. This inner line is ascribed to the 10·0 reflection from an abnormal hexagonal close-packed (h.c.p.) form in the case of each of the metals. A weak band extends from the 10·0 ring to the f.c.c. 200 ring and is believed to indicate a gradual transition from h.c.p. to f.c.c. throughout the film. Presumably the first atoms deposited form a close-packed two-dimensional array, and a few subsequent layers superimpose in h.c.p. rather than the normal f.c.c. manner. One electro-deposited silver specimen was found to be purely h.c.p. These thin layer structures are closely analogous to the transitional structures that form in solid-solid transformations (*cf.* Chap. XXII, page 461).

<sup>1</sup> G. I. FINCH and A. G. QUARRELL, *Proc. Roy. Soc. (London)*, vol. A141, p. 398, 1933.

<sup>2</sup> A. G. QUARRELL, *Proc. Phys. Soc. (London)*, vol. 49, p. 279, 1937.

There is another source of extra rings that has received much consideration. If crystals are sufficiently small or thin, the diffraction pattern for each particle may be that characteristic of a two-dimensional grating rather than a three-dimensional one. The diffraction rings built up from rotating a two-dimensional grating will, of course, differ from those of a three-dimensional one, and in general there will be bands in the pattern that have a sharp limit on their inside edge.

The **depth of penetration** of electrons may be estimated by depositing layers of various thicknesses on substrates of a different metal. Nickel deposited on copper begins to give a recognizable pattern by reflection, when the thickness reaches about  $10\text{\AA}$ ; a  $200\text{\AA}$  layer diffracts strongly,

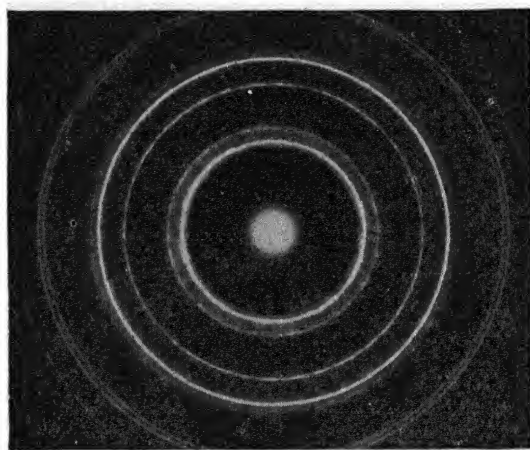


FIG. 6.—Pattern made by transmission through electrodeposited silver. Shows band overlapping the inner ring of Fig. 5 and shows the extra ring inside it. (*Finch.*)

and a  $400\text{\AA}$  layer obliterates the effect of the base.<sup>1</sup> These figures are a function of the roughness of the surface—on some surfaces a monomolecular layer or two or three atomic layers can be detected. The upper limit is imposed by the inelastic impacts of the electrons, which destroy their ability to cooperate in building the diffraction pattern. With heavy metals a film must be less than  $10^{-6}$  cm. ( $100\text{\AA}$ ) if the background scattering from inelastic impacts is to be small, and patterns cannot be expected if films are uniformly thicker than  $10^{-5}$  cm.

There have been many investigations of oxidation with electron diffraction.<sup>2</sup> The various layers in the oxide scale that forms when iron is heated in air can be dissected and the various surfaces studied sepa-

<sup>1</sup> W. COCHRANE, *Proc. Phys. Soc. (London)*, vol. 48, p. 723, 1936.

<sup>2</sup> Extensive reviews and bibliographies are given by G. P. Thomson and W. Cochran, "Theory and Practice of Electron Diffraction," Macmillan & Company, Ltd., London, 1939; B. Lustman, dissertation, Carnegie Institute of Technology, Pittsburgh, Pa., 1940.

rately. For example, when the film has just increased in thickness through the color stage and has turned black, it consists of hexagonal  $\alpha\text{-Fe}_2\text{O}_3$  with a pattern illustrated in Fig. 7. When the scale has grown thick enough to be chipped off, the underside shows the spectrum of  $\text{Fe}_3\text{O}_4$ .<sup>\*</sup> Numerous studies of the oxides of aluminum have shown the

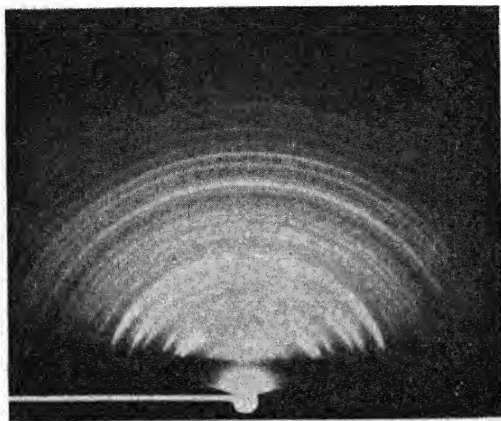


FIG. 7.—Surface-reflection pattern of hexagonal  $\alpha\text{-Fe}_2\text{O}_3$ . (Nelson.)

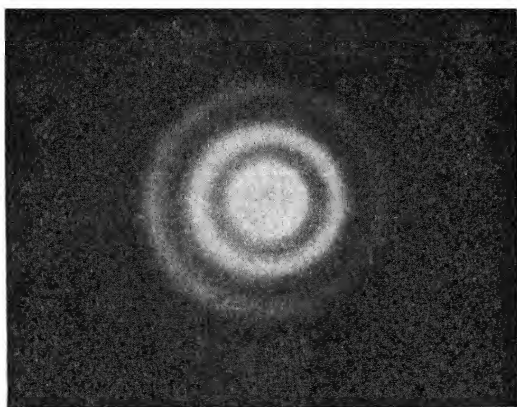


FIG. 8.—Transmission pattern for electrodeposited arsenic. Very small crystals, substantially amorphous. (Finch, Quarrell, and Wilman.)

value of this method for identifying the various structures, their grain size, and their orientation.

The **grain size** in a thin-film transmission specimen is indicated by the breadth of the diffraction lines, just as with x-rays. An electrodeposit of arsenic with exceedingly small crystals—substantially amorphous—gives the pattern reproduced in Fig. 8.† Crystallites with a mean

<sup>\*</sup> H. R. NELSON, *J. Applied Phys.*, vol. 9, p. 623, 1938.

† G. I. FINCH, A. G. QUARRELL, and H. WILMAN, *Trans. Faraday Soc.*, vol. 31, p. 1051, 1935.

dimension along an edge of  $L$  cm. will produce a line whose width at half maximum intensity is approximately

$$b = \frac{0.94\lambda}{L \cos \theta} \cong \frac{\lambda}{L} \quad \text{radians}$$

provided that the natural width due to the electron beam is negligible.<sup>1</sup>



FIG. 9.—Reflection pattern showing preferred orientation in electrodeposited iron. (Finch.)

**Preferred Orientations.**—It is usual for the thin deposits to have a preferred orientation of some sort. This is revealed in the patterns by a lack of uniformity in the intensity of each ring on the photographic plate or, in certain cases, by abnormal intensities of certain rings.

The interpretation of the texture patterns is exactly as with x-rays, except that here the angle of incidence is so small one can consider  $\theta = 0$  and the reflection circle is a great circle. An oriented electrodeposit of iron is illustrated in the reflection photograph of Fig. 9, and the texture of a specimen of gold leaf is shown by the intensity maxima in the rings of Fig. 10. Germer<sup>2</sup> found the orientations illustrated in Fig. 11 on the surface of a galena crystal after filing. When the beam struck the filed surface parallel to the direction of filing, a regular array of spots was produced (Fig. 11*b*) which is a rotation pattern with the axis of rotation horizontal and perpendicular to the beam. On the other hand, arcs are formed when the beam is perpendicular to the

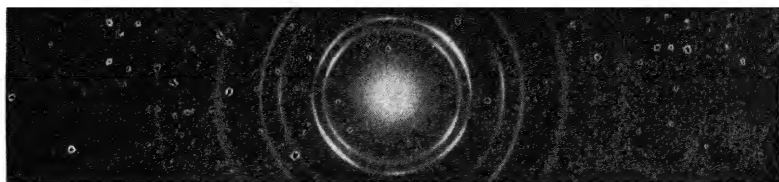


FIG. 10.—Transmission pattern of gold leaf showing preferred orientation. (Fuller.)

direction of filing (Fig. 11*c*), for the beam is then parallel to the axis of rotation of the crystallites. These spectra represent the etched condition of the filed surface; the unetched surface produces complete Debye rings, as in Fig. 11*a*, indicating a random orientation.

<sup>1</sup> Small particles yield much sharper lines in electron diffraction patterns than in x-ray patterns.

<sup>2</sup> L. H. GERMER, *Phys. Rev.*, vol. 50, p. 659, 1936.

One source of error in judging preferred orientations by electron diffraction has recently been discovered.<sup>1</sup> Etching a surface to prepare it for the electron microscope actually leaves, on grains of certain orientations, a surface contour exceptionally favorable for diffraction, and these selected grains predominate in forming the pattern. The diffraction pattern therefore represents a *weighted* sampling rather than a *random* sampling under such conditions—and this may be the rule rather than the exception.

**Polished Surfaces.**—There has been—and perhaps will be—no end to the arguments about the nature of the polished surface of metals. The discussion centers in Sir George Beilby's suggestion made early in the century that the polishing operation distorts the crystals until all crystallinity is lost so that the atoms at the very surface have only the haphazard arrangement characteristic of an amorphous material, such as a supercooled liquid. This amorphous-metal theory has had many ups and downs during its tempestuous life, and much of the controversy about it has arisen from the interpretation of electron-diffraction experiments.

When a beam of electrons falls with glancing incidence upon a polished metal surface, the resulting diffraction pattern consists merely of two very broad, diffuse rings. The striking diffuseness of the pattern is interpreted by many experimenters to indicate a lack of crystallinity in the surface material and to furnish direct proof of the amorphous-metal hypothesis. Many experiments upon which this theory was based, however, were ambiguous. A layer may give diffuse rings by *reflection* and yet give sharp rings when

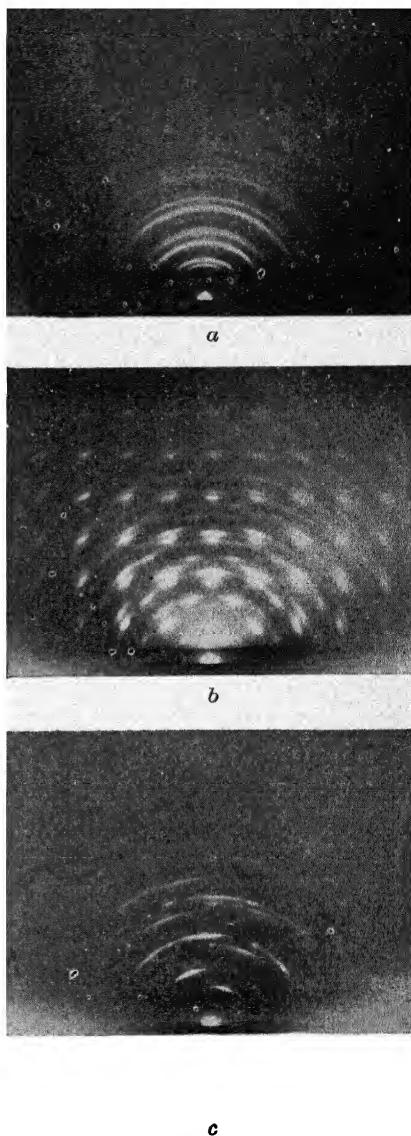


FIG. 11.—Surface-reflection patterns for filed surface of galena crystal. (a) Unetched surface, random texture; (b) etched, beam parallel to direction of filing; (c) etched, beam perpendicular to direction of filing. (Germer.)

<sup>1</sup> R. P. JOHNSON and W. R. GRAMS, *Phys. Rev.*, vol. 62, p. 77, 1942.

examined by *transmission*,<sup>1</sup> as Germer has shown with examples of the sort reproduced in Fig. 12. Kirchner<sup>2</sup> has also pointed out this fact and has shown that a pair of diffuse halos can be obtained by reflection from electrodeposits which give sharp transmission patterns.

These experiments are definite evidence that the crystalline nature of a surface cannot be judged safely by the reflection technique. The explanation of this probably lies in the effect of slight surface unevenness upon the diffracted rays; for if the electrons enter and leave the *same* surface, the direction of the diffracted rays that emerge will be altered through refraction by changes in the slope of the surface. Thus if the

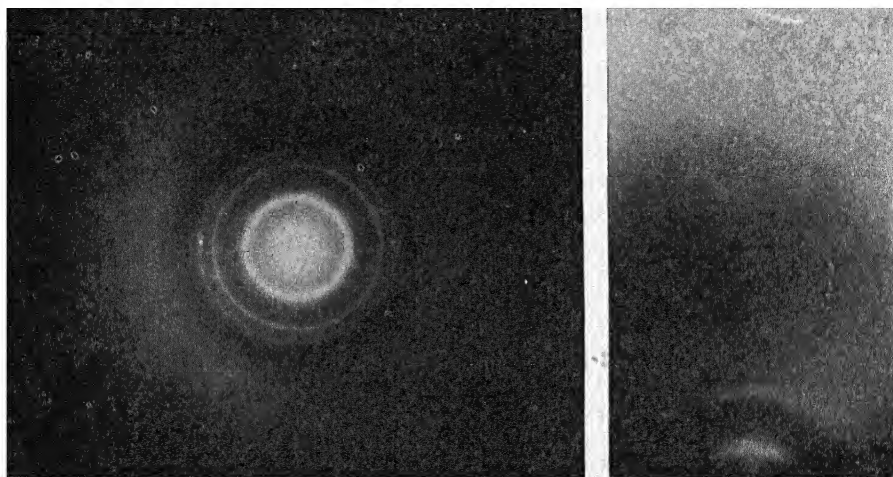


FIG. 12.—A transparent film of zinc sulphide,  $8 \times 10^{-6}$  in. in thickness, gives a crystalline ring pattern by transmission (on the left) and a diffuse amorphous-type pattern by reflection (on the right). (Germer.)

surface is wavy the diffracted rays will emerge in various directions and there will be a corresponding diffuseness in the diffraction pattern. On the other hand, if the beam enters and leaves *different* surfaces—or passes through thin projecting edges—this factor is not effective and a sharp pattern is possible.

In addition to uncertainties from the reflection technique there are the usual uncertainties as to whether each experimenter in this field has actually examined the polished metal or whether he has merely recorded the pattern of an invisible oxide or a contaminated surface. Oxidation of copper during polishing was noted by Dobinski.<sup>3</sup>

<sup>1</sup> L. H. GERMER, *Phys. Rev.*, vol. 43, p. 724, 1933.

<sup>2</sup> F. KIRCHNER, *Nature*, vol. 129, p. 545, 1932; *Trans. Faraday Soc.*, vol. 31, p. 1114, 1935.

<sup>3</sup> S. DOBINSKI, *Nature*, vol. 138, p. 31, 1936; *Phil. Mag.*, vol. 23, p. 397, 1937.



One of the more conclusive experiments on the subject was Cochrane's,<sup>1</sup> in which a gold deposit was laid on nickel and polished and the nickel subsequently etched away. There were three diffuse rings on a *transmission* pattern of this polished film, indicating an amorphous or semiamorphous structure (unless there was some blurring induced by the etching or by concentration gradients from interdiffusion of the layers). After 15 hr. at room temperature the grains had grown to a size giving sharp rings.

There is little doubt that metal is disturbed to a depth of 100 to 10,000 Å in polishing and that a preferred orientation exists in this layer,<sup>2</sup> with (110) planes lying parallel to the surface in the case of copper and gold. The outer 30 to 40 Å is the region that may be amorphous. Cochrane's experiment and Bridgman's severe torsion experiment (*cf.* page 370) seem to indicate that amorphous metal *can* be produced by severe cold work. This statement should apply only to those metals having reasonably high recrystallization temperatures, of course, and it must also be recognized that distortion and fragmentation of lesser degree are the rule in cold-worked metals, as has been discussed in Chap. XVII (page 367). Wulff and his collaborators have applied electron diffraction to the study of phase transformation induced in stainless steel (18% Ni, 8% Cr) by polishing, grinding, sanding, superfinishing, and cold rolling.<sup>3</sup> The surface layers resulting from dry or wet grinding are austenitic, indicating that they have been heated above 200°C. Below this austenitic layer is a layer that has been reduced to ferrite by cold work; the ferritic layer is about  $6 \times 10^{-4}$  cm. below the surface in samples that have been ground. Samples that have received any type of polishing contain a ferritic layer at the surface  $1.5 \times 10^{-5}$  cm. (1500 angstroms) or less in thickness. The ferrite layer in sheet reduced 50 percent by cold rolling extends about  $1 \times 10^{-4}$  cm. below the surface.

**Diffraction from Single Crystals.**—The Laue equations must be satisfied for electrons to diffract, just as in the case of x-rays. The chief difference between the two cases lies in the fact that the electron wavelengths are much smaller than the x-ray wavelengths, and the interaction between the electrons and the atoms of the crystal is much greater, so that thinner layers are effective in diffraction.

Let us consider a small cubic crystal with an electron beam parallel to the *a* axis. The Laue conditions represent concentric sets of cones around *a*, *b*, and *c* axes. The cones around the *a* axis will intersect the

<sup>1</sup> W. COCHRANE, *Proc. Roy. Soc. (London)*, vol. A166, p. 228, 1938.

<sup>2</sup> H. G. HOPKINS, *Trans. Faraday Soc.*, vol. 31, p. 1095, 1935. C. S. LEES, *Trans. Faraday Soc.*, vol. 31, p. 1102, 1935.

<sup>3</sup> J. WULFF, *Trans. A.I.M.E.*, vol. 145, p. 295, 1941; J. T. BURWELL and J. WULFF, *Trans. A.I.M.E.*, vol. 135, p. 486, 1939.

photographic plate as circles much smaller than the circles for x-ray diffraction, while the cones around *b* and *c* will be opened wide and intersect the plate nearly in straight lines. If the first Laue condition is relaxed, the second two will therefore produce two sets of nearly

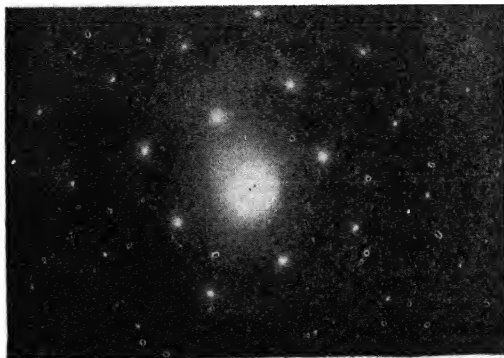


FIG. 13.—Transmission through aluminum along a cube edge of a crystal. Polycrystalline aluminum also present, giving rings. (*Finch, Quarrell, and Wilman.*)

straight lines intersecting the photographic plate at the points of a square network. Figure 13 is a photograph of a single crystal of aluminum made with the beam parallel to the cube edge; the square array of reflections is very prominent.<sup>1</sup> A striking example of the network is seen in the photograph of a graphite crystal, Fig. 14.



FIG. 14.—Transmission pattern from very thin crystal of graphite. Two-dimensional diffraction. (*Finch.*)

It can be shown by cleaving mica crystals to various thicknesses of the order of  $10^{-6}$  to  $10^{-7}$  cm. that only the thinnest ones produce these

<sup>1</sup> G. I. FINCH, A. G. QUARRELL, and H. WILMAN, *Trans. Faraday Soc.*, vol. 31, p. 1051, 1935.

regular point networks. As a thicker specimen is used, those spots of the network which satisfy the third Laue condition increase in intensity, while the others gradually disappear. The diffraction is best understood in terms of the reciprocal lattice. Each reciprocal lattice point becomes elongated in the direction of the thin dimension of the crystal; the extension of the region of intensity around each point can be computed from the equation for diffracted intensities from a parallelepiped formed of unit cells. If there are  $N_1$ ,  $N_2$ , and  $N_3$  cells along the three axes, respectively, and if the path differences between the waves scattered by the origin and the other extremities of the axes are  $A_1$ ,  $A_2$ , and  $A_3$  wavelengths, the intensity will be proportional to

$$\frac{\sin^2 (\pi N_1 A_1)}{\sin^2 \pi A_1} \cdot \frac{\sin^2 (\pi N_2 A_2)}{\sin^2 \pi A_2} \cdot \frac{\sin^2 (\pi N_3 A_3)}{\sin^2 \pi A_3}.$$

Now the effect of reducing the number of cells along the  $a$  axis is to reduce  $N_1$  in the first term. This first factor may become zero a number of times, and it will first reach zero when  $A_1 = \pm 1/N_1$ . Thus if the specimen is only two unit cells thick, its reciprocal lattice points are elongated halfway to the next reciprocal lattice point, while if it is four unit cells thick the first minimum is one-fourth of the way to the next point. A reciprocal lattice of elongated points is sketched in Fig. 15. Reflection occurs when the reflection sphere touches any part of the elongated points. When there is considerable elongation, the diffraction pattern shows the network of reflections that is characteristic of a two-dimensional grating. This network is the more evident because of the short wavelength of the electron waves, for in reciprocal space this corresponds to a reflection sphere of very large radius. The sphere is, in fact, almost a plane, as will be seen from the plot in Fig. 15, which is drawn to scale for a mica crystal  $10^{-6}$  cm. thick.

Slight imperfections in orientation, slight distortion of the crystal, or nonparallelism in the incident beam permit the reflection sphere to touch a large number of reciprocal lattice points and cause a network of reflections, even when the points are not elongated by the thinness of the crystal. It will be found a great convenience in interpreting an electron diffraction pattern to remember that it is practically a plane

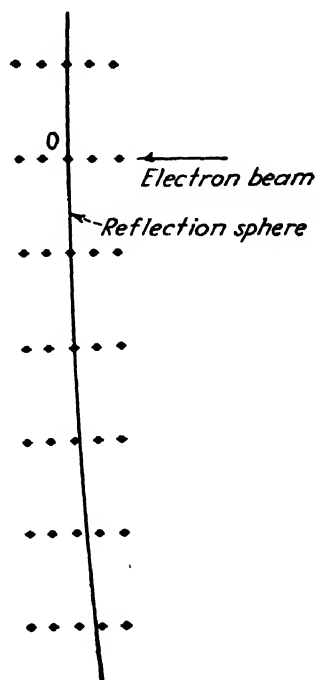


FIG. 15.—Reciprocal lattice with elongated points and reflection sphere.

section through the reciprocal lattice, a fact which makes the assignment of indices very simple.

**Intensity of Scattering.**—The intensity of an electron beam scattered by a crystal is proportional to the efficiency of scattering of individual atoms. With x-ray scattering we use an atomic scattering factor,  $f$ , to take account of this efficiency; similarly with electrons we can use a factor  $E$  for the purpose. Both  $E$  and  $f$  are functions of the angle  $\theta$ . The value of  $f$  depends upon the number of electrons in the scattering atom,  $Z$ , but  $E$  depends on the quantity  $(Z - f)$  because of scattering of electrons by the nucleus as well as by the outer electrons in the atom. The factor  $E$  has the value

$$E = (Z - f) \left( \frac{\lambda}{\sin \theta} \right)^2 \cdot c$$

where  $\lambda$  is expressed in angstroms, and  $c$  is a constant involving the electronic charge and mass and Planck's constant ( $c = e^2m/2h^2$ ). The value of  $E$  decreases with angle like  $f$ , though somewhat more abruptly, but the numerical value of  $E$  at small angles is about 10<sup>4</sup> times greater than  $f$ ; hence, electrons scatter much more intensely than x-rays. This is the reason electron diffraction can detect such minutely thin films of material. To compute the relative intensities of reflections from a crystal the usual x-ray formulas for  $F(hkl)$  are used, with  $E$  substituted for  $F$ .

**Secondary Effects.**—A complex pattern of black and white lines appears when a mica crystal is too thick to give good patterns of the type illustrated above. The **Kikuchi lines**,<sup>1</sup> as they are called, are illustrated in Fig. 16.<sup>2</sup> The nature of these straight lines is adequately accounted for by assuming that electrons entering a crystal are scattered in various directions and that some of the scattered electrons find themselves going in exactly the right directions to reflect from some plane in the crystal. In Fig. 17,  $AB$ ,  $A'B'$  represent reflecting planes in a crystal. Diffusely scattered electrons that would have followed the path  $OP$  are reflected to  $P'$ , while the scattered ray  $OQ$  is reflected to  $Q'$ . Now the intensity of the scattered ray in the direction  $OP$  is greater than in the direction  $OQ$ , and so the energy robbed from the ray  $P$  is not fully returned by the reflected ray  $Q'$  and there is a net loss in the direction  $OP$ ; similarly, there is a net gain in the direction  $OQ$ . Thus there will appear on the plate a white (weakened) line and a black (enhanced) line parallel to the projection of each crystal plane and equidistant from it. Sometimes there are so many lines at slight angles to each other, tangent

<sup>1</sup> S. KIKUCHI, *Proc. Imp. Acad. (Tokyo)*, vol. 4, pp. 271, 354, 1928; *Japan. J. Phys.*, vol. 5, p. 83, 1928.

<sup>2</sup> G. I. FINCH and H. WILMAN, *Proc. Roy. Soc. (London)*, vol. A155, p. 245, 1936.

along a curve, that the curved envelope of the lines becomes a prominent feature of the pattern.

Owing to the fact that the internal potential of a crystal is higher than that of free space, electrons entering a crystal act as if they were entering a medium of different refractive index. Their path is bent by



FIG. 16.—Transmission pattern for a relatively thick graphite crystal, showing Kikuchi lines. (*Finch and Wilman.*)

**refraction.** This effect is negligible in transmission photographs of thin films, but it becomes of importance when the primary beam of electrons enters the crystal very obliquely. It produces a distortion of the diffracted beam; each diffracted beam is drawn toward the shadow of the

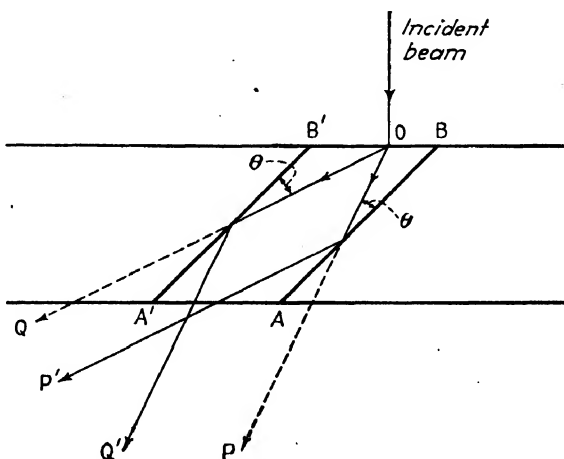


FIG. 17.—Origin of Kikuchi lines.

crystal surface on the photographic plate, and the nearer the beam to the shadow the greater the displacement. If the surface is wavy, the amount of this distortion is variable from point to point and blurred images result. This is presumably the reason for the diffuseness in Fig. 12.



## APPENDIX I

### CRYSTAL GEOMETRY

Zone relationships, which apply to the Miller indices of all systems, are as follows:

1. The plane  $(hkl)$  belongs to the zone  $[uvw]$  (i.e., is parallel to the line  $\{uvw\}$ ) if

$$hu + kv + lw = 0.$$

2. The plane  $(hkl)$  belongs to the two zones  $[u_1v_1w_1]$  and  $[u_2v_2w_2]$  if  $h:k:l = (v_1w_2 - v_2w_1):(w_1u_2 - w_2u_1):(u_1v_2 - u_2v_1)$ .

This relation may be remembered by the following operation:

$$\begin{array}{ccccccc} u_1 & \left| \begin{array}{c} v_1 \\ w_1 \end{array} \right. & \begin{array}{c} \nearrow \\ \searrow \end{array} & \begin{array}{c} u_1 \\ w_1 \end{array} & \begin{array}{c} \nearrow \\ \searrow \end{array} & \begin{array}{c} v_1 \\ w_1 \end{array} & \left| \begin{array}{c} u_1 \\ w_1 \end{array} \right. \\ & & & & & & \\ u_2 & \left| \begin{array}{c} v_2 \\ w_2 \end{array} \right. & \begin{array}{c} \nearrow \\ \searrow \end{array} & \begin{array}{c} u_2 \\ w_2 \end{array} & \begin{array}{c} \nearrow \\ \searrow \end{array} & \begin{array}{c} v_2 \\ w_2 \end{array} & \left| \begin{array}{c} u_2 \\ w_2 \end{array} \right. \end{array}$$

3. The zone  $[uvw]$  contains the two planes  $(h_1k_1l_1)$  and  $(h_2k_2l_2)$  if  $u:v:w = (k_1l_2 - k_2l_1):(l_1h_2 - l_2h_1):(h_1k_2 - h_2k_1)$ . This is analogous to the preceding formula and may be remembered in the same way.

4. The plane  $(h_3k_3l_3)$  will be among those belonging to the same zone as  $(h_1k_1l_1)$  and  $(h_2k_2l_2)$  if

$$h_3 = h_1 + h_2, \quad k_3 = k_1 + k_2 \quad \text{and} \quad l_3 = l_1 + l_2$$

The same will be true if

$$h_3 = h_1 - h_2, \quad k_3 = k_1 - k_2 \quad \text{and} \quad l_3 = l_1 - l_2$$

or if, in general,

$$h_3 = mh_1 \pm nh_2, \quad k_3 = mk_1 \pm nk_2 \quad \text{and} \quad l_3 = ml_1 \pm nl_2$$

where  $m$  and  $n$  are integers.

These and other relations may be derived from the equations of planes and lines that pass through the origin.<sup>1</sup>

The following formulas are useful in lattice computations:

1. The distance  $d_{hkl}$  between adjacent lattice planes in the simple space-lattices is most conveniently expressed in terms of  $1/d_{hkl}^2$ , given in the following formulas:

<sup>1</sup> J. D. H. DONNAY, *Am. Mineral.*, vol. 19, p. 593, 1934. Consider, for example, the three planes  $(h_1k_1l_1)$ ,  $(h_2k_2l_2)$ ,  $(h_3k_3l_3)$  which pass through the origin and intersect

System:

### Triclinic

$$\frac{1}{d^2} = \frac{1}{V^2} (S_{11}h^2 + S_{22}k^2 + S_{33}l^2 + 2S_{12}hk + 2S_{23}kl + 2S_{31}hl)$$

### Monoclinic

$$\frac{1}{d^2} = \frac{h^2}{a^2 \sin^2 \beta} + \frac{k^2}{b^2} + \frac{l^2}{c^2 \sin^2 \beta} - \frac{2hl \cos \beta}{ac \sin^2 \beta}$$

### Orthorhombic

$$\frac{1}{d^2} = \left(\frac{h}{a}\right)^2 + \left(\frac{k}{b}\right)^2 + \left(\frac{l}{c}\right)^2$$

### Hexagonal

$$\frac{1}{d^2} = \frac{4}{3} \cdot \frac{h^2 + hk + k^2}{a^2} + \left(\frac{l}{c}\right)^2$$

### Rhombohedral (rhombohedral coordinates)

$$\frac{1}{d^2} = \frac{(h^2 + k^2 + l^2) \sin^2 \alpha + 2(hk + kl + hl)(\cos^2 \alpha - \cos \alpha)}{a^2(1 - 3 \cos^2 \alpha + 2 \cos^3 \alpha)}$$

along the same straight line. This is equivalent to saying that the following three equations for the planes have one system of solutions:

$$\begin{aligned} h_1 \frac{x}{a} + k_1 \frac{y}{b} + l_1 \frac{z}{c} &= 0 \\ h_2 \frac{x}{a} + k_2 \frac{y}{b} + l_2 \frac{z}{c} &= 0 \\ h_3 \frac{x}{a} + k_3 \frac{y}{b} + l_3 \frac{z}{c} &= 0 \end{aligned}$$

This will be the case if the determinant of the coefficients is equal to zero,

$$\begin{vmatrix} h_1 & k_1 & l_1 \\ h_2 & k_2 & l_2 \\ h_3 & k_3 & l_3 \end{vmatrix} = 0$$

for when all the elements of a row are multiplied by the same factor, the determinant is multiplied by that factor. If this determinant is expanded by cofactors, the condition that the planes belong to the same zero may be written

$$\begin{vmatrix} k_2 & l_2 \\ k_3 & l_3 \end{vmatrix} h_1 + \begin{vmatrix} l_2 & h_2 \\ l_3 & h_3 \end{vmatrix} k_1 + \begin{vmatrix} h_2 & k_2 \\ h_3 & k_3 \end{vmatrix} l_1 = 0$$

which by expansion and substitution gives the formula under 1 above,

$$h_1 u + k_1 v + l_1 w = 0$$

where

$$u = k_2 l_3 - k_3 l_2 \quad v = l_2 h_3 - l_3 h_2 \quad w = h_2 k_3 - h_3 k_2$$



**Tetragonal**

$$\frac{1}{d^2} = \frac{h^2 + k^2}{a^2} + \frac{l^2}{c^2}$$

**Cubic**

$$\frac{1}{d^2} = \frac{h^2 + k^2 + l^2}{a^2}$$

where

$$\begin{aligned} S_{11} &= b^2 c^2 \sin^2 \alpha & S_{12} &= abc^2 (\cos \alpha \cos \beta - \cos \gamma) \\ S_{22} &= a^2 c^2 \sin^2 \beta & S_{23} &= a^2 bc (\cos \beta \cos \gamma - \cos \alpha) \\ S_{33} &= a^2 b^2 \sin^2 \gamma & S_{13} &= ab^2 c (\cos \gamma \cos \alpha - \cos \beta) \end{aligned}$$

$V$  = volume of the unit cell (see following paragraph)

2. The formulas for the volume of the unit cell,  $V$ , are as follows:

System:

**Triclinic**

$$V = abc \sqrt{1 - \cos^2 \alpha - \cos^2 \beta - \cos^2 \gamma + 2 \cos \alpha \cos \beta \cos \gamma}$$

**Monoclinic**

$$V = abc \sin \beta$$

**Orthorhombic**

$$V = abc$$

**Hexagonal**

$$V = \frac{\sqrt{3}}{2} a^2 c = 0.866 a^2 c$$

**Rhombohedral** (rhombohedral coordinates)

$$V = a^3 \sqrt{1 - 3 \cos^2 \alpha + 2 \cos^3 \alpha}$$

**Tetragonal**

$$V = a^2 c$$

**Cubic**

$$V = a^3$$

3. The angle,  $\phi$ , between two crystal planes  $(h_1 k_1 l_1)$  and  $(h_2 k_2 l_2)$  is determined by the following relations. [The quantities  $d$  and  $d'$  are the

interplanar spacings for  $(h_1k_1l_1)$  and  $(h_2k_2l_2)$  planes from the formulas under 1 above;  $S_{11}$ , etc., are defined above.]

System:

### Triclinic

$$\cos \phi = \frac{dd'}{V^2} [S_{11}h_1h_2 + S_{22}k_1k_2 + S_{33}l_1l_2 + S_{23}(k_1l_2 + k_2l_1) + S_{13}(l_1h_2 + l_2h_1) + S_{12}(h_1k_2 + h_2k_1)]$$

### Hexagonal

$$\cos \phi = \frac{h_1h_2 + k_1k_2 + \frac{1}{2}(h_1k_2 + h_2k_1) + \frac{3}{4}\frac{a^2}{c^2}l_1l_2}{\sqrt{\left(h_1^2 + k_1^2 + h_1k_1 + \frac{3}{4}\frac{a^2}{c^2}l_1^2\right)\left(h_2^2 + k_2^2 + h_2k_2 + \frac{3}{4}\frac{a^2}{c^2}l_2^2\right)}}$$

### Orthorhombic

$$\cos \phi = \frac{\frac{h_1h_2}{a^2} + \frac{k_1k_2}{b^2} + \frac{l_1l_2}{c^2}}{\sqrt{\left(\frac{h_1^2}{a^2} + \frac{k_1^2}{b^2} + \frac{l_1^2}{c^2}\right)\left(\frac{h_2^2}{a^2} + \frac{k_2^2}{b^2} + \frac{l_2^2}{c^2}\right)}}$$

The tetragonal equation is the same as the orthorhombic with  $a = b$ ; the cubic is the same with  $a = b = c$ .

4. The shortest distance between identical points, the "identity distance," along a direction  $[uvw]$  for the simple space-lattices is given by the following formulas:

General case:

$$I_{uvw} = \sqrt{a^2u^2 + b^2v^2 + c^2w^2 + 2bcvw \cos \alpha + 2cawu \cos \beta + 2abuv \cos \gamma}$$

Special cases:

### Hexagonal

$$I_{uvw} = a \sqrt{u^2 + v^2 + \frac{w^2c^2}{a^2} - uv}$$

### Orthorhombic

$$I_{uvw} = \sqrt{u^2a^2 + v^2b^2 + w^2c^2}$$

Cubic and tetragonal are special cases of the orthorhombic.

5. The area of the smallest unit parallelogram on the lattice plane  $(hkl)$  in simple space-lattices is

$$A_{hkl} = \sqrt{S_{11}h^2 + S_{22}k^2 + S_{33}l^2 + 2S_{12}hk + 2S_{13}hl + 2S_{23}kl}$$

for the triclinic lattice; others are special cases of this.

6. The angle between the direction  $[uvw]$  and the plane  $(hkl)$  in terms of quantities defined above is, for the general case,

$$\sin \rho = \frac{abc \sqrt{1 + 2 \cos \alpha \cos \beta \cos \gamma - \cos^2 \alpha - \cos^2 \beta - \cos^2 \gamma}}{A_{hkl} \cdot I_{uvw}}$$

The direction  $[uvw]$  lies in the plane  $(hkl)$  or is parallel to the plane  $(hkl)$  when

$$hu + kv + lw = 0,$$

and the direction is perpendicular to the plane when

$$hu + kv + lw = \frac{A_{hkl} \cdot I_{uvw}}{abc \sqrt{1 + 2 \cos \alpha \cos \beta \cos \gamma - \cos^2 \alpha - \cos^2 \beta - \cos^2 \gamma}}.$$

7. The angle between the lattice directions  $[u_1v_1w_1]$  and  $[u_2v_2w_2]$  is given by

$$\cos \rho = \frac{a^2u_1u_2 + b^2v_1v_2 + c^2w_1w_2 + bc(v_1w_2 + v_2w_1) \cos \alpha + ac(w_1u_2 + w_2u_1) \cos \beta + ab(u_1v_2 + u_2v_1) \cos \gamma}{I_{u_1v_1w_1} \cdot I_{u_2v_2w_2}}.$$

Special cases:

### Hexagonal

$$\cos \rho = \frac{u_1u_2a^2 + v_1v_2b^2 + w_1w_2(c/a)^2 - \frac{1}{2}(u_1v_2 + u_2v_1)}{\sqrt{u_1^2 + v_1^2 - u_1v_1 + w_1^2(c/a)^2} \cdot \sqrt{u_2^2 + v_2^2 - u_2v_2 + w_2^2(c/a)^2}}$$

### Orthorhombic

$$\cos \rho = \frac{u_1u_2a^2 + v_1v_2b^2 + w_1w_2c^2}{\sqrt{u_1^2a^2 + v_1^2b^2 + w_1^2c^2} \cdot \sqrt{u_2^2a^2 + v_2^2b^2 + w_2^2c^2}}$$

Tetragonal and cubic are special cases of this, the cubic formula being

$$\cos \rho = \frac{u_1u_2 + v_1v_2 + w_1w_2}{\sqrt{u_1^2 + v_1^2 + w_1^2} \cdot \sqrt{u_2^2 + v_2^2 + w_2^2}}.$$

The directions  $[u_1v_1w_1]$  and  $[u_2v_2w_2]$  are mutually perpendicular when the numerators in these expressions are zero; for example, in the cubic case

$$u_1u_2 + v_1v_2 + w_1w_2 = 0.$$

# APPENDIX II

## EMISSION AND ABSORPTION WAVELENGTHS

TABLE XXXI.—*K* EMISSION LINES AND *K* ABSORPTION EDGES, ÅNGSTRÖMS<sup>1</sup>

Element	Atomic number	Emission line					Absorption edge
		$\alpha_2$	$\alpha_1$	$\beta_3$	$\beta_1$	$\beta_2$	
		Intensities					
		Strong	Very strong	Very weak	Weak	Very weak	
Sodium.	11	11 885		Not resolved from $\beta_1$	11 594	$\beta_2$ is not observed with elements lighter than nickel	
Magnesium	12	9 869			9 539		9 4962
Aluminum	13	8.3205			7 965		7.9356
Silicon . . . .	14	7.11106			6.7545		6.7310
Phosphorus.	15	6.1425			5 7921		5 7749
Sulphur . . . .	16	5 3637	5.3613		5 0211		5 0088
Chlorine..	17	4.7212	4.7182		4 3942		4 3838
Potassium	19	3.73707	3.73368		3 4468		3 4310
Calcium	20	3 35495	3 35169		3 0834		3.0643
Scandium.	21	3.02840	3.02503		2.7739		2.7517
Titanium	22	2 74681	2.74317		2 5090		2 4912
Vanadium . .	23	2.50213	2 49835		2 2797		2 2630
Chromium. .	24	2 28891	2 28503		2 0806		2 0659
Manganese . .	25	2 10149	2 09751		1 90620		1.8916
Iron . . . . .	26	1 936012	1.932076		1 753013		1 7394
Cobalt . . . . .	27	1 78919	1 78529		1 61744		1 6040
Nickel . . . . .	28	1 65835	1 65450		1 49705		1 4839
Copper . . . . .	29	1 541232	1.537395		1 38935		1.3774
Zinc . . . . .	30	1.43603	1 43217		1 29255		1.2805
Gallium . . . . .	31	1.34087	1 33715	1.20520	1.1902		
Germanium . .	32	1.25521	1 25130	1.12671	1.1146		
Arsenic . . . . .	33	1 17743	1 17344	1 05510	1.04263		
Selenium . . . .	34	1.10652	1.10248	0.99013	0.97773		
Bromine . . . . .	35	1.04166	1.03759	0 93087	0.91809		
Krypton . . . . .	36	0.978		0.875			
Rubidium . . . .	37	0.92776	0.92364	0.82749	0 81476	0.81410	
Strontium . . . .	38	0.87761	0.87345	0.78183	0.76921	0 76837	
Yttrium . . . . .	39	0 83132	0 82712	0 73972	0 72713	0.7255	
Zirconium . . .	40	0 78851	0.78430	0.70083	0.68850	0.68738	
Niobium	41	0.74889	0.74465	0.66496	0.65280	0.65158	

<sup>1</sup> M. SIEGBAHN, "Spektroskopie der Röntgenstrahlen," 2d ed., Springer, Berlin, 1931.

TABLE XXXI.—K EMISSION LINES AND K ABSORPTION EDGES, ÅNGSTRÖMS.<sup>1</sup>—  
(Continued)

Element	Atomic number	Emission line					Absorption edge
		$\alpha_2$	$\alpha_1$	$\beta_3$	$\beta_1$	$\beta_2$	
		Intensities					
		Strong	Very strong	Very weak	Weak	Very weak	
Molybdenum.	42	0.712805	0.707831	0.631543	0.630978	0.619698	0.61848
Ruthenium	44	0.64606	0.64174	0.57193	0.57131	0.56051	0.5584
Rhodium.	45	0.61637	0.61202	0.54509	0.54449	0.53396	0.53303
Palladium ..	46	0.58863	0.58427	0.52009	0.51947	0.50918	0.50795
Silver.	47	0.56267	0.55828	0.49665	0.49601	0.48603	0.48448
Cadmium	48	0.53832	0.53390	0.47471	0.47408	0.46420	0.46313
Indium	49	0.51548	0.51106	0.45423	0.45358	0.44408	0.44298
Tin. ...	50	0.49402	0.48957	0.43495	0.43430	0.42499	0.42394
Antimony ..	51	0.47387	0.46931	0.41623		0.40710	0.40609
Tellurium	52	0.45491	0.45037	0.39926		0.39037	0.38926
Iodine ..	53	0.43703	0.43249	0.38392	0.38315	0.37471	0.37344
Xenon	54	0.417			0.360		
Cesium	55	0.40411	0.39959	0.35436	0.35362	0.34516	0.34404
Barium	56	0.38899	0.38443	0.34089	0.34022	0.33222	0.33070
Lanthanum	57	0.37466	0.37004	0.32809	0.32726	0.31966	0.31814
Cerium	58	0.36110	0.35647	0.31572	0.31501	0.30770	0.30626
Praseodymium	59	0.34805	0.34340	0.30439	0.30360	0.29625	0.2951
Neodymium	60	0.33595	0.33125	0.29351	0.29275	0.28573	0.28458
Samarium.	62	0.31302	0.30833	0.27325	0.27250	0.26575	0.2644
Europium	63	0.30265	0.29790	0.26386	0.26307	0.25645	0.2548
Gadolinium	64	0.29261	0.28782	0.25471	0.25394	0.24762	0.2462
Terbium	65	0.28286	0.27820	0.24629	0.24551	0.23912	0.2376
Dysprosium	66	0.27375	0.26903	0.23787	0.23710	0.23128	0.2301
Holmium	67	0.26499	0.26030	.....	.....	.....	0.22264
Erbium	68	0.25664	0.25197	0.22300	0.22215	0.21671	
Thulium	69	0.24861	0.24387	0.21558	0.21487	.....	0.2085
Ytterbium	70	0.24098	0.23628	0.20916	0.20332	0.20834	0.2016
Lutecium..	71	0.23358	0.22882	0.20252	0.20171	0.19649	0.1951
Hafnium..	72	0.22653	0.22173	0.19583	0.19515	0.19042	0.1901
Tantalum. . .	73	0.21973	0.21488	0.18991		0.18452	0.1836
Tungsten	74	0.21345	0.20862	0.18422		0.17898	0.17822
Osmium ..	76	0.20131	0.19645	0.17361		0.16875	0.16755
Iridium..	77	0.19550	0.19065	0.16850		0.16376	0.16209
Platinum . .	78	0.19004	0.18223	0.16370		0.15887	0.15770
Gold . . . .	79	0.18483	0.17996	0.15902		0.15426	0.15320
Thallium. ....	81	0.17466	0.16980	0.15011		0.14539	0.14441
Lead . . .	82	0.17004	0.16516	0.14606		0.14125	0.14049
Bismuth . . .	83	0.16525	0.16041	0.14205		0.13621	0.13678
Thorium . . .	90	0.1368	0.1323	0.1169		0.1134	0.11270
Uranium. . . .	92	0.13095	0.12640	0.11187		0.10842	0.10658?

<sup>1</sup> M. SIEGBÄHN, "Spektroskopie der Röntgenstrahlen," 2d ed., Springer, Berlin, 1931.

TABLE XXXII.—*L* EMISSION SPECTRA AND *L*<sub>III</sub> ABSORPTION EDGES, ANGSTROMS<sup>1</sup>

Element	Atomic number	Emission lines											Absorption edge $L_{III}$	
		$l$	$\eta$	$\alpha_2$	$\alpha_1$	Intensities								
						$\beta_1$	$\beta_2$	$\beta_3$	$\beta_4$	$\beta_5$	$\gamma_1$			
Very weak	Very weak	Weak	Very strong	Strong	Medium	Weak	Very weak	Very weak	Weak					
Copper.....	29	15.190	14.830	13.306	13.030	11.960	11.160	11.160	6.9681	6.8413	6.3620	5.9444	5.5610	
Zinc.....	30	13.950	13.610	12.230	11.960	11.010	10.153	9.395	8.912	6.3582	6.3018	6.0857	5.2121	
Gallium.....	31	12.890	12.560	11.270	10.415	9.652	8.972	8.358	6.8486	6.7694	6.5081	6.0777	4.9042	
Germanium...	32	11.922	11.587	10.415	9.652	8.972	8.358	6.8486	6.7694	6.5081	6.0777	5.9444	4.8604	
Arsenic.....	33	11.048	10.711	9.652	8.972	8.358	6.8486	6.7694	6.5081	6.0777	5.9444	5.5610	4.1212	
Selenium.....	34	10.272	9.939	8.972	8.358	6.8486	6.7694	6.5081	6.0777	5.9444	5.5610	5.2121	3.9039	
Bromine.....	35	9.564	9.235	8.358	6.8486	6.7694	6.5081	6.0777	5.9444	5.5610	5.2121	3.7986	3.6908	
Rubidium.....	37	.....	.....	.....	.....	.....	.....	.....	.....	.....	.....	.....	3.3280	
Ruthenium.....	38	7.822	7.506	6.8486	6.7694	6.5081	6.0777	5.9444	5.5610	5.2121	3.9039	3.7164	3.4963	
Strontium.....	39	.....	7.0310	6.4357	6.0567	5.8236	5.5742	5.2971	5.0047	4.7684	4.5126	4.2328	3.1493	
Yttrium.....	40	6.899	6.5939	6.0567	5.8236	5.5742	5.2971	5.0047	4.7684	4.5126	4.2328	3.9357	3.7164	
Zirconium.....	41	6.510	6.196	5.718	5.4803	5.2260	4.9100	4.6110	4.3619	4.1221	3.9007	3.6811	3.4963	
Niobium.....	42	.....	5.836	5.401	5.3950	5.1665	4.9100	4.6110	4.3619	4.1221	3.9007	3.6811	3.4963	
Molybdenum.....	44	5.4864	.....	4.8437	4.8357	4.6110	4.3619	4.1221	3.9007	3.6811	3.4963	3.3280	3.1553	
Ruthenium.....	45	0.2070	4.9112	4.5956	4.5878	4.3640	4.1221	3.9007	3.6811	3.4963	3.3280	3.1553	2.9949	
Rhodium.....	46	4.9396	4.6502	4.3666	4.3585	4.1373	3.9007	3.6811	3.4963	3.3280	3.1553	2.9949	2.8164	
Palladium.....	47	4.6976	4.4101	4.1538	4.1456	3.9266	3.6938	3.4643	3.2348	3.0053	2.7758	2.5463	2.3168	
Silver.....	48	4.4713	4.1875	3.9564	3.9478	3.7301	3.5064	3.2827	3.0590	2.8353	2.6116	2.3879	2.1642	
Cadmium.....	49	4.2593	3.9761	3.7724	3.7637	3.5478	3.3312	3.1145	2.8978	2.6811	2.4644	2.2477	2.0310	
Indium.....	50	4.0633	3.7818	3.6011	3.5922	3.3779	3.1679	2.9579	2.7479	2.5379	2.3279	2.1179	1.9079	
Tin.....	50	4.0633	3.7818	3.6011	3.5922	3.3779	3.1679	2.9579	2.7479	2.5379	2.3279	2.1179	1.9079	

Antimony	51	3 8803	3 5996	3 4408	3 4318	3 2184	3 0166	3 1451	3 1843	3 1078	2 8451	2 9907
Tellurium	52	3 7101	..	3 2910	3 2820	3 0700	2 8761	2 8013	2 9400	2 9644	2 7065	2 8457
Iodine	53	3 5497	..	3 1509	3 1417	2 9309	2 7461	2 6682	2 9059	2 8805	2 5775	2 7139
Cesium	55	3 2596	2 9833	2 8956	2 8861	2 6778	2 5064	2 6229	2 6605	2 5875	2 3425	2 4674
Barium	56	3 1287	2 8571	2 7790	2 7696	2 5622	2 3993	2 5110	2 5498	2 4772	2 2366	2 3568
Lanthanum	57	3 000	2 734	2 6689	2 6597	2 4533	2 2980	2 4053	2 4438	2 3739	2 1372	2 2537
Cerium	58	2 9857	2 6147	2 5651	2 5560	2 3510	2 2041	2 3059	2 3442	2 2769	2 0443	2 1595
Praseodymium	59	2 7781	2 507	2 4676	2 4577	2 2539	2 1148	2 2124	2 2501	2 1859	1 9568	2 0728
Neodymium	60	2 6703	2 4042	2 3756	2 3653	2 1622	2 0314	2 1222	2 1622	2 0993	1 8738	1 9907
Samarium	62	2 477	2 214	2 2057	2 1950	1 9936	1 8781	1 9580	1 9964	1 9422	1 7231	1 8408
Europium	63	2 3903	..	2 1273	2 1163	1 9163	1 8082	1 8827	1 9221	1 8705	1 6543	1 7717
Gadolinum	64	2 3071	..	2 0826	2 0419	1 8425	1 7419	1 8109	1 8493	1 8031	1 586	1 7060
Terbium	65	2 2290	..	1 9823	1 9715	1 7727	1 6790	1 7425	1 7814	1 7375	1 5266	1 6453
Dysprosium	66	2 1540	1 8922	1 9156	1 9046	1 7066	1 6198	1 6777	1 7167	1 6777	1 4697	1 576
Holmium	67	2 0821	1 8220	1 8521	1 8410	1 6435	1 5637	1 6160	1 6553	1 6188	1 4142	1 5322
Erbium	68	2 0151	1 7548	1 7914	1 7804	1 5834	1 5106	1 5579	1 5964	1 5636	1 3623	1 47919
Thulium	69	1 9511	1 6923	1 7339	1 7228	1 5268	1 4602	1 5023	1 5412	1 5115	1 3127	1 4299
Ytterbium	70	1 890	1 631	1 6789	1 6678	1 4725	1 4128	1 4494	1 4882	1 4627	1 2648	1 38264
Luycium	71	1 8318	1 5738	1 62636	1 61551	1 4207	1 3672	1 3982	1 4372	1 4143	1 2203	1 3375
Hafnium	72	1 7774	1 5197	1 57704	1 56607	1 3711	1 3235	1 3497	1 3893	1 3711	1 1765	1 2930
Tantalum	73	1 7249	1 4679	1 52978	1 51985	1 32423	1 28190	1 30409	1 34307	1 3284	1 13558	1 2517
Tungsten	74	1 6750	1 4181	1 48438	1 47336	1 27917	1 24203	1 25992	1 29879	1 2870	1 09630	1 2129
Rhenium	75	1 6273	1 3706	1 4410	1 42997	1 23603	1 2041	1 2176	1 2563	1 2481	1 0587	1 1755
Osmium	76	..	..	1 39866	1 38859	1 19490	1 16884	..	..	..	1 02296	1 1390
Iridium	77	..	1 2817	1 3598	1 34847	1 15540	1 13297	1 13847	1 17715	1 17545	0 98876	1 1088
Platinum	78	1 4964	1 2403	1 32155	1 31033	1 11758	1 09974	1 10165	1 13986	1 14100	0 95599	1 0710
Gold	79	1 4569	1 2003	1 28502	1 27377	1 08128	1 06801	1 06550	1 10422	1 10863	0 92461	1 0382
Mercury	80	1 41841	1 1616	1 24951	1 23863	1 04652	1 03770	1 03046	1 0692	1 0768	0 8946	1 0075
Thallium	81	1 3819	1 1254	1 21626	1 20493	1 01299	1 00822	0 99850	1 03699	1 04748	0 86571	0 9778
Lead	82	1 3474	1 0900	1 18408	1 17258	0 98083	0 98083	0 96721	1 00563	1 01906	0 83801	0 9492
Bismuth	83	1 3137	1 0565	1 15301	1 14150	0 95002	0 95324	0 93666	0 97501	0 99131	0 81143	0 9221
Thorium	90	1 1128	0 8528	0 96585	0 95405	0 76356	0 79192	0 75324	0 79192	0 82646	0 65176	0 7600
Protactinium	91	1 0885	0 8278	0 9427	0 9309	0 7407	0 7721	0 7307	0 7683	0 8062	0 6325	0 7208
Uranium	92	1 0649	0 8035	0 92062	0 90874	0 71851	0 75307	0 70879	0 7464	0 78679	0 61359	0 7208

# APPENDIX III

## ABSORPTION COEFFICIENTS

MASS ABSORPTION COEFFICIENTS ( $\mu/\rho$ ) OF ELEMENTS, INCLUDING SCATTERING<sup>1</sup>

Radiation .		Ag $K\alpha$	Rh $K\alpha$	Mo $K\alpha$	Cu $K\alpha$	Ni $K\alpha$	Fe $K\alpha$	Cr $K\alpha$
Absorber	Z	$\lambda 0.5604$	0.6149	0.7097	1.5392	1.6565	1.9344	2.2869
He	2	0.16	0.16	0.18				
Li	3	0.18	0.20	0.22				
Be	4	0.22	0.25	0.30	1.35	1.80	3.24	4.74
B	5	0.30	0.35	0.45	3.06	3.79	5.80	9.37
C	6	0.42	0.51	0.70	5.50	6.76	10.73	17.9
N	7	0.60	0.70	1.10	8.51	10.7	17.3	27.7
O	8	0.80	1.00	1.50	12.7	16.2	25.2	40.1
F	9	1.00	1.32	1.93	17.5	21.5	33.0	51.6
Ne	10	1.41	1.80	2.67	24.6	30.2	46.0	72.7
Na	11	1.75	2.25	3.36	30.9	37.9	56.9	92.5
Mg	12	2.27	2.93	4.38	40.6	47.9	75.7	120.1
Al	13	2.74	3.60	5.30	48.7	58.4	92.8	149
Si	14	3.44	4.52	6.70	60.3	75.8	116.3	192
P	15	4.20	5.36	7.98	73.0	90.5	141.1	223
S	16	5.15	6.65	10.03	91.3	111.5	175	273
Cl	17	5.86	7.50	11.62	103.4	125.6	199	308
A	18	6.40	8.00	12.55	112.9	141	217	341
K	19	8.05	10.7	16.7	143	179	269	425
Ca	20	9.66	12.8	19.8	172	210	317	508
Sc	21	10.5	13.8	21.1	185	222	338	545
Ti	22	11.8	15.8	23.7	204	247	377	603
Va	23	13.3	17.7	26.5	227	275	422	77.3
Cr	24	15.7	20.4	30.4	259	316	490	89.9
Mn	25	17.4	22.6	33.5	284	348	63.6	99.4
Fe	26	19.9	25.8	38.3	324	397	72.8	114.6
Co	27	21.8	28.1	41.6	354	54.4	80.6	125.8
Ni	28	25.0	32.3	47.4	49.2	61.0	93.1	145
Cu	29	26.4	34.0	49.7	52.7	65.0	98.8	154
Zn	30	28.2	37.7	54.8	59.0	72.1	109.4	169
Ga	31	30.8	39.7	57.3	63.3	76.9	116.5	179
Ge	32	33.5	42.8	63.4	69.4	84.2	128.4	196
As	33	36.5	46.0	69.5	76.5	93.8	142	218
Se	34	38.5	49.0	74.0	82.8	100.6	152	235
Br	35	42.3	53.5	82.2	92.6	112.4	169	264
Kr	36	45.0	57.5	88.1	100.4	121.9	182	285
Rb	37	48.2	62.8	94.4	109.1	132.9	197	309
Sr	38	52.1	68.3	101.2	119	145	214	334
Y	39	55.5	74.0	108.9	129	158	235	360
Zr	40	61.1	80.9	117.2	143	173	260	391

<sup>1</sup> Values are from "Internationale Tabellen zur Bestimmung von Kristallstrukturen," vol. II, Borntrager, Berlin, 1935.



MASS ABSORPTION COEFFICIENTS ( $\mu/\rho$ ) OF ELEMENTS, INCLUDING SCATTERING.<sup>1</sup>—

(Continued)

Radiation.....		Ag $K\alpha$	Rh $K\alpha$	Mo $K\alpha$	Cu $K\alpha$	Ni $K\alpha$	Fe $K\alpha$	Cr $K\alpha$
Absorber Z		$\lambda 0.5604$	$0.6149$	$0.7097$	$1.5392$	$1.6565$	$1.9344$	$2.2869$
Nb 41		65 8	86.0	18 7	153	183	279	415
Mo 42		70.7	91 6	20 2	164	197	299	439
Ru 44		$\left\{ \begin{smallmatrix} \alpha_1 79\ 9 \\ \alpha_2 12\ 2 \end{smallmatrix} \right\}$	15.4	23 4	185	221	337	488
Rh 45		13.1	16.6	25 3	198	240	361	522
Pd 46		13 8	17 6	26 7	207	254	376	545
Ag 47		14 8	19.1	28.6	223	276	402	585
Cd 48		15 5	20 1	29 9	234	289	417	608
In 49		16.5	21 7	31.8	252	307	440	648
Sn 50		17.4	22.9	33 3	265	322	457	681
Sb 51		18.6	24.6	35 3	284	342	482	727
Te 52		19 1	25 0	36 1	289	347	488	742
I 53		20 9	27 3	39 2	314	375	527	808
Xe 54		22 1	28 5	41 3	330	392	552	852
Cs 55		23 6	30 0	43 3	347	410	579	844
Ba 56		24 5	31 1	45 2	359	423	599	819
La 57		26 0	33 0	47 9	378	444	632	218
Ce 58		28 4	35 8	52 0	407	476	636	235
Pr 59		29 4	37 2	54 5	422	493	624	251
Nd 60		30 5	38 8	57 0	437	510	651	263
Sm 62		33 1	41 2	62 3	467	519	183	289
Eu 63		35 0	44 5	65 9	461	498	193	306
Gd 64		35 8	45 7	68.0	470	509	199	316
Tb 65		37 5	47 9	71 7	435	140	211	333
Dy 66		39 1	49 9	75 0	462	146	220	345
Ho 67		41 3	52 7	79 3	128	153	232	361
Er 68		42 6	54 6	82 0	133	159	242	370
Tm 69		44 8	57 6	86 3	139	168	257	387
Yb 70		46 1	59 4	88 7	144	174	265	396
Lu 71		48 4	62 6	93 2	151	184	281	414
Hf 72		50 6	65 0	96 9	157	191	291	426
Ta 73		52 2	67 7	100.7	164	200	305	440
W 74		54 6	70 7	105 4	171	209	320	456
Os 76		58.6	76 3	112 9	186	226	346	480
Ir 77		61 2	80 0	117.9	194	237	362	498
Pt 78		64 2	83 8	123	205	248	376	518
Au 79		66.7	87 1	128	214	260	390	537
Hg 80		69 3	90 1	132	223	272	404	552
Tl 81		71 7	92 4	136	231	282	416	568
Pb 82		74 4	95 8	141	241	294	429	585
Bi 83		78 1	100 4	145	253	310	448	612
Nt 86		84 7	109.1	159	278	341	476	657
Ra 88		91 1	117	172	304	371	509	708
Th 90		97.0	119	143	327	399	536	755
U 92		104 2	129	153	352	423	566	805

<sup>1</sup> Values are from "Internationale Tabellen zur Bestimmung von Kristallstrukturen," vol. II, Bohn-träger, Berlin, 1935.

# APPENDIX IV

## REFLECTING PLANES OF CUBIC CRYSTALS

The quadratic form for the cubic system can be written

$$\log \sin^2 \theta = 2 \log \lambda - \log 4 - 2 \log a + \log (h^2 + k^2 + l^2).$$

The following table gives values of  $\log (h^2 + k^2 + l^2)$  and indicates the reflections that are possible from face-centered (*F*), body-centered (*B*), and diamond cubic (*D*) lattices. All entries are possible reflections for simple cubic space-lattices.

$h^2 + k^2 + l^2$	$\log (h^2 + k^2 + l^2)$	Lattice	$hkl$
1	0.00000	. .	100
2	0.30103	<i>B</i>	110
3	0.47712	<i>FD</i>	111
4	0.60206	<i>BF</i>	200
5	0.69897	....	210
6	0.77815	<i>B</i>	211
7			
8	0.90309	<i>BFD</i>	220
9	0.95424	.	300, 221
10	1.00000	<i>B</i>	310
11	1.04139	<i>FD</i>	311
12	1.07918	<i>BF</i>	222
13	1.11394	.	320
14	1.14613	<i>B</i>	321
15			
16	1.20412	<i>BFD</i>	400
17	1.23045	. . .	410, 322
18	1.25527	<i>B</i>	411, 330
19	1.27875	<i>FD</i>	331
20	1.30103	<i>BF</i>	420
21	1.32222	....	421
22	1.34242	<i>B</i>	332
23			
24	1.38021	<i>BFD</i>	422
25	1.39794	....	500, 430
26	1.41497	<i>B</i>	510, 431

$h^2 + k^2 + l^2$	$\log (h^2 + k^2 + l^2)$	Lattice	$hkl$
27	1.43136	<i>FD</i>	511, 333
28			
29	1.46240	. .	520, 432
30	1.47712	<i>B</i>	521
31			
32	1.50515	<i>BFD</i>	440
33	1.51851	....	522, 441
34	1.53148	<i>B</i>	530, 433
35	1.54407	<i>FD</i>	531
36	1.55630	<i>BF</i>	600, 442
37	1.56820	....	610
38	1.57978	<i>B</i>	611, 532
39			
40	1.60206	<i>BFD</i>	620
41	1.61278	. .	621, 540, 443
42	1.62325	<i>B</i>	541
43	1.63347	<i>FD</i>	533
44	1.65321	<i>BF</i>	622
45	1.66276		630, 542
46	1.67210	<i>B</i>	631
47			
48	1.68124	<i>BFD</i>	444
49	1.69020	.	700, 632
50	1.69897	<i>B</i>	710, 550, 543
51	1.70757	<i>FD</i>	711, 551
52	1.71600	<i>BF</i>	640
53	1.72428	....	720, 641
54	1.73239	<i>B</i>	721, 633, 552
55			
56	1.74819	<i>BFD</i>	642
57	1.75587	.	722, 544
58	1.76343	<i>B</i>	730
59	1.77084	<i>FD</i>	731, 553

## APPENDIX V

### THE INTENSITY OF X-RAY REFLECTIONS

To determine the structure of a complex crystal a crystallographer must analyze the intensities of the reflections he observes, first computing true intensities from his films and then relating these intensities to the distribution of atoms in the unit cell. Several factors are involved in such analyses: the scattering power of individual electrons, of groups of electrons in atoms, of atoms in the unit cell, of crystals at different

temperatures, and of crystals mounted in various x-ray cameras that require their individual geometrical correction factors. These have received only brief mention in Chaps. IV to VIII.

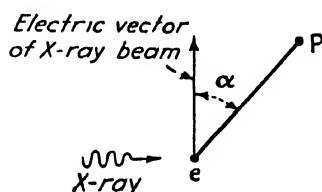


FIG. 1.—Scattering from an electron.

**Scattering by an Electron.**—J. J. Thomson<sup>1</sup>

derived the classical-theory formula for the intensity of x-rays that would be scattered by a free electron or by an electron that is held under negligible constraining forces. Consider a polarized beam of x-rays falling on an electron at *e*, Fig. 1. The electric field of the incident beam will accelerate the electron with a vibratory motion and cause it to radiate electromagnetic waves of the same wavelength as the original beam. The intensity,  $I_e$ , of this secondary radiation at the point *P* will be related to the intensity of the primary beam,  $I_0$ , the distance *r*, and the angle  $\alpha$  between the direction of observation and the direction of the electric vector of the incident radiation. The relation derived by Thomson is

$$I_e = \frac{I_0 e^4}{r^2 m^2 c^4} \sin^2 \alpha \quad (1)$$

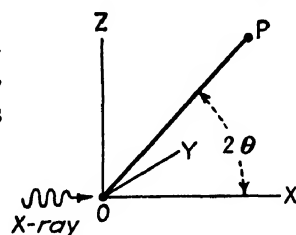


FIG. 2.—Coordinates for scattered ray.

where *e* and *m* are the charge and mass of the electron and *c* is the velocity of light.

We shall apply Thomson's formula to an electron at the origin of the coordinate axes of Fig. 2, with the incident beam proceeding along the *X* axis and the scattered rays observed at point *P* in the *XZ* plane. Let

<sup>1</sup> J. J. THOMSON, "Conduction of Electricity through Gases," 2d ed., p. 325, University Press, Cambridge, Mass., 1928, reviewed in A. H. Compton and S. K. Allison, "X-rays in Theory and Experiment," p. 117, Van Nostrand, New York, 1935.

the angle between  $OP$  and the  $X$  axis be  $2\theta$  (since  $\theta$  will then correspond to the angle in Bragg's law). If the electric vector of a polarized beam is parallel to  $Z$  and if the beam has intensity  $I_z$ , the intensity at  $P$  according to Eq. (1) will be

$$I_e = \frac{I_z e^4}{r^2 m^2 c^4} \cos^2 2\theta; \quad (1a)$$

while if the electric vector of the polarized beam is parallel to  $Y$  and of intensity  $I_y$ , the intensity at  $P$  will be

$$I_e = \frac{I_y e^4}{r^2 m^2 c^4}. \quad (1b)$$

Now under ordinary conditions the incident beam is unpolarized, and the electric vector  $E_0$  of the primary ray may be resolved into components  $E_y$  along  $Y$  and  $E_z$  along  $Z$  such that

$$E_y^2 + E_z^2 = E_0^2.$$

With unpolarized rays the electric vector occurs with equal probability at all angles; therefore, on the average, its component along  $Y$  is equal to its component along  $Z$ . On the average, therefore,

$$E_y^2 = E_z^2 = \frac{1}{2} E_0^2;$$

and since the intensity is equal to the square of the amplitude, it follows that

$$I_y = I_z = \frac{1}{2} I_0.$$

The intensity for an unpolarized beam is obtained by adding the contributions of the two components specified in (1a) and (1b), giving

$$\begin{aligned} I_e &= \frac{e^4}{r^2 m^2 c^4} (I_y + I_z \cos^2 2\theta) = \frac{e^4}{r^2 m^2 c^4} \left( \frac{1}{2} I_0 + \frac{1}{2} I_0 \cos^2 2\theta \right) \\ &= \frac{I_0 e^4}{r^2 m^2 c^4} \frac{(1 + \cos^2 2\theta)}{2}. \end{aligned} \quad (2)$$

The factor  $\frac{1}{2}(1 + \cos^2 2\theta)$  in this equation appears in subsequent formulas for intensities of reflection from crystals and is known as the "polarization factor."

**Scattering by an Atom.**—In an atom that is much smaller than the wavelength of the incident x-rays, the electrons oscillate back and forth together so that the atom acts as a unit of mass  $Zm$  and charge  $Ze$ , where  $Z$  is the number of electrons in the atom. Equation (2) then becomes

$$I_a = \frac{I_0 (Ze)^4}{r^2 (Zm)^2 c^4} \frac{(1 + \cos^2 2\theta)}{2} = Z^2 I_e. \quad (3)$$

In x-ray diffraction work, however, the wavelengths used are of the same order of magnitude as the atomic diameters. Consequently, the electrons within an atom do not scatter in phase and the intensity is less than the value predicted by Eq. (3).

It is customary to use a quantity  $f$ , the **atomic scattering factor**, by which the efficiency of the cooperation among the electrons in the atom may be expressed. The definition of  $f$  is given by the relation

$$f^2 = \frac{I_a}{I_e} \quad (4)$$

or by the equivalent statement—since the intensity of a wave is the square of its amplitude—that  $f$  is the ratio of the amplitude scattered by the atom to that scattered by an electron. When  $\theta$  is very small,  $f$  approaches the atomic number  $Z$ , because the electrons scatter nearly in phase, as assumed in Eq. (3). But  $f$  falls as  $\theta$  increases because the waves from the individual electrons must traverse increasingly unequal paths. Some of the radiation is scattered incoherently with a modified wavelength (Compton scattering); this forms an increasing fraction of the total intensity at the larger angles.

The atomic scattering factor is directly related to the distribution of electricity in the atom. Every part of the electron cloud surrounding the nucleus of the atom scatters radiation in proportion to its density. For the atom at rest (not “blurred” by thermal motion in the crystal) the formula for the atomic scattering factor is

$$f_0 = \int_0^\infty U(r) \frac{\sin kr}{kr} dr \quad (5)$$

where  $k = 4\pi(\sin \theta)/\lambda$ ,  $\lambda$  is the wavelength of the radiation, and  $U(r)$  represents the radial distribution of electric-charge density.  $U(r)dr$  is the number of electrons between  $r$  and  $r + dr$  from the center of the atom, which is assumed to be spherical,<sup>1</sup> and

$$\int_0^\infty U(r) dr = Z.$$

<sup>1</sup> It is immaterial whether  $U(r)$  is considered as the probability of finding an electron at a radius between  $r$  and  $r + dr$  or whether it is assumed that a continuous charge is distributed in the atom with a density that varies as  $U(r)$ . In the language of wave mechanics, the function  $\psi$  of Schrödinger's wave equation is such that  $|\psi|^2 dv$  is the probability of finding an electron in the element of volume  $dv$  at the point considered, and it has been shown that Eq. (5) gives the coherent scattering from an atom if we let  $U(r) = 4\pi r^2 |\psi|^2$ . Thus, wave mechanical models of an atom can predict  $f_0$ , and, conversely, experimental  $f_0$  curves afford a test of atomic models. By using a Fourier analysis of experimental  $f_0$  curves it is possible to calculate directly the electric-charge density of atoms—thus *mathematically* to “see” the atoms with an “x-ray microscope.”

It will be seen from Eq. (5) that  $f_0$  is a function of  $(\sin \theta)/\lambda$ , so that a curve in which  $f_0$  is plotted against  $(\sin \theta)/\lambda$  can be used for various wavelengths. The  $f_0$  curve calculated for cesium by a method based on wave mechanics is plotted in this way in Fig. 3. These curves can also be determined by direct measurement in certain cases; this has been done by measuring the intensities of diffracted beams from crystals with simple structures (NaCl, MgO, KCl, Al, etc.) and in another way by measuring the intensity of scattering at different angles from the atoms of a gas.<sup>1</sup> It has been found that there is good agreement between  $f_0$  values calculated by the method of Hartree (or in the case of heavy atoms by an approximate method of Thomas and Fermi) and the various experimental results. This gives confidence both in the theory of diffraction and in the atom models used. The tables of calculated  $f_0$  values which are now available for nearly all atoms and some of the common ions are accurate enough to be highly useful in crystal analysis.<sup>2</sup>

The atomic scattering factors  $f_0$  in Table XXXIII are given for a series of values of  $(\sin \theta)/\lambda$  and are therefore applicable to various wavelengths; they apply to atoms at rest and have not been modified by the temperature factor.

In using  $f_0$  tables it must be remembered that they refer to atoms at rest and all values will be reduced by the thermal motions of the atoms in crystals. This correction, which will be discussed later, is often an important one. For example, it reduces the intensity of the tenth-order reflection from (100) planes in NaCl at room temperature to a third the intensity for atoms at rest. While  $f_0$  is tabulated for different values of  $(\sin \theta)/\lambda$  so as to be applicable to all wavelengths, experiment shows that marked anomalies are introduced when  $\lambda$  is near an absorption edge of an atom in the diffracting crystal;  $f_0$  is decreased several units under these conditions.<sup>3</sup>

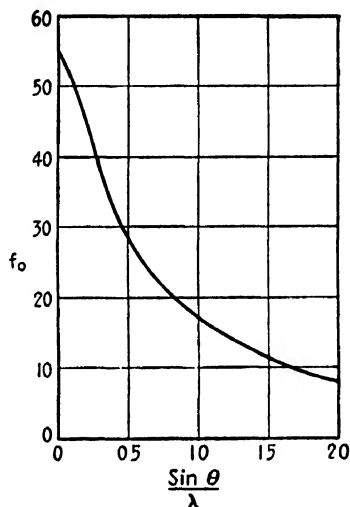


FIG. 3.—Plot of structure factor for cesium.

<sup>1</sup> For summaries of this field of physics see E. O. WOLLEN, *Rev. Modern Phys.*, vol. 4, p. 205, 1932; A. H. COMPTON and S. K. ALLISON, "X-rays in Theory and Experiment," Van Nostrand, New York, 1935; J. T. RANDALL, "Diffraction of X-rays and Electrons by Amorphous Solids, Liquids, and Gases," Wiley, New York, 1934; P. P. EWALD, "Handbuch der Physik," vol. XXIII/2, Springer, Berlin, 1933.

<sup>2</sup> R. W. JAMES and G. W. BRINDLEY, *Phil. Mag.*, vol. 12, pp. 81, 104, 1931; *Z. Krist.*, vol. 78, p. 490, 1931. W. L. BRAGG and J. WEST, *Z. Krist.*, vol. 69, p. 118, 1928. LINUS PAULING and J. SHERMAN, *Z. Krist.*, vol. 81, p. 1, 1932.

<sup>3</sup> This has been made use of to increase the difference between scattering powers of

**Scattering from a Unit Cell.**—Let us now consider the intensity of the diffracted beams that arise from the cooperation of the coherently scattered waves from each atom in the unit cell. Each atom scatters as a unit with an amplitude proportional to  $f$  and with a certain phase dependent upon its position. To compute the intensity of the diffracted beam it is necessary to add sine waves of different amplitude and phase but of the same wavelength and to determine the amplitude of the sine wave that results. The intensity of the diffracted wave is the square of this amplitude. Differences in atomic scattering power lead to different amplitudes of the waves from individual atoms, while differing positions of the atoms along the path of the incident and diffracted beams determine the relative phases of these waves.

If the amplitude of each wave is represented by the length of a vector and its phase by the direction of the vector, the resultant diffracted beam

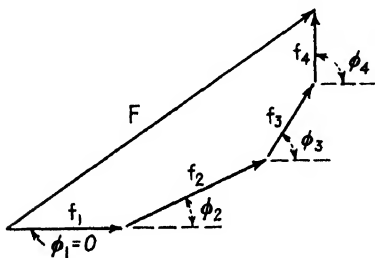


FIG. 4.

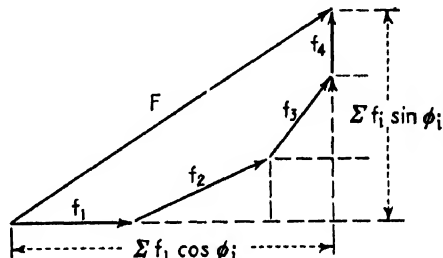


FIG. 5.

FIGS. 4 and 5.—Vector addition of diffracted rays from individual atoms.

will be represented by the vector sum of all the individual waves. This is indicated in Fig. 4 where four vectors of lengths  $f_1$ ,  $f_2$ ,  $f_3$ , and  $f_4$  are drawn to represent the atomic scattering factors for four atoms of a unit cell, and the angles  $\phi_1$ ,  $\phi_2$ ,  $\phi_3$ , and  $\phi_4$  are drawn to represent the phases of the waves scattered by these individual atoms. The square of the length of the resultant vector,  $|F|^2$ , is proportional to the intensity that will be observed.

Reference to Fig. 5 shows that each vector may be resolved into a horizontal and a vertical component of lengths  $f \cos \phi$  and  $f \sin \phi$ , respectively; these components when added give two sides of a right triangle whose hypotenuse is  $F$ . The square of the hypotenuse is given by the sum of the squares of the sides, and so we may write

$$\begin{aligned} |F|^2 &= (f_1 \cos \phi_1 + f_2 \cos \phi_2 + \dots)^2 + (f_1 \sin \phi_1 + f_2 \sin \phi_2 + \dots)^2 \\ &= (\sum_i f_i \cos \phi_i)^2 + (\sum_i f_i \sin \phi_i)^2 \end{aligned} \quad (6)$$

where the summation is to be carried out over all atoms in the unit cell,

Cu and Zn atoms in  $\beta$ -brass in order to show up their distribution on the lattice points, a distribution otherwise masked by the great similarity in their scattering power (F. W. Jones and C. Sykes, *Proc. Roy. Soc. (London)*, vol. A161, p. 440, 1937).



TABLE XXXIII.—ATOMIC SCATTERING FACTORS\*

$10^{-8} \times \frac{(\sin \theta)}{\lambda}$	0 0	0.1	0.2	0.3	0.4	0.5	0.6	0.7	0.8	0.9	1.0	1.1	1.2
H	1	0.81	0.48	0.25	0.13	0.07	0.04	0.3	0.02	0.01	0.00	0.00	
He	2	1.88	1.46	1.05	0.75	0.52	0.35	0.24	0.18	0.14	0.11	0.09	
Li <sup>+</sup>	2	1.96	1.8	1.5	1.3	1.0	0.8	0.6	0.5	0.4	0.3	0.3	
Li	3	2.2	1.8	1.5	1.3	1.0	0.8	0.6	0.5	0.4	0.3	0.3	
Be <sup>++</sup>	2	2.0	1.9	1.7	1.6	1.4	1.2	1.0	0.9	0.7	0.6	0.5	
Be	4	2.9	1.9	1.7	1.6	1.4	1.2	1.0	0.9	0.7	0.6	0.5	
B <sup>+</sup>	2	1.99	1.9	1.8	1.7	1.6	1.4	1.3	1.2	1.0	0.9	0.7	
B	5	3.5	2.4	1.9	1.7	1.5	1.4	1.2	1.2	1.0	0.9	0.7	
C	6	4.6	3.0	2.2	1.9	1.7	1.6	1.4	1.3	1.16	1.0	0.9	
N <sup>+</sup>	2	2.0	2.0	1.9	1.9	1.8	1.7	1.6	1.5	1.4	1.3	1.16	
N <sup>+</sup>	4	3.7	3.0	2.4	2.0	1.8	1.66	1.56	1.49	1.39	1.28	1.17	
N	7	5.8	4.2	3.0	2.3	1.9	1.65	1.54	1.49	1.39	1.29	1.17	
O	8	7.1	5.3	3.9	2.9	2.2	1.8	1.6	1.5	1.4	1.35	1.26	
O <sup>-2</sup>	10	8.0	5.5	3.8	2.7	2.1	1.8	1.5	1.5	1.4	1.35	1.26	
F	9	7.8	6.2	4.45	3.35	2.65	2.15	1.9	1.7	1.6	1.5	1.35	
F <sup>-</sup>	10	8.7	6.7	4.8	3.5	2.8	2.2	1.9	1.7	1.55	1.5	1.35	
Ne	10	9.3	7.5	5.8	4.4	3.4	2.65	2.2	1.9	1.65	1.55	1.5	
Na <sup>+</sup>	10	9.5	8.2	6.7	5.25	4.05	3.2	2.65	2.25	1.95	1.75	1.6	
Na	11	9.65	8.2	6.7	5.25	4.05	3.2	2.65	2.25	1.95	1.75	1.6	
Mg <sup>+2</sup>	10	9.75	8.6	7.25	5.95	4.8	3.85	3.15	2.55	2.2	2.0	1.8	
Mg	12	10.5	8.6	7.25	5.95	4.8	3.85	3.15	2.55	2.2	2.0	1.8	
Al <sup>+</sup>	10	9.7	8.9	7.8	6.65	5.5	4.45	3.65	3.1	2.65	2.3	2.0	
Al	13	11.0	8.95	7.75	6.6	5.5	4.5	3.7	3.1	2.65	2.3	2.0	
Si <sup>+</sup>	10	9.75	9.15	8.25	7.15	6.05	5.05	4.2	3.4	2.95	2.6	2.3	
Si	14	11.35	9.4	8.2	7.15	6.1	5.1	4.2	3.4	2.95	2.6	2.3	
P <sup>+</sup>	10	9.8	9.25	8.45	7.5	6.55	5.65	4.8	4.05	3.4	3.0	2.6	
P	15	12.4	10.0	8.45	7.15	6.5	5.65	4.8	4.05	3.4	3.0	2.6	
P <sup>-3</sup>	18	12.7	9.8	8.4	7.45	6.5	5.65	4.85	4.05	3.4	3.0	2.6	
S <sup>+</sup>	10	9.85	9.4	8.7	7.85	6.85	6.05	5.25	4.5	3.9	3.35	2.9	
S	16	13.6	10.7	8.95	7.85	6.85	6.0	5.25	4.5	3.9	3.35	2.9	
S <sup>-2</sup>	18	14.3	10.7	8.9	7.85	6.85	6.0	5.25	4.5	3.9	3.35	2.9	
Cl	17	14.6	11.3	9.25	8.05	7.25	6.5	5.75	5.05	4.4	3.85	3.35	
Cl <sup>-</sup>	18	15.2	11.5	9.3	8.05	7.25	6.5	5.75	5.05	4.4	3.85	3.35	
A	18	15.9	12.6	10.4	8.7	7.8	7.0	6.2	5.4	4.7	4.1	3.6	
K <sup>+</sup>	18	16.5	13.3	10.8	8.85	7.75	7.05	6.41	5.9	5.3	4.8	4.2	
Ca <sup>++</sup>	18	16.8	14.0	11.5	9.3	8.1	7.35	6.7	6.2	5.7	5.1	4.6	
Sc <sup>++</sup>	18	16.7	14.0	11.4	9.4	8.3	7.6	6.9	6.4	5.8	5.35	4.85	
Ti <sup>+</sup>	18	17.0	14.4	11.9	9.9	8.5	7.85	7.3	6.7	6.15	5.65	5.05	
Rb <sup>+</sup>	36	33.6	28.7	24.6	21.4	18.9	16.7	14.6	12.8	11.2	9.9	8.9	
Sr	38	34.4	29.0	24.5	20.8	18.4	16.4	14.6	12.9	11.6	10.5	9.5	8.7
Y	39	35.4	29.9	25.3	21.5	19.0	17.0	15.1	13.4	12.0	10.9	9.9	9.0
Zr	40	36.3	30.8	26.0	22.1	19.7	17.5	15.6	13.8	12.4	11.2	10.2	9.3
Nb(Cb)	41	37.3	31.7	26.8	22.8	20.2	18.1	16.0	14.3	12.8	11.6	10.6	9.7
Mo	42	38.2	32.6	27.6	23.5	20.8	18.6	16.5	14.8	13.2	12.0	10.9	10.0
Ma	43	39.1	33.4	28.3	24.1	21.3	19.1	17.0	15.2	13.6	12.3	11.3	10.3
Ru	44	40.0	34.3	29.1	24.7	21.9	19.6	17.5	15.6	14.1	12.7	11.6	10.6
Rh	45	41.0	35.1	29.9	25.4	22.5	20.2	18.0	16.1	14.5	13.1	12.0	11.0
Pd	46	41.9	36.0	30.7	26.2	23.1	20.8	18.5	16.6	14.9	13.6	12.3	11.3
Ag	47	42.8	36.9	31.5	26.9	23.8	21.3	19.0	17.1	15.3	14.0	12.7	11.7
Cd	48	43.7	37.7	32.2	27.5	24.4	21.8	19.6	17.6	15.7	14.3	13.0	12.0
In	49	44.7	38.6	33.0	28.1	25.0	22.4	20.1	18.0	16.2	14.7	13.4	12.3
Sn	50	45.7	39.5	33.8	28.7	25.6	22.9	20.6	18.5	16.6	15.1	13.7	12.7
Sb	51	46.7	40.4	34.6	29.5	26.3	23.5	21.1	19.0	17.0	15.5	14.1	13.0
Te	52	47.7	41.3	35.4	30.3	27.9	24.0	21.7	19.5	17.5	16.0	14.5	13.3
I	53	48.6	42.1	36.1	31.0	27.5	24.6	22.2	20.0	17.9	16.4	14.8	13.6
Xe	54	49.6	43.0	36.8	31.6	28.0	25.2	22.7	20.4	18.4	16.7	15.2	13.9
Cs	55	50.7	43.8	37.6	32.4	28.7	25.8	23.2	20.8	18.8	17.0	15.6	14.5

TABLE XXXIII.—ATOMIC SCATTERING FACTORS\*.—(Continued)

$10^{-3} \times \frac{(\sin \theta)}{\lambda}$	0.0	0.1	0.2	0.3	0.4	0.5	0.6	0.7	0.8	0.9	1.0	1.1	1.2
Ba	56	51.7	44.7	38.4	33.1	29.3	26.4	23.7	21.3	19.2	17.4	16.0	14.7
La	57	52.6	45.6	39.3	33.8	29.8	26.9	24.3	21.9	19.7	17.9	16.4	15.0
Ce	58	53.6	46.5	40.1	34.5	30.4	27.4	24.8	22.4	20.2	18.4	16.6	15.3
Pr	59	54.5	47.4	40.9	35.2	31.1	28.0	25.4	22.9	20.6	18.8	17.1	15.7
Nd	60	55.4	48.3	41.6	35.9	31.8	28.6	25.9	23.4	21.1	19.2	17.5	16.1
Il	61	56.4	49.1	42.4	36.6	32.4	29.2	26.4	23.9	21.5	19.6	17.9	16.4
Sm	62	57.3	50.0	43.2	37.3	32.9	29.8	26.9	24.4	22.0	20.0	18.3	16.8
Eu	63	58.3	50.9	44.0	38.1	33.5	30.4	27.5	24.9	22.4	20.4	18.7	17.1
Gd	64	59.3	51.7	44.8	38.8	34.1	31.0	28.1	25.4	22.9	20.8	19.1	17.5
Tb	65	60.2	52.6	45.7	39.6	34.7	31.6	28.6	25.9	23.4	21.2	19.5	17.9
Dy	66	61.1	53.6	46.5	40.4	35.4	32.2	29.2	26.3	23.9	21.6	19.9	18.3
Ho	67	62.1	54.5	47.3	41.1	36.1	32.7	29.7	26.8	24.3	22.0	20.3	18.6
Er	68	63.0	55.3	48.1	41.7	36.7	33.3	30.2	27.3	24.7	22.4	20.7	18.9
Tu	69	64.0	56.2	48.9	42.4	37.4	33.9	30.8	27.9	25.2	22.9	21.0	19.3
Yb	70	64.9	57.0	49.7	43.2	38.0	34.4	31.3	28.4	25.7	23.3	21.4	19.7
Lu	71	65.9	57.8	50.4	43.9	38.7	35.0	31.8	28.9	26.2	23.8	21.8	20.0
Hf	72	66.8	58.6	51.2	44.5	39.3	35.6	32.3	29.3	26.7	24.2	22.3	20.4
Ta	73	67.8	59.5	52.0	45.3	39.9	36.2	32.9	29.8	27.1	24.7	22.6	20.9
W	74	68.8	60.4	52.8	46.1	40.5	36.8	33.5	30.4	27.6	25.2	23.0	21.3
Re	75	69.8	61.3	53.6	46.8	41.1	37.4	34.0	30.9	28.1	25.6	23.4	21.6
Os	76	70.8	62.2	54.4	47.5	41.7	38.0	34.6	31.4	28.6	26.0	23.9	22.0
Ir	77	71.7	63.1	55.3	48.2	42.4	38.6	35.1	32.0	29.0	26.5	24.3	22.3
Pt	78	72.6	64.0	56.2	48.9	43.1	39.2	35.6	32.5	29.5	27.0	24.7	22.7
Au	79	73.6	65.0	57.0	49.7	43.8	39.8	36.2	33.1	30.0	27.4	25.1	23.1
Hg	80	74.6	65.9	57.9	50.5	44.4	40.5	36.8	33.6	30.6	27.8	25.6	23.6
Tl	81	75.5	66.7	58.7	51.2	45.0	41.1	37.4	34.1	31.1	28.3	26.0	24.1
Pb	82	76.5	67.5	59.5	51.9	45.7	41.6	37.9	34.6	31.5	28.8	26.4	24.5
Bi	83	77.5	68.4	60.4	52.7	46.4	42.2	38.5	35.1	32.0	29.2	26.8	24.8
Po	84	78.4	69.4	61.3	53.5	47.1	42.8	39.1	35.6	32.6	29.7	27.2	25.2
—	85	79.4	70.3	62.1	54.2	47.7	43.4	39.6	36.2	33.1	30.1	27.6	25.6
Em (Rn, Nt)	86	80.3	71.3	63.0	55.1	48.4	44.0	40.2	36.8	33.5	30.5	28.0	26.0
—	87	81.3	72.2	63.8	55.8	49.1	44.5	40.7	37.3	34.0	31.0	28.4	26.4
Ra	88	82.2	73.2	64.6	56.5	49.8	45.1	41.3	37.8	34.6	31.5	28.8	26.7
Ac	89	83.2	74.1	65.5	57.3	50.4	45.8	41.8	38.3	35.1	32.0	29.2	27.1
Th	90	84.1	75.1	66.3	58.1	51.1	46.5	42.4	38.8	35.5	32.4	29.6	27.5
Pa	91	85.1	76.0	67.1	58.8	51.7	47.1	43.0	39.3	36.0	32.8	30.1	27.9
U	92	86.0	76.9	67.9	59.6	52.4	47.7	43.5	39.8	36.5	33.3	30.6	28.3

\* Values are from R. W. James and G. W. Brindley (*Z. Krist.*, vol. 78, p. 470, 1931) and from "Internationale Tabellen zur Bestimmung von Kristallstrukturen," vol. II, Borntrager, Berlin, 1935; values for the lighter elements were computed by Hartree's method or by interpolation; elements heavier than rubidium were computed by the Thomas-Fermi method.

as indicated by the subscript  $i = 1, 2, 3 \dots$ . Since  $f_i$  is the ratio of the amplitude of scattering by the  $i$ th atom to that scattered under the same conditions by an electron, the resultant intensity is proportional to  $I_e |F|^2$ . The quantity  $F$  is the *structure factor* or *structure amplitude* and is the ratio of the amplitude of the wave scattered in a given direction by all the atoms in a unit cell to that scattered by a single electron under identical conditions.

**Relation of Phase,  $\phi$ , to Atomic Position.**—A simple formula gives the value of the phase,  $\phi$ , of Eq. (6) for an atom at the position  $uvw$  in a unit cell and for the  $hkl$  reflection. Consider first only the atoms on a

simple lattice. A set of parallel planes in this lattice will produce diffracted beams going in directions (given by Bragg's law) such that neighboring planes of the set will contribute waves exactly in phase with one another. The phase difference between waves from adjacent planes of the simple lattice will thus be  $2\pi$  in the first order and  $2\pi n$  in the  $n$ th order. However, the  $n$ th-order reflection of a plane is conventionally treated as the first-order reflection from a fictitious set of planes of  $1/n$ th the spacing and having indices  $n$  times the Miller indices. The interplanar distance for these fictitious planes in a cubic crystal with a lattice constant  $a_0$  is given by

$$d = \frac{a_0}{\sqrt{h^2 + k^2 + l^2}} \quad (\text{cubic}) \quad (7)$$

where  $h, k, l$  are the reflection indices. The phase difference between waves from neighboring planes of the set is proportional to the path difference for these rays and is equal to  $2\pi$ .

The path difference for the planes  $A, A'$  of spacing  $d$  is indicated in Fig. 6 by a heavy line. Consider a set of interleaved planes  $B, B'$  having the same spacing as these  $A$  planes. If the distance to the  $B$  plane is  $p$ , then the path difference to this plane is  $p/d$  of that to the  $A'$  plane, as will be seen from the heavy lines in the figure. Consequently, the phase difference between the ray reflected by the first  $A$  plane and the first  $B$  plane will be given by  $2\pi p/d$ . It can be shown geometrically that, with the same convention as used in formula (7), an atom at coordinates  $uvw$  in the unit cell will lie on a set of planes with indices  $(hkl)$  such that the plane next to the origin will be at a distance from the origin given by the equation

$$p = \frac{a_0(hu + kv + lw)}{\sqrt{h^2 + k^2 + l^2}} \quad (\text{cubic}). \quad (8)$$

Hence Eqs. (7) and (8) give the required expression for the phase of the wave from this atom,

$$\phi = \frac{2\pi p}{d} = 2\pi(hu + kv + lw).$$

Upon substituting in Eq. (6), the complete expression for the structure factor becomes

$$|F|^2 = [\sum f_i \cos 2\pi(hu_i + kv_i + lw_i)]^2 + [\sum f_i \sin 2\pi(hu_i + kv_i + lw_i)]^2 \quad (9)$$

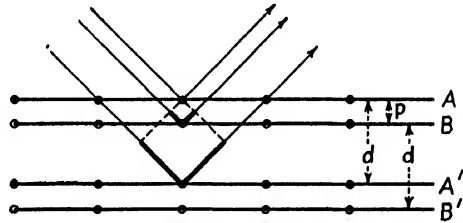


FIG. 6.—Reflection from interleaved planes. Path differences are indicated by heavy lines.

where  $u_i$ ,  $v_i$ , and  $w_i$  are the coordinates of the  $i$ th atom of the unit cell whose atomic scattering factor is  $f$ , and where  $hkl$  are the indices of the reflection. The summation extends over all atoms in the unit cell.

The above discussion has been limited for simplicity to cubic crystals, but the same principles hold for other systems of axes, and *Eq. (9) is true for all crystal systems*. It is an equation of the utmost importance in crystallography, for the determination of atomic positions in crystals is always based on this relation between the coordinates of the atom in a unit cell and the intensity with which they will scatter x-rays in the different spectra. This equation has been applied to each of the 230 space groups, and the characteristic features of the reflections for each space group have been derived from it and tabulated.<sup>1</sup> There will be

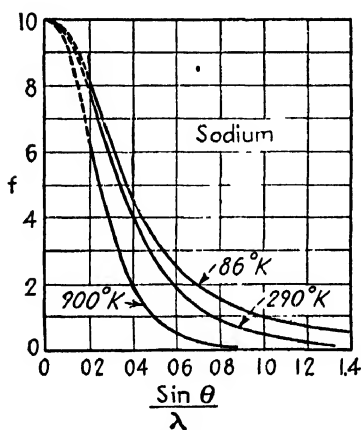


FIG. 7.—Structure factor for sodium at different temperatures. (R. W. James and E. Firth, *Proc. Roy. Soc. (London)*, vol. A117, p. 62, 1927.)

certain reflections absent from the diffraction pattern of a crystal because  $|F|^2 = 0$  for these. By comparing a list of the missing reflections with the tables it is usually possible to determine to which one (or more) of the space groups the crystal might belong. When the space group has been determined, to find how the atoms are arranged in the unit cell it is necessary to employ the structure-factor equation, either in the general form, *Eq. (9)*, or more conveniently in a simplified form appropriate to the particular space group in question.

The equation will give one value of the structure factor of a reflection for each arrangement of atoms in the cell, and the problem is essentially one of choosing an arrangement such that the coordinates for all atoms, when inserted in the structure-factor equation, will predict the intensities actually observed for each of the reflections of the diffraction pattern. This extremely tedious procedure has been shortened and simplified in many ways, some of which are discussed in *Chap. VIII*, page 149, and in *Appendix VI*.

<sup>1</sup> "Internationale Tabellen zur Bestimmung von Kristallstrukturen," vol. I, Borntrager, Berlin, 1935. K. LONSDALE, "Simplified Structure Factor and Electron Density Formulae for the 230 Space Groups of Mathematical Crystallography," G. Bell, London, 1936.

$$|F|^2 = [\sum_i f_i \cos 2\pi(hu_i + kv_i + lw_i)]^2. \quad (10)$$

**The Temperature Factor.**—In the section on the atomic scattering factor it was assumed that the atom was at rest. In crystals, however, the atoms are oscillating constantly and very rapidly about their mean position. The effect of this thermal motion is to smear the electron distribution to larger radii and to decrease the scattering factor,  $f$ , below the value for the atom at rest,  $f_0$ . The higher the temperature the more blurred the atom will appear and the more rapidly  $f$  will decrease with increasing angle, as will be seen from the curves of Fig. 7 for sodium atoms in crystals of rock salt at different temperatures.

It has been calculated that for an atom vibrating as a whole

$$f = f_0 e^{-M} \quad (11)$$

where

$$M = 8\pi^2 \bar{U}^2 \left( \frac{\sin \theta}{\lambda} \right)^2,$$

$\bar{U}^2$  being the mean square displacement of the atoms from their mean position measured at right angles to the reflecting planes. The value of  $\bar{U}^2$  can be calculated with fair accuracy by theories developed by Debye and Waller.<sup>1</sup>

<sup>1</sup> The formula deduced by Debye (after Waller's correction for a numerical error of a factor of 2.0 that occurred in his original paper) is

$$M = \frac{6h^2}{mk\Theta} \left[ \frac{\phi(x)}{x} + \frac{1}{4} \right] \left( \frac{\sin \theta}{\lambda} \right)^2$$

where  $m$  is the mass of the atom,  $h$  is Planck's constant,  $k$  is the gas constant,  $\Theta$  is the characteristic temperature which is discussed in theories of specific heat,  $x = \Theta/T$ , where  $T$  is the absolute temperature of the crystal,  $\phi(x)$  is a function evaluated and tabulated by Debye, and  $\theta$  is the glancing angle of Bragg's law. In the formula given above, the crystal is assumed to have a zero-point energy of one-half quantum per degree of freedom at absolute zero. The formula may be derived by considering the crystal as an isotropic elastic solid having a series of elastic waves in it, forming a frequency spectrum extending up to a maximum frequency of  $\nu_m$ . The characteristic temperature,  $\Theta$ , is equal to  $h\nu_m/k$ , and  $\nu_m$  is given by

$$\nu_m^3 = 4\pi \left( \frac{9n}{\frac{2}{g_t^3} + \frac{1}{g_l^3}} \right)$$

where  $n$  is the number of vibrating atoms per cubic centimeter, and where  $g_t$  and  $g_l$  are the velocities of transverse and longitudinal waves in the crystal, which are supposed constant for all frequencies and directions in the crystal. At temperatures small compared with  $\Theta$ , one can take  $\phi(x)/x = (\pi^2/6)(T^2/\Theta^2)$ . For tables of the  $\phi(x)$  and  $\Theta$ , see R. W. James and G. W. Brindley, *Phil. Mag.*, vol. 12, p. 81, 1931; or "Internationale Tabellen zur Bestimmung von Kristallstrukturen," vol. II, Bornträger, Berlin, 1935; for a detailed summary of the temperature factor, see F. C. Blake, *Rev. Modern Phys.*, vol. 5, p. 169, 1933. Waller has derived an expression for  $\bar{U}_z^2$  that can be evaluated for simple crystals and is in good agreement with x-ray intensities from NaCl at temperatures below 500° abs. (see summaries mentioned).

Since the atoms in a unit cell may have displacements that differ among themselves, the values of  $M$  may be different for each atom, and, strictly, Eq. (9) should be written

$$|F|^2 = [\sum f_0 e^{-M} \cos 2\pi(hu + kv + lw)]^2 + [\sum f_0 e^{-M} \sin 2\pi(hu + kv + lw)]^2 \quad (12)$$

with the appropriate values of  $M$  inserted for each atom; furthermore,  $M$  may vary with the direction of the crystal planes, thus with the

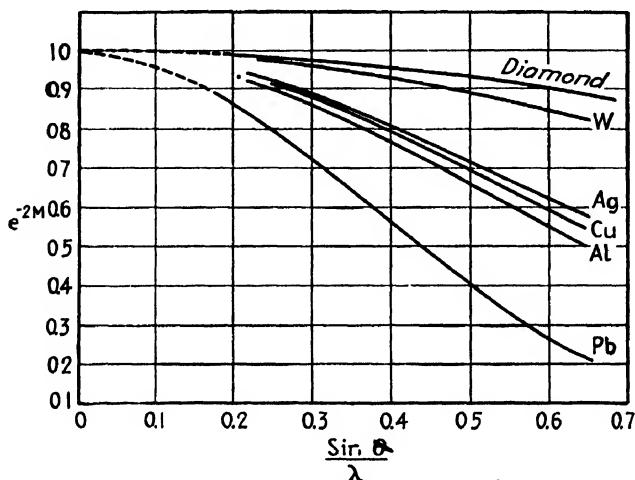


FIG. 8.—Values of temperature factor for different elements. (F. C. Blake, *Rev. Modern Phys.*, vol. 5, p. 169, 1933.)

indices ( $hkl$ ). In practice, it is common to make the simplifying assumption that the mean displacement is the same for all atoms and all crystal planes; so Eq. (9) may be written

$$|F|^2 = |F_0|^2 e^{-2M} = e^{-2M} \{ [\sum f_0 \cos 2\pi(hu + kv + lw)]^2 + [\sum f_0 \sin 2\pi(hu + kv + lw)]^2 \}. \quad (13)$$

Figure 8 shows the values of the factor  $e^{-2M}$  for a number of common crystals, and it will be noticed that it is a function that falls slowly with increasing diffraction angle. When the temperature factor is unknown or uncertain, it is best in comparing calculated and observed intensities of x-ray reflections to make all comparisons within groups of reflections having approximately similar  $\theta$  values, since only small variations in  $e^{-2M}$  are to be expected within small ranges of  $\theta$ .

#### Geometrical Factors Influencing Intensities of Diffracted X-rays.—

In the preceding sections it has been pointed out that the intensity of a diffracted beam depends on the structure factor, and this in turn on the temperature and also on the state of polarization of the primary beam. But additional factors belong in formulas giving diffracted beam intensities; these will now be presented. A summary at the end of this

appendix lists the more important formulas. In practice, many structures have been determined without corrections for temperature, absorption, or extinction and with intensities estimated by eye with an error of some 25 percent, and so the amount of effort that should be put on these corrections is a matter on which opinion differs.

1. THE LORENTZ FACTOR.—A perfect crystallite can reflect a monochromatic beam of x-rays not only under the exact value of the glancing angle  $\theta$  given by Bragg's law but also with smaller intensities at angles deviating some seconds of arc from this value. Darwin and others have calculated the total energy in the diffracted beam, taking into account this variable reflecting power near the angle  $\theta$ .

The factor in the intensity equation that takes this into account differs for the different methods of diffraction (Laue, rotating crystal, powder, etc.), and a derivation would be too lengthy for presentation here. For our purposes it is sufficient to know the results. The total

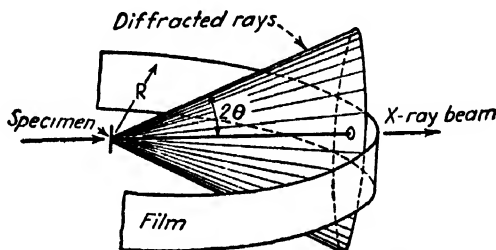


FIG. 9.—Geometry of a Debye ring in a powder camera.

energy per second diffracted from a set of crystal planes ( $hkl$ ) in the powder method is proportional to  $1/\sin \theta$ . This energy, however, spreads out along the generators of a cone and intersects the film to form a ring. In the powder method (Debye-Scherrer-Hull method) we observe only a fraction of the total circumference of this ring on a cylindrical film, and the blackening of the ring will depend not only upon the total energy contributing to the ring but also on the circumference over which this is spread.

If the radius of a cylindrical powder camera is  $R$ , Fig. 9, the film will intersect a circle of circumference  $2\pi R \sin 2\theta$ , from which it follows that the energy per centimeter along the circumference of this circle will be the product of the factor  $1/\sin \theta$  mentioned in the preceding paragraph and the factor  $1/(2\pi R \sin 2\theta)$ , and the blackening of the powder diffraction line will thus be dependent upon this product, the so-called **Lorentz factor**,  $1/(\sin 2\theta \sin \theta)$ , which may also be written  $1/(2 \sin^2 \theta \cos \theta)$ . The various constants that go with these factors to make up the complete formula are of little interest to us in the usual crystallographic problems since they are the same for all lines on a given powder diffraction pattern

(as, for example, the radius of the camera,  $R$ ) and do not influence the relative intensities of lines in the pattern.

Tables of the combined Lorentz and polarization factors for the more important x-ray diffraction methods have been published.<sup>1</sup> Buerger has shown that the Lorentz and polarization factor can be automatically corrected for in certain cameras by a high-speed rotating template in front of the film.<sup>2</sup>

2. THE MULTIPLICITY FACTOR,  $p$ .—It is obvious that with several different sets of planes diffracting to a given spot on a photographic film the intensity at that spot will be greater than it would be with only one set of planes contributing. Since the reflections from the different sets are independent of one another, the intensity from  $p$  sets of equivalent planes contributing to the same area on the film will be  $p$  times the intensity from one set. In the powder method all planes of the same interplanar spacing will contribute to the same ring on the film, and  $p$  for any crystal will then be equal to the number of permutations of indices  $h$ ,  $k$ ,  $l$  that give identical values of  $\sin^2 \theta$  in the quadratic form for the crystal. In cubic crystals of the most common classes,  $O_h$ ,  $O$ , and  $T_d$ , the "multiplicity factor"  $p$  has the following values:

Planes . . . . .	{100}	{111}	{110}	{ $hk0$ }	{ $hhl$ }	{ $hkl$ }
Multiplicity . . . . .	6	8	12	24	24	48

Any higher order reflections from these planes will have the same multiplicity factors as the listed ones. The multiplicity factor is determined by the crystal symmetry and for the powder method is tabulated in many crystallographic reference books.

Certain points should be kept in mind in connection with this factor.

(1) It is only in the powder method that *all* planes of similar spacing can superpose their reflections, and so it is only for this method that the tabulated values of  $p$  hold. In the rotating-crystal or oscillating-crystal methods the orientation of the equivalent planes with respect to the axis of rotation will determine how many different sets give superimposed reflections, and  $p$  will usually be less than the values for the powder

<sup>1</sup> See "Internationale Tabellen zur Bestimmung von Kristallstrukturen," vol. II, pp. 556–568, Bornträger, Berlin, 1935, for discussion and tables of the Lorentz polarization factors. At the end of the present appendix will be found a list of the intensity formulas for each method. The factor for the Laue method is derived and tables given in E. Schiebold, "Die Lauemethode," pp. 115–120, Akademische Verlagsgesellschaft m.b.H., Leipzig, 1932. For other derivations and discussions of the subject see F. C. Blake, *Rev. Modern Phys.*, vol. 5, p. 169, 1933, A. Schleede and E. Schneider, "Röntgenspektroskopie und Kristallstrukturanalyse," vol. II, pp. 240–245, Gruyter & Co., Leipzig, 1929.

<sup>2</sup> M. J. BUEGER, *Proc. Natl. Acad. Sci.*, vol. 25, p. 383, 1939.



method.<sup>1</sup> (2) Planes of different forms may have the same interplanar spacings and superposed reflections; both sets of planes must then be taken into account. For example, in face-centered cubic crystals, {333} and {511} planes have identical spacings and contribute to the same Debye ring with different structure factors and multiplicity factors. (3) For the rotating- and oscillating-crystal methods the multiplicity factor depends on the orientation of the crystal in the camera; in the oscillating-crystal method, it also depends upon the range of oscillation.

3. THE ABSORPTION FACTOR,  $A(\theta)$ .—The path of the reflected beam within the crystalline specimen varies with the angle of reflection and results in a reduction of intensity that changes with  $\theta$  and with the shape of the specimen. The "absorption factor" that is inserted into intensity formulas to correct for this is one of the slowly varying factors that does not have an important influence on the relative intensities of *neighboring* reflections. It has been neglected by most experimenters, but Claassen,<sup>2</sup> Rusterholtz,<sup>3</sup> and Blake<sup>4</sup> have given detailed discussions of it and have presented curves for predicting it from the known dimensions and absorption coefficient of the sample when the sample is a cylindrical rod in the powder method. While it is frequently an unimportant factor, as when molybdenum radiation is used on small specimens of low absorption coefficient, it may change manyfold when soft radiation is used. Calculations of the absorption factor,  $A(\theta)$ , by Blake are represented in Fig. 10, in which the ratio of the factor at angle  $\theta$  compared with the factor at  $\theta = 90^\circ$  is plotted against  $\theta$  for cylindrical samples. The radius of the sample is assumed small compared with the radius of the cylindrical camera (*e.g.*, about 0.02-cm.-diameter samples in ordinary Debye cameras). In this figure,  $r$  is the sample radius in centimeters and  $\mu$  is the linear absorption coefficient for the rays in the powdered sample—not in the solid crystal—and the curves are plotted for different values of the product  $\mu r$ .\*

<sup>1</sup> Tables will be found in F. Halla and H. Mark, "Röntgenographische Untersuchung von Kristallen," p. 236, Barth, Leipzig, 1937; and for the powder method in R. W. G. Wyckoff, "Structure of Crystals," 2d ed., p. 177, Chemical Catalog Co., New York, 1931. For certain crystals of lower symmetry (with parallel-face hemihedrism) the structure factor of certain superposed reflections may differ from others, *i.e.*, the different faces of a form will not have equal reflecting powers. This should be taken into account in evaluating  $p$ .

<sup>2</sup> A. CLAASSEN, *Phil. Mag.*, vol. 9, p. 57, 1930.

<sup>3</sup> A. RUSTERHOLTZ, *Helv. Phys. Acta*, vol. 4, p. 68, 1931.

<sup>4</sup> F. C. BLAKE, *Rev. Modern Phys.*, vol. 5, p. 169, 1933.

\* Tables will be found in "Internationale Tabellen zur Bestimmung von Kristallstrukturen," vol. II, Bornträger, Berlin, 1935. For powders of 200 mesh or smaller,  $\mu r$  is perhaps 0.6 of the value for a homogeneous solid.

The absorption factor for the Laue method is, of course, entirely different and is complicated by the fact that the wavelength, and therefore the absorption coefficient, are different for nearly every spot;<sup>1</sup> one must consider the critical absorption limits of atoms in the sample which may cause important changes in absorption coefficients at certain wavelengths. The quantitative estimation of intensities by the Laue method is very difficult and is seldom attempted. Nevertheless, relative intensities of certain pairs of reflections are directly comparable if the pairs are chosen so that they involve the same wavelength and the same length of path in the crystal.

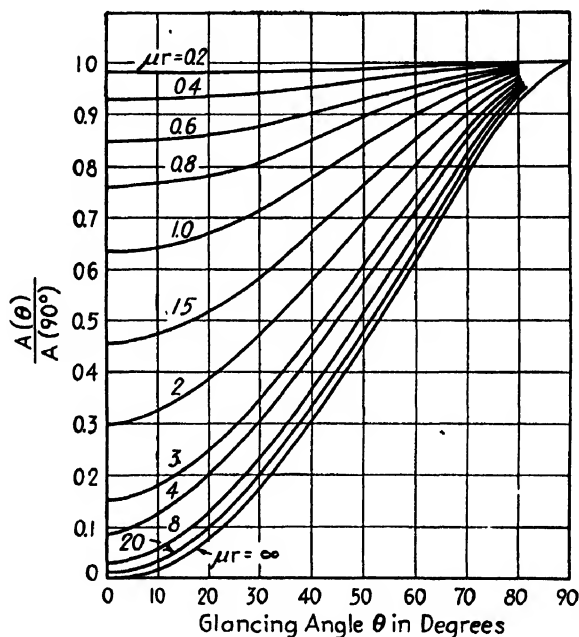


FIG. 10.—Absorption factor for cylindrical specimens. (Blake.)

At the time of writing, the absorption factor for the rotating-crystal method has been treated only for the zero layer line of reflections.<sup>2</sup> Wells<sup>3</sup> and Buerger<sup>4</sup> have discussed absorption in Weissenberg photographs for crystals that have certain external forms, but such corrections are complicated and are best avoided by making the crystals so small that absorption is negligible.

<sup>1</sup> R. W. G. WYCKOFF, "The Structure of Crystals," p. 148, Chemical Catalog Co., New York, 1931; E. SCHIEBOLD, "Die Lauemethode," p. 124, Akademische Verlagsgesellschaft m.b.H., Leipzig, 1932.

<sup>2</sup> A. J. BRADLEY, *Proc. Phys. Soc. (London)*, vol. 47, p. 879, 1935; O. P. HENDERSHOT, *Rev. Sci. Instruments*, vol. 8, p. 324, 1937.

<sup>3</sup> A. F. WELLS, *Z. Krist.*, vol. 96, p. 451, 1937.

<sup>4</sup> M. J. BUEGER, *Z. Krist.*, vol. 99, p. 189, 1938.

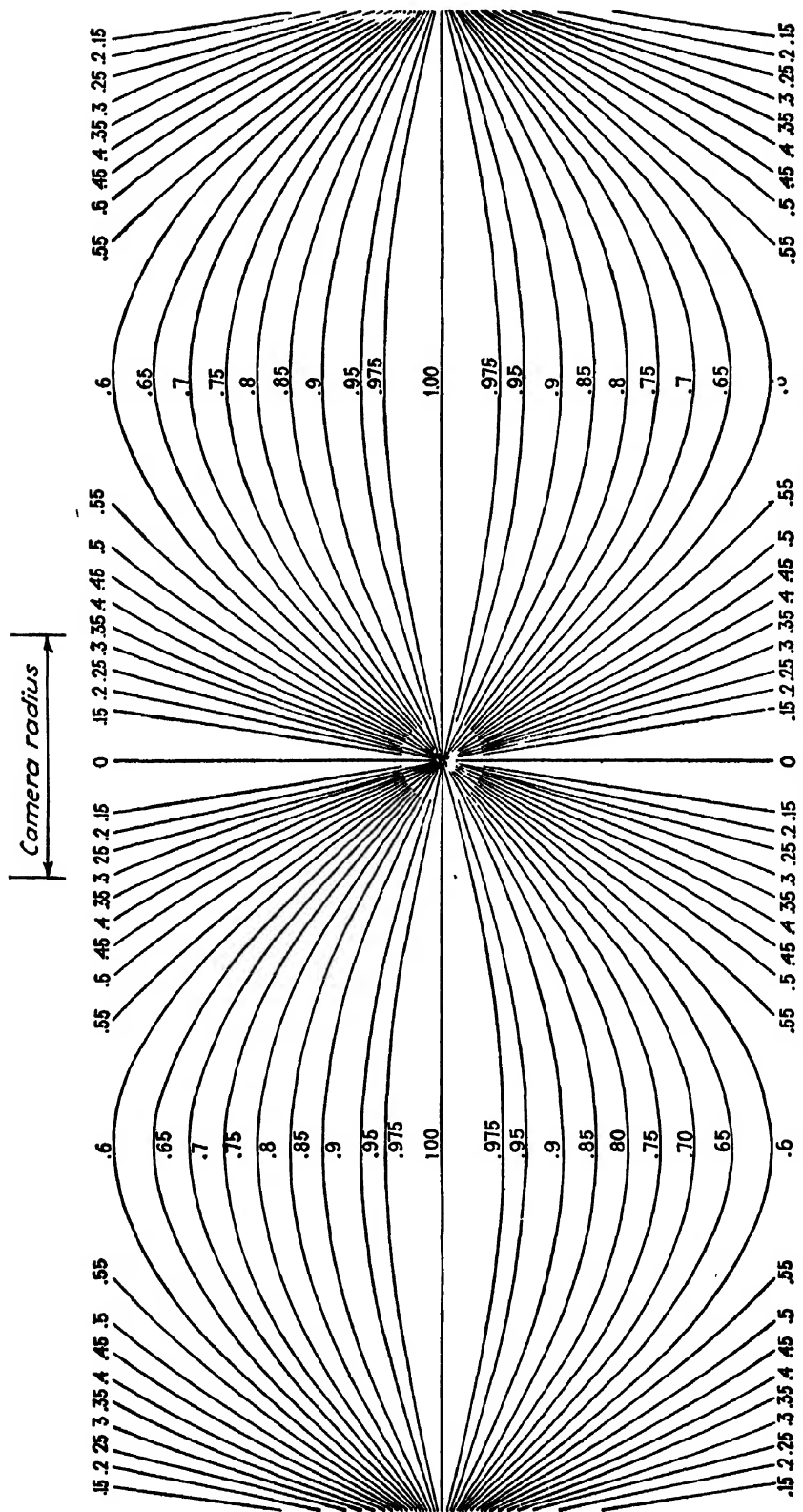


Fig. 11.—Velocity factor for rotating crystal photographs on cylindrical film.

4. THE VELOCITY FACTOR,  $V(\theta)$ , IN ROTATING- AND OSCILLATING-CRYSTAL METHODS.—When a single crystal is turned about an axis with constant angular velocity, the crystal planes have various lengths of time in which to reflect, times that are inversely proportional to the rate of change of the glancing angle  $\theta$  as the crystal rotates. Only for those planes which reflect to the equatorial line of spots (the planes whose zone axis coincides with the rotation axis) is  $V(\theta)$ , the velocity factor, equal to unity; it is less than unity for all spots above or below the equator and depends on the position of the spot in a way shown graphically in Fig. 11 for a cylindrical film.<sup>1</sup> If this figure is placed on a rotating- or oscillating-crystal pattern reduced to the same scale, the factor applicable to any spot can be read directly from the line that falls on that spot. Spots lying approximately above or below the direct beam at the center of the chart always give untrustworthy intensity data. The factor for Weissenberg photographs has been treated by Tunell<sup>2</sup> and by Warren and Fankuchen.<sup>3</sup>

5. EXTINCTION.—The ability of a crystal to reflect is influenced by the degree of perfection of the crystal; unless the crystal is very imperfect, the reflected intensities are abnormally low. It happens that this effect is seldom of importance in metallurgical work, for imperfection is the rule in metals and alloys.<sup>4</sup> Even in crystals such as quartz, Rochelle salt, or fluorite, where the high perfection would require important corrections for extinction, the correction can be reduced to negligible amounts by powdering the crystals. The severe strains from cleaving a crystal into minute fragments introduce sufficient imperfection to reduce extinction to a negligible amount. The reflecting power of relatively perfect crystals can also be increased by grinding the surface or roughening it with abrasives, for this process reduces extinction in the surface layers. Internal strains induced in a quartz crystal by piezoelectric oscillations cause increased reflecting power at various points throughout the interior of the crystal.<sup>5</sup> The extinction effect has been troublesome chiefly in precision intensity determinations (spectrometer studies).<sup>6</sup>

<sup>1</sup> E. G. COX and W. F. B. SHAW, *Proc. Roy. Soc. (London)*, vol. A127, p. 71, 1930. Other references are H. ORT, *Z. Physik*, vol. 88, p. 699, 1934; E. SCHIEBOLD, "Methoden der Kristallstrukturbestimmung mittels Röntgenstrahlen," vol. II, Die Drehkristallmethode, Akademische Verlagsgesellschaft m.b.H., Leipzig, 1932; H. ORT, "Handbuch der Experimentalphysik," Wien and Harms, vol. VII/2, Akademische Verlagsgesellschaft m.b.H., Leipzig, 1928; A. HETTICH, *Z. Krist.*, vol. 90, p. 473, 1935. For Weissenberg photographs (inclined), see G. TUNELL, *Am. Mineral.*, vol. 24, p. 448, 1939.

<sup>2</sup> G. TUNELL, *Am. Mineral.*, vol. 24, p. 448, 1939.

<sup>3</sup> B. E. WARREN and I. FANKUCHEN, *Rev. Sci. Instruments*, vol. 12, p. 90, 1941.

<sup>4</sup> See the determinations of R. M. Bozorth and F. E. Haworth, *Phys. Rev.*, vol. 45, p. 821, 1934, for example.

<sup>5</sup> C. S. BARRETT and C. E. HOWE, *Phys. Rev.*, vol. 39, p. 889, 1932.

<sup>6</sup> See A. H. COMPTON and S. K. ALLISON, "X-rays in Theory and Experiment," Van Nostrand, New York, 1935.

**Summary of Formulas for Relative Intensities.**

1. Powder method, cylindrical film (Debye-Scherrer-Hull cameras):

$$I \propto \frac{(1 + \cos^2 2\theta)}{\sin^2 \theta \cos \theta} \cdot p \cdot |F|^2 \cdot A(\theta). \quad (14)$$

2. Rotating- and oscillating-crystal method, assuming negligible absorption:

$$I \propto \frac{(1 + \cos^2 2\theta)}{\sin 2\theta} \cdot p' \cdot |F|^2 \cdot V(\theta). \quad (15)$$

For flat films,  $V(\theta) = 1/\sin \beta$ , where  $\beta$  is the angle in Fig. 12 between  $OP$  and  $OA$ , where  $O$  is the central spot,  $P$  the diffracted spot, and  $OA$  the

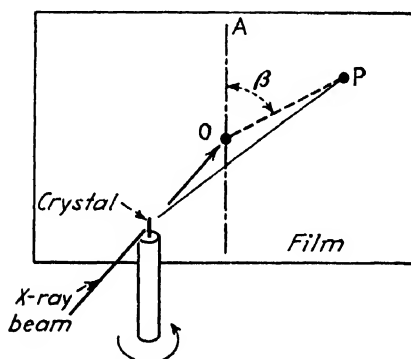


FIG. 12.—Angle  $\beta$  in the velocity factor.

projection on the film of the axis of rotation. For cylindrical films, see Fig. 10. The multiplicity factor  $p'$  must be calculated for each spot; in photogoniometers, such as the Weissenberg,  $p'$  is always unity.

3. Laue method:

$$I \propto \frac{(1 + \cos^2 2\theta)}{\sin^2 \theta} \cdot |F|^2 \cdot A'(\theta) \cdot f(\lambda) \quad (16)$$

where  $f(\lambda)$  takes account of the variation with wavelength of the photographic efficiency and the incident intensity.

## APPENDIX VI

### DETERMINATION OF CRYSTAL STRUCTURE WITH FOURIER SERIES

**Electron Density Expressed by Fourier Series.**—The density of the diffracting material in a crystal (the electron density) varies periodically along any direction through the lattice, going through a complicated cycle of peaks and minima with the same spatial periodicity as the distribution of atoms of the lattice. Therefore, it is possible to describe the electron distribution by a Fourier series,<sup>1</sup> as can be done for any periodic function. Let us consider first the general case, which is not convenient to use in structure analysis, and then treat certain special cases and modifications.

Let  $\rho(uvw)$  represent the electron density at a point whose coordinates in the unit cell are  $uvw$ . If a Fourier series for  $\rho(uvw)$  is set up, each term in the series represents a stationary system of density waves. Each set of waves is capable of diffracting x-rays with a certain intensity,  $|F(hkl)|^2$ , for the successive parallel sheets of density act as reflecting planes. A set of standing waves parallel to the  $(hkl)$  plane in the crystal is represented by a Fourier term having  $F(hkl)$  as a coefficient, and summing all terms gives the series

$$\rho(uvw) = \frac{1}{V} \sum_{h=-\infty}^{+\infty} \sum_{k=-\infty}^{+\infty} \sum_{l=-\infty}^{+\infty} F(hkl) e^{2\pi i(hu+kv+lw)} \quad (1)$$

where  $V$  is the volume of the unit cell. Carrying out the summation is thus equivalent to superimposing the sheets of electron density, crossing each other in all directions, and also results in adding a constant term  $F(000)$  which is equal to the total number of electrons in the unit cell. The relation is stated using the complex quantity  $i = \sqrt{-1}$  because this is a convenient way to take account not only of the amplitude but also of the change of phase of the beam when it is scattered.<sup>2</sup>

<sup>1</sup> Reviews of this field will be found in W. L. BRAGG and J. WEST, *Phil. Mag.*, vol. 10, p. 823, 1930. W. L. BRAGG, "The Crystalline State," Macmillan, New York, 1934. A. H. COMPTON and S. K. ALLISON, "X-rays in Theory and Experiment," Van Nostrand, New York, 1935. J. M. ROBERTSON, "Reports on Progress in Physics," vol. IV, pp. 332-367, Physical Society, (London), 1938.

<sup>2</sup> Usually  $|F(hkl)| = |F(\bar{h}\bar{k}\bar{l})|$  (Friedel's law) when the wavelength used is not near an absorption edge of any atom in the crystal and when the phase change on scattering is the same for all the electrons.

This expression takes a simple form when the crystal has a center of symmetry, for then the imaginary parts vanish and

$$\rho(uvw) = \frac{1}{V} \sum_{k=-\infty}^{+\infty} \sum_{l=-\infty}^{+\infty} \sum_{l=-\infty}^{+\infty} F(hkl) \cos 2\pi(hu + kv + lw). \quad (2)$$

A direct determination of crystal structure is suggested by this relation: if one determines a great many  $F(hkl)$  values for various planes and solves the series for different points  $(uvw)$  in the unit cell, a plot results that shows the distribution of electrons throughout the cell with peaks occurring at the position of atom centers. There are serious hindrances to this procedure, however. In the first place, there is an ambiguity as to the sign of each term, for the intensities are proportional to  $|F(hkl)|^2$ , not to  $F(hkl)$ . It requires an approximate knowledge of the structure of the crystal to determine these signs, for they are positive or negative depending on whether the diffracted waves have a phase the same as or opposite to that of a wave scattered by the origin. The second hindrance to the use of Eq. (2) is the tremendous number of calculations involved.

By projecting the electron density in the unit cell onto one of the principal planes of the crystal the number of terms to be calculated can be diminished from several thousand to several hundred. Suppose the electron density is projected parallel to the  $a$  axis so as to form a density pattern on the plane containing the  $b$  and  $c$  axes; Eq. (2) then reduces to

$$\rho(vw) = \frac{1}{A} \sum_{k=-\infty}^{+\infty} \sum_{l=-\infty}^{+\infty} F(0kl) e^{2\pi i(kv + lw)} \quad (3)$$

or, if the projection has a center of symmetry at the origin,

$$\rho(vw) = \frac{1}{A} \sum_{k=-\infty}^{+\infty} \sum_{l=-\infty}^{+\infty} F(0kl) \cos 2\pi(kv + lw) \quad (4)$$

where  $A$  is the area of the face of the unit cell on which the projection is made. It will be seen that the only data needed for this projection are the reflections from planes of the type  $(0kl)$  (prism reflections), which belong to a single zone  $[100]$ . A plot of this function is shown in Fig. 1 for the crystal shown in a similar projection in Fig. 2.<sup>1</sup> The same uncertainty as to signs of the terms has to be dealt with by preliminary determinations of the structure.

This method has received considerable attention since its development by W. L. Bragg. Other types of projection somewhat analogous to this

<sup>1</sup> W. L. BRAGG, *Z. Krist.* vol. 70, p. 475, 1929.

were devised earlier by A. H. Compton and others but are less used in structure analysis. Lonsdale<sup>1</sup> has published simplified electron-density formulas for each of the space groups; these speed the computations relating reflection intensities to atom positions.

It should be noticed that series which predict structure factors from an assumed distribution of atom positions [Chap. IV, page 79] are just the inverse of the series of this chapter, which deduce structures from observed  $F$  values.

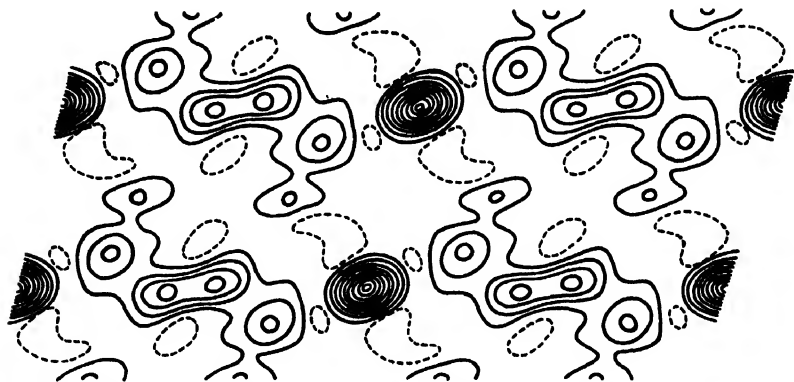


FIG. 1.—Electron density of diopside (calcium-magnesium silicate) projected upon (010) plane. (W. L. Bragg.)

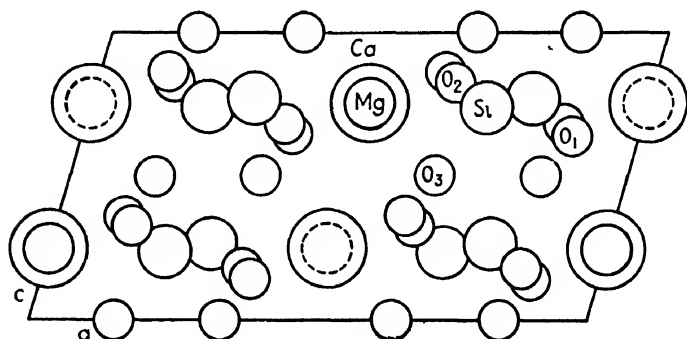


FIG. 2.—Atom positions in diopside, projected as in Fig. 1. (W. L. Bragg.)

**The  $F^2$  Series of Patterson.**—A later development by Patterson<sup>2</sup> and its modification by Harker<sup>3</sup> stem from the same fundamental principles and will find wide usage in solving complex structures. It is possible to set up a Fourier series in which  $|F(hkl)|^2$  occurs, and information about the atomic positions can be derived from it *without making assumptions as to the signs of the coefficients* as is necessary in  $F(hkl)$

<sup>1</sup> K. LONSDALE, "Simplified Structure Factor and Electron Density Formulae for the 230 Space Groups of Mathematical Crystallography," G. Bell, London, 1936.

<sup>2</sup> A. L. PATTERSON, *Z. Krist.*, vol. 90, pp. 517, 543, 1935; *Phys. Rev.*, vol. 46, p. 372, 1934.

<sup>3</sup> D. HARKER, *J. Chem. Phys.*, vol. 4, p. 381, 1936.



series. Patterson's series for three dimensions is

$$P(uvw) = \sum_{h=-\infty}^{+\infty} \sum_{k=-\infty}^{+\infty} \sum_{l=-\infty}^{+\infty} |F(hkl)|^2 e^{2\pi i(hu+kv+lw)}.$$

This reduces to the cosine form (either with or without a center of symmetry in the crystal),

$$P(uvw) = \sum_{h=-\infty}^{+\infty} \sum_{k=-\infty}^{+\infty} \sum_{l=-\infty}^{+\infty} |F(hkl)|^2 \cos 2\pi(hu + kv + lw). \quad (5)$$

The function  $P(uvw)$  represents the product of the electron density at any point in the unit cell whose coordinates are  $xyz$  and the electron density at another point whose coordinates are  $x + u, y + v, z + w$ . Thus, if there is an atom in the crystal at  $xyz$  and another at  $x + u, y + v, z + w$ , there will be two peaks in the electron density  $\rho(xyz)$ , their distance apart will be given by the vector whose components are  $uvw$ , and there will be a maximum in  $P(uvw)$  at the point  $uvw$  corresponding to this pair of atoms. In other words, Eq. (5) defines an electron-density product  $P(uvw)$  that has maxima at distances and directions from the origin corresponding to the distances and directions between pairs of atoms in the crystal. The amplitudes of the peaks of  $P(uvw)$  correspond to the products of the electron densities at the two points considered (roughly products of the two atomic numbers).

This triple Fourier series cannot be employed without a prohibitive amount of labor in calculation, but it becomes manageable if  $P(uvw)$  is projected on one of the faces of the unit cell. With projection along the  $c$  axis onto the (001) plane, for instance, the projected function is

$$p(uw) = \int_0^1 P(uvw) dw = \sum_{h=-\infty}^{+\infty} \sum_{k=-\infty}^{+\infty} |F(hk0)|^2 \cos 2\pi(hu + kv). \quad (6)$$

A two-dimensional "Patterson plot" can then be made of the function  $p(uw)$  with contours drawn to show the distribution of this function throughout the projection, as shown in Fig. 3.<sup>1</sup> A peak at  $uw$  on this plot corresponds to an interatomic distance in the crystal whose components along the  $x$  and  $y$  axes are  $u$  and  $v$ . It is to be noted that there is a certain ambiguity in interpreting the plot because it shows only the  $uw$  components of the interatomic vectors rather than the true vectors with components  $uvw$ ; thus if there are two interatomic vectors with  $u$  and  $v$  components the same but with the  $w$  component different, these will superpose on the  $P(uw)$  plot.

<sup>1</sup> A. L. PATTERSON, *Z. Krist.*, vol. 90, pp. 517, 543, 1935. It is frequently unnecessary to plot more than a half or a quarter of a unit cell, if symmetry elements supply the rest.

In practice, the operations involved in using Eq. (6) are as follows: The intensities of all available reflections of the [001] zone are measured. This may be done by visual estimation of intensities from a film, using a set of graded exposures as a comparison standard. The intensities are then corrected by the Lorentz and polarization factors, and perhaps by additional factors, so as to yield  $|F(hkl)|^2$  values. The series is then computed for a large number of values of  $u$  and  $v$ —perhaps 60 values of each variable—each value of  $p(uv)$  being determined by some 20 to 200 values of  $|F(hkl)|^2$ . The computed values are plotted on a projection, and points of equal value are connected by contour lines as in Fig. 3.

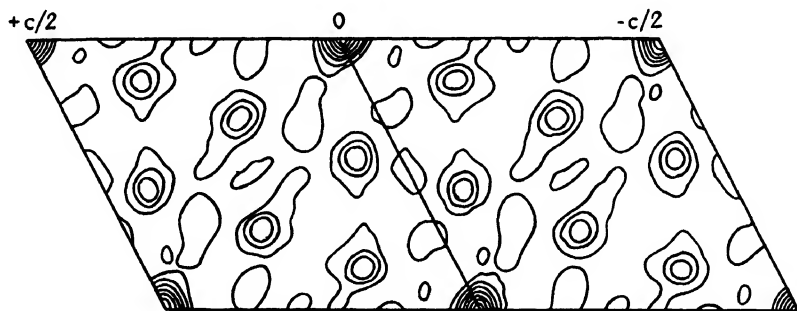


FIG. 3.—Contour-line plot of  $F^2$  series for  $C_6Cl_6$ . (Patterson.)

**The Patterson-Harker  $P^2$  Series.**—Harker<sup>1</sup> has applied Eq. (5) in such a way as to make use of knowledge of the symmetry elements in crystals, thus simplifying the method. When preliminary analysis has determined the space group to which a crystal belongs, a knowledge of the symmetry elements makes it possible to write down all the possible equivalent positions that atoms can occupy. Suppose there is a **twofold axis** parallel to the  $b$  axis of the crystal; then an atom at  $xyz$  has an equivalent atom at  $\bar{x}y\bar{z}$ , and the vector between these two has components  $2x, 0, 2z$ . These values substituted in Eq. (5) will yield a maximum value of  $P(uvw)$  at the point  $u = 2x, v = 0, w = 2z$ , which will be a point in the plane  $v = 0$ . Every other atom will also be paired with an equivalent atom in the same way and will lead to maxima in the same plane. Therefore, the  $u$  and  $w$  coordinates of every atom in the crystal can be found by evaluating  $P(uvw)$  for the special case of  $v = 0$ . Equation (5) then becomes

$$\begin{aligned}
 P(u0w) &= \sum_{h=-\infty}^{+\infty} \sum_{k=-\infty}^{+\infty} \sum_{l=-\infty}^{+\infty} |F(hkl)|^2 \cos 2\pi(hu + lw) \\
 &= \sum_{h=-\infty}^{+\infty} \sum_{l=-\infty}^{+\infty} C_{hl} \cos 2\pi(hu + lw)
 \end{aligned} \tag{7}$$

<sup>1</sup> D. HARKER, *J. Chem. Phys.*, vol. 4, p. 381, 1936.

where

$$u = 2x, \quad w = 2z, \quad C_{hl} = \sum_{k=-\infty}^{+\infty} |F(hkl)|^2.$$

On the two-dimensional plot of  $P(u0w)$  there is now no confusion arising from interatomic vectors that are not parallel to the planes  $y = a$  constant, for these vectors do not appear. The maxima on the plot will show directly the values of the parameters  $x$  and  $z$  of the atoms in the unit cell. A two-dimensional series  $P(u0w)$  is used for all symmetry elements that are axes of rotation parallel to  $b$ , and similar ones with appropriate cyclic changes apply to rotation axes parallel to the other crystal axes.

With a **twofold screw axis** parallel to  $b$  an atom at  $xyz$  is equivalent to one at  $\bar{x}$ ,  $y + \frac{1}{2}$ ,  $\bar{z}$ , and interatomic vectors have components  $2x$ ,  $-\frac{1}{2}$ ,  $2z$ . Thus  $P(uvw)$  must be evaluated for  $v = -\frac{1}{2}$  [or, since  $P(uvw)$  has a center of symmetry, for  $v = \frac{1}{2}$ ],

$$\begin{aligned} P(u\frac{1}{2}w) &= \sum_{h=-\infty}^{+\infty} \sum_{k=-\infty}^{+\infty} \sum_{l=-\infty}^{+\infty} |F(hkl)|^2 \cos 2\pi \left( hu + \frac{k}{2} + lw \right) \\ &= \sum_{h=-\infty}^{+\infty} \sum_{l=-\infty}^{+\infty} C_{hl} \cos 2\pi(hu + lw) \end{aligned} \quad (8)$$

where

$$C_{hl} = \sum_{k=-\infty}^{+\infty} (-1)^k |F(hkl)|^2 \quad u = 2x, \quad w = 2z$$

The "Patterson-Harker plot" for a twofold screw axis parallel to  $b$  thus will be a two-dimensional plot having peaks from which the coordinates  $u$  and  $w$  of the interatomic vectors may be obtained. Other screw axes lead to related series.<sup>1</sup>

<sup>1</sup> The table below gives the form of series required for each type of symmetry axis parallel to  $b$  and for each type of symmetry plane perpendicular to  $b$ . Cyclic interchange will yield the corresponding cases for elements parallel and perpendicular to  $a$  and  $c$  axes.

Symmetry Element	Form of $P(uvw)$
(a) Axes parallel to $b$ :	
2, 4, 4 <sub>2</sub> , 6, 6 <sub>2</sub> .....	$P(u0w)$
2 <sub>1</sub> , 4 <sub>1</sub> , 4 <sub>2</sub> , 6 <sub>1</sub> , 6 <sub>4</sub> .....	$P(u\frac{1}{2}w)$
3 <sub>1</sub> , 6 <sub>2</sub> , 6 <sub>4</sub> .....	$P(u\frac{1}{3}w)$
(b) Planes perpendicular to $b$ :	
Reflection plane.....	$P(0vw)$
Glide plane with glide of $\frac{1}{2}a_0$ .....	$P(\frac{1}{2}v0)$
Glide plane with glide of $\frac{1}{2}c_0$ .....	$P(0v\frac{1}{2})$
Glide plane with glide of $\frac{1}{2}(a_0 + c_0)$ .....	$P(\frac{1}{2}v\frac{1}{2})$
Glide plane with glide of $\frac{1}{4}(a_0 + c_0)$ .....	$P(\frac{1}{4}v\frac{1}{4})$
Glide plane with glide of $\frac{1}{4}(3a_0 + c_0)$ .....	$P(\frac{3}{4}v\frac{1}{4})$

Whenever possible, a plane of symmetry or a glide plane is used as a basis for the series, since for these cases Eq. (5) can be reduced to a one-dimensional series that is quickly computed. For a **plane of symmetry** perpendicular to  $b$ , equivalent atoms are at  $xyz$  and  $x\bar{y}z$  with interatomic vector components  $0, 2y, 0$  giving maxima in  $P(uvw)$  on the  $b$  axis only. Then

$$\begin{aligned} P(0v0) &= \sum_{h=-\infty}^{+\infty} \sum_{k=-\infty}^{+\infty} \sum_{l=-\infty}^{+\infty} |F(hkl)|^2 \cos 2\pi kv \\ &= \sum_{k=-\infty}^{+\infty} B_k \cos 2\pi kv \end{aligned}$$

where

$$B_k = \sum_{h=-\infty}^{+\infty} \sum_{l=-\infty}^{+\infty} |F(hkl)|^2 \quad \text{and} \quad v = 2y.$$

**$F^2$  Series in Structure Determination.**—A Patterson-Harker plot effectively focuses all the diffraction data from a crystal on a certain feature in the structure, for instance on the interatomic distances for atoms on a certain plane in the unit cell. The resolving power that results is correspondingly higher than is found in a two-dimensional Patterson plot which uses only reflections from planes of a single zone [*e.g.*,  $(hk0)$  reflections in Eq. (6)]. Furthermore, this resolving power can be brought to focus on any plane the investigator believes will be most illuminating; or on a whole series of planes in turn that are spaced at intervals through the cell, giving a series of cross sections; or on a line that is run through the cell at any important position where a hint as to the structure might be found. The method thus can be an extremely powerful aid in solving complex crystal structures. The review by Robertson is recommended for a detailed discussion of the use of series of all types in structure determination.<sup>1</sup>

None of the methods, of course, avoids the difficulty inherent in any Fourier method that the phases of the terms are not determined by the diffraction data. Phases must be assumed or determined otherwise or the whole question of phases must be circumvented by plotting  $F^2$  series, which give less complete data but do not involve the phase uncertainty.<sup>2</sup> The  $F^2$  series method contains the ambiguity that results from the

<sup>1</sup> J. M. ROBERTSON, "Reports on Progress in Physics," vol. IV, pp. 332-367, Physical Society, London, 1938.

<sup>2</sup> It is interesting that two different crystal structures have been found with the same  $|F|^2$  values, but with different signs for  $F$  values. These were found in the two forms of Bixbyte,  $(\text{FeMn})_2\text{O}_8$ , in the space group  $T_h^1 - Ia3$ . A. L. Patterson has remarked that a similar ambiguity in determining structures from Fourier series could occur in  $O_h^{10} - Ia3d$  and perhaps in some other space groups.

fact that it is not directly possible to decide which pair of atoms in the crystal belongs to a given interatomic vector. However, in some crystals there are only a few heavy atoms of large scattering power, and these can be identified readily.

**Computing Aids for Series.**—The labor of computing any of the Fourier series mentioned above or any modifications of them is considerable, and much thought has been given lately to methods of shortening the work. Without shortcuts, some crystal projections that have been published would require over 500,000 separate terms to be evaluated and summed. Robertson<sup>1</sup> has employed cards on which are printed appropriate sine and cosine functions. A semimechanical sorting device picks out the proper set to be added for a series summation. Lipson and Beevers<sup>2</sup> have made up sets of numbered strips or slide rules with some of the computations already performed on them, which, when placed on a board in proper positions, make visible a column of numbers that are the individual terms of the series to be summed. The same operations are accomplished in a different way by a smaller set of strips and templates devised by Patterson and Tunell.<sup>3</sup> By using one of these strip devices it is possible to compute a series in two or three days that would have required as many weeks by the older methods. Methods based on extensive use of card sorting and computing machines may ultimately replace the strip methods and reduce the task to simply punching buttons.

**Optical Synthesis of Fourier Series.**—A field of research that holds much promise for crystal-structure workers in the future is the summation of Fourier series by physical methods rather than mathematical ones. W. L. Bragg<sup>4</sup> opened the field by using an optical method of summing the terms of a Fourier series so as to produce photographically the projected electron density in a unit cell. He prepared a photographic plate with alternating light and dark bands on it that transmitted light with intensities varying approximately according to the cosine of the distance from one edge of the plate. When this was placed in an enlarging camera, it projected the bands upon a film or printing paper and recorded them; by varying the exposure time and the projection distance the amplitude, phase, and period of these bands could be varied, and a series of these exposures could be summed simply by superimposing them on the same film or print. Each exposure was made to correspond with a single term in a Fourier series and represented the sheets of electron density that produced the given term. The final print was then a

<sup>1</sup> J. M. ROBERTSON, *Phil. Mag.*, vol. 21, p. 176, 1936.

<sup>2</sup> H. LIPSON and C. A. BEEVERS, *Proc. Phys. Soc. (London)*, vol. 48, p. 772, 1936.

<sup>3</sup> A. L. PATTERSON and G. TUNELL, *Am. Mineralogist*, vol. 27, p. 655, 1942.

<sup>4</sup> W. L. BRAGG, *Z. Krist.*, vol. 70, p. 475, 1929.

synthesis of the electron density in the unit cell projected on one of the faces of the cell. The photograph confirmed the computed results. Huggins<sup>1</sup> has refined this method so that a lantern-slide projector can be used at a fixed distance from the printing paper. Lantern slides are prepared with bands at appropriate spacings and orientations for the different series terms, both positive and negative, and from this set the operator picks out and projects the proper slide for each term in the series. Early results obtained by Huggins are illustrated by Fig. 4 for fluorite ( $\text{CaF}_2$ ).<sup>2</sup> An unwanted uniform background on the resulting photograph can be eliminated by the use of a suitable type of photographic

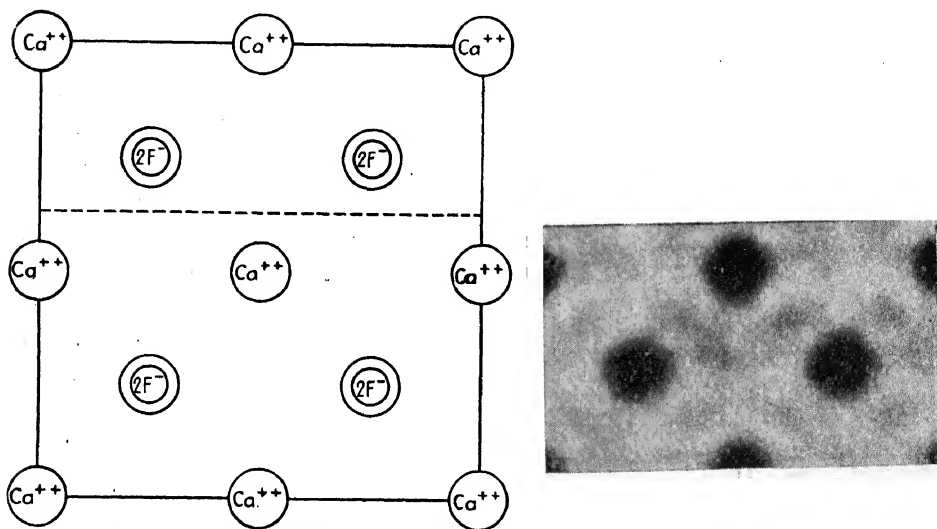


FIG. 4. Structure of  $\text{CaF}_2$  by optical summation of Fourier series. (Huggins.)

emulsion which is insensitive to this amount of exposure. A 50-term summation can be made in half an hour by this optical-summation method. It can be employed not only for electron-density plots in which there is a center of symmetry, but also for nonsymmetrical projections, provided that the phases of the terms are known, and for Patterson and Patterson-Harker plots.

M. J. Buerger has been developing methods for the synthesis of Fourier series by optical diffraction. He has shown that it is possible to drill a metal plate with holes spaced according to the points in a layer of a reciprocal lattice and by placing this plate in a lens system to form a diffraction image of the light passing through the holes. The diffraction image is the Patterson or the Harker plot of the data drilled into the

<sup>1</sup> M. L. HUGGINS, *J. Am. Chem. Soc.*, vol. 63, p. 66, 1941..

<sup>2</sup> Contributed by M. L. Huggins. The data used were from R. J. Havighurst, *Phys. Rev.*, vol. 28, p. 869, 1926.

plate. By adjusting the amount of light that passes through each hole in the plate (for example, by varying the size of the holes) the various  $F$  values for each reflection can be represented and the projected image can be made to show all the large and small peaks that are found on the mathematically computed plots. Further developments of this principle appear likely.

## APPENDIX VII

### CRYSTAL STRUCTURES OF THE ELEMENTS

The following table has been obtained from summaries by M. C. Neuberger (*Z. Krist.*, vol. 93, p. 1, 1936) and by H. S. Rawdon and H. C. Vacher (*Metals Progress*, vol. 40, pp. 187, 581, 715, 1941) and references given in these articles. It represents a critical review of the data as of 1941.

An asterisk indicates the ordinary form of an element that exists (or is thought to exist) in more than one form. Included in the list is the *A* symbol used by P. P. Ewald and C. Hermann in the "Strukturbericht" (*Z. Krist.*, vol. 66ff., Akademische Verlagsgesellschaft m.b.H., Leipzig).

Modification	Element	Type of structure	Lattice constants in Å			Temperature for which constants apply	Distance of closest approach, Å
			<i>a</i>	<i>b</i>	<i>c</i> or axial angle		
	Actinium						
	Alabamine						
	Aluminum	F c c. A1	4 0414		.....	25°C	2 8577
	Antimony	Rhombohedral A7	4 4976		$\alpha = 57^{\circ}6.5'$	25°C.	2 8795
	Argon	F c c. A1	5 42		.....	-233°C.	3 83
	Arsenic	Rhombohedral A7	4 135		$\alpha = 54^{\circ}7.5'$	Room	2 507
	Barium	B c c. A2	5 015		.....	Room	4 343
$\alpha$	Beryllium*	H c p. A3	2 2680		3 5942	20°C.	2 2236
$\beta$	Beryllium	Hexagonal	7 1		10 8	Room	
	Bismuth	Rhombohedral A7	4 7356		$\alpha = 57^{\circ}14'2''$	18 5°C	3 1036
	Boron	Probably hexagonal					
	Bromine	Orthorhombic	4 48	6 67	8 72	-150°C.	2 27
	Cadmium	H c p. A3	2 9731		5 6069	25°C.	2 9731
$\alpha$	Calcium*	F c c. A1	5.560		.	20°C.	3 932
$\beta$	Calcium						
$\gamma$	Calcium	H c p. A3	3 94		6 46	460°C.	3 94
	Carbon	Diamond cubic A4	3 561		.....	18°C.	1 511
	Carbon (graphite)*	Hexagonal A9	2 46		6 78	Room	1 42
$\alpha$	Cerium	H c p. A3	3 65		5 91	Room	3 63
$\beta$	Cerium*	F c c. A1	5 143		.....	Room	3 637
	Cesium	B.c.c. A2	6 05		.....	-173°C	5 24
$\alpha$	Chlorine	Tetragonal	8 56		6.12	< -110°C.	1 88
$\alpha$	Chromium*	B.c.c. A2	2 8786		.....	17°C	2 492E
$\beta$	Chromium	H c p. A3	2 717		4 418	Room	2 709
$\gamma$	Chromium	Cubic A12	8 717		.....	Room	1 043
$\alpha$	Cobalt*	H c p. A3	2 507		4 072	Room	2 499
$\beta$	Cobalt	F.c.c. A1	3 545		..	Room	2 506
	Columbium	B c c. A2	3 2941		..	20°C	2 8527
	Copper	F.c.c. A1	3 6080		..	20°C.	2 5512



Modification	Element	Type of structure	Lattice constants in Å			Temperature for which constants apply	Distance of closest approach, Å
			a	b	c or axial angle		
Para-	Dysprosium	H.c.p. A3	3.74		6.09	Room	3.73
	Erbium*						
	Europium						
	Fluorine						
	Gadolinium						
	Gallium	Orthorhombic, 1-face centered A11	4.517	4.511	7.645	Room	2.437
	Germanium	Diamond cubic A4	5.647	.	.....	Room	2.445
	Gold	F.c.c. A1	4.0700	.	.....	20°C.	2.8779
	Hafnium	H.c.p. A3	3.200	.	5.077	Room	3.139
	Helium						
	Holmium	H.c.p. A3	3.557		5.620	Room	3.480
	Hydrogen	Hexagonal	3.75		6.12	-271°C.	
	Illium						
	Indium	Face-centered tetragonal A6	4.585		4.941	22°C.	3.242
	Iodine	Orthorhombic, 1-face centered A14	4.795	7.255	9.180	Room	2.70
	Iridium	F.c.c. A1	3.8312	.		19°C.	2.7091
	Iron*	B.c.c. A2	2.8610			20°C.	2.4777
	Iron	F.c.c. A1	3.564			20°C.	2.520
			3.642			950°C.	2.580
	Iron	B.c.c. A2	2.93			1425°C.	2.53
			5.68			-191°C	4.02
α	Krypton	F.c.c. A1	5.68			-191°C	4.02
	Lanthanum*	H.c.p. A3	3.75		6.06	Room	3.73
	Lanthanum	F.c.c. A1	5.296			Room	3.754
	Lead	F.c.c. A1	4.9389			20°C.	3.4924
	Lithium	B.c.c. A2	3.5016			20°C	3.033
	Lutecium						
	Magnesium	H.c.p. A3	3.2022		5.1991	20°C.	3.1899
	Manganese*	Cubic A12	8.894			Room	1.065
	Manganese	Cubic A13	6.300			Room	2.368
	Manganese	Face-centered tetragonal A6	3.774		3.526	Room	2.582
α	Masurium						
	Mercury	Rhombohedral A11	2.999		α = 70°31.7'	-46°C	2.999
	Molybdenum	B.c.c. A2	3.1403		..	17°C.	2.7196
	Neodymium*	H.c.p. A3	3.657		5.88	Room	3.620
	Neon	F.c.c. A1	4.52			-268°C.	3.20
	Nickel	H.c.p. A3	2.49		4.08	Room	2.49
	Nickel*	F.c.c. A1	3.5169		.	25°C.	2.4868
	Nitrogen	Cubic	5.66			-252°C	1.06
	Nitrogen	Hexagonal	4.34		6.59	-234°C.	
	Osmium	H.c.p. A3	2.7298		4.3104	20°C.	2.670
α	Oxygen	Orthorhombic	5.50	3.82	3.44	-252°C.	
	Oxygen	Rhombohedral	6.19		α = 99.1°	-238°C.	
	Oxygen	Cubic	6.83			-225°C.	
	Palladium	F.c.c. A1	3.8817	...		20°C.	2.7448
	Phosphorus*	Orthorhombic A16	3.31	4.38	10.50	Room	2.17
	Platinum	F.c.c. A1	3.9158	..	.	20°C.	2.7689
				β = 92°			
	Polonium	(Probably) monoclinic	7.42	4.29	14.10	Room	3.4
	Potassium	B.c.c. A2	5.333	.	..	Room	4.618
	Praseodymium*	H.c.p. A3	3.657		5.924	18°C.	3.64
	Protoactinium						
Black							

Modification	Element	Type of structure	Lattice constants in Å			Temperature for which constants apply	Distance of closest approach, Å
			a	b	c or axial angle		
	Radium						
	Radon						
$\alpha$	Rhenium	H.c.p. A3	2 7553		4 4493	20°C.	2 7340
	Rhodium	Cubic	9 21			Room	
$\beta$	Rhodium*	F.c.c. A1	3 7956			18°C.	2 6839
	Rubidium	B.c.c. A2	5 62			-173°C.	4 87
$\alpha$	Ruthenium*	H.c.p. A3	2 6987		4 2740	18°C.	2 6447
	Samarium						
$\alpha$	Scandium*	F.c.c.	4 532			Room	3 925
$\beta$	Scandium	H.c.p. A3	3 30		5 23	Room	3 23
	Selenium*	Hexagonal A8	4 337		4 944	Room	2 316
$\alpha$	Selenium	Monoclinic		$\beta = 91^{\circ}34'$			
			8 992	8 973	11 52	Room	
$\beta$	Selenium	Monoclinic		$\beta = 93^{\circ}4'$			
			12 74	8 04	9 25	Room	
	Silicon	Diamond cubic A4	5 4173			20°C.	2 3457
	Silver	F.c.c. A1	4 0778			25°C.	2 8835
	Sodium	B.c.c. A2	4 2820			20°C.	3 708
	Strontium	F.c.c. A1	6 075			Room	4 296
$\alpha$ (Yellow)	Sulphur*	Face-centered orthorhombic A17	10 48	12 92	24 55	Room	2 12
				$\beta = 83^{\circ}16'$			
$\beta$	Sulphur	Monoclinic	10 90	11 02	10 96	103°C.	
	Tantalum	B.c.c. A2	3 2959			Room	2 8544
	Tellurium	Hexagonal A8	4 445		5 912	Room	2 858
	Terbium						
$\alpha$	Thallium*	H.c.p. A3	3 450		5 520	Room	3 404
$\beta$	Thallium	F.c.c. A1	4 841			Room	3 423
	Thorium	F.c.c. A1	5 077			Room	3 590
	Thulium						
$\alpha$ (gray)	Tin	Diamond cubic A4	6 46			18°C.	2 80
$\beta$ (white)	Tin*	Body-centered tetragonal	5 8194		3 1753	20°C.	3 0161
$\alpha$	Titanium*	H.c.p. A3	2 953		4 729	Room	2 915
$\beta$	Titanium	B.c.c. A2	3 32			900°C.	2 88
$\alpha$	Tungsten	Cubic A1	5 038			20°C.	2 519
$\beta$	Tungsten*	B.c.c. A2	3 1586			25°C.	2 7354
	Uranium	Orthorhombic	2 852	5 865	4 945	Room	2 76
	Vanadium	B.c.c. A2	3 0338			25°C.	2 6274
	Vanadium						
	Xenon	F.c.c. A1	6 24			-185°C.	4.41
	Ytterbium						
	Yttrium	H.c.p. A3	3 663		5 814	Room	3 595
	Zinc	H.c.p. A3	2 6595		4 9368	25°C.	2 6595
$\alpha$	Zirconium*	H.c.p. A3	3 223		5 123	Room	3 166
$\beta$	Zirconium	B.c.c. A2	3 61			867°C.	3 18

\* Ordinary form of an element that exists (or is thought to exist) in more than one form.

# APPENDIX VIII

## INTERNATIONAL ATOMIC WEIGHTS<sup>1</sup>

Element	Sym- bol	Atomic number	Atomic weight	Element	Sym- bol	Atomic number	Atomic weight
Aluminum . . . . .	Al	13	26.97	Molybdenum.....	Mo	42	95.95
Antimony.....	Sb	51	121.76	Neodymium. . .	Nd	60	144.27
Argon. . . . .	A	18	39.944	Neon . . . . .	Ne	10	20.183
Arsenic . . . . .	As	33	74.91	Nickel . . . . .	Ni	28	58.69
Barium . . . . .	Ba	56	137.36	Nitrogen.. . . .	N	7	14.008
Beryllium . . . .	Be	4	9.02	Osmium.....	Os	76	190.2
Bismuth . . . . .	Bi	83	209.00	Oxygen . . . . .	O	8	16.0000
Boron . . . . .	B	5	10.82	Palladium . . . .	Pd	46	106.7
Bromine . . . . .	Br	35	79.916	Phosphorus . . .	P	15	30.98
Cadmium . . . . .	Cd	48	112.41	Platinum . . . .	Pt	78	195.23
Calcium . . . . .	Ca	20	40.08	Potassium . . . .	K	19	39.096
Carbon . . . . .	C	6	12.010	Praseodymium	Pr	59	140.92
Cerium . . . . .	Ce	58	140.13	Protoactinium	Pa	91	231
Cesium . . . . .	Cs	55	132.91	Radium . . . . .	Ra	88	226.05
Chlorine . . . . .	Cl	17	35.457	Radon . . . . .	Rn	86	222
Chromium . . . . .	Cr	24	52.01	Rhenium . . . . .	Re	75	186.31
Cobalt . . . . .	Co	27	58.94	Rhodium . . . . .	Rh	45	102.91
Columbium . . . .	Cb	41	92.91	Rubidium . . . .	Rb	37	85.48
Copper . . . . .	Cu	29	63.57	Ruthenium . . . .	Ru	44	101.7
Dysprosium . . . .	Dy	66	162.46	Samarium . . . . .	Sm	62	150.43
Erbium . . . . .	Er	68	167.2	Scandium . . . . .	Sc	21	45.10
Europium . . . . .	Eu	63	152.0	Selenium. . . . .	Se	34	78.96
Fluorine . . . . .	F	9	19.00	Silicon . . . . .	Si	14	28.06
Gadolinium . . . .	Gd	64	156.9	Silver . . . . .	Ag	47	107.880
Gallium . . . . .	Ga	31	69.72	Sodium . . . . .	Na	11	22.997
Germanium . . . .	Ge	32	72.60	Strontium . . . .	Sr	38	87.63
Gold . . . . .	Au	79	197.2	Sulfur . . . . .	S	16	32.06
Hafnium . . . . .	Hf	72	178.6	Tantalum . . . . .	Ta	73	180.88
Helium . . . . .	He	2	4.003	Tellurium . . . .	Te	52	127.61
Holmium . . . . .	Ho	67	164.94	Terbium . . . . .	Tb	65	159.2
Hydrogen . . . . .	H	1	1.0080	Thallium . . . . .	Tl	81	204.39
Indium . . . . .	In	49	114.76	Thorium . . . . .	Th	90	232.12
Iodine . . . . .	I	53	126.92	Thulium . . . . .	Tm	69	169.4
Iridium . . . . .	Ir	77	193.1	Tin . . . . .	Sn	50	118.70
Iron . . . . .	Fe	26	55.85	Titanium . . . . .	Ti	22	47.90
Krypton . . . . .	Kr	36	83.7	Tungsten . . . . .	W	74	183.92
Lanthanum . . . .	La	57	138.92	Uranium . . . . .	U	92	238.07
Lead . . . . .	Pb	82	207.21	Vanadium . . . . .	V	23	50.95
Lithium . . . . .	Li	3	6.940	Xenon . . . . .	Xe	54	131.3
Lutecium . . . . .	Lu	71	174.99	Ytterbium . . . .	Yb	70	173.04
Magnesium . . . .	Mg	12	24.32	Yttrium . . . . .	Y	39	88.92
Manganese . . . . .	Mn	25	54.93	Zinc . . . . .	Zn	30	65.38
Mercury . . . . .	Hg	80	200.61	Zirconium . . . .	Zr	40	91.22

<sup>1</sup> *J. Am. Chem. Soc.*, vol. 63, p. 850, 1941.

## APPENDIX IX

### PHYSICAL CONSTANTS<sup>1</sup> AND NUMERICAL FACTORS

Planck's constant  $h = (6.6242 \pm 0.0024) \times 10^{-27}$  erg-sec.

Charge on the electron  $e = (4.8025 \pm 0.001) \times 10^{-10}$  abs. e.s.u.

Mass of electron at rest  $m_0 = 9.1066 \times 10^{-28}$  g.

Velocity of light  $c = (2.99776 \pm 0.00004) \times 10^{10}$  cm. per sec.

Boltzmann's constant  $k = 1.38047 \times 10^{-16}$  erg per deg.

Gas constant  $R = Nk = 1.9869$  cal. per deg. per mol

$= 8.31436 \times 10^7$  ergs per deg. per mol

Avogadro's number  $N = 6.0227 \times 10^{23}$  per mol

Mechanical equivalent of heat  $J = 4.1855$  abs. joules per cal. (15°C.)

Mass of atom of unit atomic weight  $1/N = 1.67339 \times 10^{-24}$  g.

Ice point  $T_0 = 273.15^\circ K$ .

Faraday constant  $F = 9648.7 \pm 1$  abs. e.m.u. per gram equivalent

$= 2.89247 \times 10^{14}$  abs. e.s.u. per gram equivalent

1 electron volt  $= 1.602 \times 10^{-12}$  erg

1 electron volt per molecule  $= 23.05$  kcal. per mol

1 kcal.  $= 4.185 \times 10^{10}$  ergs

1 electron volt  $= 11,500k$

1 cal. (15°C.)  $= 4.182$  joules

1 volt  $= 1/300$  e.s.u.  $= 10^8$  e.m.u.

1 radian  $= 57.29578$  deg.

1 in.  $= 2.5400$  cm.

1 Å  $= 10^{-8}$  cm.

1 micron  $= 10^{-3}$  mm.  $= 10^4$  Å

1 psi.  $= 1422$  kg. per sq. mm.

$\ln x = \log_e x = 2.302585 \log_{10} x$

The base of natural logarithms,  $e = 2.718$

<sup>1</sup> R. T. Birge, 1941.

# INDEX

## A

Aborn, 267  
 Absolute reflecting power, 83  
 Absorption coefficients, 520  
 Absorption factor, 537  
 Adamantine compounds, 210  
 Age hardening, 340, 461-474  
 Aluminum, rolled, preferred orientations  
     in, 395-401, 425  
 A.S.T.M. card index of x-ray data, 138  
 Amorphous metal, 1  
     electron diffraction studies of, 503-  
     505  
 Amorphous solids, 229  
 Andersen, 188, 191  
 Andrade, 290-294  
 Angles, formulas for, 511-515  
     table for cubic crystals, 35  
 Anisotropy, in crystals, 453-460  
     in polycrystalline metals, 371, 443-  
     453  
 Annealing, sharpening of lines during, 86,  
     375-377  
 Ansel, 290, 324  
 Antimony, explosive, 229, 440  
 Antimony structure, 200  
 Archer, 461  
 Arsenic, amorphous, 229, 440, 501  
 Astbury, 146  
 Asterism, 82, 350-362  
     in age hardening alloys, 470-474  
 Atomic percentage, formula for, 205  
 Atomic scattering factor  $f$ , 77  
 Atomic weights, 555  
 Atoms, determining positions of, 150  
     radii of, 150, 216-218  
 Austenite, 203, 476  
 $AX$  and  $AX_2$  compounds, 209-218  
 Axes, choice of, 145  
     principal, secondary, tertiary, 24  
     systems of, 3  
     table of, 4

## B

Bain, 230, 476, 478  
 Bainite, 479  
     habit planes, 485  
     orientations, 484  
 Bakarian, 162, 411, 414  
 Baldwin, 427-429, 446, 450  
 Bardeen, 253  
 Barkhausen effect, 263  
 Bauschinger effect, 329  
 Beck, 449  
 Becker, 239, 473  
 Becker-Orowan theory, 333  
 Bend test, effect of orientations on, 412-  
     415  
 Berg, 361  
 Bernal, 98, 107, 109  
 Beta phases, 211, 232, 265  
 Bethe, 238-240  
 Binary diagrams, determination of, 178-  
     185  
 Birge, 556  
 Bitter, 264, 432, 433, 451  
 Bjurstrom ruler, 129, 151  
 Blake, 536, 537  
 Boas, 373, 429, 437, 458, 459  
 Boas and Schmid's theory, 387  
 Body-centered cubic structure, 197  
 Body-centered lattices, absent reflec-  
     tions from, 77, 127, 146  
     rotating crystal patterns of, 101  
 Bohr theory of atom, 49  
 Boron nitride structure, 209  
 Bozorth, 34, 125, 221, 403, 432, 451,  
     453  
 Bradley, 117, 119, 133-135, 187-195, 234,  
     538  
 Bragg, 44, 142, 350, 356, 542-549  
 Bragg spectrometer, 83  
 Bragg-Williams theory, 236, 241, 248  
 Bragg's law, 70, 75-77, 134  
     in reciprocal space, 105

- Brass, line widths from, 374-377  
     phases in, 180, 211-215  
     rolled, directional properties in, 443-446  
     preferred orientations in, 395-402, 424-429
- Bravais lattices, 2
- Brick, 293, 397, 402, 416, 425, 430
- Bridgman, 1, 173, 370
- Brill, 373
- Brillouin zones, 257
- Brindley, 367-374, 527, 533
- Buerger, 98, 114, 135, 145, 221, 536, 538
- Burgers, 334, 359, 422, 448, 475
- Burghoff, 445
- C**
- Calcium fluorite structure, 210
- Calibration of films, densities, 65  
     for  $\theta$ , 84, 121, 132-137
- Cameras, back-reflection Laue, 167-172  
     back-reflection powder, 81, 85, 122, 124, 135, 280  
     Buerger, 111, 113  
     Davey-Wilson, 165-167  
     de Jong-Bouman, 114  
     focusing, 84, 121  
     for grain distortion, 361, 362  
     high temperature, 98, 119  
     Laue, 80, 88, 89, 172  
     low temperature, 98, 120  
     pinhole, 87, 88  
     powder, 84, 89, 97, 115-125  
     for preferred orientations, 87, 163  
     rotating crystal, 82, 89, 97  
     precision, 145  
     Sauter, 114  
     for stress measurement, 270, 274, 279  
     universal, 89, 97  
     Weissenberg, 111
- Canfield, 344
- Carbon black, 358
- Castings, textures in, 435-437
- Cementite, 476
- Cesium chloride structure, 209, 232
- Chalmers, 311, 314, 325, 345, 347
- Characteristic x-rays, 47
- Charts, Davey-Wilson, 164, 166  
     Greninger, back reflection, 170  
     Hull-Davey, 128-130  
     stereographic, 29  
     Wever, pole figure, 160, 161
- Chemical affinity effect, 206
- Chemical analysis, by x-ray diffraction, 86, 139  
     by x-ray emission, 44, 49
- Claassen, 537
- Clark, 56, 142, 410
- Classes, symmetry, 13-18
- Cleavage, 317-324
- Cleavage planes, analysis of, stereographic, 37
- Cochrane, 496, 500, 505
- Cohen, 135-138
- Cohen's analytical extrapolation, 136
- Cohesion, in metals, 251, 254
- Cold work, asterism from, 350-363  
     effect of, on physical properties, 460  
     from fatigue stressing, 377-380  
     vs. line intensities, 372-375  
     vs. line widths, 363-372  
     residual energy from, 339, 364  
     revealed by x-rays, 86  
     theory of resistance from, 261
- Colloidal state, 229
- Colloids, diffraction lines from, 142
- Compressibility, 253
- Compression, deformation textures from, 385-387  
     recrystallization textures after, 422, 424  
     theories of textures, 387-395
- Compton, 52, 527, 542
- Compton effect, 58
- Conductors, theories of, 254-261
- Constitution diagrams, determination of, 86, 178-195
- Continuous spectrum, 46, 93
- Conversion factors, 556
- Coolidge tubes, 59, 61
- Coordinates, of atoms, 3  
     of equivalent points, 18, 24  
     of lattice points, 4  
     of reciprocal lattice points, 103, 106
- Copper, line widths from, 369, 371, 377
- Covalent binding, 196
- Cox, 540
- Creep, 344-348
- Cristobalite structure, 209
- Cross rolling, recrystallization textures after, 433
- Crossed-grating diffraction, in age-hardening alloys, 470

- Crossed-grating diffraction, in crystals,  
     356, 358  
     in electrons, 500  
     Laue equations, for 73  
 Crystal, definition of, 1  
 Crystal structure, of adamantine com-  
     pounds, 210  
     of amorphous solids, 229  
     of elements, 196–201  
         table, 552  
     of Hume-Rothery phases, 211–216, 265  
     imperfections, 219–223  
         (See also Imperfection in crystals)  
     of intermediate phases, 208–219, 265  
     of interstitial compounds, 216  
     of liquids, 224–229  
     of normal valency compounds, 208–211  
     reference books on, 196  
     of solid solutions, 201–208, 266  
     superlattices, 230–240  
     use of term, 3  
 Crystal-structure determination, Fourier  
     series methods, 144, 542–551  
     fundamental methods, 76–85, 114  
     by Laue method, 93  
     outline of steps, 144–153  
     by powder method, 125  
     x-ray, limitations of, 114, 144–148  
 Crystal systems, table of, 4  
 Crystallographic formulas, 511–515  
 Cube texture, 425–430, 446  
 Cubic system, angles between planes, 34,  
     35, 511  
     diffraction lines from, 126, 522  
 Cylindrical coordinates, 106
- D
- Dahl, 425, 428, 444, 451  
 Darwin, 220  
 Davenport, 480, 484  
 Davey, 118, 127, 133, 165, 221, 403, 405  
 Debye, 533  
 Debye equation, for liquids, 225  
 Debye-Scherrer-Hull method, 83, 115–  
     143  
 Decrement, 341  
 Deep drawing, textures from, 417  
 Deformation bands, 305, 360, 391–395  
     asterism from, 360  
 Dehlinger, 366, 370
- de Jong, 114  
 Densities, of crystals, calculated, 138  
     photographic, 65  
     in Laue patterns, 93  
 Derge, 482  
 Diamond cubic structure, absent reflec-  
     tions from, 127  
 Diamond structure, 199, 210  
 Diffraction, discovery of, 44  
     of electrons, 493–510  
     from lattices and space groups, 146–148  
     of x-rays by crystals, 69–87  
 Directional properties, 443–460  
 Disappearing phase method, 181, 187  
 Dislocation theory, 334–348  
 Dislocations, diffraction from, 366  
     resistance arising from, 261  
 Dixit, 440  
 Domains, in ferromagnetic metals, 263  
     in superlattices, 239  
 Domes, 19  
 Donnay, 146, 511  
 Drude-Lorentz theory, 254
- E
- Easthope, 238, 240  
 Eccentricity errors, 134–137  
 Edmunds, 414, 436, 447, 449  
 Elam, 294, 304–307  
 Elastic aftereffect, 329  
 Elastic constants, 268, 278, 453–458  
     of superlattices, 247  
 Electrodeposits, line broadening from,  
     229, 368, 501  
     textures in, 437–439  
 Electron compounds, 211–216  
 Electron density, in crystals, 542–551  
 Electron diffraction, 493–509  
     apparatus, 494  
     extra rings, 498  
     identification of phases, 497  
     particle-size determination by, 501  
     reciprocal lattice relations, 106  
 Electron microscope, 142, 223  
 Electron theory, of metals, 251–266  
 Electron waves, 254  
 Electronegative valency effect, 206  
 Electrons, atomic energy states of, 49–52  
     in x-ray tube, 46

Elements, structures of, 552-554  
 symmetry, 13, 19, 21  
 Elmore, 264  
 Enantiomorphic crystals, 16  
 Endurance limit vs. x-ray patterns, 377-380  
 Energy levels, 49-52, 255-266  
 Epsilon phases, 212-214, 265  
 Equi-inclination photograph, 113  
 Equivalent points, 18, 19, 24  
 Errors in powder cameras, 132-137  
 Etch pits, 174, 223  
 orientations by, 173-177  
 Eutectoid reactions, 475-492  
 Evaporated films, 439-442  
 Evaporation, metal deposited by, 229, 439  
 Ewald, 552  
 Exposure, measures of, 65  
 Extinction, 369, 374, 540  
 Extrapolation of errors, 135

## F

$f$ , atomic scattering factors, 77, 372, 526  
 table of, 529  
 $F$ , structure factor, 79, 528-532  
 $F^2$  series, 544-551  
 Face-centered cubic structure, 197  
 Face-centered lattices, absent reflections  
 from, 127, 146  
 rotating crystal patterns of, 101  
 Faces, growth, 144  
 Fankuchen, 540  
 Farnam, 422  
 Fatigue, A.S.T.M. committee reports, 378  
 deformation of grains by, 369, 377-380  
 effect of, on residual stresses, 282  
 Ferrite, 203, 476  
 Ferromagnetism, 241, 248  
 theory, 261-264  
 Fiber textures, 154-158, 381-395  
 Films, calibration of, 84, 132-137  
 calibration of densities, 65  
 characteristic curve of, 65  
 efficiency of, 65-68  
 methods of reading, 280  
 shrinkage of, 132-135, 271  
 Filters, x-ray, 56, 125

Finch, 496-509  
 Fink, 461-468, 478  
 Fisher protractor, 33  
 Fluorescent x-rays, 52, 85  
 Fluorite structure, 209  
 Focusing cameras, 84, 121  
 Foote, 183  
 Form, planes of, 8, 18, 19  
 Fourier analysis of structure, 144, 542-551  
 Fowler, 242  
 Fracture, 317-324  
 Furth's theory of, 321  
 Fricke, 374  
 Friedel's law, 89  
 Fuller, 412, 449, 498

## G

Gallium liquid, 227  
 Gamma phases, 213-216, 265  
 Gas, structure of, 1  
 Geisler, 467-474  
 Gensamer, 268, 328, 407, 416, 431  
 Germer, 441, 493-504  
 Glassy state, 1, 229  
 Glide plane symmetry, 21  
 Glocker, 268-282, 424, 426  
 Gnomonic projection, 43, 90  
 Goldschmidt, 150, 208, 209  
 Goniometers, for crystal orientation, 165-173  
 for preferred orientation, 163  
 Goss, 409, 416, 424, 432, 451  
 Gough, 310, 378  
 Grain boundaries, effect of deformation, 325  
 Grain size, after cold work, 1, 363-375  
 determination of, by line broadening, 142, 363-372  
 by spot size, 82  
 Graphical methods, for powder patterns, 127, 134  
 Greenland, 292, 298  
 Greninger, 167, 477-491  
 Greninger chart, 170  
 Griffith, 332  
 Groth, 145  
 Guinier, 471  
 Guinier-Preston zones, 470-474



## H

- Habit planes, austenite decomposition, 484-491
- Hanawalt, 413, 414
- Hanawalt's chemical analysis system, 139-141, 497
- Hardness, vs. grain size, 326  
vs. line widths, 375, 376  
of solid solutions, 326, 340  
of superlattices, 246
- Harker, 544, 546
- Haworth, 221, 365-370
- Heindlhofer, 323
- Hemihedral symmetry, 16
- Hemimorphic crystals, 16
- Hendricks, 358, 496
- Hermann-Mauguin notation, space-lattices, 6, 22  
symmetry elements, 16, 17
- Heusler alloys, 234, 248
- Hexagonal close-packed structure, 197
- Hexagonal crystals, axes of, 4  
indices of, 9  
interpretation of patterns from, 131  
stereographic projection of, 37  
unit cell of, 7
- Holohedral symmetry, 16
- Homopolar binding, 196
- Hot rolling textures, 416
- Howe, 305
- Huggins, 550
- Hull, 139
- Hull-Davey charts, 128
- Hume-Rothery, 120, 184, 185, 476
- Hume-Rothery 8 - *N* rule, 199
- Hume-Rothery structurally analogous phases, 211-216, 265

## I

- Imperfection in crystals, 82, 219-223  
asterism from, 358
- Indices, determination of, metallographically, 41  
of directions, 8  
of Laue spots, 90  
law of rational, 12  
Miller, 7  
Miller-Bravais, 9, 10  
of planes of form, 8, 18

- Indices, in powder patterns, 126  
of reflected beams, 75, 84  
in rotating crystal patterns, 100  
transformation of, 11  
in Weissenberg patterns, 111  
zone, 8, 13
- Insulators, theories of, 254-261
- Intensities of reflections, absolute, 83  
for electron diffraction, 508  
formulas (x-rays), 79, 541  
Laue spots, 81, 93, 538  
along Laue streaks, 351  
measurement of, 65, 83  
relation of, to crystal structure, 78-80, 524-551
- Intermetallic compounds, 204
- Internal friction, 341-344
- Interplanar spacings, 76, 126
- Interstitial compounds, 216
- Inversion, center of, 14
- Iodine structure, 200
- Ionic binding, 196
- Ionization spectrometer, 83
- Iron, line widths from, 376  
microstructure from transformation, 40  
preferred orientations in, 386, 391, 394, 402-410, 417, 424, 431-433

## J

- James, 527, 533
- Jay, 234
- Jeffries, 424, 461
- Jette, 121, 124, 138, 188, 203
- Jetter, 464-471
- Jevons, 447, 450
- Johansson, 230, 241
- Johnson, 53
- Jones, 265

## K

- K* series, 47, 85
- Kaiser, 470
- Kanter, 345
- Kauzmann, 345
- Kettman, 134
- Kies, 379
- Kikuchi, 508
- Knot theory of age hardening, 461
- Koeler, 336-339

Kommers, 378  
 Kurdumow-Sachs orientation relation-  
 ship, 481

## L

Lark-Horowitz, 498  
 Lattice complex, 148  
 Lattice constants, precision determina-  
 tion, 132-139  
     theoretical calculations, 253  
 Lattices, 2  
     types of, 5, 6  
     use of term, 3  
 Laue, 44  
 Laue equations, 71-74  
     in rotating-crystal method, 98  
 Laue method, 80, 88-96  
     asterism, 350-362  
     shapes of spots, 93  
 Layer lines, 82, 98, 108  
 Lees, 419, 505  
 Leonhardt, 94  
 Lester, 267  
 Limiting sphere, 106  
 Line broadening, from cold work, 363-372  
     from particle size, 142, 370-372, 501,  
     502  
 Lineage structure, 221  
 Lipson, 476, 549  
 Liquid, structure of, 1, 224-229  
 Liquid crystals, 2  
 Local-curvature theory, 356, 359-362  
 Ionsdale, 149, 532, 544  
 Lorentz factor, 535  
 Lustman, 431

## M

McCandless, 491  
 McKeehan, 126, 264, 314  
 Magnesium, directional properties in, 449  
     preferred orientations in, 410-414, 433  
 Magnetic domains, 263  
 Magnetism, changes during annealing,  
     375  
     theory of, 261-265  
 Marsh, 194  
 Martensite, 478  
     Greninger-Troiano theory of, 483  
     habit planes, 483-485  
     orientations, 480-484

Martensitic transformation, in  $\beta$ -brass,  
     309  
 Mathewson, 308-313, 323, 388  
 Mehl, 202, 239, 407, 464-492  
 Mercury, 227  
 Merica, 461  
 Mesomorphic state, 2  
 Metallic binding, 196, 251  
 Meteorites, structure of, 464  
 Mica, structure of, 2  
 Microcreep, 348  
 Microstructure, during age hardening,  
     461-470  
     in steel, 475-491  
     vs. strength, 328  
 Molecular binding, 196  
 Moller, 270-282  
 Monochromator, 118, 125  
 Mosaic blocks, 219-223  
     effect of, on dislocations, 337, 338  
     on intensities, 372  
     on line widths, 363-371  
 Moseley's law, 48  
 Mott, 468, 470  
 Multiplicity factor, 536

## N

Nabarro, 468, 470  
 Nelson, 501  
 Neuberger, 552  
 Neumann bands, 308  
 Nickel arsenide structure, 210, 216  
 Nishiyami, 482  
 Nishiyami orientation relationship, 482  
 Nitride needles (plates), 42  
 Nix, 231, 436  
 Norbury, 215  
 Normalizing, random texture from, 433  
 Northcott, 437  
 Norton, 283-285, 417

## O

Omega ( $\omega$ ) coordinate, 106, 112  
 Optical synthesis of series, 549  
 Order of reflections, 71, 75  
     in Laue spots, 81  
     in reciprocal lattices, 102  
 Order in superlattices, 230-250  
     long range, 235

- Order-disorder transformations, 230–250  
Orientation of crystals, determination,  
    stereographic, 38, 40, 41  
    of precipitate, 466–474  
    preferred, 87, 381–442  
    representation of, 34  
Orthohexagonal axes, 11  
Orthorhombic crystals, diffraction lines  
    from, 131  
    example of structure determination,  
        151  
Oscillating crystal method, 109  
Overgrowths, 491
- P
- Parameters (atom positions), 149  
Parametric method, 182, 187  
Particle-size determination, 142, 370, 502  
Patterson  $P^2$  series, 544  
Patterson-Harker series, 546  
Pauli's exclusion principle, 255  
Pauling, 151, 527  
Pearlite, 477  
    orientations in, 484  
Penfield protractors, 28, 33  
Periodic table, 198, 219  
Permallov, line widths from, 365, 368  
Pfeil, 305  
Phase changes, stereographic analysis of,  
    in iron, 40  
    (See also Transformations)  
Phase diagrams, determination of, 178–  
    195  
Phase rule, 180  
Phases, determination of, in alloys,  
    178–195  
    in Fe-C alloys, 475–480  
    identification of, by x-rays, 86  
    intermediate, structure of, 208–219  
    theories of, 265  
Phillips, 447, 458  
Physical constants, table of, 556  
Piezoelectric crystals, 16  
Pinacoids, 19  
Planck constant, 50  
Plane of symmetry, 14  
Planes, indices of, 7  
    intersection of, 38  
    spacing of, 12  
    traces on two surfaces, 37–42  
Plastic deformation, grain distortion  
    from, 362  
    mechanism of, 288–330  
    theories of, 332–348  
Point groups, 13  
    table, 17  
Points, coordinates of, 18, 24  
Pole figures, cold rolling, 398–416  
    compression textures, 386, 392, 393  
    deep-drawn pail, 418  
    plotting of, 158–162  
Poles of planes, 25, 33, 37–42  
Polished metal, 1  
Polished surfaces, electron diffraction  
    studies of, 503–505  
Post, 403, 410  
Powder cameras, errors in, 132–137  
Powder method, 80, 83, 115–143  
    absorption errors, 135–137  
    for binary diagrams, 179–185  
    choice of camera dimensions, 119  
    choice of radiation, 85, 125, 138  
    interpretation of films, 125–143, 151  
    specimens, 118, 121, 122, 184  
    for ternary diagrams, 185–195  
Precipitation, during age hardening,  
    461–474  
    of planes, analysis of, 37–42  
Precision lattice constants, 86, 132–139  
Preferred orientations, 87, 381–442  
    analysis of, 154–163  
    in castings, 435–437  
    causing asterism, 351–354  
    from cold drawing, 417  
    from cold rolling, 395–415  
    from compression, 385–395  
    after compression and recrystalliza-  
        tion, 422–424  
    from cross rolling, 415  
    from deep drawing, 417  
    in deposited films, 439–442  
    directional properties from, 443–452  
    effect of, on properties, 381, 443–453  
    electron diffraction evidence of, 502, 503  
    from hot rolling, 416  
    from machining and polishing, 418  
    recrystallization, theories, 420, 428  
    in rolled sheet recrystallized, 424–434  
    from torsion, 417  
    from wire drawing, 381–395  
    in wires, recrystallized, 420–424

Preston, 357, 471  
 Primitive space-lattices, 6  
 Primitive translations, 2  
 Principal stresses, 269  
   measurement of, 270-287  
 Prisms (crystal forms), 19  
 Projections, gnomonic, 42, 90  
   reflection, 43  
   spherical, 25, 31, 32  
   standard, 33  
   stereographic, 25  
     nets, 29, 30  
 Protractors, stereographic, 28, 33  
 Pyramids, 19  
 Pyroelectric crystals, 16

## Q

Quantum numbers, 258  
 Quarrell, 499, 501, 506  
 Quasi-binary lines, 194  
 Quick, 379

## R

Radii, atomic, 150, 216-218  
 Radiography, 54  
   voltages used, 46  
 Radius errors, 134-137  
 Randall, 527  
 Ransley, 415, 448  
 Rational indices, law of, 12  
 Reactions, orientation and habit in, 491  
 Read, 335-343  
 Reciprocal lattice, 101, 472  
   for electron diffraction, 507  
 Reciprocity law, x-ray, 67  
 Recovery, 375  
   revealed by x-rays, 86  
 Recrystallization, 375  
   accompanying age hardening, 463, 464  
   revealed by x-rays, 86  
 Recrystallization textures, 420-434  
   table, iron and its alloys, 432  
 Reference sphere, 25, 42  
 Reflection, of x-rays, 70-87  
   table of reflecting planes, 522  
 Reflection projection, 43  
 Reflection sphere, 103  
 Refraction error, 138  
 Relative valency effect, 206

Resistivity, changes during annealing,  
   375, 376  
   vs. magnetism, 264  
   in superlattices, 243-245, 248, 261  
   theories of, 254-261  
 Robertson, 542, 548, 549  
 Rock salt structure, 209  
 Rolling and recrystallization, textures  
   from, 424-434  
 Rolling textures, 395-417  
   theories of, 406, 407  
 Röntgen, 44  
 Ross filters, 58  
 Rotating crystal camera, 145  
 Rotating crystal methods, 80, 82, 97-114  
 Rotation axes, of symmetry, 13  
 Rotation-inversion axes, 14  
 Rutile structure, 209

## S

Sachs, 270, 283, 286, 330, 354, 364, 395-  
   431, 463, 481  
 Sauter, 114  
 Sauveur, 485  
 Scattering of x-rays, 53, 77, 524, 534  
 Scherrer, 142  
 Scherrer particle size formula, 142, 370  
 Schiebold, 536  
 Schmid, 382-459  
 Schoenflies, space-group notation, 6, 22  
   symmetry-class notation, 15, 17  
 Screens, intensifying, 67  
 Screw axes, 21  
   table of, 22  
 Seeman-Bohlin camera, 121  
 Seitz, 251, 335-342, 345, 454  
 Semiconductors, 260  
 Shear, in twinning, 315-317  
 Shear stress, for slip, 294-302, 332, 341  
 Shearing fracture, 321  
 Shockley, 231, 240, 241, 251  
 Shrinkage errors, 132-137  
 Schrödinger equation, 257  
 Siegbahn, 138  
 Sisson, 408, 410  
 Sixtus, 432, 452  
 Size factor, 206  
 Slide rule, for cubic patterns, 127  
 Slip, crystallography of, 288-294, 304  
   rotation caused by, 302-307

- Slip, stress required for, 294-302, 332-340  
     theories of, 332-341  
 Slip lines, 291, 338  
     analysis of, stereographic, 37-42  
     precipitation along, 462  
 Slits, design of, 117  
 Smekal, 332  
 Smith, C. S., 445  
 Smith, D. W., 461-468, 474, 484, 485  
 Smith, G. V., 484, 485, 491  
 Sodium, liquid structure of, 226  
 Solid solutions, in iron alloys, 219  
     structure of, 201-208  
     theory of, 266  
 Sommerfeld's theory, 258  
 Space groups, 19  
     determination of, 146  
     tables of, 148  
 Space-lattices, 2  
     determination of, 146  
     drawings of, 5  
     table of, 6  
     x-ray determination of, 114, 126, 146, 151  
 Spacings, interplanar, 76, 126  
 Specific heats, of metals, 256  
     of superlattices, 242  
 Specimen preparation, 118, 121, 122, 184  
     for pole figures, 162  
 Spectrometer, ionization, 83  
 Sphere of reflection, 103  
 Spots, shapes of, 93-96  
 Spretnak, 409, 496  
 Sputtered films, 439-442  
 Steel, rolled, diffraction from, 158, 161, 162  
     directional properties in, 447, 452  
     preferred orientations in, 402-405, 407-410, 415-418, 431-433  
     for transformers, 432  
 Stereographic projection, 25-43  
     angle measurement on, 26, 32, 33  
     applications, 25, 37, 145  
     of Laue asterism, 351-354  
     of Laue equations, 73, 74  
     nets and their use, 29-33  
     of orientation of crystals, 34, 40, 163-177  
     of preferred orientations, 155-162  
     (See also Pole figures)  
 Stereographic projection. protractors, 28, 33  
     standard projections, 33  
 Stibitz, 365  
 Stickley 368, 371  
 Stillwell, 151  
 Strain hardening, 298-302, 326-330, 335-338  
 Strains, macroscopic, measurement of, by x-rays, 267-287  
 Stress coat, 380  
 Stress measurement, by sectioning, 286  
     by x-rays, 86, 267-287  
 Stresses, in age hardening alloys, 467, 468  
     altered by fatigue, 282  
     vs. asterism, 354  
     for cleavage, 317-324  
     macroscopic vs. microscopic, 363  
     for slip, 294-302  
     for twinning, 315, 322  
     from welding, 281-285  
 Structurally analogous phases, 211-216  
 Structure, use of term, 3  
 Structure factor  $F$ , 79, 127  
 Sublimation energy, 253  
 Superlattices, 230-250  
     origin of resistance in, 261  
 Symmetry, determination of, 81, 144-148  
     of point positions, 148  
     rotation axes of, 13  
     of x-ray patterns, 89  
 Symmetry elements, 13, 19  
     reflection characteristics of, 147, 546  
 Systems, crystal, 2, 6
- T
- Tamman, 230  
 Tarasov, 451, 452  
 Taylor, 304, 330, 334-336, 364, 388-390  
 Tellurium structure, 200  
 Ternary alloys, recrystallization textures in, 430  
 Ternary diagrams, 185-195  
 Tetrahedral symmetry, 16  
 Tetragonal crystals, diffraction lines from, 129  
 Texture (see Preferred orientations)  
 Thermal vibrations, asterism from, 357  
 Thomas, 127  
 Thomassen, 374-377

- Thomson, 493, 496, 524  
 Torsion textures, 417  
 Traces of planes, 37-42  
 Transformations, in age hardening alloys, 466-474  
   asterism from, 356  
   of metals, 474  
   in steel, 475-492  
 Translation, repetition by, 21  
 Translation groups, 2  
 Troiano, 483, 485  
 Tubes, x-ray, 59-64  
 Tunell, 540, 549  
 Twinning, atom movements in, 313-315  
   crystallography of, 307-313  
   effect of, on pole figures, 413-415  
   in magnesium, 449  
   shear in, 315-317  
   stresses for, 315, 322  
 Twinning planes, analysis of, stereographic, 37-42
- U
- Ulrey, 45  
 Unckel, 444  
 Unit cell, 3  
   atoms in, determination of, 148  
   choice of, 145  
   determination of, 145  
     Laue, 93  
     rotating crystal, 100, 107  
   hexagonal, 7  
   volume of, 102  
 Uranium, structure of, 151
- V
- Vacher, 397, 552  
 Valency compounds, 208-211  
 Vegard's law, 202  
 Velocity factor, 540  
 Vilella, 477, 480  
 von Hevesy, 44, 52
- W
- Waller, 533  
 Warren, 142, 151, 226, 358, 540  
 Wasserman, 411-422, 439-449, 470-483  
 Wavelengths, electron, 254  
   x-ray, table of, 516-519  
 Wavelengths, of x-rays, 45-49, 138  
   true scale vs. Siegbahn, 138  
 Weissenberg goniometer, 111  
 Welding stresses, 281-285  
 West, 542  
 Westgren, 121  
 Westgren-Phragmén camera, 121  
 Wever, 133, 134, 219  
 Wever chart, for pole figures, 160-162  
 White radiation, 45-47, 94  
 Widmanstätten figures, analysis of, stereographic, 41, 42  
   table of data, 486  
 Wires, deformation textures in, 381-385  
   recrystallization textures in, 421-424  
   theories of, 387-395  
 Wollen, 527  
 Wood, 285, 368-378, 437, 438  
 Wooster, 111, 454  
 Wright, 33, 43  
 Wulff, 505  
 Wulff net, 29  
   uses of, 38-42  
 Wurtzite structure, 210  
 Wyckoff, 22, 88, 93, 151, 196, 537, 538
- X
- X-bands, 305  
 X-constituent in steels, 480  
 X-ray tubes, 59-64  
 X-rays, absorption of, 51, 53  
   absorption coefficients, 520  
   characteristic spectrum, 47, 85, 516  
   chemical analysis by, 44, 49  
   choice of, powder method, 85, 125  
   continuous spectrum, 46  
   diffraction fundamentals, 69-87  
   discovery of, 44  
   efficiency of production, 45, 47  
   filtering, 56  
   fluorescent, 52  
   generating equipment, 59-64  
   intensity measurement, 65  
   *K* and *L* series lines, 47-49  
   line intensities vs. voltage, 52  
   photographic effects of, 65-68  
   properties of, 44, 45  
   protection from, 64  
   scattered, 58, 69  
   true wavelengths, 138  
 Xi ( $\xi$ ) coordinate, 106, 112

## Y

Young, 466, 483

## Z

Zachariasen, 151, 356–358

Zener, 341–344

Zernike-Prins formula, 225

Zeta ( $\zeta$ ) coordinate, 106, 112

Zinc, rolled, directional properties in, 449

Zinc, rolled, preferred orientations in,  
410–414, 433

standard projection of, 37

Zinc blende structure, 209

Zinc-sulphide screens, 68

Zintl, 217

Zone axes, 12

determination of, 39

Zone theory, 257–266

Zones, 12

in Laue patterns, 81, 90 .















